DETECTION OF DEFECTS IN CONCRETE STRUCTURES USING VIBRATION TECHNIQUE

Thesis presented for the Degree of

Doctor of Philosophy

of the University of Strathclyde

by

Henricus Priyosulistyo, Ir.,M.Sc.

Department of Civil Engineering

University of Strathclyde

February, 1992

C O N T E N T S

ACKNOWLEDGEMENTS

The author wishes to thank to the Government of Indonesia for granting leave and financial support to undertake this study.

He is deeply grateful to Professor H.D.Wright for his encouragement, valuable discussions and guidance in writing up the thesis. He also would like to thank Dr.J.Marshall for the technical guidance, thoughtful criticism and friendship throughout this research.

Thanks are also due to Professor I.A.MacLeod for the use of the laboratory and computing facilities, to Mr.J.D.Allan for his supports, to the structure laboratory staff of the department in particular to Messrs. J.Morrin, J.Harper, J. McLean and T.Towers for their technical advice and friendship during the course of the experimental work and to Mr.R.Barron and Mr.D.Evan for their helps on dealing computer problems.

The author also wishes to thank the CPIU-Jakarta and the British Council for organising this study and mutual communication.

Finally, to my beloved wife and son the author wishes to record their patience and understanding.

ABSTRACT

This thesis investigates the dynamic behaviour of reinforced concrete beams as they are loaded to failure. Four beams have been investigated. Two types of crack pattern and two types of reinforcement pattern were the main variable parameters. Partially bonded reinforcement as artificially created (by greasing the bars) and positioned at the center third span in two of the four beams investigated. The remaining two beams had conventional bonded reinforcement. Flexural and diagonal splitting patterns were created by loading mechanisms individually applied on two beams of each type of reinforcement. Stage by stage application of static loadings was used. Steady state vibration tests were applied at prior to loadings the beams and at several load stages as gradually increasing defects occurred. There are four parts to this investigation and these are presented in this thesis.

The first part investigates the accuracy of several techniques dealing with signal parameters from a digital response spectrum in the signal processing. A logic geometry was developed and was applied on the line spectra of the response spectrum. Numerical evaluation found that the error induced in the proposed technique decreased exponentially with increasing numbers of cycles. A maximum of 0.17% errors may exist when

examining 100 cycles of the frequency of interest. A regression analysis was used to achieve further accuracy of the results.

The second part investigates the jump phenomenon of mechanical exciters and the sharp drop phenomenon of magnetic exciters. Both of which may confuse the analysis of structural dynamic behaviour. By accounting for the stiffness of the magnetic field of the magnetic exciter in a mathematical model, the jump phenomena was shown to be due to the effect of the reflected force in the excited structure. Practical equations were also proposed to relate absolute to relative parameters.

The third part of the thesis concerns the algorithms required in filter processing and includes the development of a computer solution. Two algorithms were developed to obtain coefficients of a polynomial equation which was set up from elementary equations and from a rational function respectively. The algorithms were simple and easy to program.

The last part of the thesis discusses the detection of flexural and diagonal splitting defects and non-linear behaviour of the beams during the vibration tests. Static and dynamic comparisons are also discussed.

Based on the characteristics of the polar diagrams it was found that several possible types of non-linear damping were demonstrated in the experiments. The typical viscous and non-linear higher polynomial damping existed

mostly in the models although the crack pattern and intensity of cracks contributed to changes in the type of damping. In addition the beam models in almost all conditions showed non-linear soft spring behaviour. Diagonal splitting crack patterns can be identified from a small decrease of resonant frequency and from the sharp drop of resonant amplitude. The presence of single deep cracks greatly reduced the stiffness. The experiments show that a sharp decrease of resonant frequency indicates that a large amount of residual strain exists.

It is concluded that defects of the reinforced concrete beams can be identified from the changes of the dynamic parameters using the proper digital signal analyses. The jump phenomenon is shown to be due to the effect of the reflected force on the moving exciter mass rather than due to the presence of the non-linear soft spring system.

NOMENCLATURE

a = coefficient of amplitude

a_0 = a_1 = b_1 = coefficients of the Fourier series

a_k = roots of polynomial equation

A = relative dynamic amplitude coefficient

An = spectra level associated with frequency fn

At = attenuation of pass band frequency.

A_c = angular stop band

A_s = angular pass band

= total area of steel section

$\bar{A}$ = absolute dynamic amplitude coefficient

A(w) = coefficient of the w^{th} regression analysis

b = amplitude coefficient

= breadth of beam section

B = absolute dynamic amplitude coefficient

B_s = Polynomial equation in Laplace form

B(w) = coefficient of the w^{th} regression analysis.

c = viscous damping coefficient

c_r = critical damping coefficient

C = coefficient of analog to digital transformation

C_c = total force of concrete in compression

C1 = C2 = Cn = coefficients

CF = corrective factor

[C] = matrix of damping coefficients

d = damping ratio = c/c_r

= clear depth of beam section

dB = decibels = $20\log_{10}$(Ratio)

[e] = matrix of eigenvectors

$[e]^T$ = transpose matrix of eigenvectors

E_c = modulus elasticity of concrete

E_s = modulus elasticity of steel

f = analog frequency in Hertz.

fr = predicted frequency

f_{cu} = compressive stength of concrete (N/mm^2)

fn = frequency with amplitude denoted by An

f_s = allowable stress of steel (N/mm^2)

f_y = yield stress of steel (N/mm^2)

F = static force

F_0 = static force from the magnetic field

F(t) = F sin ωt = time dependence force of excitation

[F(t)]= matrix of time dependence force of excitation

h = hysteretic damping coefficient

= total height of beam section

h(t) = time dependence function

$h(\tau)$ = time dependence function

H(f) = transformed function of h(t)

H(s) = transformed function in Laplace form

H(z) = transformed function in z-form

i = coefficient of integration

i(t) = time dependence function

I(f) = transformed function of i(t)

I_o = initial inertia

I_k = inertia of region-k

j = $\sqrt{-1}$ = imaginary root

j(t) = time dependence function

J = number of divisions

J(f) = transformed function of j(t)

k = stiffness of system

= coefficient of integration (integer value)

k(t) = time dependence function

K(f) = transformed function of k(t)

K = stiffness of system

[K] = stiffness matrix

l = coefficient of integration

L = total amount of data executed

= span (m)

m = mass of system

m_r = M/m = ratio of mass

M = mass of system

[M] = mass matrix

n = order of polynomial equation

= E_s/E_c = modulus equivalence

N = normal force

= number of coefficients of polynomial equation

p = angular natural frequency

p_k = k^{th} angular natural frequency

p_r = p_2/p_1 = ratio of angular frequencies

q = distributed load (kN/m)

Q_{self} = self weight load (kN/m)

r = ω/p = frequency ratio

= B/A = amplitudes ratio of excited beam/structure to moving excitation mass

r_u = ω/p_u = frequency ratio

r_a = $(1 + 0.75\ \alpha\ A^2)$

R ≃ $(\mu\ F)$ = Coulomb friction force

sgn($\dot{x}$) = vector in phase with velocity

s = bilinear transformation coefficient

t = time

Δt = time interval = time increment

T = executable time

T_s = total force of steel in tension

T_o = 1/f = period of signal

T(max) = Kinetic energy

u = coefficient of integration

v = shear stress (kN/mm^2)

V = shear force (kN)

V(max) = Strain energy

x = x(t) = time dependence function

$\dot{x}$ = first derivative of x to time = velocity

$\ddot{x}$ = second derivative of x to time = acceleration

x_1 = relative dynamic displacement of the moving exciter mass to the excited beam/structure.

x_2 = absolute dynamic displacement of the excited beam/structure

x_3 = absolute displacement of the moving exciter mass

x(t) = time dependence function

X(f) = transformed function of x(t)

$y(t)$ = time dependence function

$Y(f)$ = transformed function of $y(t)$

$[z]$ = displacement matrix

α = measured relative phase angle of the moving exciter mass to the excited beam/structure.

= coefficient in filter design

β = $\varphi - \alpha$ = different phase angle between the true and measured relative phase angles.

= coefficient in filter design

Δf = frequency resolution

Δt = time interval

γ = stiffness parameter

$\psi(x)$ = general shape function in x-axis

λ = $2\pi f/F_s$ = digital frequency range

μs = micro strain (10^{-6} strain)

$\nu(x)$ = shape function in x-axis

ρ = coefficient of friction

τ = time

φ = true relative phase angle of the moving exciter mass and the excited beam/structure.

ω = angular frequency of excitation

ω_0 = $2\pi f_0$

INTRODUCTION

1. INTRODUCTION

This thesis concerns the evaluation of the structural condition of reinforced concrete beam elements by monitoring their dynamic response to forced excitation.

1.1. General.

Any structure may be thought of as being composed of many constituent elements. Each element may be considered 'alive' in that it has specific sensitivities. Reactions to stimulus may be various and include static deflection, thermal reaction and sensitivity to vibration. In this latter case the maximum responses are known as indications to the natural frequencies of the structure. If different maximum responses may be sustained they provide many modes of vibration. The modes of vibration may be thought of as being dependent on a number of idealised lumped masses and the axes of vibration of those lumped masses. The number of independent mass times axis situations defines the degree of freedom of the system. When one of the natural frequencies is intentionally excited the elements respond. The amplitude response of the individual element depends on its mass, stiffness and damping. Loading or damage causes changes in the response of individual elements and therefore the structure as a

whole. The changes of response may be due to the changes of one or more of the dynamic parameters, i.e. natural frequencies, damping, amplitudes and stiffness. Structural defects may be caused by the failure to design against environmental hazards such as that caused by heavy traffic disturbance, water waves or from heavy machinery involved in or close to the structure. Alterations to the structure or its use may also cause defects. In addition earthquake loads or impact from bomb blasts on or near the structure will affect the reliability and integrity of the structure. This study covers the specific defect of flexural and diagonal splitting cracks on simply supported reinforced concrete beams and investigates the characteristics of its dynamic parameters. The evaluation of the dynamic parameters includes signal processing and the evaluation techniques used for this are developed in the study.

1.2. Review of Vibration Studies.

Several researchers have studied the effect of damage on the dynamic response of simply supported reinforced concrete beams.

Tourk [1] studied the effect of the presence and propagation of cracks in the concrete on the characteristics of the dynamic response. In his experiment on nine reinforced concrete beams having nominal dimensions of 1300mm x 50mm x 75mm he attached

strong steel frames at the ends of the reinforced concrete beams perpendicular to the beam axis and applied static load by pulling on a steel bar connecting the frame's tips. The eccentric load created an almost even moment over the length of the beam. A magnetic vibrator was positioned at the centre of the span, under the concrete beam, and was anchored to the floor. A loading ring was used to measure the induced load and was attached between the vibrator head and the bottom of the beam. The eccentric load was not removed while the steady state vibration test was being carried out. The static moment as well as the the excitation force, which was 5 Newtons, was maintained constant over the vibration test during which scanning for natural frequency between 50 to 200 Hz took place. Tourk [1] found that the natural frequencies exponentially decreased as the static moment increased. In addition the damping ratios increased with the increasing static moments. The natural frequencies found from the experiments did not agree well with analytical results. This error was reported to be due to the incorrect idealisation of the analytical model or the fact that existing micro cracks might have changed the natural frequencies. Furthermore, it was noted that the amplitudes of excitation caused variation in the natural frequencies. The higher the amplitudes of excitation the lower the natural frequencies found.

Sim [2] improved the analytical techniques used by Tourk [1] by remodelling the cracks in the finite element model. The linear program was modified to accept the existing cracks by zeroing the element stiffness around the cracks. A step by step or iterative analysis was applied in the program and this corresponded to the propagation of the cracks. The model consisted of many layers and the stiffness was updated as each concrete layer cracked. Sim found from these numerical results that the natural frequencies decreased as the cracks increased. The finite element program produced static load-deflection results which were also in good agreement with those obtained experimentally.

Hashim [3] improved the loading scales applied in the eccentric bar as used by Tourk [1]. Hashim applied an excitation force of 50 Newton over the frequency range of 50 to 200 Hz in the steady state vibration test and examined successfully eight singly and doubly reinforced concrete beams. He commented that the static loading device affected the damping. Moreover he also found that the natural frequencies decreased as the beam approached its failure moment.

Tan [4] examined three types of beam, i.e. under , balanced and over reinforced concrete beams. The methods of creating cracks and the analytical comparisons were the same as those used by Sim [2]. However, instead of applying steady state vibration tests as used by Tourk

[1], Hashim [3] and Sim [2] Tan carried out impact tests. The damping ratio from the impact test was included in the computational analysis. The computational result of the later technique was in good agreement with the experiment.

Several research studies on the dynamic characteristics of structures composed of materials other than concrete have also been carried out.

Research on steel beam elements was carried out by Christides and Barr [5]. Solid cross section steel beams were examined in this study. Artificially created symmetrical cracks were introduced and successive steady state excitation experiments were carried out. A parameter was evaluated from the experimental tests and included in the proposed equation of motion. This allowed the equation to take account of the effect of stress about the cracks. The equation was a satisfactory fit to the experimental results. Furthermore, It was also reported that the natural frequency was not sensitive to the presence of the crack unless the crack was very extensive. A parabolic curve showing the relationships between the ratio of the natural frequency and the ratio of crack depth for various numbers of artificial cracks was produced. The cracks were intentionally made quite wide to avoid nonlinear characteristics that could occur due to the opening and closing of the more narrow cracks.

Hassan [6] studied the characteristics of a lattice tower under vibration tests. Two types of test were dealt with, i.e. steady state vibration tests and 'pull-sudden release' tests. From the 'pull-sudden release' tests Hassan found a relationship between amplitudes of excitation and damping. She stated that the damping characteristics were dependent on the amplitude of excitation. At a certain higher range of amplitude of excitation the increase in amplitudes of excitation increased the damping ratio. The structure relating to this observation was viscously damped. On the other range the increase of amplitudes of excitation decreased the damping ratio. She illustrated this characteristic as an asymptotic curve in a cartesian axis. The structure relating to this later observation was dry damped. Furthermore the two ranges met at a point where the half power band width method most accurately predicted the damping ratio.

Ibanez [7] reviewed several analytical techniques to improve structural dynamic models in the study of the safety and reliability of pressure vessels and piping systems in nuclear power plants. He included experimental data to improve the dynamic model of the structure under test. The model could then be used for simulation. Numerous practical examples were described and were shown to be of value. It was commented that the dynamic characteristics of the structure changed with

greater amplitudes of excitation. Many other experimental aspects were also discussed in the paper.

The work discussed above was carried out without much consideration of the non-linearities of the structure or the material. Several standard references dealing with vibration of structures in this elastic range are also available such as in [8,9.10,11.12,13]. Several papers are now reviewed which include the study of non-linear structures and material response.

White [14,15] conducted experimental and theoretical work on the non-linearities arising from large deflections. A steel plate was hinge-supported at its four edges so as to maintain the possibility of the membrane effect. The non-linear hard spring behaviour became the main topic of the study. White [14,15] found a solution to the determination of resonance of a structure having non-linear hard spring behaviour. The maximum rate of arc spacing criterion derived from a cubic equation on the polar diagram (a diagram representing the real and imaginary part of the response) was proposed to identify resonance. Steady state excitations were applied at a steady frequency increment. Details of this phenomena will be covered in chapter-2. Furthermore White in [14] as well as in [16] studied the effects of the non-linearity on the dynamic parameters from the impulse response of a structure using a Fourier transform of the proposed perturbation method. It was

reported that although the time history of the perturbation method was not accurate the predicted natural frequencies were in agreement with those derived from a Fourier transform program.

Hartog [45] in his study of a system damped by a combination of Coulomb and Viscous friction described the variety of possible damping types on structural behaviour. He stated at least four types met most frequently, i.e. the viscous damping where the damping force is proportional to the velocity, the Coulomb damping where the force is independent of the velocity, the air resistance damping where the force is proportional to the square or higher order of the velocity and the internal hysteresis/ hysteretic damping where the force is independent of the velocity and depends only on the amplitude of motion. He presented an exact solution of a single degree of freedom system with the mixed damping just mentioned. The increase of Coulomb friction decreased amplitude response.

Yeh [46] developed the work of Hartog [45]. An exact solution for a two degree of freedom system with one Coulomb and two viscous dampers was established. The solution had a range of accuracy when applied only to motions that did not come to rest.

Tomlinson et al.[17] referring to the work of Hartog [45] and Yeh [46] further investigated, in detail the dynamic characteristics of a structure with lightly

viscous damping and coulomb friction damping using the harmonic balance method, a method of equating coefficients of the lower terms of a trigonometric equation. Tomlinson reported that the presence of coulomb damping no longer allowed the response to conform to a locus of a circle of the polar diagram in the resonant region. The distorted pattern in the polar diagram was evaluated on the basis of the in-phase and quadrature power dissipated when exciting the normal mode. This effect was also studied by Tomlinson in [18] which the distorted pattern was proved to be due to the presence of non-linear coulomb damping and not to be due to limitations imposed by the approximate method.

Rades [19] referred to the work of Tomlinson [17,18] in dealing with the parameter identification of a structure with coulomb friction and hysteretic damping. Rades developed a technique to evaluate the coefficient of the non-linearity by using several polar diagrams. Rades claimed that the way the isochrones, i.e. lines connecting the points of constant frequency from different curves, bent into a concave shape as shown in the family of polar diagrams can identify the presence of coulomb damping especially when the distorted curves were not obviously apparent. Furthermore, Rades in [20] revealed the validity of the isochrones to identify the presence of quadratic damping, a damping which is associated with the turbulent flow of a fluid through an

orifice. Rades claimed that this type of damping cause the isochrones to bend into a convex shape and the curves therefore distorted like a flattened ball. Another result was achieved when Rades [21] examined the effects of non-linear stiffness in a resonance test. He examined the cubic stiffness term in the governing equation using the harmonic balance method. He demonstrated the effect of a jump phenomena in the polar diagram and used the isochrones to identify a type of stiffness non-linearity. Rades carried out experiments using rubber or polyurethane materials for vibration isolation purposes. Since non-linear stiffness can not be identified by a single polar diagram Rades strongly recommended that only families of polar diagrams and their isochrones be used for identification of non-linear stiffness. Further discussions are available in chapter-2.

Many standard references discuss the mathematics of non-linear structures as seen in [22,23]. These will not be discussed here.

A recent application of the vibration tests using mechanical vibrators to relieve residual stress was discussed by Claxton [47,48]. He [47] commented that his technique was a complementary technique to the existing thermal treatment technique. One or more resonant frequencies were induced on the structure under tests at certain levels of amplitude where the yield point of the material was exceeded. About 2000 cycles at every

resonance were applied within 10 minutes frequency scanning which was described as the mass and stiffness dependence. He [47,48] claimed that his technique was successful and many problems were dealt with using the technique.

1.3. Review of Signal Processing.

Apart from the non-linear response problems signal processing obviously plays a significant role in determining correct dynamic parameters. This subject includes the problems of digitizing data, Fourier transformation and filter design. These subjects are available in many standard references such as in [10,24,25,26,27,28,29]. Only reference to specific parts of the standard references, related papers and reports will be discussed below.

To enable analog signals to be analysed digitally using a proposed Fast Fourier Transform program a digitising machine or digitiser is demanded. The accuracy of the digitiser input data to the software controlling the digitiser plays an important role. The accuracy of the digitiser can be defined in the specification of the digitiser . The higher the 'bits' the better the results. A twelve 'bits' digitiser can represent a unit analog output in 2^{12} integer numbers. The accuracy of the digital numbers may be achieved at plus or minus 1 digit. Further more the output is also

dependent on the input scaling factor. Errors due to improper factor selection, known as round off error, may decrease the accuracy of the digital output. Further discussion of this matter may be found in [25].

Parameters of a signal may be more simply analysed in the frequency domain rather than in the time domain. Since digital data is involved in the analysis a classical method, the Discrete Fourier Transform as seen in reference [25], may be used for small amounts of data. To avoid repeated executions occurring in the DFT method an algorithm derived on the basis of the prime number of 2, known as the Fast Fourier Transform (FFT), was originally proposed by Cooley and Tukey [30]. This algorithm saves considerable executable time over the DFT method. Algorithms on the basis of prime numbers of other than two have also been available [24,27]. The latest algorithm is able to execute any amount of data (namely the self sorted Radix Mixed FFT). This algorithm is more flexible in practice especially if a lot of data is executed as has been used in weather forecasting by Temperton [31,32,33]. Moreover the radix mixed algorithm can be adopted in any computer memory and analysis can be carried out without disposing out any amount of data. Further discussions of the Fourier transformation are found in chapter-2.

The FFT method was adopted by Hassan [6] in the research to analyse the dynamic parameters from steady

state vibration tests. Hassan introduced an empirical formula to deal with the resonant frequency of the response. The accuracy of the results using the formula depended on the frequency resolution. Further discussions in this matter are found in chapter-4.

Signal processing inevitably involves filter designs. To gain executable time in on line process two complementary cascade Fast Fourier Transformers proposed by O'leary [34] may be simultaneously used to transform two dependent data blocks. The two sets of transformed non-recursive filter functions can be stored in the computer memory. Continuous filtering may then be performed by cascading the transformed pairs and the sets of the filter spectrum. Word rates in excess of 3MHz are possible with available hardware. O'leary [34] applied this design in the radar communications areas.

Kormylo at al. [35] proposed a two-pass recursive digital filter to avoid the phase-lag imposed in the filtering process. The initial and reverse time transients were evaluated and an overlapped scheme was proposed.

Czarnach [36] introduced an overlap-save algorithm in terms of matriculation to identify the time transients involved in the filtering process of non-causal recursive systems. Systematic errors were detected in the process using cascade connections.

Chan et al.[37] proposed filter coefficients derived

from a finite impulse response (FIR) using the Wiener-Lee decomposition technique. An analog transfer function was decomposed into the Wiener-Lee decomposed form. Coefficients were evaluated using the integral transformation proposed. The recursive filter was achieved by truncating the non-recursive filter using a window function after applying a bilinear transformation. The technique avoided overflow which is likely to happen in the non-recursive filters. The time transients are detectable from the filter function words. Further band stop attenuation may be increased by applying window function on the impulse filter response. The advantage of this recursive filter over the other recursive filters was that the band pass/band stop specifications may be changed as easily as the non-recursive filter.

Following Chan's proposal Kwong [38] simplified the computation of the Wiener-Lee decomposition method. He proposed an expansion of the transformed filter function into a Laurent series. Inverse transformation may then be carried using standard z-transformations.

Chan et al.[39] again introduced a non causal filter using the Wiener-Lee transformation technique. He managed to deal with the phase-lag which normally occurred in any convolution process. In comparison with the two-pass non causal recursive filter proposed by Kormylo et al.[35] this technique occupied a small amount of computer memory because of the short transient word.

therefore. it required a small group delay.

The technique proposed by Chan [37,39] and Kwong [38] is employed in the program and a long division algorithm is developed in the process. Further discussion of the filtering technique is found in chapter-2 and chapter-6.

1.4. Summary of Existing Research and Formulation of the Problem.

The dynamic parameters of reinforced concrete beams under vibration tests have been studied by several authors [1,2,3,4]. Most experiments were under constant external load whilst the vibration tests were carried out. This enabled the cracks to open during the vibration tests. As the amplitudes of excitation were not excessive the effects of non-linearity due to opening and closing of the cracks were not apparent. The decreasing natural frequencies observed with the increase in the amplitudes of excitation were possibly due to the soft spring behaviour of the structures. The increase in cracking, due to an increase in the flexural moment, reduced the natural frequencies. This has been accepted in all previous research. The curve relating natural frequency to crack depth proposed by Christide et al. [5] is different from the similar curve relating natural frequency to the flexural moment proposed by Tourk [1]. The steel material having artificial wide open cracks

produced an inverse exponential curve (convex shape upward) and the presence of cracks were found to be not sensitive to the natural frequencies. An exponential curve was reported by Tourk [1] in the natural frequency - applied moment relationships of the reinforced concrete beams.

Theoretical equations of motion developed for the homogeneous material proposed by Christide et al. [5] may not be directly applied to reinforced concrete structures due to the complexities of the structure. Reinforcement obviously contributes to the behaviour of the beam as it cracks under load. This is especially noted during dynamic experiments if the external load was removed as reported by this author in [40]. Mathematical studies have shown that it is still not possible to predict closely the dynamic behaviour of reinforced concrete beams. The finite element method employed by previous researchers predicted results far from the experimental values despite improvements by Sim [2] on the element mesh making it resemble more the experimental model. Numerical studies and the experimental studies have consumed almost equal amounts of researchers' time. It was, therefore, decided that this research should concentrate on experimental work and in particular the effects of different crack patterns and their identification from the study of the dynamic parameters. Several suggestions are made to achieve more accurate

dynamic parameters.

It was reported that the natural frequencies resulting from the polar diagram overestimated natural frequencies from the response spectrum [15]. This was possibly due to the fact that the measured phase did not represent the relative phase of the exciter to the structure under test. A study on this phenomena has been carried out and formulae for correction purposes are presented.

There are two possible non-linear stiffness problems imposed by the reinforced concrete beams under tests. Under considerably low amplitudes of excitation the beams exhibit quasi-softening behaviour. If the beams are excited excessively they may exhibit rectification phenomenon. Correct experimental procedures and settings play an important role in accurate analysis of the results. Furthermore non-linear damping may also be exhibited in the experiment. Under relatively high amplitudes of excitation the concrete beams may demonstrate viscous damping. In contrast under considerably low amplitudes of excitation dry friction or Coulomb friction or non-proportional damping may exist.

The empirical equation proposed by Hassan [6] to deal with the peak frequency response numerically depended on the frequency resolution. Since only peak frequencies were of interest the additional zero data values to suit the base-2 algorithm or the application of the window function may be acceptable. As vibration tests include

many aspects where response spectra should be proper and any signal in the frequency domain can be performed in the time domain with the radix-2 FFT. the window function and the additional zero data values should not be employed. An alternative solution using a proposed logic geometry applied on the spectra level is proposed. Errors induced in the results are analyzed via the radix mixed FFT which is capable of accepting any amount of data. From the response spectra an equation for correction has been derived.

1.5. Scope and Layout of the Thesis.

The general objective of the study was to monitor defects of reinforced concrete beams by means of vibration tests. Appropriate methods and improvements on existing experimental procedures and analyses are examined to produce more accurate values of the dynamic parameters.

Basic linear and non-linear equations of motion are described briefly in chapter-2. General transformation of the Fourier series into Fourier integral and its associated physical characteristics are then described. The signal processing involved in obtaining dynamic parameters and the presentation of the response are also discussed in this chapter.

The experimental setup and procedures are discussed in chapter-3. Typical specimens, positions of the

vibration pick-ups and their considerations are described. Comments and confirmations on the experimental procedure and results are described at the end of the chapter.

To improve the dynamic parameters corrective coefficients based on a proposed geometry are described in chapter-4. Comparisons are made with the available techniques and comments on the applications of the proposed technique are also included.

Relationships between the exciter and the excited structure and their affects on the response spectrum are evaluated in chapter-5. Corrections to the results are proposed.

The general output quality of any vibration tests depends on the amount of data analysed. A large amount of data is processed using a computer program. Two algorithms are established to enable the long division theory and the setting up of polynomial equations to be applied in the developed computer program. These discussions are obtained in chapter-6.

Results and analyses of the vibration tests are separately discussed in chapter-7 due to the dependency of several evaluations made in chapter-4 to chapter-6.

Discussions of the results are outlined in chapter-8 following the conclusions and suggestions for further research given in chapter-9.

CHAPTER - 2

2. CHARACTERISTICS OF VIBRATING STRUCTURES.

2.1. General.

Applications of the theory of vibration in monitoring defects in structures are developed in this chapter. A brief discussion of the linear behaviour and a rather deeper discussion of the non-linear behaviour of structures are described. Several possible mathematical solutions may be constructed which depend on the types of excitation applied to the system. This chapter will only emphasise the solutions of the equation of motion of steady state excitation problems.

Most researchers present graphs showing dynamic parameters in terms of frequency response. Response form, namely polar diagram or polar plot, may also be produced by decomposing the amplitudes into their real and imaginary parts and plotting them in the form of an Argand diagram. This technique has several advantages over frequency response techniques, especially when non-linearity exists. The technique will be described further in this chapter.

Signal processing involving Fourier transformations and filter designs will also be discussed. Parameters of a signal, i.e. amplitude, frequency and phase angle rely on the accuracy of the signal processing employed. On the basis of this knowledge those parameters can be used for analysis.

2.2. Equation of Motion of Linear Vibratory Systems.

A basic equation of motion of a single degree vibratory system can be expressed as follows.

$$m\ddot{x} + c\dot{x} + kx = F(t) \qquad \ldots\ldots\ldots (2.1)$$

The particular solution to equation (2.1) for a steady state excitation is

$$x_p = a \sin \omega t + b \cos \omega t$$

By substituting the particular solution and its derivatives in eq.(2.1) and equating the coefficients of the lower order of the trigonometric equation, the amplitude response of the system may be established. Further details of this substitution is available in Appendix [A-1]. The response spectra and the associated stiffness diagrams are shown in fig.(2.1).

A continuous structure can be idealised as a system having a series of lumped masses, springs and dampers. This idealisation simplifies the complicated dynamic parameters which usually occur in real structures. Decoupling the equations of motion enables the dynamic parameters of the system to be analysed independently. The general equation for multi degree vibratory systems can be written as follows :

$$[e]^T[M][e]\ [\ddot{z}] + [e]^T[C][e]\ [\dot{z}] + [e]^T[K][e]\ [z] = [e]^T[F(t)] \qquad (2.2)$$

A complete derivation of equations (2.2) can also be found in Appendix (A-2).

2.3. Equation of Motion of Non-linear Vibratory Systems.

The equation of motion described in (2.1) subject to a steady state force of excitation includes two parameters, c and k which cause the system to behave in a non-linear way. If there is non-linear stiffness the equation becomes

$$m\ddot{x} + c\dot{x} + k(x \pm \gamma x^3) = F(t) \qquad \ldots\ldots (2.3)$$

Equation (2.3) suggests that if the stiffness parameter, γ is zero then equation (2.3) is exactly the same as equation (2.1).

The solution to equation (2.3) can be approximated for small non-linearities by employing a method of harmonic balance as described in references [11,22,23]. By applying a particular solution, $x = A \cos(\omega t + \varphi)$, and an excitation force $F(t) = F_0 \cos \omega t$ into equation (2.3) and omitting the higher harmonics the relationship between the relative amplitude and frequency is obtainable. The technique is fully described in Appendix (A-2) and (A-3) and is partly shown below.

$$(r)^2_{1,2} = (r_a^2 - 2d^2) \pm \left[\frac{F_0^2}{k^2 A^2} - 4d^2(r_a^2 - d^2) \right]^{0.} \qquad (2.4)$$

$$\varphi = \tan^{-1}\left[\frac{2dr}{r_a^2 - r^2}\right] \qquad (2.5)$$

If a resonant frequency of the structure tends to increase as the applied force increases such that the frequency ratio, ω/p, at resonance, is greater than one then the system is referred to as a 'hard spring' system. Mathematically this characteristic is achieved by

adjusting positive γ. The higher the stiffness parameter, γ the larger the non-linearity as seen in fig.(2.2). The line connecting the resonance points of different force of excitation is referred to as the 'skeleton'. Equation (2.4) is a polynomial equation where at a certain frequency of excitation, ω/p it provides three different values of amplitude, A. At this stage the system is within the unstable condition where in practice this produces a 'jump phenomenon'. The stability boundary can mathematically be derived as seen in Appendix (A-4) or reference [22].

On the other hand if the resonant frequency of the structure tends to decrease as the applied force increases the system is referred to as a 'soft spring' system where a negative stiffness parameter, γ is mathematically appropriate. This can be seen in fig.(2.3).

White [14,15] in the study of the effects of non-linearity due to large deflections in resonance testing revealed the existence of the 'jump phenomenon' due to the significant effect of the membrane forces.

Non-linear damping in the frequency domain has similar effects to the 'soft spring' behaviour [22,23]. Coulomb friction damping occurs in some structures where the normal force perpendicular to the friction plane plays a significant role. The equation of non-linear damping was studied by Tomlinson [17] and Rades [19]. Tomlinson

described in [17] that the existence and position of Coulomb friction in a system could be identified, though it could not be identified directly when the system had many Coulomb devices. The combined effect of hysteretic and Coulomb friction was studied in [23]. The equation was presented in the form

$$m\ddot{x} + \frac{h}{\omega}\dot{x} + R\,\mathrm{sgn}(\dot{x}) + kx = F(t) \qquad \text{.....(2.6)}$$

where : $R\,\mathrm{sgn}(\dot{x})$ is the Coulomb damping where the sign is dependant on the relative velocity ($\dot{x}$) with which the friction force, $R \triangleq (\rho N)$ is associated.

On the basis of equation (2.3) and (2.6) equations for multi degree vibratory systems can be built up in terms of matrices as described in Appendix (A-1). A similar equation based on equation (2.6) was developed by Tomlinson [17] to enable hysteretic and friction damping to work on a multi degree vibratory system.

2.4. Polar Diagram.

By decomposing absolute amplitudes into their real and imaginary parts associated with cosines and sines respectively and plotting them on a form of Argand diagram results in a polar diagram. The tangent, φ is associated with the phase angle of the excitation force to the response signal. The technique has several advantages over the frequency response diagram in terms of its capability to improve improper amplitudes arising from difficulties in the instrumentation.

White [15] studied the rate of change of phase angles of a single degree vibratory system as shown in fig.(2.4). He derived an equation proposing the maximum frequency spacing criterion in the polar diagram to identify the natural frequency. The technique was further extended by Rades [19,21].

Rades [21] studied in more detail the effect of non-linearity in polar diagrams. He suggested a method of identifying non-linearity using a series of experiments having different forces of excitation. Looking at the lines connecting the same frequencies (isochrones) the types of non-linearity can be identified as shown in fig.(2.5) and fig.(2.6). Furthermore he also derived a stability boundary equation in the polar diagram. He noted that the 'jump phenomenon' starts at a certain phase angle where the tangent of the isochrone coincides with the tangent of the polar diagram. The stability boundary equation is represented as a hyperbolic equation with the center axis at 135 degree of phase angle. The complete derivation of the equations are obtainable in Appendix (A-5). Rades [19] identified the non-linear damping as a distorted shape of the polar plots as shown in fig.(2.7). Tomlinson [17] commented that the techniques proposed by White [15] did not hold true for a system having Coulomb friction damping. He provided a set of equations to deal with such a phenomenon as shown in fig.(2.8).

2.5. Signal Processing.

As amplitudes, frequencies and phases are measured in vibration testing the analysis of the results must include signal processing. A brief introduction to the Fourier series theory and a more detailed description of the Fourier Transformation are given below.

2.5.1. Fourier Series.

The Fourier theory states that any periodic signal can be decomposed into a series of components of sinusoidal form and of different frequency. The formulation of the statement as described by Ramirez [25] is

$$Y = \frac{1}{2}a_0 + \sum_{1=1}^{1=\infty} (a_1 \text{Cos } 1x + b_1 \text{Sin } 1x) \qquad \ldots\ldots (2.7)$$

The equation must be periodic with time and for all time (i.e time must begin at minus infinity and continue to plus infinity). For practical purposes the observable time can be selected in such away that it does not reduce very much the quality of the results. Furthermore, the conditions for the existence of a Fourier series are referred to as the Dirichlet conditions [25] which are associated with the finite numbers existing in the function, the existence of maximum and minimum values and that the function is integrable in any period.

Equation (2.7) can be modified to relate amplitudes, frequencies and phases as follows.

$$x(t) = a_0 + \sum_{1=1}^{1=\infty} [\ a_1 \cos 1\omega_0 t + b_1 \sin 1\omega_0 t\ ] \qquad \ldots(2.8)$$

where: $\omega_0 = 2\pi f_0$; $a_0 = \frac{1}{T}\int_0^T x(t)\,dt$

$a_1 = \frac{2}{T}\int_0^T x(t) \cos 1\omega_0 t/dt$

$b_1 = \frac{2}{T}\int_0^T x(t) \sin 1\omega_0 t/dt$

T = executable time

As long as a periodic waveform can be mathematically described that meets the Dirichlet conditions, equation (2.8) can be used.

2.5.2. Fourier Integral.

Whilst the Fourier series can deal with a periodic waveform, the Fourier integral can deal with non-periodic waveforms. Thus, it can include periodic waveforms where the period is allowed to approach infinity.

Based on the mathematical identities

$$e^{-j1\omega_0 t} = \cos 1\omega_0 t - j \sin 1\omega_0 t \quad \text{and}$$

$$e^{j1\omega_0 t} = \cos 1\omega_0 t + j \sin 1\omega_0 t$$

for $\omega_0 = 2\pi f_0$ and $j = \sqrt{-1}$ gives

$$\text{Cos } 2\pi 1 f_0 t = \frac{e^{j2\pi f_0 t} + e^{-j2\pi f_0 t}}{2}$$

$$\text{Sin } 2\pi 1 f_0 t = \frac{e^{j2\pi f_0 t} - e^{-j2\pi f_0 t}}{2j}$$

and substituting these into equation (2.8) gives

$$x(t) = \sum_{1=-\infty}^{1=\infty} C_1 \, e^{j2\pi 1 f_0 t} dt \qquad \ldots\ldots\ldots (2.9)$$

By analogy with equation (2.8) C_1 can be evaluated for n $= -\infty$ to n $= +\infty$ using

$$C_1 = \frac{1}{T}\int_{-T/2}^{T/2} x(t)\, e^{-j2\pi 1 f_0 t} dt$$

In knowing that each harmonic is separated by $\Delta f = 1/T$ and manipulating the above equations the

amplitude-frequency relationship can be described as :

$$x(t) = \lim_{\Delta f \to 0} \frac{1}{T} \sum_{l=-\infty}^{l=\infty} X(lf)\, e^{j2\pi l f t} \Delta f \quad \text{or}$$

$$x(t) = \int_{-\infty}^{\infty} X(f)\, e^{j2\pi f t}\, df \qquad \ldots\ldots\ldots (2.10)$$

The coefficient X(f) of equation (2.10) is equal to

$$X(f) = \int_{-\infty}^{\infty} x(t)\, e^{-j2\pi f t} dt \qquad \ldots\ldots\ldots (2.11)$$

Equation (2.10) and (2.11) respectively represent the Inverse Fourier Transform (IFT) and the Direct Fourier Transform (DFT). Again, for practical purposes the observable time is limited to -T to +T.

2.5.3. Physical Characteristics of Fourier Integral.

As a result of limiting the observable time as mentioned in (2.5.2) the Fourier integral has some physical characteristics which affect the performance of the frequency domain spectrum.

a. Initial Condition, T :

The frequency domain resolution, Δf, is inversely proportional to the period, T. Therefore, the longer the period the higher the frequency resolution (approaching a continuous spectrum).

The Fourier integral is defined over frequencies and time from minus infinity to plus infinity, consequently, it involves negative as well as positive frequencies. In addition to this the amplitudes in the positive as well as in the negative frequency domain, especially for real signals, are equally

divided.

Phase angles in the positive frequency domain are duplicated in the negative frequency domain, except that the images are inverted.

If the Fourier integral is represented in terms of complex numbers, Re(f) + j Im(f), the amplitude can be determined as the absolute values.The inverse tangent of the Imaginary to the Real parts represents the phase angle.

b. Even and Odd Functions.

Mathematically even functions are shown as f(t) = f(-t) and are associated with a cosine waveform. In terms of polar plots the even function is associated with real values. On the other hand odd functions are associated with a sine waveform or imaginary values in the polar form. The odd functions are mathematically represented as f(t) = -f(-t).

c. Time Shifting.

It has been described in (2.5.3.b) that time shifting changes the status of an odd function to an even function or vice versa. Thus, this does affect both the real and imaginary values on which the phase angle relies.

2.5.4. Windowed Waveform.

For the purpose of practical analysis signals can be treated as periodic or non-periodic waveforms

depending on the assumption made when treating the signals (i.e using the Fourier series or Fourier integral). If a square or a rectangular truncation (window) is applied the transformation of the rectangular function in the frequency domain is represented by

$$X(f) = 2T_0 \frac{\sin 2\pi f T_0}{2\pi f T_0} + j0 \qquad \ldots\ldots (2.12)$$

The equation contains a major lobe with decaying side lobes. Other windows have been developed to achieve a maximum major lobe and minimum side lobes as referred to in [10,25,27].

In general the concept of treating windowed signals is equal to multiplying the original signal by a function in the time domain or convoluting their frequency domain transforms. This process can be expressed mathematically as,

$$y(t) = \int_{\tau=-\infty}^{\infty} h(\tau)\, x(t-\tau)\, d\tau \qquad \ldots\ldots\ldots (2.13)$$

Further discussions concern windowed waveforms and convolution are obtainable in chapter (2.5.7) and Appendix (D-1).

2.5.5. Digital Fourier Analysis

Fourier integrals have become more useful after the invention of the digital converter which converts analog data into integer numbers. The accuracy of the digital data relies on the 'bit' of the digital converter.

a. Discrete Fourier Transform

Equation (2.11) may be slightly modified to accept digital data which is kept in arrays. The equation is known as the Digital Fourier Transform and is shown below.

$$X(k.\Delta f)= \Delta t \sum_{l=0}^{L-1} x(l\Delta t)\ e^{-j2\pi klf\Delta t} \qquad \ldots\ldots (2.14)$$

Consequently inverse transformation can also be performed by

$$x(l.\Delta t)= \Delta f \sum_{l=0}^{L-1} X(k\Delta f)\ e^{j2\pi klf\Delta t} \qquad \ldots\ldots (2.15)$$

Including $\Delta t=1$ and $\Delta f=1/(L\ \Delta t)$, for L = amount of data executed, into both equations (2.14) and (2.15) give

$$X(k) = \sum_{l=0}^{L-1} x(l)\ e^{-j2\pi kl/L} \qquad \ldots\ldots (2.16)$$

$$x(l) = \frac{1}{L} \sum_{l=0}^{L-1} X(k)\ e^{j2\pi kl/L} \qquad \ldots\ldots (2.17)$$

Some programming-languages do not accept complex numbers this can be overcome by substituting $e^{\pm\varphi} = \cos\varphi \pm j \sin\varphi$ into equation (2.16) and (2.17). This method requires considerable time when the amount of data to be analysed is large.

b. Fast Fourier Transform.

An attempt to reduce the number of multiplications and additions in the DFT process was made by Cooley-Tukey [30]. This is referred to as the Fast Fourier Transform (FFT) [25] or Radix-2 FFT [24] or FFT Base-2. This technique has great savings in computation if the amount of data has a prime number of two. Later studies were carried out by Temperton [31.32.33] and these are based on prime numbers other than two. The executable time

increases if the amount of data can not be decomposed into prime numbers of 2,3 or 5. The technique is referred to as the self sorted radix-mixed FFT.

2.5.6. Physical Characteristics of the DFT

There are several considerations that must be taken into account when digitising signals.

a. Frequency range of interest.

The frequency range is set by the sampling rate. The lower the sampling rate the wider the frequency range. The maximum frequency is referred to as the Nyquist frequency [25] which can be obtained by inverting the doubled sampling rate.

b. Frequency resolution.

When two or more frequencies occur in the signal it requires a certain resolution in order to distinguish the frequencies themselves within the frequency domain. The relationship between frequency resolution and the number of cycles required defines the minimum recording time as follows.

$$\text{Number of cycles} \geq \frac{2 \times \text{Frequency Range of Interest}}{\text{Frequency Resolution}}$$

c. Amount of data.

The amount of data will be automatically established after determining the Nyquist frequency and the frequency resolution.

Amount of data $\geq$ 2 x Number of cycles.

d. Harmonic frequency.

If a signal is not purely sinusoidal transformation will result in harmonics which are integer multiplication of the fundamental frequency.

e. Round-off and Jitter.

As a result of losing horizontal time stability an analog to digital converter or a digitiser can cause a 'jitter'. In addition, a low bit digitiser or very low signal can cause round-off error. These errors are usually apparent as noise. They may contribute a significant error in determining phase angles.

f. Periodicity.

When an integer number of cycles of a signal is acquired the peak of the transformed window (main lobe) meets one of the line spectrum of the periodic signal, therefore, the amplitude will be a maximum. In contrast if there is not an integer number of cycles the amplitude will vary from about 70% to 100% of the maximum amplitude. Therefore, non-integer numbers of cycles of the signal produce leakage. This is due to the fact that the line spectra do not coincide with the zeros of the window's side lobes as normally occurs when an integer number of cycles is sampled. Further discussion is given in chapter-4. To overcome such a leakage other types of window are described in references [24,25].

g. Aliasing.

The Nyquist condition requires that two sets of data to be acquired per cycle of frequency of interest. If less than two sets of data per cycle are sampled the signal in the frequency domain will move back to a lower frequency. If an unexpected signal appears in the range of frequency, it may belong to a higher than maximum frequency range.

Actual freq. = Nyquist + (Nyquist-Unexpected freq.)

h. Frequency, Amplitude and Phase.

To achieve proper frequencies and amplitudes of interest using frequency domain spectra several methods have been suggested in references [6,10]. It was referred to by Harris [10] that frequencies and amplitudes can be obtained from a graph showing relationships between attenuation (dB) of the maximum to the highest adjacent line spectra and the coefficient of the improvement as seen on fig.(2.9). This technique employs the Hanning Window.

Hassan [6] used an empirical formula relating the relationships between the two adjacent line spectra about the peak amplitude and the frequency of interest as seen on fig.(2.10).

i. Effects of applying a window.

All windows have major lobe heights, side lobes and band widths resulting from the mathematical transformation. Rectangular windows have high side

lobes, thus, these side lobes create leakage especially when a non-periodic signal is transformed. The leakage obstructs the existence of some frequencies having very low amplitudes. Further discussions are obtainable in chapter-4.

2.5.7. Filters.

Some signals have very low amplitudes and it is likely that noise interferes in such a way that it masks the signals. The noise may be from the structural supports, the environment, the electronic circuitry or from the friction between the components of the structure itself.

Filters attempt to separate the signal from the noise. There are many types of filters available. The choice depends on the frequency bands of interest. Low pass, high pass and band pass - band stop filters are the common classifications. There are many types of filter function available. In general the functions can be classified into the Finite Impulse Response (FIR) and the Infinite Impulse Response (IIR).

Referring to equation (2.13) convolution in the discrete time can be expressed as follows.

$$y(l) = \sum_{k=-\infty}^{k=\infty} x(k)\ h(l-k)$$

Assuming the system is linear-time invariant it can also be expressed in terms of

$$y(l) = \sum_{i=-\infty}^{i=\infty} x(l-i)\ h(i) \qquad \ldots\ldots\ldots (2.18)$$

where h(v) must be causal/physically realizable and be infinite.

The advantage of the use of FFT lies in the reduction of the executable time. The transformation of a filter function is usually in terms of the rational transfer function,H(z). The IIR-Butterworth filter will be discussed because it is simple to understand and is flexible to adjust in the pass, transition and stop bands as referred to by Peled [28]. Appendix (D-1) provides further discussions for the following filters.

a. Low pass filter.

Derived from an analog filter Laplace transform of the filter function as described in reference [25] the transfer function of the IIR-Butterworth filter gives

$$H(s) = \frac{1}{B_n(s)} \qquad \ldots\ldots (2.19)$$

where $B_n(s)$ is a polynomial of degree n with roots at

$$a_k = e^{j(0.5n+0.5+k)\pi/n} \qquad \ldots\ldots (2.20)$$

where : k varies from 0 to n-1

Noting the prescribed attenuation,At in dB, in the stop band whilst the attenuation in the pass band is maintained to be less than 3 dB the required minimum degree n of the polynomial function,f(n) can be established using the equation

$$n = 0.5\ \frac{Log(10^{At/10}-1)}{Log(\Omega_s)} \qquad \ldots\ldots (2.21)$$

where :

$$\Omega_s = Tan(A_s/2)\ /\ Tan(A_c/2)$$

A_s and A_c are respectively the pass band and the stop band frequencies.

By substituting the appropriate value of n into equation (2.20) the polynomial equation, $B_n(s)$ is established. The transfer function,H(z) can be obtained by including

$$s = C\,\frac{(z-1)}{(z+1)} \quad \text{for } C = \cot(A_c/2)$$

into equation (2.19).

b. High pass filter.

By inverting the low pass analog to digital transformation curve, this provides a means of inverting the pass band and the stop band of the previous low pass filter.

c. Band pass and band stop filter.

The procedure is slightly different from the low pass and high pass filters. Both sets of the pass band and stop band frequencies must be given. As a result of these two transition bands the equivalent polynomial equations of degree n are obtainable by considering the maximum value of Ω_s for both transition bands.
The FIR-Butterworth filter as referred to by Chan et.al. [37] has several advantages over the IIR-Butterworth filter. The filter is more appropriate where the executable time required is short. The main difference from the IIR-Butterworth is that the filter coefficients are reduced after decomposing the rational function of

the IIR-Butterworth,H(z) using the Wiener-Lee decomposition method.

The technique enables the filter coefficients to be reduced considerably. Details of both filter types can be obtained in Appendix (D-1).

2.5.8. Physical Characteristics of Filter Function.

a. Phase.

It is understandable from the mathematical point of view that most convolutions delay the phase angle. The phase angle becomes important when considering the time history of a signal. Two pass digital filter techniques can be used to restore the phasing to the original position as suggested by Kormylo et al. [35]. Chan et.al [39] proposed a non-causal filtering which allows users to calculate the phase delay if necessary. In addition Chan et al. in [37] proposed using FIR-Butterworth filter when a short phase delay is required.

b. Amplitude.

The IIR-Butterworth filter results in increasing gains in amplitude beyond the pass band frequency. The pass band frequency can be set to a certain value. In this case the pass band frequency is set at -3dB while the stop band attenuation is dependent on request. With the FIR-Butterworth filter the pass band attenuation varies with the number of coefficients requested, although it is detectable.

c. Transient Signal.

The transfer function is always periodic, from 0 to π, but the signal captured is arbitrary, therefore, in most cases, the filtering process results in transient signals or words. The length of the transient words depends on the transition band width. The narrower the transition band width the longer the length of the transient words [26,44]. Czarnach [36] investigated the length of the transient words of IIR filters and eliminated them through an algorithm he proposed. Chan et.al. [39] commented on the work of Czarnach [36] that the method required a lot of data and a large group delay when a two cascade connection was carried out. He proposed a non-causal filter which comprises a recursive filter,H(z) and a stable non-recursive filter to approximate the transfer function,$H(z^{-1})$. The technique allows small group delay and small memory requirements. The phase angle is determinable from the equation he proposed. Moreover, Chan et.al.[36] proposed a new FIR filter using the Wiener-Lee decomposition method. This method has advantages in that its transition band is easily adjusted and that the length of transient words is determinable by its transfer function length.

Furthermore, he commented that the method avoids overflow which usually occurs with the IIR filters especially with the IIR-Butterworth. When a small number of filter coefficients are employed this reduces the gain factors

in the passband and in the stop band due to the non-periodicity of the filter coefficients. The auto search Humming window was proposed to increase the gain factor (attenuation) in the stop band.

An algorithm of the bilinear transformation based on matrices was presented by Power [42] and was improved by Davies [43]. On the basis of the long division theorem Kamen [44] presented a program but the logic of the program was not obvious. The author ran the program but it was not successful. A proposed algorithm will be described in chapter-6.

2.6. Concluding Remarks.

The non-linear stiffness parameter, γ is dependent on the amplitude of excitation, F(t). This results in different resonant frequencies for different amplitudes of excitation. From the frequency response point of view the natural frequencies can not be justified from a single response unless the amplitude of excitation is small. At this stage the natural frequencies are approximately equal to the resonant frequencies.

Polar diagrams allow more accurate determination of the resonant frequencies. The correction is carried out by approximating the relative phase angle at resonance. The use of Mixed Radix FFT allows any amount of data to be analysed without any data subtraction or addition which can decrease the frequency resolution and increase

leakage respectively. Furthermore, characteristics imposed on any signal processing should be recognised since they affect mainly amplitudes and phase angles.

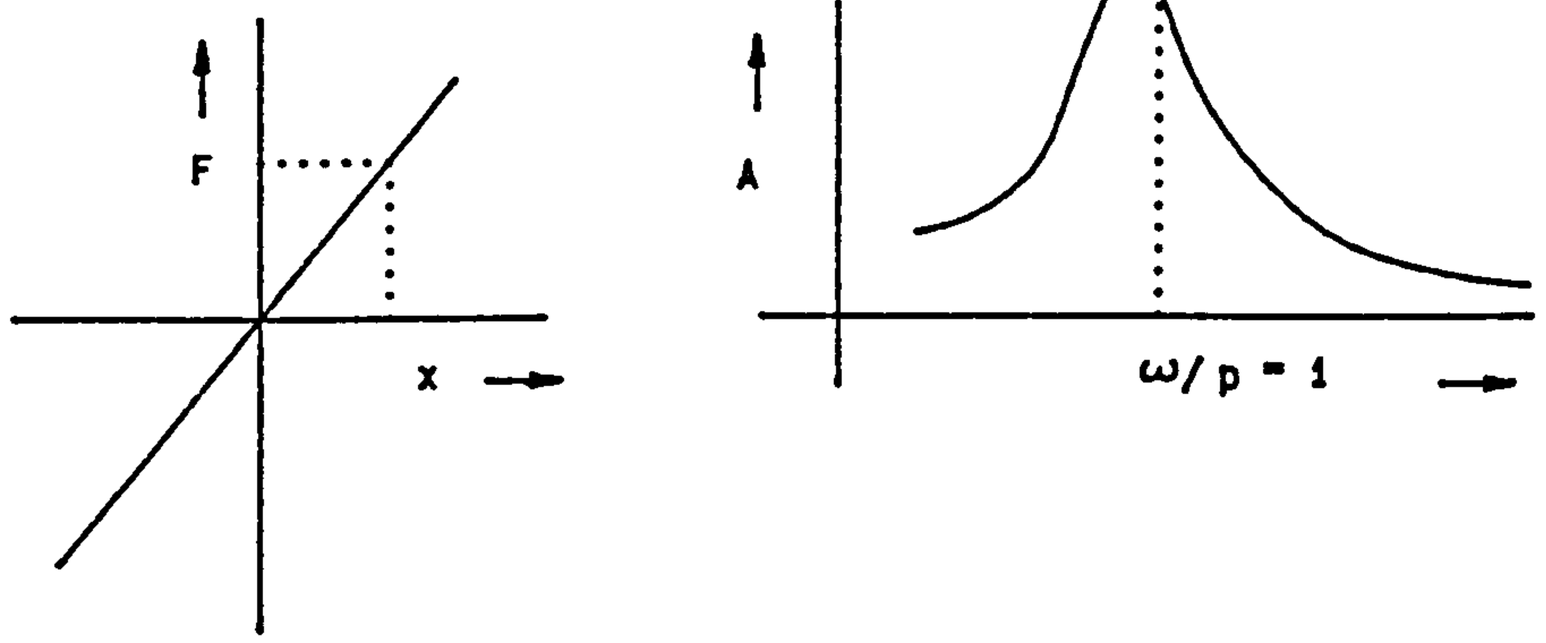

F = Force

x = Displacement

ω/ p = Frequency Ratio

A = Dynamic Amplitude

ω = Frequency of Excitation

p = Natural Frequency

FIG.2.1.FORCE-DISPLACEMENT DIAGRAM AND FREQUENCY RESPONSE OF LINEAR SPRING SYSTEMS.

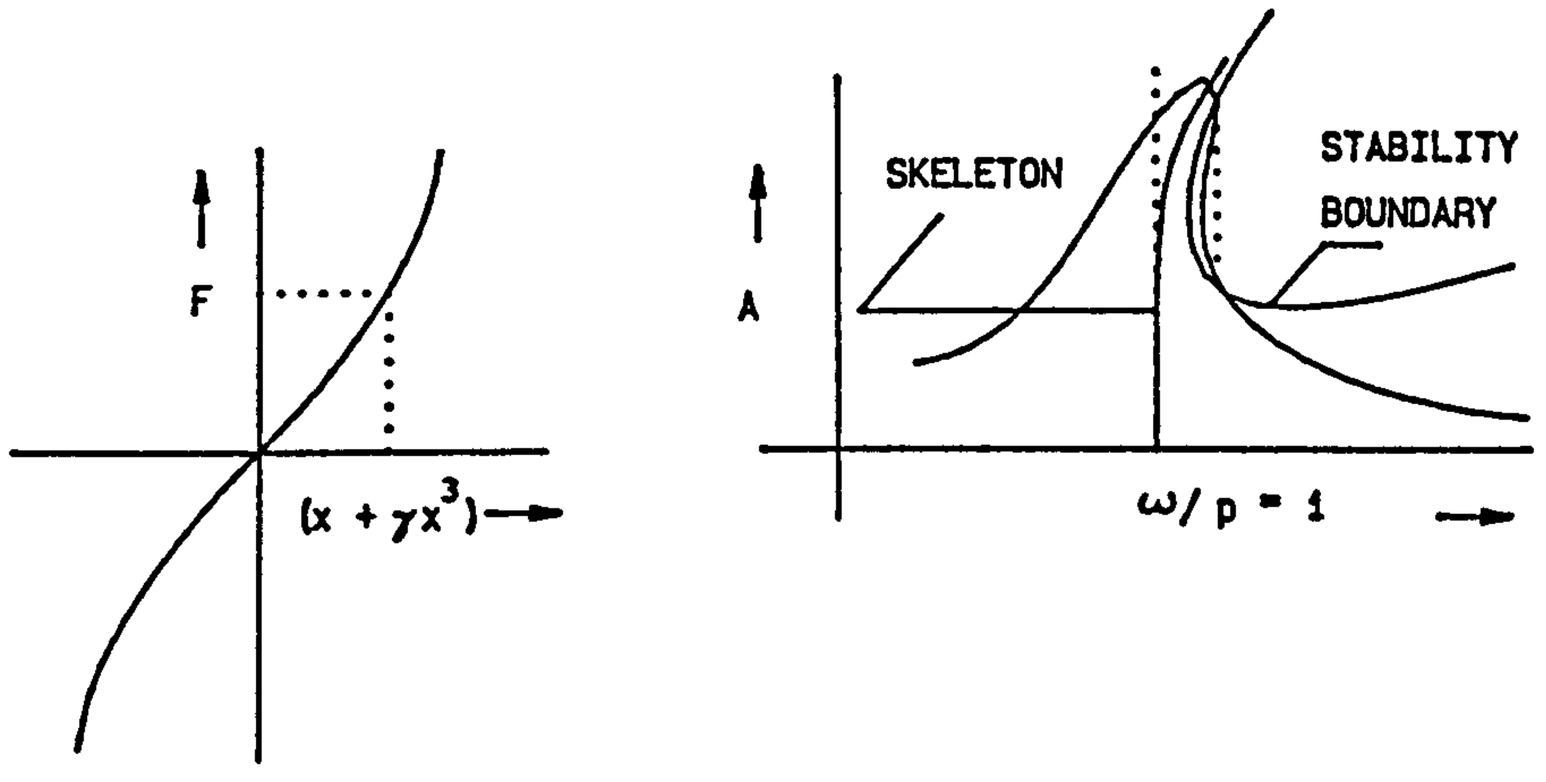

F = Force

x = Displacement

γ = Nonlinear Stiffness factor

ω/ p = Frequency Ratio

A = Dynamic Amplitude

ω = Frequency of Excitation

p = Natural Frequency

FIG.2.2.FORCE-DISPLACEMENT DIAGRAM AND FREQUENCY RESPONSE OF HARD SPRING SYSTEMS.

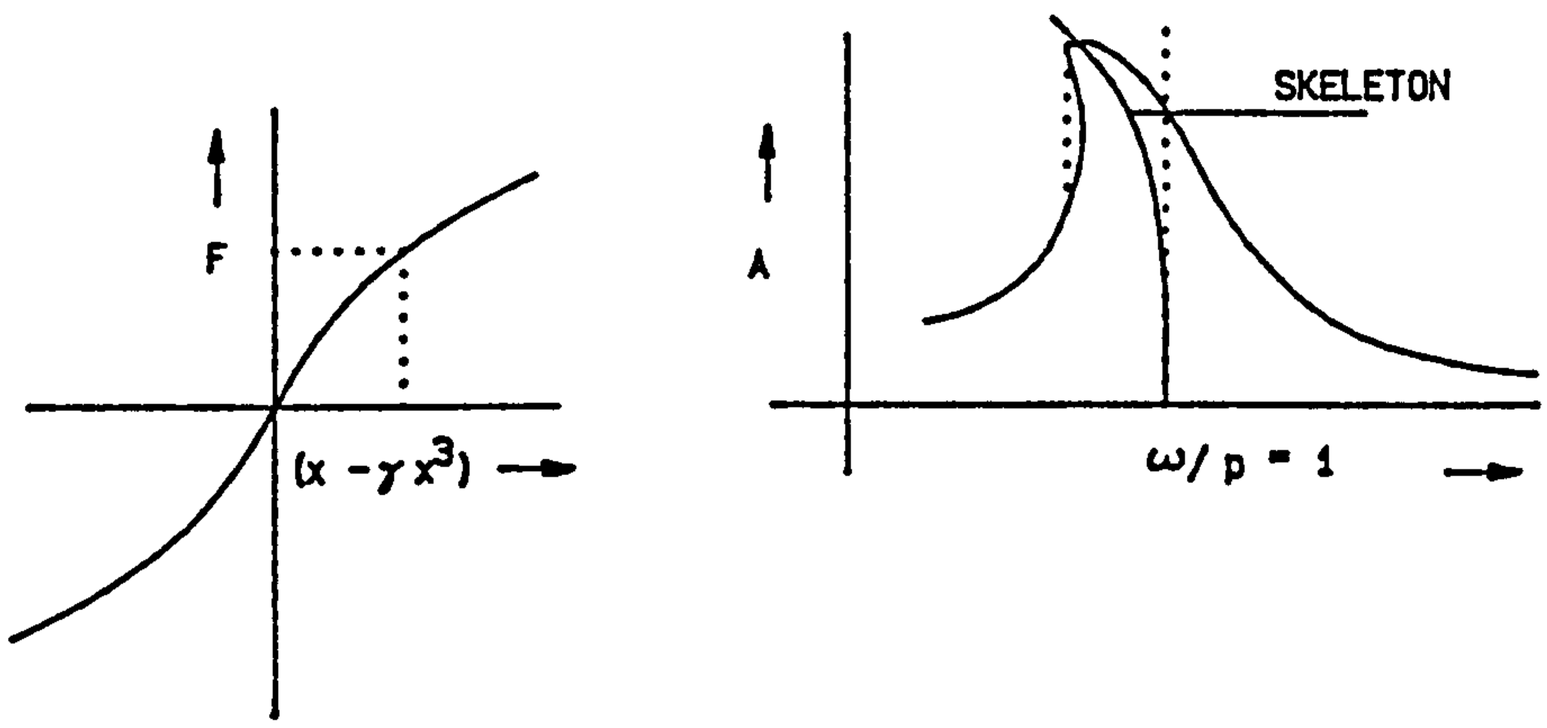

F = Force

x = Displacement

γ = Nonlinear Stiffness Factor

ω/p = Frequency Ratio

A = Dynamic Amplitude

ω = Frequency of Excitation

p = Natural Frequency

FIG.2.3.FORCE-DISPLACEMENT DIAGRAM AND FREQUENCY RESPONSE OF SOFT SPRING SYSTEMS.

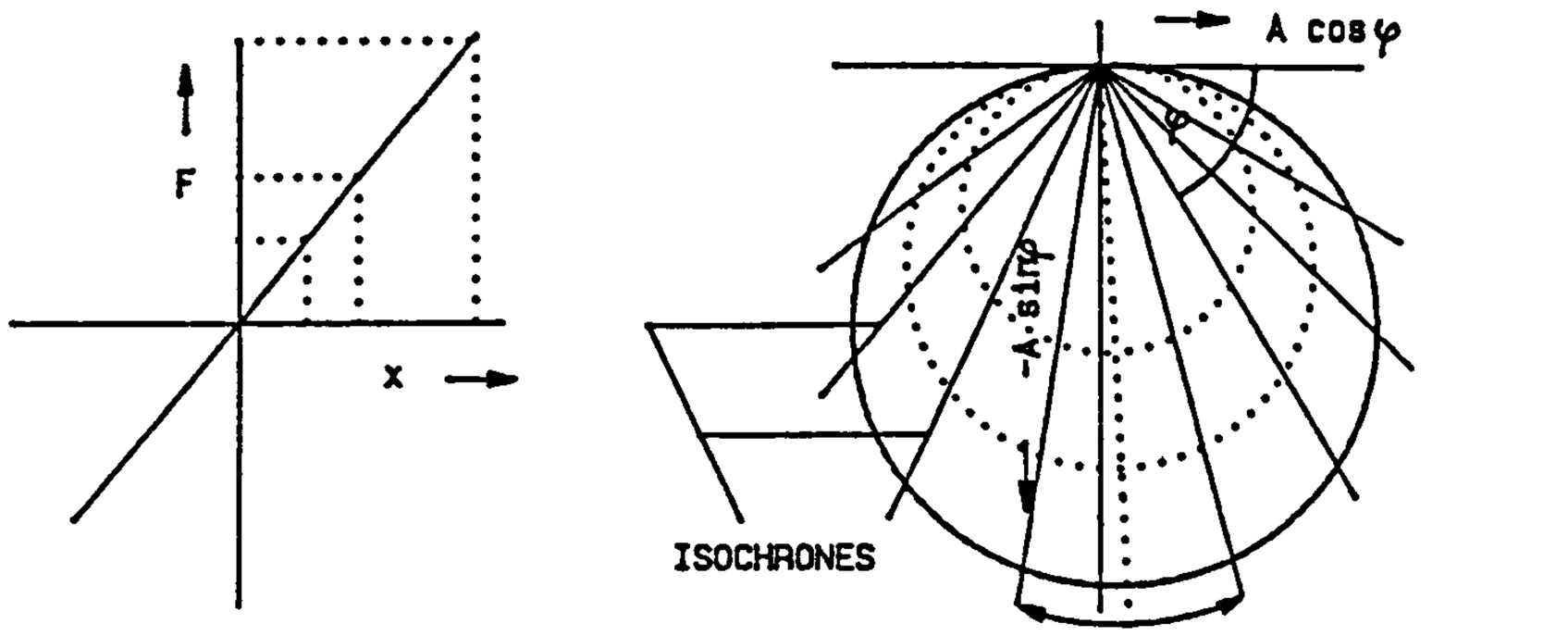

F = Force

x = Displacement

x = A cos φ , real axis

y = -A sin φ , imaginary axis

A = Dynamic Amplitude

φ = Phase Angle

FIG.2.4.FORCE-DISPLACEMENT AND POLAR DIAGRAMS OF LINEAR SPRING SYSTEMS AT DIFFERENT FORCES OF EXCITATION

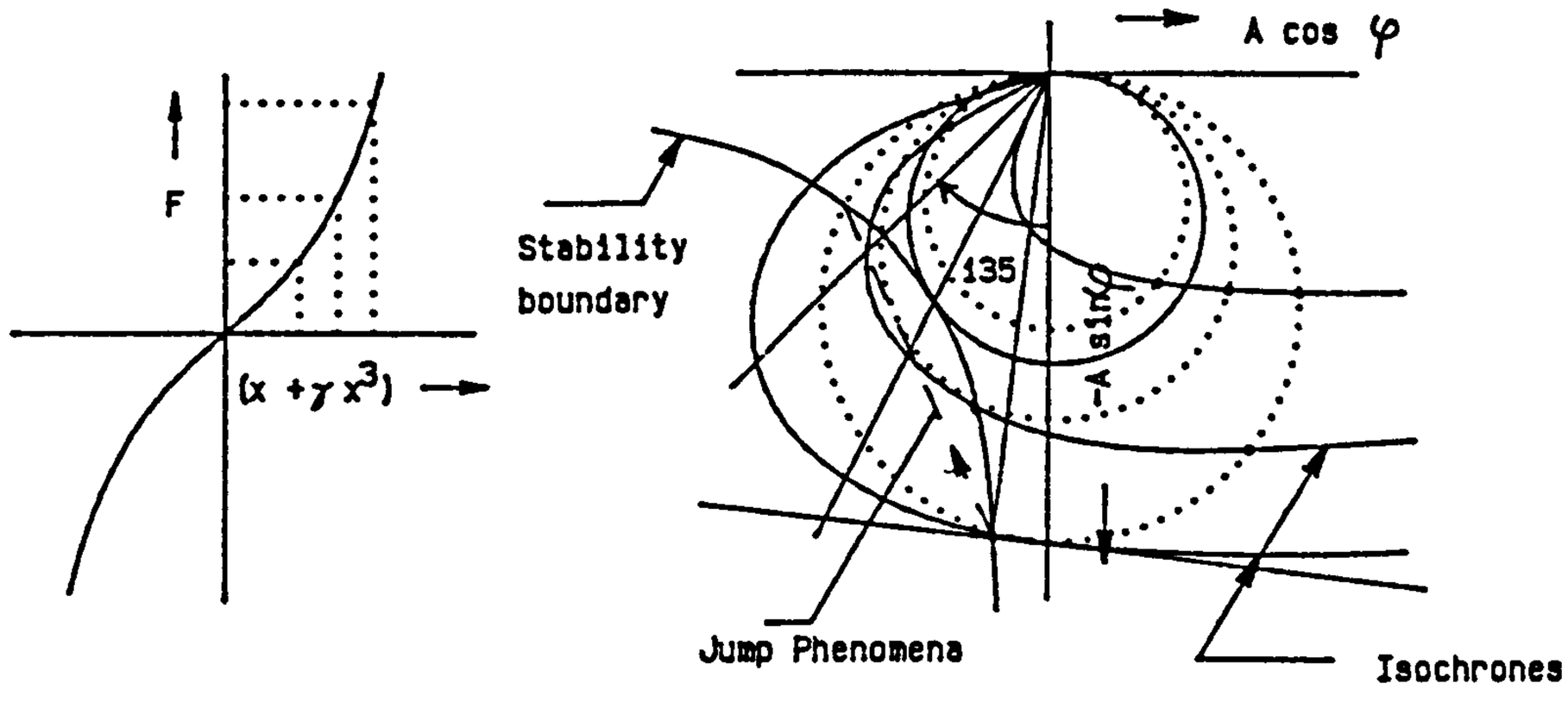

F = Force

x = Displacement

γ = Nonlinear Stiffness Factor

x = A cos φ , real axis

y = -A sin φ , imaginary axis

A = Dynamic Amplitude

φ = Phase Angle

FIG.2.5.FORCE-DISPLACEMENT AND POLAR DIAGRAMS OF HARD SPRING SYSTEMS AT DIFFERENT FORCES OF EXCITATION

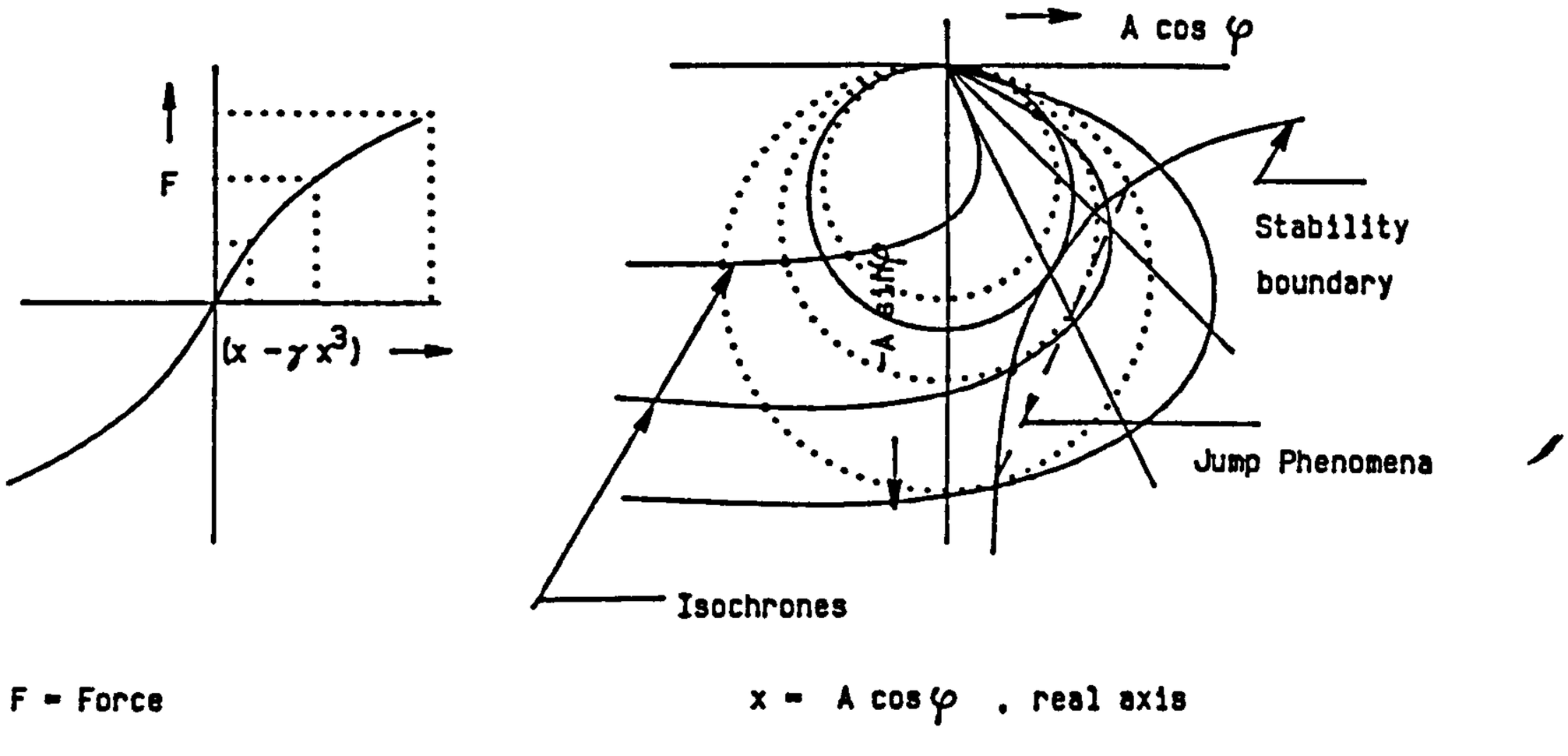

F = Force

x = Displacement

γ = Nonlinear Stiffness Factor

x = A cos φ , real axis

y = -A sin φ , imaginary axis

A = Dynamic Amplitude

φ = Phase Angle

FIG.2.6.FORCE-DISPLACEMENT AND POLAR DIAGRAMS OF SOFT SPRING SYSTEMS AT DIFFERENT FORCES OF EXCITATION

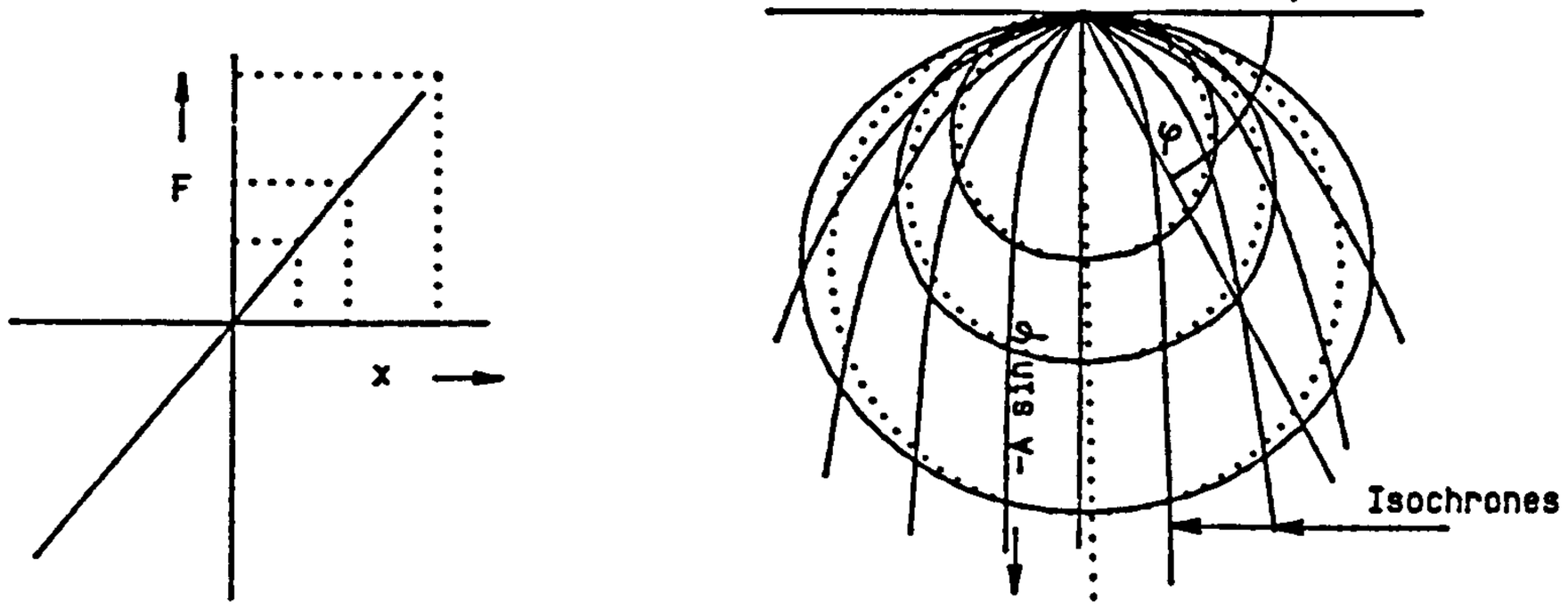

F = Force

x = Displacement

x = A cos φ , real axis

y = -A sin φ , imaginary axis

A = Dynamic Amplitude

φ = Phase Angle

FIG.2.7.FORCE-DISPLACEMENT AND POLAR DIAGRAMS OF COMBINED VISCOUS AND QUADRATIC DAMPING SYSTEMS AT DIFFERENT FORCES OF EXCITATION

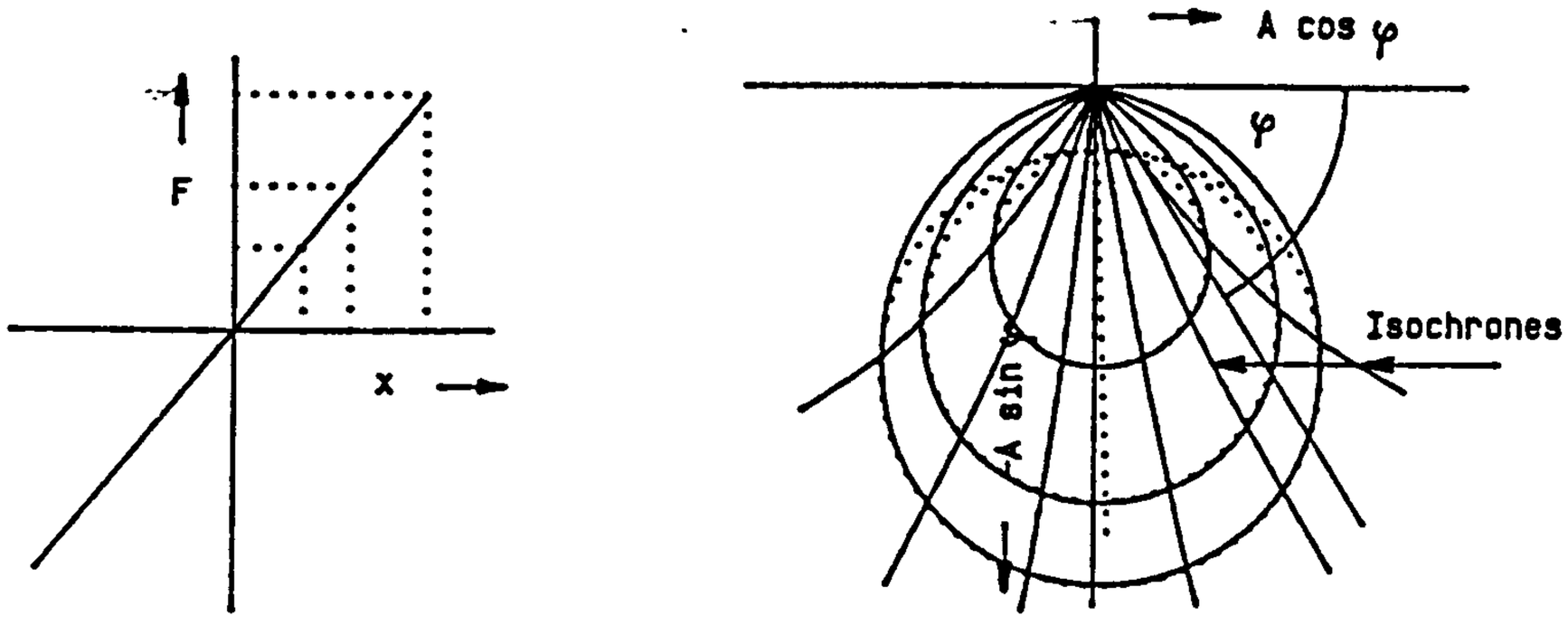

F = Force

x = Displacement

x = A cos φ , real axis

y = -A sin φ , imaginary axis

A = Dynamic Amplitude

φ = Phase Angle

FIG.2.8.FORCE-DISPLACEMENT AND POLAR DIAGRAMS OF COMBINED VISCOUS AND COULOMB DAMPING SYSTEMS AT DIFFERENT FORCE OF EXCITATION

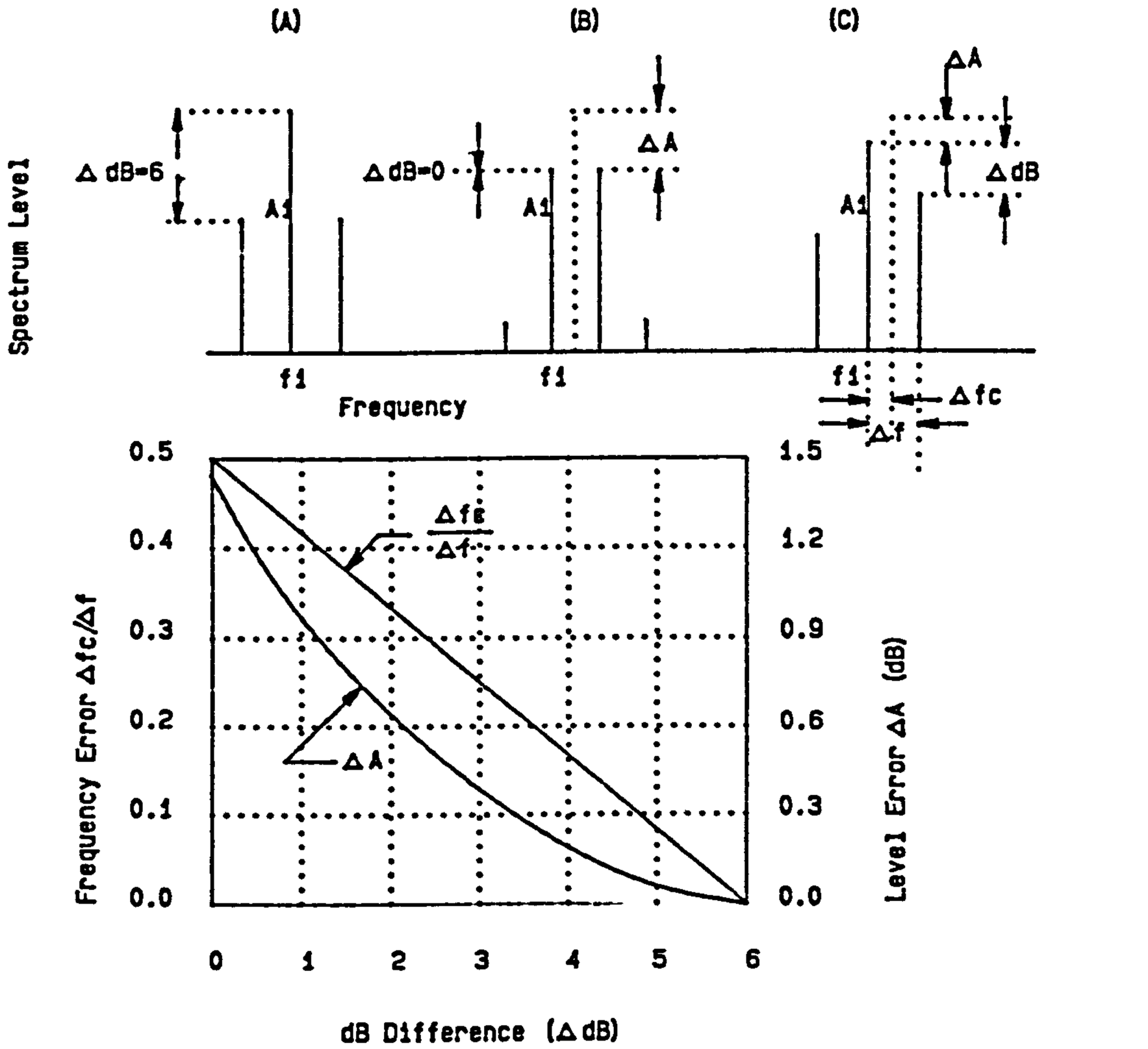

Δ f = Frequency resolution (Hz) : ΔA = Corrective Amplitude

Δfc = Corrective Frequency : A = A1 + ΔA = Predicted Amplitude

fr = f1 + Δfc = Predicted Frequency

FIG.2.9.PICKET FENCE CORRECTION FOR HANNING FUNCTION

(CITED FROM REF.10)

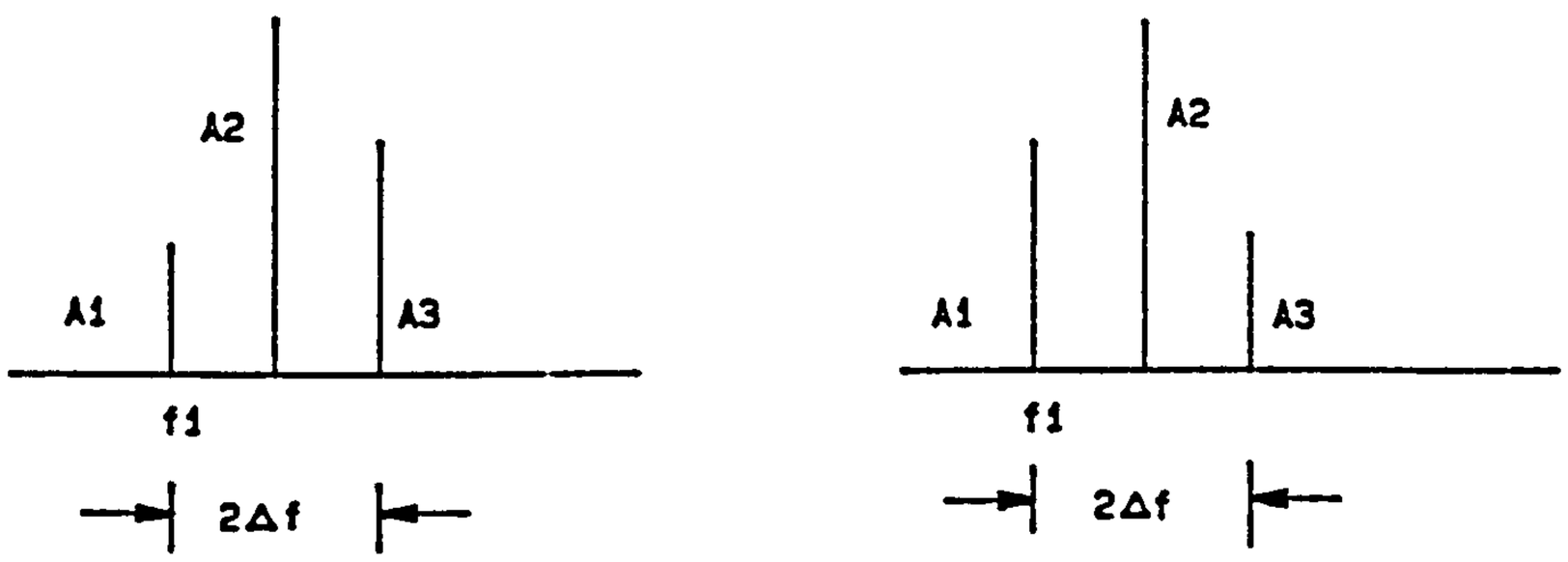

K = A3/(A1+A3)

fr= f1 + 2Δf * K

FIG.2.10.EMPIRICAL FORMULA PROPOSED BY HASSAN [REF.6]

CHAPTER - 3

3. EXPERIMENTAL STUDIES.

3.1. General.

This chapter will describe the experimental work carried out on four simply supported reinforced concrete beams. Included in the experiments were the investigation of the jump phenomenon which was found when reexamining the data as reported by the author in [40] and the non-linear behaviour in relation to the detection of the flexural and diagonal splitting crack patterns for beams with fully bonded and partially bonded reinforcement. In addition calibrations of the instrumentation will also be described. The use of a mechanical exciter as well as a magnetic exciter in relation to the jump phenomenon will also be discussed in this chapter. Due to the limit of the frequency range of the mechanical exciter the experiment mainly used the magnetic exciter.

In general there are three main dynamic tests as implied in references [6,7,26] :

a. Steady state vibration tests employ a steady state input signal, which is normally a sinusoidal, induced by an exciter and is used in references [1,3,4,5,20,21,22,36].

b. Transient tests, including impact and 'pull-sudden release' or step-relaxation and snap back, are used if only certain low natural frequencies are of concern

[5.7.19.20].

c. Further tests, involving random vibration (pure, pseudo and periodic), may be applied when either tests a) and b) are not possible. These tests involve statistics and long recordings.

The tests carried out in this study used the steady state vibration technique. A typical lay out of the experiments is shown in fig.(3.1).

3.2. Models.

3.2.1. Types and General Properties.

Two types of simple concrete beam were investigated in the experiments; the fully bonded and partially bonded beams. Each type (2 samples) were tested and each sample had a specific crack pattern, i.e. flexural or diagonal splitting crack patterns. The mechanical exciter has a range of frequency up to 50Hz whilst the magnetic exciter has a range up to 10kHz. Based on the specifications of the mechanical exciter and the material properties the dynamic properties of the fully and partially bonded beams were calculated. By arranging the beam's dimensions the natural frequencies can be approximated by the Rayleigh method [8]. All beams were of the same overall dimensions being nominally 100mm wide, 150mm deep and 3050mm long. The first natural frequencies of the fully and partially bonded beams based on this specification were calculated as

26.09Hz and 24.74Hz respectively.

The concrete strengths were designed to comply with BS8110 having nominal cube strengths of 30 N/mm^2. Two plain mild steel bars of 12mm nominal diameter were used as the reinforcement. The beams were simply supported without any significant shear reinforcement to enable simple experiments to be carried out and to avoid interference resulting from other parameters such as from support systems. Three 4mm diameter links having triangular shape were used to keep the reinforcement in position when casting. The typical reinforcement is shown in fig.(3.2) and the procedure for the design calculation is available in Appendix (B-1) to (B-3).

3.2.2. Strain Gauging.

Two sets of two gauges were positioned at the mid span and at the quarter span to measure strains in tension and compression at both sections. Two gauges were attached to one of the two mild steel reinforcement bars. A single 4 mm diameter mild steel bar was positioned in the compression area to accommodate the other two gauges. The gauges were attached to the reinforcement parallel to the axis of the beam. The process was summarised as follows :

1. Consecutive dry and wet abradings with 200-grit emery cloth and 400-grit silicon carbide paper respectively were applied to the surface of the steel bars.

2. 'M-Prep Conditioner A' was applied repeatedly and was then scrubbed with a cleanex medical wipe until the surface was clean.
3. 'M-Prep Neutraliser 5' was applied and was carefully dried with a cotton bud.
4. The 2mm long foil strain gauge with a gauge factor 2.13 and 119.8 Ohm resistance of SHOWA products was attached on a cellophane tape for ease of handling and was positioned on the surface prepared in (1) to (3).
5. Lifting up one of the cellophane tape ends and applied 'M-Bond 200 catalyst' on the steel surface for quick hardening. Two drops of M-Bond 200 adhesive were applied at the edge of the strain gauge position such that when the cellophane was folded down this adhesive flowed in contact with the strain gauge.
6. Immediately applying firm thumb pressure for one minute to let the adhesive work properly.
7. Wiring the gauge by soldering the terminal was done carefully after removing the cellophane tape. To insulate the active gauge from the terminals a piece of 5mm paper tape was stuck across the gauge length separating the active gauge from the terminal area.
8. To protect the gauge from damage while casting the concrete 'M-Coat D Air Drying Acrylic' was coated on the gauge and an ordinary mastic for insulation was also applied around the steel bar over the gauge area.

3.2.3. Mix Design and Manufacture.

In general the minimum material properties should comply with the BS-8110 for normal concrete. All beams were designed to have nominal concrete cube stress, fcu of 30N/mm^2, the yield steel stress, f_s of 312N/mm^2 and a slump of 10-30mm. From those specifications the equivalent area of steel to concrete, m is found to be 7.69 for elastic design/check calculations.

The beam was cast using a steel mould. Slump and VB tests were carried out before casting to ascertain the in situ quality of the concrete mix to the design mix. A concrete vibrator was applied to achieve sufficient compaction. Two concrete cubes, two concrete cylinders and one concrete beam specimen were tested after 28 days. The beams as well as the specimens were cured under the natural laboratory environment.

The procedure for calculation of the mix design and the ultimate moment and shear of the fully and partially bonded beams are available in Appendix (B-1), Appendix (B-2) and (B-3) respectively.

3.2.4. Support System.

To relate the relationships between the static and dynamic behaviour of concrete structures with defects, a simply-supported system with self aligning and roller bearings as seen in fig.(3.3) was used in this work. Thus, twisting resistance was negligible. This support

system reduced the complex behaviour resulting from parameters other than those directly under investigation. Two pieces of solid steel shaft having 2 inches diameter were positioned at about the neutral axis of the beam at both ends to fit the support bearings. One set of the bearings was bolted down on a massive steel column to create a hinge. The other set of bearings was bolted down on a horizontally movable platform to create a rolling support. The movable platform was designed to resist uplifting movements. Two strips of hardened steel rollers enabled the platform to move horizontally upon another fixed steel platform. The massive steel columns supporting the fixed steel platform as well as the hinge were anchored down on the floor of the laboratory.

3.2.5. Static Loading.

To create flexural and diagonal splitting crack patterns where the sensitivity of the dynamic parameters to those types of crack pattern were investigated two types of loading points were applied. The first type positioned the loading points at the third of the span and the second type was at 200mm inward from the supports. Four loading stages were applied to beam-1 to beam-3 and six loading stages to beam-4. More accurate load readings were carried out by averaging the output of two load cells employed. Each load cell was positioned in between the hydraulic jack and the laboratory floor.

Strains were also measured through strain gauges. The very small change of resistance resulting in a small change of potensial can not be measured directly. Amplifiers were required to increase the strain gauges output. The typical static loading arrangements are shown in fig.(3.4).

3.2.6. Dynamic Loading.

Vibration tests were carried out on the intact beam and successively after the static loading stages over the beam models. Steady state vibration tests were applied mostly using the magnetic exciter with the exception for the jump phenomenon investigation which occurred on the mechanical exciter. The magnetic exciter as well as the mechanical exciter were positioned at similar points on the span. The moving out of balance mass of the mechanical exciter produces axial tension and compression on the beam and also produces variable extra moments due to the eccentric axis of the shaft to the beam. These parameters are assumed to be small and will not be considered. The force of the magnetic exciter was presumed to be perpendicular to the beam axis.

3.3. Instrumentation.

The main instrumentation used in the experiment consisted of an exciter with a signal generator and amplifier, several vibration pick-ups, two tape recorders

and several additional monitoring devices. Static loading devices were employed to create crack patterns which mainly consisted of a loading machine, hydraulic jacks, load cells, strain gauge amplifiers and loading frames (harnesses). The typical wiring arrangement of the experiment and the loading set up are portrayed in fig.(3.5).

3.3.1. Exciters and Signal Generators.

The mechanical exciter used by author in reference [40] was also used in the experiments to investigate the jump phenomenon. Rotating frequencies were induced via a speed controller. The three phase AC exciter possessed a frequency limit at 50 Hz and a low torque at lower frequencies. The force of excitation is proportional to the squared frequency, the mass and the radius of gyration. A maximum centrifugal load of 250 lbs may be achieved with this 14.5kg mechanical exciter. A similar set up was also considered when using the magnetic exciter driven by an integral amplifier. The Derritron magnetic exciter type VP-2 had a maximum 10N output and 1kg weight. This was positioned on the beam 250mm from the mid span position. The maximum range of frequency was above 1 kHz.

3.3.2. Dynamic Transducers.

Several B&K piezoelectric accelerometers were

employed in the experiments. The charge sensitivities of the B&K accelerometers type 4332 and 4366 (3 pieces, around 30 gr each) were 73.2, 49.1, 53.5, 51.0 pc/g at 50Hz respectively whilst the other B&K accelerometers type 4338 (2 pieces, around 60gr each) were 97.8 and 100.7 pc/g at 50Hz. The resonant frequency of the lower weight accelerometers was above 10kHz whilst for the other it was about 5kHz. The linear operation range of the accelerometers were from about 15Hz to 10kHz. The velocity probe (Schenck type T77) has a sensitivity of 75mV/mm/sec at 80Hz. Below 15Hz the output was low and unreliable although 20 to 2000Hz range of operation was recommended by the manufacturer. As the output was not linear within the operation range a calibration was required. The LVDT type DCT 2000A were also employed in the experiment. This device had a sensitivity of 6.52mV/V/mm. To obtain reasonable results when working in very low displacements a sufficient DC input was necessary (maximum of ± 15V may be fed). The maximum frequency range of 200Hz was normally applied to such displacement meters. Inevitably the phase delay was not reported in the certificate therefore, a calibration was required for this.

The number of monitoring locations depended on several considerations such as the availability of transducers, the capacity of the signal recorders and the data acquisition card. Seven locations were dealt with :

Accelerometer no.3 was positioned on the moving exciter mass of the magnetic exciter measuring absolute accelerations and another (no.1) was positioned adjacent to the exciter to measure the absolute accelerations of the beam. From these transducers the relative relationship between them can be obtained and will be discussed in chapter-5. Accelerometer no.6 was positioned at the mid span to measure amplitudes of the beam at the first natural frequency. The velocity probe and accelerometer no.5 were respectively intended to monitor the second and the third natural frequencies and were positioned at the fourth and the sixth locations of the span. Finally, another two accelerometers (no.2 and no.4) were used to monitor the behaviour of the beams ends.

The accelerometers were connected to the charge amplifiers, to enable adequate signal output to be recorded. The charge amplifiers have several optional unit output/modes (displacement, velocity and acceleration). Improper selections of the low pass filter settings available on the charge amplifiers may cause changes in the signal properties and these effects are discussed in chapter-2 or Appendix (D-1). The output relationships of the displacement, velocity and acceleration are given in Appendix (B-4.A). Unlike accelerometers the velocity probe is designed on the basis of the Eddy current method. The output is designed

in such away that it does not require amplifiers. The output (mV) relating to the velocity (mm/sec) is supplied by the manufacturer and graphically shown in Appendix (B-4.B).

3.3.3. Tape Recorder and Data Acquisition Card.

Racal magnetic tape recorders provide several advantages over the use of direct acquisition. Slow down replays can be carried out which allow flexibility and the ability to achieve a certain amount of data per cycle. Seven selectable speeds from 2.38 cm/sec to 152.4 cm/sec were available.

To allow the signals to be analysed digitally a data acquisition card type PCL-812PG was installed on an Atari Personal Computer PCC-1415 286/30. The data acquisition card has a maximum speed of reading of 33.33 micro seconds. The 12 bits machine provides a digital data range of -2048 to +2048 with an accuracy of ± 1 digit. Capturing higher frequencies requiring a large amount of data. The number of cycles may not be achieved using direct acquisition but the tape recorder can be replayed at a slower speed than at recording.

3.3.4. Static Loading Devices.

The hydraulic loading machine (Riehle) was able to provide hydraulic pressure up to 10000psi. Pressure to load conversion was calculated by multiplying the area of

the 20 tons capacity hydraulic jacks which were positioned beneath the laboratory floor in the basement. A force of more than 35kN at each loading position was required to create diagonal splitting cracks. The load cells with +10V DC input provided a maximum load of 25 tons. These were used for accurate load readings. The loading machine was linked to the hydraulic jacks pulling the harnesses down and leaving the load cells compressed. To provide diagonal splitting cracks a simply supported hollow steel section was put over the concrete beam in such away that the loads from the hydraulic jacks were transferred to positions close to the supports. As well as measuring strains via the output of the strain gauges attached the hysteretic deflections at the mid span were also recorded using a dial gauge.

3.4. Calibrations.

The results of the experiment rely on the instrumentation employed. Almost all devices used in the experiment were checked and were related to each other. Several calibration tests were carried out prior to the vibration tests and are described in this sub chapter.

3.4.1. Accelerometers.

Response of the accelerometers was examined by linking up a specific accelerometer to a specific charge amplifier and putting the accelerometers on a larger

magnetic exciter table (Derritron VP-3) which was freely put on the floor. Frequency excitations over the range of frequency (20Hz to 400Hz) were carried out and an established signal analyser program was used to analyse the signal parameters.

The phase angles between accelerometer no.3 and no.1 were especially monitored in this calibration (these were positioned on the moving exciter mass and the adjacent to it) as the polar diagrams rely on these measurements. The comparison of these accelerometers output are shown in fig.(3.6) and fig.(3.7). The accelerometers were reliably accepted since the comparison of the amplitudes and phases over the range of the frequency of interest were almost constant.

3.4.2. Velocity Probe.

The velocity probe and an accelerometer were put on a Derritron magnetic exciter,VP-3 and stage by stage frequency excitation and the amplitude readings were successively carried out. The signals from both pick-ups were recorded, digitised and were analysed using a program set up for this experiment as described in chapter-6. Output of the velocity probe (mV) was compared to the output of the accelerometer.

Characteristics of the velocity probe depend on the frequency of excitation. To ascertain their relationships and to enable the velocity probe to be used

for direct computer calculations a set of several curve fitting equations are provided as follows :

a.For frequency 6-13.7Hz :

$$C = 52.143 - 18.151\,f + 2.391\,f^2 - 0.06532\,f^3$$

b.For frequency 13.7-23.8Hz :

$$C = -615.321 + 104.3\,f - 4.9139\,f^2 + 0.07492\,f^3$$

c.For frequency 23.8-70Hz :

$$C = 178.29 - 6.021\,f + 0.1309\,f^2 - 1.252E\text{-}03\,f^3 + 4.38E\text{-}06\,f^4$$

d.For frequency 70-2000Hz :

$$C = 70.0 + 4.3008\,(2000 - f)/1930$$

where : f = frequency of interest (Hz)

C = converting factor (mV/mm/sec)

The fitted curve is seen in fig.(3.8).

3.4.3. Signal Recorders.

Input-output as well as the speed of the Racal recorders were also examined by inputting known signals from an alkaline battery and also from a signal sweep generator and analysing the amplitude and phase using the signal analyser program. The speed and amplitude of the racal recorders indicated their reliability. Less than 1% difference in speed and less than 3% difference in amplitude from the known input signal were achieved.

3.4.4. Digitiser.

A similar calibration to the racal recorders was

also carried out to the PCL-812PQ card installed on the Atari Personal Computer type PCC 1415 before using it in the main experiment. The amplitude and frequency of a known signal, using a digital VLF meter and oscilloscope, were fed into the input channel of the PCL-812PQ card. The analysis was carried out using the signal analyser program. It was of interest to note that an attempt to input a reading rate or interval time less beyond its capability (33.33μs) and also an attempt to read an open input circuit resulted in arbitrary digital signals. Within the published range of frequency the PCL-812PQ showed its conformity. To avoid round-off error which may occur in any digitiser is necessary to rescale the analog input in such a way that it is still less than but close enough to the maximum input of the digitiser.

3.4.5. Magnetic Exciter.

Before applying the magnetic exciter the force characteristics were investigated. A force transducer (B&K type 8200) was screwed down on a thick steel plate which was firmly anchored on the laboratory floor. Upon this force transducer the magnetic exciter was mounted. An accelerometer and a weight were also mounted on the moving exciter mass giving a total mass of 0.12853 grams. To avoid the additional effect of resonance of the body of the exciter on reading the data of the force transducer only a low amplitude and a certain range of

frequency of excitation were applied. Comparisons of the results are shown in fig.(3.9.A) and the lay out of the experiment is portrayed in fig.(3.9.B).

3.5. Test Procedures.

This sub-chapter discusses the test procedures of the experiments investigating the jump phenomenon, the absolute to relative relationship, the non-linear behaviour and the effect of the flexural and diagonal splitting crack patterns and defects on the dynamic parameters.

3.5.1. Jump Phenomenon.

It was reported by author in reference [40] that the response of the steady state tests using the mechanical exciter was jagged about the resonance due to a sudden change of the dynamic properties. Further study of this phenomenon was carried out in this research by setting up two exciters, i.e. the mechanical exciter and the magnetic exciter, mounted on similar concrete beams at about the same position and exciting the beams over their resonance frequencies. These two experiments were important since the jump phenomenon always occurred around resonance.

The out of balance mass of the mechanical exciter produces force proportional to its squared frequency as reported by the author in [40]. Therefore, increasing

the frequency of excitation by a speed controller results in higher force of excitation. A linear change of force of excitation can be carried out by adjusting the out of balance mass which comprise two sets of solid half circle steel attached at both ends of the exciter shaft as seen in fig.(3.10). Two different series of force of excitation were applied on the beam over the first mode which was about 25Hz. Forward and reverse frequency excitations were also carried out to examine the behaviour of the jump phenomenon.

When applying the higher force of excitation (the angle between the two half circle steel plate, α at 30 degree) it was found in the forward excitations that at about the resonant frequencies the speed of the out of balance mass did not proportionally increase with the increase of the speed controller. At a certain stage a slight change on the speed controller resulted in a sudden change of speed of the out of balance mass which was referred to as the jump phenomenon. The frequency at which the jump started in forward excitations were different from the reverse excitations. This jump phenomenon decreased with the force of excitation (the angle between the two half circle steel plate at 15 degree). The second experiment indicated that the effect of the excited beam on the moving out of balance mass was significant.

3.5.2. Absolute to Relative Relationship.

A further study using the magnetic exciter was carried out. The magnetic exciter (Derritron VP-2) was positioned on the beam at similar distance from the centre of the beam as the mechanical exciter. To increase the force of excitation 80 grams of mass and 29.93 grams of an accelerometer mass were added to the 18.6 grams of the built up moving mass. The force of excitation can be obtained by multiplying the total moving exciter mass which was 128.53 grams by its relative acceleration as described in later sub chapter. The experimental set up is shown in fig.(3.11). A relative measuring device, the LVDT, was mounted to measure the relative displacement of the moving exciter mass to the body of the device. The frequency of excitation was controled by turning the analog knob available on the integral amplifier. A low frequency digital indicator was employed to monitor the manually adjusted frequency increments. A decrease of voltage and an increase in ampere of the amplifier controlling the magnetic exciter about the beam resonance was indicated for both forward and reverse experiments.

3.5.3. Non-linear Properties.

The experiment investigated the non-linear behaviour of the beam before and after inducing cracks. This experiment was conducted within the experiments of

beam-2. partially bonded, flexural crack pattern. The procedure was similar to that relating absolute to relative parameters as discussed in (3.5.2) with the exception that this experiment was carried out on two condition, i.e. before and after inducing cracks. Three different sets of force of excitation were applied on each condition.

3.5.4. Flexural and Diagonal Splitting Defects.

There were several similar test procedures for the experiments applied to each fully and partially bonded beam and are described as follows :

Before lifting the beam from the casting mould the strains were always recorded. It was found that the strain differences due to each beam deflecting under its self weight were about 20-30μs which was considered negligible. The strains were also recorded once the beam had been set in position on its bearings and was ready to test.

Four loading stages were applied on beam-1 to beam-3 and six loading stages were applied on beam-4. Load increments of 0.47kN and 1.18kN were needed to create flexural and diagonal splitting crack patterns respectively. At each increment the strains, deflection and the load were recorded. Similar mid span tensile strains for both fully and partially bonded beams were kept in each stage of loading. This criterion was used

to highlight the possibility that the load-strain curve of the partially bonded beam would be different from the fully bonded beam.

Steady state excitations were carried out over three natural frequencies. Input-output signals were recorded on two 4-channel Racal recorders where the first channel of each recorder was assigned to be the common channel. Finer frequency increments were applied around the resonant frequency. Frequency increments of less than 0.1Hz were difficult to achieve for higher frequencies,i.e. above 50Hz, therefore, frequency increments of 0.2 to 0.5Hz were applied about the second resonance and 0.5 to 1.0 Hz were applied about the third resonance.

3.5.4.1. Beams Containing Flexural Crack Patterns.

Two types of sample were examined and will be described as follows.

a. Fully Bonded Beam.

Before applying external loading points a vibration test over the three natural frequencies was conducted. Following the first vibration test the first static loading at the third span was applied. Visible cracks at about the mid span were created at 1.74kN. The strain in the tensile reinforcement at the mid span was 381.7μs. The load was further increased until it reached 2.18kN where the strain in the tensile reinforcement at the mid

span was 591.5μs. This meant that the strain had theoretically reached 37.9% of the yield strain. The number of cracks were 5 spread over the third span and the maximum visible crack depth was 35-40mm.

After releasing the static loading the second vibration test was carried out in a similar way to the first vibration test. Following the second vibration the second static loading was applied. The static loading was terminated at 4.21kN when the strain in the tensile reinforcement at the mid span was 1219μs. This, theoretically, approached 78.1% of the yield strain. There were 10 cracks 60-70 mm deep spread over the midle third of the span.

The third vibration test was again similar to the previous vibration tests. Further static loading was applied until the yield strain in the tensile reinforcement was approached. Wider cracks were concentrated in the middle third of span and finer cracks spread over the rest of the span. The maximum static load at this stage was of 5.26kN and the strain in the tensile reinforcement at the mid span was 1512μs. Theoretically it had approached 96.9% of the yield strain. A total of 11 cracks had developed with average depth of 70-80mm and spread over the beam's length.

The fourth vibration test measured the dynamic characteristics of the beam at close to flexural failure. This last static loading stage aimed to find the maximum

load and the typical crack pattern at failure. This load was assumed to occur when large increments were recorded on the dial gauge positioned at the mid span. The maximum load was about 7.78kN and the strain in the tensile reinforcement approached 1930μs. This meant that the yield strain had been exceeded by 23% that specified by the supplier (312 N/mm^2).

b. Partially Bonded Beam.

The range of the frequency excitations was from about 20 Hz to 280Hz. Three modes of vibration were excited within this range. Following the first vibration test with no load on the beam static loading at the same positions as with the fully bonded beam was applied. The load created a crack at 0.76kN resulting in a sudden change of strain in the tensile reinforcement at the mid span from 163μs to 533μs. The static loading was increased to 1.76kN where the strain in the tensile reinforcement at the mid span approached 806.8μs (51.7% yield strain). No further significant additional cracks appeared although the single crack opened significantly. This 110mm deep crack was situated at about the mid span.

The second vibration test was then applied. A significant difference on the first and the third natural frequencies were indicated at this test. Slightly unstable signals known as beating signals were recorded and were presumed due to the presence of bond within the

debonded reinforcement after cracking. A further static loading stage resulted in no further significant cracks. After approaching 2.75kN, which gave 1057μs in the tensile reinforcement at the mid span the load was removed.

The third vibration test was carried out within the similar range of frequency of the previous vibration tests. Strains of 1391μs (89.16% yield strain) of the tensile reinforcement at the mid span were achieved at 3.77kN. No further new cracks were developed but the depth of the single crack increased slightly.

The last vibration test of this series produced a similar set of excitations to the previous tests. Following the vibration test the last loading stage was applied until the beam failed. Prior to the yield failure five additional cracks developed in the middle third of the mid span. The load was terminated when the yield strain in the tensile reinforcement at the mid span approached 2343μs. This meant that it exceeded the specified yield strain by 50%.

3.5.4.2. Beams Containing Diagonal Splitting Crack Patterns.

Two types of sample were examined and will be described as follows.

a. Fully Bonded Beam.

The experiment was initiated by applying a vibration

test on the beam. The frequency excitations were carried out over the three vibration modes which were of the same range as the previous tests. The diagonal splitting crack patterns was created by applying two external point loads near to the supports.

Strains of 406μs (26% yield strain) in the tensile reinforcement at the mid span were achieved at 9.27kN and were sufficient to develop flexural cracks at mid span. Eight cracks of 35-50mm deep were created within the two point load positions.

The second vibration test was applied after releasing the static loading rig. The steady state frequency excitations were applied over the three vibration modes. Further static loading created a total number of 21 cracks, 50-60mm deep, spread over almost the whole beam length. A maximum static load of 15.84kN was applied in this stage producing strains of 876μs (56% yield) in the tensile reinforcement at the mid span. At this stage diagonal splitting cracks were still not visible.

The third static loading stage was aimed to create apparent diagonal splitting crack patterns. This was achieved at 18.47kN or at a strain of 1028μs (65.89% of the tensile reinforcement capacity) at the mid span.

Again, the fourth vibration test was conducted over the three vibration modes. Further static loading created diagonal splitting cracks at the roller support at 22.35kN or at 1272μs (81.5% yield strain) in the

tensile reinforcement at the mid span before the beam failed of diagonal splitting at 35.34kN. The last recorded strains of the tensile reinforcement at the mid span were 1947μs. This strain was 24.8% higher than that specified by the supplier.

b. Partially Bonded Beam.

The frequency excitations were carried out over the three vibration modes to represent the initial conditions of the dynamic parameters. The range of the frequency excitation was from 0 to 280Hz. Sudden change of strains and displacement were found due to cracks suddenly occurring in this type of beam. The single wide crack 120 mm deep at the mid span occurred at 4.49kN or at 661.2μs (42.3% yield strain) in the tensile reinforcement at the mid span.

The second vibration test was conducted after releasing the static loading rig. Unstable amplitude readings of the signal were recorded. The second static loading stage followed and the second vibration test was then conducted. The maximum load at this stage was 7.01kN or at 917μs (58.7% yield strain). No significant additional cracks were produced at this loading stage. It was expected that at this loading stage initial diagonal splitting cracks had started.

The third vibration test was aimed to evaluate the effects of the initial diagonal splitting crack patterns

on the characteristics of the dynamic parameter.

Following this vibration test the third static loading stage was carried out and aimed to create visible diagonal splitting cracks at a similar strain as in the fully bonded beam under a similar loading pattern. This aim was not successful, no visible diagonal splitting cracks propagated.

The fourth loading stage again attempted to create diagonal splitting crack patterns by increasing the load to 21.484kN which was 1.71kN higher than that the fully bonded beam with similar loading pattern but there was still no indication of the visible diagonal splitting cracks. The load was released and checks were carried out throughout the apparatus and loading frame positions. No indications of misreading or mechanical fault were found.

The fifth loading stage was then applied. At this stage the diagonal splitting cracks were apparent at 25.418kN or at 2000μs (128.2% yield strain) in the tensile reinforcement at the mid span.

The fifth vibration test was aimed to evaluate the effect of the visible diagonal splitting cracks on the characteristics of the dynamic parameter.

Further load was applied until the beam failed of diagonal splitting mode.This was achieved at 30.455kN or at 2316μs in the tensile reinforcement at the mid span. This strain was 48.4% higher than specified.

3.6. Test Result and Comment.

3.6.1. Jump Phenomenon.

Normalised frequency responses to the square of the frequency excitation in the hysteretic experiment (using the mechanical exciter) for different sets of force of excitation are shown in fig.(3.12). This experiment indicates that the unstable region causing the jump phenomenon depends on the force of excitation. The higher the force of excitation the larger the unstable region. This phenomenon is similar to non-linear hard spring behaviour demonstrated by White and Rades [15,21]. The non-linear behaviour demonstrated by White and Rades [15,21] was found from the membrane effect of a steel plate with simply supported hinges at its four edges and rubber or polyurethane pads for vibration isolation purposes. The simple support system applied in the concrete reinforced beam experiment should not allow the non-linear hard-spring behaviour as demonstrated by White [15] to occur. Thus, the unstable condition must have been due to something else. The non-linear behaviour may arise from the opening and closing of cracks or bonding and debonding of the steel reinforcement.

The normalised response of a concrete beam subject to four sets of the same force of excitations is shown in fig.(3.13) and demonstrates non-linear soft spring behaviour. The higher amplitude at lower frequency response shows that the concrete beam is predominantly

controlled by the stiffness rather than by the damping. Typical viscous damping exists in this response. Since the peak amplitude and resonant frequency are of importance the jump phenomenon is further investigated in chapter-5.

3.6.2. Absolute to Relative Relationship.

This experiment using a magnetic exciter confirms that the jump phenomenon was not due to the non-linear hard-spring behaviour. The response spectrum of the concrete beam subjected to a lower force of excitation (20-30 times lower) as shown in fig.(3.14) indicates that the jump phenomenon does not apparently exist. In contrast the amplitude of the moving exciter mass (both absolute and relative as shown by accelerometer on the moving exciter mass and the LVDT respectively) sharply decreases as the frequencies of excitation approaches the resonance. This phenomenon does not conform with the calibration as shown in fig.(3.9). Fig.(3.14) also confirms the presence of the absolute and relative amplitudes which are of interest when discussing normalised force of excitation.The reflected force of the excited beam is supposed to affect the amplitude of the moving exciter mass. A further phenomenon is also indicated that the relative amplitudes of the LVDT are lower than the absolute amplitudes of the accelerometer before approaching resonance and reversed after

resonance. The relative phase difference measured from the LVDT to the excited beam and from the accelerometer to the excited beam is shown in fig.(3.15) and confirms the phenomenon mentioned above. Further discussions about these observations are found in chapter-5.

3.6.3. Non-linear Behaviour.

This experiment was carried out on the second beam, partially bonded, before applying flexural cracks. The three sets of force of excitation gave rise to different relative force of excitation as shown in fig.(3.17) (a further discussion of the relative force will be given in chapter-5). This indicates the presence of non-linear soft spring behaviour. To establish better relationships between the dynamic parameters before and after the beam had cracked a similar experiment was repeated on the same beam as it approached failure and the results are shown in fig.(3.18) and (3.19). Different resonant frequencies and amplitudes may be seen in the graphs. These figures confirm the effect of the reflected force from the excited beam on the moving exciter mass and the presence of the non-linear soft spring behaviour. Normalised responses of fig.(3.17) and (3.19) as shown in fig.(3.20) and (3.21) show an interesting phenomenon. Before the beam was artificially cracked the normalised responses of the three sets of force of excitation resulted in almost similar peak

amplitudes. This reveals that the beam possessed a very low non-linearity as shown in fig.(3.20). The same beam, possessing a large number of cracks, fig.(3.21) indicates that the increase in the force of excitation decreases the peak amplitudes at lower natural frequencies. This phenomenon confirms the finding of the research carried out by Hassan [6] from her analysis of the 'pull back - sudden release' experiments. Frictional damping predominantly controlled the response of the beam. Further discussions on this is obtained in chapter-7.

Polar diagrams were shown by Rades [19,20,21], Tomlinson [17,18] and White [15,16] to possess unique properties which could define the existence of non-linearities. The polar diagram of fig.(3.12) as shown in fig.(3.22) represents a non-linear hard spring behaviour. This unlikely and confusing result is further discussed in chapter-5. The isochrones of polar diagram in fig.(3.23) which related to fig.(3.20) indicates clearly the non-linear soft spring behaviour. This should be viewed in comparison with the spectral representations in fig.(3.17). This also applies to the comparison between fig.(3.24) and fig.(3.19). As proposed by White [14,15] the resonant frequencies can be found at the maximum rate of change of curvature if constant intervals of frequency of excitation can be applied.

3.6.4. Result from Applying Flexural and Diagonal Splitting Crack Patterns.

Four specimens have been examined consisting of two fully bonded reinforced concrete beams (FB) and of two partially bonded reinforced concrete beams (PB). Two types of loading have been applied to the both types of beam, i.e. loading type-1 (L1) to create flexural crack patterns and loading type-2 (L2) to create diagonal splitting crack patterns. Static loading increments for loading type-1 and loading type-2 were 0.47kN and 1.18kN respectively. A summary of the material properties measured is given in table (3.1) and the more detailed static properties are given in the following sub-chapters.

The dynamic properties of all beams required to be normalised and the normalisation procedure is discussed in chapter-5. The response of the beams subject to dynamic excitations will be discussed in chapter-7.

3.6.4.1. Beams Containing Flexural Crack Patterns.

a. Fully bonded beams (FB/L1).

From table (3.1) it can be seen that the slump test of this beam shows the concrete mix to be rather stiff. This was corrected by carrying out thorough compaction using a concrete mix vibrator. This also improved the result of the compressive stress of the cubes, modulus elasticity and the tensile stress of the concrete beam.

The other test results were close to their design values. During the static loading of the beam early fine cracks started soon after the first loading stage had been reached and simultaneously spread over the midle third of the span. The load-displacement as well as the load-strain graphs detected these propagating cracks as a decreasing slope of the related curves as seen in fig.(3.25.A and 3.25.B). Within the first loading stage the tensile strain distribution was affected by the bond. The increase in cracks implying a decrease of bond between the tensile reinforcement and the concrete and is shown as the decrease of slope of the load-displacement or load-strain curve. Fig.(3.25.C) did not respond very much to the propagating cracks as the load was positioned at the quarter span positions. Residual strains are indicated at all positions of the gauge as seen in fig.(3.25) as the non-zero initial conditions of the displacement as well as the strain after reversing the load.

The residual strains decreased with the increase of load. This may indicate a small loss of bond surrounding the reinforcement bars. This implies that the residual strains in the load deformation do not relate significantly to the number of cracks as shown at the third stage where twelve additional cracks were induced without a significant change of the shift. Almost linear relationships are found at the third and the fourth

loading stages as shown in the three curves in fig.(3.25).

At the load at which yield occurred in the tensile reinforcement close to one of the harnesses it was noted that the strains were not evenly spread along the length of the reinforcement, thus the 'folded back' strain curve in fig.(3.25.B) was expected to occur at a strain gauge close to the failure point. The load-displacement curve of fig.(3.25.A) would have shown an increase in displacement at the yielding load however it was decided to remove the dial gauge before this deformation had been reached (due to the shortage of the movement of the arm). The load-displacement diagram therefore does not represent properly this last stage of loading. The maximum load, strain and displacement of each stage of the static loading and the yield crack patterns are highlighted in table (3.2) and fig.(3.26) respectively.

b. Partially bonded beams (PB/L1).

Tests of specimen materials show that most results are slightly higher than prediction with the exception of the Young's Modulus of elasticity. The in situ slump was slightly over the requirement. This was probably due to an excessive water-cement ratio.

A sudden single crack within the first loading stage resulted in a residual strain and displacement as portrayed in fig.(3.27.A) and (3.27.B). Since

fig.(3.27.C) is a response of the gauges within the fully bonded region this sudden change of crack was not recorded as residual strains.

Two further loading stages did not apparently increase the number of cracks. Only a slight change in depth of crack was indicated for the single wide open crack at the second and the third loading stages. Fig.(3.27.B) and (3.27.C) imply that the beam behaved elastically in the unbonded area and only a small loss of bond in the bonded areas. In comparison with the fully bonded beam under the same loading pattern where a more visible number of cracks were developed this beam possessed a lower dry friction but higher stiffness in certain area. The dynamic characteristics of this beam will be discussed in chapter-7.

The last loading stage gave rise to several additional cracks within the centre third of the span. At failure the compressive strain at the mid span position above the single wide crack was excessive and as a result of this the concrete crushed.

A 'folded back' strain curve as well as the elongated load- displacement curve at the yielding load are demonstrated in fig.(3.27.A) and (3.27.B). The load-displacement curve is typical of an under reinforced beam failing due to flexural moment. Further detailed maximum load, strain and displacement and the flexural crack patterns are presented in table (3.3) and

fig.(3.28) respectively.

3.6.4.2. Beams Containing Diagonal Splitting Crack Patterns.

a. Fully bonded beams (FB/L2).

Although the slump test of this beam complied with the specification it was found that the Young's Modulus of elasticity was far from the BS8110 calculated value. This was probably due to inadequate compaction. Other results for this beam were close to the design values.
A slightly uneven strain distribution was indicated by the gauges positioned near to the loading point as seen in fig.(3.29.C). More significant residual strains are found in fig.(3.29) under first and second loading stages which were respectively 26% and 45% of the maximum load. The cyclic loading shapes of the first and second loading stages are different from the third cyclic loading stage. Eight and twenty one flexural crack were developed in this beam within the first and second loading stages respectively. The more the number of cracks the more non-linear damping friction and the lower the stiffness expected. In contrast the damping and the stiffness control the amplitude of vibration acted in opposite ways. These phenomena are discussed in chapter-7. The third loading stage was expected to develop diagonal splitting cracks. An audible sound 'tick' was heard just before the diagonal splitting cracks were visible at the

hinge. The diagonal splitting crack occurred at the supporting shaft close to the loading point at 56% of the maximum load. The different cyclic loading shape at this stage is shown as a less significant shift and is due to a change of load distribution. This is also shown as a small increase of the crack depths. This change of load distribution may also change the dynamic characteristics of the beam as will be discussed in chapter-7.

A loud sound was heard at failure of diagonal splitting as the cage surrounding the beam end was cut off.

The load-displacement and load-strain relationships are almost straight at the last loading stage. This complies with the design calculation where it was predicted that the beam should fail in diagonal splitting whilst the main reinforcement should be and was within the elastic range. Detailed maximum load- strain and load-displacement values at each stage and the failure crack patterns are shown in table (3.4) and fig.(3.30) respectively.

b. Partially bonded beam (PB/L2)

Test results of the slump, Young's Modulus and the cube stress complied with the design values as described in Appendix (B-1).

Within the first loading stage a crack suddenly occurred at the unbonded area. This crack occurred at about 10% of the maximum load and its effect is apparent from the

graphs shown in fig.(3.31.A) and (3.31.B) as residual strains. No further new cracks and only small changes of depth of the single crack is indicated by the flatter shapes of the cyclic curve at the second and third loading stages in comparison with the shapes of the fully bonded beam under the same loading pattern in fig.(3.29). This effect is more clearly shown in fig.(3.31.B) where the gauge was positioned at the unbonded area. From the type and the number of cracks the dynamic characteristics of this beam may be easily distinguished from the fully bonded beam under the same loading pattern. This will be covered in chapter-7. The fourth loading stage does not show obvious change in the load distribution. A residual strain is just apparent in fig.(3.31.A) and (3.31.C). This indicates that the diagonal splitting propagation is followed by flexural cracks. Six flexural cracks were visible at about 56% of the maximum load prior to the diagonal splitting crack propagation at roller. At this stage the diagonal splitting cracks were not clearly initiated by the 'tick' sound as reported in the fully bonded beam under the same loading pattern. The last loading stage developed another diagonal splitting cracks at the hinge before the beam collapsed. Table (3.5) summarises the maximum load-deflection and load-strain whilst fig.(3.32) shows collapse patterns of the beam.

3.7. Concluding Remarks.

3.7.1. Design, Experimental Procedure and Calibration .

The simply supported reinforced concrete beam models enable the investigation of the effect of bond, number of cracks, crack depth and the typical flexural and diagonal splitting crack patterns on the static characteristics of the beam. The dynamic characteristics of these beams will be discussed in chapter-7 and should confirm these investigations.

The normal concrete mix and the mild tensile steel in the design of beams should and did give rise to under reinforced concrete beams.

To provide perfect beam specimens without ends twisting was complex. The self aligning bearings helped to reduce this difficulty. The rods anchoring the supports onto the laboratory floor possessed their own natural frequencies, and these did not significantly affect the dynamic tests.

The number of vibration pick-ups used was adequate as only the first few modes of vibration were investigated. The constant connections between the vibration pick-ups and the charge amplifiers ensured constant results in the tests. Simple calibrations used in this experiment also helped to ascertain the output quality of the vibration pick-ups. The accuracy of other instrumentation used which may have affected the quantity and quality of the signal was proved.

The maximum load in each loading stage was different from one beam to another due to different capacity of the beams. Strains at the mid span of the beams were used as indications of the maximum loading at each stage.

3.7.2. Jump Phenomenon.

Three experiments have been carried out which affect the quality of the responses of the beams. The first experiment using the mechanical exciter shows a non-linear hard spring behaviour.

3.7.3. Absolute to Relative Relationship

The second experiment using a magnetic exciter shows the effect of the reflected force from the excited beam on the moving exciter mass. This effect was demonstrated as a sharp drop in the amplitude of the moving exciter mass when approaching resonance.

3.7.4. Non-linear Properties.

The third experiment displays the non-linear soft spring behaviour of the beams. The greater number of cracks produced the higher non-linearity. The first two experiments will be further discussed in chapter-5 and the third experiment in chapter-7.

3.7.5. Detection of Defects.

Four samples of reinforced concrete beam have been

tested and the general characteristics have been reviewed.

The number of cracks created in the fully bonded beam (FB/L1) were more than those created in the partially bonded beam (PB/L1). No further cracks were propagated and only a small increase of depth of the single open crack in the partially bonded beam (PB/L1) occurred before the last loading stage was applied. The residual strains and displacement were more visible in the fully bonded beam (FB/L1) than in the partially bonded beam (PB/L1). The 'folded back' curves showed that the typical under reinforced concrete beam behaviour was displayed on both samples.

The second two samples possessed diagonal splitting crack patterns. The first of the two samples was fully bonded and the second was partially bonded. The fully bonded beam (FB/L2) displayed larger residual strains than that of the partially bonded beam (PB/L2). An almost zero shift was apparent from the partially bonded beam (PB/L2) at the mid span. The change of the load distribution is recognised as the flattened cyclic load-strain or load-displacement curve and the lower residual strains.

The dynamic characteristics of these beams depend on the solution of the jump phenomenon therefore, these results will be discussed in chapter-7.

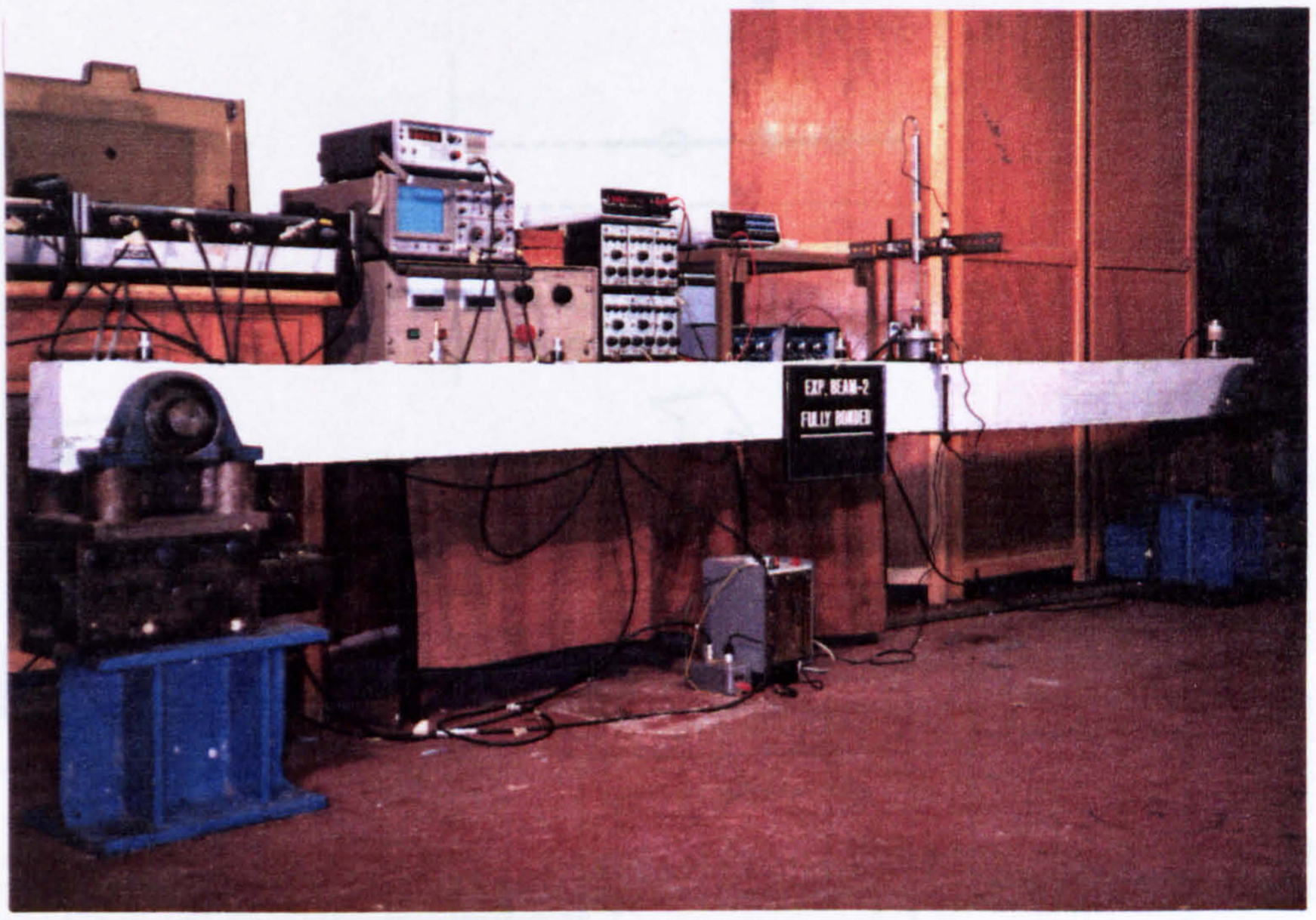

FIG.3.1.TYPICAL LAY OUT OF EXPERIMENTS.

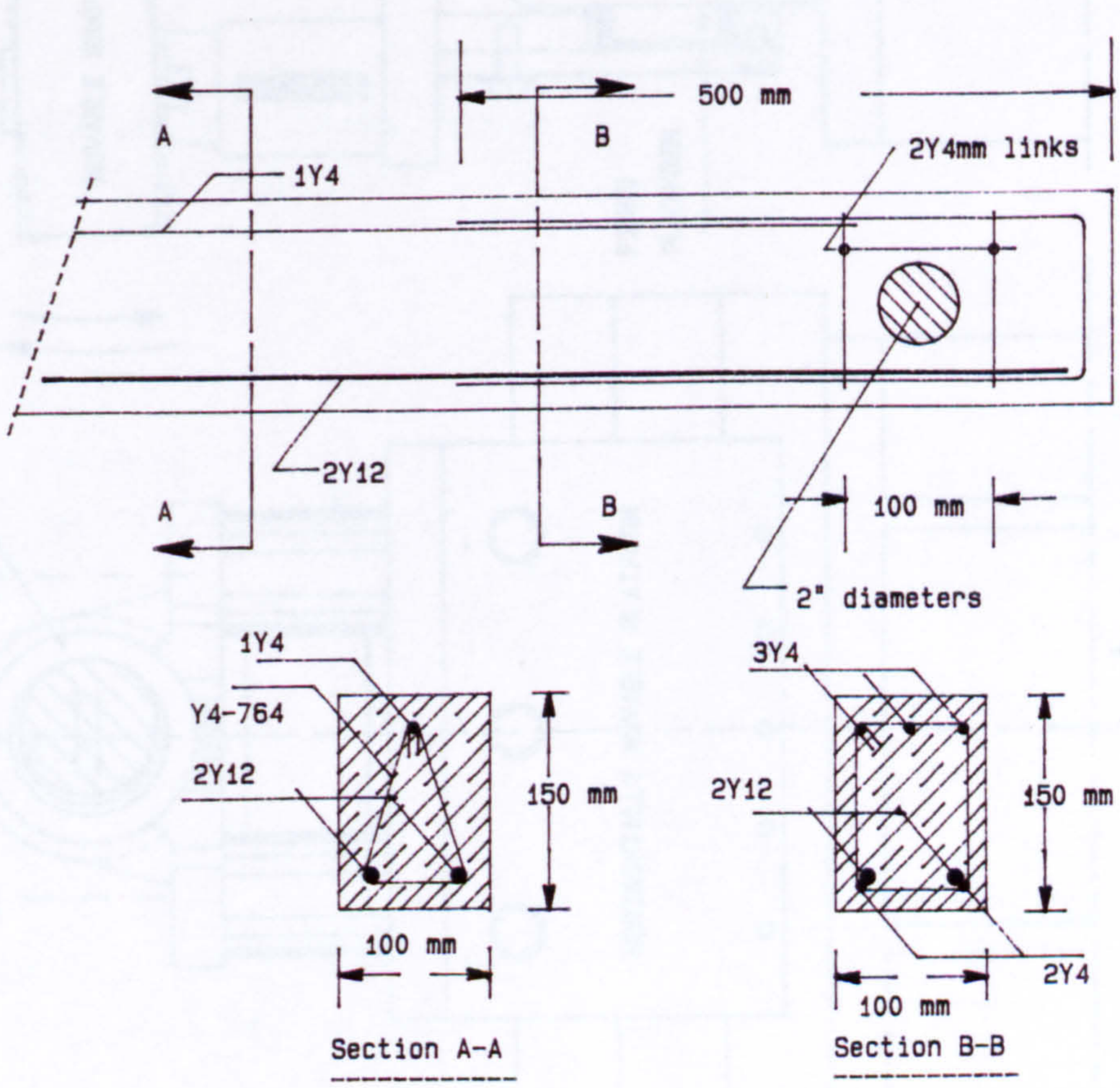

FIG.3.2.TYPICAL DETAILS OF REINFORCEMENT.

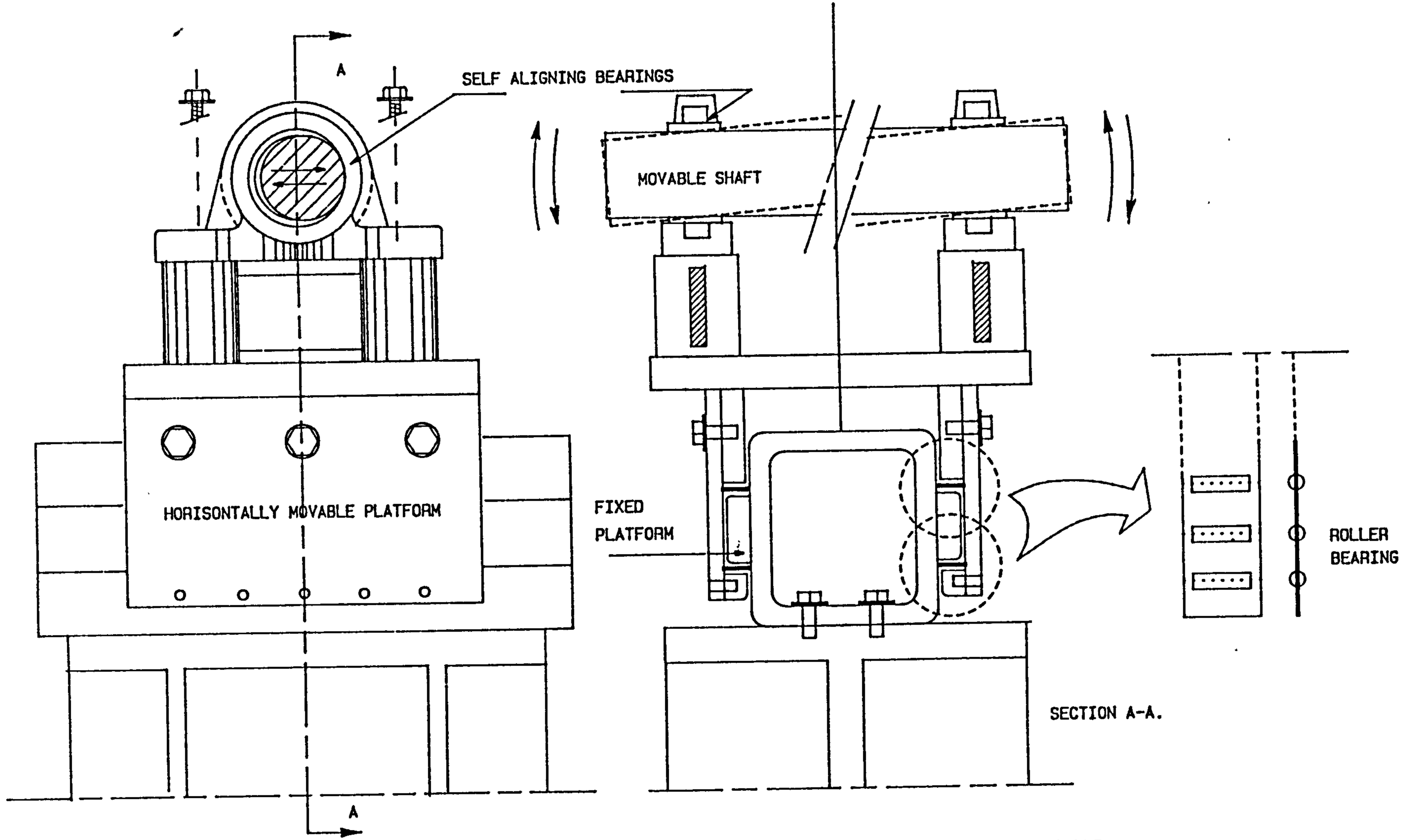

FIG.3.3.SKETCHES OF SELF ALIGNING AND ROLLER BEARINGS.

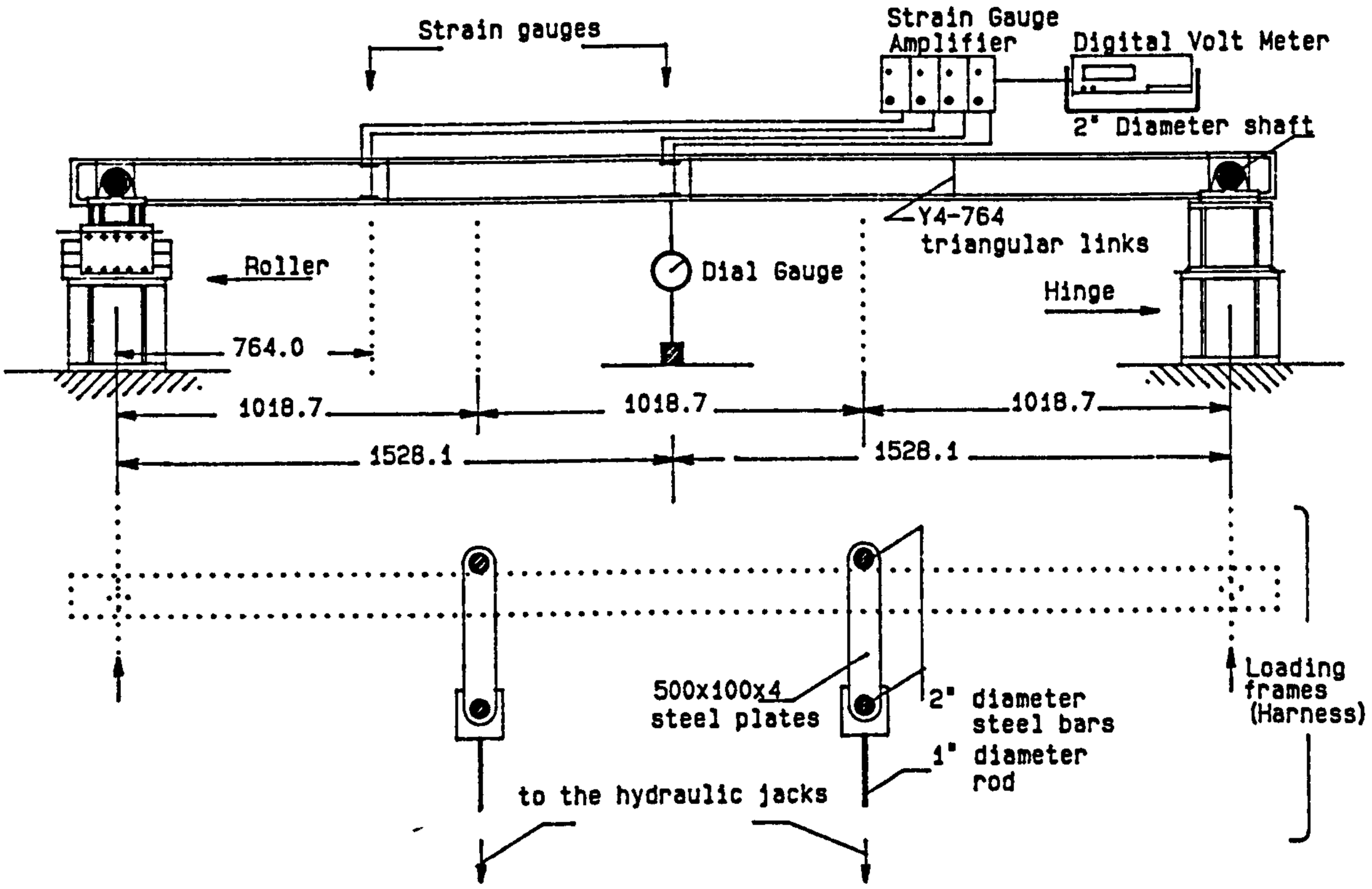

A) .TYPICAL LAY OUT OF FLEXURAL LOADING.

(UNITS IN mm, UNLESS STATED)

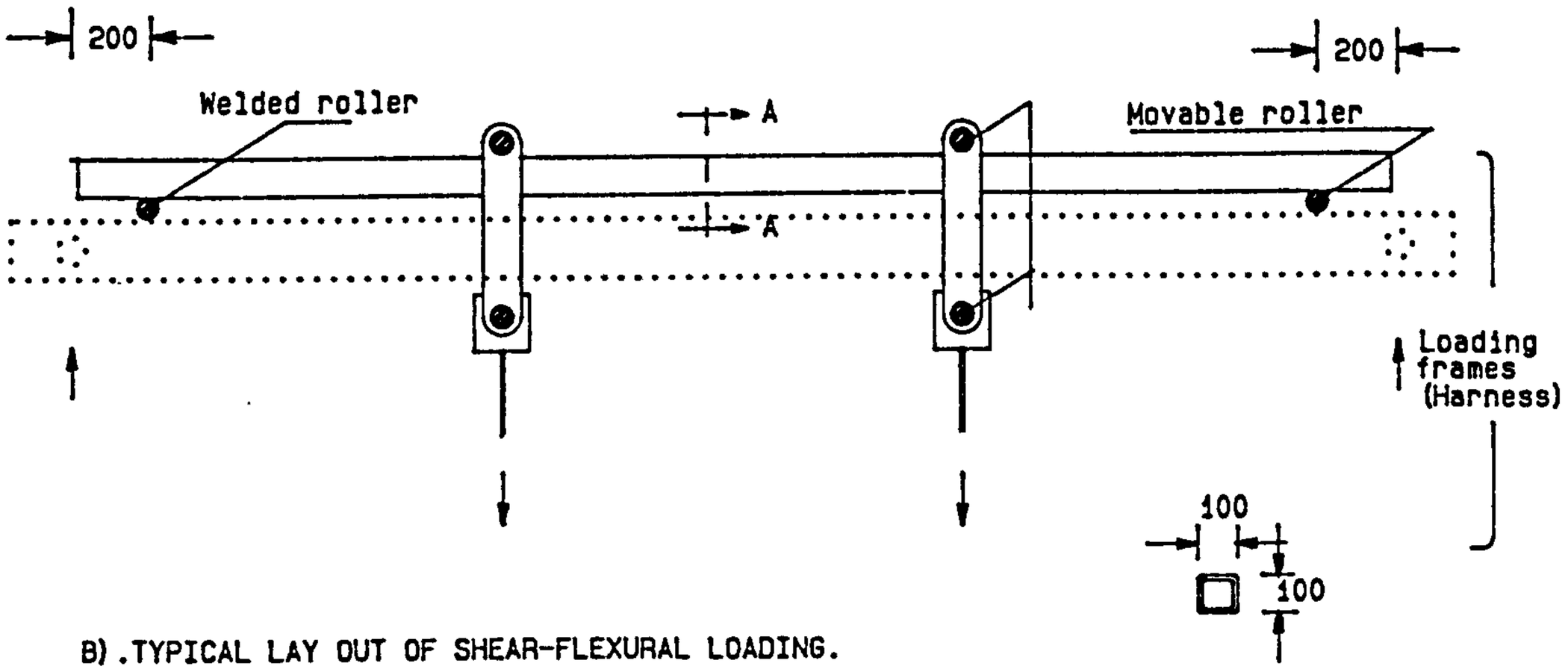

B) .TYPICAL LAY OUT OF SHEAR-FLEXURAL LOADING.

(UNITS IN mm, UNLESS STATED)

FIG.3.4.TYPICAL LAY OUT OF STATIC LOADING.

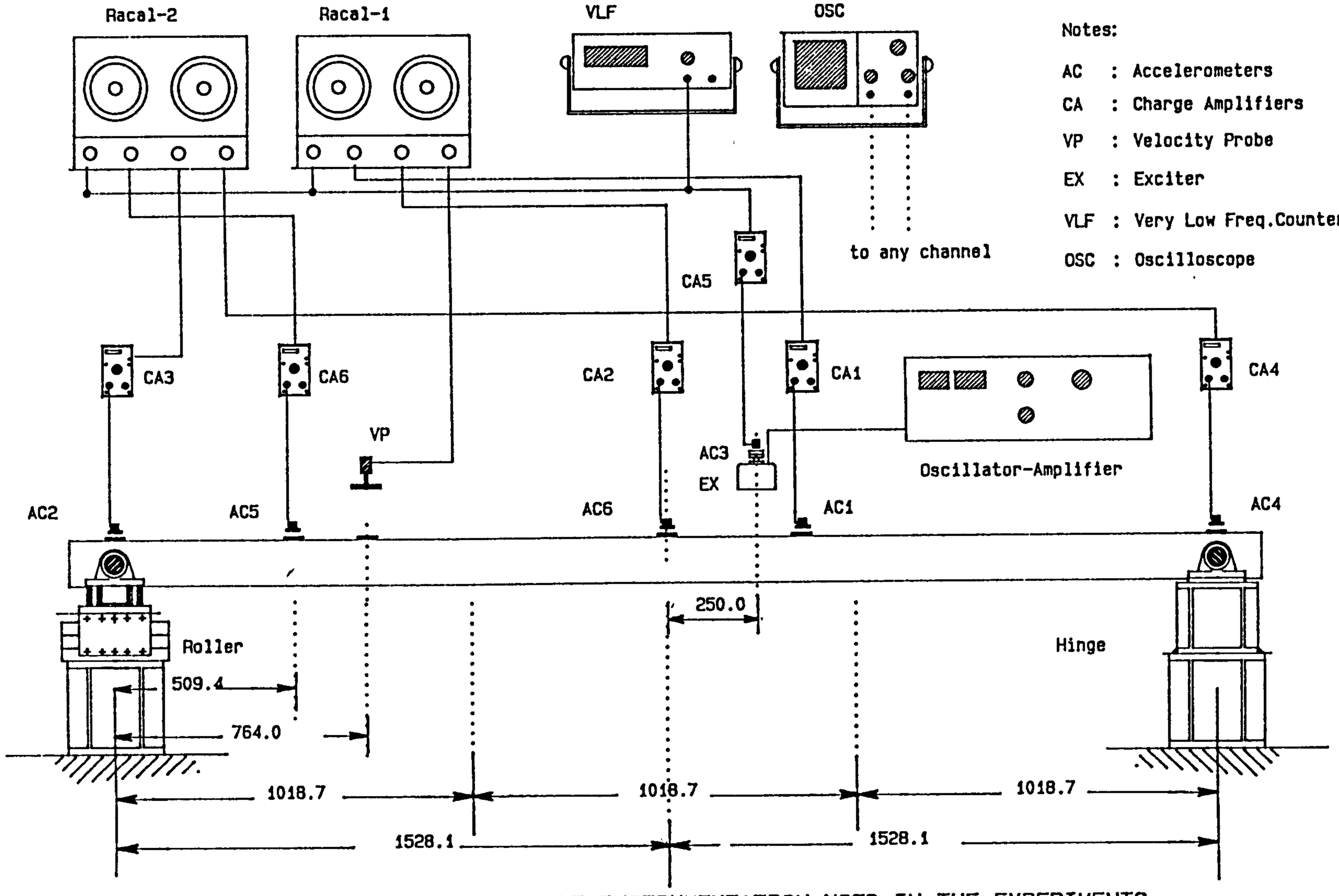

FIG.3.5.WIRING DIAGRAM OF INSTRUMENTATION USED IN THE EXPERIMENTS

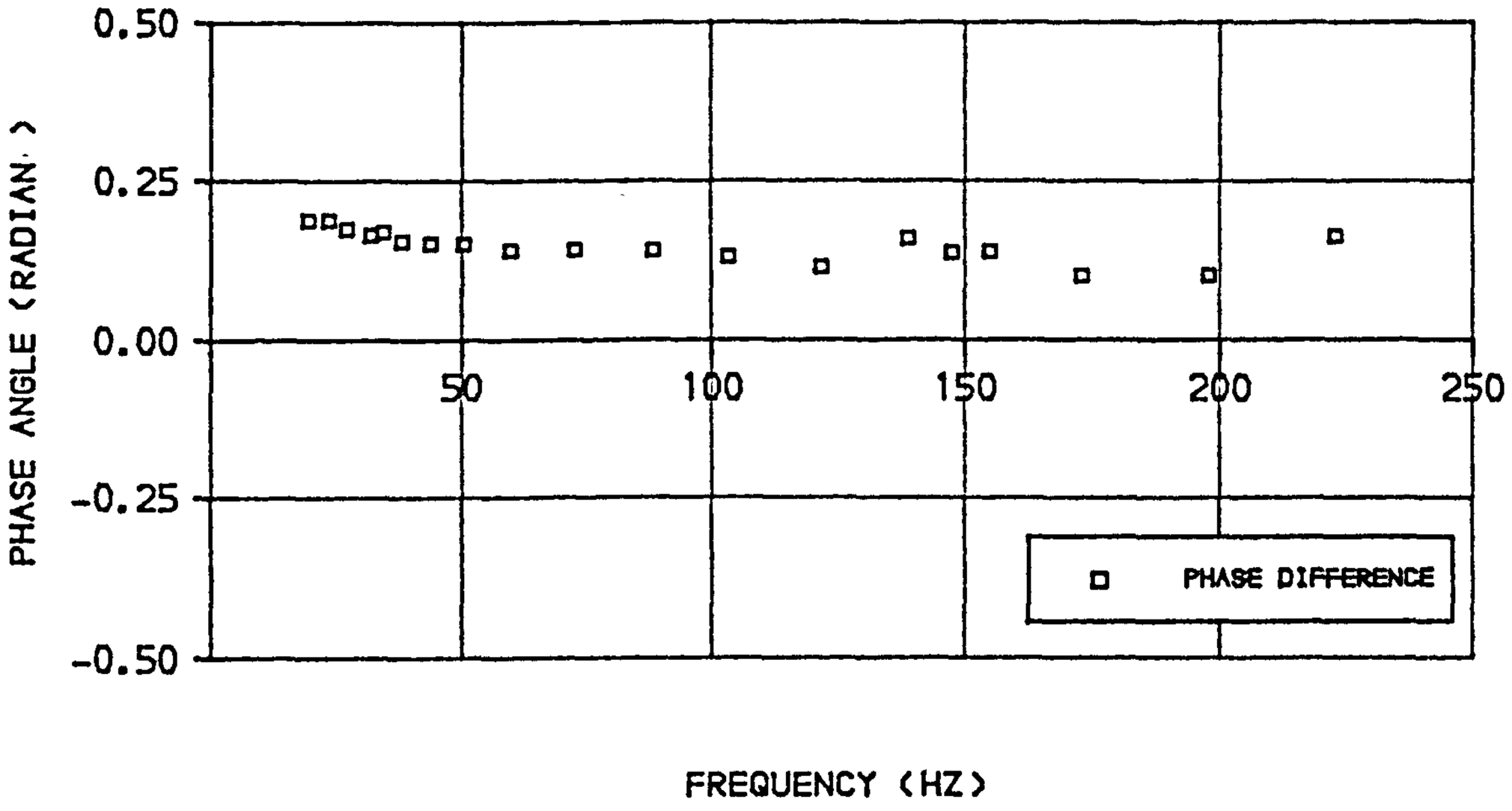

FIG.3.6. INHERENT RELATIVE PHASE DIFFERENCE OF ACCELEROMETER NO.1 (ADJACENT TO EXCITER) TO ACCELEROMETER NO.3 (ON THE MOVING EXCITER MASS)

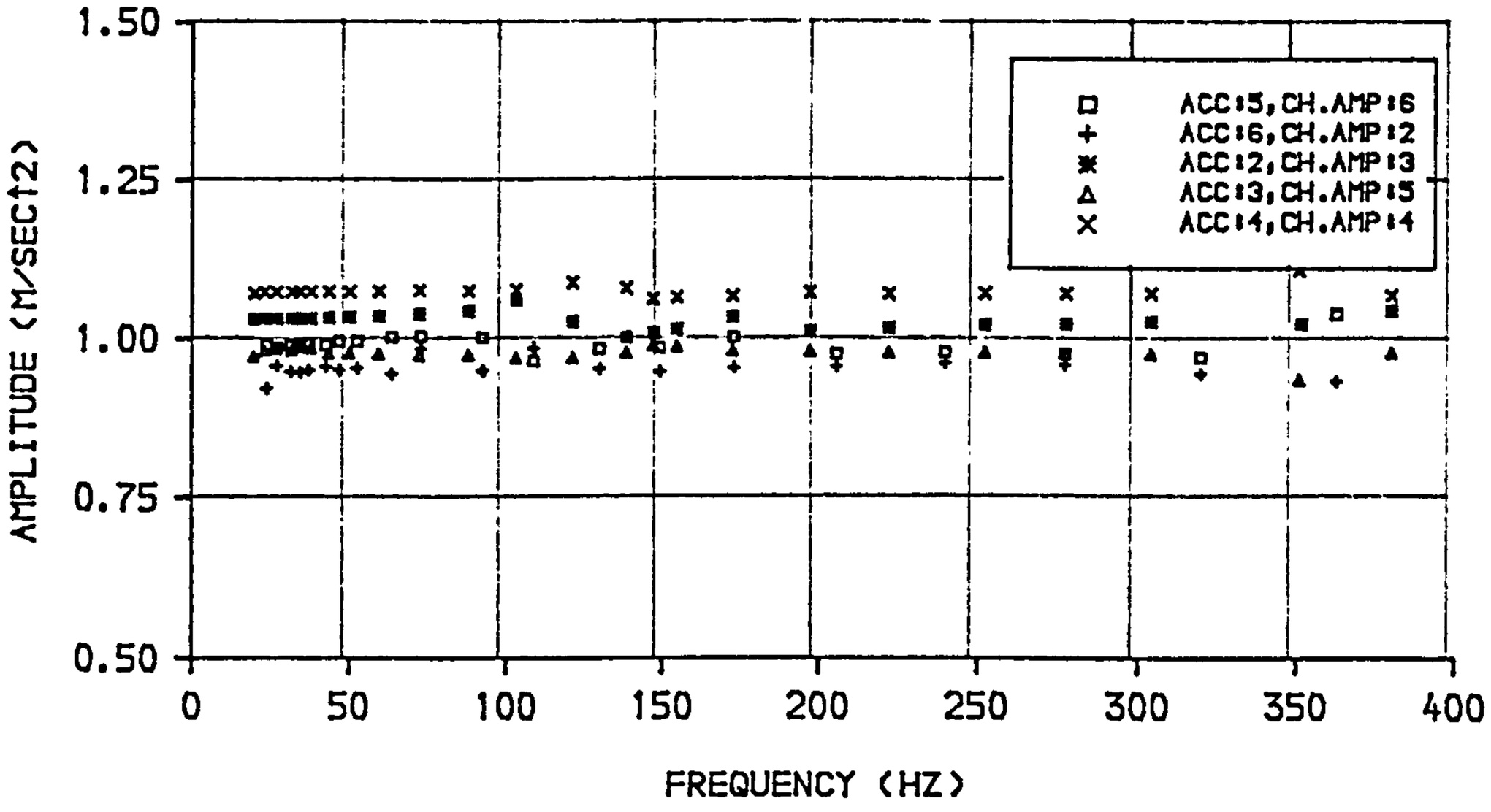

FIG.3.7. AMPLITUDE RATIO OF ACCELEROMETERS (B&K NUMBER: 2 TO 6) TO ACCELEROMETER (B&K NUMBER: 1)

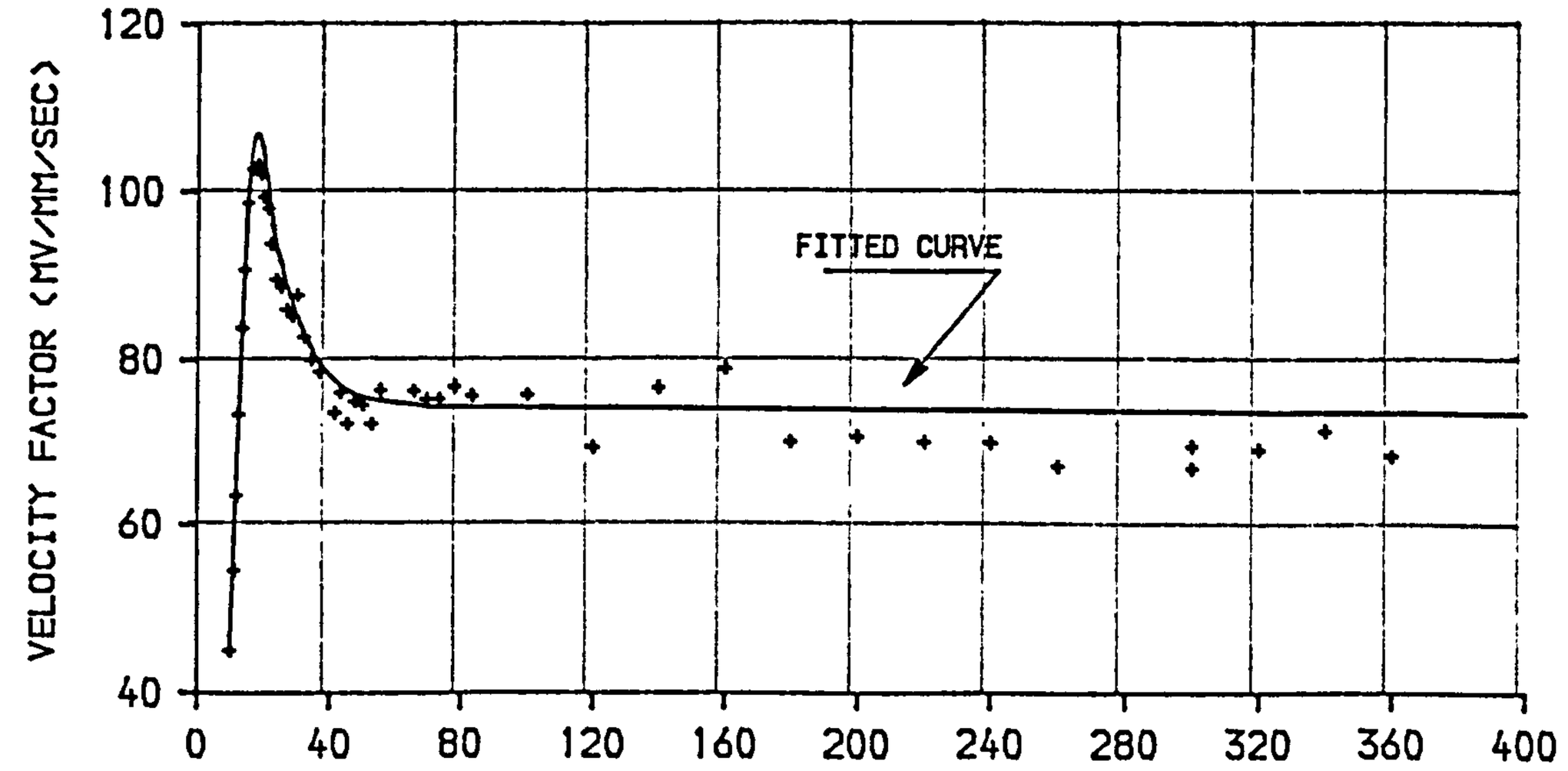

FIG.3.8. AMPLITUDE RATIO OF VELOCITY PROBE (T-77 IN MV) TO ACCELEROMETER (B&K NUMBER: 1 IN MM/SEC)

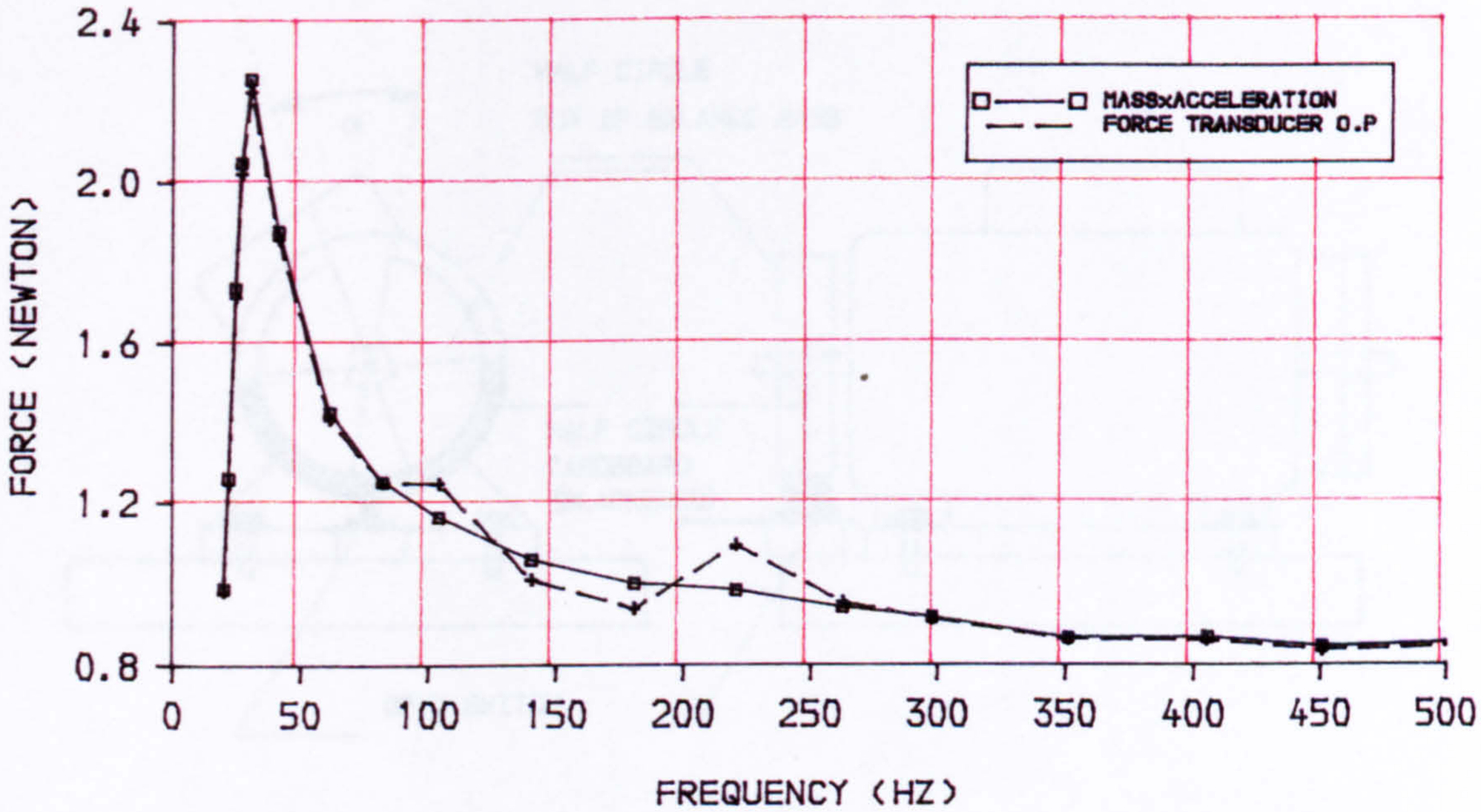

A. COMPARISON BETWEEN FORCE FROM MASS*ACCELERATION AND FORCE-TRANSDUCER OUTPUT (B&K TYPE 8200)

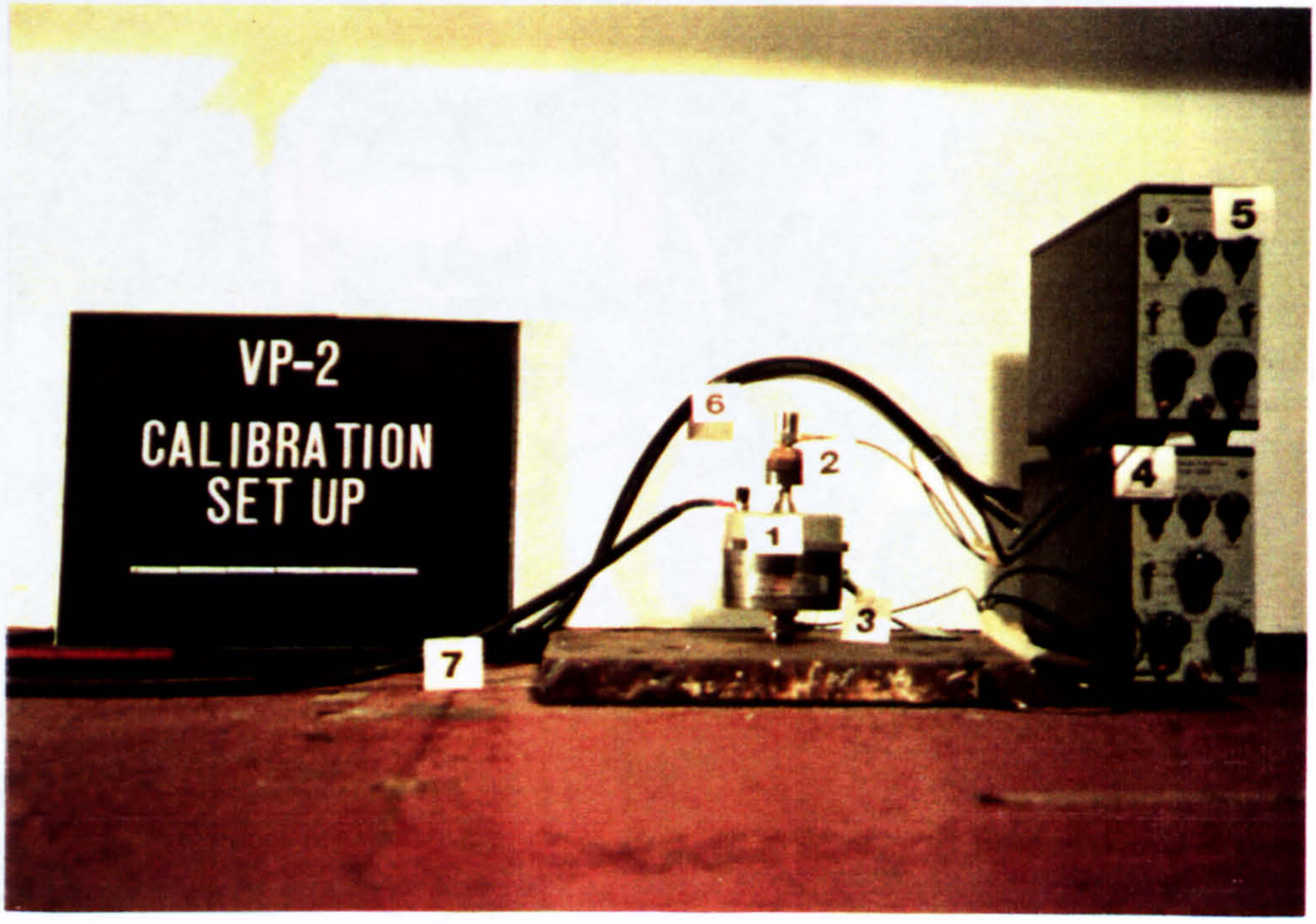

(1) = MAGNETIC EXCITER (3) = FORCE TRANSDUCER (B&K8200) (6) = TO TAPE RECORDER

(2) = ACCELEROMETER (4) = (5) = CHARGE AMPLIFIERS (7) = FROM POWER SUPPLY

B. SET UP OF INSTRUMENTATION

FIG.3.9.CALIBRATION SET UP CONFIRMING FORCE OF EXCITATION

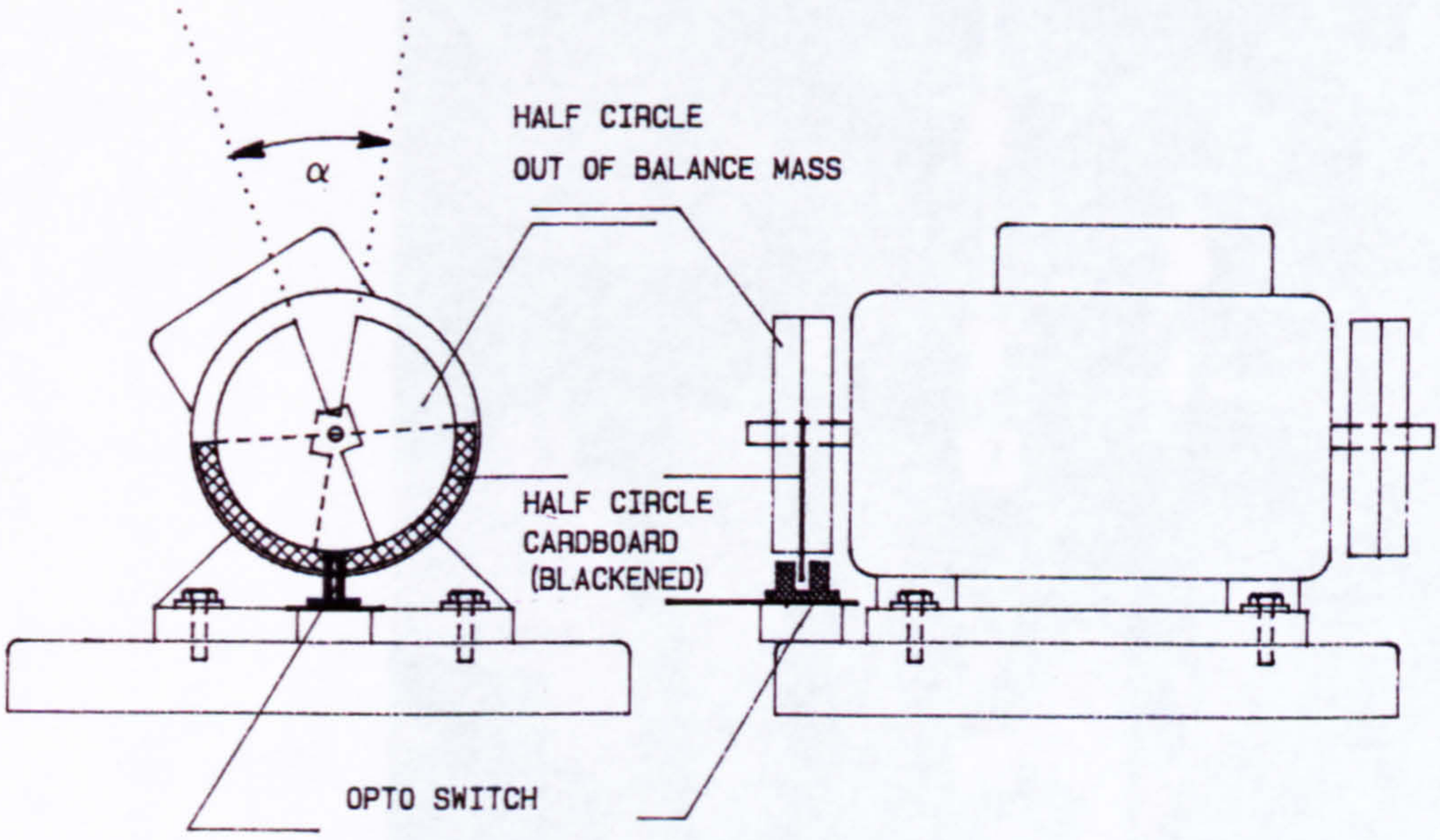

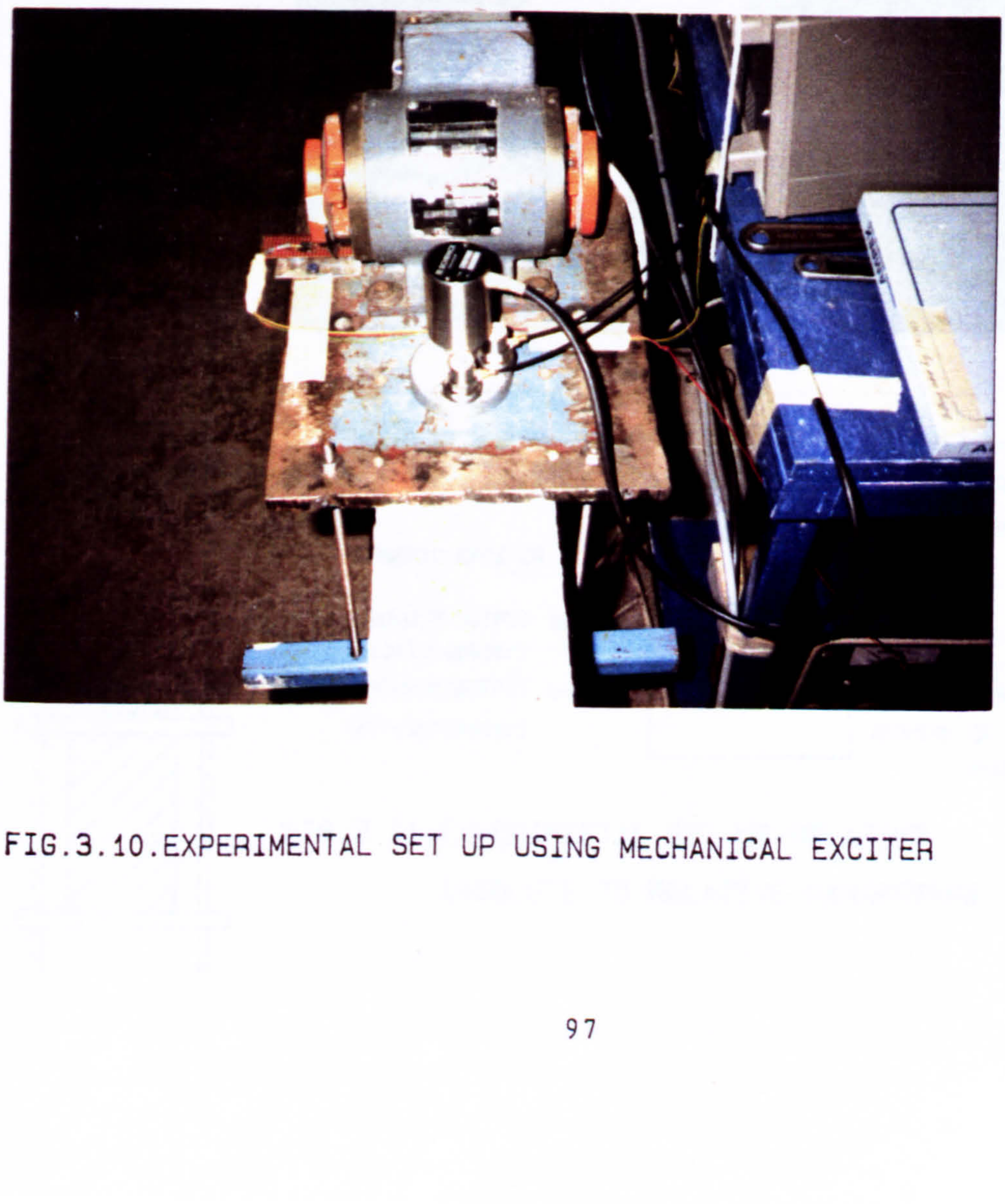

FIG.3.10.EXPERIMENTAL SET UP USING MECHANICAL EXCITER

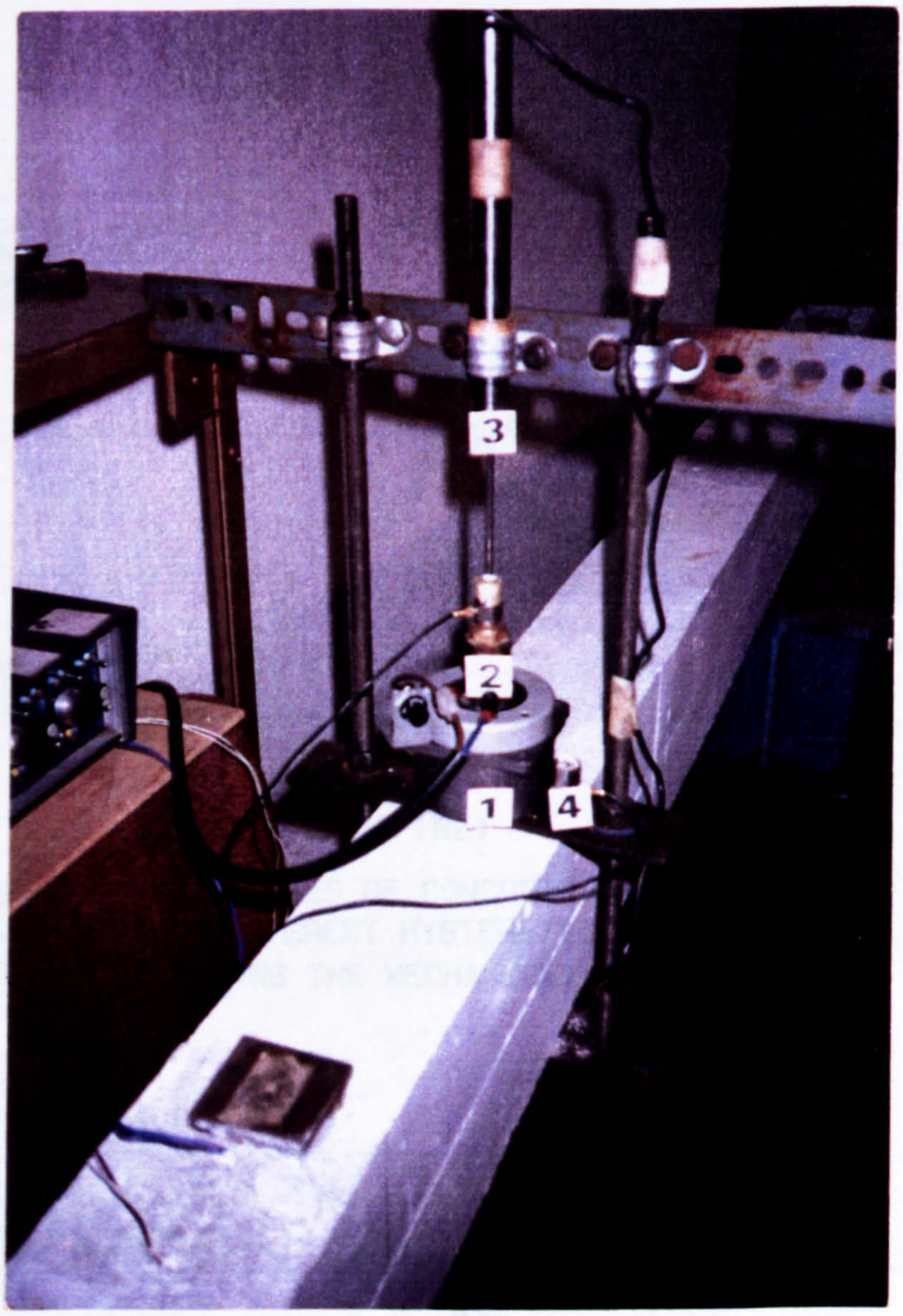

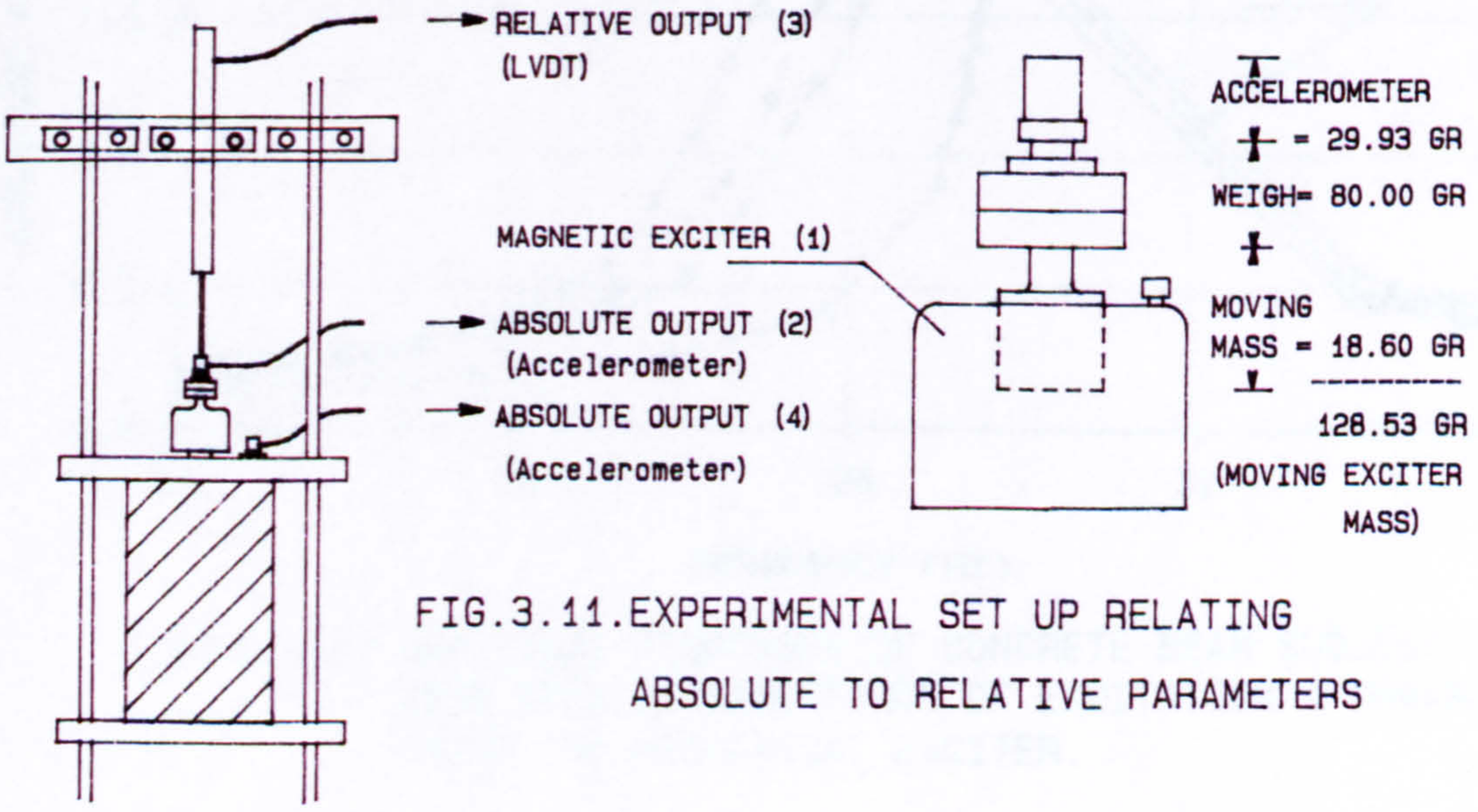

FIG.3.11.EXPERIMENTAL SET UP RELATING
ABSOLUTE TO RELATIVE PARAMETERS

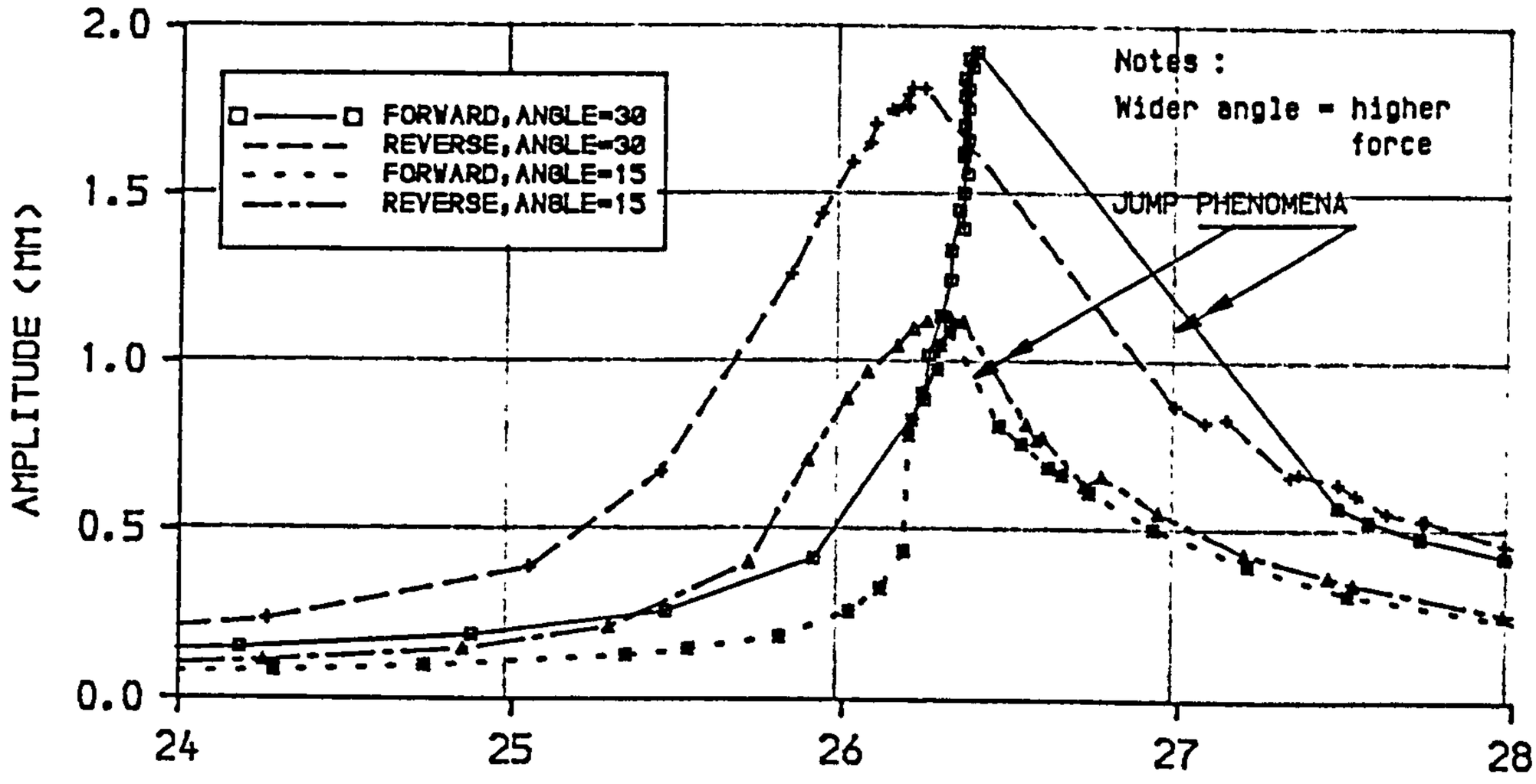

FIG.3.12. AMPLITUDE RESPONSES OF CONCRETE BEAM SUBJECT TO TWO SETS OF DIFFERENT HYSTERETIC FORCE OF EXCITATION USING THE MECHANICAL EXCITER.

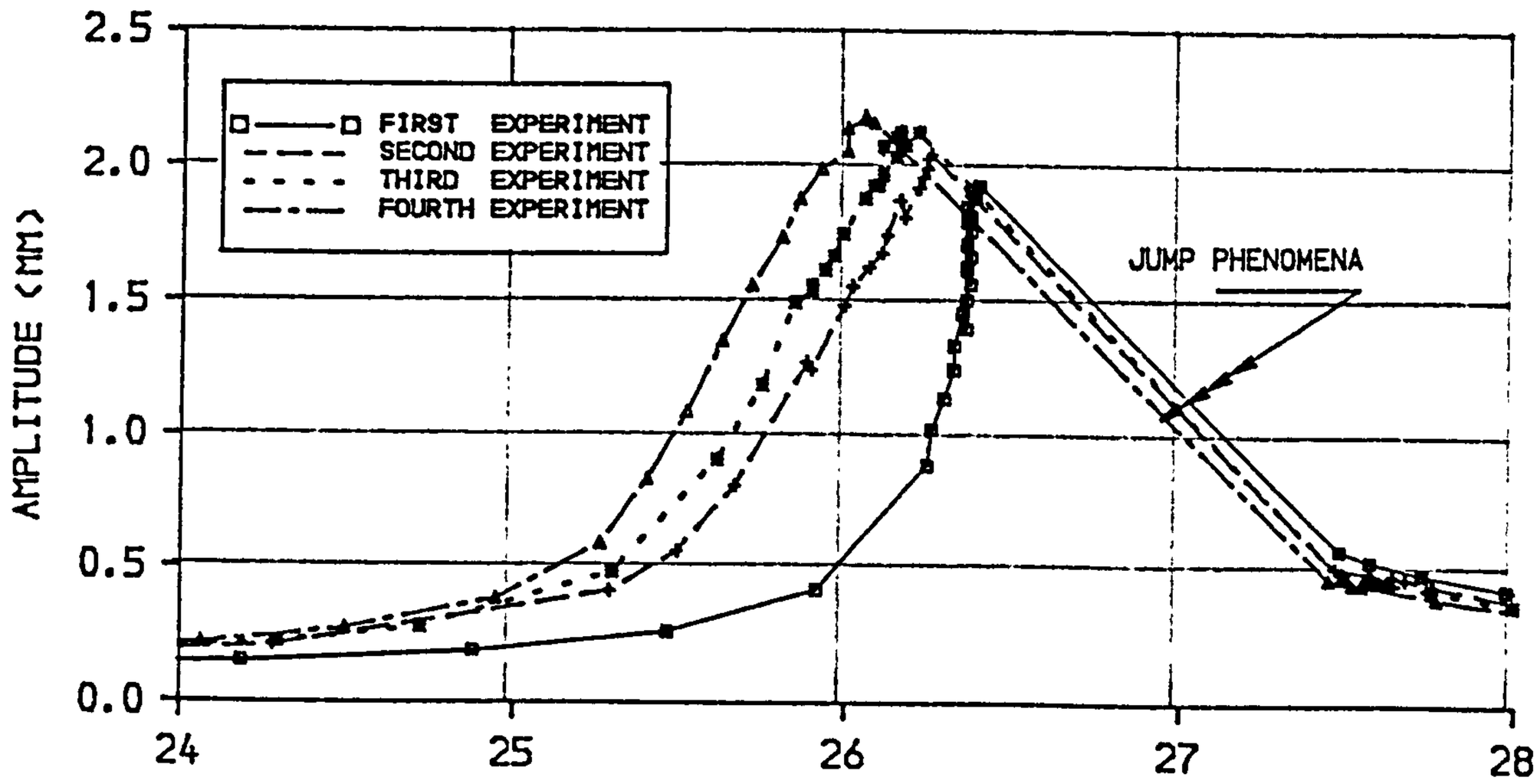

FIG.3.13. AMPLITUDE RESPONSES OF CONCRETE BEAM SUBJECT TO FOUR SETS OF SAME FORCE OF EXCITATION (FORWARD) USING THE MECHANICAL EXCITER.

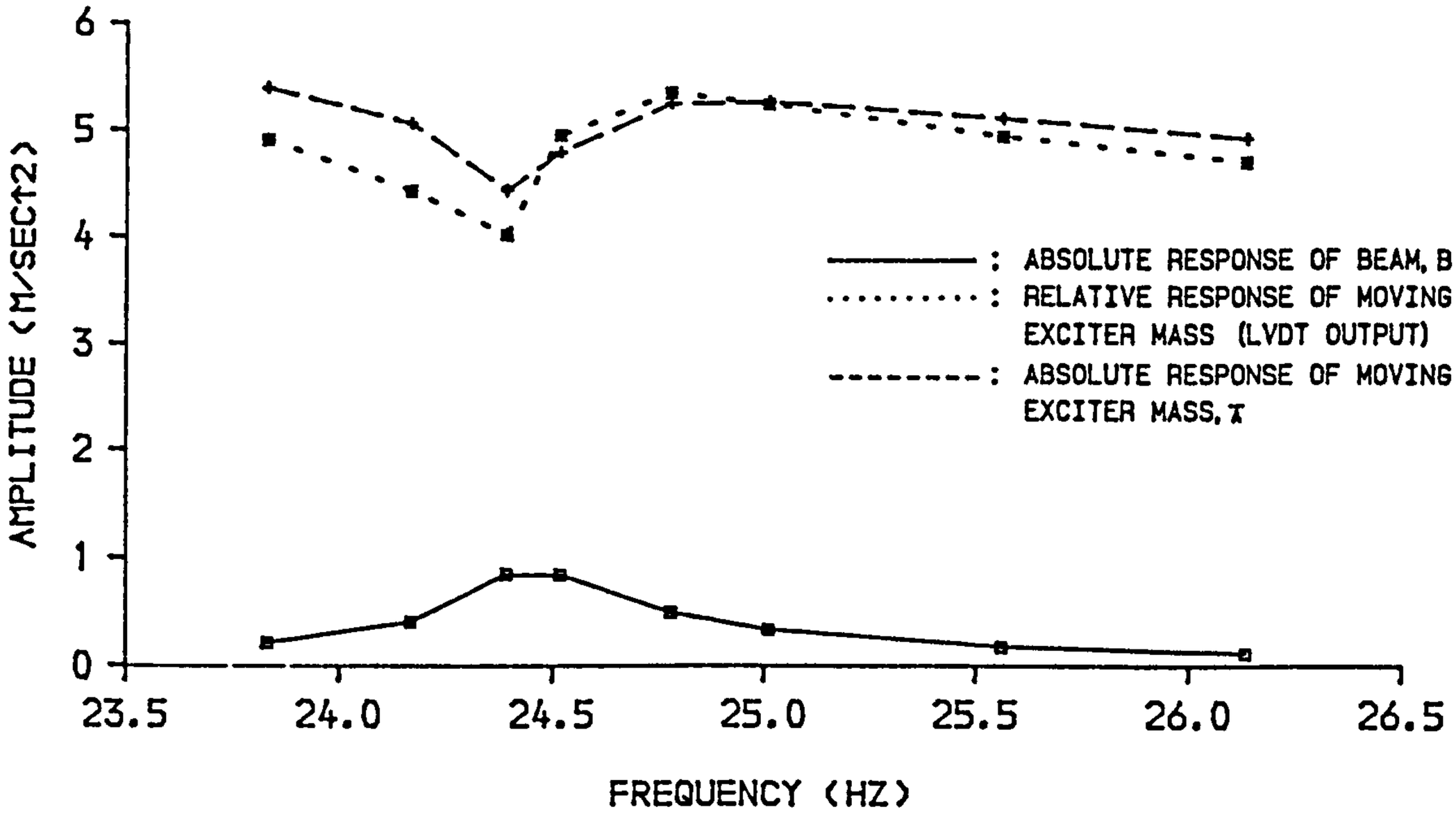

FIG.3.14.RESPONSES OF AMPLITUDE OF MOVING EXCITER MASS, LVDT AND BEAM-1 (FB/L1), SUBJECT TO A SET OF FORCES OF EXCITATION USING THE MAGNETIC EXCITER, FULLY BONDED, FIRST MODE.

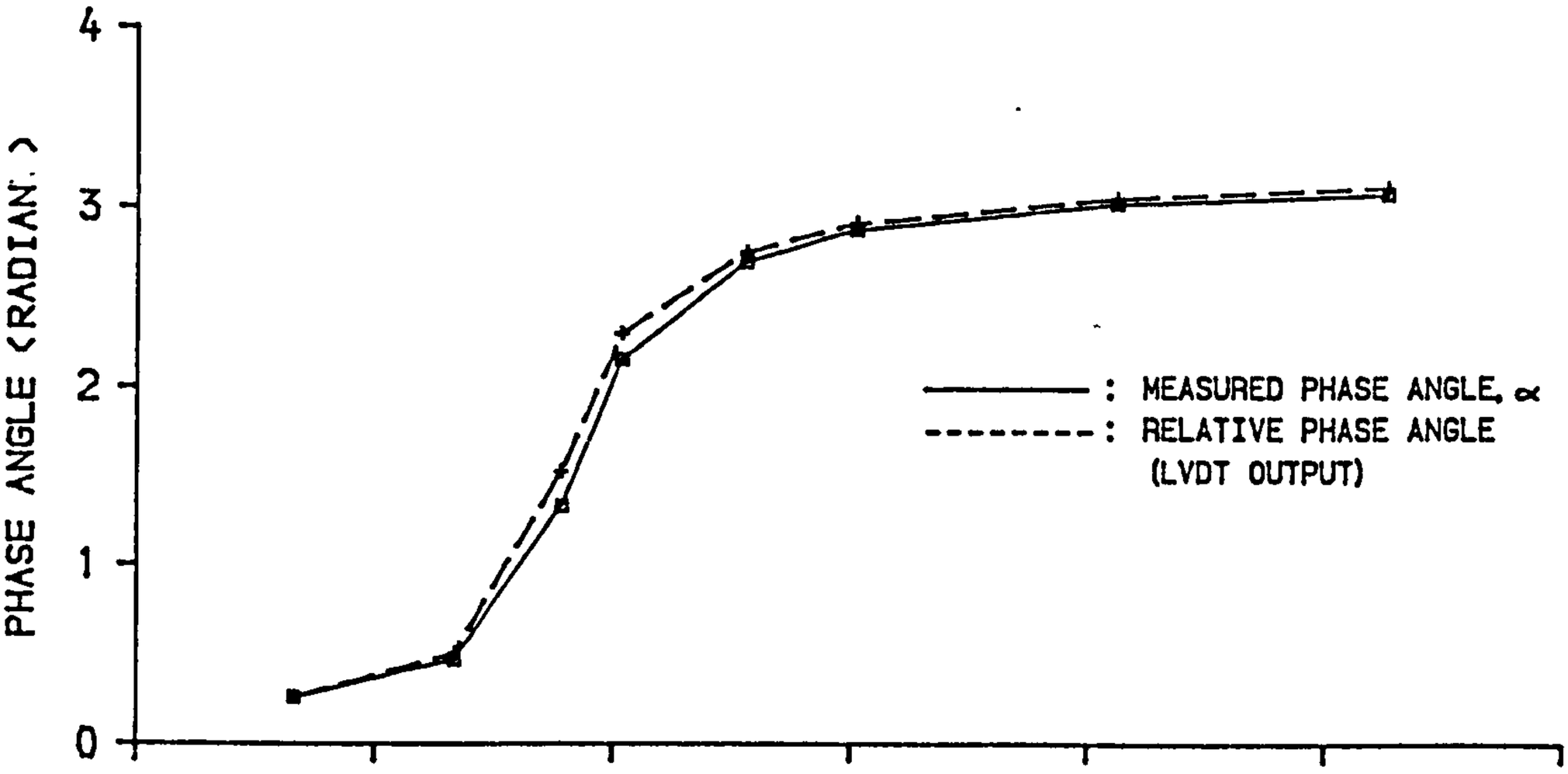

FIG.3.15.RESPONSES OF PHASE ANGLE BETWEEN MOVING EXCITER MASS AND BEAM-1 (FB/L1) (REFER TO FIG.3.14)

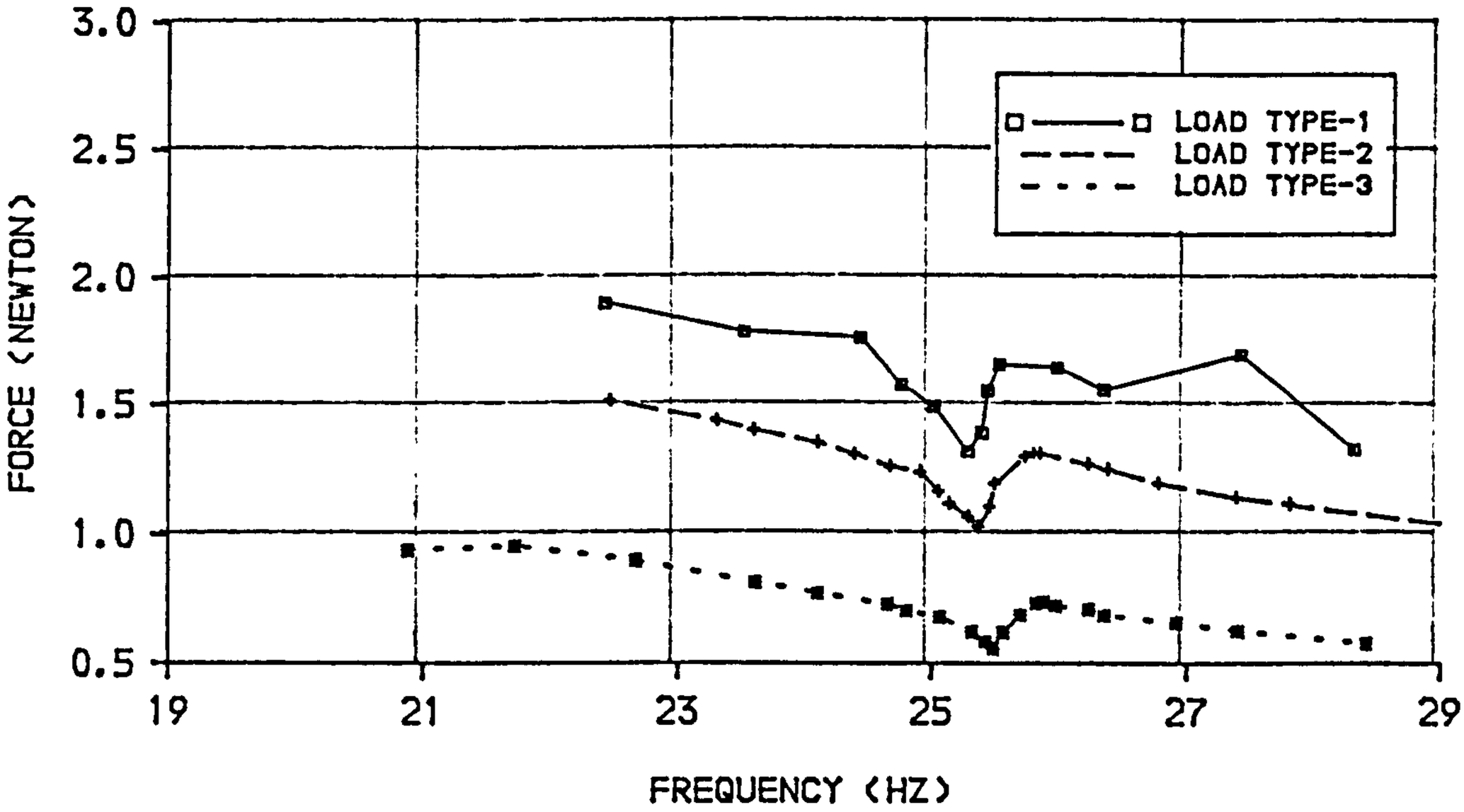

FIG.3.16.RESPONSES OF THREE SETS OF FORCE OF EXCITATION ON BEAM-2 (PB/L1), PARTIALLY BONDED, FIRST MODE, BEFORE APPLYING FIRST LOADING STAGE.

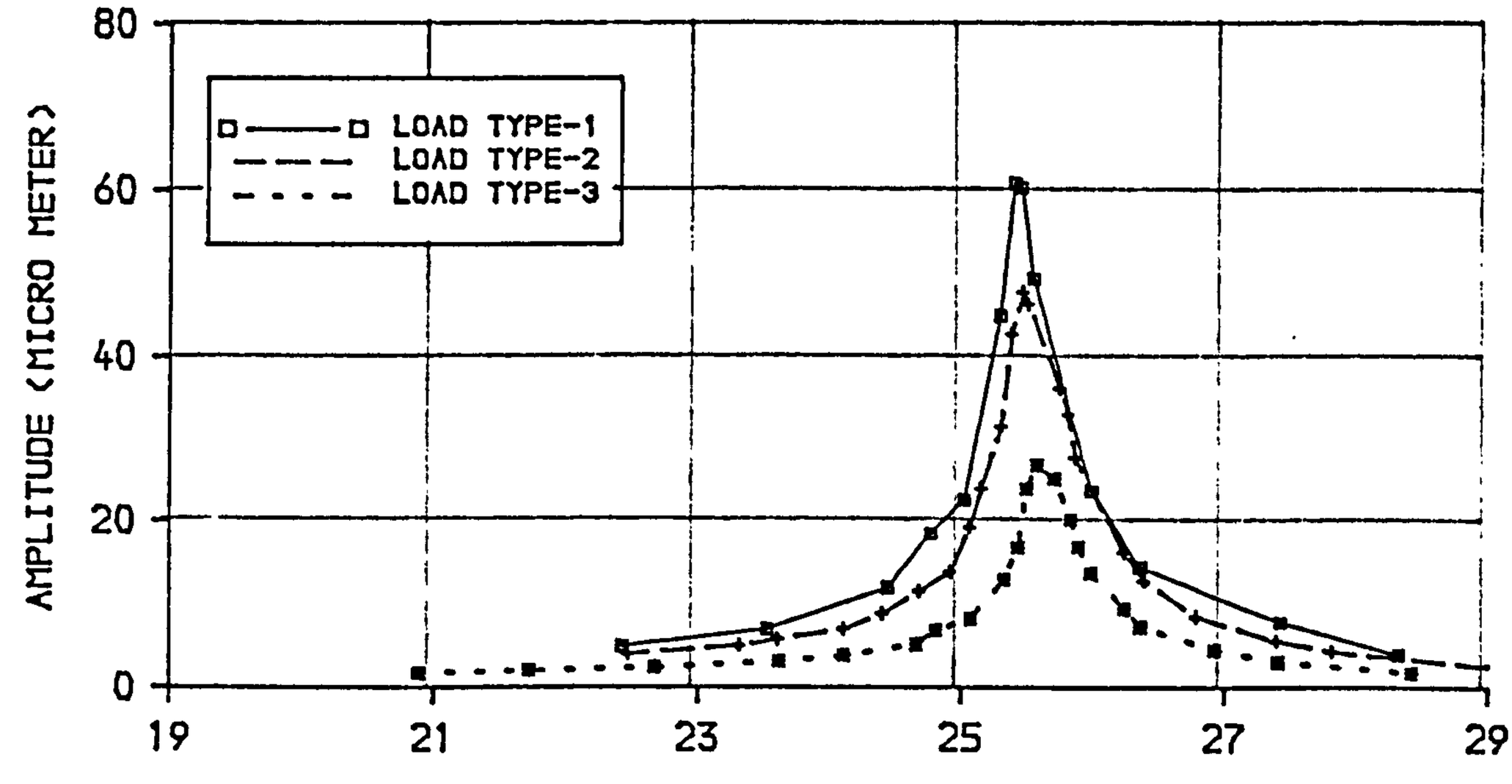

FIG.3.17.RESPONSES OF BEAM-2 (PB/L1), PARTIALLY BONDED, FIRST MODE, BEFORE APPLYING FIRST LOADING STAGE (REFER TO FIG.3.16)

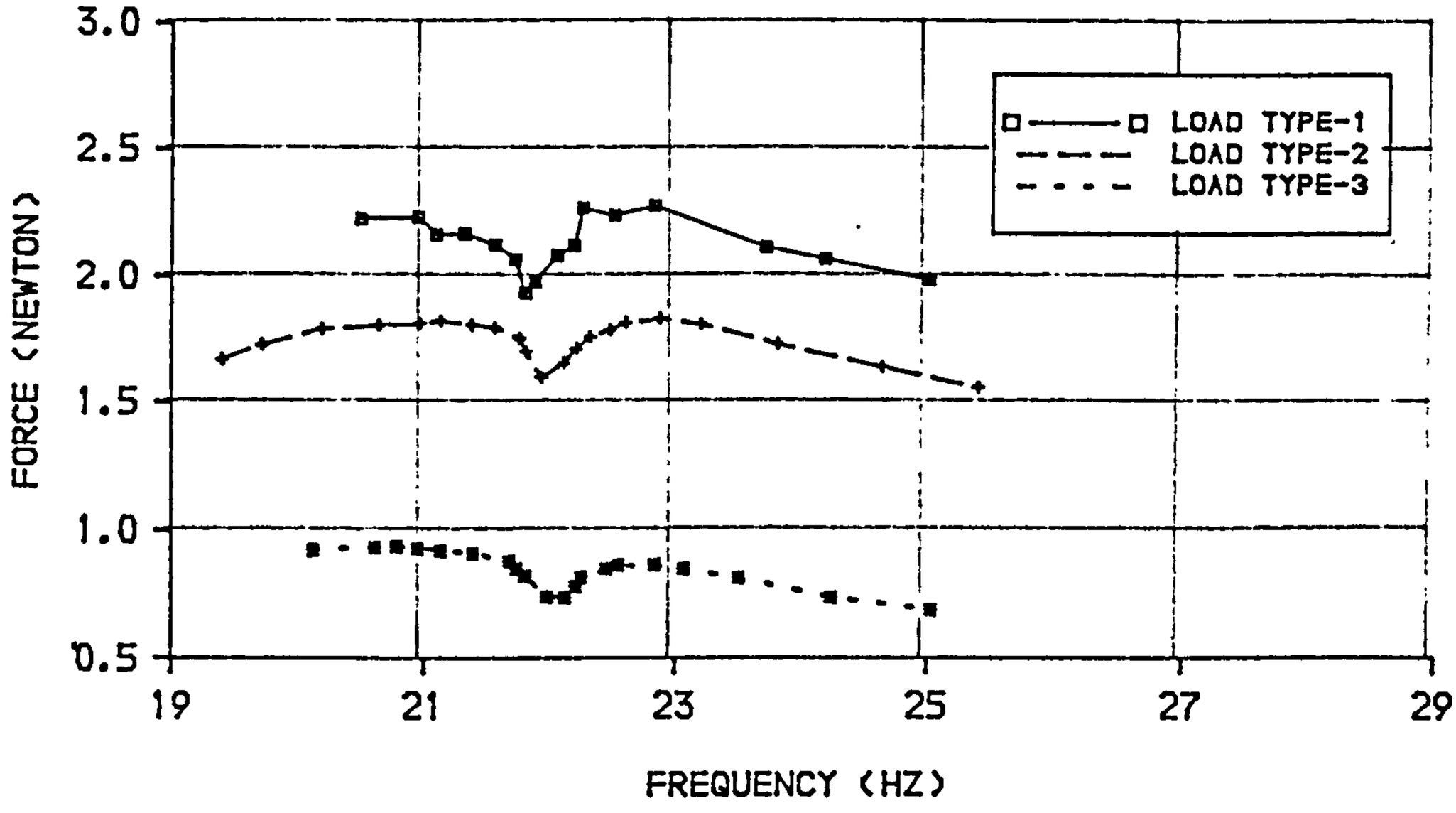

FIG.3.18.RESPONSES OF THREE SETS OF FORCE OF EXCITATION ON BEAM-2 (PB/L1), PARTIALLY BONDED, FIRST MODE, AFTER APPLYING THIRD LOADING STAGE.

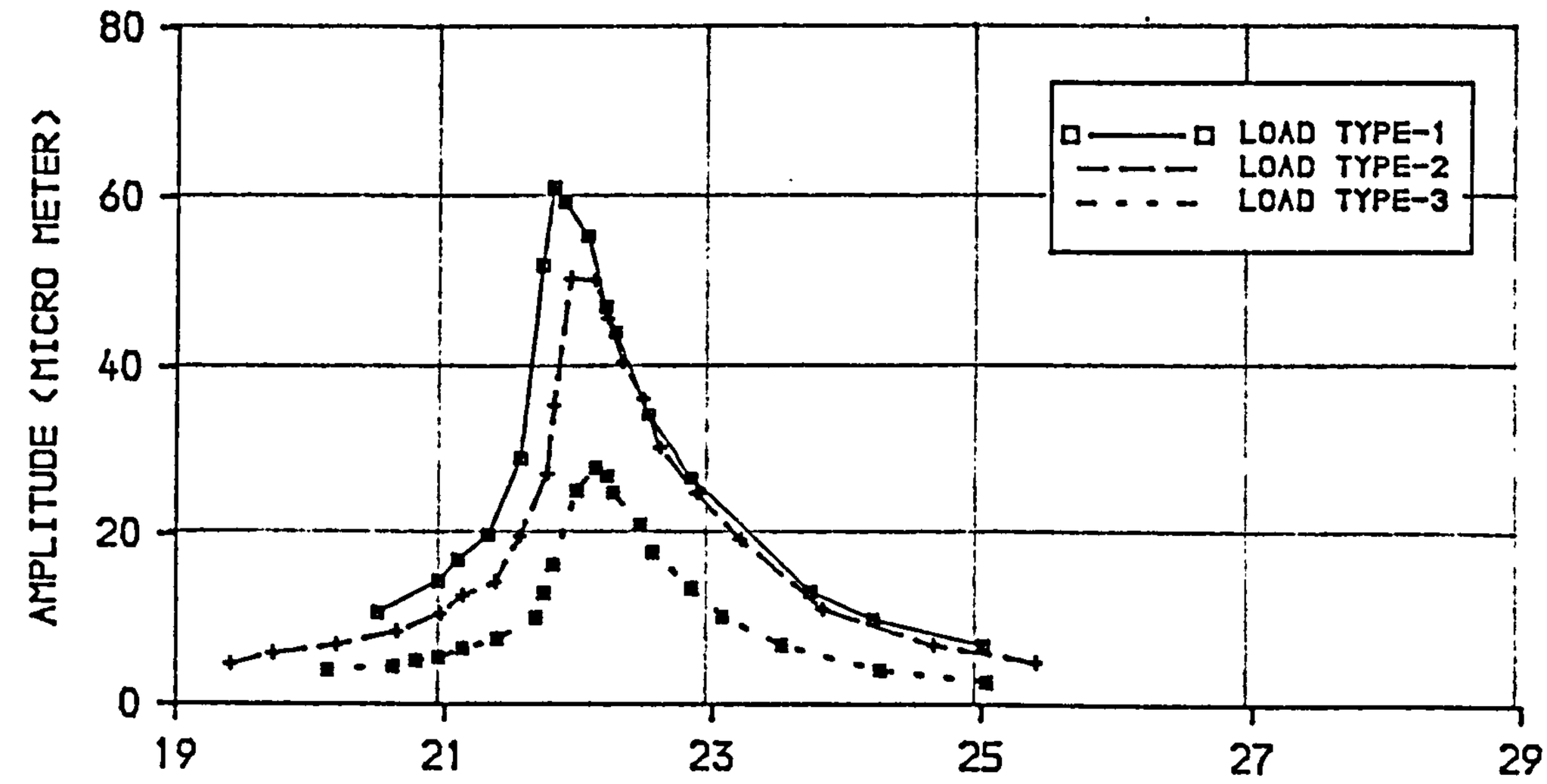

FIG.3.19.RESPONSES OF BEAM-2 (PB/L1), PARTIALLY BONDED, FIRST MODE, AFTER APPLYING THIRD LOADING STAGE (REFER TO FIG.3.18)

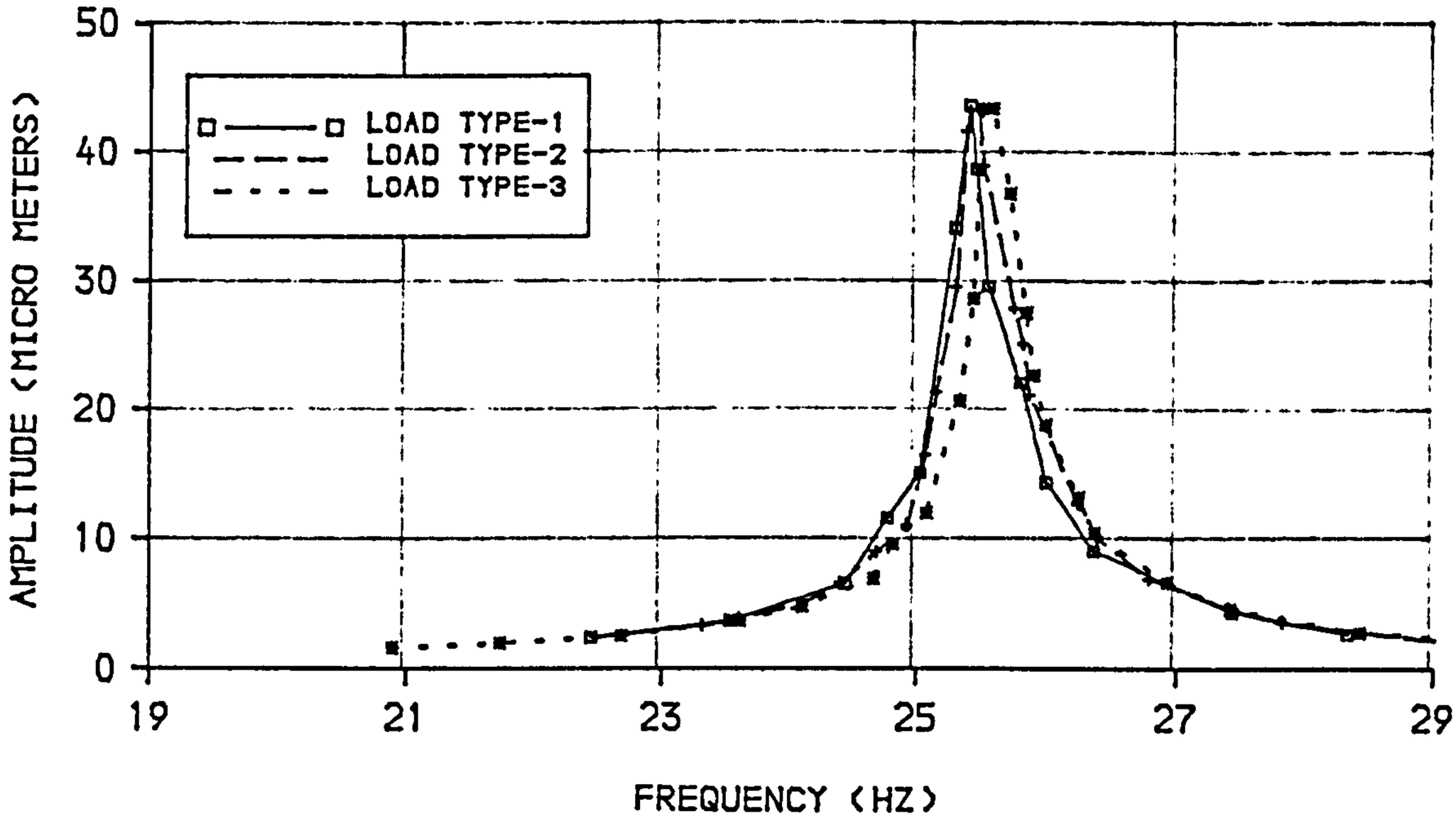

FIG.3.20.NORMALISED RESPONSES OF BEAM-2 (PB/L1), PARTIALLY BONDED, FIRST MODE (REFER TO FIG.3.16 AND 3.17)

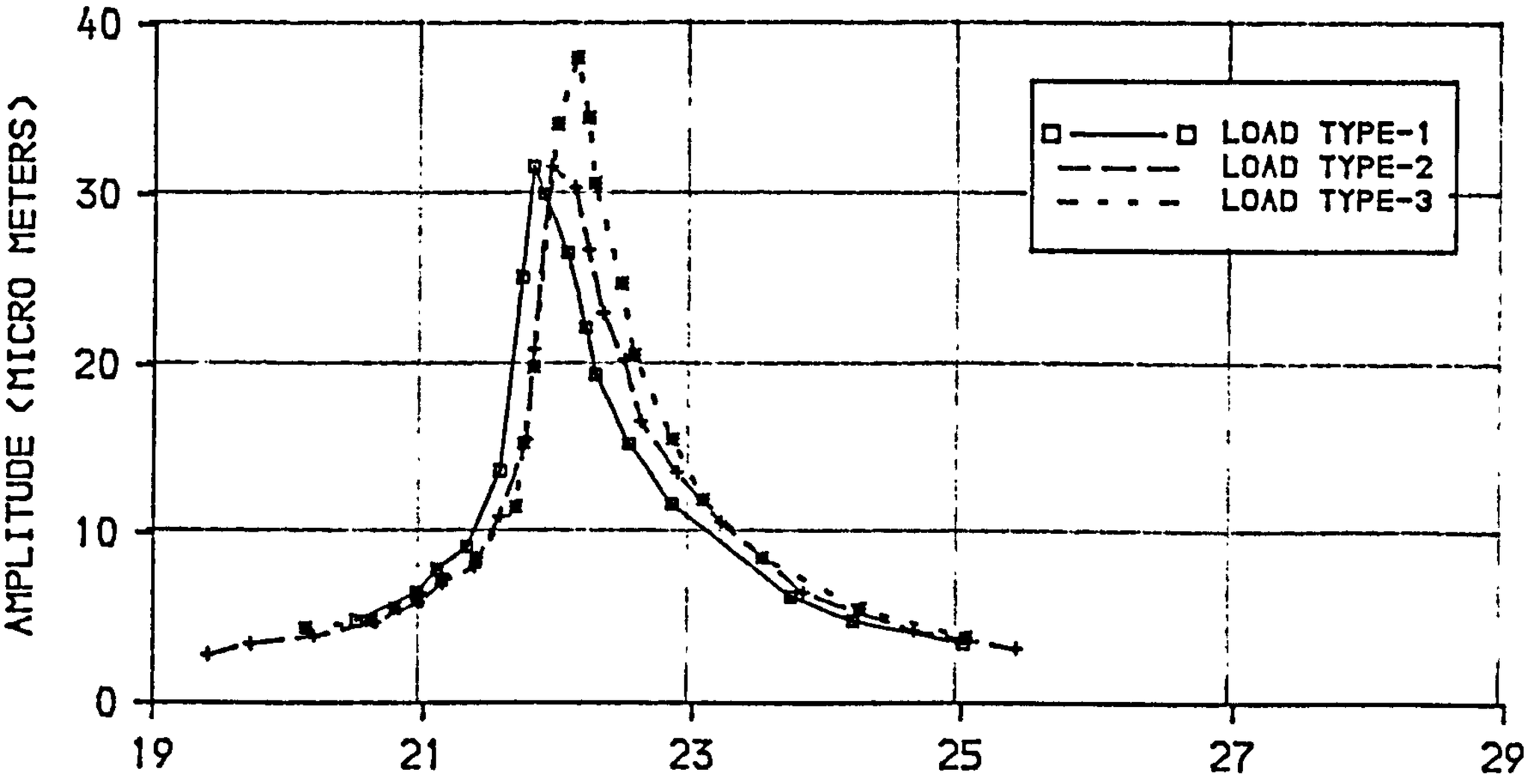

FIG.3.21.NORMALISED RESPONSES OF BEAM-2 (PB/L1), PARTIALLY BONDED, FIRST MODE (REFER TO FIG.3.18 AND 3.19)

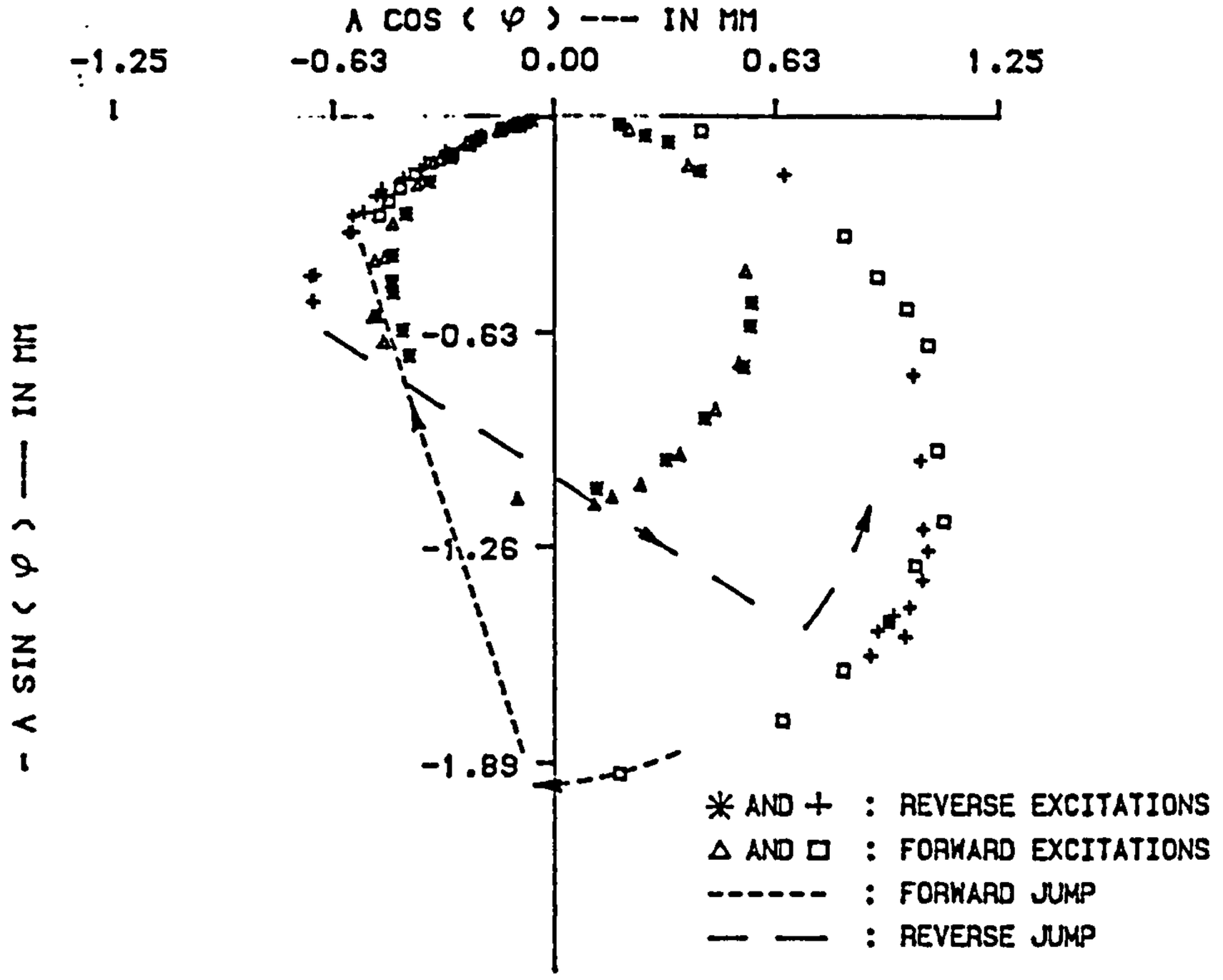

FIG.3.22.POLAR DIAGRAMS OF BEAM SUBJECT TO TWO SETS OF DIFFERENT HYSTERETIC FORCE OF EXCITATION (REFER TO FIG.3.12)

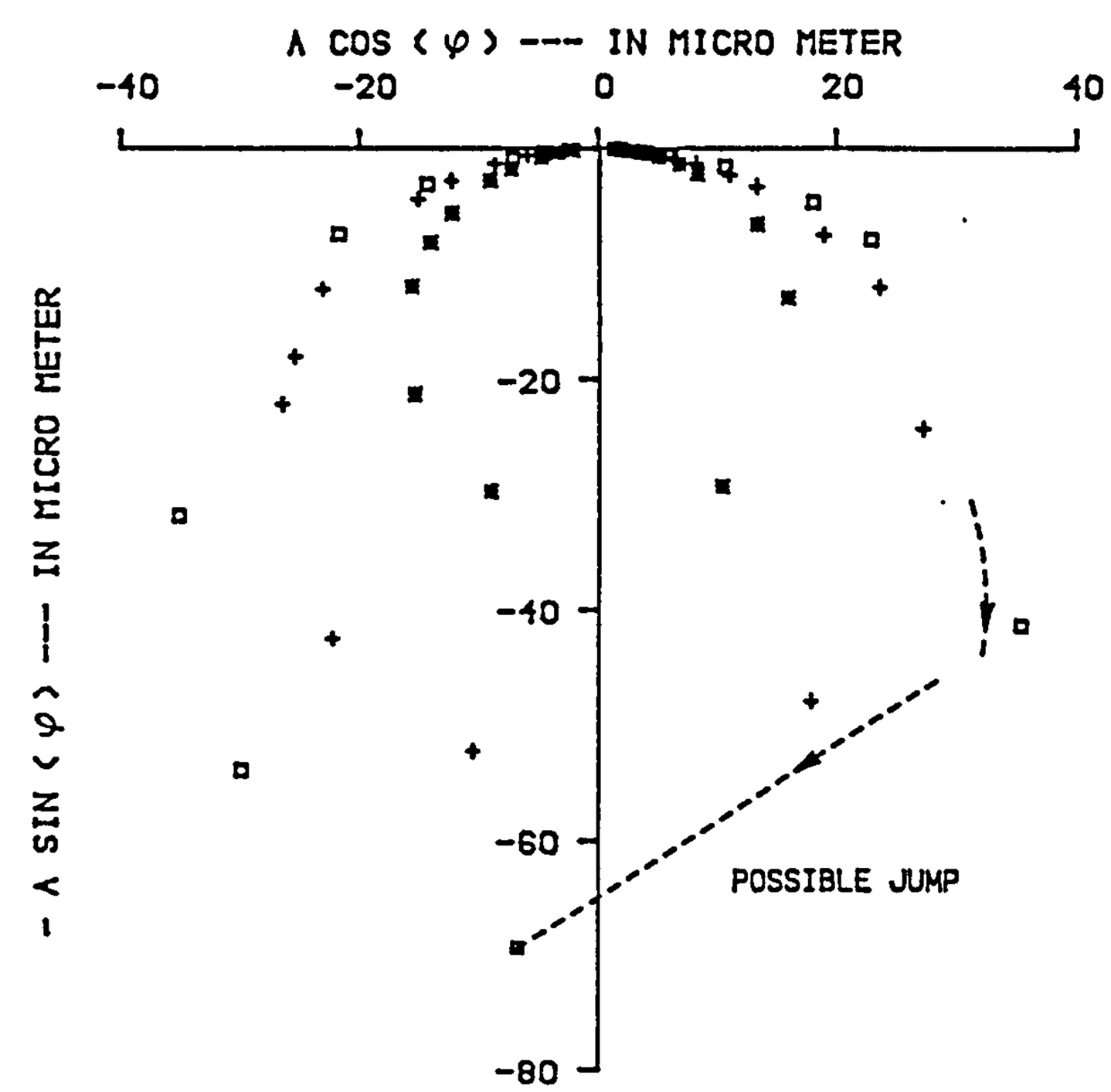

FIG.3.23.POLAR DIAGRAMS OF BEAM-2 (PB/L1), PARTIALLY BONDED, SUBJECT TO THREE DIFFERENT SETS OF EXCITATION (REFER TO FIG.3.20)

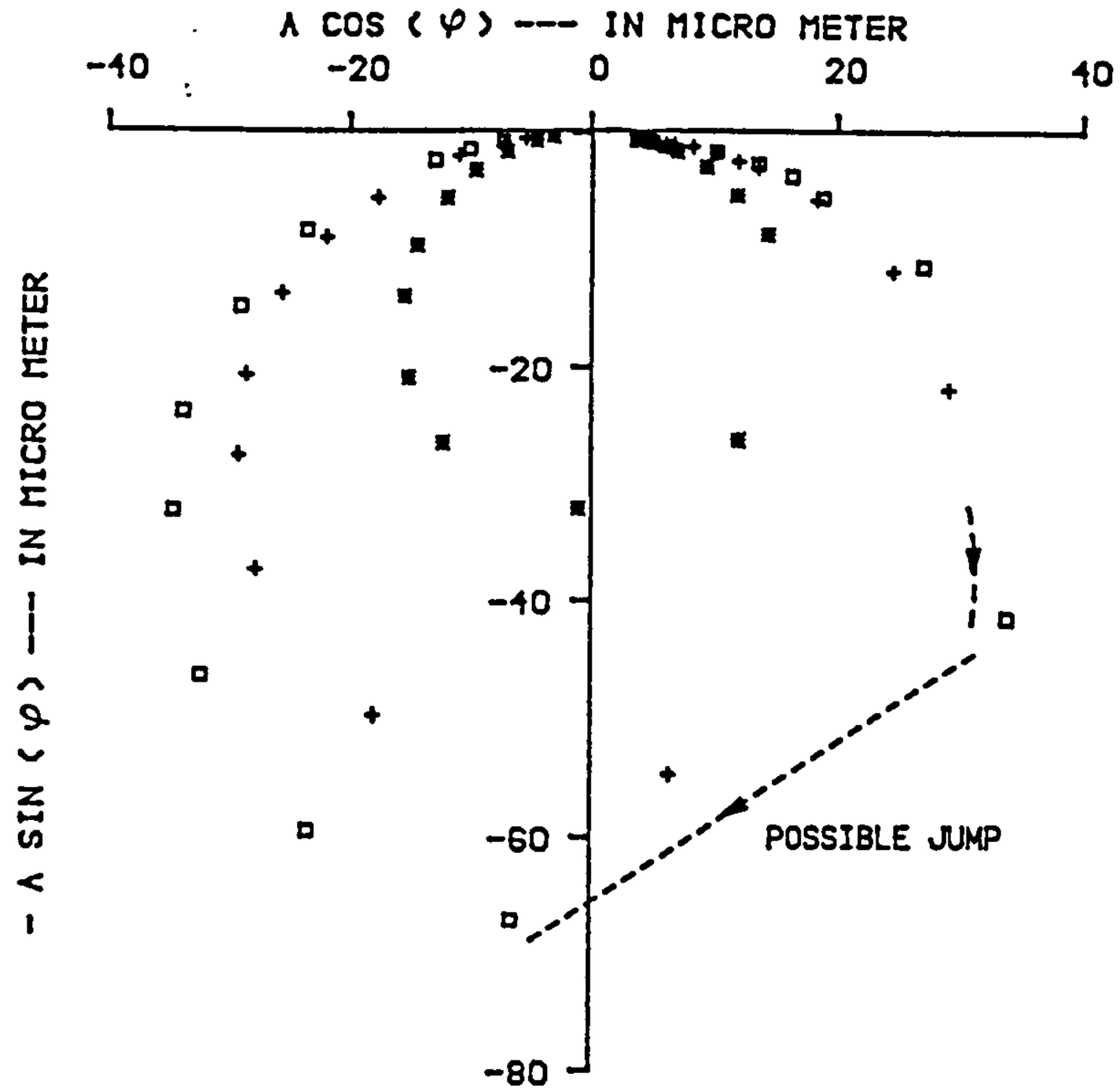

FIG.3.24.POLAR DIAGRAMS OF BEAM-2 (PB/L1) SUBJECT TO THREE DIFFERENT SETS OF FORCE OF EXCITATION (REFER TO FIG.3.21)

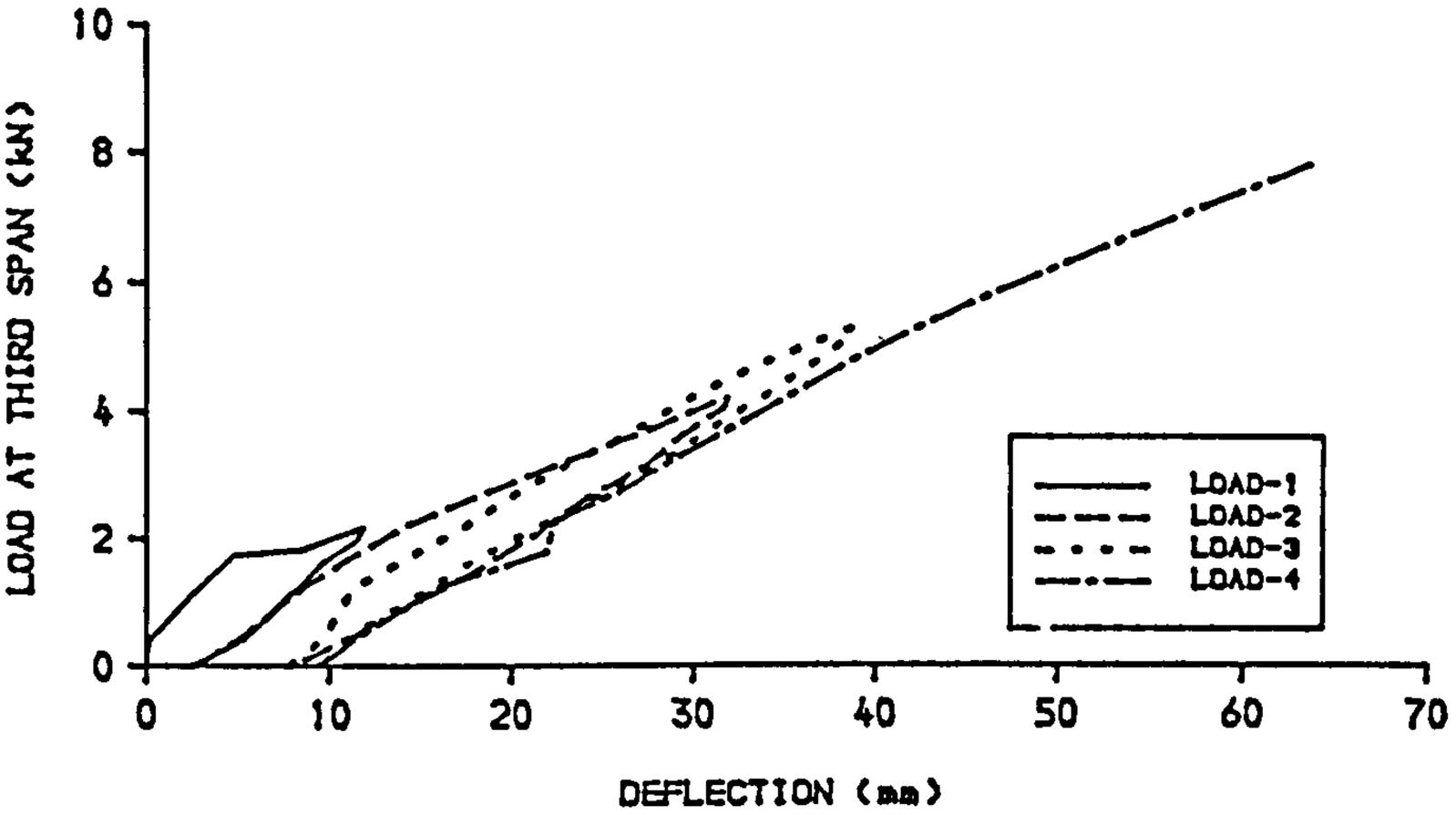

A) .LOAD-DEFLECTION CHARACTERISTICS AT MID SPAN

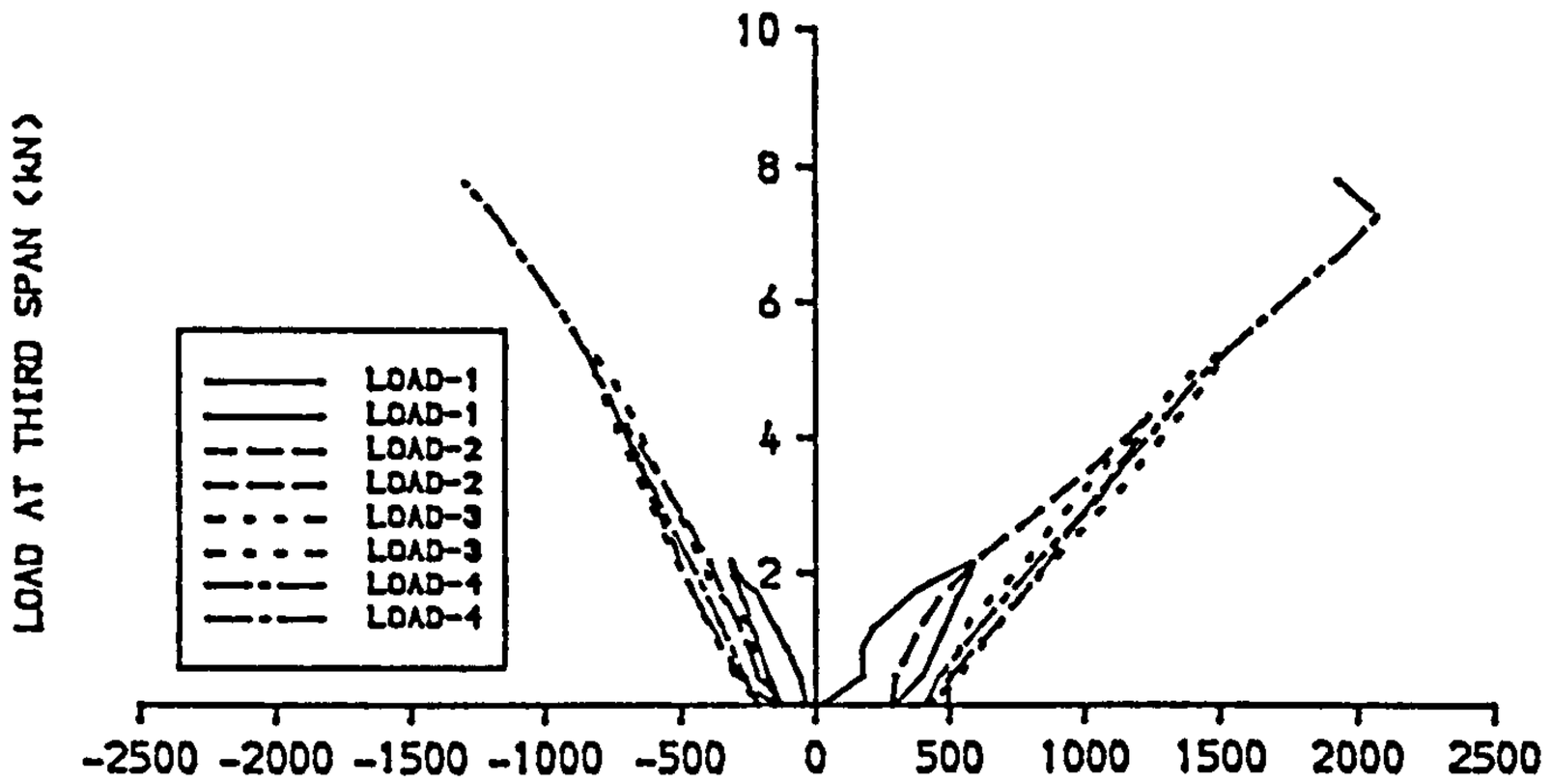

B) .LOAD-STRAIN CHARACTERISTICS AT MID SPAN

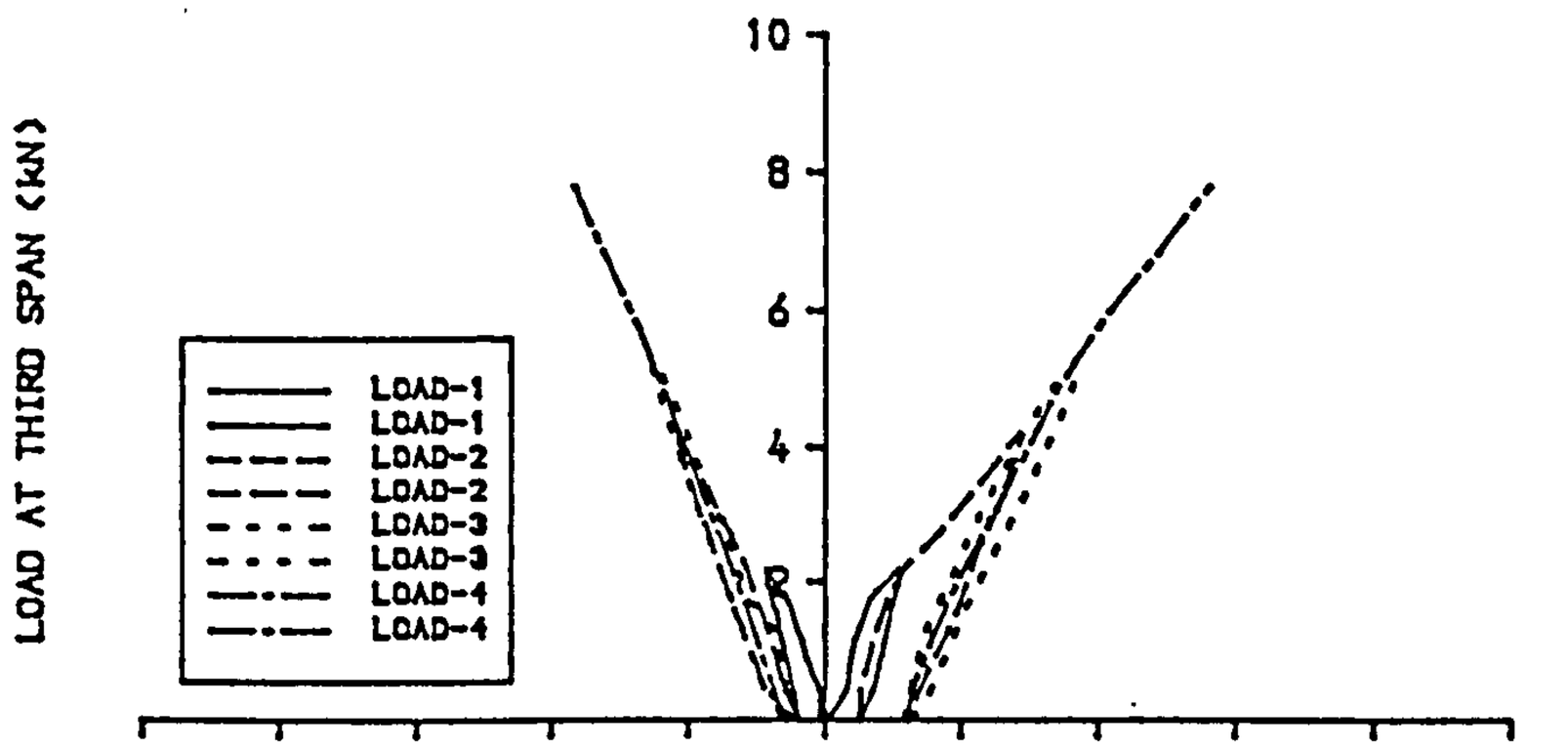

C) .LOAD-STRAIN CHARACTERISTICS AT QUARTER SPAN

FIG.3.25.LOAD-DEFLECTION AND LOAD-STRAIN CHARACTERISTICS OF BEAM-1 (FB/L1), FULLY BONDED, FLEXURAL CRACK PATTERN.

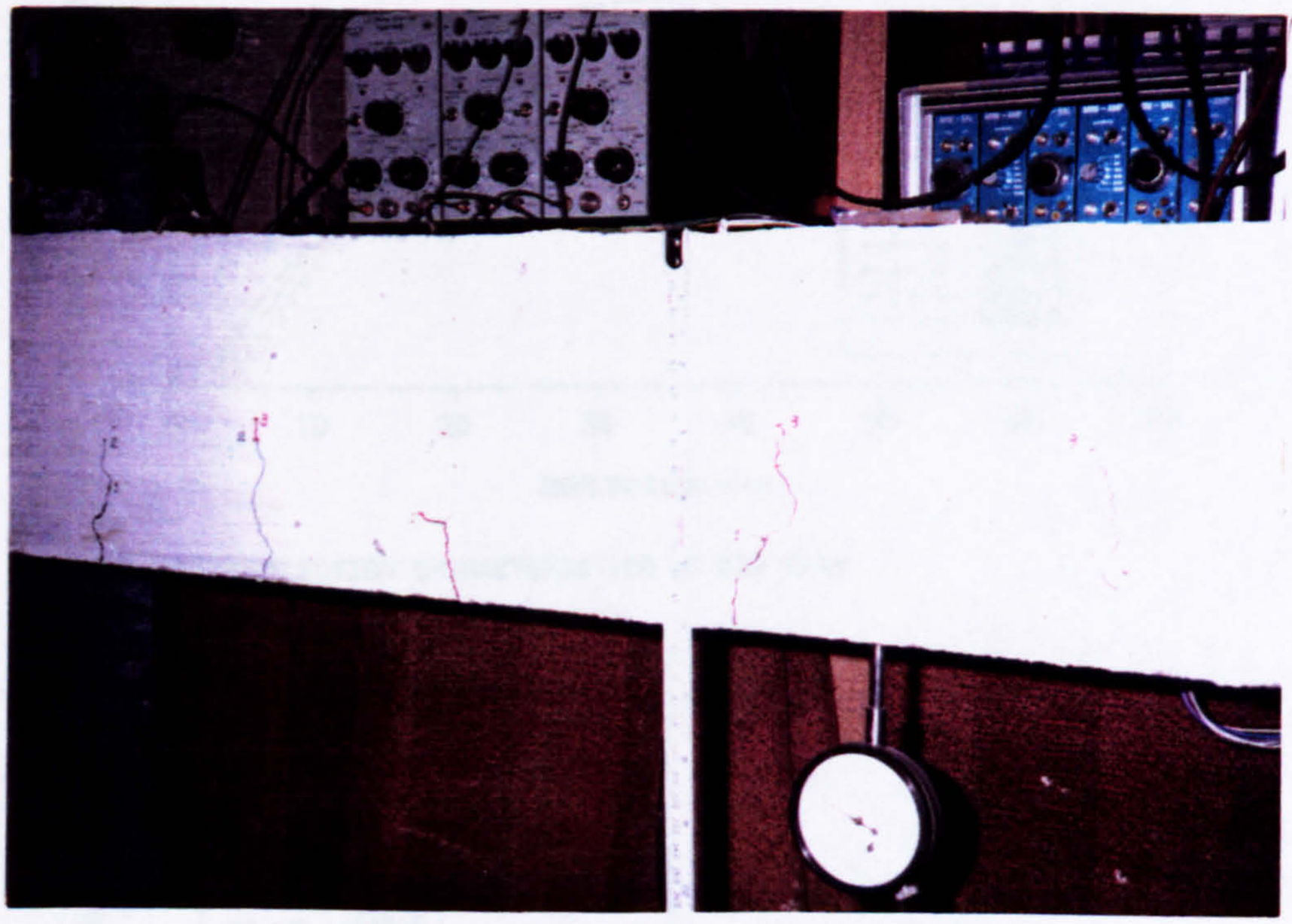

A. BEAM BEFORE FAILURE.

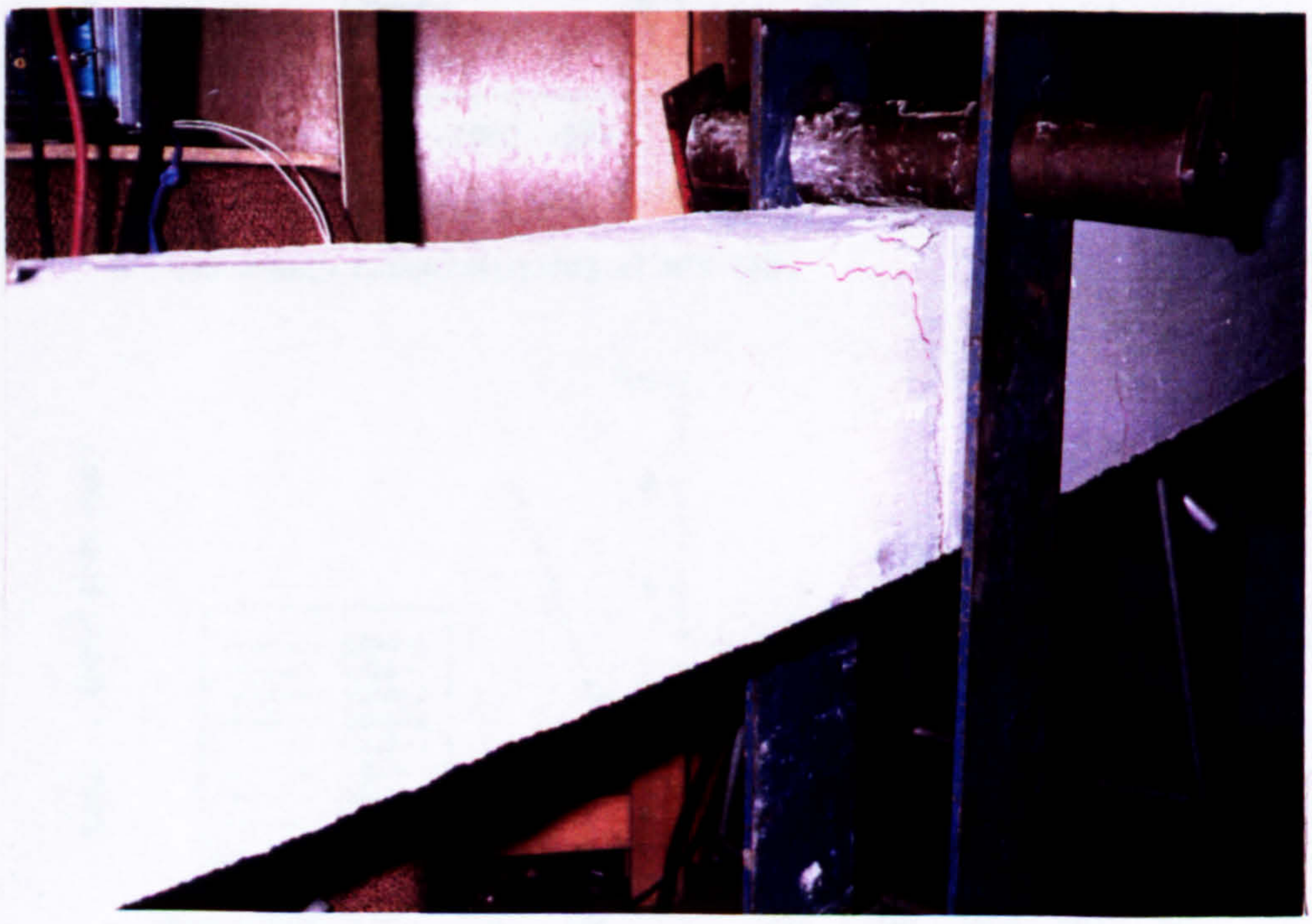

B. BEAM AT FAILURE.

FIG.3.26.FLEXURAL CRACK PATTERNS BEFORE AND AT FAILURE OF BEAM-1 (FB/L1), FULLY BONDED.

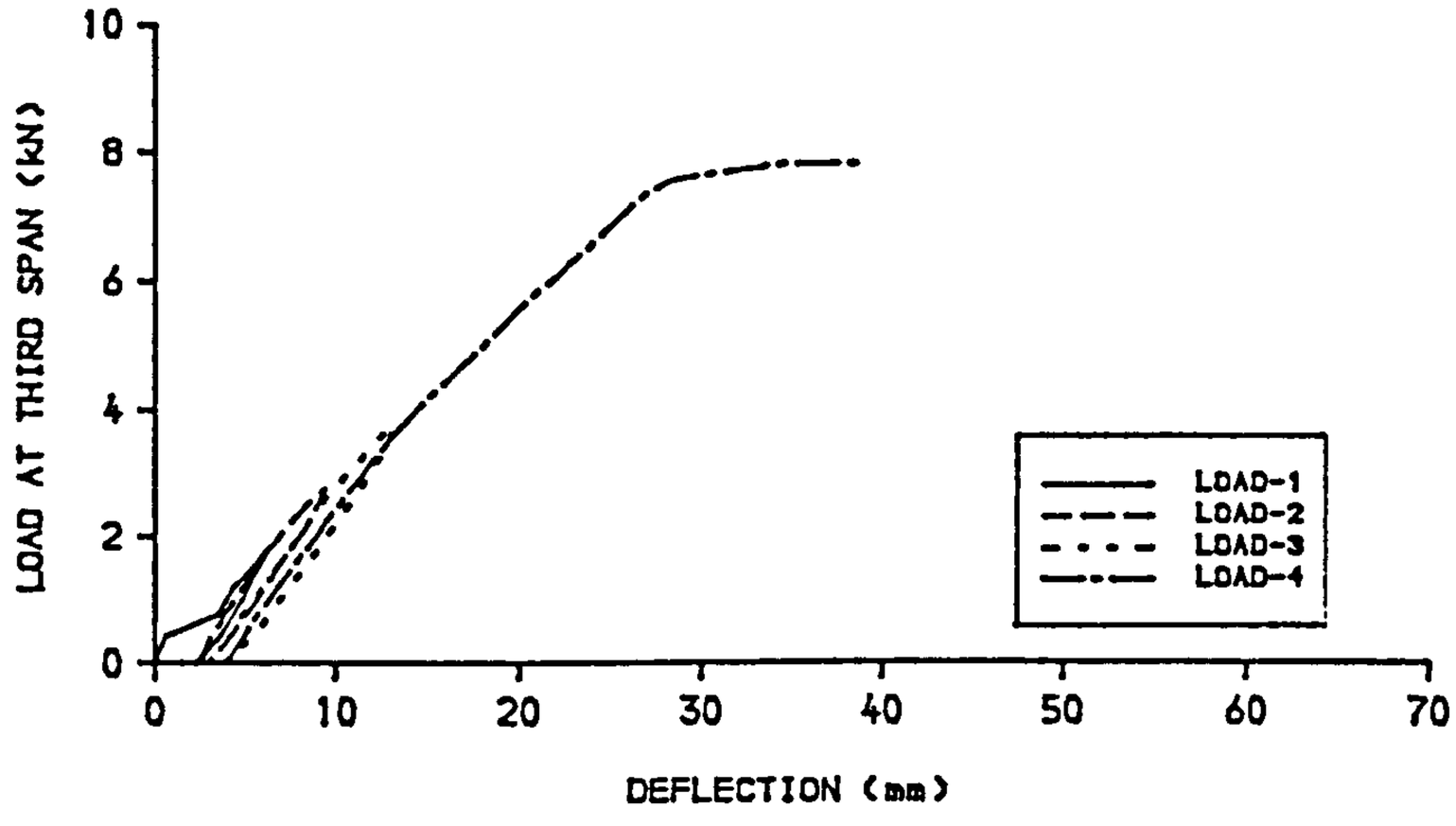

A) .LOAD-DEFLECTION CHARACTERISTICS AT MID SPAN

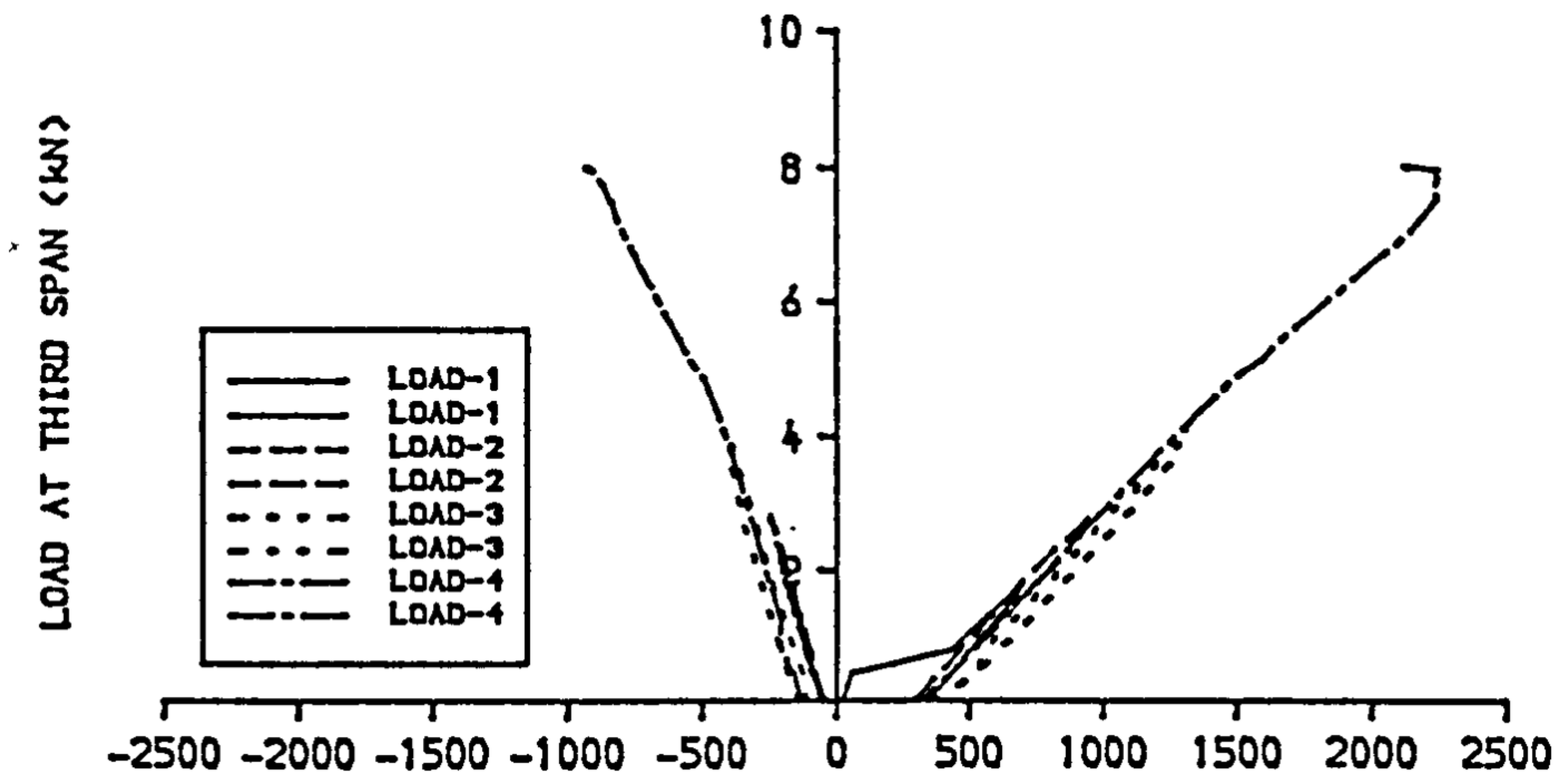

B) .LOAD-STRAIN CHARACTERISTICS AT MID SPAN

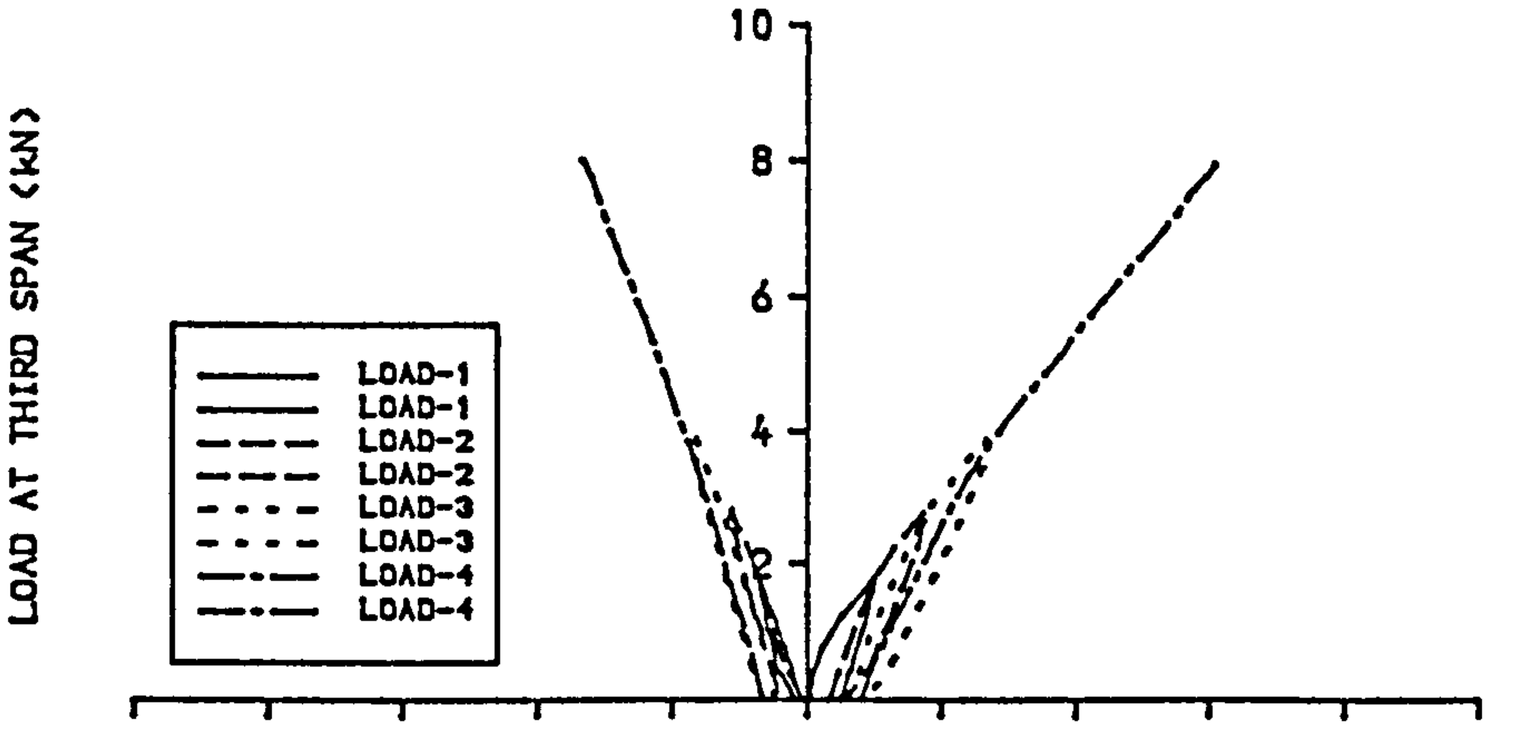

C) .LOAD-STRAIN CHARACTERISTICS AT QUARTER SPAN

FIG.3.27. LOAD-DEFLECTION AND LOAD-STRAIN CHARACTERISTICS OF BEAM-2 (PB/L1), PARTIALLY BONDED, FLEXURAL CRACK PATTERN.

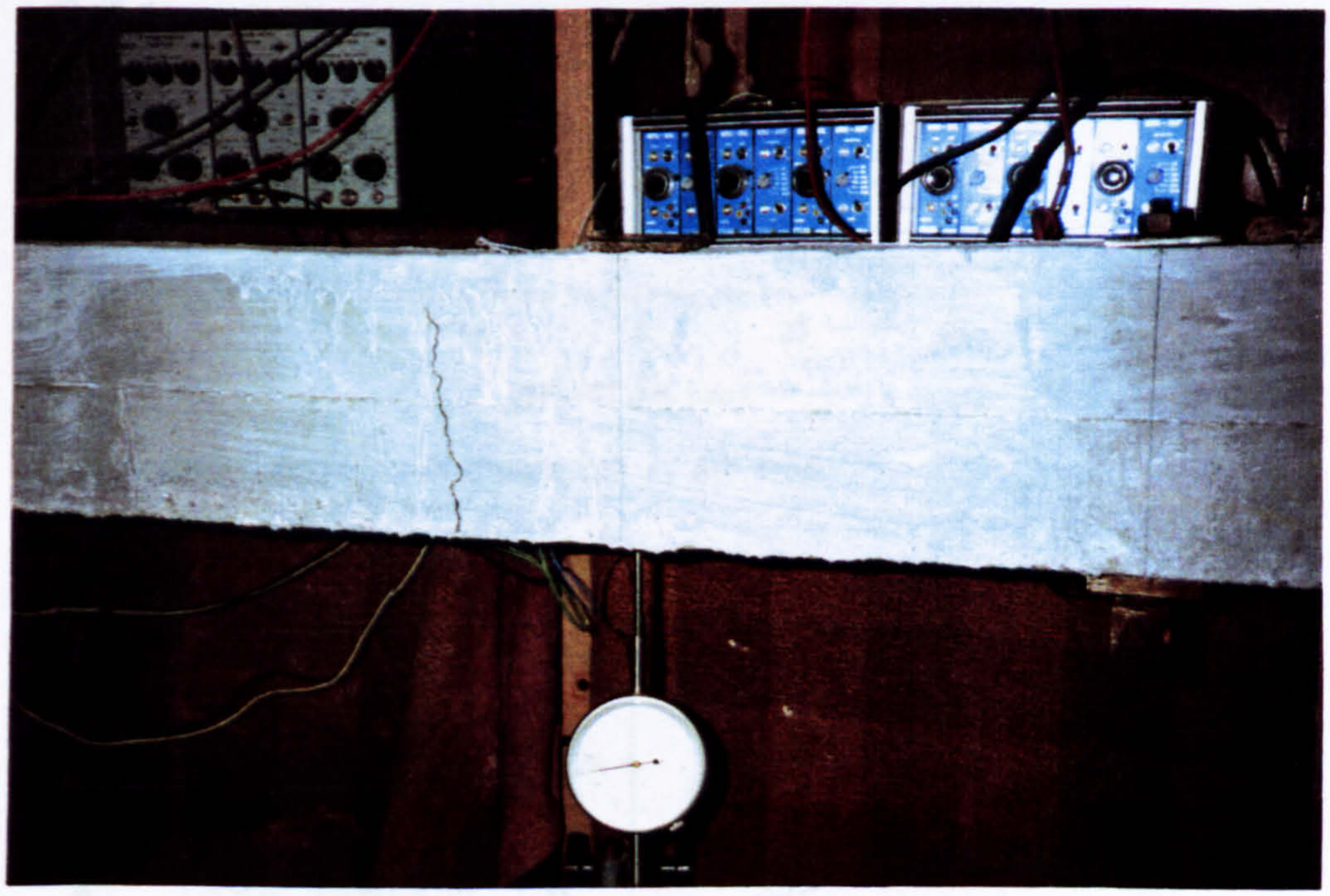

A. BEAM BEFORE FAILURE.

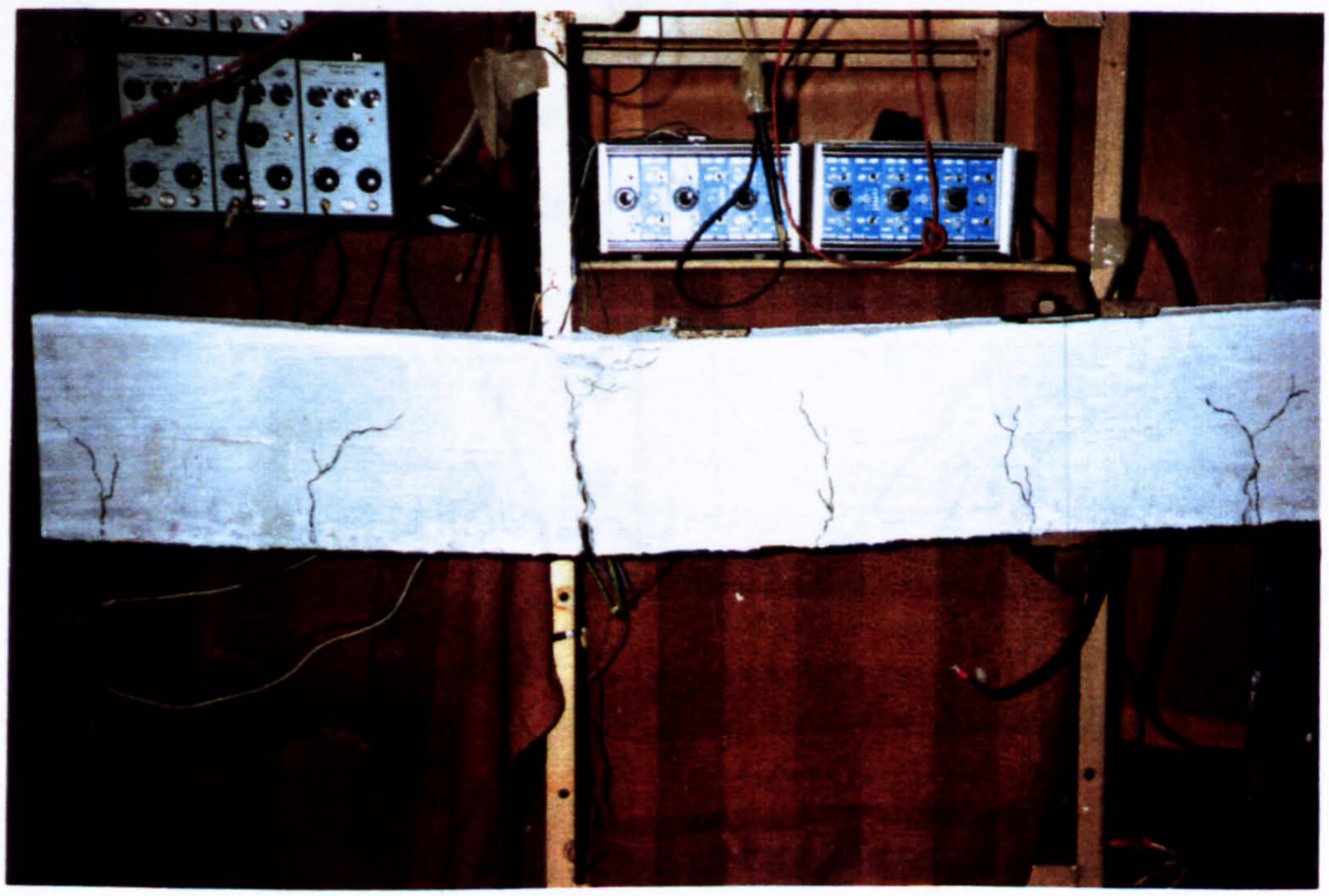

B. BEAM AT FAILURE

FIG.3.28.FLEXURAL CRACK PATTERNS BEFORE AND AT FAILURE
OF BEAM-2 (PB/L1), PARTIALLY BONDED

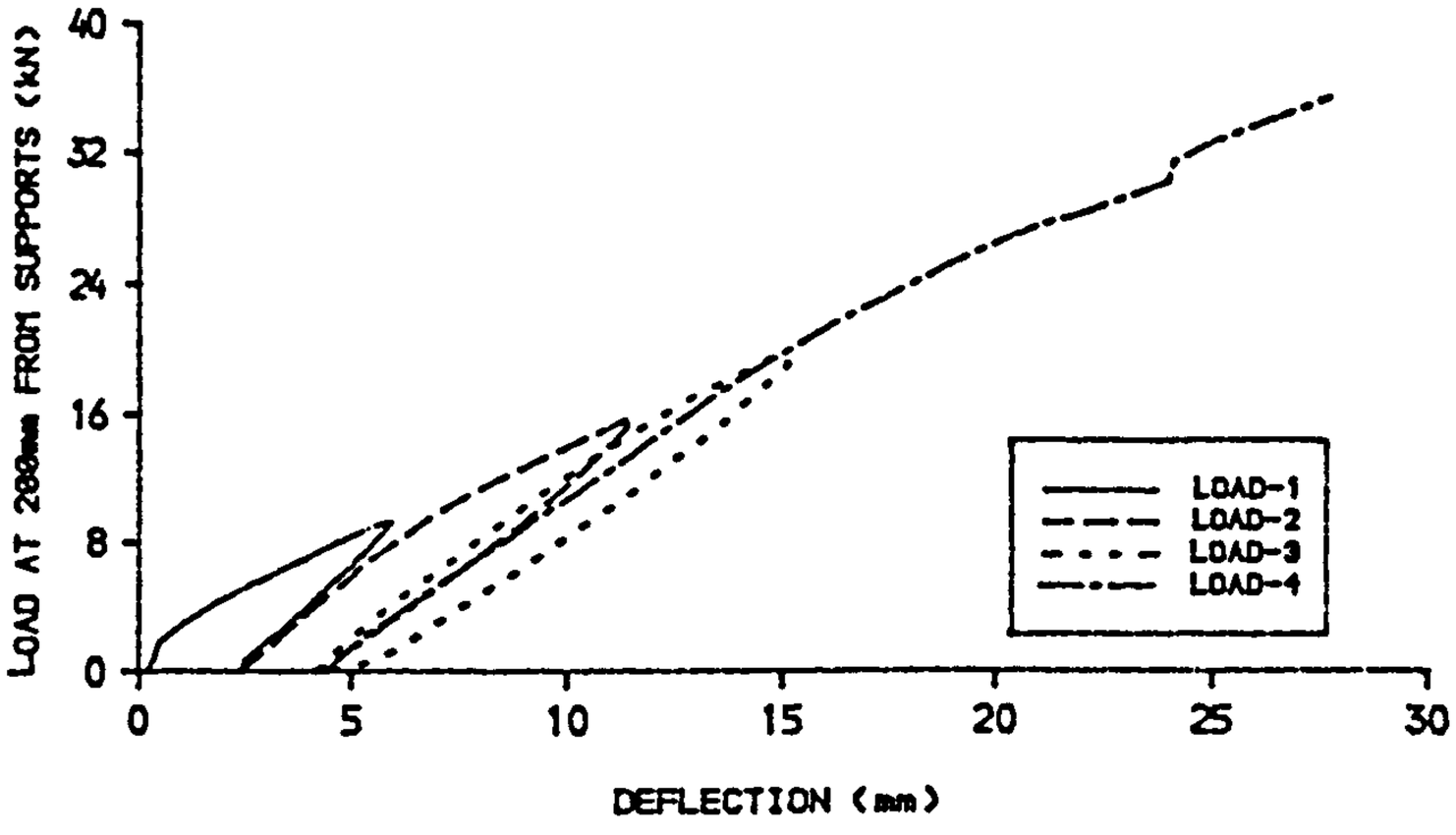

A) .LOAD-DEFLECTION CHARACTERISTICS AT MID SPAN

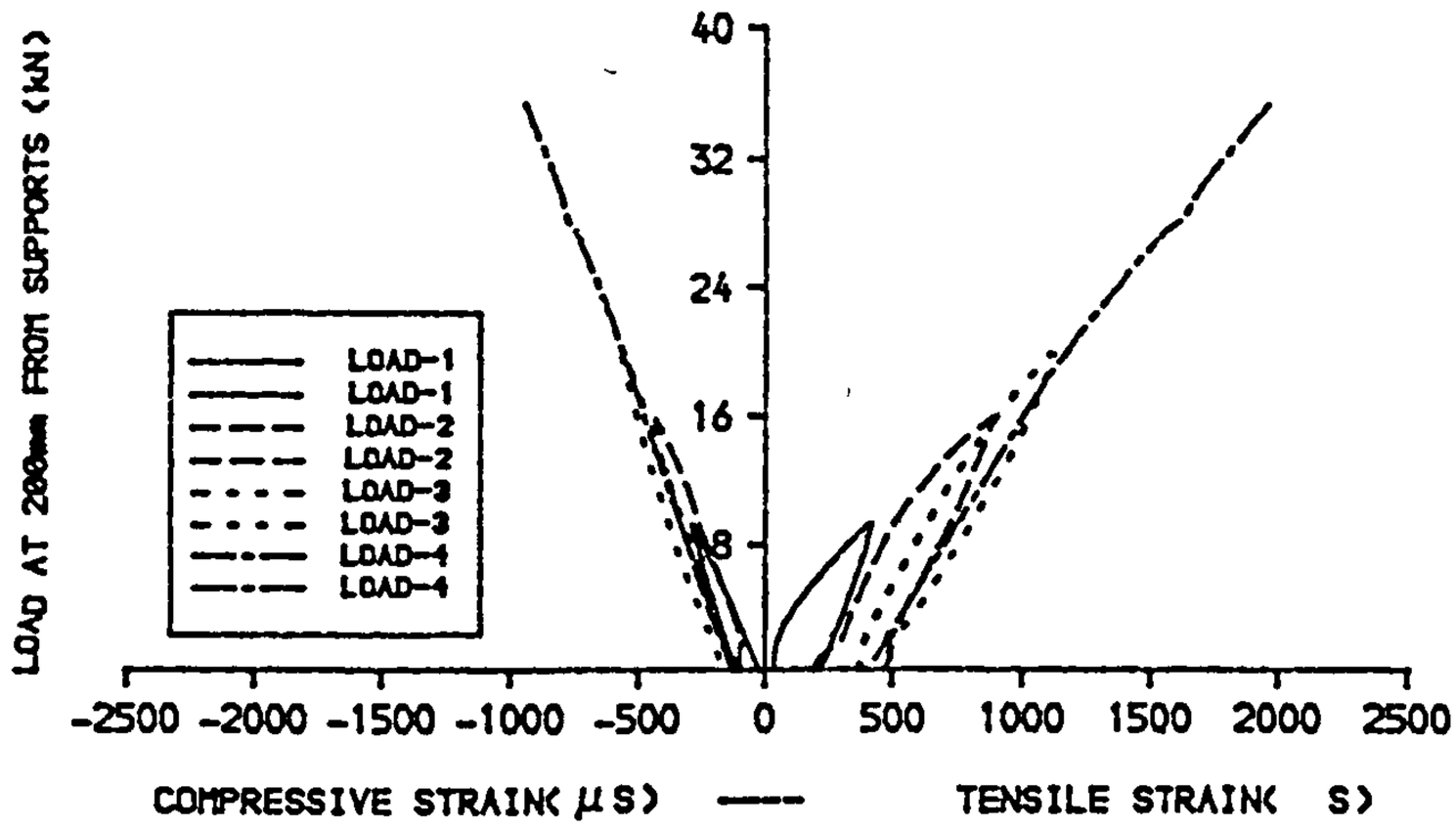

B) .LOAD-STRAIN CHARACTERISTICS AT MID SPAN

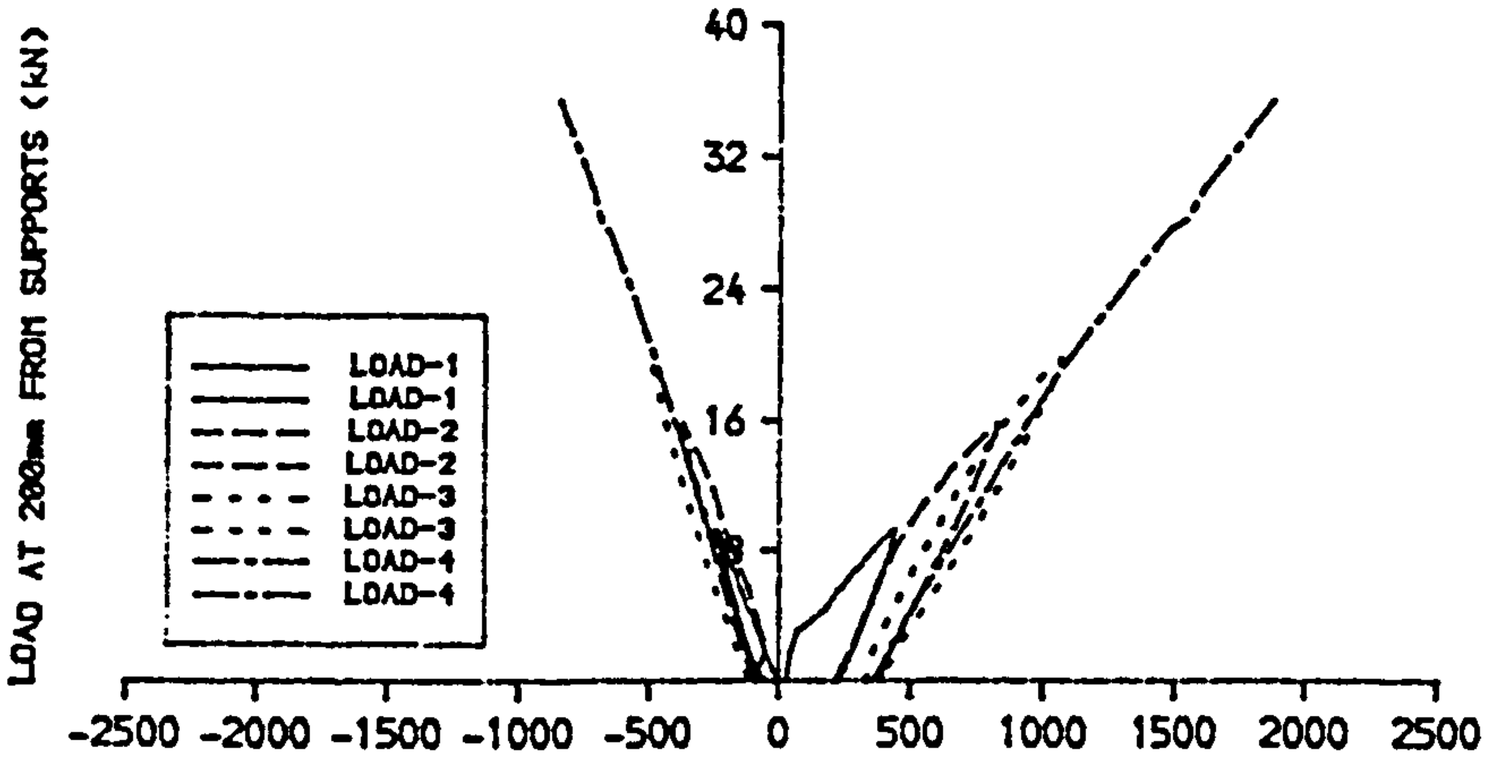

C) .LOAD-STRAIN CHARACTERISTICS AT QUARTER SPAN

FIG.3.29.LOAD-DEFLECTION AND LOAD-STRAIN CHARACTERISTICS OF BEAM-3 (FB/L2), FULLY BONDED, DIAGONAL SPLITTING CRACK PATTERN.

A. BEAM JUST BEFORE FAILURE

B. BEAM AT FAILURE

FIG.3.30.DIAGONAL SPLITTING CRACK PATTERNS JUST BEFORE AND AT FAILURE OF BEAM-3 (FB/L2), FULLY BONDED (AT HINGE).

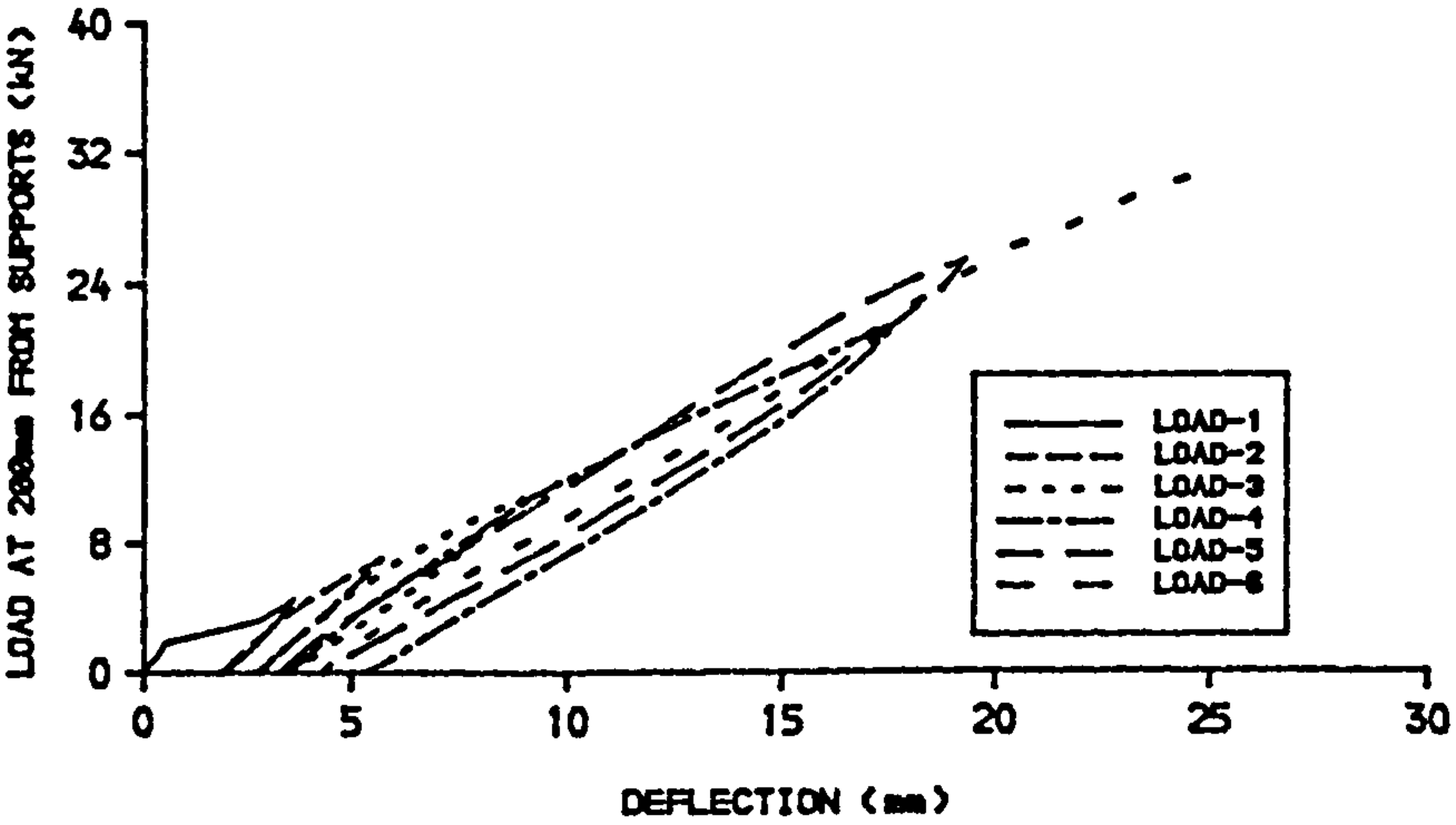

A) .LOAD-DEFLECTION CHARACTERISTICS AT MID SPAN

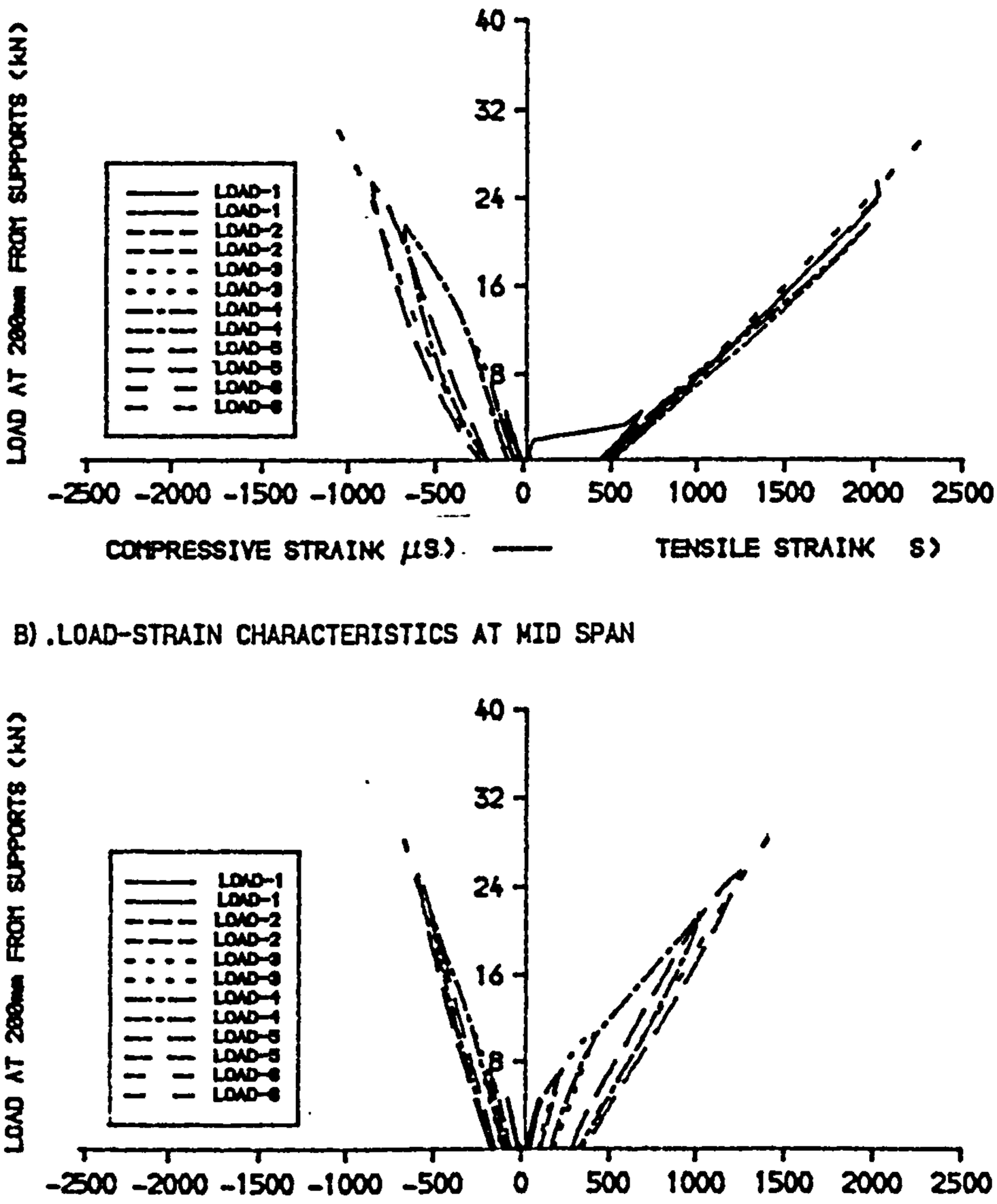

B) .LOAD-STRAIN CHARACTERISTICS AT MID SPAN

C) .LOAD-STRAIN CHARACTERISTICS AT QUARTER SPAN

FIG.3.31. LOAD-DEFLECTION AND LOAD-STRAIN CHARACTERISTICS OF BEAM-4 (PB/L2), PARTIALLY BONDED, DIAGONAL SPLITTING CRACK PATTERN.

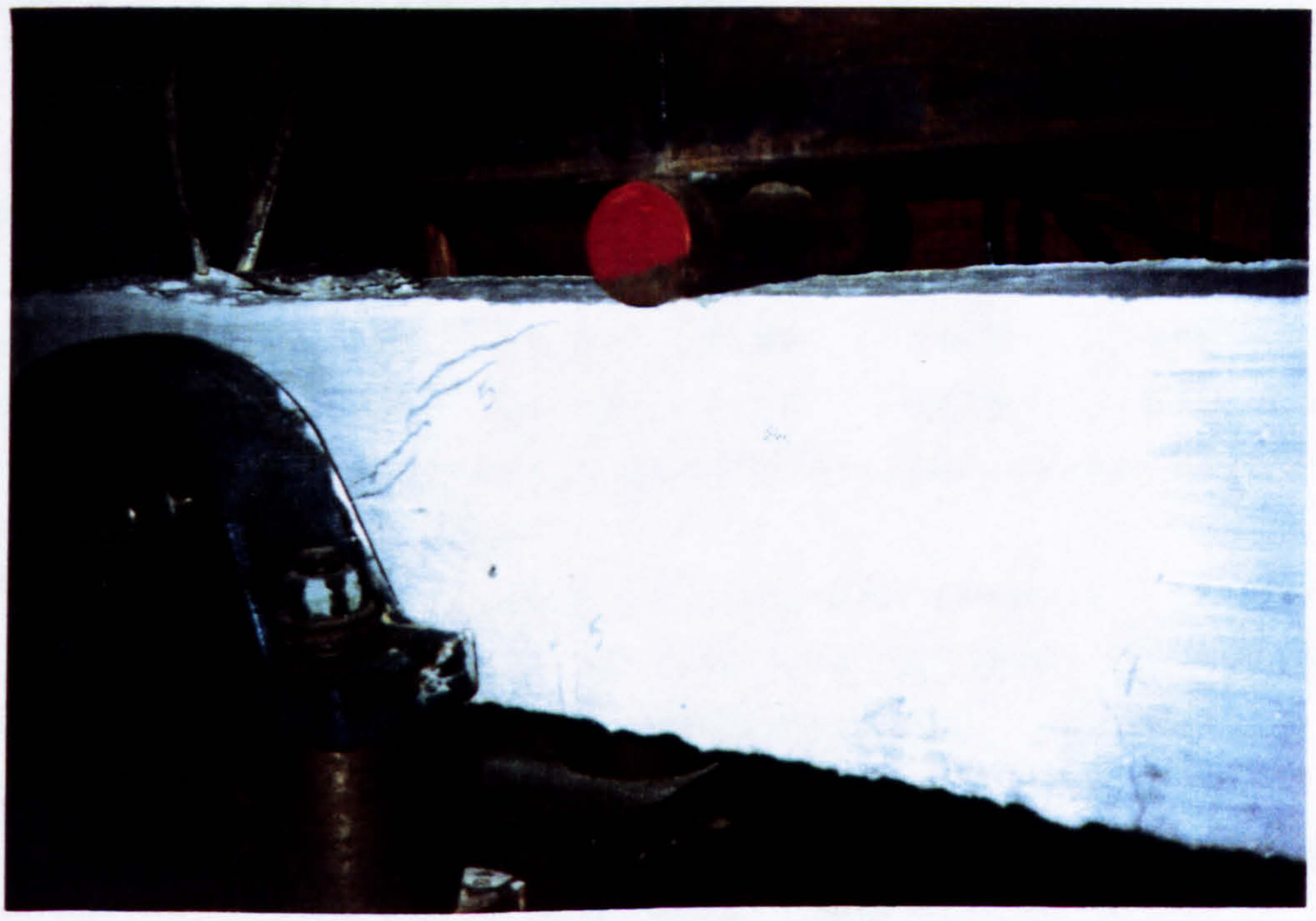

A. BEAM FAILURE AT ROLLER.

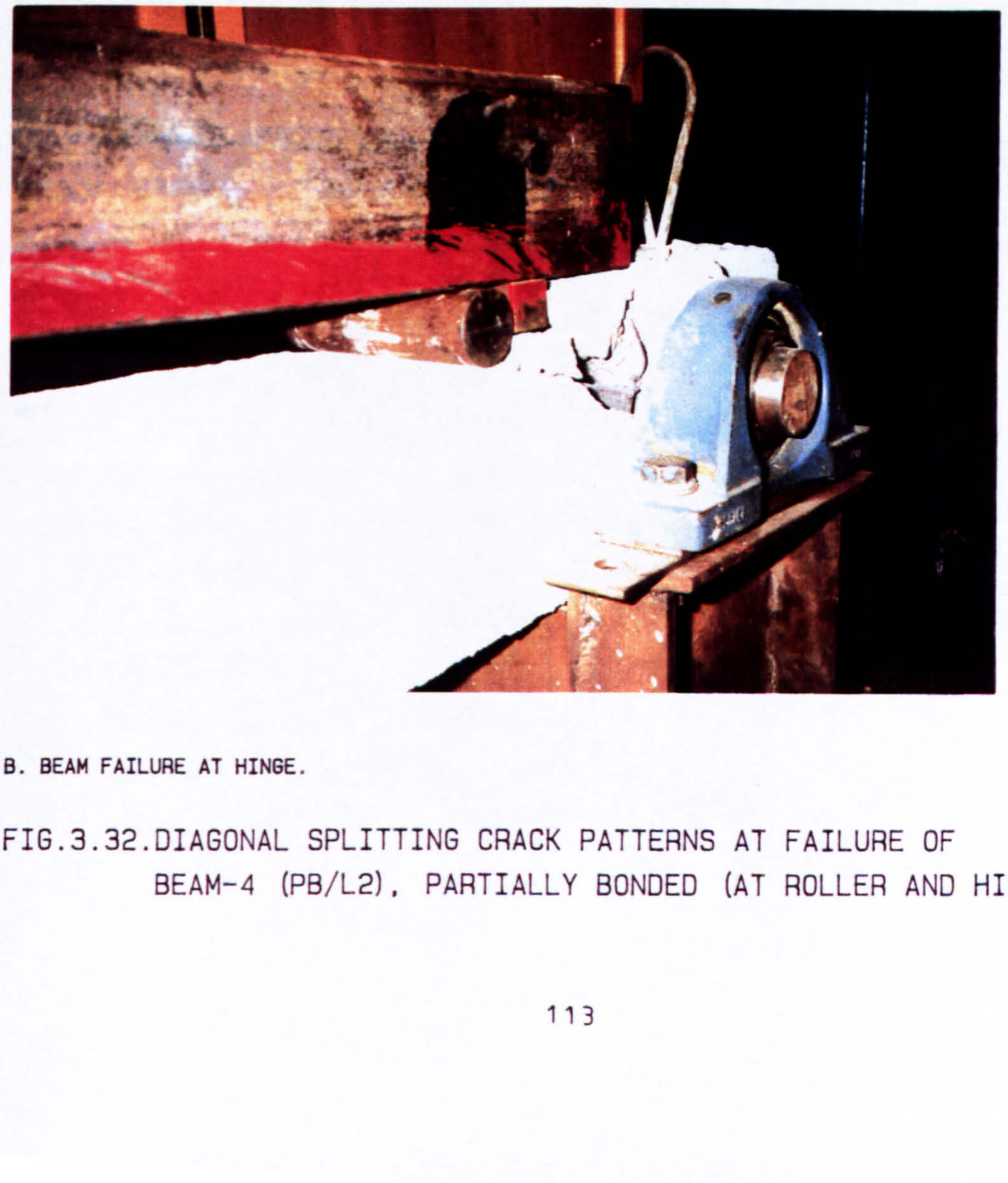

B. BEAM FAILURE AT HINGE.

FIG.3.32.DIAGONAL SPLITTING CRACK PATTERNS AT FAILURE OF BEAM-4 (PB/L2), PARTIALLY BONDED (AT ROLLER AND HINGE).

Table.3.1. Material Properties.

[1]	[2]	[3]	[4]	[5]	[6]	[7]
BEAM-1(R)	39.16	23.26	4.65	6/12	312	FB/L1
BEAM-2(U)	49.02	17.56	5.11	25/5	312	PB/L1
BEAM-3(S)	44.92	15.51	4.66	10/7	312	FB/L2
BEAM-4(V)	46.91	24.38	4.18	21/5	312	PB/L2

[1]=experimental codes.

[2]=compressive strength of concrete cubes, f_{cu} (N/mm^2)

[3]=modulus elasticity of concrete cylinder, E_{c_2} (kN/mm^2)

[4]=tensile strength of concrete beam, f_1 (N/mm^2)

[5]=slump/VB test (mm/sec)

[6]=tensile strength of steel reinforcement, f_s (N/mm^2)

FB =fully bonded reinforcement beam

PB =partially bonded reinforcement beam

L1 =flexural crack patterns

L2 =diagonal splitting crack patterns

Table.3.2. Load - Strain - Displacement of BEAM-FB/L1

Load Stage	Maximum Load (kN)	Maximum Strain (μs) [1]	[2]	[3]	[4]	Displ. m.sp. (mm)	Vis.Crack Depth (mm)	Vis.Crack Number
1	2.181	592	273	-316	-214	4.68+)	40	5
2	4.210	1220	716	-703	-537	12.57	65	6
3	5.264	1513	920	-823	-621	15.28	75	18
4	7.632	1931	1411	-1295	-920	*)21.52	%)	%)

+) =flexural crack initiated within this stage

*) =displacement before removing dial gauge.

%) =failure crack patterns (see associated photographs)

[1]=tensile strain at mid span

[2]=tensile strain at quarter span

[3]=compressive strain at mid span

[4]=compressive strain at quarter span

Table.3.3. Load - Strain - Displacement of BEAM-PB/L1

Load Stage	Maximum Load (kN)	Maximum Strain (μs) [1]	[2]	[3]	[4]	Displ. m.sp. (mm)	Vis.Crack Depth (mm)	Vis.Crack Number
1	1.764	807	297	-544	-533	6.19+)	120	1
2	2.756	1058	485	-618	-631	9.40	125	1
3	3.777	1391	708	-762	-762	13.10	130	1
4	7.808	2224	1598	-1319	-1197	38.94	%)	%)

+) =sudden flexural crack pronounced

%) =failure crack patterns (see associated photographs)

Table.3.4. Load - Strain - Displacement of BEAM-FB/L2.

Load Stage	Maximum Load (kN)	Maximum Strain (μs) [1]	[2]	[3]	[4]	Displ. m.sp. (mm)	Vis.Crack Depth (mm)	Vis.Crack Number
1	9.271	406	425	-304	-265	5.72+)	50	8
2	15.841	876	810	-447	-390	11.30	57	21
3	19.773	1113	1051	-584	-516	14.88+)	57	23
4	35.347	1947	1854	-961	-871	27.63	%)	%)

+) =flexural crack initiated within this stage

+) =diagonal splitting crack pronounced

%) =failure crack patterns (see associated photographs)

NOTES TO ALL TABLES :

[1]=tensile strain at mid span

[2]=tensile strain at quarter span

[3]=compressive strain at mid span

[4]=compressive strain at quarter span

Table.3.5. Load - Strain - Displacement of BEAM-PB/L2.

Load Stage	Maximum Load (kN)	Maximum Strain (μs) [1]	[2]	[3]	[4]	Displ. m.sp. (mm)	Vis.Crack Depth (mm)	Vis.Crack Number
1	4.496	661	79	-124	-105	3.55+)	120	1
2	7.011	917	196	-207	-206	5.56	120	1
3	10.796	1190	390	-303	-298	8.78	120	1
4	21.484	1948	990	-693	-537	17.42	121	1
5	25.418	2000	1220	-885	-624	19.32*)	125	6
6	30.455	2316	1479	-1086	-745	24.64**)	%	%

+) =flexural crack initiated within this stage (3.19kN)

*) =diagonal splitting crack at roller (25.418kN)

**)=diagonal splitting crack at hinge (26.850kN)

%) =failure crack patterns (see associated photographs)

[1]=tensile strain at mid span

[2]=tensile strain at quarter span

[3]=compressive strain at mid span

[4]=compressive strain at quarter span

CHAPTER - 4

4. DETERMINATION OF SIGNAL PARAMETERS.

4.1. General.

Signal parameters comprising the natural frequency, peak amplitude or resonance amplitude and the damping, can be obtained from the frequency response or the polar diagram. Frequencies and amplitudes obtained from the Fast Fourier Transform construct a frequency response whilst amplitudes and phases construct polar diagram. The discrete data resulting from the digitising process may be truncated arbitrarily. This arbitrary digital truncation create problems in the determination of the signal parameters using the FFT analysis. These problems and their solution in digital signal processing are considered in this chapter.

Corrective coefficients based on linear approximations are developed and are applicable to the rectangular window and the Hanning window functions. These coefficients are then applied in the analysis of the experimental results.

4.2. Mathematical Basis.

As the signal is truncated arbitrarily within a certain interval of time the Fourier transform which is valid only for infinite interval of time will induce errors. Instead of errors due to digital processing termed 'round off errors' errors due to the non periodic

signal also occur.

It has been discussed in chapter-2 that the transformation of the digitised signal data is accepted as the convolution of the infinite signal and the window function. The most simple window function is the rectangular window. The transform of the rectangular window function is given as follows.

$$H(f) = \int_{-T}^{T} A\, e^{-j2\pi ft}\, dt \qquad \ldots\ldots (4.1)$$

$$H(f) = A\int_{-T}^{T} \cos(2\pi ft)\, dt - jA\int_{-T}^{T} \sin(2\pi ft)\, dt$$

By omitting the second odd integrand gives

$$H(f) = 2AT\,\frac{\sin(2\pi Tf)}{2\pi Tf} \qquad \ldots\ldots (4.2)$$

where : A = amplitude of the impulse

T= time starts from -T to + T

f = frequency resolution

The transformed function,H(f) is a diminishing sinusoidal function with respect to the frequency as seen in figure (4.1-A.1). The largest amplitude and the diminishing amplitudes are respectively referred to as the main lobe and the side lobes in many references. The transformed function of an even signal,x(t) and an odd signal,y(t) are respectively given below.

$$X(f) = \int_{-\infty}^{\infty} a\cos(2\pi f_0 t)\, e^{-j2\pi ft}\, dt$$

$$= (a/2)\int_{-\infty}^{\infty} [e^{+j2\pi f_0 t} + e^{-j2\pi f_0 t}]\, e^{-j2\pi ft}\, dt$$

$$= (a/2)\,\delta(f-f_o) + (a/2)\,\delta(f+f_o) \qquad \ldots\ldots (4.3)$$

$$Y(f) = \int_{-\infty}^{\infty} a\sin(2\pi f_0 t)\, e^{-j2\pi ft}\, dt$$

$$= (a/2)\int_{-\infty}^{\infty} [e^{+j2\pi f_0 t} - e^{-j2\pi f_0 t}]\, e^{-j2\pi ft}\, dt$$

$$= j(a/2)\ \delta(f+fo) - j(a/2)\ \delta(f-fo) \quad \ldots\ (4.4)$$

where :

$\delta(f-fo)$ and $\delta(f+fo)$ are unit terms.

The multiplication of the rectangular window,h(t) and the periodic signal,x(t) is accepted as a convolution of the transformed function,H(f) and the continuous signal,X(f) as seen in fig.(4.1-A.4). Digital processing may be represented as sets of a unit impulse with constant interval of time. The transform of the unit impulse with time equals to minimum time,To/4 results line spectra at the maximum range of frequency,4/To as seen in fig.(4.1-A.3). Furthermore the transform of the unit impulse with time equals the total time,To and results in line spectra at every 1/To as seen in fig.(4.1-A.5). Multiplications of figures (A.1) with (A.2) and (A.3) of fig.(4.1) in the time domain, this process is equal to convolving those figures in the frequency domain and represents an infinite digitising process. The finite digitising process is achieved by convolving the impulse of the total time, shown in fig.(4.1-A.5) and the later result in the time domain, or by multiplying its transform with the later result in the frequency domain. The finite digitising process is shown in fig.(4.1-A.4). From the later figure it is shown that the maximum amplitude of the main lobe coincides with one of the line spectra and the other line spectra coincide with the zero points of the superimposing side lobes. This process,

theoretically, does not induce very much error if the number of cycles are adequate.

If a non periodic signal is truncated the digitising process is the same as the periodic signal. The result will be different due to non-coincidences of the main lobe as well as the side lobes with the line spectra. The transform of the rectangular window seen in figure B.1 of fig.(4.1) results a slightly compressed diminishing sinusoidal function because of $1/(T_o+\Delta t)$ whilst the transform of the infinite signal remains the same, $1/T_o$ as seen in fig.(4.1-B.2). Figures (4.1-B.3) also remains the same as the time interval is not changed, therefore, the maximum ranges of frequency remain the same. Due to different total time, $(T_o+\Delta t)$ the transform is slightly compressed, $1/(T_o+\Delta t)$. Figures (4.1-B.4) show that the maximum amplitude of the main lobe does not coincide with one of the line spectra and most line spectra are affected by the side lobes.

Those figures suggest that the actual maximum main lobe and the actual frequency of the signal may only be approximated by considering the amplitudes and frequencies surrounding the main lobe. Some other window functions such as Humming and Hanning window functions attempt to reduce effect of the side lobes on the main lobe, in such away that the line spectra surrounding the frequency of interest are not very much distorted. Most attempts suggest to taper the abrupt edges in such that

the head and the tail of the signal fall off smoothly to zero. The most popular use of such a window is the Hanning window function. The Hanning window function produces considerably lower side lobes. The signal parameters are obtained by considering the maximum and the second highest amplitude. The corrections to the amplitude and frequency due to the non-periodicity of the signal are performed graphically in fig.(2.9).

4.3. Corrective Coefficients.

To approximate frequencies linear coefficients based on the symmetric angular concept of the line spectra within the main lobe are developed. The transformed digitised data via the radix mixed FFT mostly results in a maximum line spectrum with two lower line spectra surrounded, if not two of equal amplitudes. The maximum and two surrounding amplitudes are considered in the method.

The frequency of interest is assumed to be within the maximum and the nearest high amplitude. The approximation is carried out by intersecting two lines forming equal angles. The first line passes through the minimum and the maximum of the three amplitudes considered. This line creates angles with respect to horizon and vertical. The second line is drawn through the medium amplitude at the angle to the vertical to form a mirror image of the first line, so that they form equal

angles as seen in fig.(4.2). If a pure sinusoidal signal is truncated arbitrarily and is digitised three possible conditions are shown in fig.(4.2). Instead of errors due to aliases, those are folded signals due to improper amount of data per cycle and are beyond the scope this discussion, this technique induces errors due to the effects of superimposing of the side lobes which are more predominant as the frequency resolution is low. The percentage errors are detected numerically as a logarithmic decrement of periodic signals where analysis via the radix mixed FFT is carried out. Fig.(4.3) shows the relationship between the errors induced and the number of cycles. Acceptable results are dependent on the frequency sensitivities of the experiment. Maximum errors of 0.17% are achieved if 100 cycles of the frequency of interest are considered in this direct technique. The longer the number of cycles the better the resolution and the lower the percentage error induced. Figure (4.4) shows that the percentage errors relate to the non-integer number of cycles. Thus, those errors are manageable and can be reduced by using corrective coefficients associated with the non-integer number of cycles. Coefficients, C_1 and C_2 are derived geometrically from fig.(4.2).

Condition-1 :

$$a = 2(A_2-A_1) \quad ; \quad b = (A_3-A_1)$$

$$c = a-b = 2(A_2-A_1)-(A_3-A_1) = 2A_2-A_1-A_3$$

$$d = a-(c/2) = 2(A_2-A_1)-[(2A_2-A_1-A_3)/2]$$

$$= (2A_2-3A_1+A_3)/2$$

$$C_1 = d/a = (2A_2-3A_1+A_3)/[4(A_2-A_1)]$$

$$= \frac{2A_2-3A_1+A_3}{4(A_2-A_1)} \qquad \ldots\ldots (4.5)$$

Condition-2 :

$$e = 2(A_2-A_3) \quad ; \quad f = (A_1-A_3)$$

$$g = e-f = 2(A_2-A_3)-(A_1-A_3) = 2A_2-A_3-A_1$$

$$h = e-(g/2) = 2(A_2-A_3)-[(2A_2-A_3-A_1)/2]$$

$$= (2A_2-3A_3+A_1)/2$$

$$C_2 = 1-h/e = 1-[(2A_2-3A_3+A_1)/4(A_2-A_3)]$$

$$= \frac{2A_2-A_3-A_1}{4(A_2-A_3)} \qquad \ldots\ldots (4.6)$$

Condition-3 :

This condition can be included into one of the two previous conditions. It depends on the technique defining the highest amplitude in the program.

After determining the geometric condition of the three frequencies appropriate the equation (4.5) or (4.6) is applied and the approximate frequency can be obtained using the formulae given below.

$$f_r = f_1 + 2\Delta f\, C_n \qquad \ldots\ldots (4.7)$$

where : $2\Delta f = | f_3 - f_1 |$

$C_n = C_1$ relates to condition-1 or

C_2 relates to condition-2

The direct technique mentioned above may be improved in situations where analysing many numbers of cycle is not possible. This technique involves regression analysis and FFT analysis to evaluate errors induced in the direct

technique.

Characteristics of the coefficients over any numbers of cycle are shown in fig.(4.4). Consistent paths are proved at number of cycles greater than 10. Thus, it can be expected that the output of the Fourier transform analysis of these periodic errors shown in fig.(4.5) consist of a series of signals having consistent frequencies but varying amplitudes with different number of cycles as shown in fig.(4.6). By examining the responses in this figure where leakage is not visible throughout several harmonics this figure suggests that phase differences do not exist significantly therefore, these will simplify the proposed governing equation.

Fig.(4.6) suggests that the error can be represented as a series of sinusoidal functions. Coefficients of the sinusoidal functions vary with the number of cycles. A power regression analysis can be applied to relate maximum errors of the series of the sinusoidal functions. On the other hand the errors also depend on the degree of the non-periodicity. This can be identified from the value of C_1 or C_2. The value of C_1 varies from 0.50 to 0.75 and the value of C_2 varies from 0.25 to 0.50. Assuming that the percentage errors are symmetric to the horizontal and vertical axes a general term relating the degree of non-periodicity and the error may be represented as an absolute value of $(0.5-C_1)$ or $(0.5-C_2)$. This value is included in the determining amplitude of

every sinusoidal function considered. The general term of the improving coefficient is given below.

$$CF = 1 \pm \sum_{n=1}^{n=\infty} A(n)\, S^{B(n)} \sin(2\pi nT) \qquad \ldots\ldots(4.8)$$

where :

S is the number of cycles at frequency of interest

A(n) and B(n) are amplitude and power regression factors.

T is the coefficient of non-periodicity and may be obtained from equation below

P = -1.6263E-18 - 2.2337E-03*T + 3.8492E-01*T^2

+9.5283E-01*T^3 + 5.7285E-01*T^4

P = | C1 - 0.5 | for condition-1

P = | C2 - 0.5 | for condition-2

Acceptable improvements are obtained by considering several harmonics. Four harmonics result in the following four sets of coefficients

A(1) = 0.162345	B(1) = -0.986026
A(2) = 0.024498	B(2) = -1.019394
A(3) = 0.007502	B(3) = -0.943649
A(4) = 0.003198	B(4) = -1.028459

Transformation of an odd function,a $\sin(2\pi ft)$ in the frequency domain results in amplitude down to $a/\sqrt{2}$. Corrections due to non-periodicity of the signal can be carried out numerically, and a fitting curve may be produced by means of a polynomial regression analysis. Fig.(4.7) relates the degree of non-periodicity and the factor required to improve the maximum amplitude found

from the Fourier transform analysis.

4.4. Validity of the Proposed Method.

Knowing that the Hanning window function reduces side lobes, the application of the direct technique using coefficients, C_1 and C_2 to the Hanning response can result frequencies in an accuracy similar to the Hanning window technique. Applying the proposed technique to the Hanning response no longer requires the graphical conversion as seen in fig.(2.9).

The empirical formula proposed by Hassan [5] provides good accuracy if adequate numbers of cycle are analysed. The formula requires attention especially in the region where the signal is periodic. This is due to the numerical instability. The two amplitudes considered may be ignored in comparison to the maximum amplitude, but if division is made the result can be far from the actual frequency of interest. Figures (4.8) and (4.9) indicates the characteristics of the formula.

The proposed direct technique relies on the number of cycles and the periodicity. For high frequencies of interest the technique saves time though it requires a reliable high speed digitiser. Since frequency domain is of interest the amount of data per cycle is not critical but it must comply with the Nyquist frequency requiring at least two data sets per cycle to avoid aliases. In fact the range of frequency of interest determines the

amount of data required.

The indirect technique reduces the inherent error when using the direct technique. The percentage error can be indicated from the values of C_1 or C_2 and the approximate number of cycles. Based on this data corrective factor,CF can be employed and evaluation to the frequency found in the direct technique can be carried out. The complementary amplitude at the frequency of interest can be estimated using a fitting curve producing corrective factors as shown in fig.(4.7).

In addition a simulation shown in fig.(4.10) demonstrates the efficiency of the direct technique and the indirect technique and the direct technique on the Hanning window function.

4.5 Concluding Remarks.

Though the numerical method proved that the proposed corrective coefficients may be applicable for any signal data to provide accurate regression curves relating the number of cycles to the errors induced requires elaborate work. Therefore, the application of equation (4.5) to a signal having more than 40 cycles at the frequency of interest is recommended.

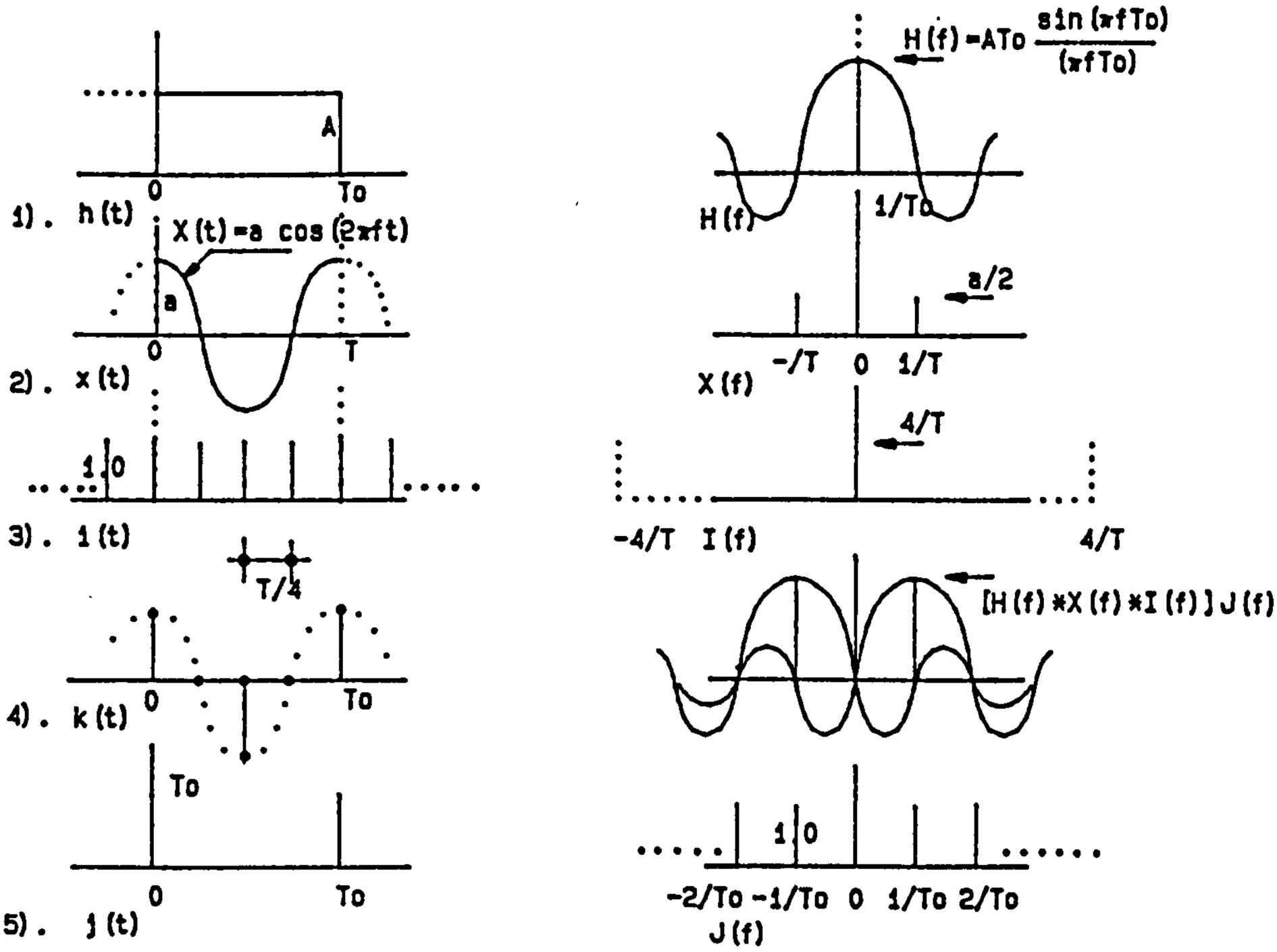

A).Periodic Truncation (Integer Number of Cycles)

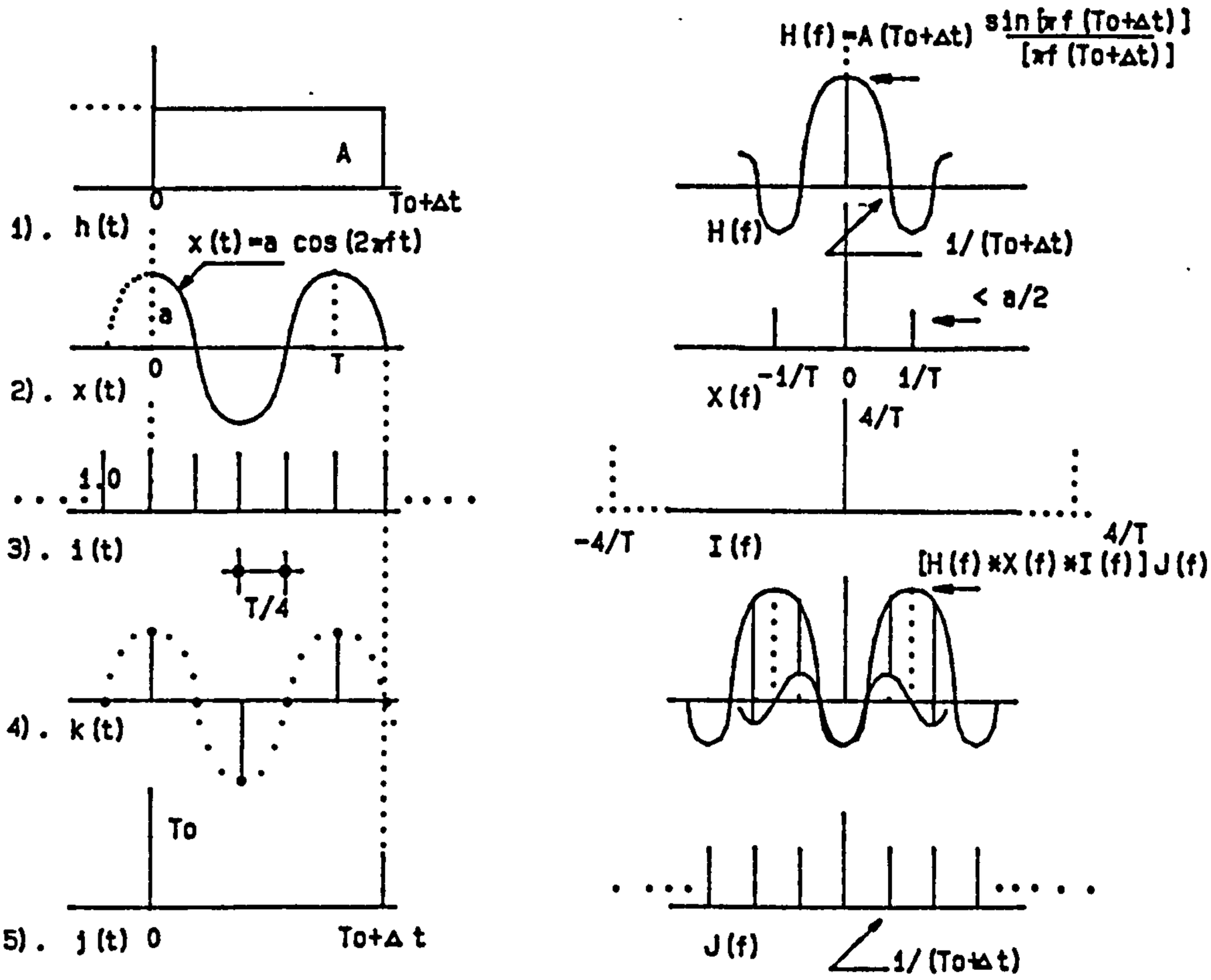

B).Non-periodic Truncation (Non-integer Number of Cycles)

FIG.4.1.EFFECT OF PERIODIC AND NON-PERIODIC TRUNCATIONS ON THE LINE SPECTRA

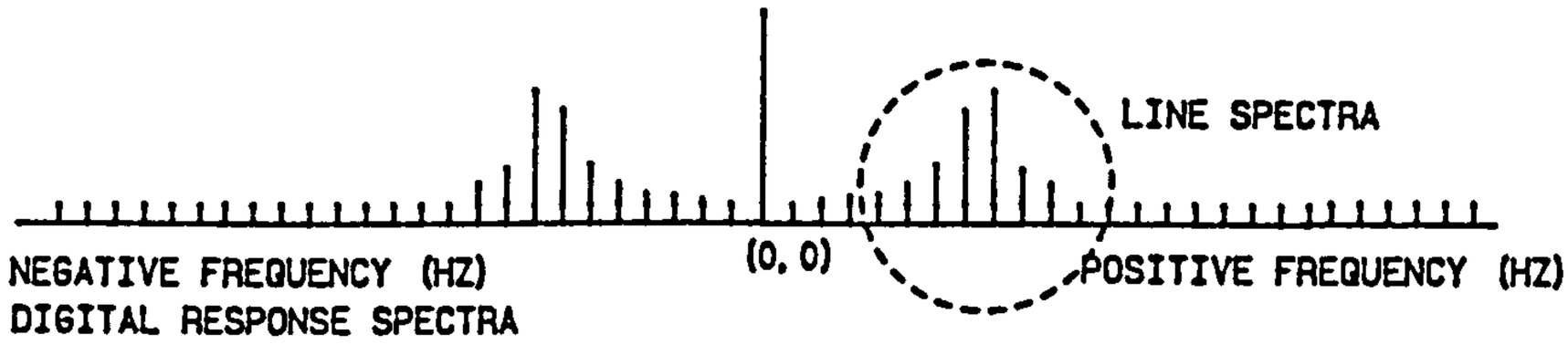

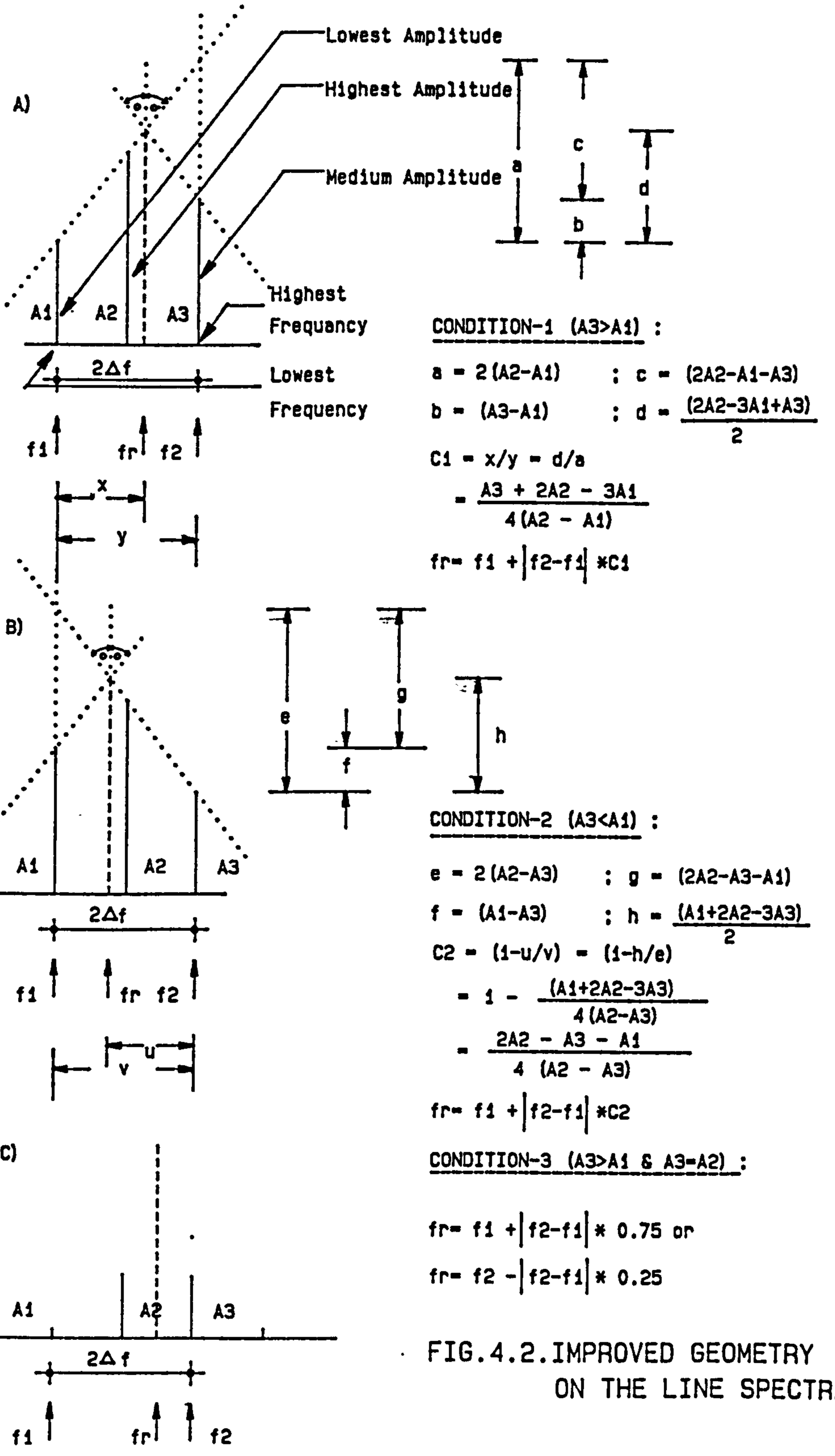

CONDITION-1 (A3>A1) :

$a = 2(A2-A1)$; $c = (2A2-A1-A3)$

$b = (A3-A1)$; $d = \frac{(2A2-3A1+A3)}{2}$

$C1 = x/y = d/a$

$= \frac{A3 + 2A2 - 3A1}{4(A2 - A1)}$

$fr = f1 + |f2-f1| * C1$

CONDITION-2 (A3<A1) :

$e = 2(A2-A3)$; $g = (2A2-A3-A1)$

$f = (A1-A3)$; $h = \frac{(A1+2A2-3A3)}{2}$

$C2 = (1-u/v) = (1-h/e)$

$= 1 - \frac{(A1+2A2-3A3)}{4(A2-A3)}$

$= \frac{2A2 - A3 - A1}{4 (A2 - A3)}$

$fr = f1 + |f2-f1| * C2$

CONDITION-3 (A3>A1 & A3=A2) :

$fr = f1 + |f2-f1| * 0.75$ or

$fr = f2 - |f2-f1| * 0.25$

FIG.4.2.IMPROVED GEOMETRY ON THE LINE SPECTRA

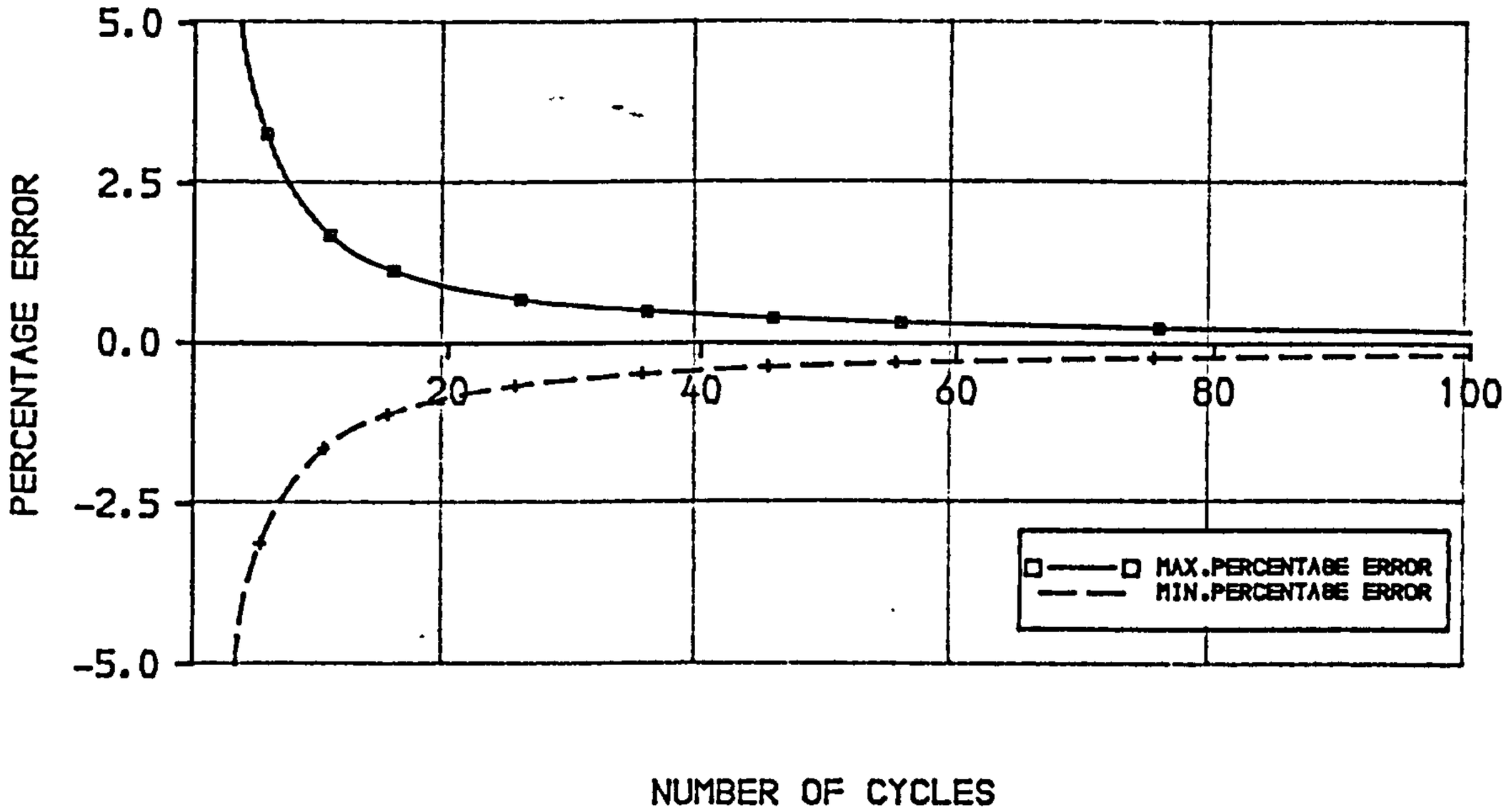

FIG.4.3.MAXIMUM AND MINIMUM PERCENTAGE ERROR USING PROPOSED TECHNIQUE.

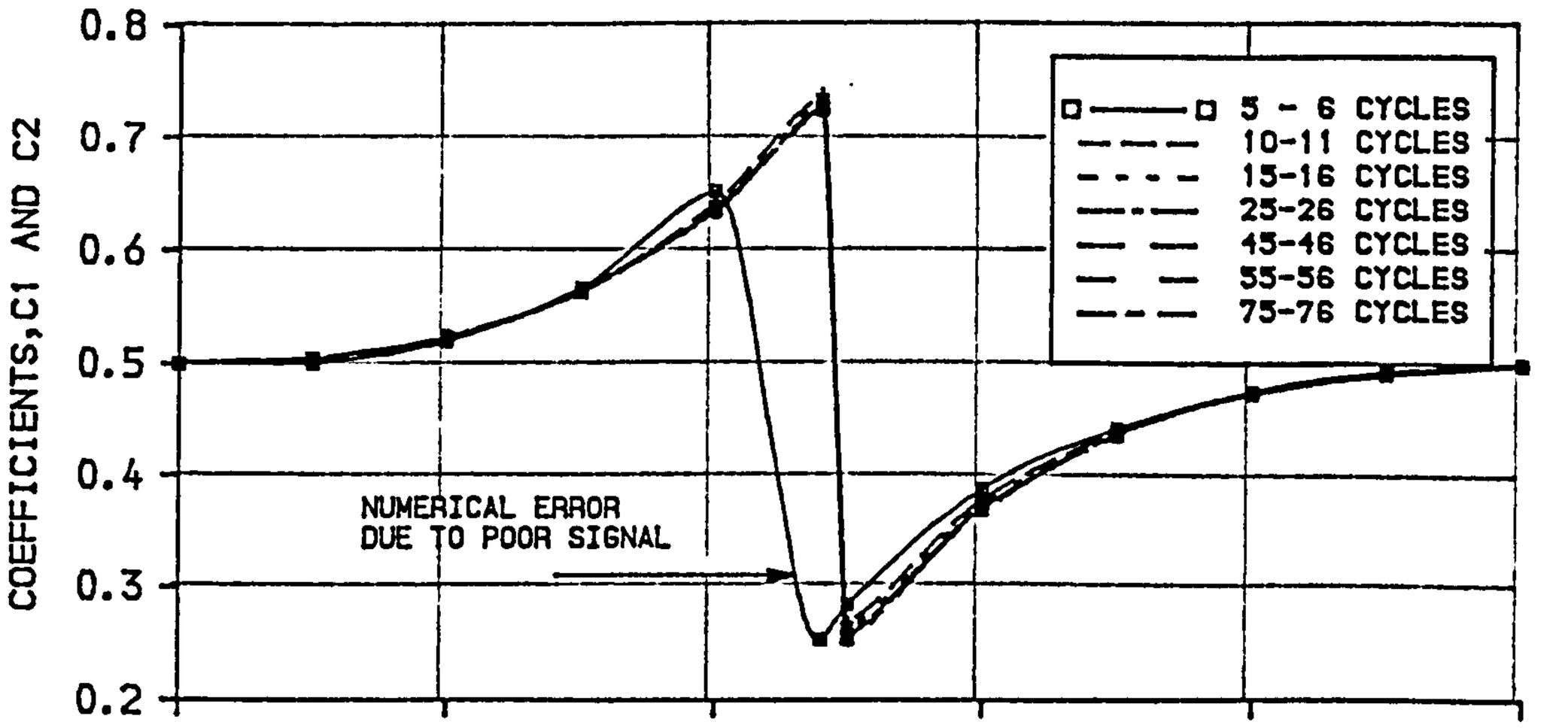

FIG.4.4.CHARACTERISTICS OF COEFFICIENT C1 AND C2 OVER NON-PERIODICITIES

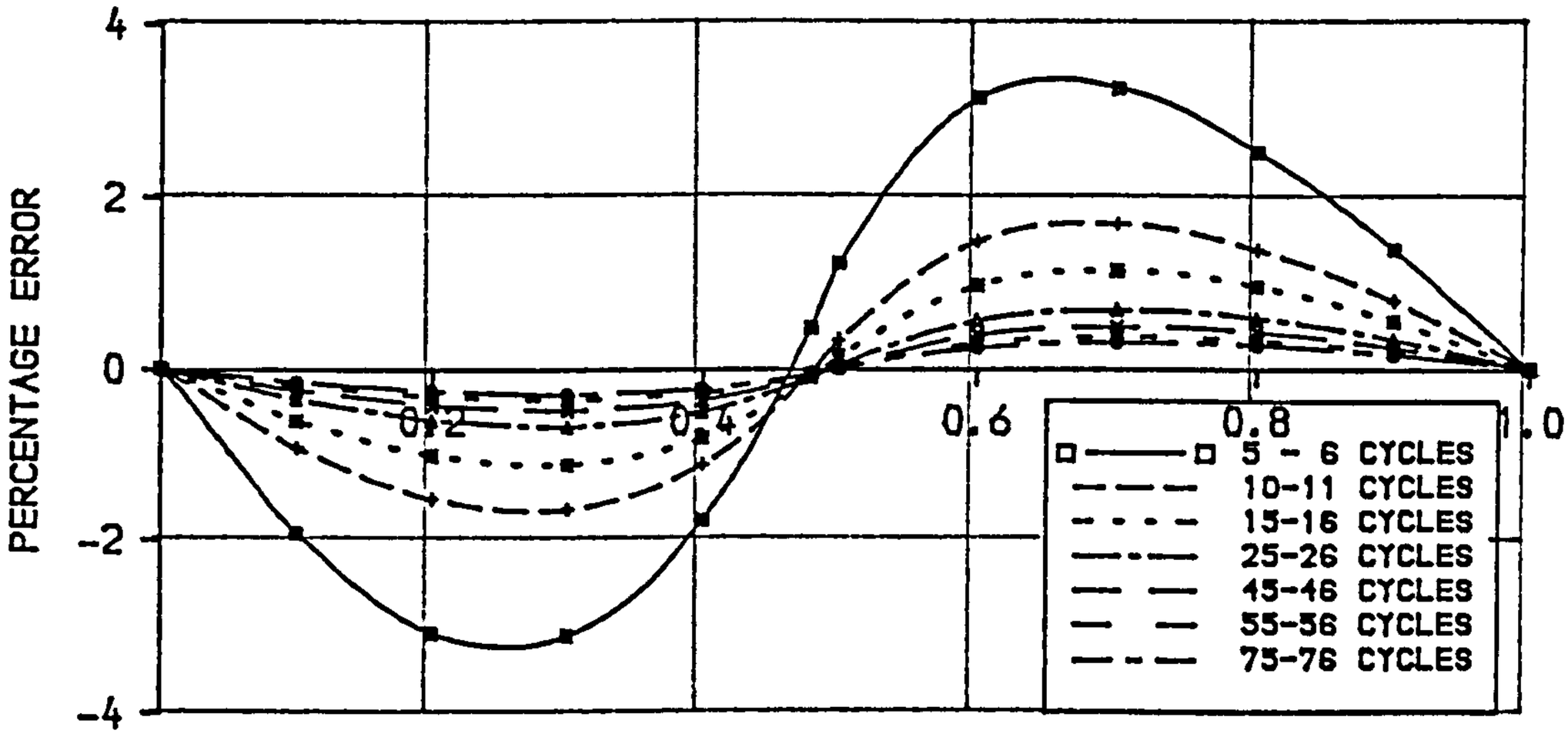

NON-PERIODICITY

FIG.4.5.PERCENTAGE ERROR OVER NON-PERIODICITIES FOR DIFFERENT NUMBER OF CYCLES.

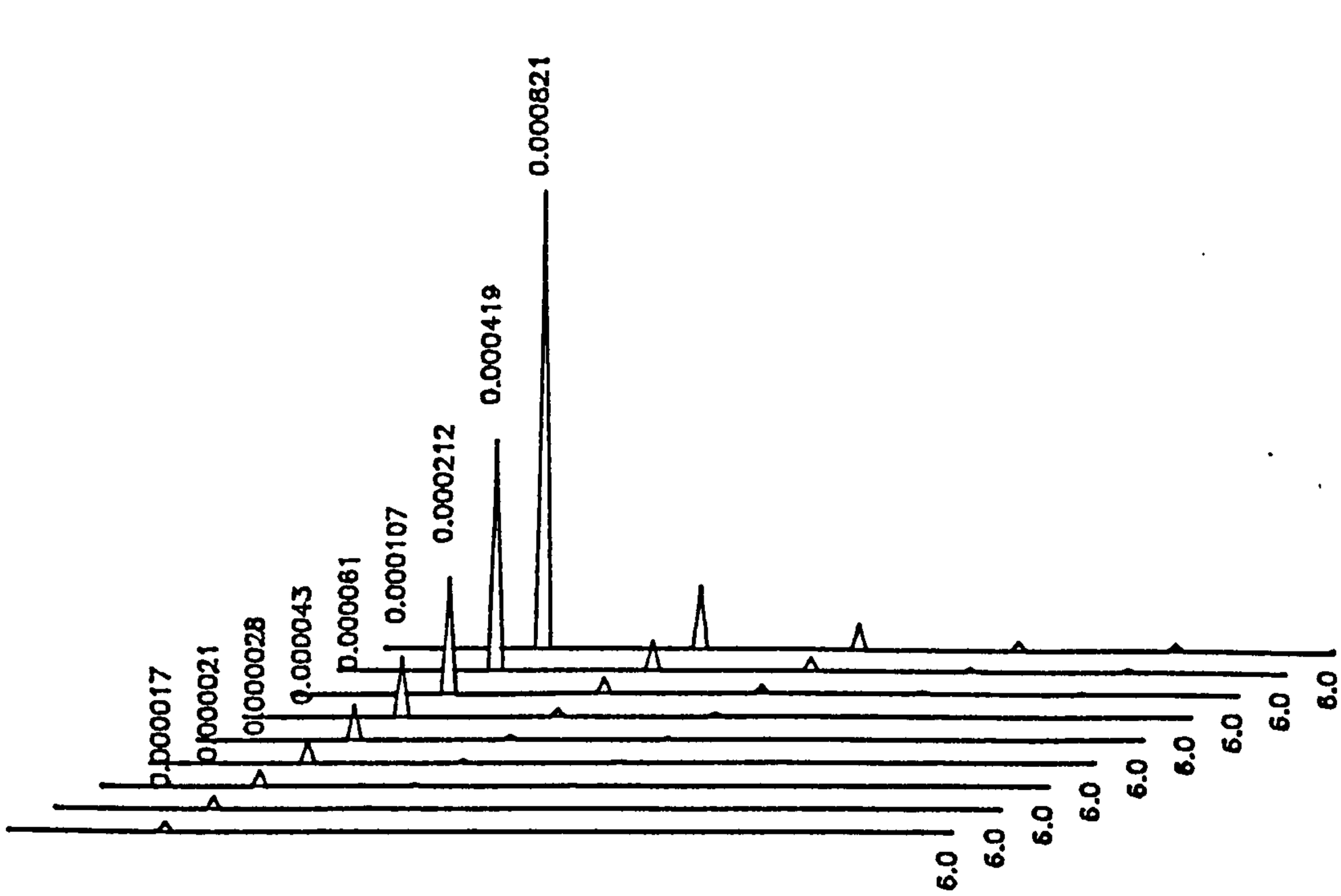

FIG.4.6.RESPONSE SPECTRA OF ERROR (%) FOR 10, 20, 40, 80, 140, 200, 300, 400 AND 500 NUMBER OF CYCLES.

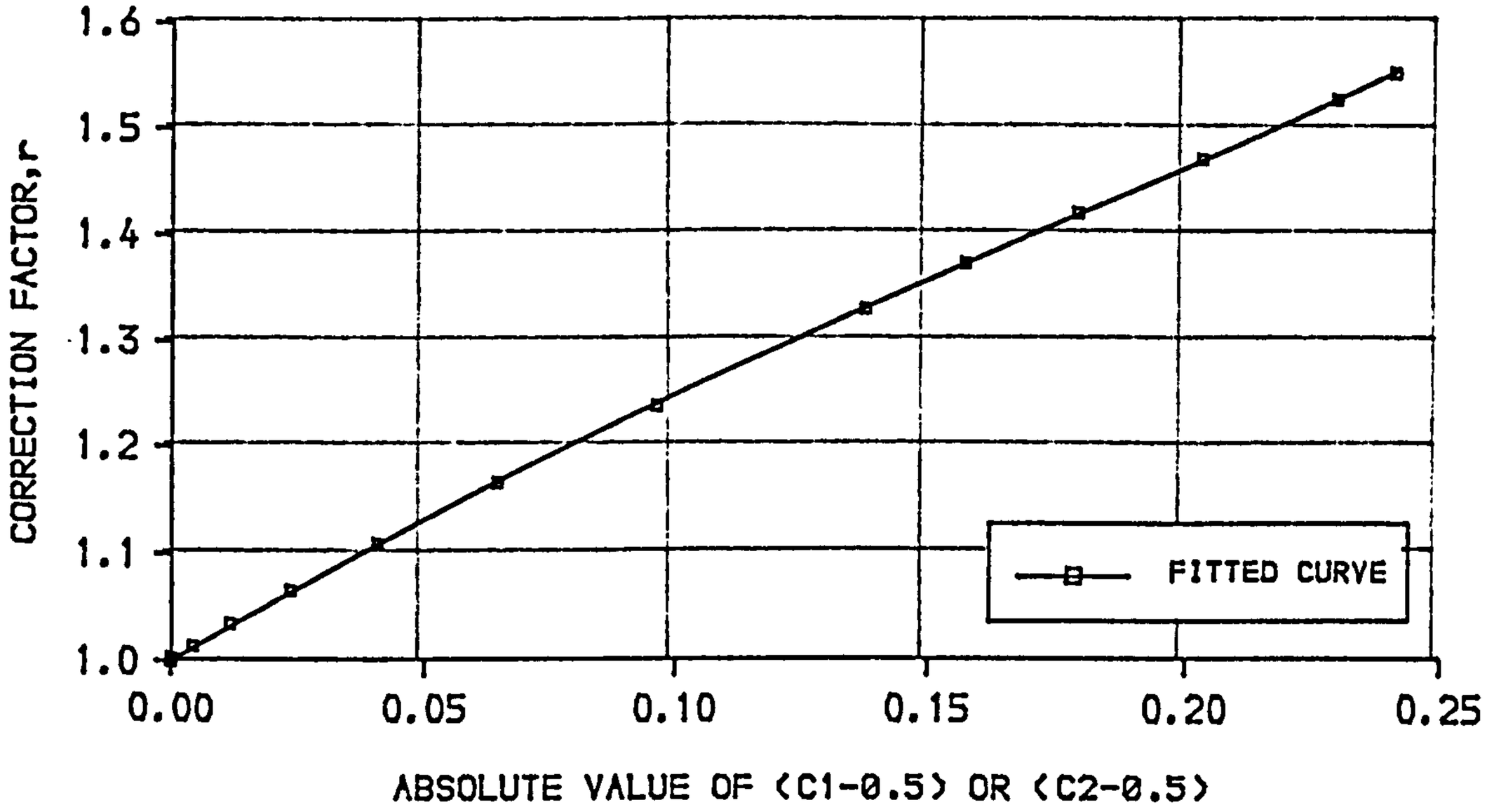

FIG.4.7.AMPLITUDE CORRECTION FACTOR APPLIED IN PROPOSED TECHNIQUE.

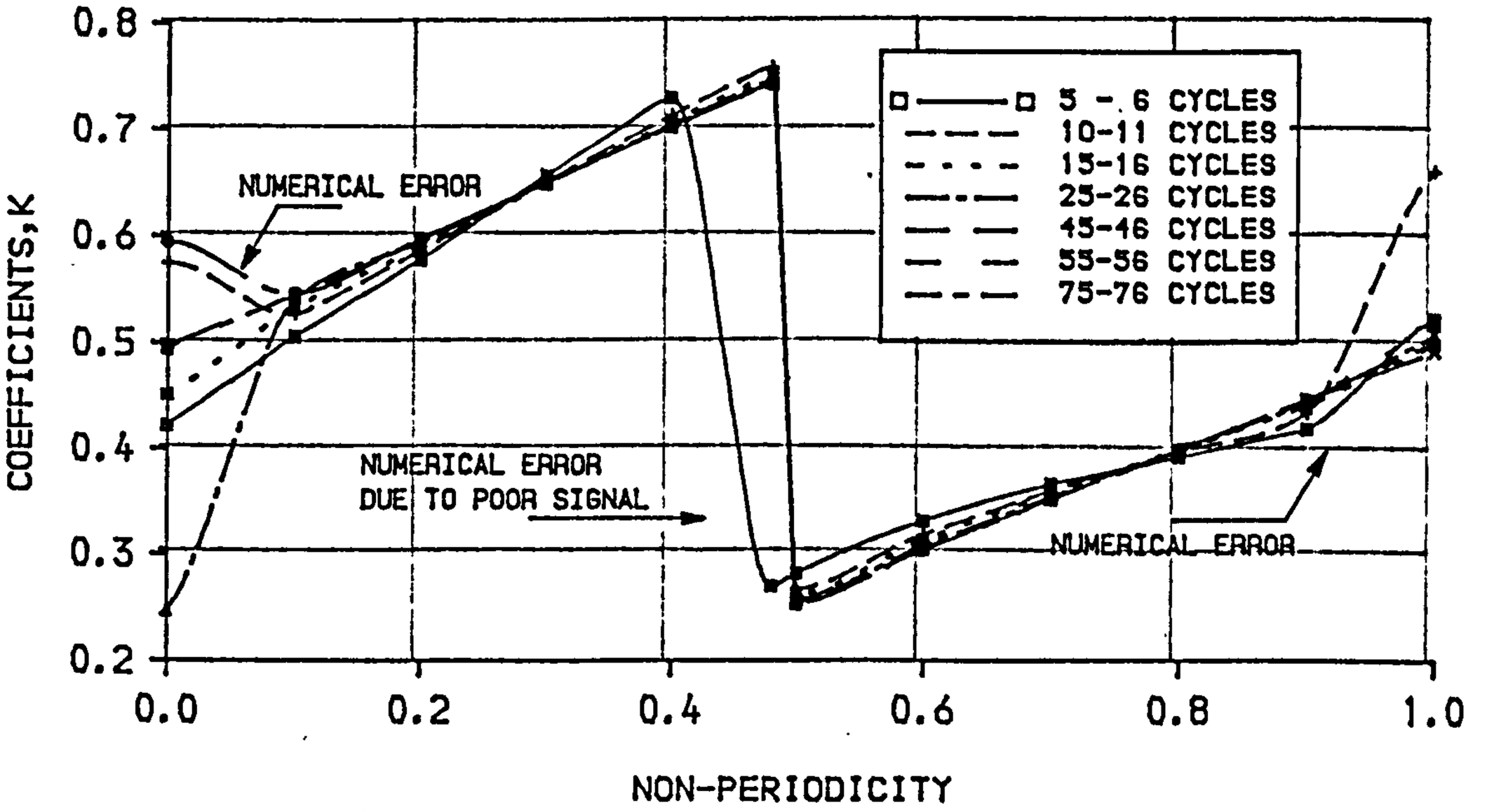

FIG.4.8.CHARACTERISTICS OF COEFFICIENT, K OVER NON-NON-PERIODICITIES AS PROPOSED BY HASSAN [6]

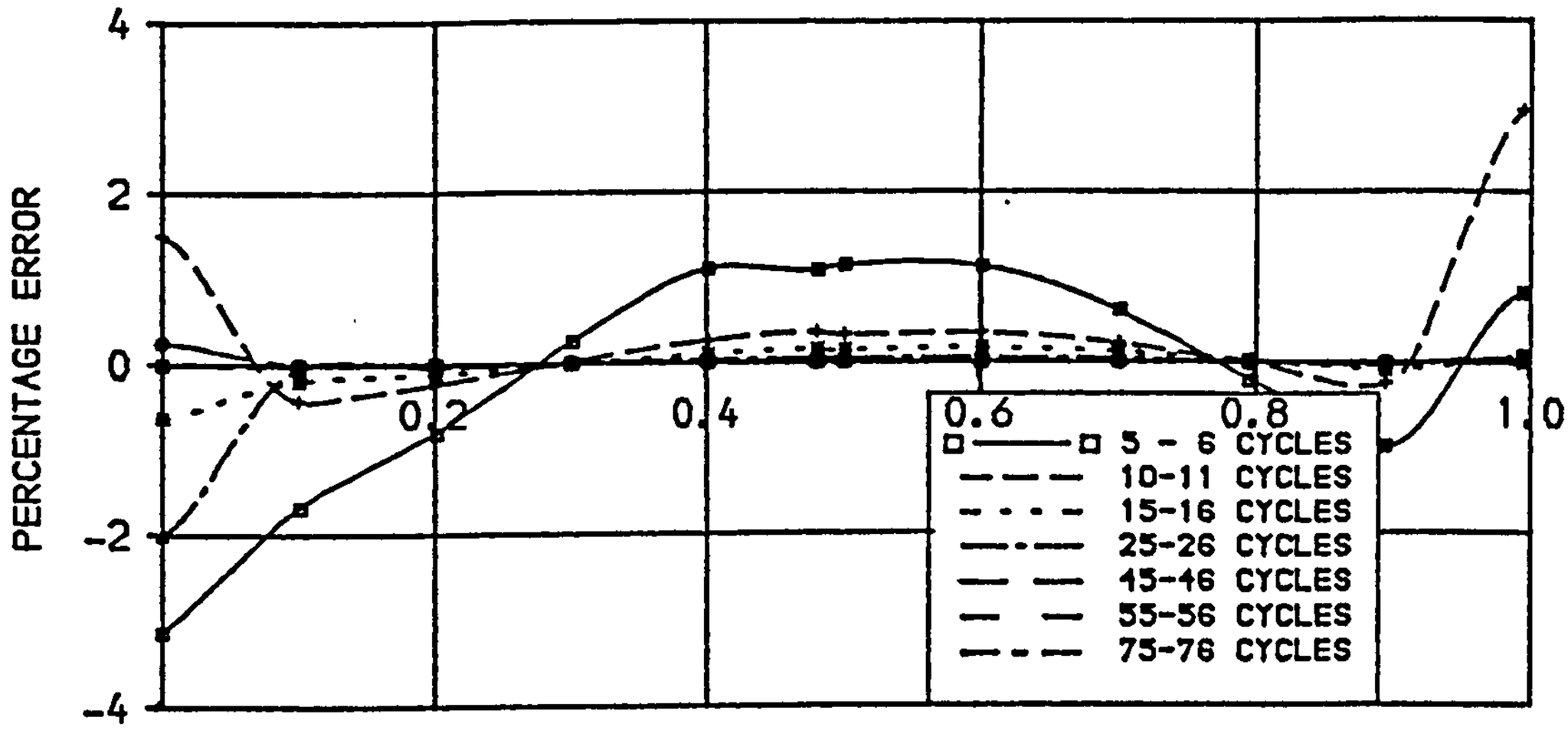

FIG.4.9.PERCENTAGE ERROR OVER NON-PERIODICITIES FOR DIFFERENT NUMBER OF CYCLES PROPOSED BY HASSAN [6]

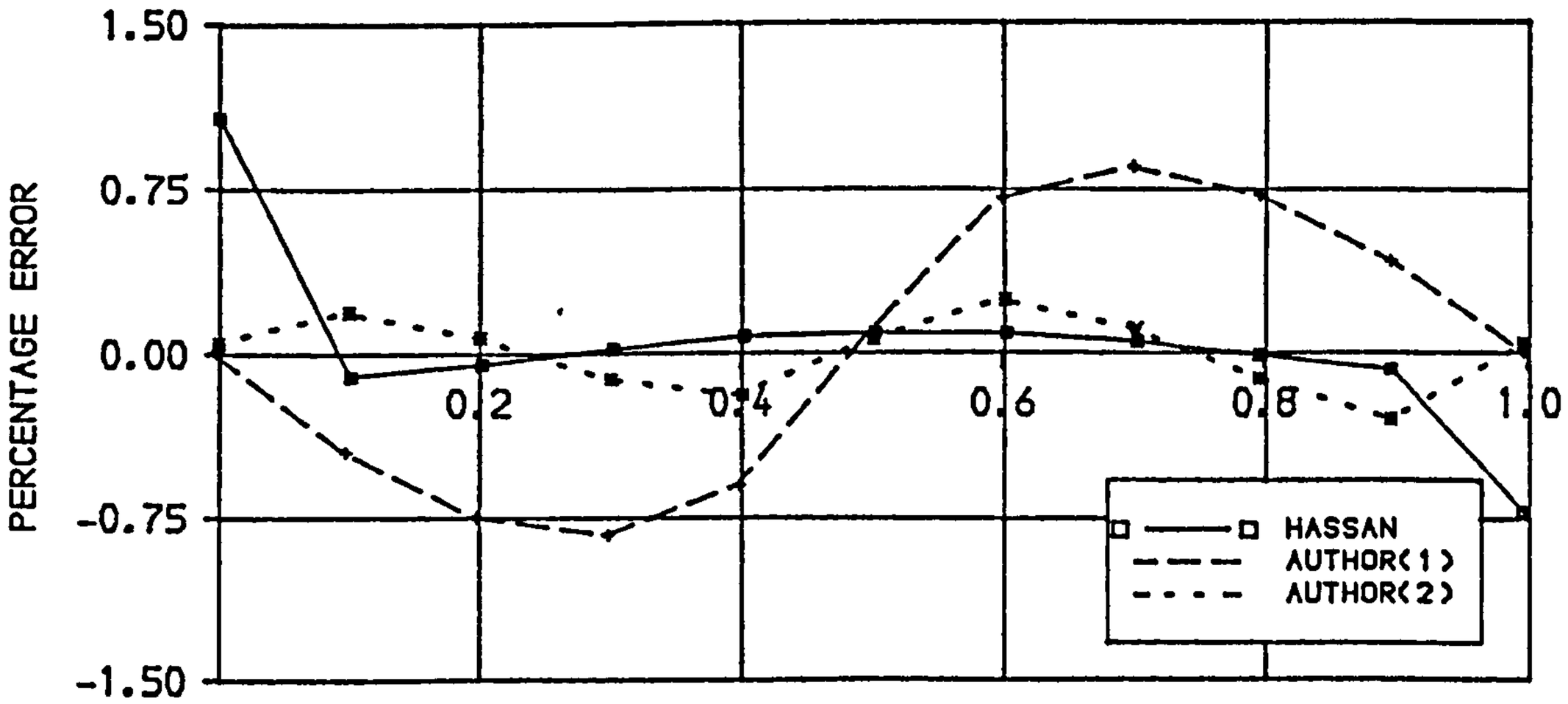

FIG.4.10.COMPARISON BETWEEN TECHNIQUES PROPOSED BY HASSAN [6] AND AUTHOR [DIRECT TECHNIQUE - AUTHOR(1) AND INDIRECT TECHNIQUE - AUTHOR(2)]

CHAPTER - 5

5. EXCITER - STRUCTURE RELATIONSHIPS.

5.1. General.

The experiments identified peculiar characteristics of two types of exciter, the magnetic and the mechanical exciters, over the resonance frequency. Since the characteristics in question affect the response it is necessary to investigate these characteristics. The phenomena are of interest since the maximum or resonance amplitude and the resonance frequency of the structure play an important role.

The phenomena were found when the exciters were anchored down onto the simply supported reinforced concrete beams. The response of the beam excited by the mechanical exciter displays a jump phenomenon and the response of the moving exciter mass of the magnetic exciter shows a sharp decrease in the amplitude about the resonance. Mathematical models have been developed which demonstrate a good correlation with the characteristics of the experimental results.

5.2. Mathematical Models.

The peculiar characteristics identified in the experiments may be clearly explainable from the mathematical point of view. Simple mathematical models normally require several assumptions such as the mass, the stiffness, the damping, the boundary condition and

the forcing function. The better the assumptions to the real model the better the results of the mathematical model. If the assumed equation of motion and the boundary conditions are appropriately chosen the simple mathematical models will demonstrate the characteristics of the system in question.

5.2.1. Absolute and Relative Parameters.

Accelerometers and velocity probes measure absolute amplitudes. This implies that they are a means of measuring amplitudes and phases with respect to an 'indefinite' reference. The relative relationships of two accelerometers measuring absolute amplitudes and phases, within the same 'indefinite' time, reference and system, may be used to overcome this problem.

Each magnetic exciter was anchored down onto the beam under tests whilst the vibration tests were conducted. To measure relative amplitudes and phases of the moving exciter mass (inside the exciter, exciting the beam) to the beam under tests two accelerometers were employed. One accelerometer was mounted on the moving exciter mass and the other accelerometer was positioned on the beam close to the exciter. Both accelerometers measured absolute amplitudes and phases. The problem was to relate them and to obtain the relative amplitudes of the moving exciter mass to the beam for the purpose of obtaining the actual excitation force.

Assuming that the exciter has a constant and high magnetic field the problem is to determine the relative phases and amplitudes of the moving exciter mass to the beam. The relationships are graphically portrayed in fig.(5.1). The relative displacement of the moving exciter mass to the beam is assumed as

$$x_1 = A \sin \omega t \qquad \ldots\ldots (5.1)$$

and the corresponding displacement response of the beam

$$x_2 = B \sin(\omega t - \varphi) \qquad \ldots\ldots (5.2)$$

The accelerometers monitored absolute displacements, thus, the amplitude and phase angle relationships between the moving exciter mass and the excited beam were required to be investigated. The absolute displacement of the accelerometer positioned on the moving exciter mass is assumed as follows.

$$x_3 = x_1 + x_2 = \bar{A} \sin (\omega t - \beta) \qquad \ldots\ldots (5.3)$$

The relationships amongst the amplitude coefficients, A , B and $\bar{A}$ which will be referred to as amplitudes for the purpose of generality, and the phase angles φ and β are portrayed graphically in fig.(5.1). Substituting trigonometric rules for x_1 and x_2 into equation (5.3) also yield

$$x_3 = A \sin \omega t + B \sin (\omega t - \varphi) \qquad \ldots\ldots (5.4)$$

Equating coefficients of equation (5.3) and (5.4) gives

$$A + B \cos \varphi = \bar{A} \cos \beta \qquad \ldots\ldots (5.5)$$

$$B \sin \varphi = \bar{A} \sin \beta \qquad \ldots\ldots (5.6)$$

To relate the phase angle eq.(5.6) is divided by eq.(5.5)

to give

$$\beta = \tan^{-1}\left[\frac{B \sin \varphi}{(A + B \cos\varphi)}\right] \qquad \ldots\ldots (5.7)$$

Further, substituting eq.(5.6) into eq.(5.5) relates the amplitudes of the moving exciter mass and the beam as

$$A = \frac{\bar{\lambda}}{\sin \varphi}[\sin (\varphi-\beta)] \qquad \ldots\ldots (5.8)$$

Introducing relative phase angle of the absolute displacement of the moving exciter mass to the absolute displacement of the excited beam, $\alpha = \varphi-\beta$ into equation (5.8), where the value of α is obtainable from experiments, yields

$$A = \frac{\bar{\lambda} \sin \alpha}{\sin \varphi} \qquad \ldots\ldots (5.9)$$

Again, substituting $\alpha = \varphi - \beta$ into eq.(5.6) and rearranging the trigonometric identities gives

$$\varphi = \tan^{-1}\left[\frac{\bar{\lambda} \sin \alpha}{(\bar{\lambda} \cos \alpha - B)}\right] \qquad \ldots\ldots (5.10)$$

Equation (5.9) shows that the magnitudes of A and $\bar{\lambda}$ depends on the ratio of $\sin \alpha/\sin \varphi$. Since the value of α is always lower than the value of φ, unless $\alpha = \varphi$ for all φ and $\alpha = \varphi$ for $\varphi = 0, \pi, 2\pi$ ....etc., there will be a ratio of one within the value of $\varphi = 0$ to π. Thus, the amplitude, A meets the amplitude, $\bar{\lambda}$ within the range of $\varphi = 0$ to π. This can be obtained by substituting $A = \bar{\lambda}$ into equation (5.9) to give $\sin \varphi = \sin \alpha$. This exists only if : a. $\varphi = 0, \pi, 2\pi, 3\pi$ .... etc

b. $\varphi \geq \pi/2$ and $\varphi \leq \pi$ since $\varphi \geq \alpha$

In other word $\sin \varphi = \sin \alpha$ is possible only if $\varphi > \pi/2$ and $\alpha < \pi/2$. At this specific point of meeting $\cos \varphi = -\cos \alpha$. Including this identity into equation (5.10)

gives

$$\frac{\sin \alpha}{-\cos \alpha} = \frac{\bar{A} \sin \alpha}{\bar{A} \cos \alpha - B} \; ; \; B = 2\bar{A} \cos \alpha \quad \ldots\ldots (5.11)$$

5.2.2. Effect of Reflected Force on Excitation Force.

The effect of the reflected force on the excitation force results in the jump phenomena appeared in the mechanical exciter response and in a peculiar drop appeared in the magnetic exciter response, as seen in chapter-3 fig.(3.7) and (3.8). To explain this a two degree of freedom system is considered. The moving exciter mass of the exciter is assumed to possess a lump mass,m and a stiffness from the magnetic field,k whilst the excited beam possesses a lump mass,M, stiffness,K and damping,c. The moving exciter mass is subjected to a force $F_0 \sin \omega t$ from the electro magnetic field. These relationships are graphically shown in fig.(5.2).

The equation of motion of the moving exciter mass can be expressed as

$$F_0 \sin \omega t = m \ddot{x}_1 + k x_1 - k x_2 \quad \ldots\ldots (5.12)$$

The particular solution to equation (5.12) may be represented as a combination of the force motion,A sin ωt and the reflected motion,C sin $(\omega t - \varphi)$ which has a phase lag relative to the moving exciter mass but is in phase with the excited beam. This combined motion can be expressed as

$$x_1 = A \sin \omega t + B \sin (\omega t - \varphi) = \bar{A} \sin (\omega t - \beta) \quad (5.13)$$

Amplitude coefficients A,B and $\bar{A}$ will be referred to as

amplitudes for the purpose of generality. The equation of motion of the excited beam is

$$0 = M \ddot{X}_2 + K x_2 + k x_2 + c \dot{x}_2 - k x_1 \quad \ldots\ldots (5.14)$$

The particular solution to eq.(5.14) is

$$x_2 = B \sin (\omega t - \varphi) \quad \ldots\ldots (5.15)$$

Including the derivatives of equations (5.13) into equation (5.12) yield

$$F \sin \omega t = - m \omega^2 \bar{A} \sin (\omega t - \beta) + k \bar{A} \sin (\omega t - \beta) - k B \sin (\omega t - \varphi)$$

$$= (k - m \omega^2) \bar{A} \sin (\omega t - \beta) - k B \sin (\omega t - \varphi) \quad \ldots\ldots (5.16)$$

and also equation (5.15) into (5.14) yield

$$0 = -M \omega^2 B \sin (\omega t - \varphi) + K B \sin (\omega t - \varphi) + k B \sin (\omega t - \varphi) + c \omega B \cos (\omega t - \varphi) - k \bar{A} \sin (\omega t - \beta)$$

$$= (k + K - M \omega^2) B \sin (\omega t - \varphi) + c \omega B \cos (\omega t - \varphi) - k \bar{A} \sin (\omega t - \beta) \quad \ldots\ldots (5.17)$$

Applying a trigonometric identity $\sin (\omega t - \beta) = \sin \omega t \cos \beta - \cos \omega t \sin \beta$ into equation (5.16) and equating coefficients give

$$F = (k - m \omega^2) \bar{A} \cos \beta - k B \cos \varphi \quad \ldots\ldots (5.18)$$

$$0 = (k - m \omega^2) \bar{A} \sin \beta - k B \sin \varphi \quad \ldots\ldots (5.19)$$

Similar procedures are applied to equation (5.17) to give

$$0 = (k + K - M \omega^2) B \cos \varphi + c \omega B \sin \varphi - k \bar{A} \cos \beta \quad \ldots\ldots (5.20)$$

$$0 = (k + K - M \omega^2) B \sin \varphi - c \omega B \cos \varphi - k \bar{A} \sin \beta \quad \ldots\ldots (5.21)$$

Multiplying $\sin \varphi$ and $\cos \varphi$ into equations (5.20) and

(5.21) respectively and summing those two equations gives

$$0 = c\ \omega\ B(\sin^2\varphi+\cos^2\varphi)-k\ \bar{\lambda}(\sin\varphi\ \cos\beta-\sin\beta\ \cos\varphi)$$

$$0 = c\ \omega\ B - k\ \bar{\lambda}\ \sin(\varphi-\beta)$$

Introducing relative phase angle $\alpha = \varphi-\beta$; $c = 2d^2M\ p_2$:

$k = m\ p_1$ gives

$$\bar{\lambda} = \frac{2d\ M\ p_2\ \omega\ B}{m\ p_1^2\ \sin\alpha}$$

Furthermore introducing $m_r = M/m$: $r_1 = \omega/p_1$; $p_r = p_2/p_1$ and $C1 = 2d\ m_r\ p_r\ r_1$ gives

$$\bar{\lambda} = C1\ B\ /\ \sin\alpha \qquad \ldots\ldots (5.22)$$

The amplitude,B of equation (5.22) can be obtained by substituting $\bar{\lambda}\cos\beta$ of equation (5.18) into (5.20).

$$0 = (k + K - M\ \omega^2)\ B\cos\varphi + c\ \omega\ B\sin\varphi - k\left[\frac{F + k\ B\cos\varphi}{(k - m\omega^2)}\right]$$

$$0 = (k - m\omega^2)\ (k + K - M\ \omega^2)\ B\cos\varphi + (k - m\omega^2)\ c\ \omega\ B\sin\varphi - kF - k^2B\cos\varphi$$

Multiplying this later equation by $(1/k^2)$ gives

$$B = \frac{F/k}{\left[(1+\frac{K-M\omega^2}{k})(1-\frac{m\omega^2}{k})\cos\varphi + \frac{c\omega}{k}(1-\frac{m\omega^2}{k})\sin\varphi - \cos\varphi\right]}$$

Introducing $K = M\ p_2^2$, $k = m\ p_1^2$, $m_r = M/m$, $p_r = p_2/p_1$, $r_1 = \omega/p_1$ and $c = 2d\ M\ p_2^2$ give

$$B = \frac{F/k}{\{1+m_r(p_r^2-r_1^2)\}(1-r_1^2)\cos\varphi + 2dm_r p_1 r_1 (1-r_1^2)\sin\varphi - \cos\varphi}$$

Substituting $C1 = 2dm_r p_1 r_1$, $C2 = 1+m_r(p_r^2-r_1^2)$ and $C3 = (1-r_1^2)$

$$B = \frac{F/k}{(\ C2\ C3\ -\ 1\ )\cos\varphi + C1\ C3\ \sin\varphi} \qquad \ldots\ldots (5.23)$$

The phase angle,φ of equation (5.23) can be obtained by substituting $\bar{\lambda}\sin\beta$ of equation (5.19) into equation

(5.21)

$$0 = (k + K - M\omega^2)\, B \sin\varphi - c\,\omega\, B \cos\varphi - k\left[\frac{k\, B \sin\varphi}{(k - m\omega^2)}\right]$$

$$0 = (k - m\omega^2)(k + K - M\omega^2) \sin\varphi - (k - m\omega^2)\, c\,\omega \cos\varphi - k^2 \sin\varphi$$

$$\tan\varphi = \frac{c\,\omega\,(k - m\omega^2)}{(k - m\omega^2)(k + K - M\omega^2) - k^2}$$

Dividing the numerator and the denominator by k^2 give

$$\tan\varphi = \frac{c\,(\omega/k)(1 - m\omega^2/k)}{(1 - m\omega^2/k)(1 + (K/k)_2 - M\omega^2/k) - 1}$$

$$= \frac{2dm_r p_r r_1 (1 - r_1^2)}{(1-r_1^2)\{(1+m_r(p_2^2-r_1^2)\} - 1}$$

and from which φ can be expressed as

$$\varphi = \tan^{-1}\left[\frac{C_1\ C_3}{C_2\ C_3 - 1}\right] \qquad \ldots\ldots (5.24)$$

To evaluate the relative phase angle, α of equation (5.22) equation (5.18) and (5.19) are multiplied by cos φ and sin φ respectively.

$$F\cos\varphi = (k - m\omega^2)\,\bar{A}\cos\beta\cos\varphi - k\,B\cos^2\varphi$$

$$0 = (k - m\omega^2)\,\bar{A}\sin\beta\sin\varphi - k\,B\sin^2\varphi$$

By summing up the later equations and introducing the trigonometric rules those equations give

$$F\cos\varphi = (k - m\omega^2)\,\bar{A}\cos(\varphi-\beta) - k\,B$$

Dividing by k the later equation gives

$$\bar{A} = \frac{(F/k)\cos\varphi + B}{(1-r_1^2)\cos\alpha} \qquad \ldots\ldots (5.25)$$

Equating (5.25) and (5.22) and introducing coefficients C_1, and C_3 gives

$$\{(F/k)\cos\varphi + B\}/C_3\cos\alpha = C_1\ B\ /\ \sin\alpha$$

where :

$$\alpha = \tan^{-1}\left[\frac{C_1\ C_3\ B}{(F/k)\cos\varphi + B}\right] \qquad \ldots\ldots (5.26)$$

5.3. Validity of the Proposed Method.

Based on the calibration experiments described in chapter (3.4) and established for those purposes the relative amplitudes are determined using equation (5.7) and (5.10). The relative amplitudes resulting from equation (5.7) rely on the ratio of the sin α / sin φ. The calculated relative phase angles, φ are dependent on the measured amplitudes, $\bar{A}$ and B and the phase angle, α. These dependencies do not seem very critical since signal processing is carried out carefully as described in (2.5) and chapter-4.

The measured relative displacements of the LVDT to the excited beam over the range of frequencies of the first mode shown in fig.(5.3) are parallel to the calculated relative amplitudes. A slight difference is possibly due to different calibration factor. The absolute displacements before resonance overestimate the relative displacements. In contrast this phenomena is reversed after resonance. The turning point represents a condition where the relative displacement, A is equal to the absolute displacement, $\bar{A}$. If the turning point is obtainable from the experiment then the relative phases can be determined from eq.(5.11) and eq.(5.10) respectively.

Further differences in the phase angles, as portrayed in fig.(5.4) for the same experiment, become significant about resonance. Those differences are obviously dependent on the amplitudes of the moving exciter mass and the excited beam.

A theoretical simulation of eq.(5.7) and eq.(5.10) over the range of excitations, i.e. 0 to π, is shown graphically in fig.(5.5) and fig.(5.6). Figure (5.5) indicates the sensitivity of the ratio of the relative to the absolute amplitudes, $A/\bar{A}$ over the phase of excitation, φ (0 to π). The higher the ratio of the absolute beam displacement to the relative amplitude of the moving exciter mass, $r = (B/A)$ then the higher the ratio, $A/\bar{A}$. This implies a means of obtaining the more significant differences between the absolute, $\bar{A}$ and the relative amplitude of the moving exciter mass, A. All curves in fig.(5.5) pass a value of $A/\bar{A} = 1$ but the intersection points of the curves moves towards the higher phase of excitation, φ as the increase of the value of r. Fig.(5.6) relates the relative phase of excitation, φ and the relative phase angle, $\beta = \varphi - \alpha$. The value of β becomes significant as the ratio, r is large. In addition the maximum relative phase angles, β also move towards the higher phase of excitation, φ.

Applying equations (5.22) to (5.26) for $m_r = 843.75$, $p_r = 14$ and d = 10% with exponentially decreasing force as shown in fig.(5.7) results in the graph of fig.(5.8) and

(5.9). Fig.(5.8) demonstrate the characteristics of the amplitude response of the beam,B and the absolute amplitude response of the moving exciter mass,$\bar{I}$. A significant drop occurs at about resonance as expected. The reflected force opposes the excitation force in such a way that it reduces the amplitudes of the excitation. Fig.(5.9) also reveals the characteristics of the relative phase angle,φ and the relative phase angle,β over the range of resonance. These later two figures are similar to the experimental results shown in fig.(3.8-A) and (3.8-B). This simulation does not show the experimental results to great accuracy due to the simplifications used in the model but the method can approximately describe the behaviour of any exciter including the mechanical exciter used. The AC-mechanical exciter has almost constant torque about the resonant frequencies. Due to the reflected force of the excited beam the out of balance mass movement was opposed. This was apparent as a decreasing speed/rotation of the out of balance mass. The reflected force reduces the force of excitation at resonance but it is not possible to achieve dynamic equilibrium as the force of excitation increases proportionally to the square of the frequency of excitation. This creates an unstable condition. Thus, increasing the frequency, by increasing input power, will only pass by unstable region so producing the jump phenomenon reported in chapter (3.4). The sensitivity of

the reflected force depends on the mass ratio, m_r, frequency ratio, p_r, and damping of the beam, d.

5.4. Proposed Corrections.

As output of vibration tests required to be normalised the problem of relating amplitudes and phases of the moving exciter mass to the excited structure will involve. Equations (5.9) and (5.10) can be employed for correcting experimental results. Thus, this involves the measurement of phases in presenting the frequency response. For practical purposes revisions of amplitude and phase are carried out only at the frequencies of interest.

In knowing the relative acceleration and the mass of the moving exciter mass the applied force is obtained by multiplying these later values. This applied force is used to normalise the whole output.

In modeling the beam the idealised force may not be ideal since it is affected by the reflected force of the excited beam. This reflected force can be applied in the model as a force moving in phase with the beam where the exciter is positioned.

5.5. Concluding Remarks.

The absolute-relative relationships of the amplitude and phase have been demonstrated. These relationships reveal an important role in the determination of the

resonance as well as the peak amplitude since relative analysis is of interest. Experimentally this requires two vibration pick-ups to obtain the relationships.

The force relationships of the exciter and the beam have also been demonstrated using the simple two degrees of freedom system. The existence of the jump phenomenon using the mechanical exciter as well as the reduction of the amplitude of the moving exciter mass using the magnetic vibrator has been demonstrated theoretically and experimentally. This phenomenon is of importance when dealing with experiments as well as mathematical models.

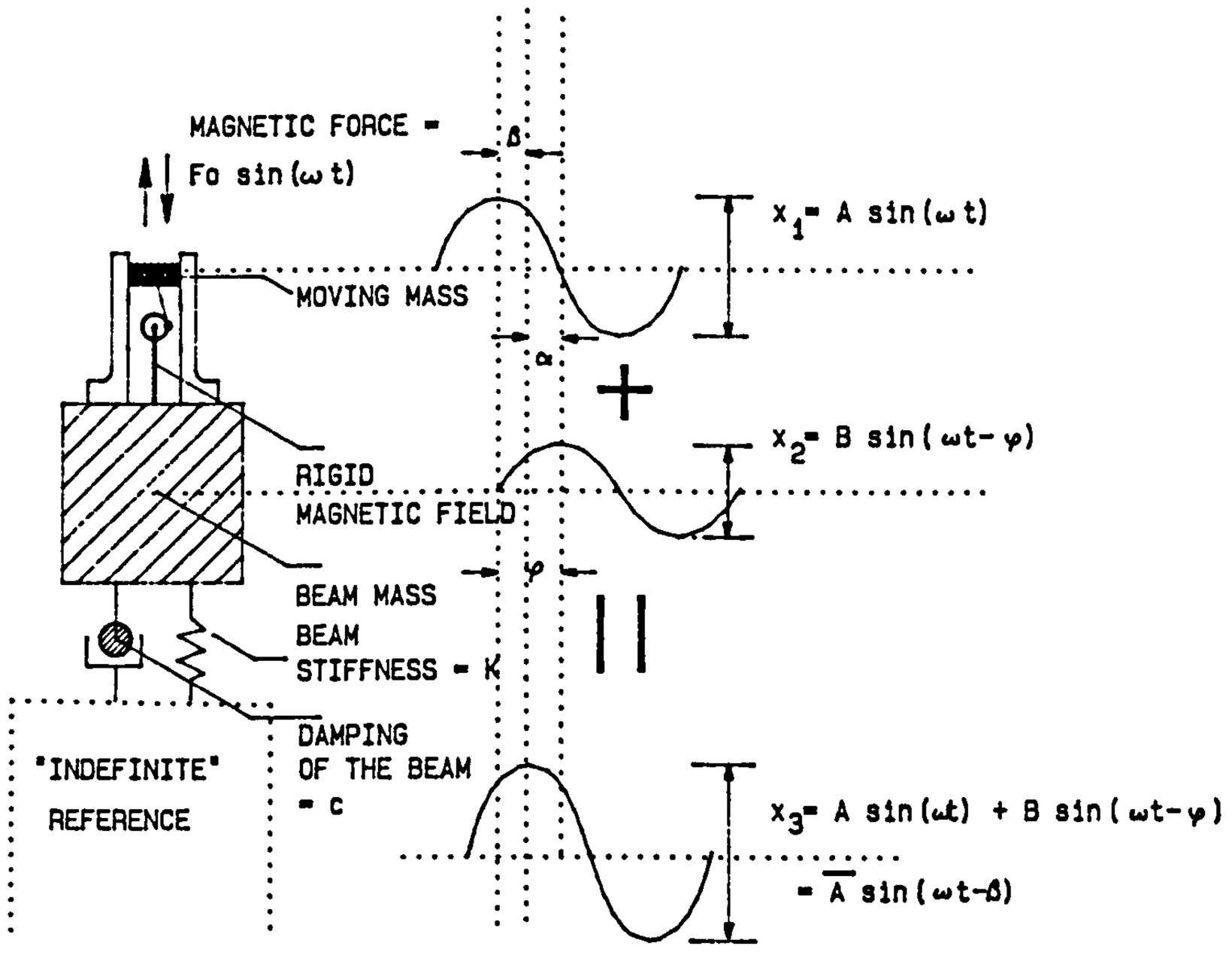

FIG.5.1.ABSOLUTE TO RELATIVE AMPLITUDES AND RELATIVE PHASES RELATIONSHIPS.

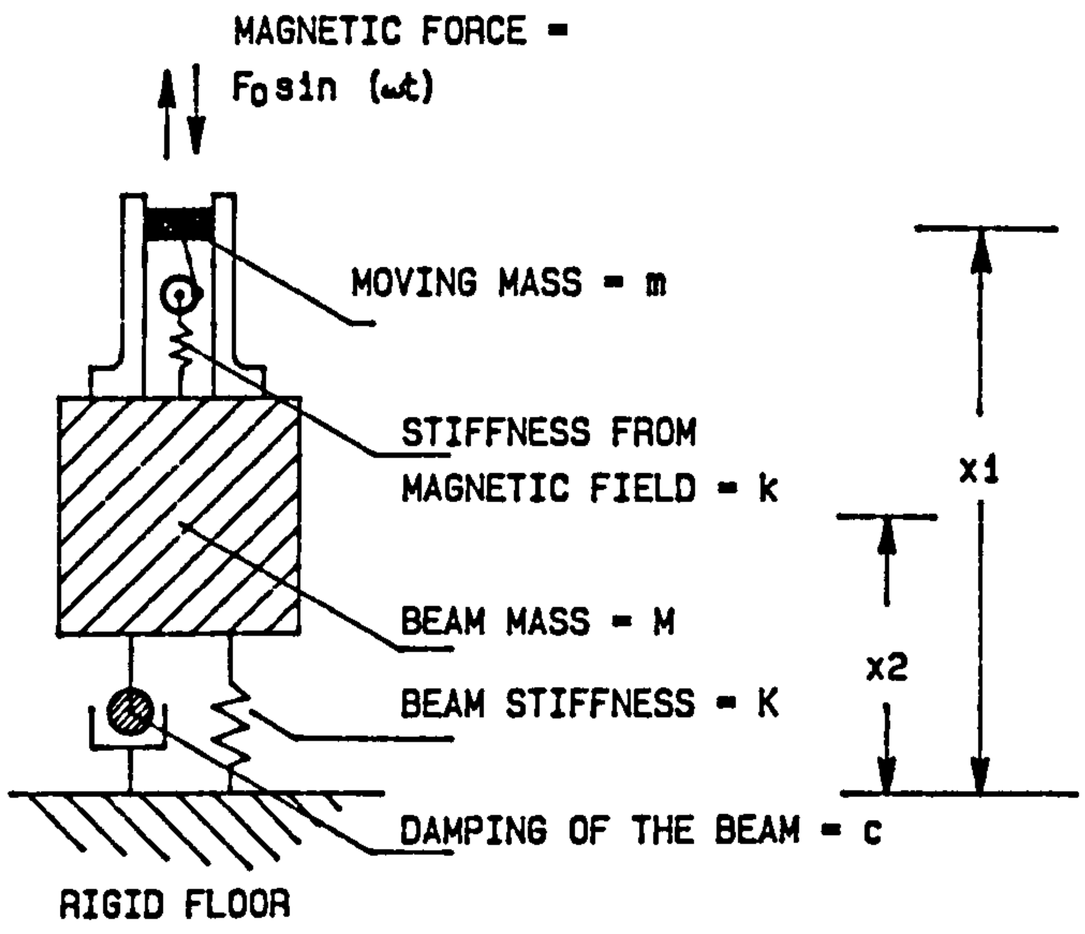

FIG.5.2.EFFECT OF APPLYING STIFFNESS FROM THE MAGNETIC FIELD ON THE FORCE OF THE MOVING MASS.

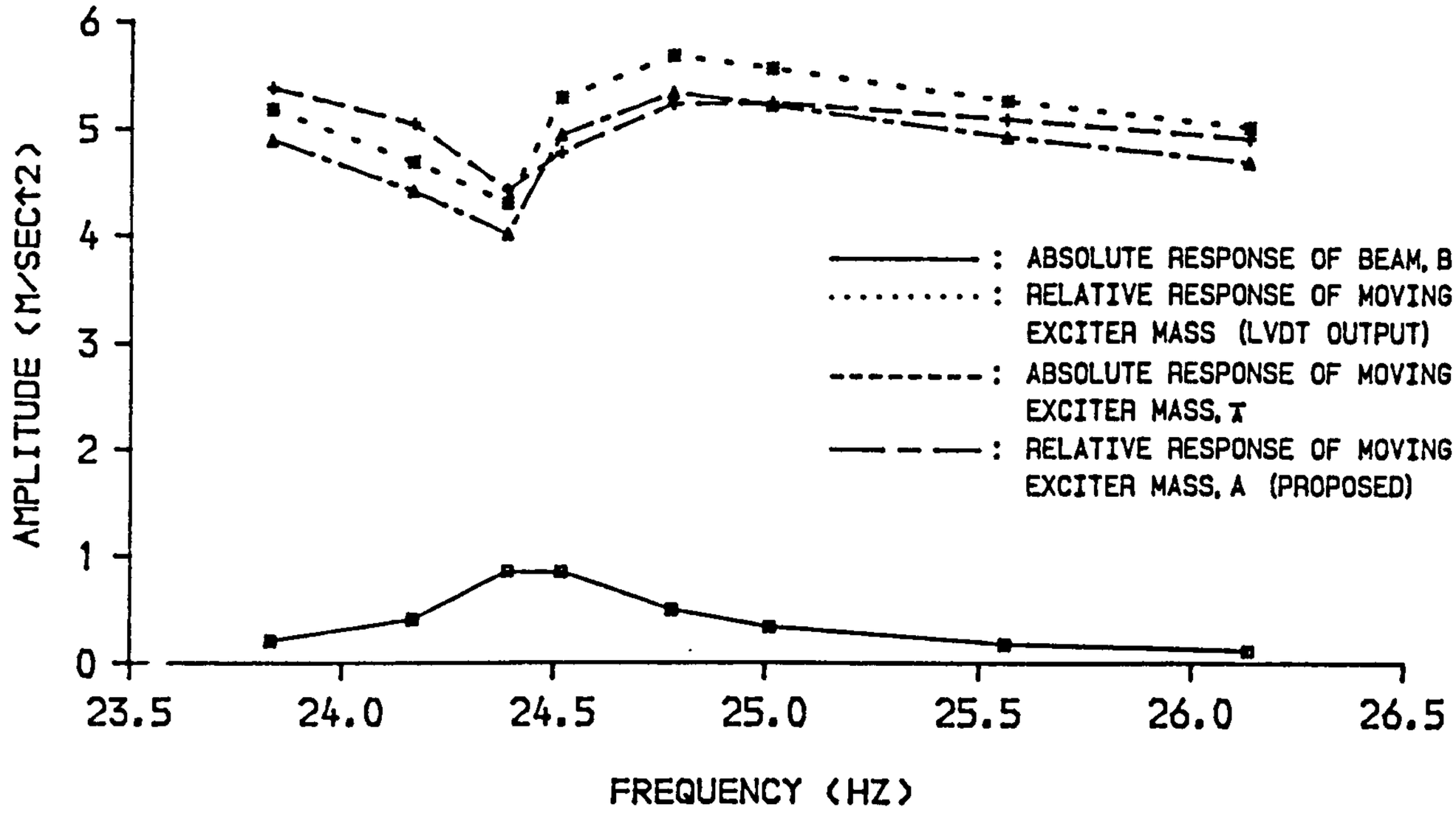

FIG.5.3. RESPONSES OF AMPLITUDE OF MOVING EXCITER MASS, LVDT AND BEAM-1 (FB/L1), SUBJECT TO A SET OF FORCES OF EXCITATION USING THE MAGNETIC EXCITER, FULLY BONDED, FIRST MODE

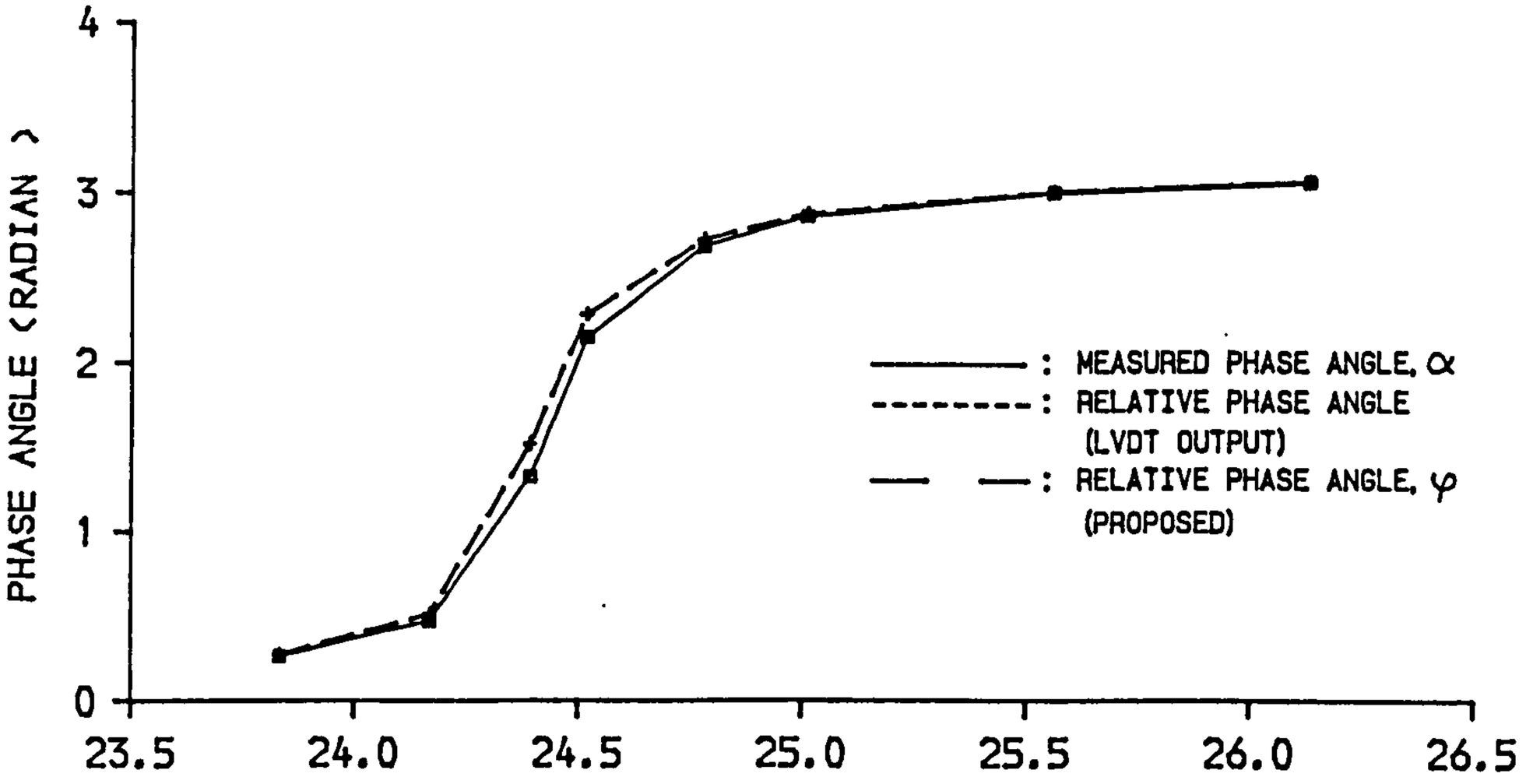

FIG.5.4. RESPONSES OF PHASE ANGLE OF MOVING EXCITER MASS TO BEAM-1 (FB/L1) (REFER TO FIG.5.3)

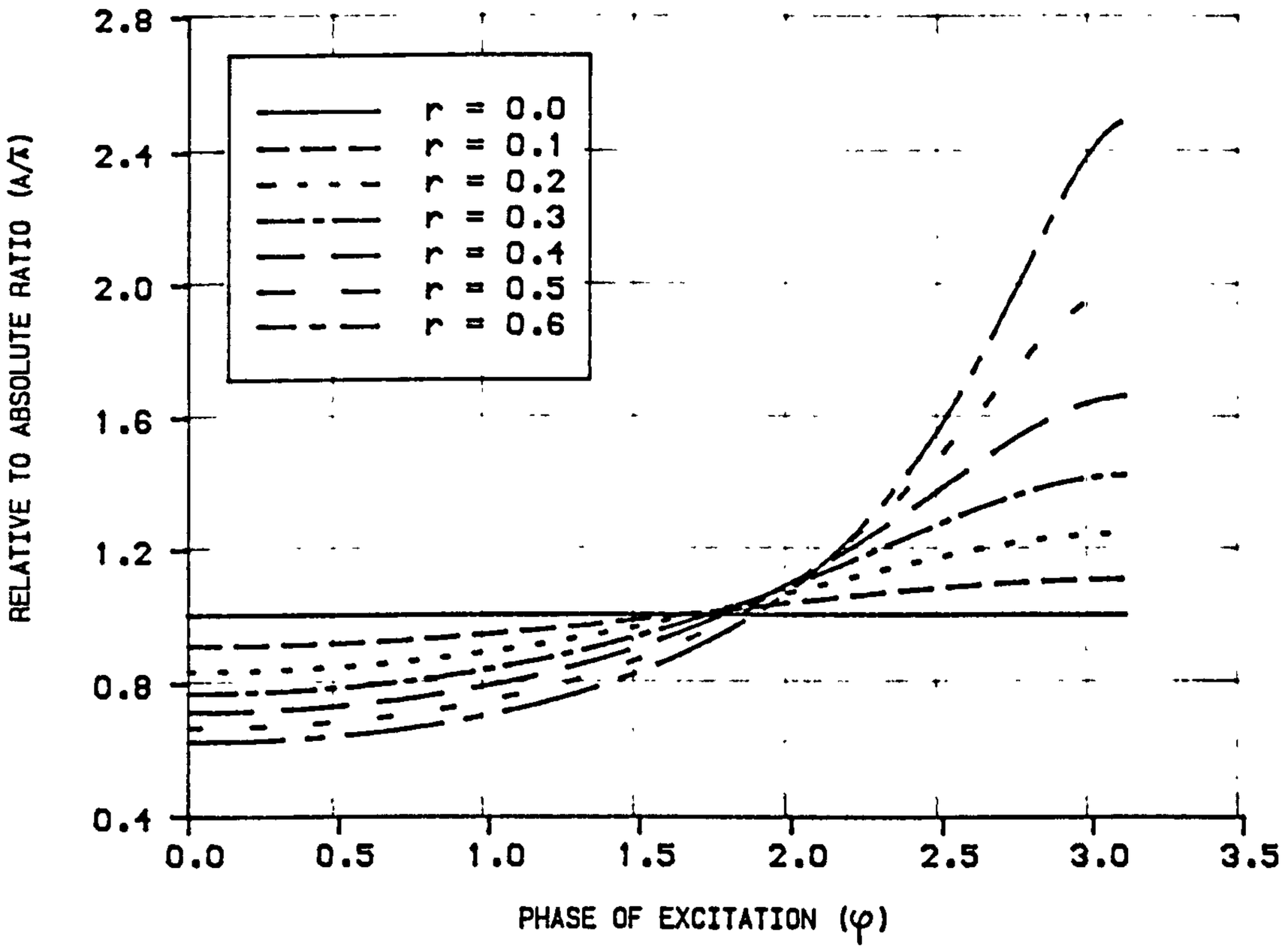

FIG.5.5.EFFECT OF AMPLITUDE OF EXCITED STRUCTURE TO AMPLITUDE OF THE MOVING EXCITER MASS.

[r = RELATIVE TO ABSOLUTE RATIO (B/A)]

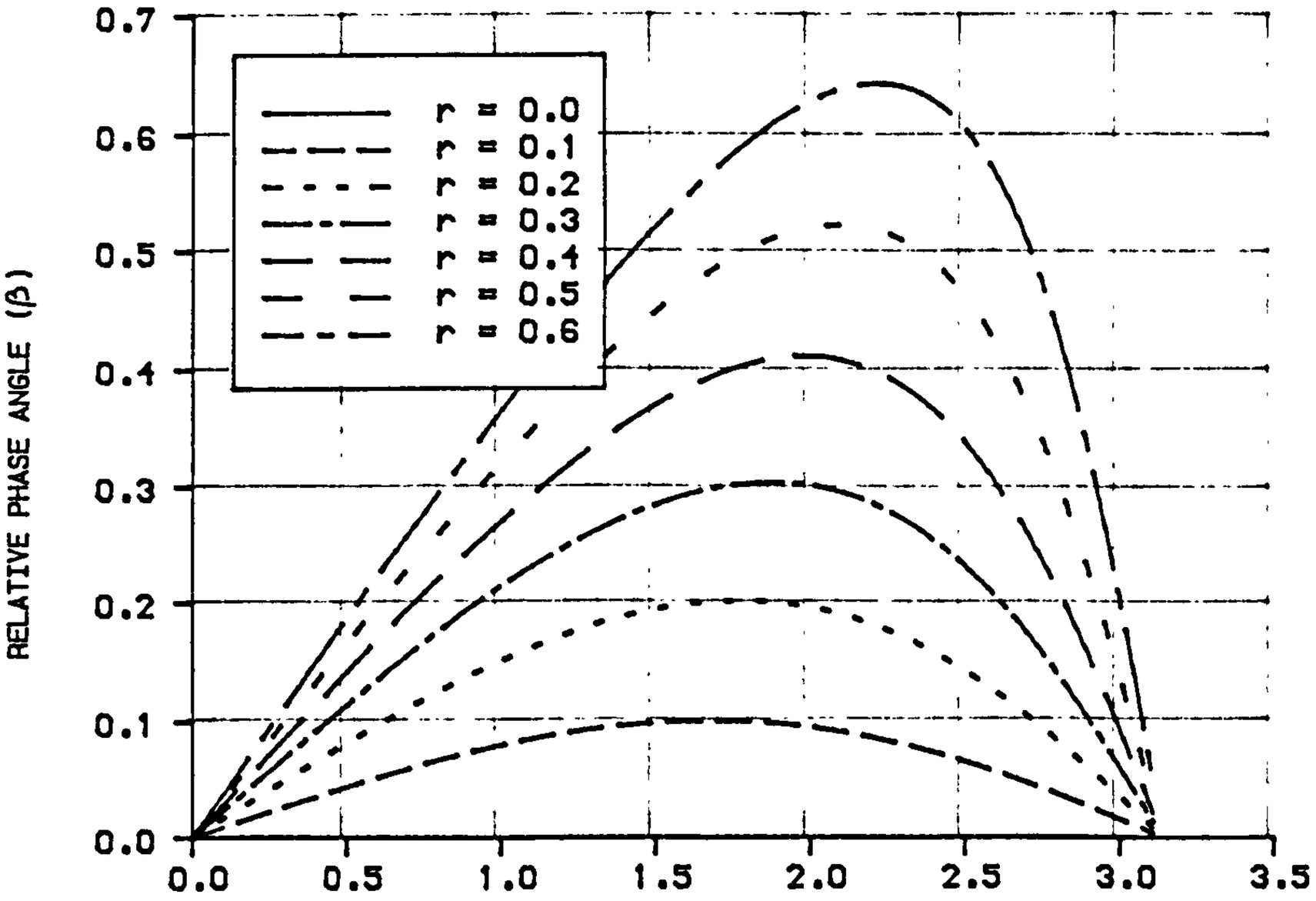

FIG.5.6.EFFECT OF AMPLITUDE OF EXCITED STRUCTURE TO RELATIVE SHIFTS OF PHASE ANGLE, β

[r = RELATIVE TO ABSOLUTE RATIO (B/A)]

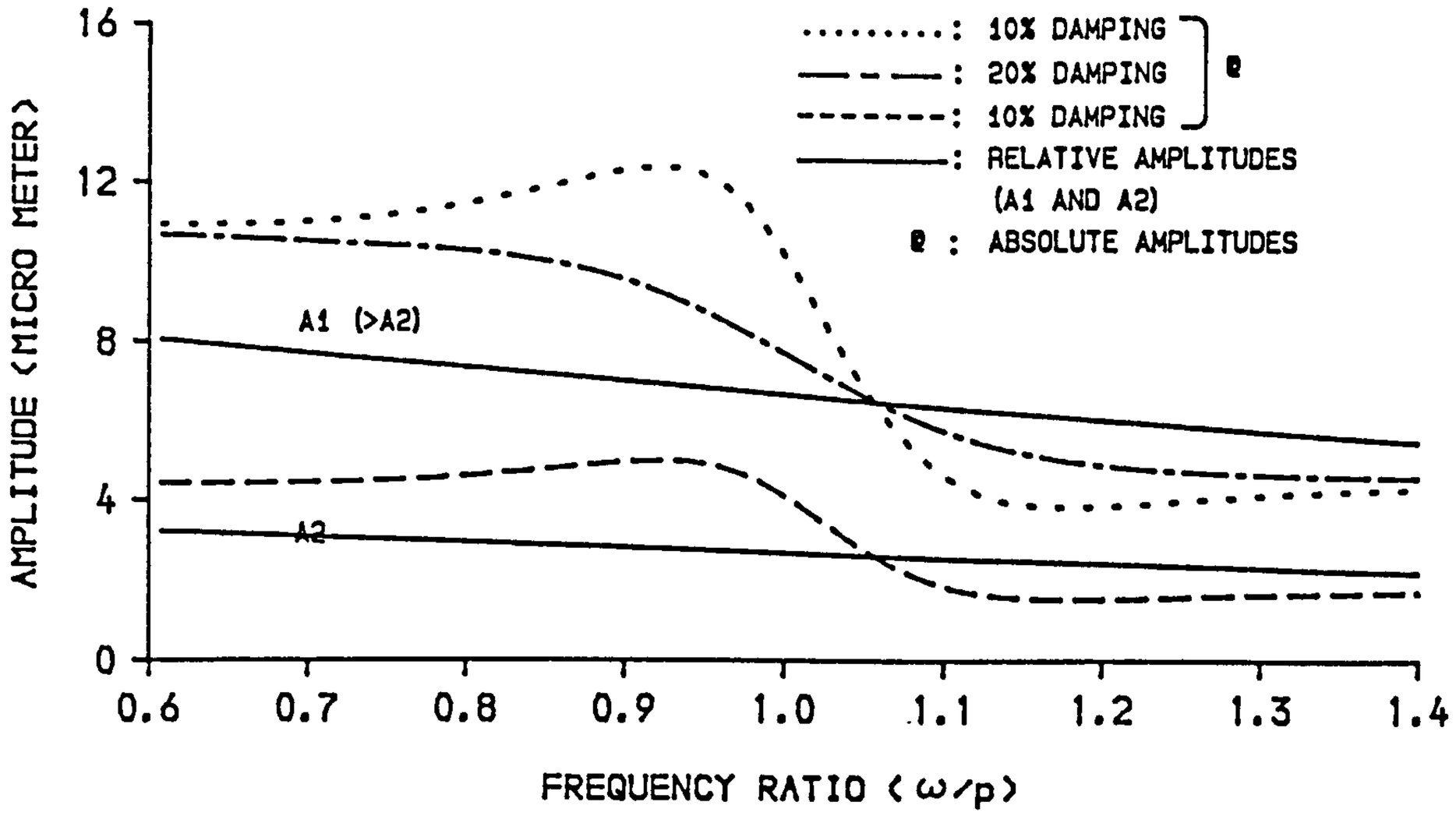

FIG.5.7.EFFECT OF DAMPING RATIOS ON ABSOLUTE AMPLITUDES AT DIFFERENT FORCES OF EXCITATION (ILLUSTRATION WAS CARRIED OUT ON A SINGLE DEGREE OF FREEDOM SYSTEM WITH m =843.75, p =14, d =10%, d =20%)

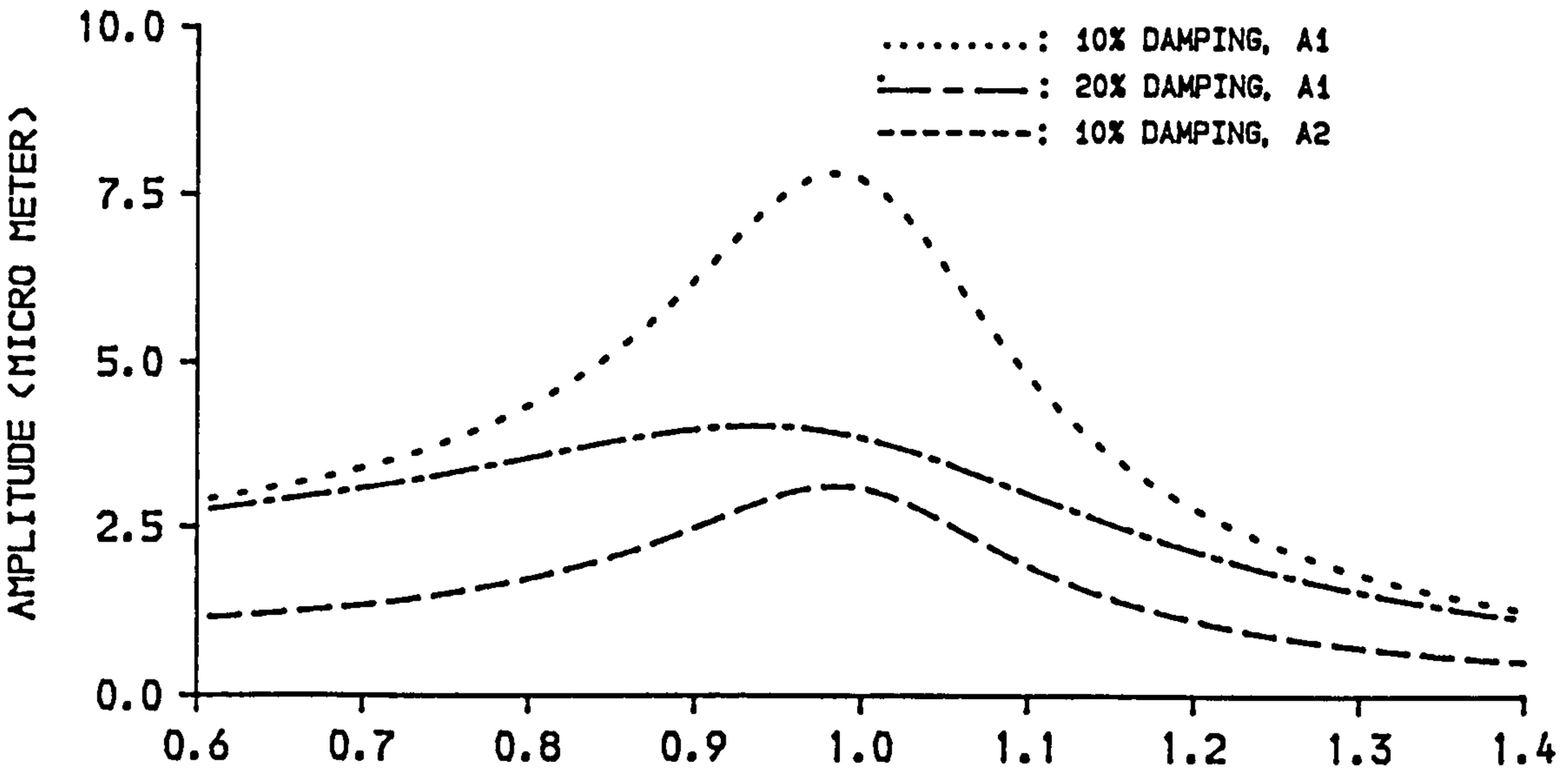

FIG.5.8.RESPONSE SPECTRA OF THE STRUCTURE (REFER TO FIG.5.7)

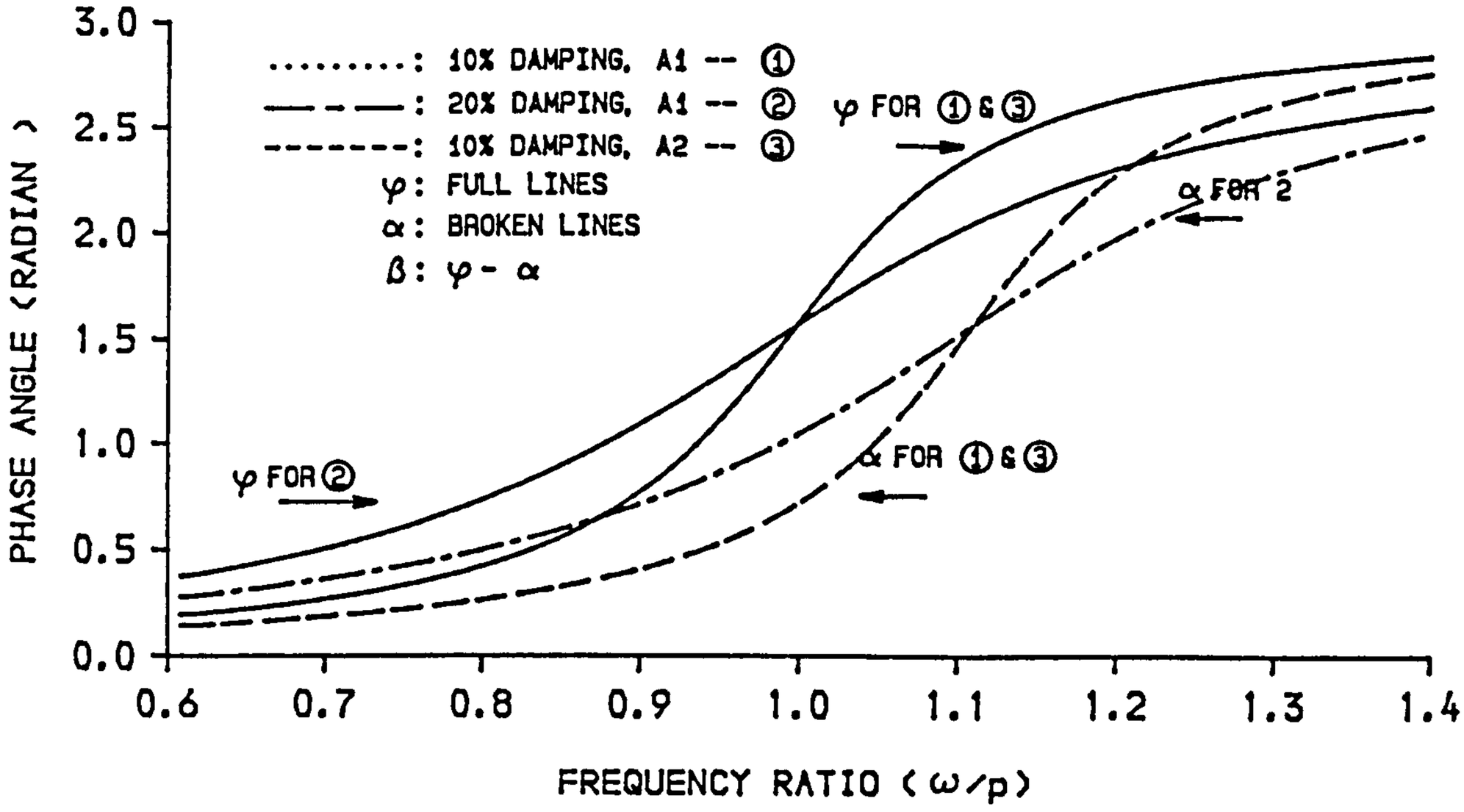

FIG.5.9.RESPONSE OF PHASE ANGLES, α , φ AND β (REFER TO FIG.5.7)

CHAPTER - 6

6. PROGRAMMING AND THE ALGORITHMS.

6.1. General.

Two computer programs have been developed. The purpose of one is to analyse the data from the experiments and the purpose of the other is to present the data as graphical output. The first program is linked to the radix mixed FFT routines installed in the VAX main frame and includes the development of the corrective coefficients on the determining frequencies and amplitudes discussed in chapter-4 and the FIR filter based on the IIR-Butterworth filter function discussed in chapter-2 and Appendix (D-1). Two algorithms are used to provide coefficients resulting from the long division process and coefficients resulting from a bilinear substitution into the polynomial function. These are installed in the program to complete the filter program routine. The fortran-77 program runs on the VAX main frame. The second program is linked to the UNIRAS-UNIRASPAK routines installed in the VAX to enable superimposed responses resulting from the first program to be plotted onto a single 4A-paper.

6.2. Programming.

6.2.1. First Program.

The input data for this program starts with a row containing a filename to describe the test. The second

row has the number of data points and the time interval between readings. These two values represent frequency resolution and the frequency range as mentioned in chapter-2. Most digitisers provide a facility to scale the analog input up or down to achieve a maximum accuracy in the digital output. The selection of the scaling or gain factors is of important in avoiding round off error as mentioned in chapters-2 and 3. These gain factors or scaling factors are included when running the digitiser program (which is a modification of the program example included in the package). After rearrangement of the output of the modified program example these gain factors are given in the third row of the data format as seen in table (6.1). The digitised data with the associated channel numbers is positioned on the fourth row and subsequent rows.

This first program is set up interactively in such a way that users can input other gain and converting factors associated with the amplifiers or signal conditioners, the accelerometers and the charge amplifiers used. These charge amplifiers have several controllers relating to the sensitivity of the accelerometers, converting factors (m/sec^2/unit output, or m/sec/unit output, or mm/unit output) and the gain factors (mV/ unit output). These later two factors are interactively included when running the program. If transducers do not require amplifiers unit input shall be included on the program.

Further interactive aspects to include the range of the frequency of interest which allows the selection of the maximum amplitude within a range. Otherwise inputting a zero frequency and any high frequency are acceptable.

If the time domain is of interest and the data is required to be filtered, further interactive input is included. Two main filter functions are installed in the program, i.e. low pass / high pass and band pass / band stop filters. Appropriate input should be given following the selection of the filter type such as the pass band (Hz), stop band (Hz), the minimum attenuation in the stop band (dB) and the number of coefficients considered. A quick report is displayed on the screen confirming the attenuations in the pass band and stop band frequencies according to the number of coefficients just included.

Output of the program is stored in several data files for further processing. The names of the data file are listed below.

1. ORIGINAL.DAT (data before filter processing)
2. FILTERED.DAT (data after filter processing)
3. SPECTRUM.DAT (spectrum after filter processing)
4. DBGAIN.DAT (impulse filter response in the frequency domain)
5. IMPULSE.DAT (impulse filter response in the time domain)

Output formats are shown in in table (6.2) to table

(6.6) and the listing program is given in Appendix (C-1).

6.2.1. Second Program.

This program is also designed interactively. The data format required is exactly the same as the output of the first program stored in SPECTRUM.DAT as seen in table (6.4). Several rows at the end of the data represent the peak amplitude and the associated frequencies in selected ranges included in the first program.

Several interactive input statements are required when running this program and this enables several X-Y axes (groups) to be created and positioned at certain levels. Each axis can accommodate several graphs. The GSURF routine within the UNIRAS-UNIRASPAK package is capable of creating superimposed graphs which can indicate the plotting order of the graphs. Results of this program are shown in chapter-7.

6.3. Algorithm for Determining Polynomial Coefficients.

The determination of polynomial coefficients arises when dealing with the bilinear transformation substitution on a polynomial equation on the linear discrete time system. Power [42] solved the problem in terms of ordinary matrices and matrices with symmetric properties, namely the Q-matrix, which were reported to considerably reduce the execution time in comparison with the classical algebraic method, i.e. substituting the

bilinear equation $s = \frac{z + 1}{z - 1}$ into the polynomial equation.s of degree n. Davis [43] commented, on the technique proposed by Power [42], that this technique was not the only alternative. Davis also commented that the technique required a matrix routine which was not fully described although he admitted that Power's proposal required a short execution time. Davis [43] proposed a simple substitution technique, namely synthetic addition, to solve the problem. This involved scaling, reciprocating and shifting of the magnitudes in such a way that no multiplication were required.

A slightly different problem from that described by Power [42] and Davis [43] will be examined in this chapter. Power [42] and Davis [43] started from a known polynomial equation such as

$$as^n + bs^{n-1} + cs^{n-2} + \ldots\ldots \text{ etc.} \qquad \ldots (6.1)$$

into which the bilinear transformation

$$s = \frac{z + 1}{z - 1} \qquad \ldots (6.2)$$

was then substituted and the coefficients of the new polynomial in Z-form were determined.

The author starts from known roots of the polynomial equation (6.1) which are established from the equation (2.20) as listed below.

$$a_k = e^{j(0.5n+0.5+k)\pi/n} \qquad \ldots (6.3)$$

Roots of equation (6.3) are substituted into a transfer function,H(s) described in chapter (2.5.7) comprising a set of element equations in the denominator

$$H(s) = \frac{1}{(s - a_1)(s - a_2)(s - a_3)(s-\ldots} \qquad \ldots (6.4)$$

Substituting the bilinear transformation (6.2) into equation (6.4) gives

$$H(z) = \frac{1}{\{(1-a_1)z - (1+a_1)\}\{(1-a_2)z - (1+a_2)\}\{\ldots}$$

$$= \frac{1}{(az - b)(cz - d)(ez - f)(gz - \ldots} \qquad \ldots (6.5)$$

Equation (6.5) shows that the bilinear transformation is a simple multiplication process of elementary linear equations. The problem is to find the coefficients of the polynomial equation itself. The number of elementary equations represent the order of the polynomial equation,n. The number of coefficients of the polynomial equation are then equal to (n+1).

Introducing : a = A(1),b = B(1)

c = A(2),d = B(2)

e = A(3),f = B(3) ..... etc.

into the denominator of equation (6.5), the multiplication process is carried out in several stages depending on the number of elementary equations substituted.

E.g : $y = (2x + 3)(4x - 2)(6x - 8)$

$= (8x^2 + 8x - 6)(6x - 8)$

$= (48x^3 - 16x^2 - 100x + 48)$

For many elementary equations this process may be easily understood from the diagram shown in fig.(6.1). The algorithm works as follows.

1. Let coefficients of the first elementary equation.A(1) be above the second elementary equation.A(2).

2. Three blocks of coefficient resulting from this multiplication are expected.
3. The first block is obtained by multiplying the first coefficients of those two elementary equations,A(1) and A(2).
4. The second block is obtained by cross multiplications of coefficients of those elementary equations,B(1)A(2) and B(2)A(1) and then sum them up.
5. The third block is obtained by multiplying the last coefficients of those elementary equations,B(1)B(2).
6. Further substitutions are made by repositioning the later coefficients (three blocks) as the first elementary equation and substituting the next equation as the second elementary equation. The process (1) to (5) is repeated with the exception that the process (4) is repeated for other intermediate coefficients after sliding the second elementary coefficients towards to the right.

A program in fortran-77 language was written for this purpose as follows.

```
C     DETERMINING COEFFICIENTS OF POLYNOMIALS
      PRINT *,'Order of Polynomial :'
      READ  *, N
      DO 10 J = 1,N
      READ  *, A(J),B(J)
10    CONTINUE
      X(1,1)  = A(1)
      X(1,2)  = B(1)
      DO 20 K = 2,N
      X(K,1)  = X(K-1,1)*A(K)
      X(K,K+1)= X(K-1,K)*B(K)
      DO 15 M = 2,K
      X(K,M)  = A(K)*X(K-1,M)+B(K)*X(K-1,M-1)
15    CONTINUE
```

```
20    CONTINUE
      END
```

Notes :

```
X(K.1)   = first coefficient of step K
X(K.K+1)= last coefficient of step K
X(K.M)   = intermediate coefficients of step K
```

6.4. Long Division Algorithm.

To achieve an inverse transform of the transfer function.H(z) described in equation (6.5) a simple form is required for digital computational reasons. Given a general term of the rational function as follows

$$H(z) = \frac{B(0)z^3 + B(1)z^2 + B(2)z + B(3) \quad ..etc.}{A(0)z^3 + A(1)z^2 + A(2)z + A(3) \quad ..etc.} \qquad (6.6)$$

An alterative solution to the determination of the coefficients of the polynomial equation (6.6) is by applying a classical long division technique. This technique is an ordinary division. The name implied by this technique requires an algorithm to be processed by the computer program. Such a computer program was set up by Kamen in reference [44] but the author was not successful in running this program. This may be due to the mistyped program listing. An attempt to investigate the problem was not made due to the algorithm being unavailable.

Therefore, an algorithm is developed in this chapter on the basis of the long division technique. The technique restricts the order of the polynomial equation of the numerator to not greater than the order of the polynomial equation of the denominator.

The simplest transformation rule in the Z-plane as

described in many references such as in [44] is carried out by equating coefficients of two identical functions. The resulting polynomial equation (6.6) is given in (6.7) below

$$H(z) = \bar{A}\, z^{0} + \bar{B}\, z^{-1} + \bar{C}\, z^{-2} + \bar{D}\, z^{-3} + \quad \ldots (6.7)$$

$$H(z) = x(0T)z^{0} + x(1T)z^{-1} + x(2T)z^{-2} + x(3T)z^{-3} + \quad (6.8)$$

where : T = interval time

From equation (6.7) and (6.8) the digital filter function.x with respect to time (kT) can be established. This time domain digital filter function is convergent at a large number of T.

E.g : $H(z) = \dfrac{2z^{2} + 3z + 5}{3z^{3} + 5z^{2} + z + 3}$

denominator | numerator | results

$3z^{3}+5z^{2}+z+3 \;|\; 2z^{2}+3z+5 \;|\; \frac{2}{3}z^{-1} + \frac{1}{9}z^{-2} + \frac{44}{27}z^{-3}$ .. etc.

$2z^{2} + \frac{10}{3}z + \frac{2}{3} + 2z^{-1}$

$-\frac{1}{3}z + \frac{13}{3} - 2z^{-1}$

$\frac{1}{3}z + \frac{5}{9} + \frac{1}{9}z^{-1} + \frac{1}{3}z^{-2}$

$\frac{44}{9} - \frac{17}{9}z^{-1} + \frac{1}{3}z^{-2}$

$\frac{44}{9} + \frac{220}{27}z^{-1} + \frac{44}{27}z^{-2}$

..... etc.

For higher orders of polynomial equation the division process is explained in the algorithm shown in fig.(6.2). The algorithm works as follows.

1. The first coefficient of the resulting equation is obtained by dividing coefficients of the same and highest order of the numerator and the denominator. B(0)/A(0).

2. The coefficients of the intermediate orders of the resulting equation are obtained by cross multiplications of the coefficients of the intermediate orders in question and the coefficients of the highest orders and then subtract them up.
3. Process (2) is repeated as needed for to obtain acceptably accurate result. Further discussion on this can be obtained in Appendix D-1.

A simple program can be set up using the algorithm.

```
C       DETERMINING COEFFICIENTS OF RATIONAL FUNCTIONS.
        PRINT *,'HIGHEST ORDER POLYNOMIAL :'
        READ  *, N
        PRINT *,'NUMBER OF COEFFICIENTS EXPECTED :'
        READ  *, J
        PRINT *,'COEFFS. OF NUMERATOR AND DENOMINATOR '
        DO 10 I = 0,N
        READ  *, B(I),A(I)
        V(0,I)  = B(I)
        S(I)    = A(I)/A(0)
10      CONTINUE
        DO 20 K = 1,J
        DO 30 I = 0,N-1
        V(K,N)  = 0.0
        V(K,I)  = S(0)*V(K-1,I+1) - S(I+1)*V(K-1,0)
30      CONTINUE
        V(K-1,0)  = V(K-1,0)/A(0)
20      CONTINUE
        END
```

Notes :

V(K-1,0)= coefficients of the new polynomial equation,
for K = 1,2,3,4 ..... etc.
S(I) = scaling factor.

6.5. Comparisons of Computing Time.

The first algorithm discussed in chapter (6.3) requires multiplications and additions. In comparison with the available techniques quoted by Davis [43] the technique proposed is much simpler as shown in the

program written above. The ordinary matrix technique proposed by Power [42] required similar number of multiplications but the number of additions is twice that required by the proposed technique. The total multiplications and additions proposed are similar to the Q-matrix with symmetric properties. The synthetic division technique proposed by Davis [43] is still superior in comparison with the proposed technique and the Ordinary matrix proposed by Power [42]. These comparisons are shown in the table (6.7).

The number of multiplication and addition of the proposed technique are respectively given

$$\text{Number of multiplication} = N^2 - N - 2$$

$$\text{Number of addition} = (N^2 - 3N + 2)/2$$

where : N = number of coefficients of a polynomial equation of order n ($N = n + 1$).

The proposed technique has an advantage over the available techniques in that the roots of the polynomial are already determined from equation (6.3) therefore, the bilinear transformation is easily carried out within the elementary equations. As the polynomial equation can be established from the elementary equations the coefficients in question are automatically obtainable. This process is different from those mentioned by Power and Davis [42,43] where the polynomial equation was already established and the bilinear substitution was carried out within the established polynomial. This

implies that the proposed technique has a specific use when the roots of the polynomial are already established; such as in the case of the IIR-Butterworth filter function.

The second algorithm described in chapter (6.4) requires multiplications. subtraction and division. Instead of the dependency on the order of the polynomial.n this algorithm also depends on the number coefficients requested,J which converge for J=∞. Those arithmetic processes can be presented in the formula

Number of divisions = J

Number of multiplications = 2J(N-1)

Number of subtractions = J(N-1)

The aim of producing a series in filter processing is that truncation can be applied to reduce transience and transformations can also be carried out in a more simple way. The effect of the truncation of the resulting series applied to the filter processing in the time domain, i.e. by applying inadequate number to J. will reduce dB gain in the stop band and increase dB gain in the pass band. Physically this reduces amplitudes of the signal passed and may still allow a certain percentage amplitude of the signal stopped to be embedded in the signal passed.

6.6. Concluding Remarks.

Instead of using Fast Fourier Convolution routines installed in the VAX computer main frame, the program requires two algorithms developed in this chapter. The comparison with other algorithms has been demonstrated. The benefit of the proposed algorithm is on its simple programming and that it may be used for any problems concerned with determining the coefficients of a polynomial equation although this will be efficient if the roots of the polynomial equation in question are given.

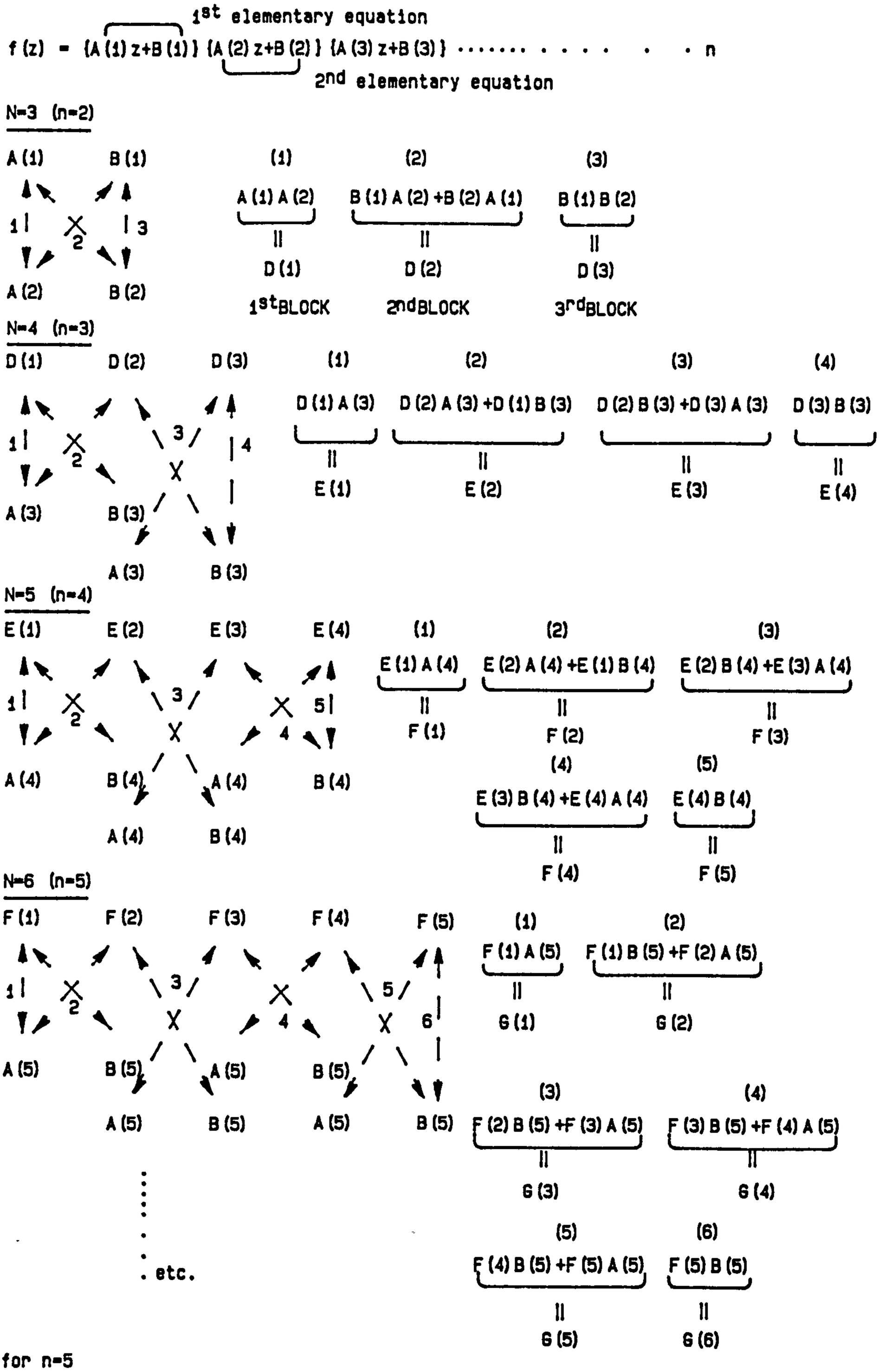

for n=5

$$f(z) = G(1)z^5 + G(2)z^4 + G(3)z^3 + G(4)z^2 + G(5)z^1 + G(6)z^0$$

FIG.6.1.ALGORITHM FOR DETERMINING COEFFICIENTS OF POLYNOMIAL EQUATION FROM ELEMENTARY EQUATIONS.

$$H(z) = \frac{B(1+0)\,z^{k} + B(1+1)\,z^{k-1} + B(1+2)\,z^{k-2} + B(1+3)\,z^{k-3} \quad B(n)\,z^{0}}{A(0)\,z^{n} + A(1)\,z^{n-1} + A(2)\,z^{n-2} + A(3)\,z^{n-3} + \cdots A(n)\,z^{0}} \qquad \text{for } k \leqslant n, \quad l = n-k$$

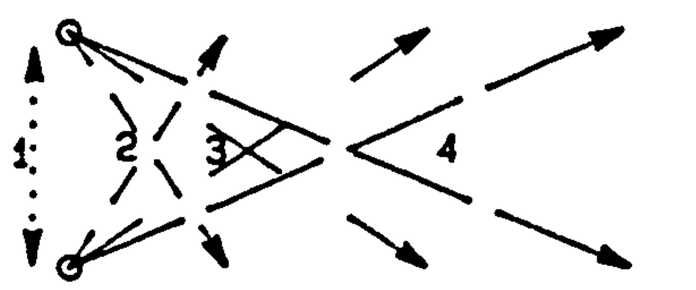

(1) $\dfrac{B(0)}{A(0)}$

(2) $\dfrac{B(1)\,A(0) - A(1)\,B(0)}{A(0)} = B^{1}(0)$

(3) $\dfrac{B(2)\,A(0) - A(2)\,B(0)}{A(0)} = B^{1}(1)$

(4) $\dfrac{B(3)\,A(0) - A(3)\,B(0)}{A(0)} = B^{1}(2)$ ..... etc.

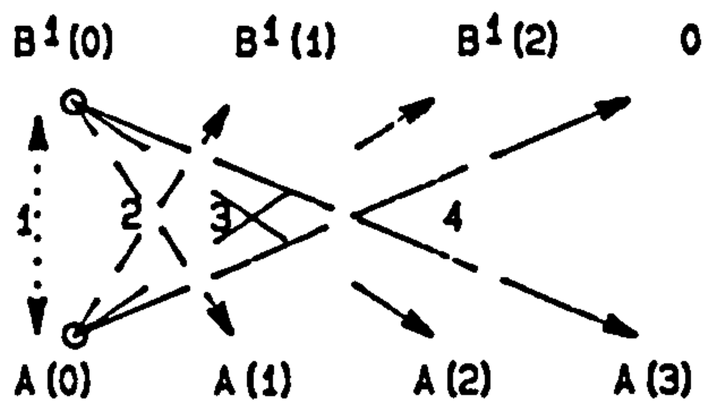

(1) $\dfrac{B^{1}(0)}{A(0)}$

(2) $\dfrac{B^{1}(1)\,A(0) - A(1)\,B^{1}(0)}{A(0)} = B^{2}(0)$

(3) $\dfrac{B^{1}(2)\,A(0) - A(2)\,B^{1}(0)}{A(0)} = B^{2}(1)$

(4) $\dfrac{0\,A(0) - A(3)\,B^{1}(0)}{A(0)} = B^{2}(2)$ ..... etc.

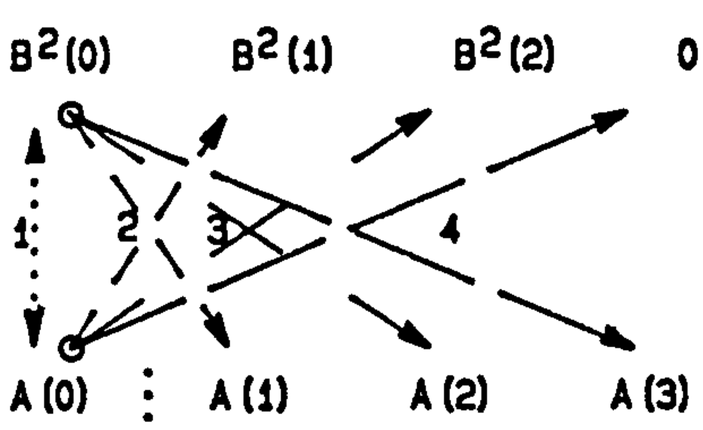

(1) $\dfrac{B^{2}(0)}{A(0)}$

(2) $\dfrac{B^{2}(1)\,A(0) - A(1)\,B^{2}(0)}{A(0)} = B^{3}(0)$

(3) $\dfrac{B^{2}(2)\,A(0) - A(2)\,B^{2}(0)}{A(0)} = B^{3}(1)$

(4) $\dfrac{0\,A(0) - A(3)\,B^{2}(0)}{A(0)} = B^{3}(2)$ ..... etc.

. etc.

$$H(z) = \frac{B(0)}{A(0)}\,z^{0} + \frac{B^{1}(0)}{A(0)}\,z^{-1} + \frac{B^{2}(0)}{A(0)}\,z^{-2} + \cdots\cdots$$

Notes :

..... : DIVISION

— — — : MULTIPLICATION

FIG.6.2. ALGORITHM FOR DETERMINING COEFFICIENTS OF POLYNOMIAL EQUATION FROM RATIONAL FUNCTION.

Table 6.1.Data Input

TEST *(file name)*				
400*(number of data)*		1.56	*(interval time in msec)*	
1.25	2.50	1.25	0.675	*(gain factor)*
1194	-315	-91	-149	*(integer data)*
757	-649	-38	-1000	
-178	-116	49	-1210	
(ch-1)	*(ch-2)*	*(ch-3)*	*(ch-4)*	

Table 6.2.Original Digital Signal

0.0000E+00	1.4915	*Gain factors and converting factors are applied in this data*
2.0300E-03	1.2293	
4.0600E-03	0.6271	
6.0900E-03	0.0862	
(time in sec)	*(amplitude)*	

Table.6.3.Filtered Data

0.0000E+00	0.1142
2.0300E-03	0.4191
4.0600E-03	0.6827
6.0900E-03	0.8796
(time in sec)	*(amplitude)*

Table.6.4.Spectrum Data.

TEST *(file name)*			
400 *(number of data)*		2 *(number of peak amplitudes)*	
1	0.0000	0.0000	0.0000
2.	1.2315	0.0069	-0.0072
3.	2.4630	0.0069	-0.0145
4.	3.6945	0.0071	-0.0291
⋮	⋮	⋮	⋮
400.	325.3458	0.0034	0.00233
1.	25.0023	1.0034	*associated number of peak amplitudes*
2.	75.4988	0.5000	
	(frequency)	*(amplitude)*	*(phase angle)*

Table.6.5.dB Gain Data.

1	0.0000	0.0000	0.0993	-0.01440
2.	0.0157	1.2315	0.9886	-0.00990
3.	0.0314	2.4630	1.0001	0.00087
4.	0.0471	3.6945	1.0012	0.01117
	(angular frequency)	*(analog frequency)*	*(gain factor)*	*(gain factor-dB)*

Table.6.6.Impulse Data.

1	5.6774E-06
2	7.6007E-05
3	4.9461E-04
4	2.0979E-03
5	6.5649E-03
	(amplitude)

Table 6.7. Comparison of the Results of Several Techniques

N	(A) Q-Matrix		(B) Synthetic Division		(C)	
	Mult.	Add.	Mult.	Add.	Mult.	Add.
5	25 (9)	20	0	30	18	6
10	100 (40)	90	0	110	88	36
15	225(104)	210	0	240	208	91
50	2500(1200)	2450	0	2550	2448	1176

Notes :
n = order of polynomial equation
A = proposed by Power [42]
B = proposed by Davis [43]
C = proposed by Author
( )= using symmetry properties

CHAPTER - 7

7. TEST RESULTS AND ANALYSIS OF VIBRATION TESTS.

7.1. General.

This chapter will discuss responses to the vibration tests described in chapter-3. The relative force of the moving exciter mass to the beam discussed in chapter-5 will be included in the analyses of the normalised response of the beams. The frequencies, amplitudes and percentage damping of the non-linear soft spring system are force dependent [6,13,15,16,21]. This dependency for the first mode of the concrete beam models will be described in this chapter and a linear frequency approximation will be applied on the basis of the experimental data described in chapter-3. Polar diagrams with ellipse or arc curves fitted and isochrones emphasising the non-linear behaviour will be described. The false selection of the peak amplitudes which may result from the experiment will also be dealt with. Several diagrams relating conditions of the beam to the dynamic parameters are presented where the flexural and diagonal splitting crack patterns can be identified.

Four to five responses of each vibration mode representing four to five conditions of the beam subjected to successively increasing flexural or diagonal splitting crack patterns will be analysed. Three vibration modes at each beam at six positions will be displayed in frequency responses. The characteristics of

the polar diagrams for the first, second and the third modes will be analysed respectively from the accelerometers at mid span, a quarter span and at a sixth span. Forces of excitation for the related responses are shown in appendix-E and the summary of those forces, the dynamic and static properties are presented in table (7.1) to table (7.3).

7.2. Effect of Non-linear Soft Spring Behaviour.

The three sets of force of excitation at two extreme conditions, i.e. intact and severe damaged beams, described in chapter-3 displayed the non-linear stiffness and non-linear damping. The non-linear stiffness was apparently greater at the severe damaged beam whilst the non-linear damping relied on the specific crack patterns. These non-linearities can be identified from the force-amplitude and force- frequency graphs. If the orgin of the graphs are not produced interpretations of the non-linearities may not be carried out simply.

Fig.(7.1) displays several possibilities which may occur in the experiments. Fig.(7.1.a) represents a linear spring with viscous or hysteretic damping systems where resonant amplitudes are linearly proportional to the forces of excitation. This system demonstrates the independence of the resonant frequency on the force of excitation. The related normalised graph displays a linear vertical line.

Fig.(7.1.b) represents the behaviour of systems with non-linear soft spring and viscous or hysteretic damping. This is clearly recognised in the normalised graph as an inclined line towards the right. The decrease of the resonant frequency will further confirm the existence of this non-linear soft spring behaviour. The third graph shown in fig.(7.1.c) displays the behaviour of systems with linear stiffness and non-linear damping. These later systems can be recognised in the normalised graph as line inclined towards the left. This graph can also represent the behaviour of hard spring systems. Thus, the recognition of frequency changes will confirm the behaviour of the system. A mixture of those figures possibly occurs in the real structure such as illustrated by the typical experiment results in fig.(7.2), (7.3) and (7.4).

Three sets of force of excitation resulted in three resonant frequencies with three peak amplitudes. Those parameters will be analysed in this chapter. The non-normalised graph in fig.(7.2) indicates that with the same force of excitation the beam with severe cracks, shown by the broken line, resulted in a lower peak amplitude compared with the intact beam, shown by the full line. The mixed non-linearity is not as clearly indicated in the normalised graph shown in fig.(7.3). The related normalised curves display similar patterns. The inclining broken line towards the left is recognised

as increasing non-linear damping.

This also happened on the intact beam as shown by the full line. The slightly inclined lines towards the left confirms the low degree of non-linear damping as well as non-linear soft spring behaviour. These hypotheses are further confirmed by the changes in the resonant frequencies as shown in fig.(7.4). As the force of excitation is increased the resonant frequency decreased. Parabolic fitted curves may be applied for the purpose of practical interpolations. Furthermore checks can be carried out from an examination of the polar diagrams shown in fig.(7.5) and (7.6).

Characteristics of the equipment have been described in chapter-3. The phase characteristic of the accelerometers measuring phase angles indicated that a shift in the phase angle was influenced by the amplitude characteristics. A small shift was executed by the proposed formulae described in chapter-4 at about 25Hz and about 10 degree shift was obtained at 100 Hz. Therefore, true phase angles are expected at the first modes and slightly rotated counter clock wise polar diagrams are expected at the second modes. Almost circular polar diagrams with maximum arc spacings showing the resonant frequencies [15] confirm the existence of the viscous damping and the small non-linear soft spring behaviour respectively of the intact beam. A more distorted circle is found for the severely damaged beam

especially at the higher force of excitation. Thus, a mixture of the non-linear soft spring with non-linear damping is possibly possessed by this beam.

7.3. Proposed Linear Correction.

From the experimental data shown in fig.(7.2) to (7.4) typical parabolic fitted curves can be established. Knowing the parabolic curves may be fitted relating force and the resonant frequencies at two conditions, i.e. on the intact and damaged beams, the intermediate frequencies at different forces of excitation may be interpolated linearly using a formula as shown in appendix (E-5.A). The resonant frequencies are stiffness dependant. Since the non-linear soft spring behaviour is exhibited in this experiment the higher force of excitation results in the lower stiffness due to the opening cracks. The resonant amplitudes which are normally indicated by the peak amplitudes are stiffness and damping dependant. The non-linear damping and non-linear stiffness affecting the resonant amplitudes as shown in fig.(7.3) possibly follow a typical parabolic curve too. The typical parabolic curve can be established from the experimental data for the two conditions of beam. Linear amplitude interpolations can then be applied for different forces of excitation using a formula as shown in appendix (E-5.B). The dependency of the peak amplitudes on the two parameters implies that

at higher forces of excitation the fitted curves based on three sets of force of excitation may be no longer valid due to the predominant effect of the non-linear soft spring behaviour which increases the lean of the curves towards the right. These linear approximations are applied on the results of all first modes only as shown in fig.(7.7) to (7.10). Slightly improvements on the resonant amplitudes and frequencies revealed that the different forces of excitation had little effects on the resonant frequencies and amplitudes.

7.4. Beams Containing Flexural Cracks.

7.4.1. Fully bonded beam (FB/L1).

Normalised responses for the first mode of the beam subjected to the four sets of similar force of excitation as shown in appendix (E.1.1) are displayed in fig.(7.11). The forces of excitation are determined by multiplying the relative accelerations and the mass of the moving exciter mass which was set to 128.53 grams. These accelerations were controlled manually from the integral amplifier. The output of the amplifier could not be constantly managed as shown in appendix (E-1.2) and (E-1.3). However, the results of the normalised responses will be not greatly affected.

The response shown in fig.(7.11) by the intact beam and the almost perfect circle of polar diagram in fig.(7.14.A) indicate that the beam at this stage

possessed viscous damping with little non-linear soft spring behaviour. After applying the first loading stage the resonant frequency decreased sharply followed by a decrease in the resonant amplitude. The induced crack apparently increased the damping, so reducing the amplitude at resonance as shown in the second response. The slightly elliptically distorted polar diagram in fig.(7.14.B) which is theoretically associated with higher polynomial damping phenomena [45] confirms the existence of the increased damping. Furthermore the second loading stage resulted in a slight change of the resonant frequency as well as in the resonant amplitude. The more distorted polar diagram in fig.(7.14.C) indicates that higher damping controlled the amplitude at resonance. The third loading stage produced more wide open cracks. This apparently reduced non-linear damping which is indicated by the last response and the associated polar diagram as an increase in the resonant amplitude and the almost circular polar diagram. Details of those parameters are summarised in table (7.1).

Response spectra on the second mode of the beam are displayed in fig.(7.12). A different trend from the first mode vibration test is displayed by these responses. The imposed flexural cracks resulted in higher resonant amplitudes. This apparently indicated small increase in damping and the presence of the lower stiffness is predominant. Furthermore checks can be made

on the associated polar diagrams shown in fig.(7.15). The polar diagrams rather shift in origin position. These were due to the different phase characteristics of the accelerometers measuring phase angles as described in chapter-3. Since a constant shift was involved within the range of frequency investigated this would not affect the interpretation of the polar diagrams. Almost circular polar diagrams were possessed by this beam at the second mode especially for the intact beam and after the third loading stage. This implied that almost viscous damping with possibly low non-linear soft spring behaviours existed over all the loading stages. Sets of force of excitation and the detail values are shown in appendix (E-1.2) and table (7.2).

The third response spectra of the four sets of force of excitation shown in appendix (E-1.3) are displayed in fig.(7.13). Higher damping is indicated from the spectra by way of a flatterer response. Several pseudo responses [14] surrounding the main response increase the complexity of the system and analysis. The opening and closing of cracks is the possibility greatest causing this phenomenon. The related polar diagrams of the response spectra displayed in fig.(7.16) show irregular patterns and distorted circles which are difficult to analyse.

7.4.2. Partially bonded beam (PB/L1).

A slightly higher resonant frequency on the intact beam-2 (PB/L1) than the fully bonded beam (FB/L1) was due to the higher material properties of the beam as recorded in the concrete cube tests. A maximum equivalent static load of 100N may theoretically be applied at mid span without creating cracks. But due to the unknown damping ratio of the beam, this load could crack whilst vibration tests took place. It was decided to reduce the force of excitation as shown in appendix (E-2.1).

An almost circle polar diagram was shown at this stage implying the existence of viscous or hysteretic damping. The first loading stage produced a sudden crack at about the mid span. The single, wide open crack resulted in a lower resonant frequency with lower resonant amplitude as shown in fig.(7.17). The presence of the crack activated the bond between the reinforcement and the concrete which increased the damping. Furthermore loading stages resulted in a further decrease of the natural frequency as well as the amplitude. This increasing damping was indicated in the greater distortion of the circles after the second and third loading stages as shown in fig.(7.20). The third loading stage produced a peculiar response spectra. The increase of resonant frequency with the increase of load should not exist unless a great change of geometry properties have occurred. An internal change of properties such as the activated bond and

interlocking between the reinforcement and the concrete had probably increased the stiffness. The wide open crack and the associated viscous damping were predominant. As a result the amplitude at resonance was higher than that after the second loading stage. From the polar diagrams shown in fig.(7.20) the presence of viscous damping with the non-linear soft spring behaviours were just apparent after applying the first and the third loading stages.

The responses of the second mode are shown in fig.(7.18). An almost similar amplitude pattern to beam-1 (fully bonded, FB/L1) after applying the first loading stage indicated that non-linear damping existed and controlled the amplitude. This non-linear damping is confirmed by the associated polar diagrams shown in fig.(7.21). The non-linear damping shown as distorted polar diagrams after the first and second loading stages was from the places where the bond was activated and deactivated simultaneously. The tensile strain of the partially bonded beam in the unbonded region was entirely governed by the steel reinforcement. In the fully bonded region the tensile strain was partly governed by the steel reinforcement. At the places where fully and partially bond meet there is a discontinuity of bond stress as well as flexural stress. This discontinuity disappears exponentially with the distance [5]. The increase of tensile strain decrease the steel area/perimeter which

may increase loss of bond. The sinusoidal force employed can result in the activate and deactivate bond.

Furthermore this second loading stage exhibited decreasing amplitude with increasing damping. The third loading stage may have released the remaining bond such that the simultaneous bonding and debonding process was deactivated. As a result the viscous damping with slightly non-linear soft spring behaviour was predominant. At this stage the decrease in stiffness was indicated clearly from the increase in amplitude at resonance. The complementary polar diagrams in fig.(7.21.D) confirmed this phenomena. The typical pseudo resonances were indicated in the polar diagrams on the intact beam and on the second loading stage as small circles within the main circles. This was possibly due to the presence of opening and closing cracks or from the activated and deactivated bond of the reinforcement that changed the stiffness as well as damping with respect to time.

The presence of the pseudo resonance is more obvious at the higher modes. The flattened responses with several pseudo resonances indicated in the third responses in fig.(7.19) confirm the complexity of the system. As a result the polar diagrams shown in fig.(7.22) are difficult to analyse.

7.5. Beams Containing Diagonal Splitting Cracks.

7.5.1. Fully Bonded beam (FB/L2).

The lower compressive strength of the materials of this beam resulted in a lower first resonant frequency. This missing point can be interpolated from the polar diagram as the type of the damping is recognised. A sharp drop in the resonant frequency after applying the first loading stage was followed by a decrease in the resonant amplitude. Again, the increasing damping can be identified from the distorted polar diagram. Furthermore the loading stage aimed to develop diagonal splitting cracks. Just before the diagonal splitting cracks became visible a vibration test was conducted. The third response indicated clearly a drastic change of the dynamic parameters. A sharp drop in resonant amplitude with little change of resonant frequency despite a similar force of excitation (as shown in appendix E-3.1) clearly distinguished this response from other responses. The vibration test at this early stage of diagonal cracking activated Coulomb friction damping [22,23]. The slight change in the crack depth and growth of flexural cracks indicated small change in the beam stiffness and resulted in only slightly lower resonant frequency. The associated polar diagram in fig.(7.26) showed a circle slightly shift in y-origin creating a 'pear shape'. This very slight change of polar shape was possibly due to the small Coulomb friction damping force which is associated

with the diagonal force,N times frictional factor,ρ. A further the loading stage created visible shear cracks and resulted in a higher resonant amplitude with a classical lower resonant frequency. The visible cracks deactivated the Coulomb friction damping in such a way that the viscous damping took the main part in controlling the resonant amplitude.

The typical increasing resonant amplitudes with decreasing resonant frequencies at the second mode were also exhibited by this beam within the flexural mode pattern. The associated polar diagrams in fig.(7.27) confirmed the presence of viscous damping with slightly non-linear soft spring behaviour. An equipment error resulting in a phase shift was also indicated in this second mode. The sharp drop of the resonant amplitude with the slight decrease of the resonant frequency was also performed in polar diagram after applying the second loading stage. The slightly distorted polar diagram is possibly due to the presence of the early non-linear damping as well as the Coulomb damping. The 'pear shape' can be detected but is not as clearly shown as in the first mode. A higher resonant amplitude at the last response than that at the second and the third clearly explains the relief of the beam from the Coulomb damping. Summary of these dynamic and static properties are obtained in table (7.2).

Responses of the third mode suggest that the higher

applied loads required to create diagonal splitting cracks have changed the supports condition in such a way that the amplitude responses of the supports became much higher. Two possible reasons for this which are either generated from the support systems or the shaft connecting the concrete beam to the support systems. In general the flatter responses with the pseudo resonances in the third mode indicate the complexity the system. The associated polar diagrams which are also slightly rotated counter clock wise in fig.(7.28) were in accordance with the phase characteristics of the accelerometers used. The last polar diagram indicated the return of the viscous damping with small non linear stiffness.

7.5.2. Partially bonded beam (PB/L2).

Five of six loading stages carefully applied on this beam as reported in chapter-3 will be analysed. The higher first resonant frequency of this intact beam was apparently proportional to the material properties of the beam. The resulting five responses from five loading stages in the first mode as shown in fig.(7.29) indicated that the large change of resonant frequency only occurred after applying the first loading stage. This was due to the single crack opened widely. The straight response approaching resonance is confirmed from the associated polar diagrams in fig.(7.32) as a missing point during

the experimental test. The lower number of cracks compared to beam-2 (PB/L1) only slightly activated non-linear damping. The slightly reduced resonant amplitudes after applying the second and third loading stages indicated the presence of viscous damping. As the damping and stiffness play an important role in defining resonant amplitudes their types and proportion will affect the response performance. The increasing load was not apparently distributed proportionally over the beam length as indicated by the lower increase in the number of cracks with the increase of loading stages. Thus, the non-linear soft spring behaviour was predominant over the expected Coulomb friction damping. As a result the Coulomb damping was no apparent as shown as in the decrease of amplitude before the cracks were visible. However, the non-increasing amplitude at the fourth response was possibly due to the presence of the non-linear damping. The change of the load distribution to produce diagonal splitting cracks is shown as slight decrease of the resonant frequency. The associated polar diagrams indicate the presence of viscous damping with a non-linear soft spring behaviour.

The second mode responses in fig.(7.30) do not clearly indicate the typical increasing resonant amplitudes with the increase in the loading stages due to the presence of significant pseudo- resonance especially after applying the fourth loading stage. This pseudo- resonance is more

clearly visible in the polar diagrams shown in fig.(7.33). Almost all polar diagrams possessed similar non-linear damping although the intensities were different. A clear pseudo resonance possibly indicated the greater bonding and debonding activity.

In general the responses of the third mode indicated increasing resonant amplitudes at each increase of loading stage. A slightly drop in amplitude after the third loading stage may indicate the presence of early shear cracks. The associated polar diagrams shown in fig.(7.34) are circles which are rotated counter clock wise and shift in y-origin. This shift in y-origin indicates the presence of Coulomb friction damping and the circles indicate viscous damping. The rotated polar diagrams are due to the phase characteristics of the measuring accelerometers. Slight pseudo resonances appear in all polar diagrams showing the complexity of the system.

7.6. Discussion.

7.6.1. Non-linearity.

The use of the polar diagram technique has demonstrated the typically higher polynomial damping of these beams [45]. In the case of beams described in this experiment the higher polynomial damping can be associated with the opening and closing of existing cracks and the bonding and debonding activity of the

reinforcement in the partially bonded beams where the damping force is transferred gradually and follows an exponential curve. This typical damping pattern which is elliptical on the polar diagrams was shown in almost all the experimental beams. Furthermore this experiment has also demonstrated the existence of Coulomb damping or dry friction damping [17.18.19] such as shown in the beam with diagonal splitting crack patterns. Low contribution from appearance of Coulomb damping in this case was possibly due to the small area of shear plane which defines the friction factor, ρ. The partially bonded beam-4 (PB/L2) did not clearly show Coulomb friction damping due to the geometric change of the partially bonded beam which attracted more flexural cracks during post loading stages. General characteristics of the polar diagram with several possible non-linearities are summarised in table (7.4).

The force of excitation can not be evenly applied over the resonance frequencies. The resulting resonant frequency and amplitude will not be achieved at the same force of excitation. Linear approximations using fitting curves may be used as the alternatives from which the approximated dynamic parameters can be obtained. Although many possible polynomial equations can fit the data, the characteristics of the structure need to be considered. This implies that the fitted curve should not be extrapolated unless the behaviour of the structure

starting from the intact and progressing to a failure under vibration tests has been completely understood. Excessive forces of excitation may attract the presence of semi hard and soft spring behaviour giving rise to rectification phenomena [23]. This emphasises the point that a fitted curves should not be extrapolated.

7.6.2. First Mode.

A graph relating strains and resonant frequencies is shown in fig.(7.35). The fully bonded beam with flexural crack patterns (FB/L1) exhibited a higher stiffness before yielding compared with the fully bonded beam which exhibited a diagonal splitting crack pattern (FB/L2). This can be deduced from the fact that more cracks existed in the diagonal splitting cracked beam (FB/L2). thus lower stiffness can be expected. More over in comparison with the partially bonded beams having the similar crack patterns (PB/L1) this beam (FB/L1) possessed much greater stiffness. The presence of early shear cracks was indicated by a very slight change of resonant frequency as observed in fig.(7.35). This was possibly due to the change in the load distribution in such a way that it only slightly changed the stiffness.

The partially bonded beam with the flexural crack patterns (PB/L1) showed a unique difference. In comparison with the beam-4 (PB/L2) this beam possessed a lower stiffness before yielding. This further confirms

that the beams with diagonal splitting crack patterns produced lower reductions in stiffness with the increase of strains compared to the beams with flexural crack patterns.

Fig.(7.36) relates strains to amplitudes. The decrease of amplitude with the increase in strain of beam-1 (FB/L1) was due to the presence of higher damping. Thus, beam-2 (PB/L1) possessed higher damping than beam-1. This can be explained from the fact that more friction occurred in the partially bonded beam. The fully bonded beam-3 with a diagonal splitting crack pattern (FB/L2) showed a significant change in the load distribution that caused a change in amplitude characteristics such as the sharp drop as observed in fig.(7.36). As the resonant amplitudes are controlled by damping instead of stiffness an observation throughout the frequency - strain graph will be beneficial. Furthermore beam-4 (PB/L2) well defined that the load distribution affected the stiffness as shown by the higher amplitudes of this beam than beam-2 (PB/L1).

7.6.3. Second Mode.

The effect of increasing flexural cracks in the fully bonded beam (FB/L1) is significant in relation to the fully bonded beam with the diagonal splitting cracks as shown in fig.(7.37) although the differences are not as sharp as in with the first mode. The different

pattern shown by beam-4 (PB/L2) in fig.(7.39) confirmed that stiffness was more sensitive to crack depth rather than the number of cracks. The increase of loading stage on beam-4 did not produce significant additional cracks. The increase of load was apparently concentrated in the increasing depth of the single crack. The non evenly distributed load over the beam length was indicated as the lower decrease of the resonant frequencies with increasing loading stages.

Fig.(7.40) relates resonant amplitudes to strains. In this second mode the beam-1 (FB/L1) raised its resonant amplitude with increasing strains. This implies that the ends of the beam at ends possessed a lower percentage of cracks or a higher stiffness in comparison with the beam as whole. In other words the cracks are most pronounced at mid span. The partially bonded beam with flexural cracks (PB/L1) displayed a similar pattern to beam-1 (FB/L1) especially at the post loading stage which there was a dramatic increase. A clear and significant drop of resonant amplitude of beam-3 (FB/L2) distinguished this beam from the fully bonded beam-1 (FB/L1). The generally higher resonant amplitudes in comparison with the beam-1 (FB/L1) indicate that the beam was much stiffer. The non evenly distributed load was indicated by the beams with diagonal splitting crack patterns (FB/L2) and (PB/L2) in that their resonant amplitudes were higher than the beams with flexural crack patterns.

7.6.4. Third Modes.

Pseudo resonances occurring at about 90 degree out of phase confuses the determination of the dynamic parameters. The resonant frequency and the peak-amplitude with respect to strain as shown in fig.(7.39) and (7.40) do not clearly indicate results similar to the previous modes. Fig.(7.39) generally indicates that the percentage decrease of the resonant frequency with the increase of strain does not vary greatly for all beam types. Fig.(7.40) also indicates that at higher modes the resonant amplitudes tend to increase with the increasing strain.

7.7. Concluding Remarks.

The partially bonded and the fully bonded beams possessed non-linear soft spring stiffness with varying damping types. The higher polynomial damping such as elliptic/ quadratic form can be fitted favourably. Since the force of excitation can not be applied constantly over the modes of interest the interpolation using polynomial curves can be applied with a reservation that extrapolation should not be carried out and the sets of force of excitation do not vary greatly. The partially bonded beam has also demonstrated that stiffness is more sensitive to crack depth rather than the number of cracks.

For beams possessing similar properties, their typical

defects can be identified from the percentage drop of resonant frequency with respect to strain. In addition a typical curve can be determined if the typical load applied on the beam was identified such as in the case of loads producing diagonal splitting crack patterns. The effect of loss of bond significantly decreases the percentage resonant frequency thus this type of beam defect is easily detected. The phenomena of the greater the number of defects the higher the damping and this can be a practical tool to identify the severity of damage to beams by comparing the decrease in the percentage resonant amplitudes. Beams with diagonal splitting cracks have showed the change of load distribution which resulted in a lower percentage decrease of the resonant frequencies. From the polar diagram point of view types of damping rely on the phase angle characteristics of the measuring equipment. If the phase characteristics are well understood the analyses can give proper results.

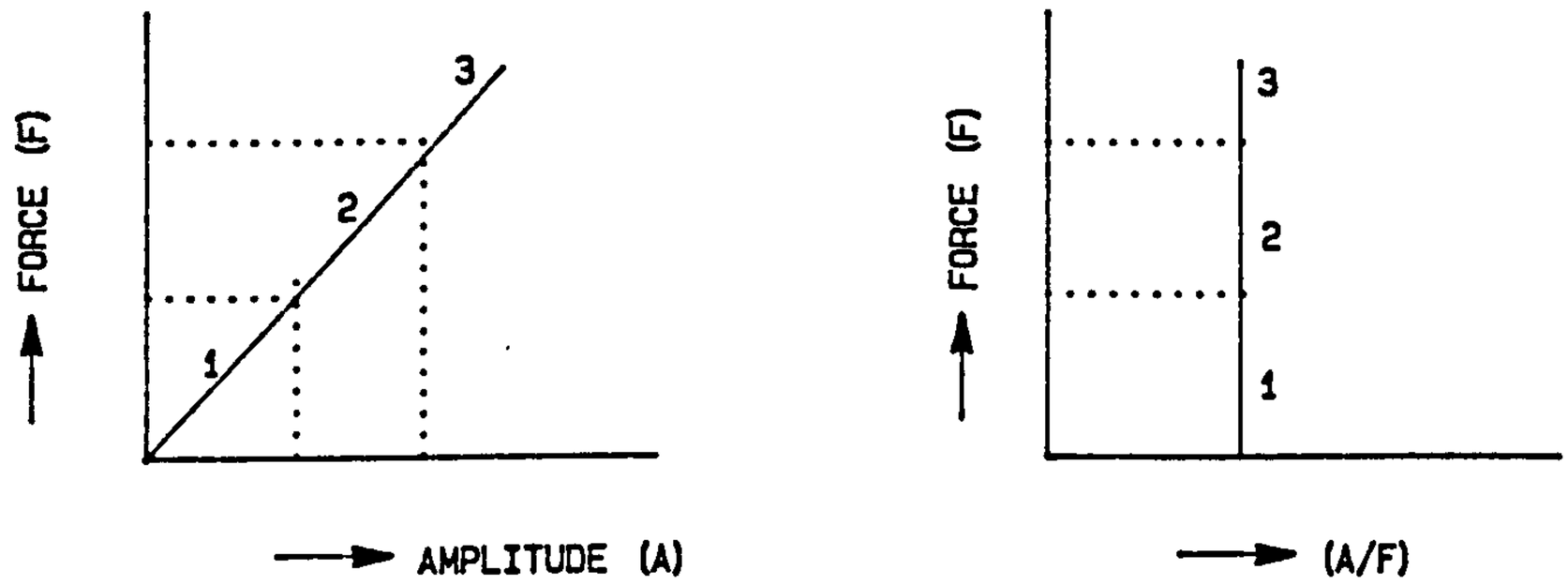

A) .NON-NORMALISED AND NORMALISED RESPONSES OF LINEAR STIFFNESS - VISCOUS DAMPING SYSTEMS (NO CHANGES IN RESONANT FREQUENCIES) .

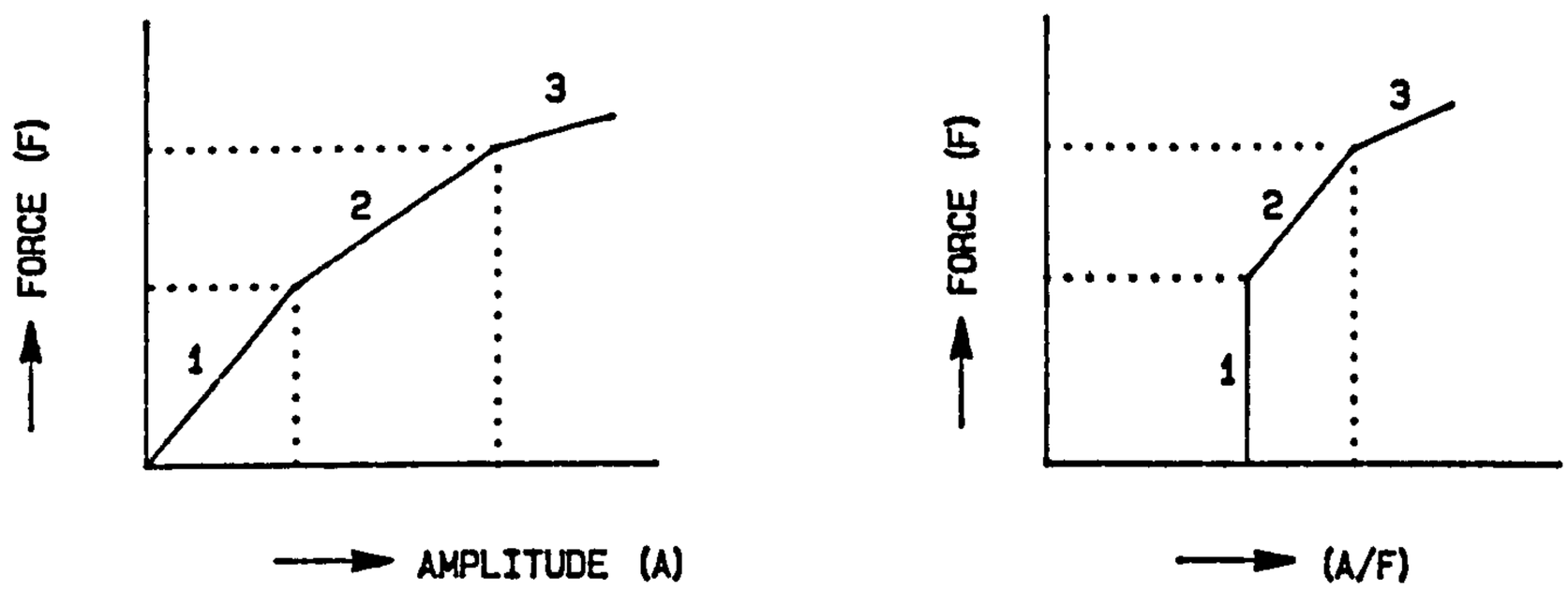

B) .NON-NORMALISED AND NORMALISED RESPONSES OF NON-LINEAR SOFT SPRING STIFFNESS - VISCOUS DAMPING SYSTEMS (FOLLOWED BY CHANGES IN RESONANT FREQUENCIES) .

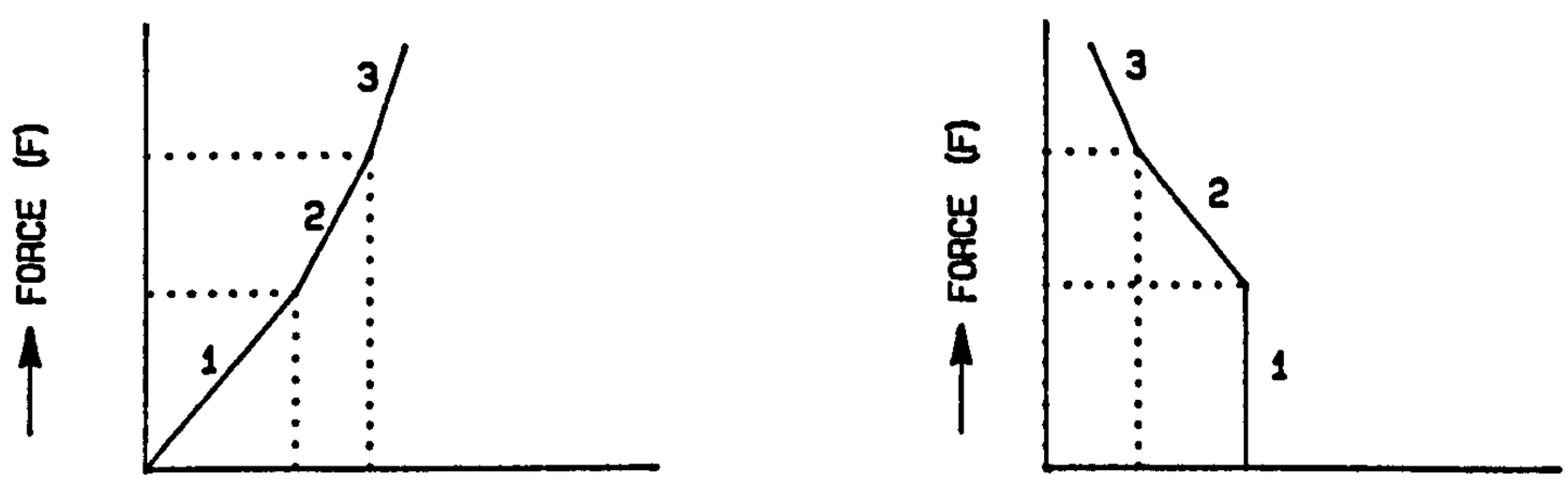

C) .NON-NORMALISED AND NORMALISED RESPONSES OF LINEAR STIFFNESS - NON-LINEAR DAMPING SYSTEMS (NO CHANGES IN RESONANT FREQUENCIES) .

FIG.7.1.SEVERAL POSSIBILITIES OF BASIC NON-NORMALISED AND NORMALISED RESPONSES.

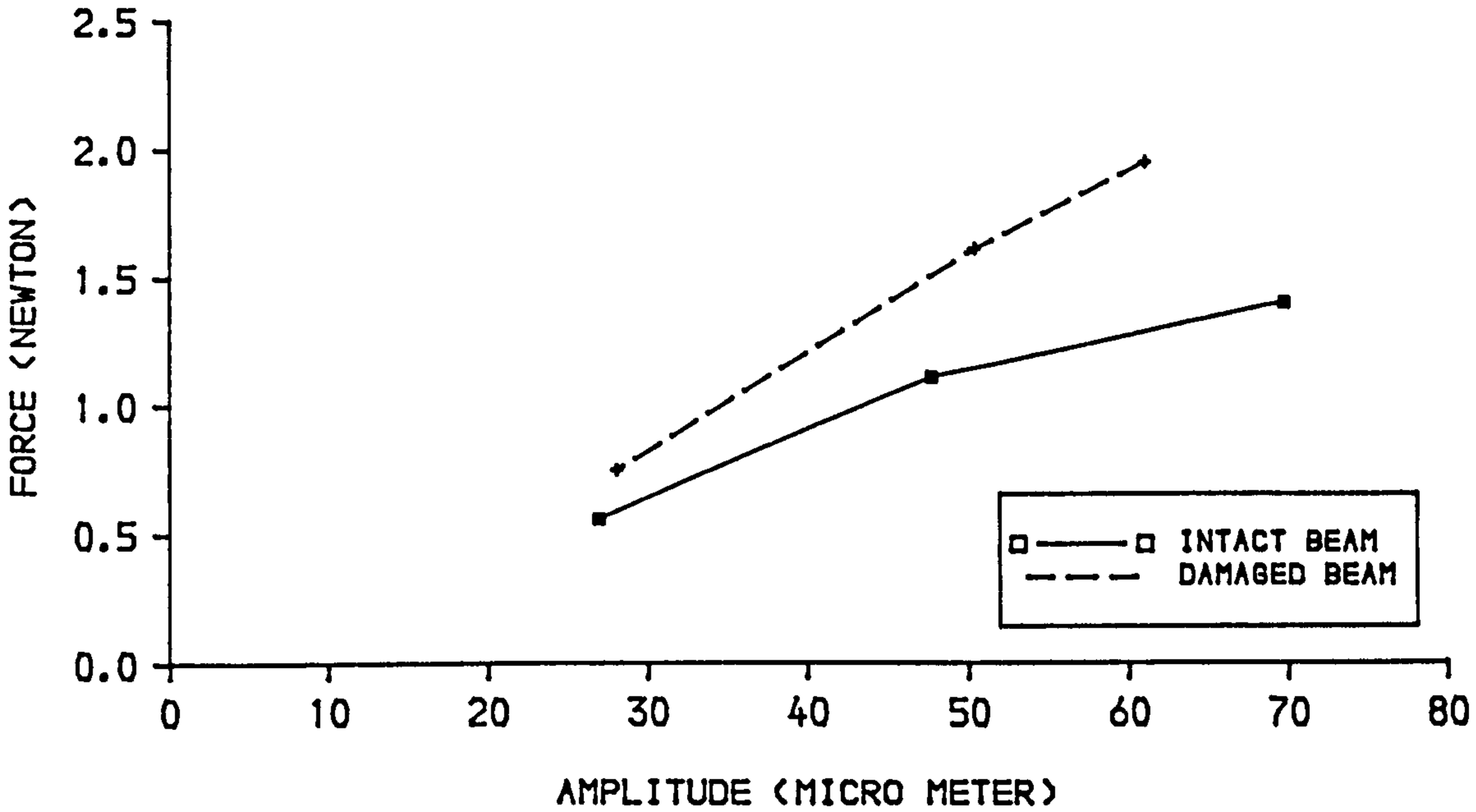

FIG.7.2.FORCE-AMPLITUDE RELATIONSHIP (NON-NORMALISED) OF INTACT AND DAMAGED BEAM-2 (PB/L1). PARTIALLY BONDED FLEXURAL CRACK PATTERN.

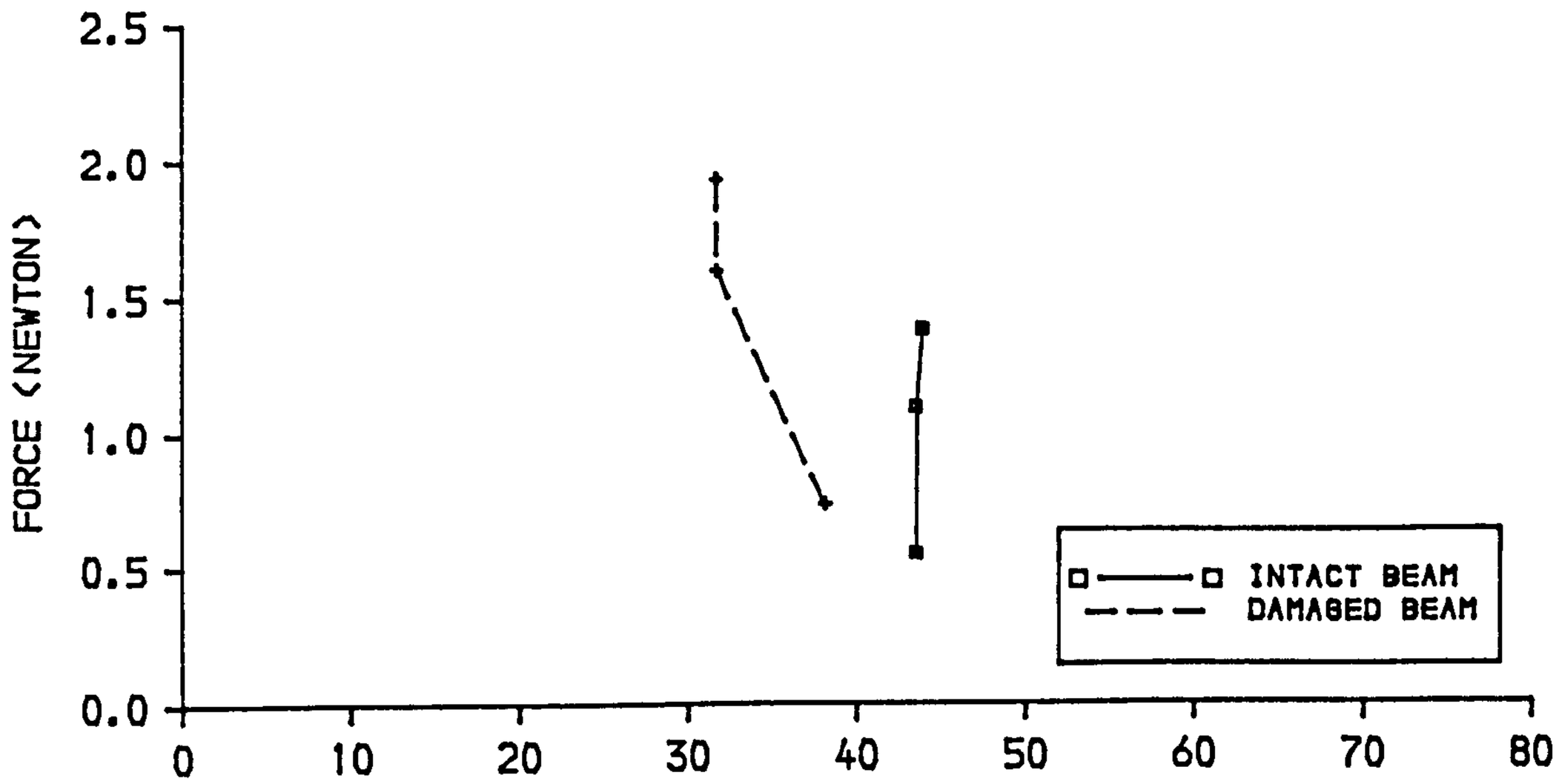

FIG.7.3.FORCE-AMPLITUDE RELATIONSHIP (NORMALISED) OF INTACT AND DAMAGED BEAM-2 (PB/L2). PARTIALLY BONDED FLEXURAL CRACK PATTERN.

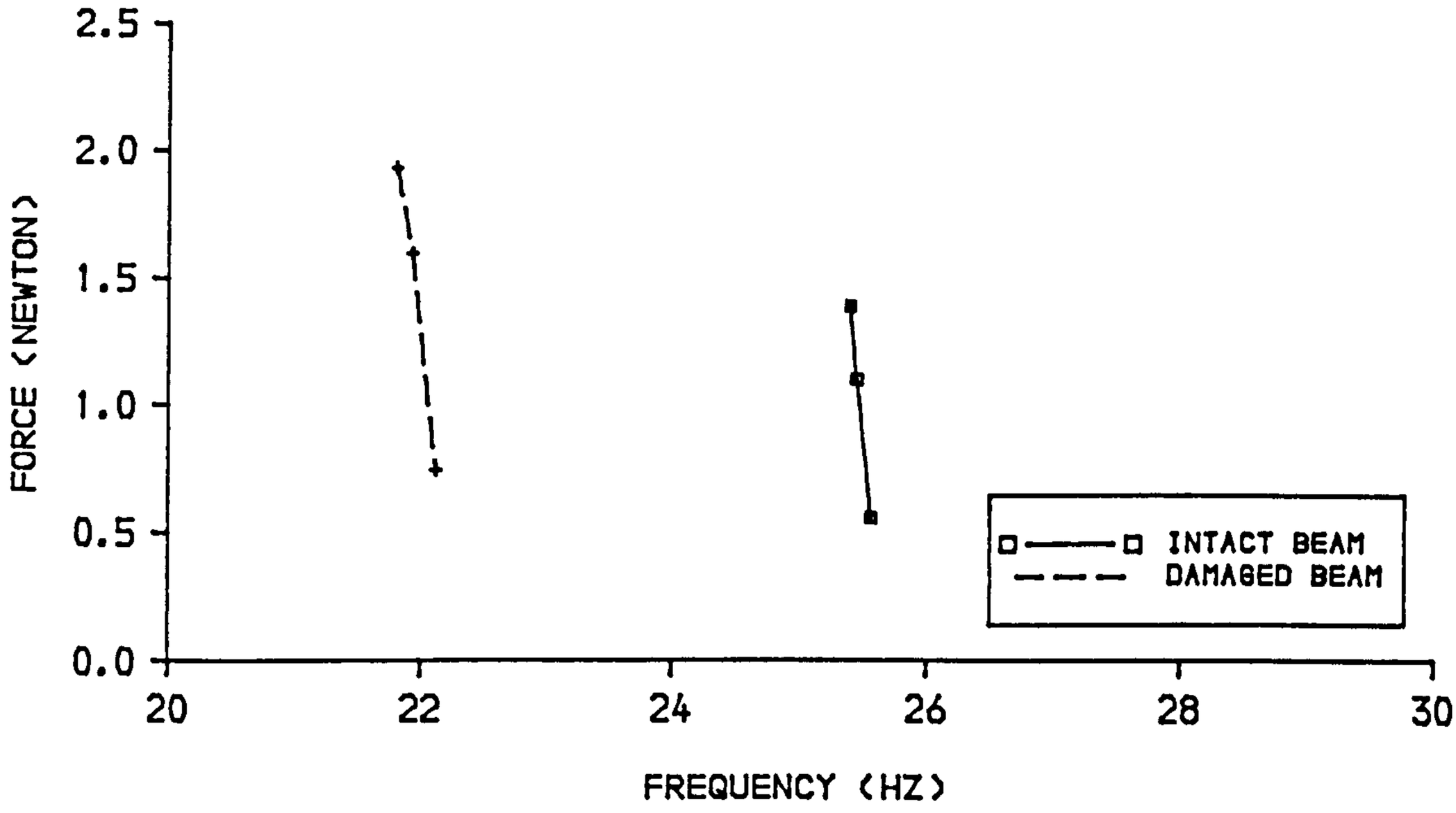

FIG.7.4.FORCE-FREQUENCY RELATIONSHIP OF INTACT AND DAMAGED BEAM-2 (PB/L2), PARTIALLY BONDED, FLEXURAL CRACK PATTERN.

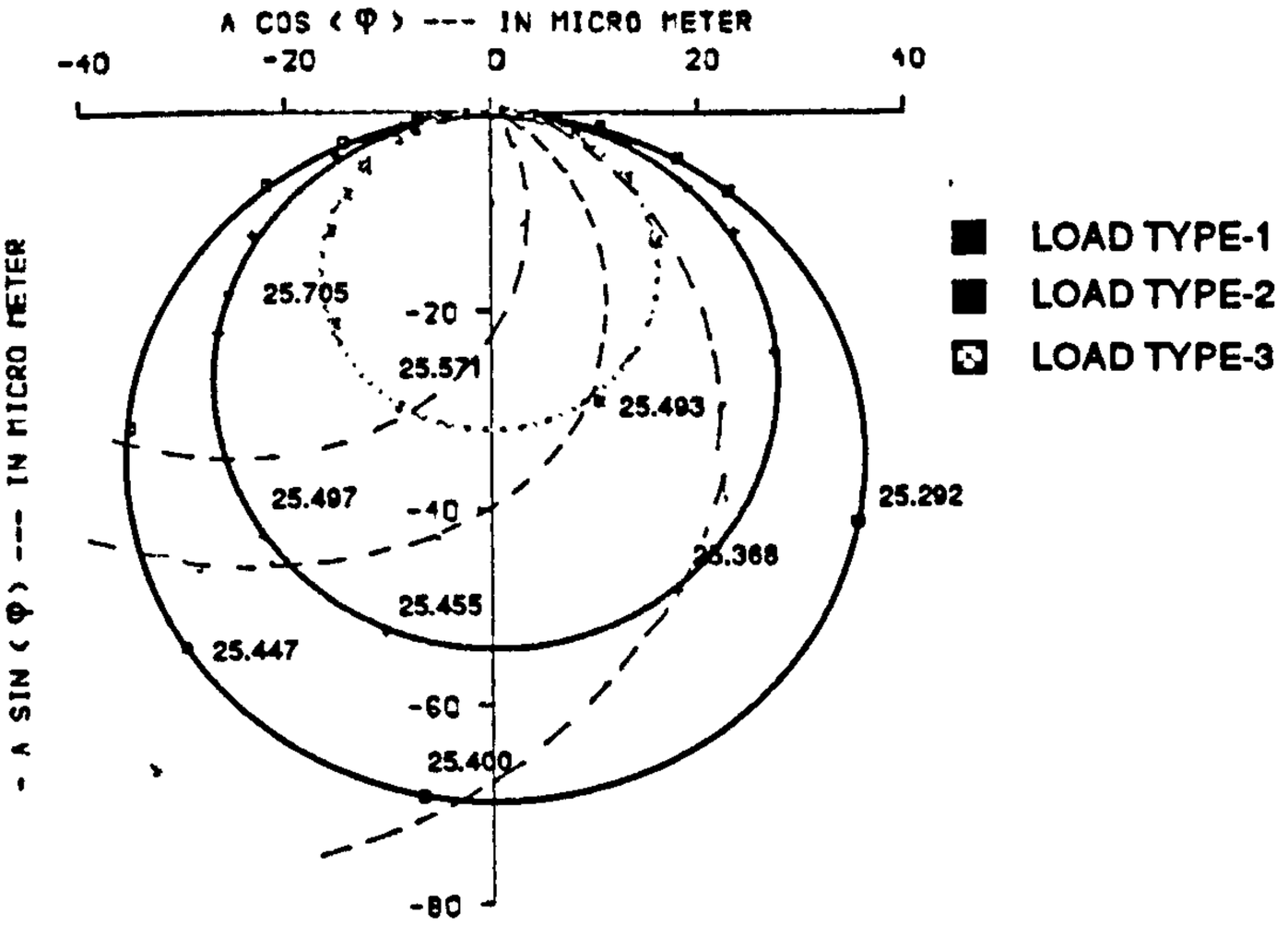

FIG.7.5. POLAR DIAGRAMS OF BEAM-2 (PB/L1), SUBJECT TO THREE DIFFERENT SETS OF FORCE OF EXCITATION FIRST MODE, INTACT BEAM (REFER TO FIG.7.2 TO 7.4)

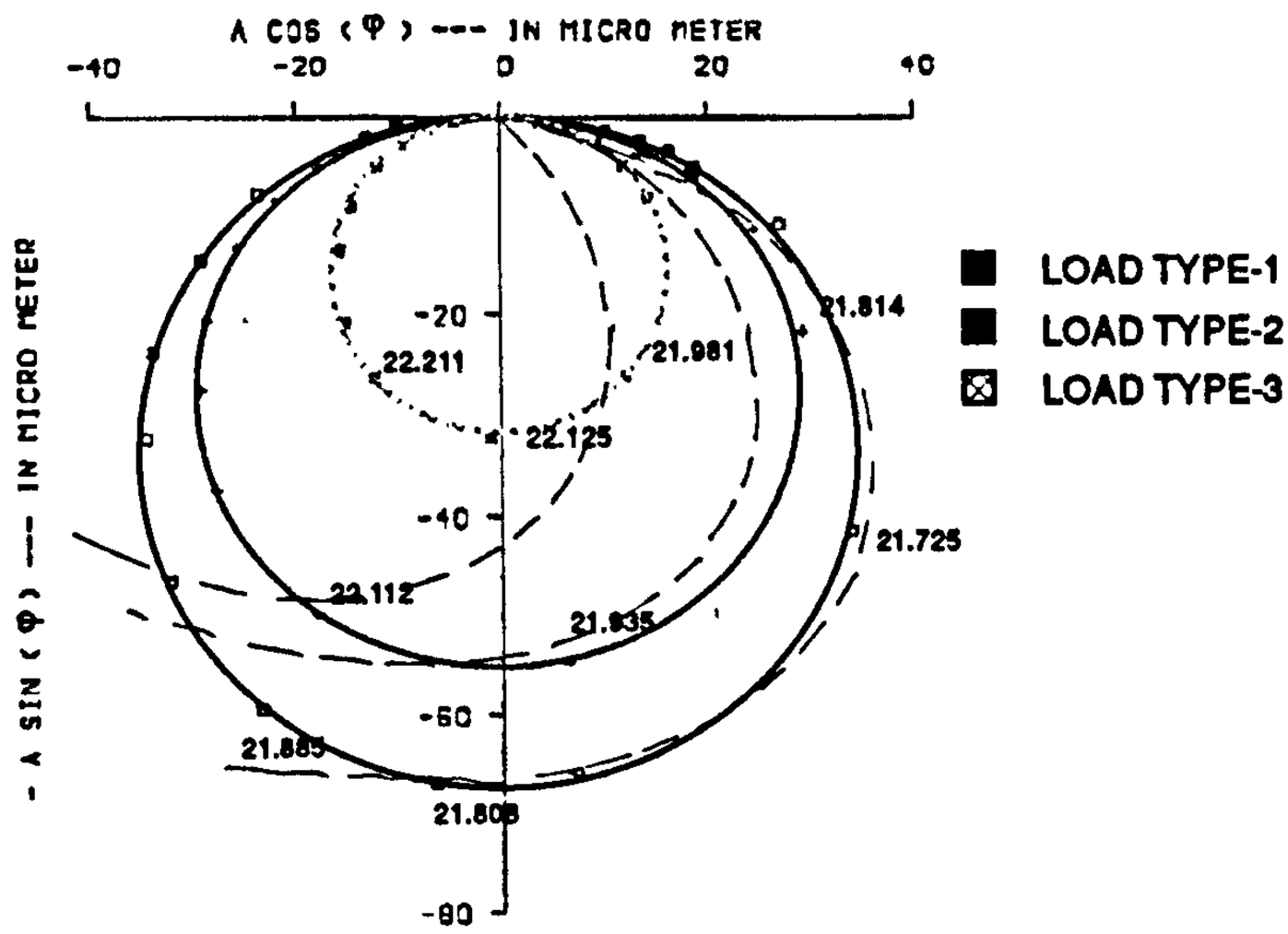

FIG.7.6. POLAR DIAGRAMS OF BEAM-2 (PB/L1), SUBJECT TO THREE DIFFERENT SETS OF FORCE OF EXCITATION FIRST MODE, DAMAGED BEAM (REFER TO FIG.7.2 TO 7.4)

NOTES TO ALL FIGURES :

φ : phase angle between force of excitation and beam response
A : displacement amplitude of beam

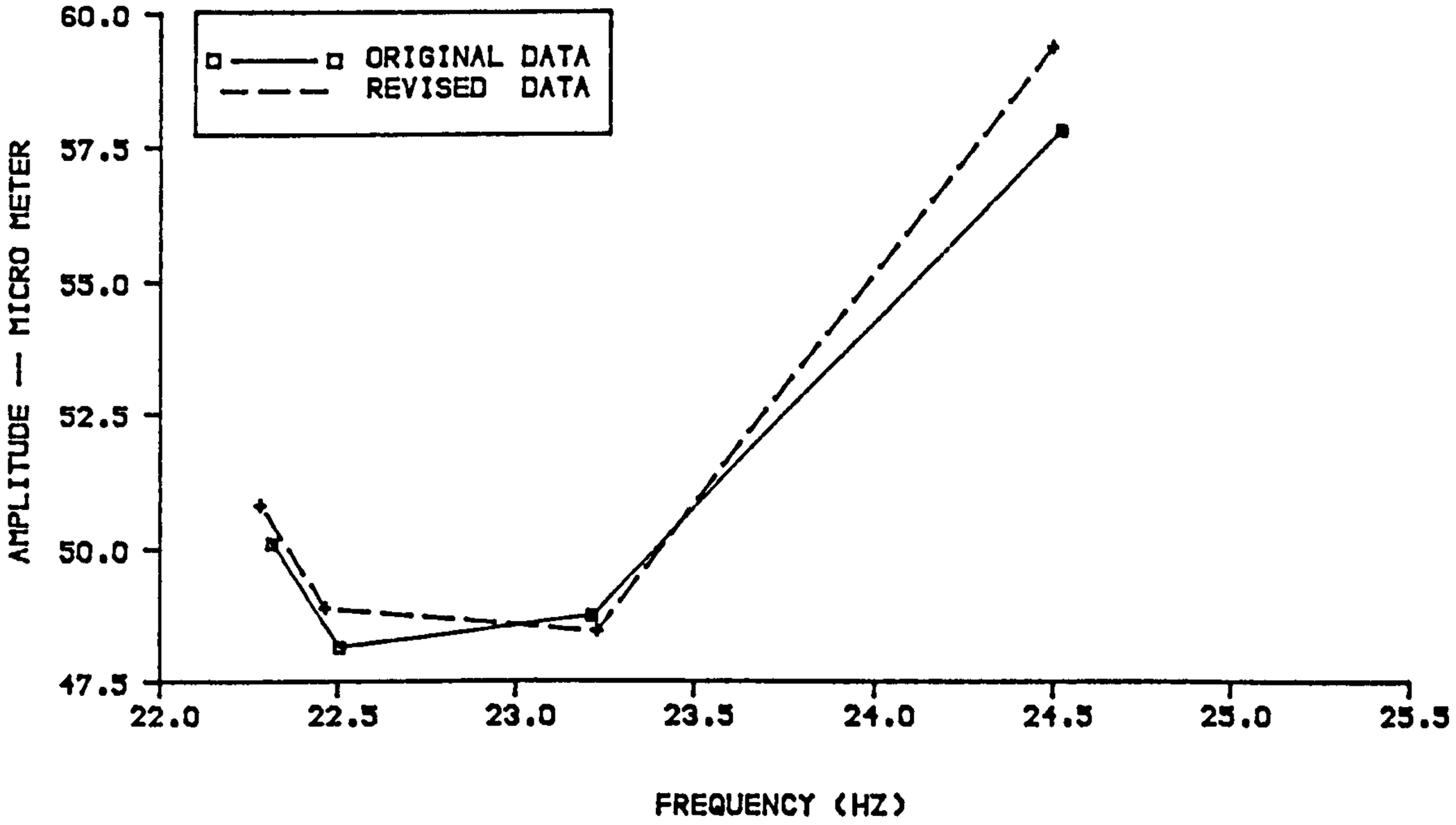

FIG.7.7.ORIGINAL AND REVISED RESONANT FREQUENCY
AND PEAK AMPLITUDE, FIRST MODE, BEAM-1 (FB/L1)

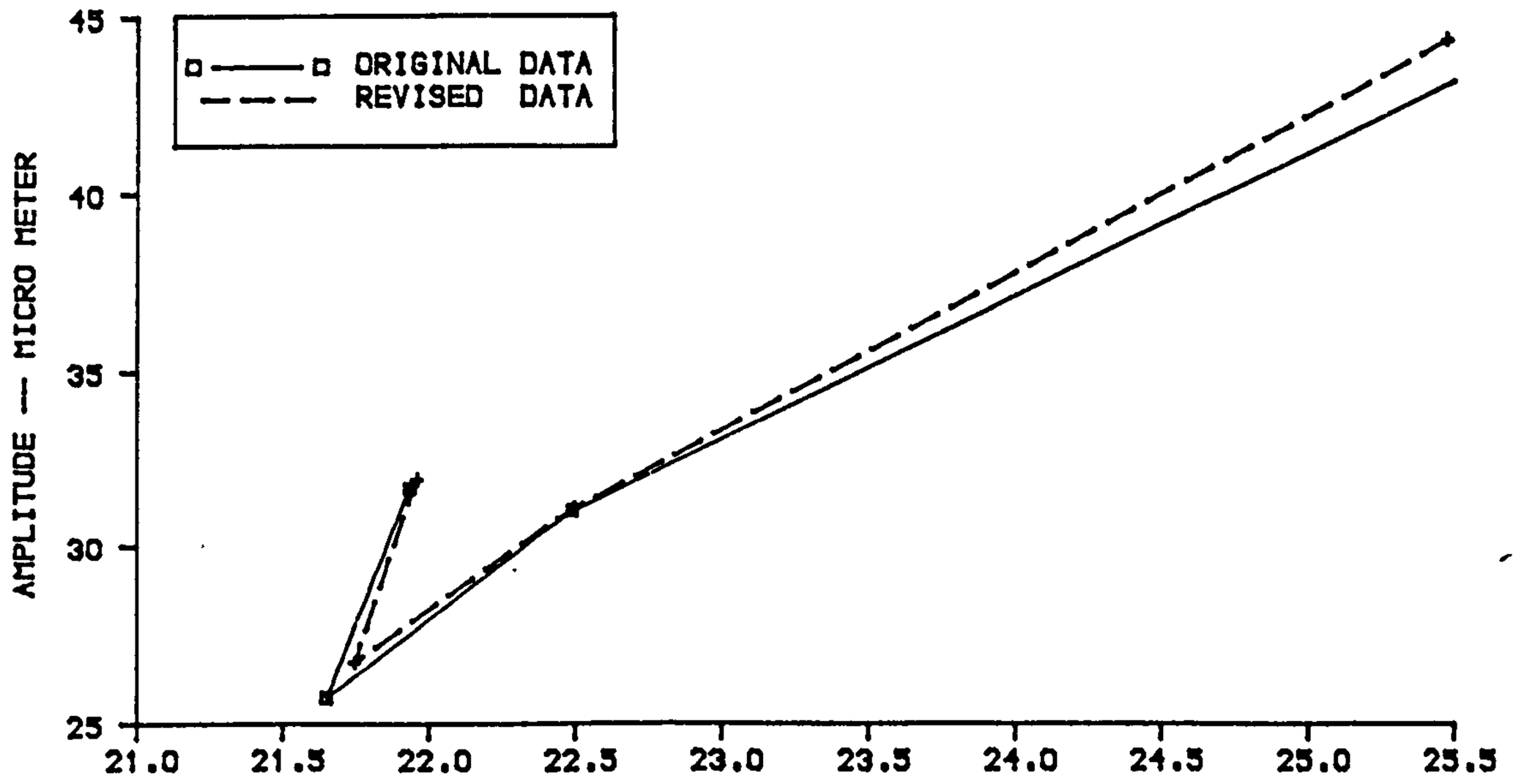

FIG.7.8.ORIGINAL AND REVISED RESONANT FREQUENCY
AND PEAK AMPLITUDE, FIRST MODE, BEAM-2 (PB/L1)

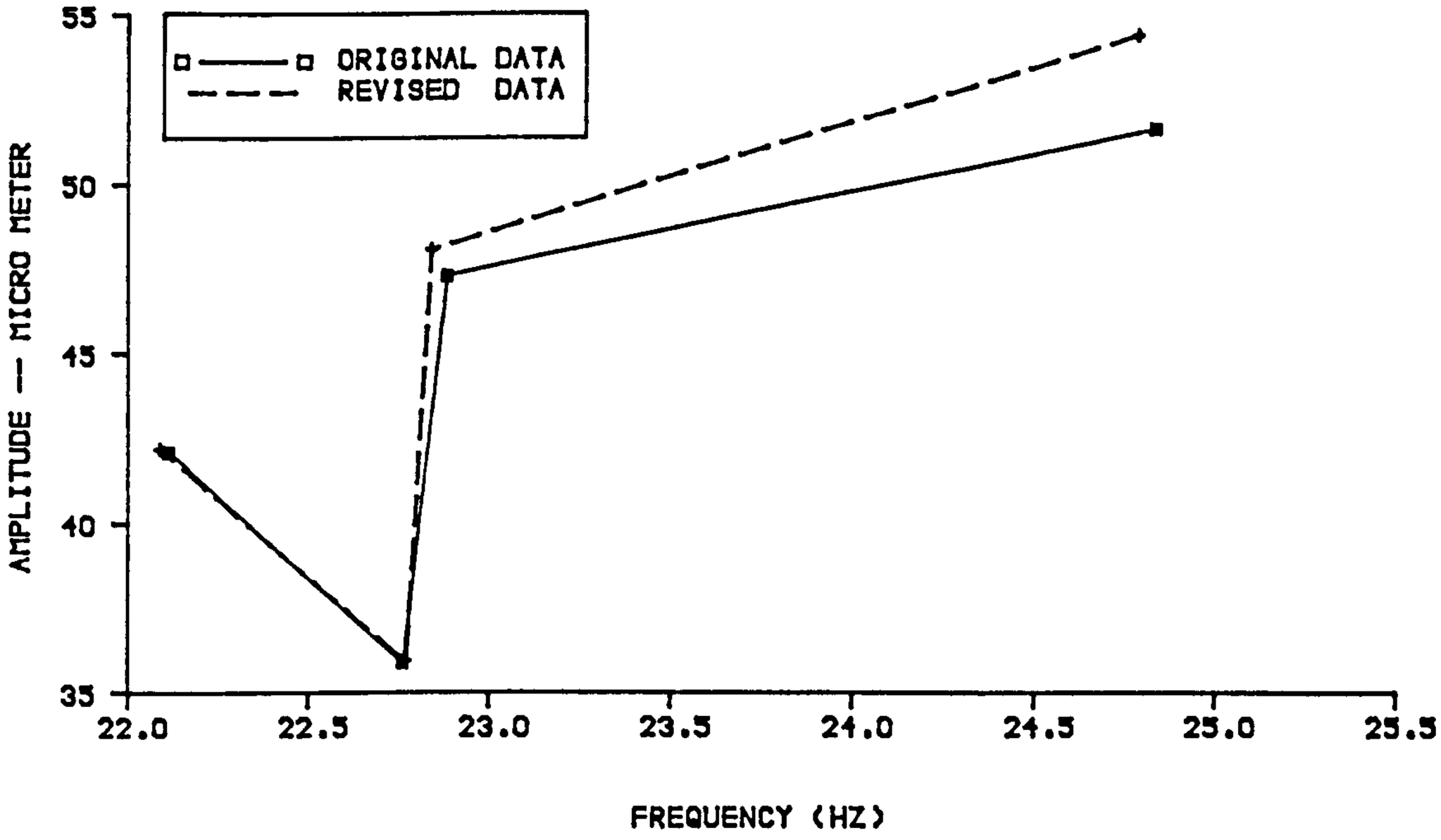

FIG.7.9.ORIGINAL AND REVISED RESONANT FREQUENCY AND PEAK AMPLITUDE, FIRST MODE, BEAM-3 (FB/L2)

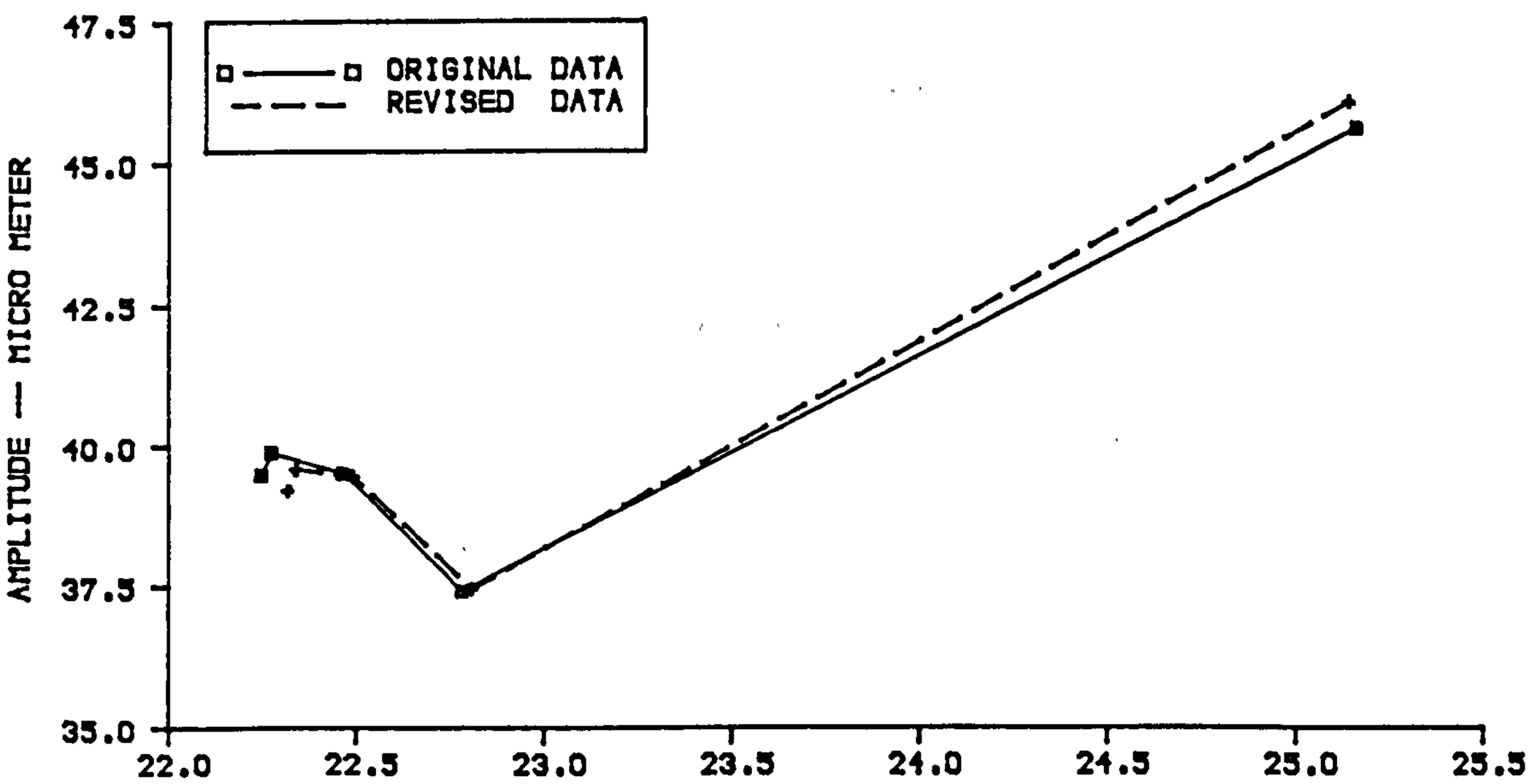

FIG.7.10.ORIGINAL AND REVISED RESONANT FREQUENCY AND PEAK AMPLITUDE, FIRST MODE, BEAM-4 (PB/L2)

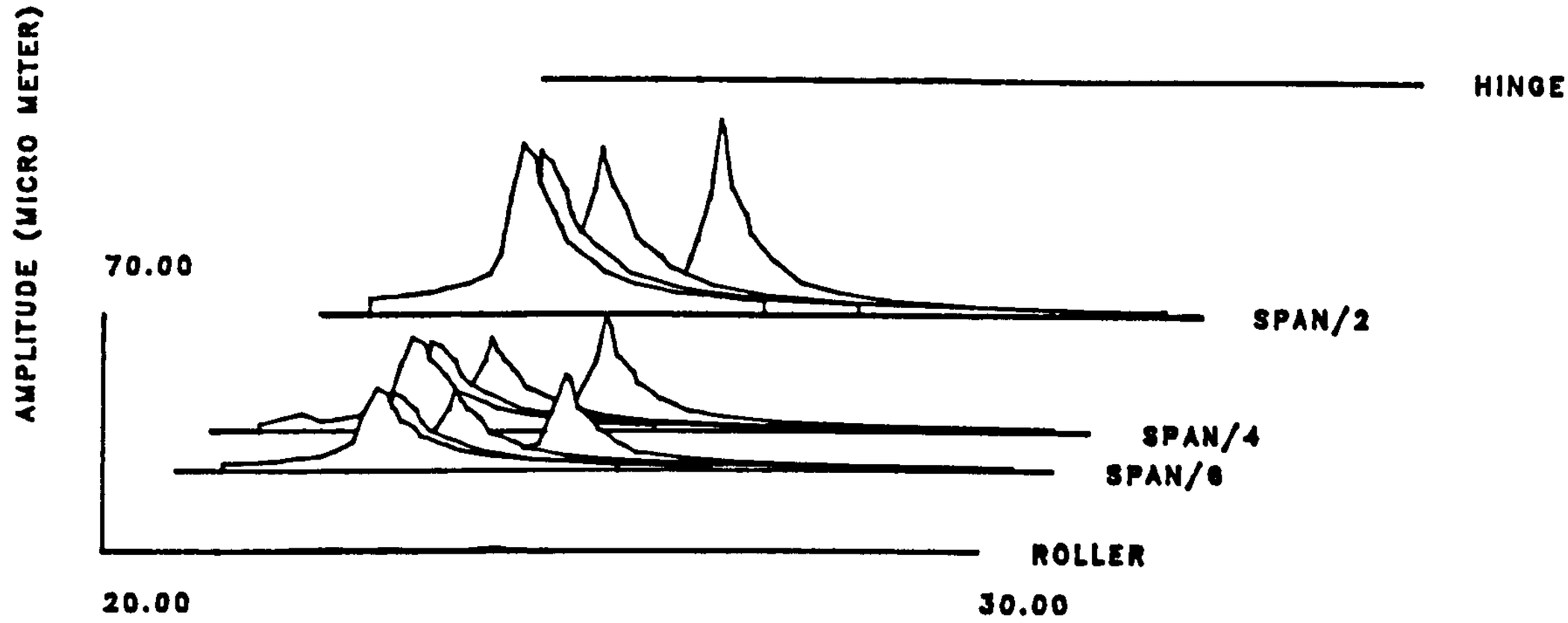

FIG.7.11.RESPONSE SPECTRA, BEAM-1 (FB/L1) SUBJECT TO FOUR LOADING STAGES, FULLY BONDED, FLEXURAL CRACK PATTERN, FIRST MODE.

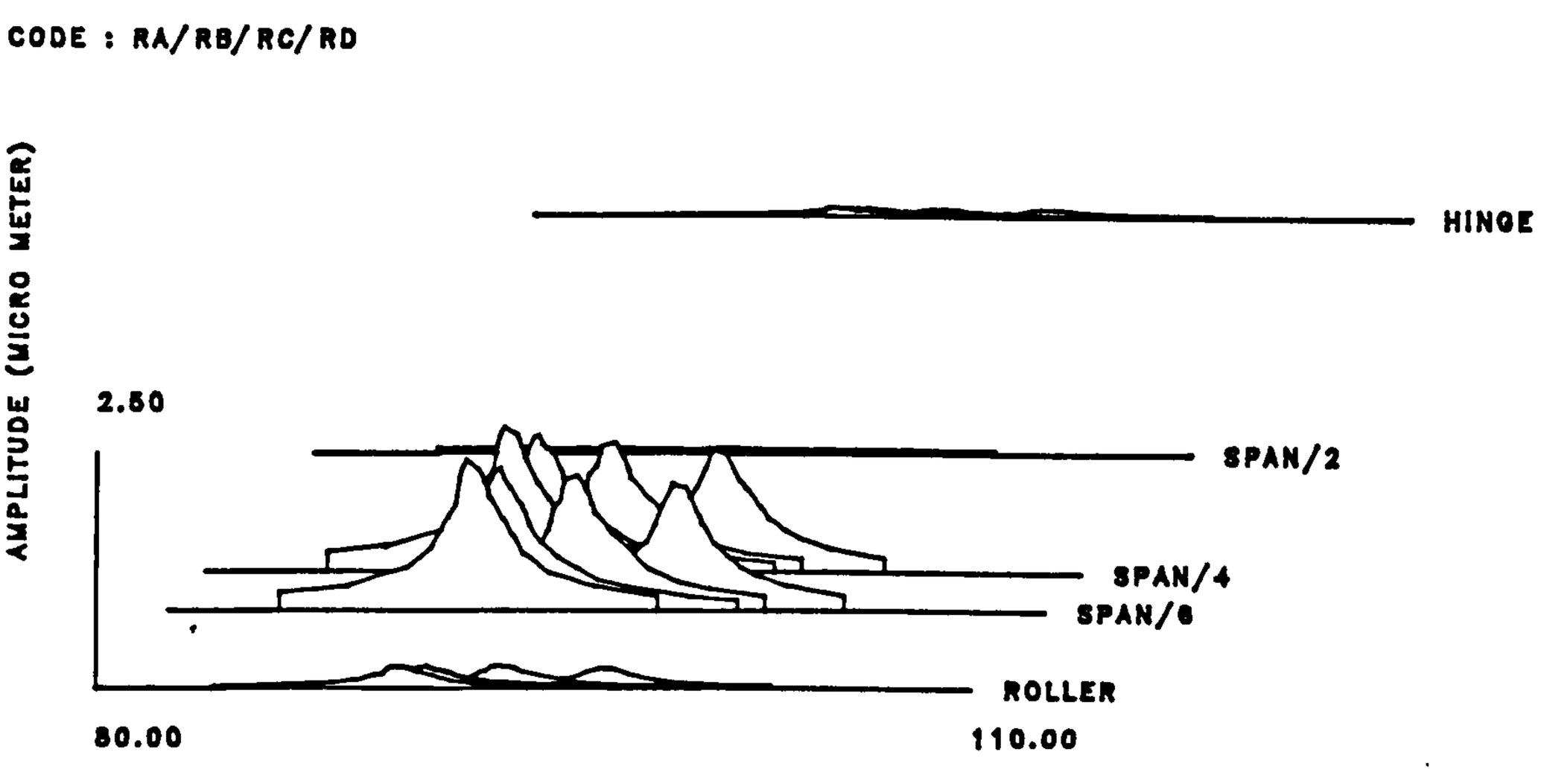

FIG.7.12.RESPONSE SPECTRA, BEAM-1 (FB/L1) SUBJECT TO FOUR LOADING STAGES, FULLY BONDED, FLEXURAL CRACK PATTERN, SECOND MODE.

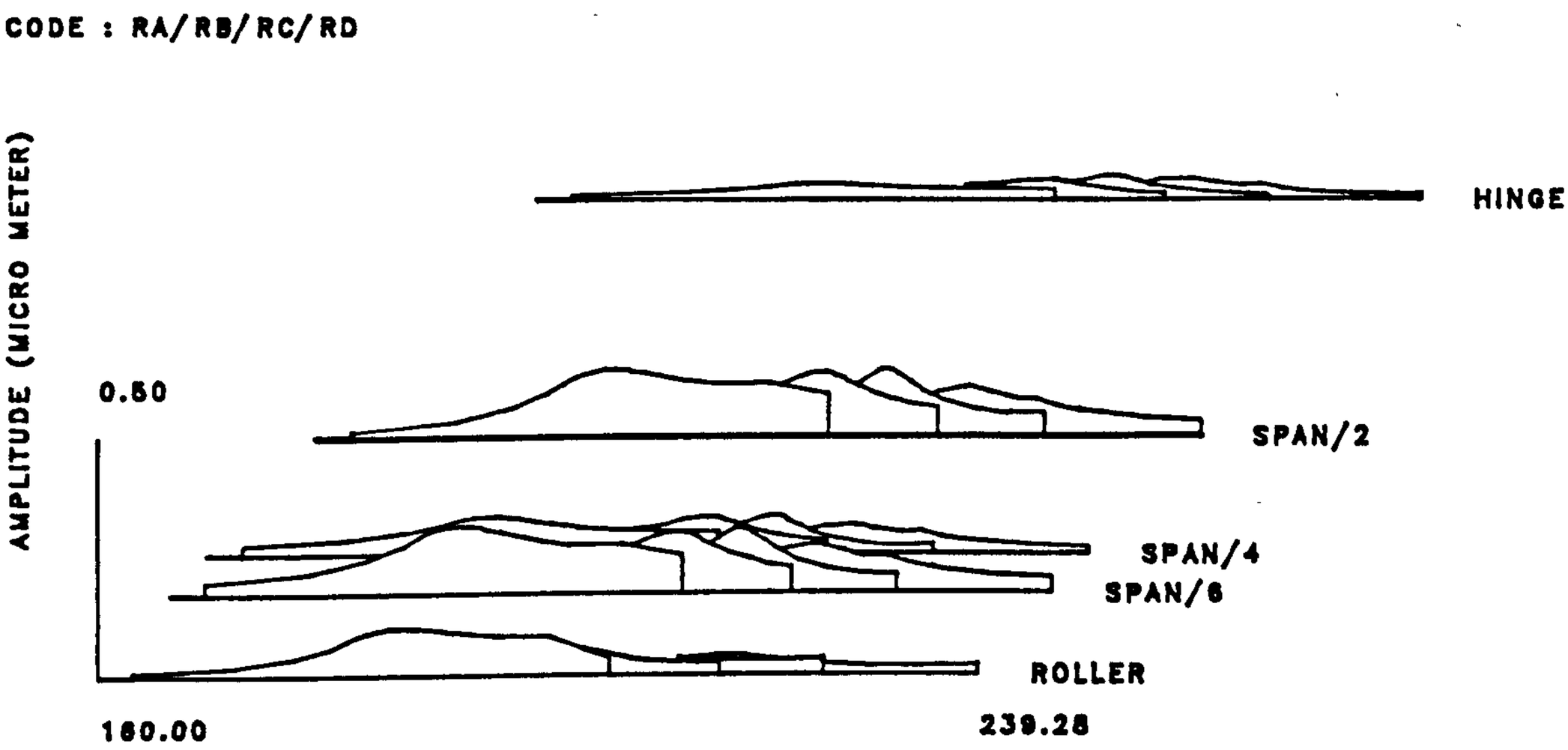

FIG.7.13. RESPONSE SPECTRA, BEAM-1 (FB/L1) SUBJECT TO FOUR LOADING STAGES, FULLY BONDED, FLEXURAL CRACK PATTERN, THIRD MODE.

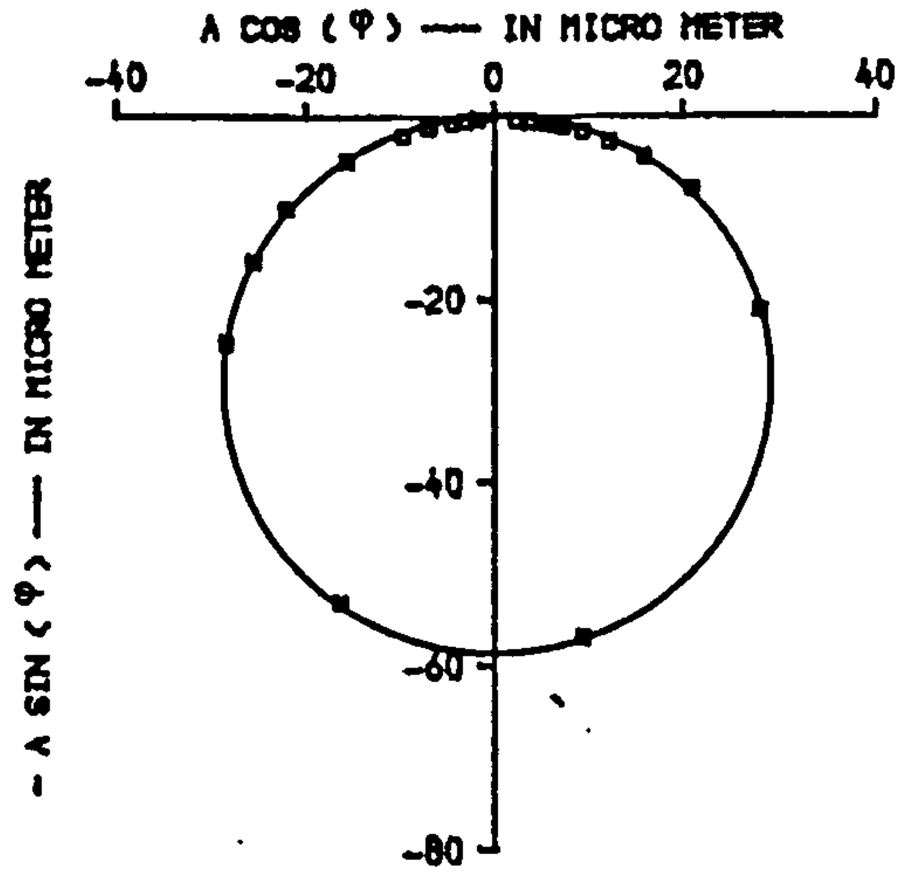

A. BEFORE APPLYING FIRST LOADING STAGE

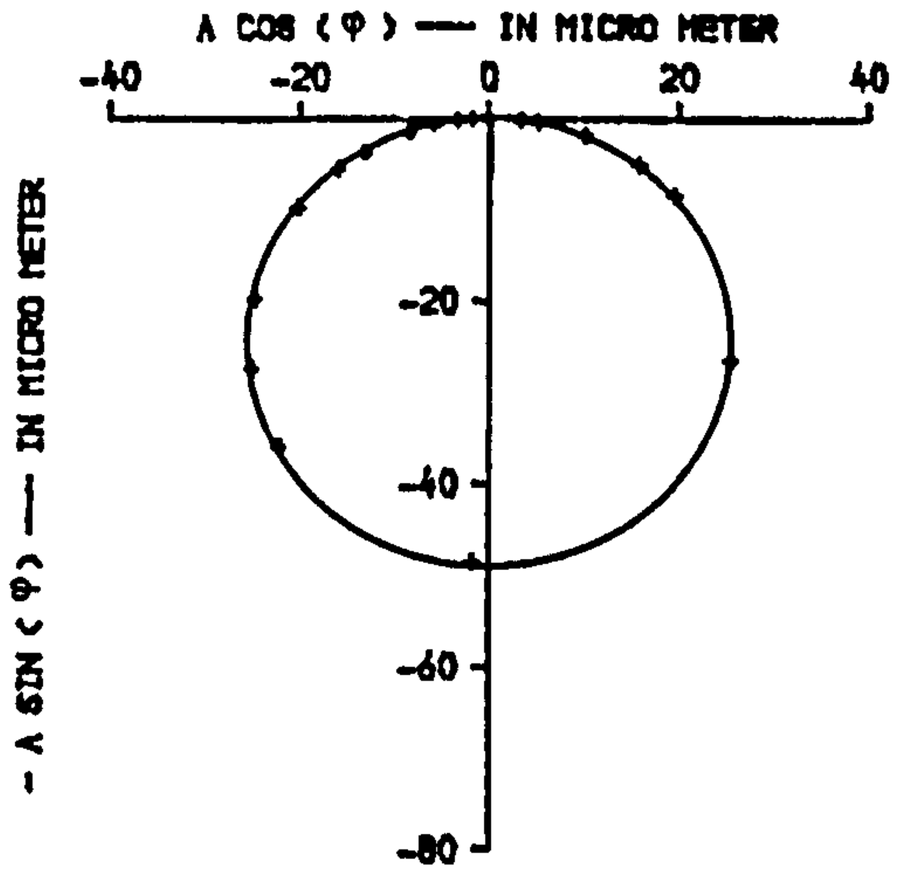

B. AFTER APPLYING FIRST LOADING STAGE

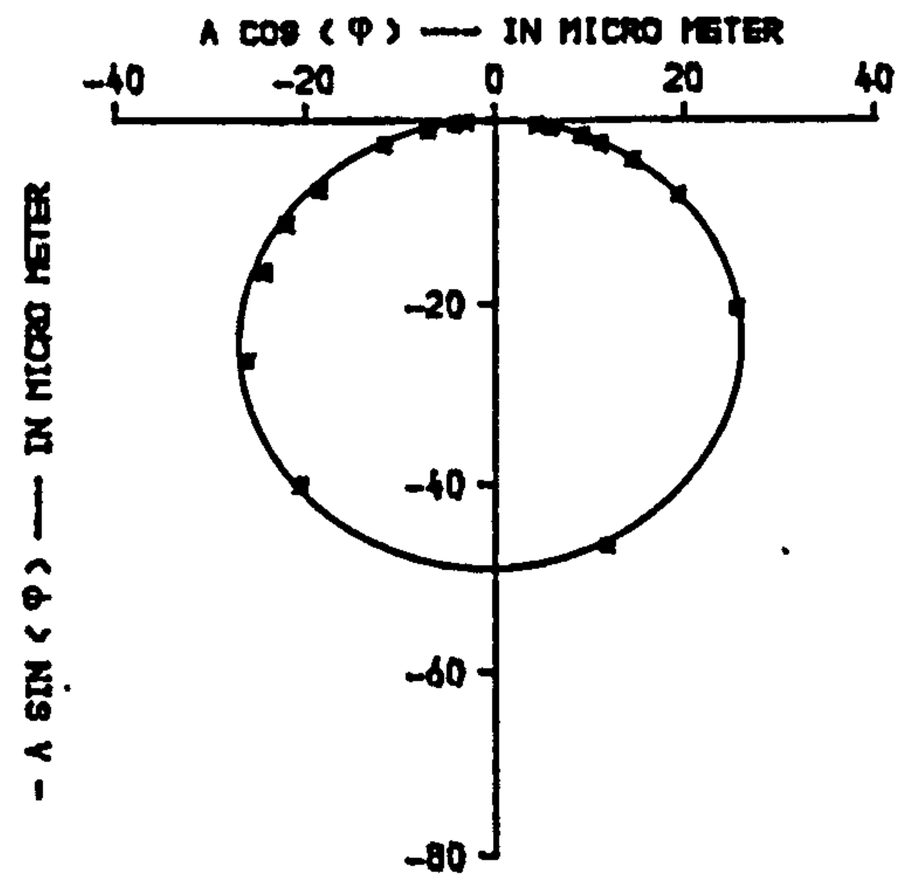

C. AFTER APPLYING SECOND LOADING STAGE

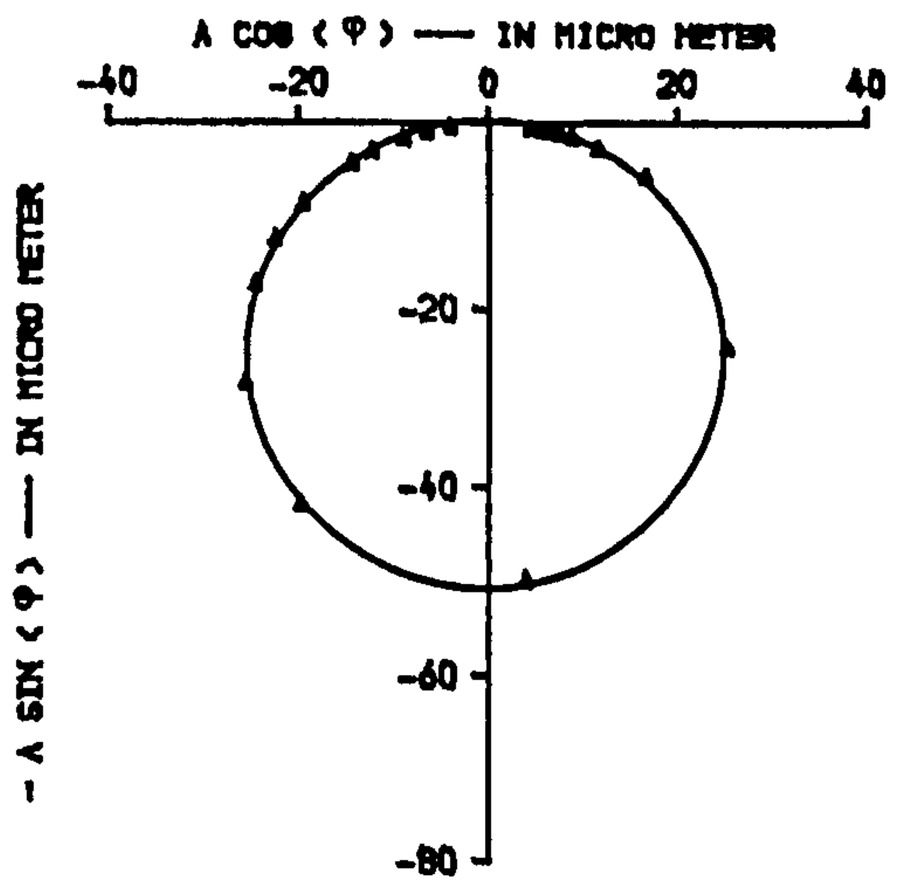

D. AFTER APPLYING THIRD LOADING STAGE

NOTES :

Φ : phase angle between force of excitation and beam response
A : displacement amplitude of beam

FIG.7.14. POLAR DIAGRAMS OF BEAM-1 (FB/L1), FULLY BONDED, FIRST MODE, AT MID SPAN, FLEXURAL CRACK PATTERN.

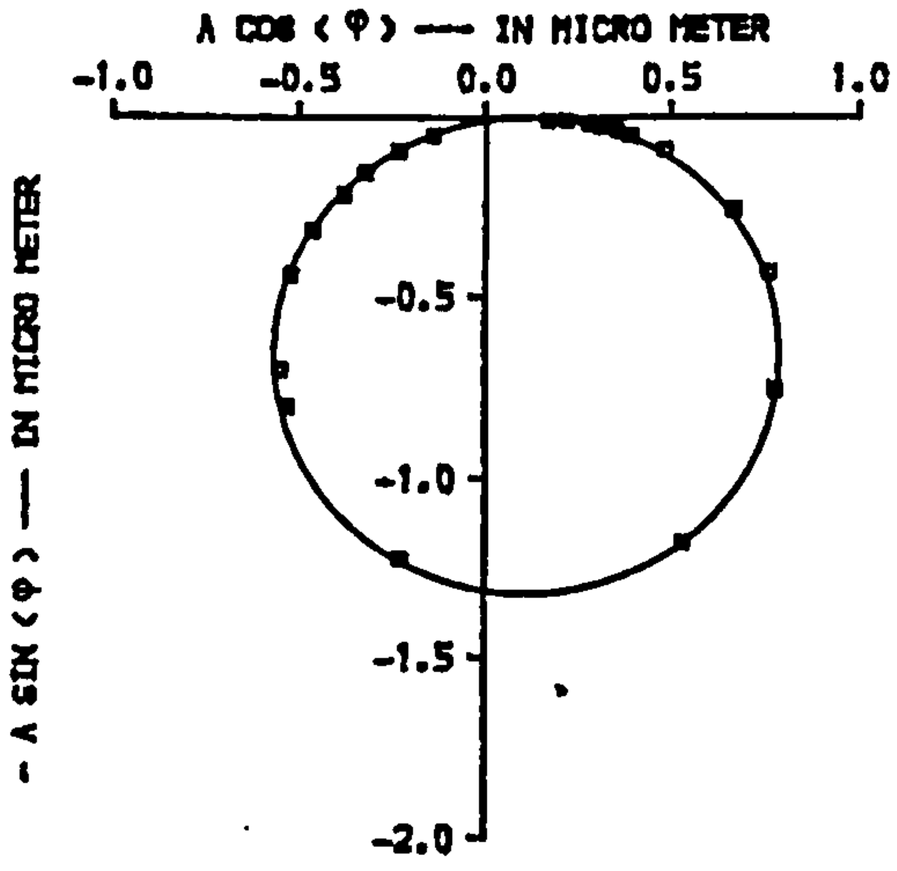

A. BEFORE APPLYING FIRST LOADING STAGE

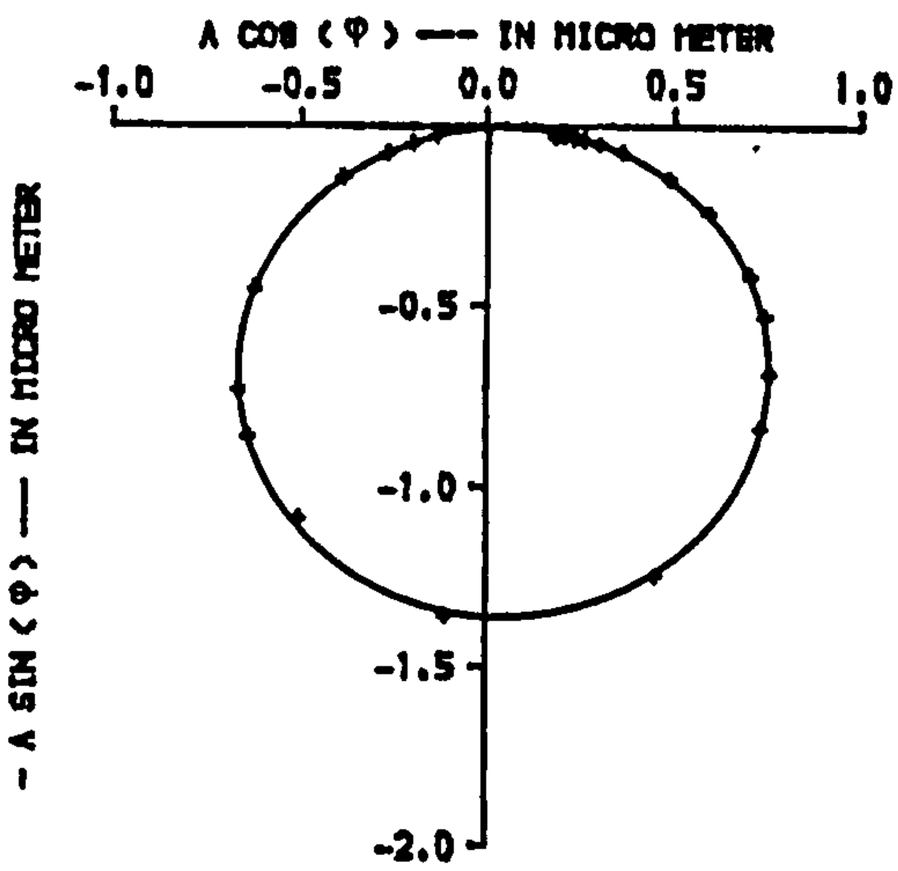

B. AFTER APPLYING FIRST LOADING STAGE

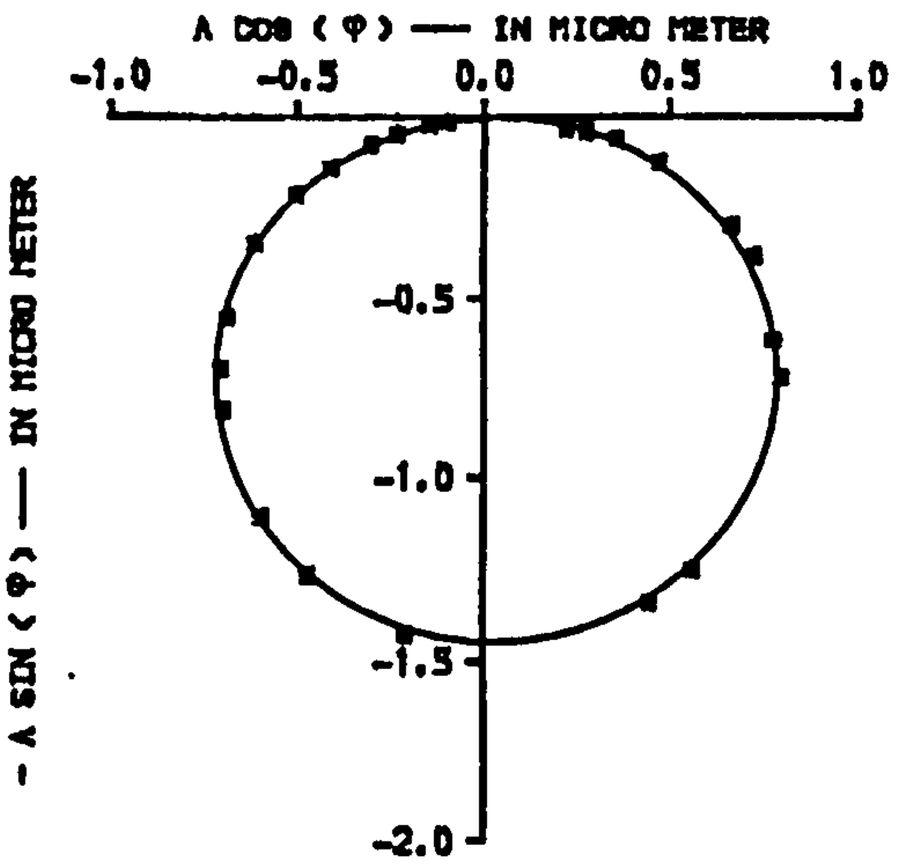

C. AFTER APPLYING SECOND LOADING STAGE

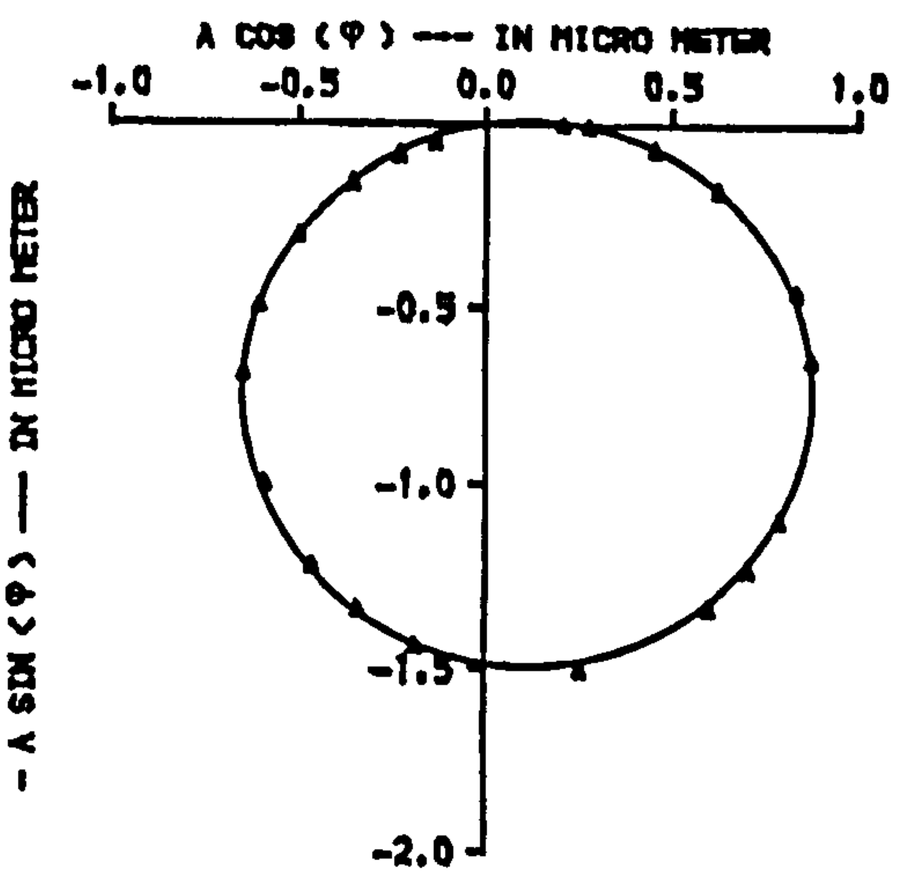

D. AFTER APPLYING THIRD LOADING STAGE

NOTES :

φ : phase angle between force of excitation and beam response

A : displacement amplitude of beam

FIG.7.15. POLAR DIAGRAMS OF BEAM-1 (FB/L1), FULLY BONDED, SECOND MODE, AT QUARTER SPAN, FLEXURAL CRACK PATTERN.

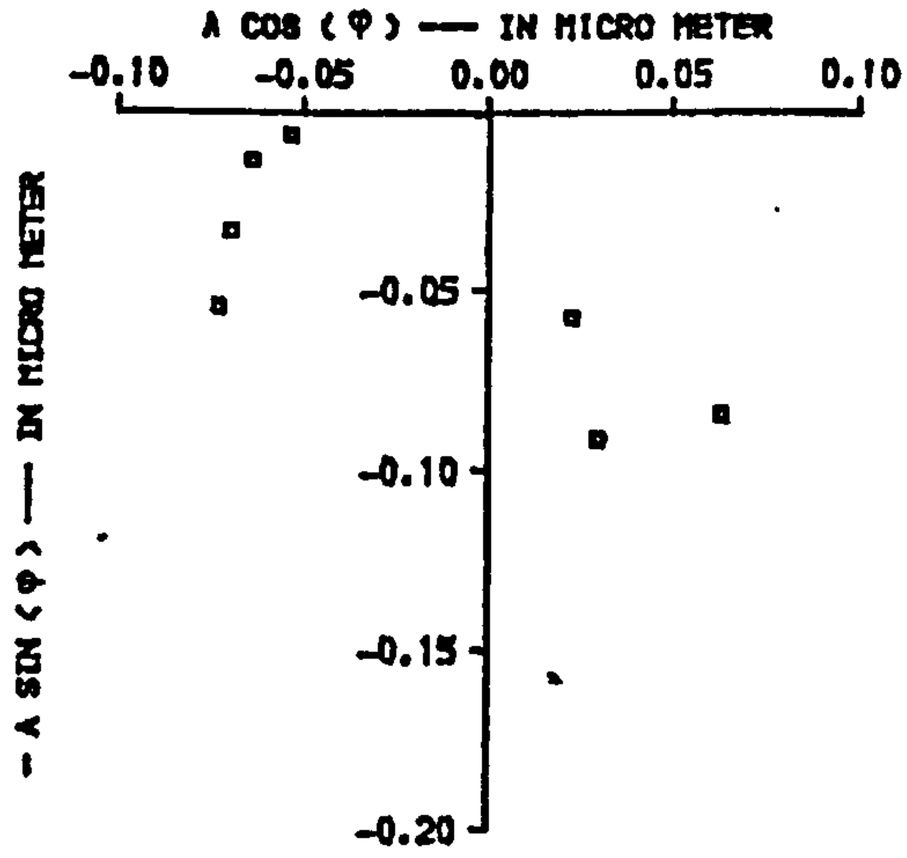

A. BEFORE APPLYING FIRST LOADING STAGE

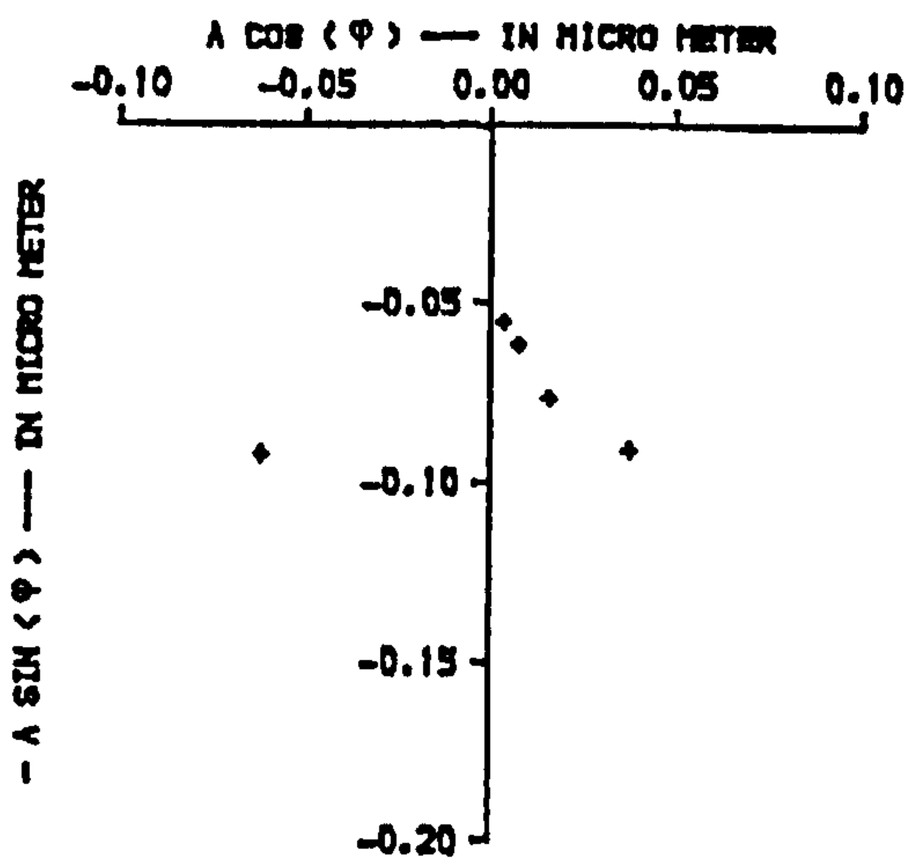

B. AFTER APPLYING FIRST LOADING STAGE

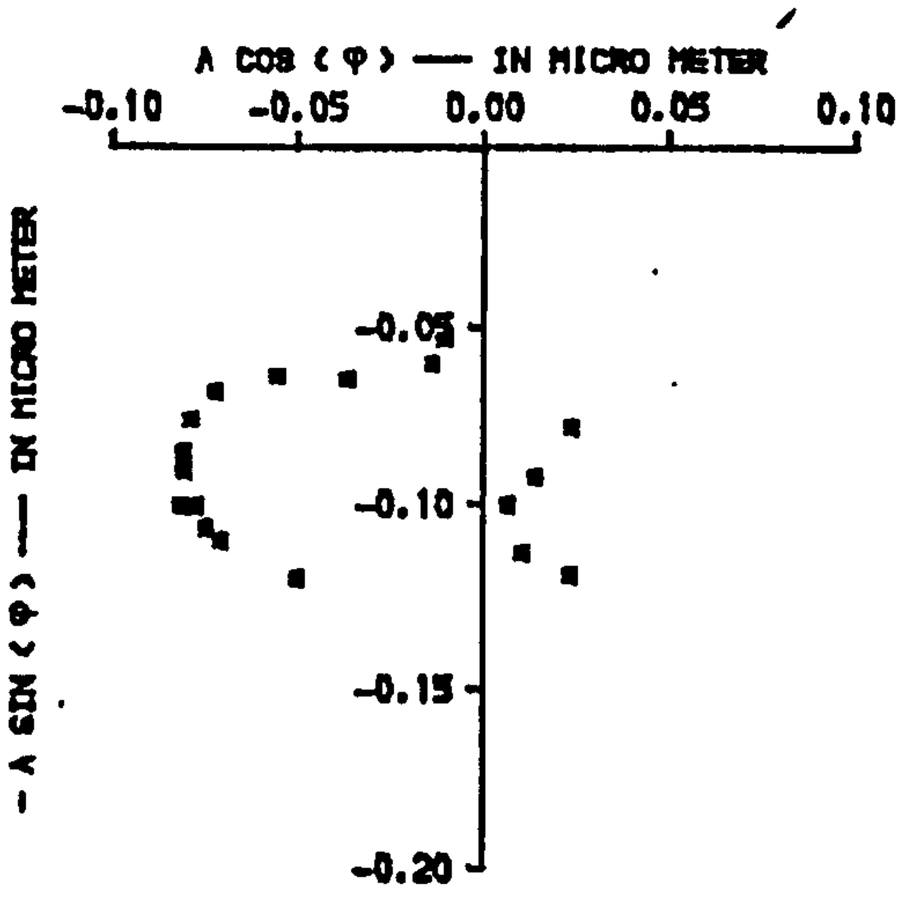

C. AFTER APPLYING SECOND LOADING STAGE

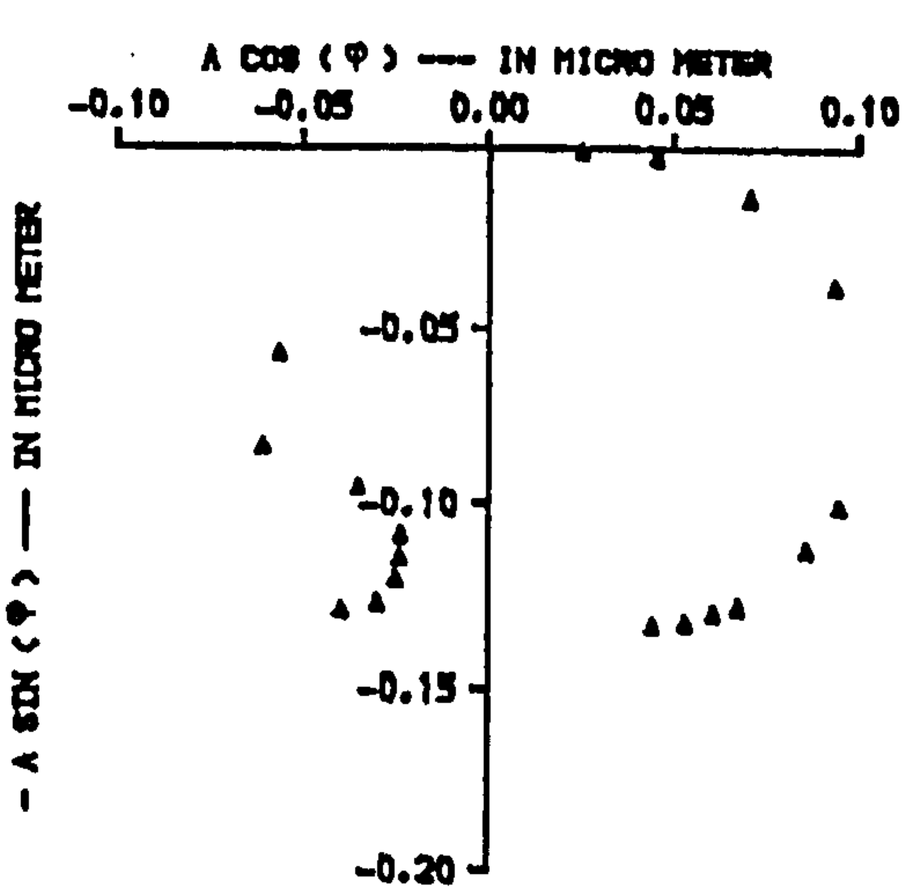

D. AFTER APPLYING THIRD LOADING STAGE

NOTES :

φ : phase angle between force of excitation and beam response

A : displacement amplitude of beam

FIG.7.16. POLAR DIAGRAMS OF BEAM-1 (FB/L1), FULLY BONDED, THIRD MODE, AT A SIXTH SPAN, FLEXURAL CRACK PATTERN.

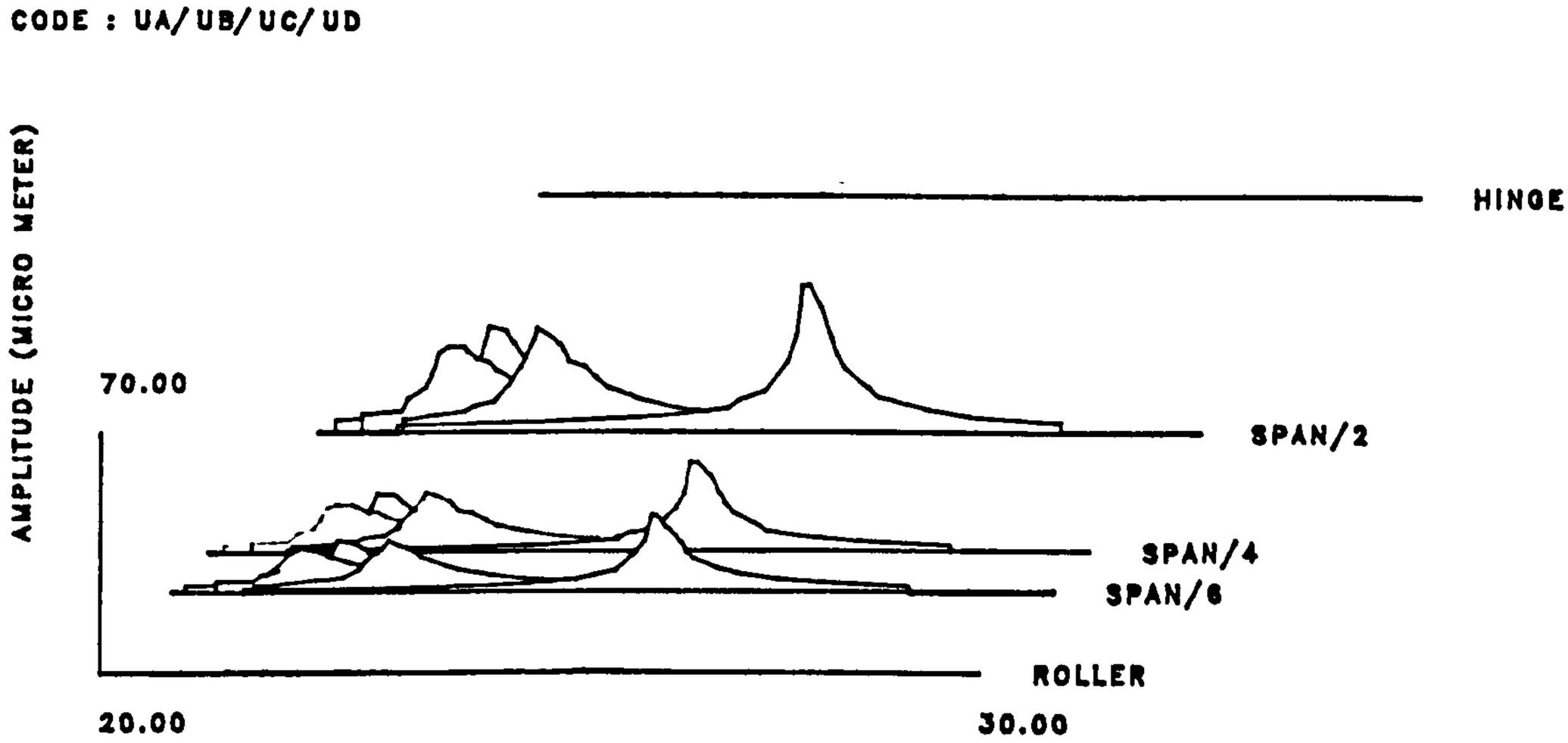

FIG.7.17.RESPONSE SPECTRA, BEAM-2 (PB/L1) SUBJECT TO FOUR LOADING STAGES, PARTIALLY BONDED, FLEXURAL CRACK PATTERN, FIRST MODE.

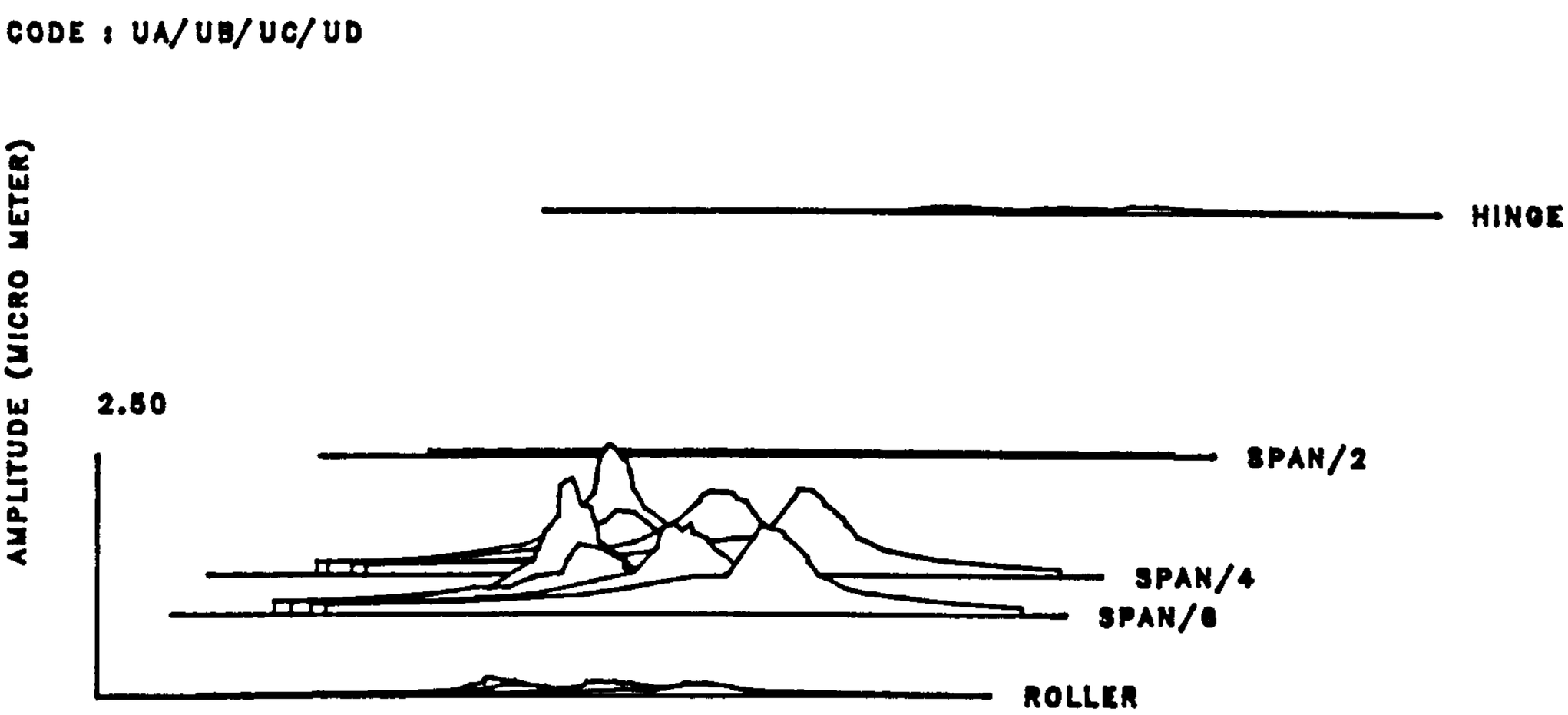

FIG.7.18.RESPONSE SPECTRA, BEAM-2 (PB/L1) SUBJECT TO FOUR LOADING STAGES, PARTIALLY BONDED, FLEXURAL CRACK PATTERN, SECOND MODE.

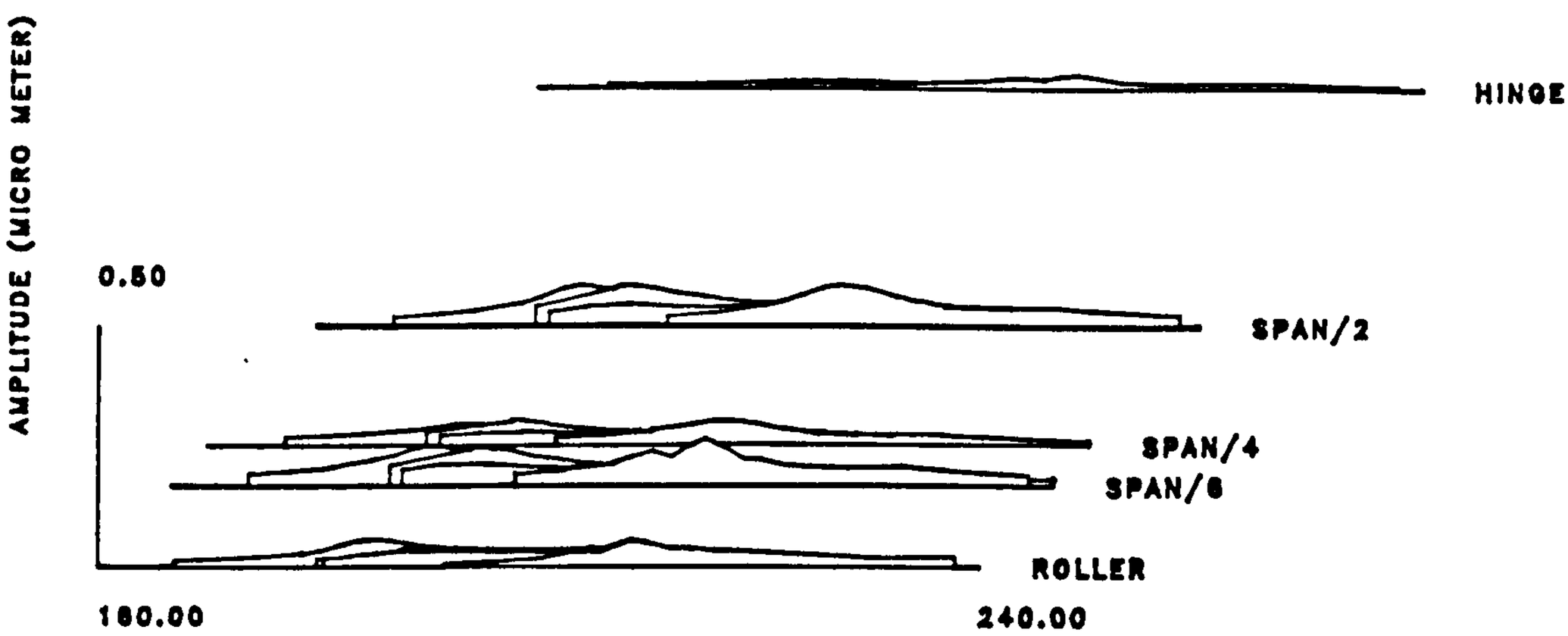

FIG.7.19.RESPONSE SPECTRA, BEAM-2 (PB/L1) SUBJECT TO FOUR LOADING STAGES, PARTIALLY BONDED, FLEXURAL CRACK PATTERN, THIRD MODE.

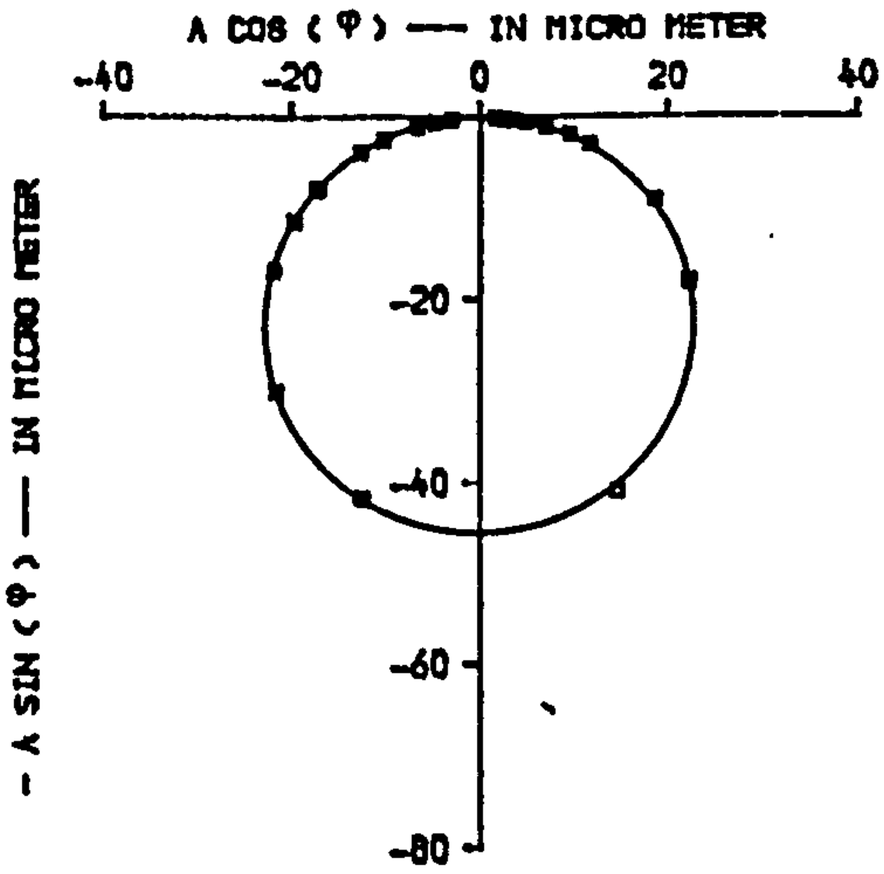

A. BEFORE APPLYING FIRST LOADING STAGE

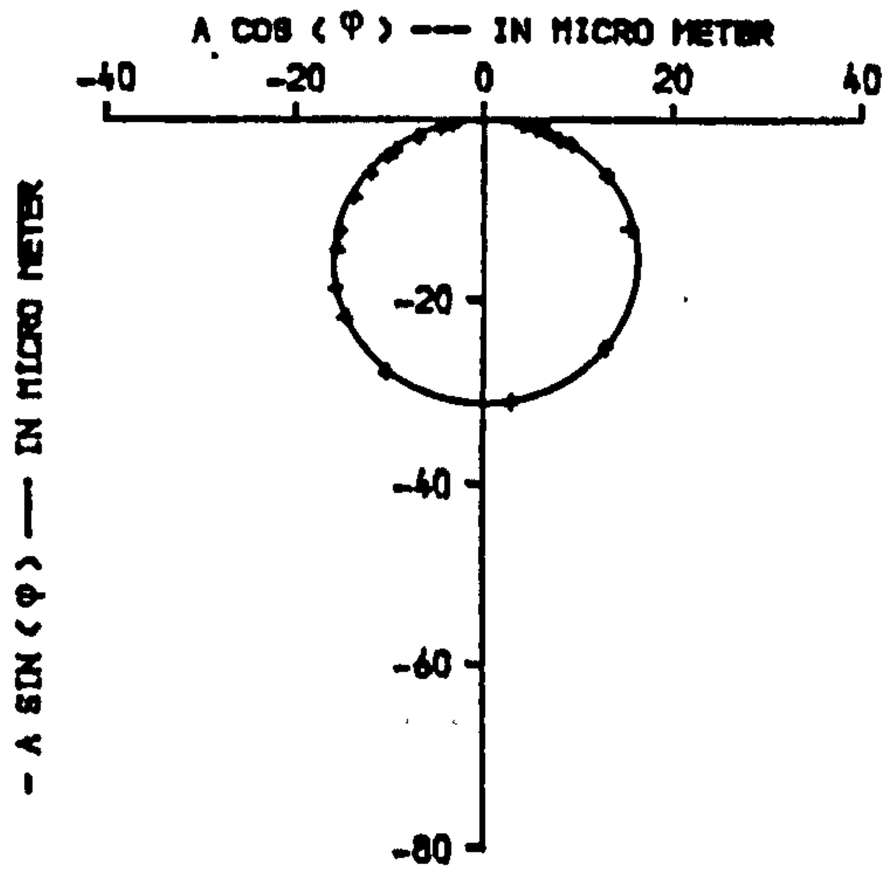

B. AFTER APPLYING FIRST LOADING STAGE

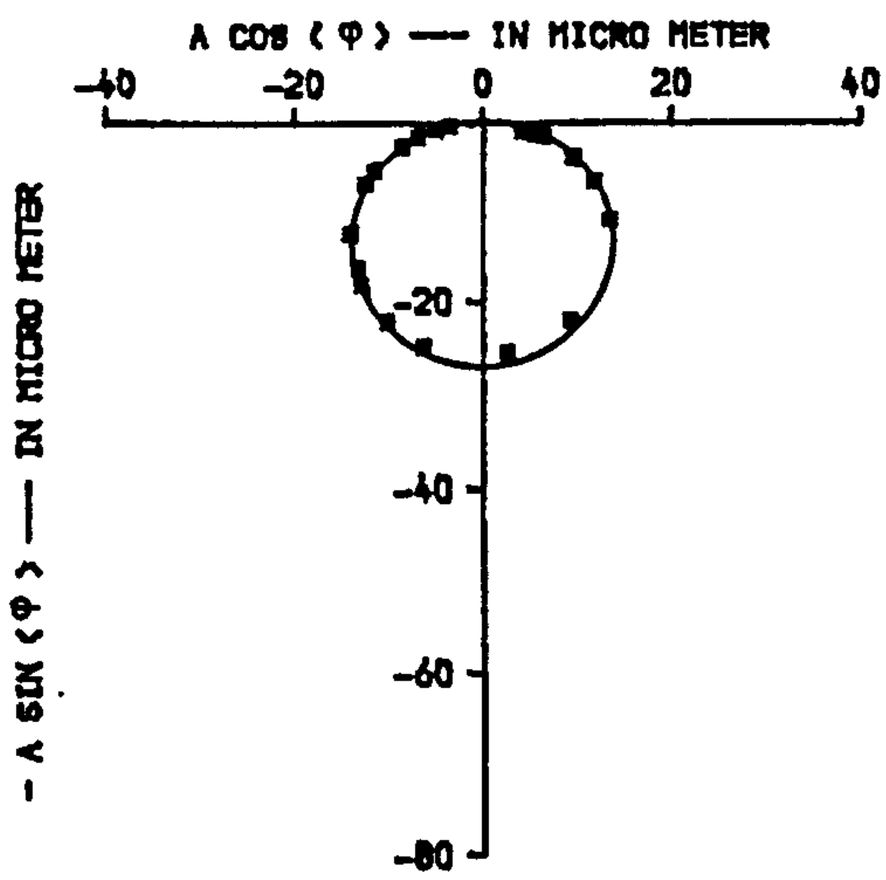

C. AFTER APPLYING SECOND LOADING STAGE

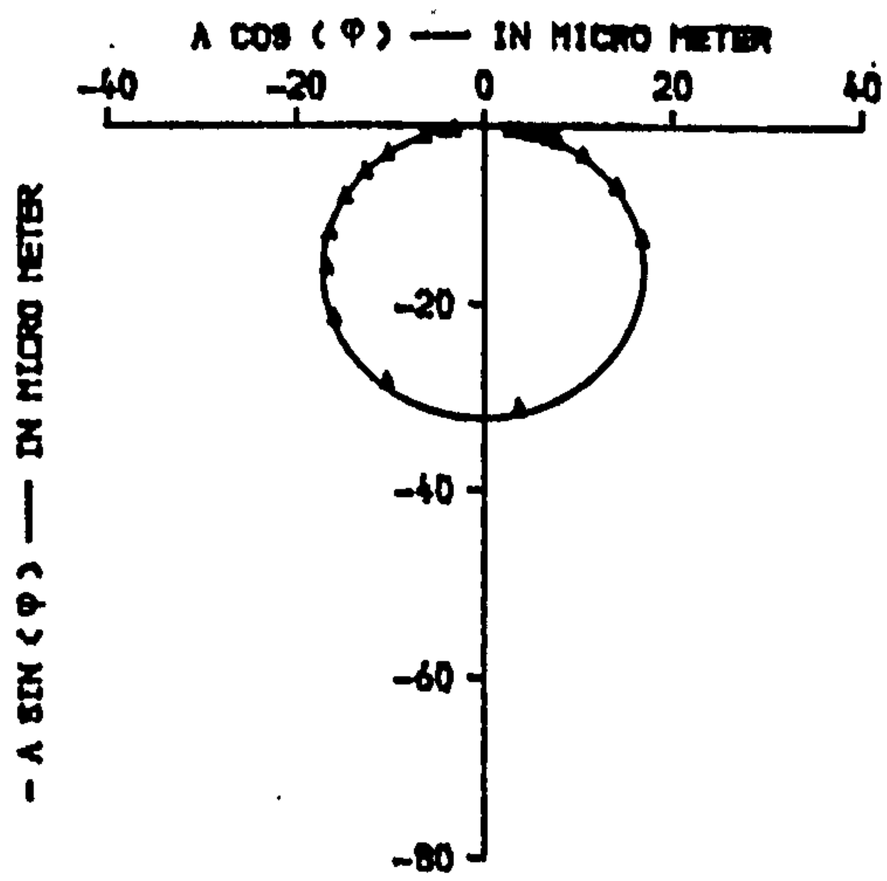

D. AFTER APPLYING THIRD LOADING STAGE

NOTES :

φ : phase angle between force of excitation and beam response
A : displacement amplitude of beam

FIG.7.20. POLAR DIAGRAMS OF BEAM-2 (PB/L1), PARTIALLY BONDED, FIRST MODE, AT MID SPAN, FLEXURAL CRACK PATTERN

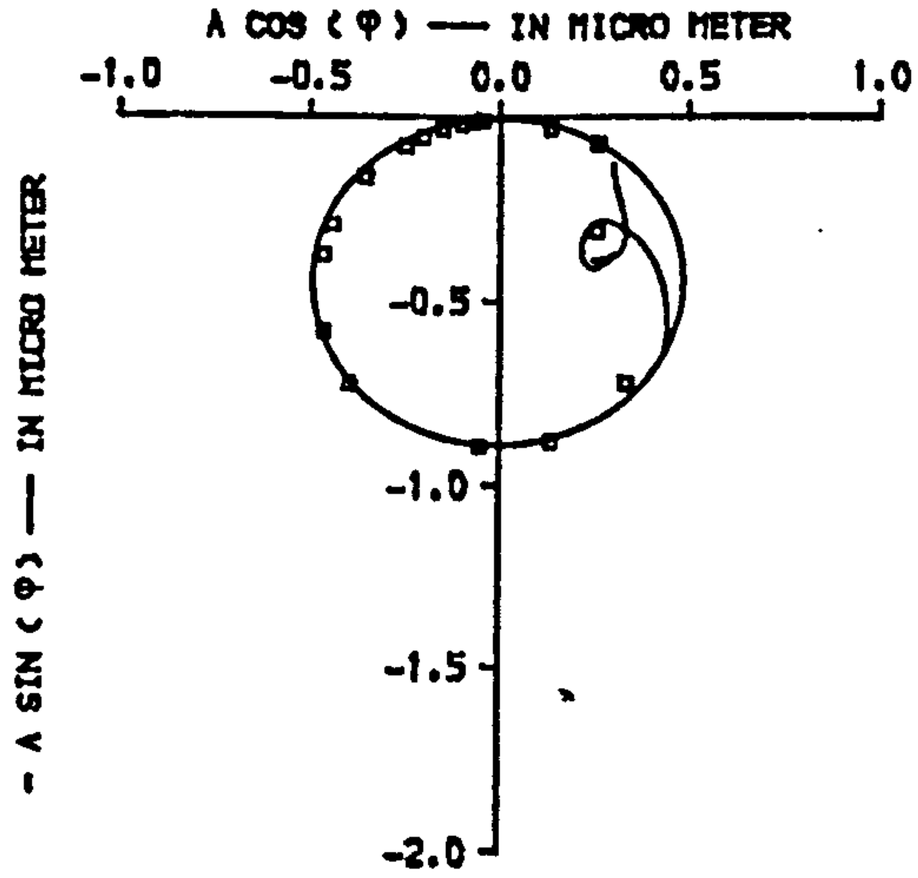

A. BEFORE APPLYING FIRST LOADING STAGE

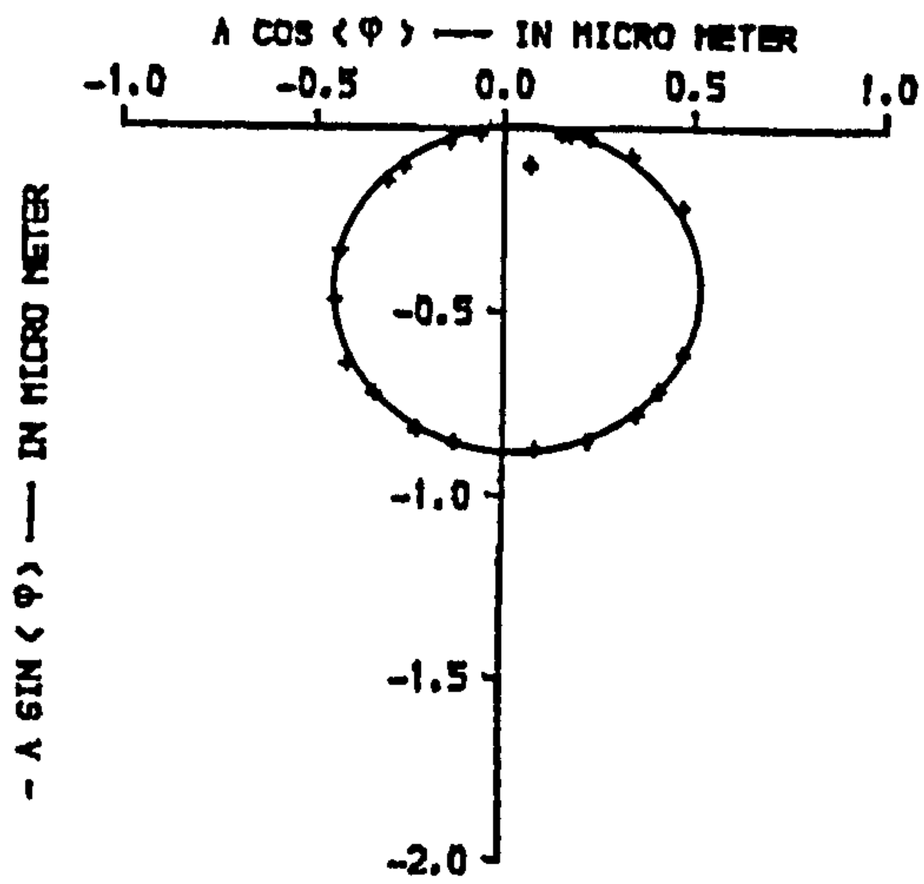

B. AFTER APPLYING FIRST LOADING STAGE

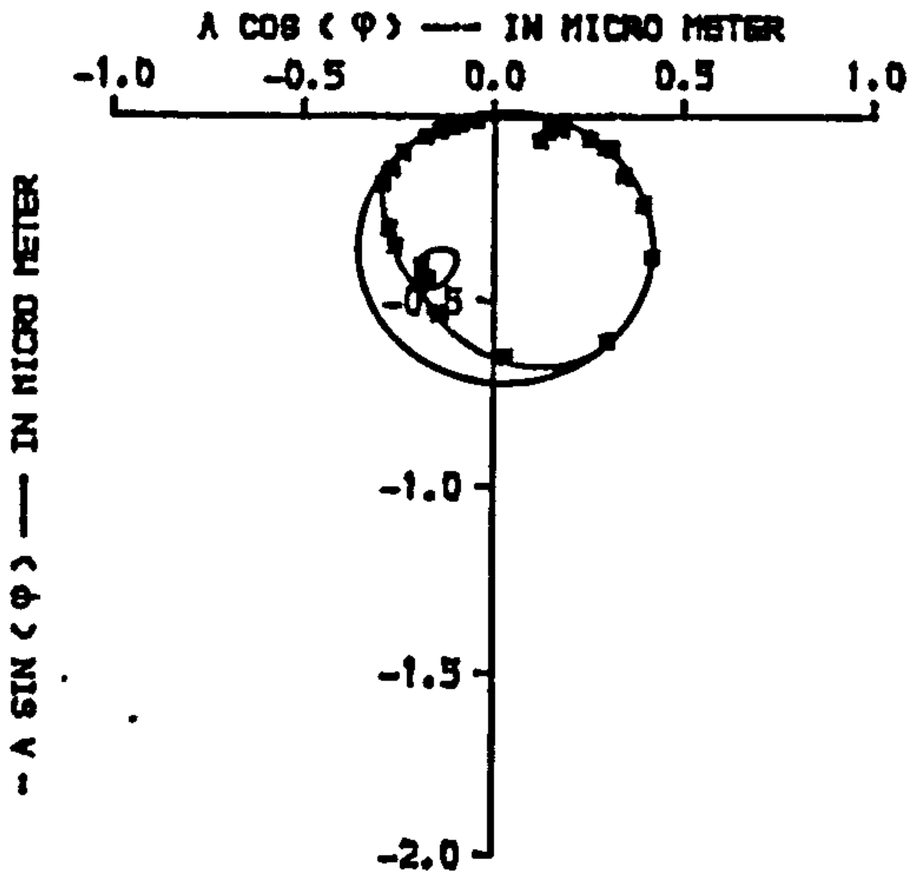

C. AFTER APPLYING SECOND LOADING STAGE

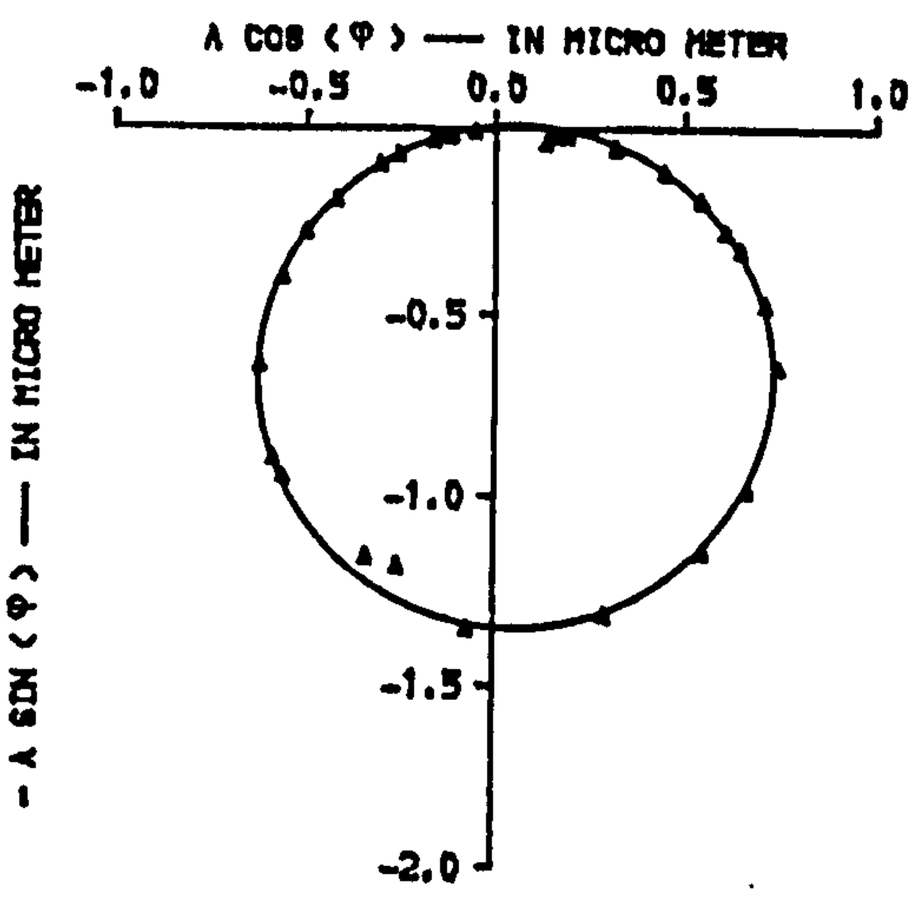

D. AFTER APPLYING THIRD LOADING STAGE

NOTES :

φ : phase angle between force of excitation and beam response
A : displacement amplitude of beam

FIG.7.21. POLAR DIAGRAMS OF BEAM-2 (PB/L1), PARTIALLY BONDED, SECOND MODE, AT QUARTER SPAN, FLEXURAL CRACK PATTERN

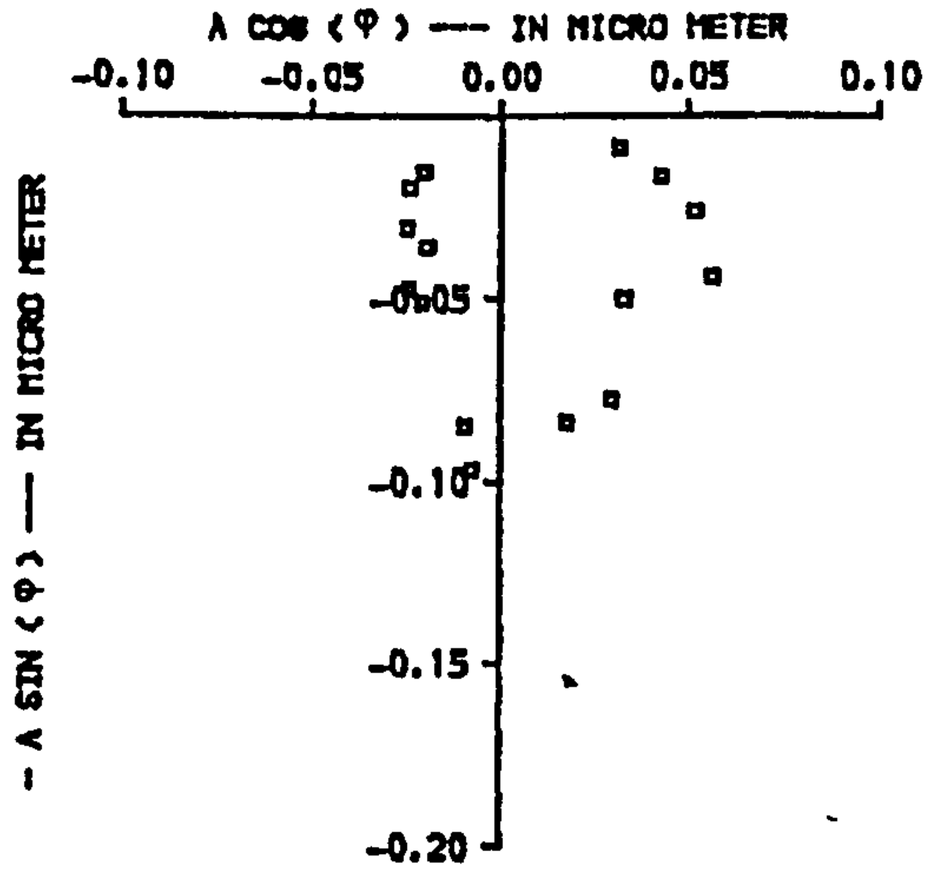

A. BEFORE APPLYING FIRST LOADING STAGE

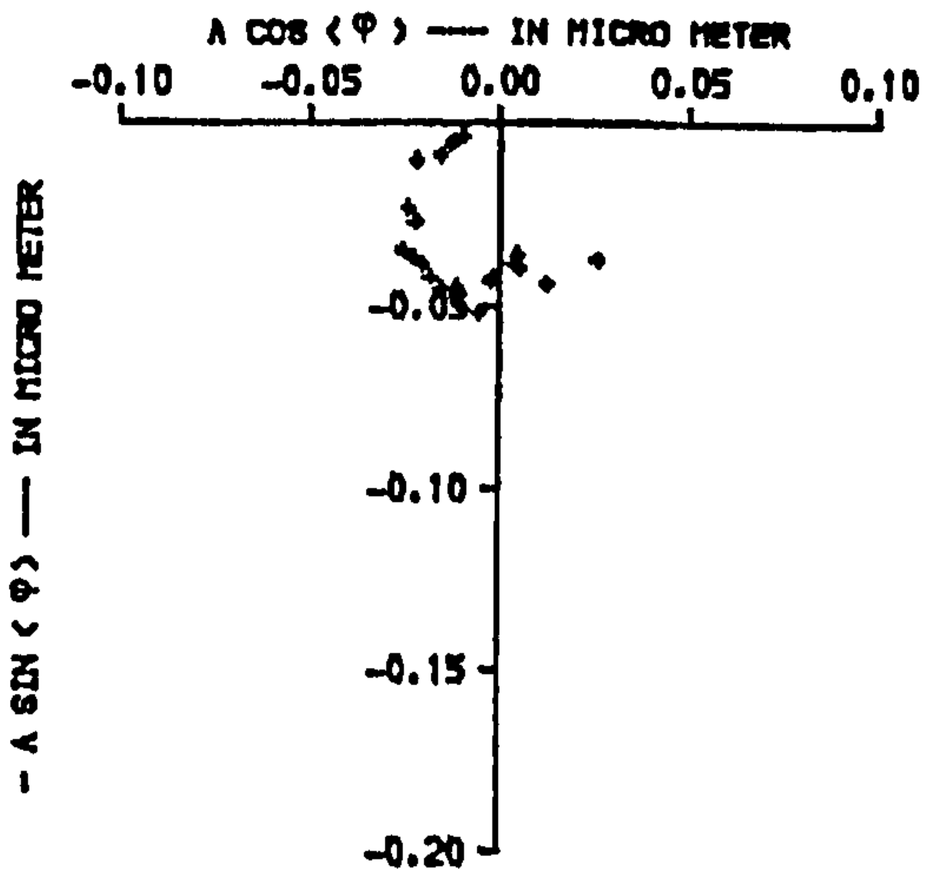

B. AFTER APPLYING FIRST LOADING STAGE

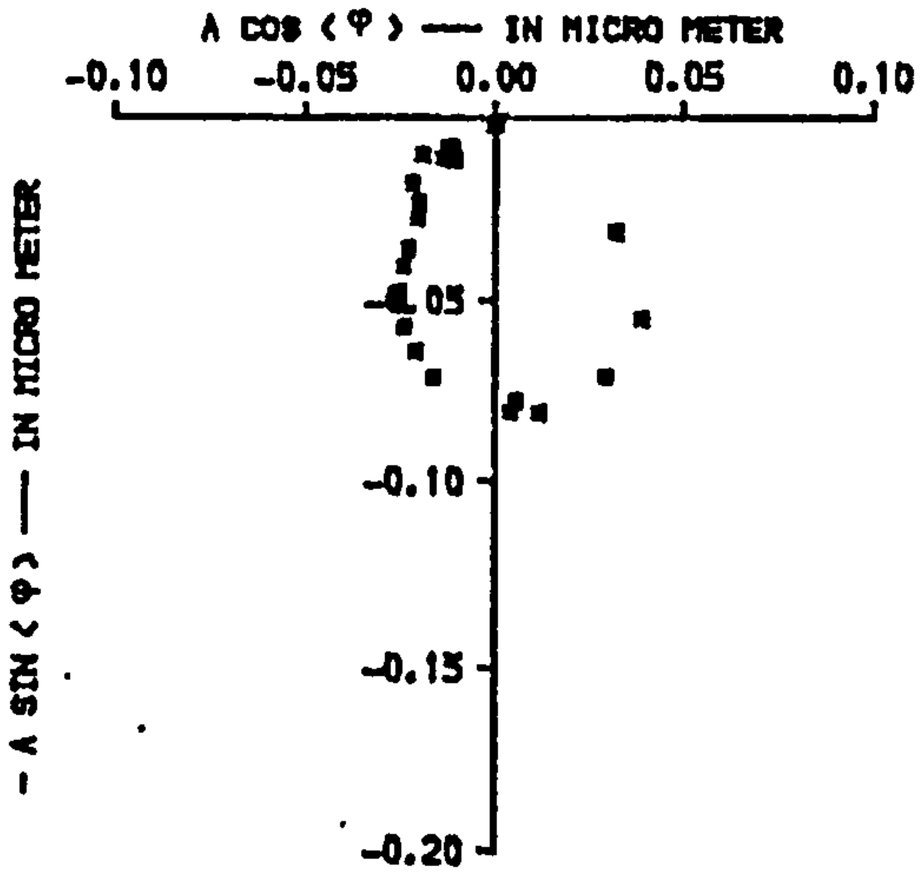

C. AFTER APPLYING SECOND LOADING STAGE

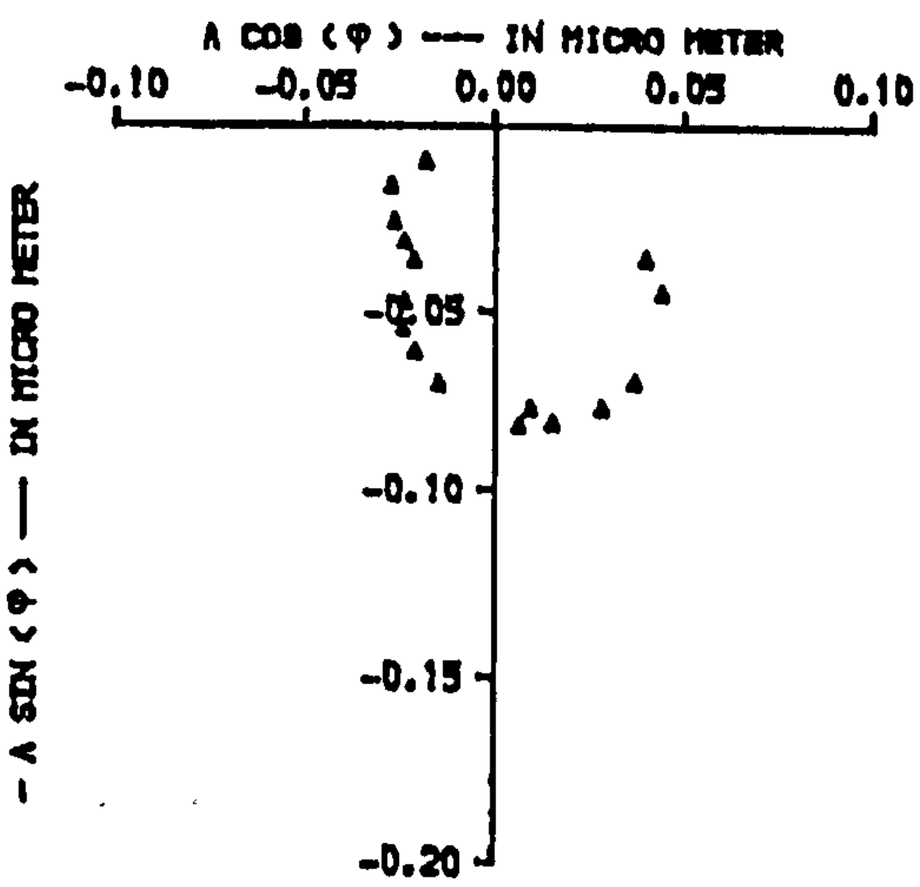

D. AFTER APPLYING THIRD LOADING STAGE

NOTES :

φ : phase angle between force of excitation and beam response
A : displacement amplitude of beam

FIG.7.22. POLAR DIAGRAMS OF BEAM-2 (PB/L1), PARTIALLY BONDED, THIRD MODE, AT A SIXTH SPAN, FLEXURAL CRACK PATTERN

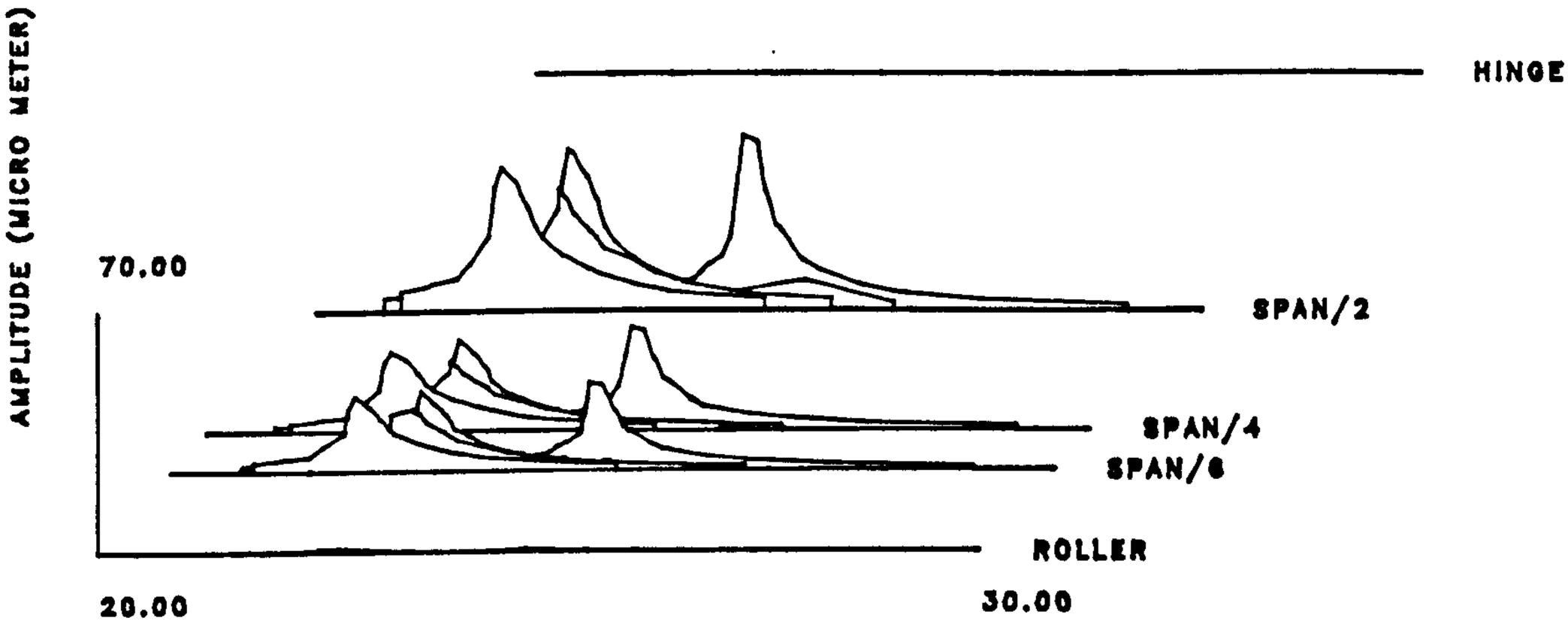

FIG.7.23. RESPONSE SPECTRA, BEAM-3 (FB/L2) SUBJECT TO FOUR LOADING STAGES, FULLY BONDED, DIAGONAL SPLITTING CRACK PATTERN, FIRST MODE.

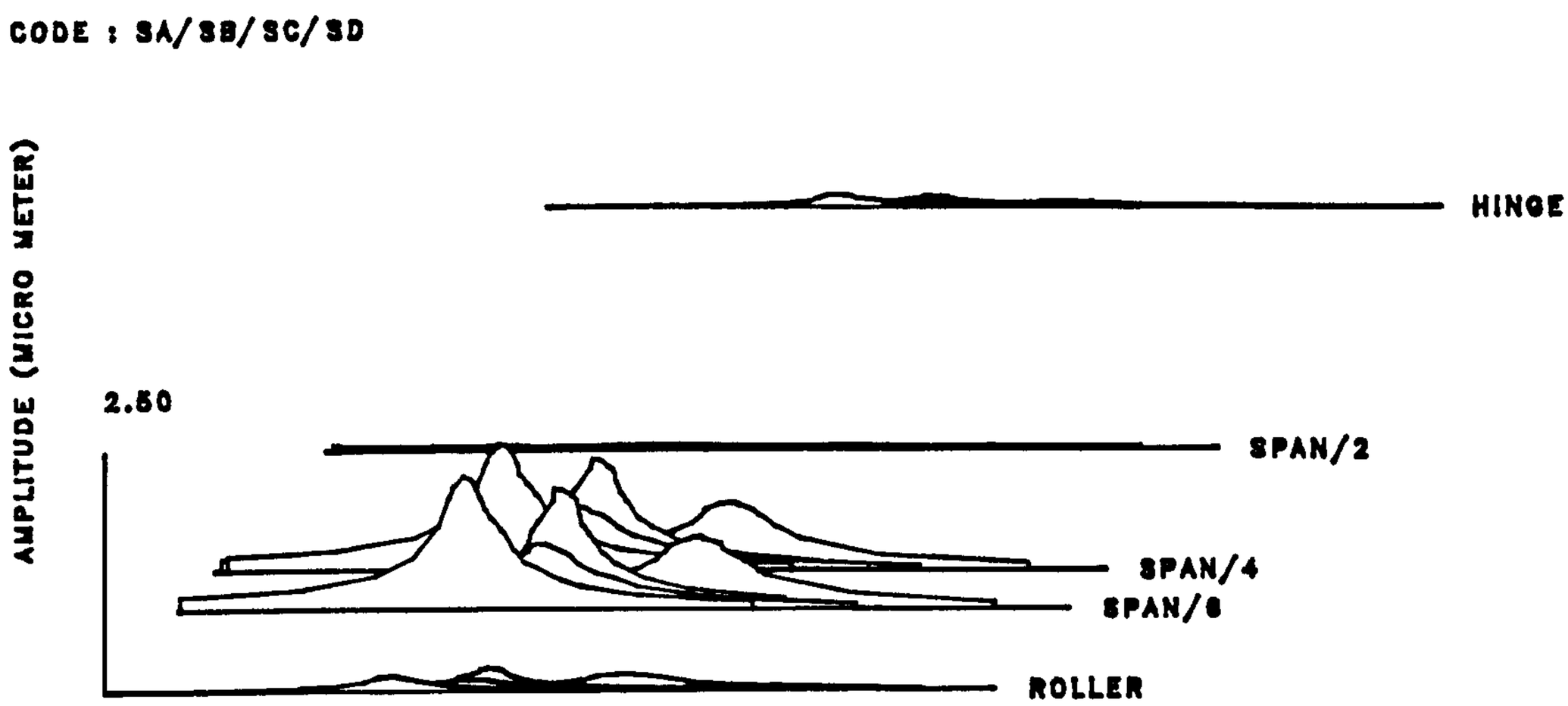

FIG.7.24. RESPONSE SPECTRA, BEAM-3 (FB/L2) SUBJECT TO FOUR LOADING STAGES, FULLY BONDED, DIAGONAL SPLITTING CRACK PATTERN, SECOND MODE.

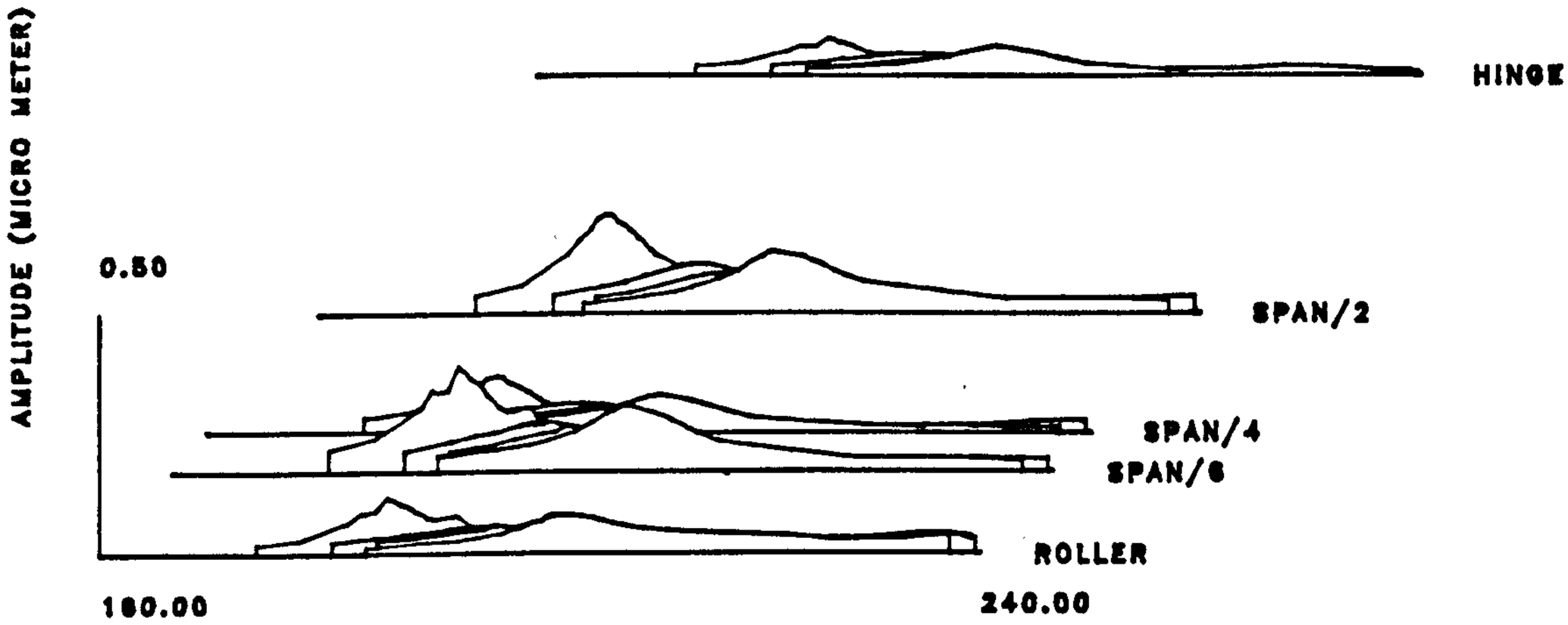

FIG.7.25. RESPONSE SPECTRA, BEAM-3 (FB/L2) SUBJECT TO FOUR LOADING STAGES, FULLY BONDED, DIAGONAL SPLITTING CRACK PATTERN, THIRD MODE.

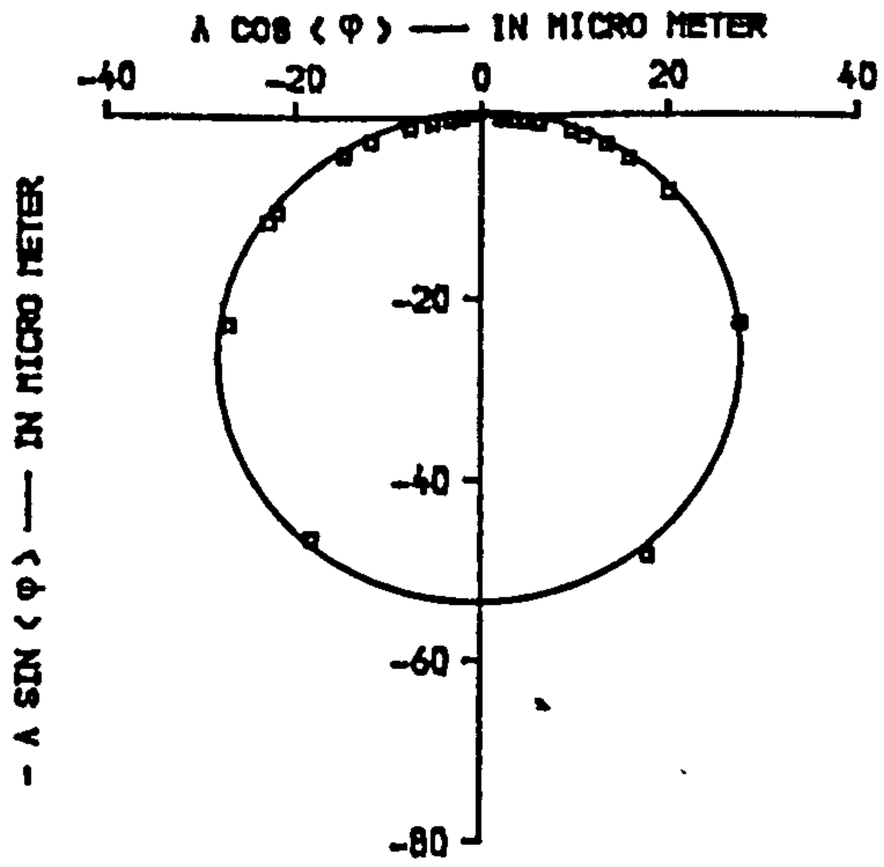

A. BEFORE APPLYING FIRST LOADING STAGE

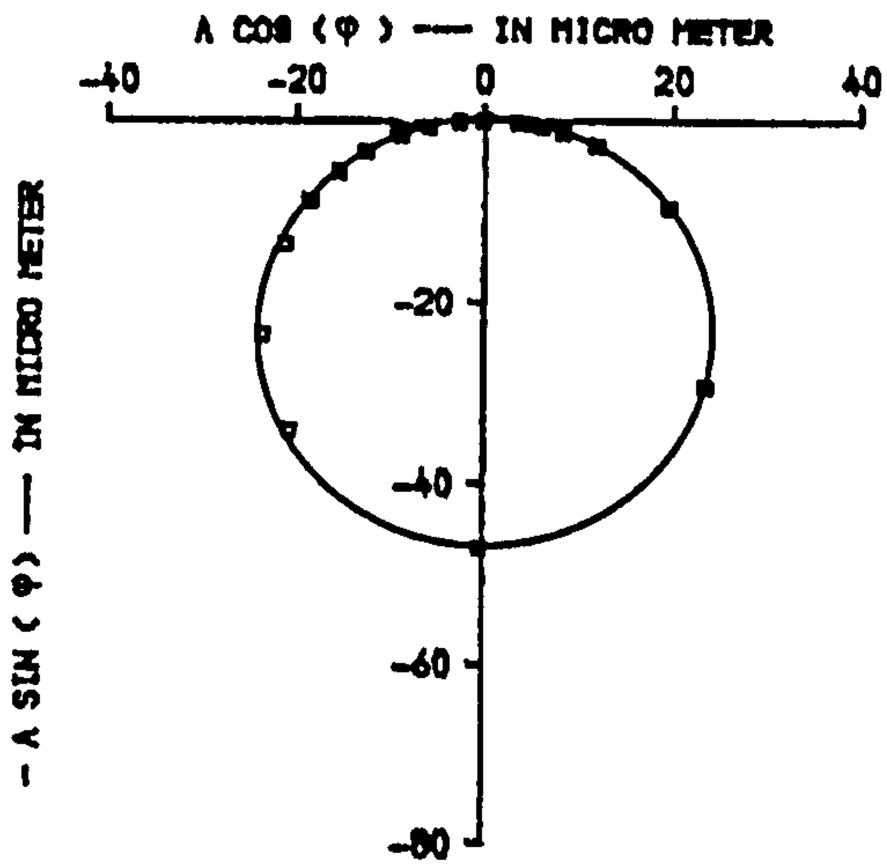

B. AFTER APPLYING FIRST LOADING STAGE

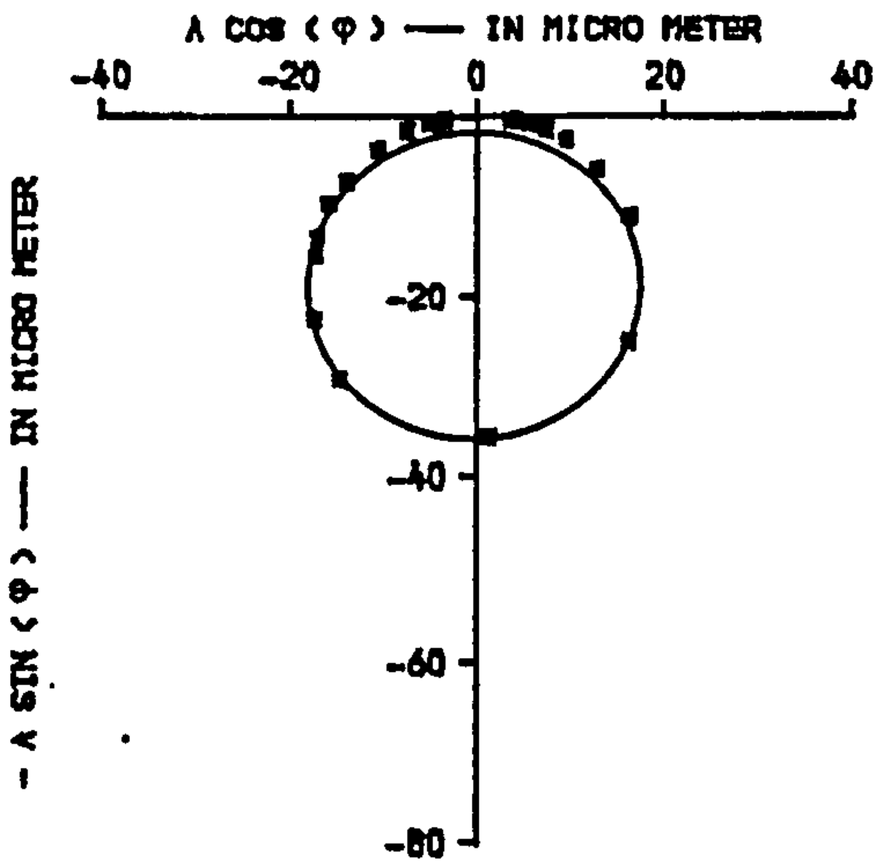

C. AFTER APPLYING SECOND LOADING STAGE

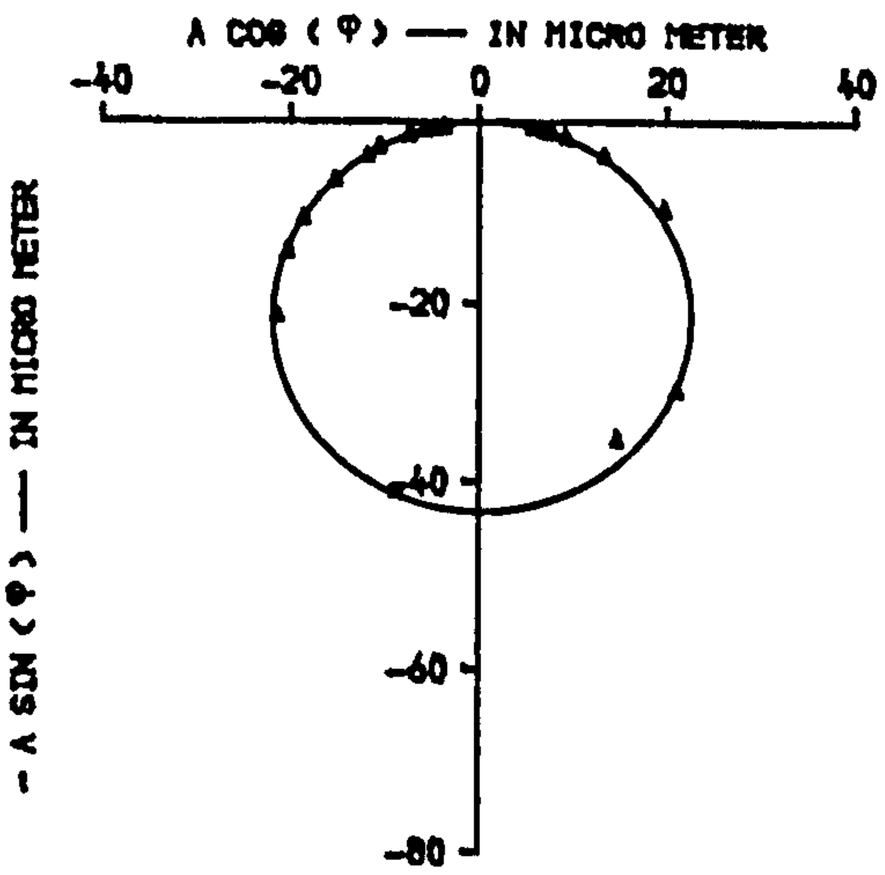

D. AFTER APPLYING THIRD LOADING STAGE

NOTES :

φ : phase angle between force of excitation and beam response
A : displacement amplitude of beam

FIG.7.26. POLAR DIAGRAMS OF BEAM-3 (FB/L2), FULLY BONDED, FIRST MODE, AT MID SPAN, DIAGONAL SPLITTING CRACK PATTERN.

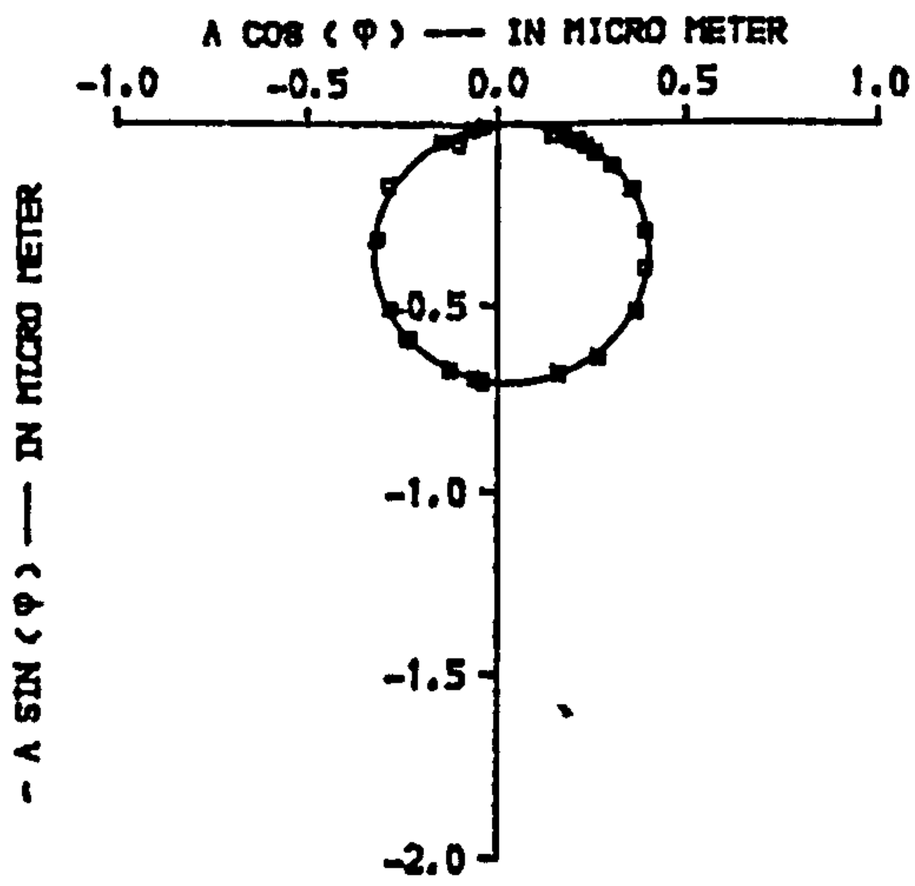

A. BEFORE APPLYING FIRST LOADING STAGE

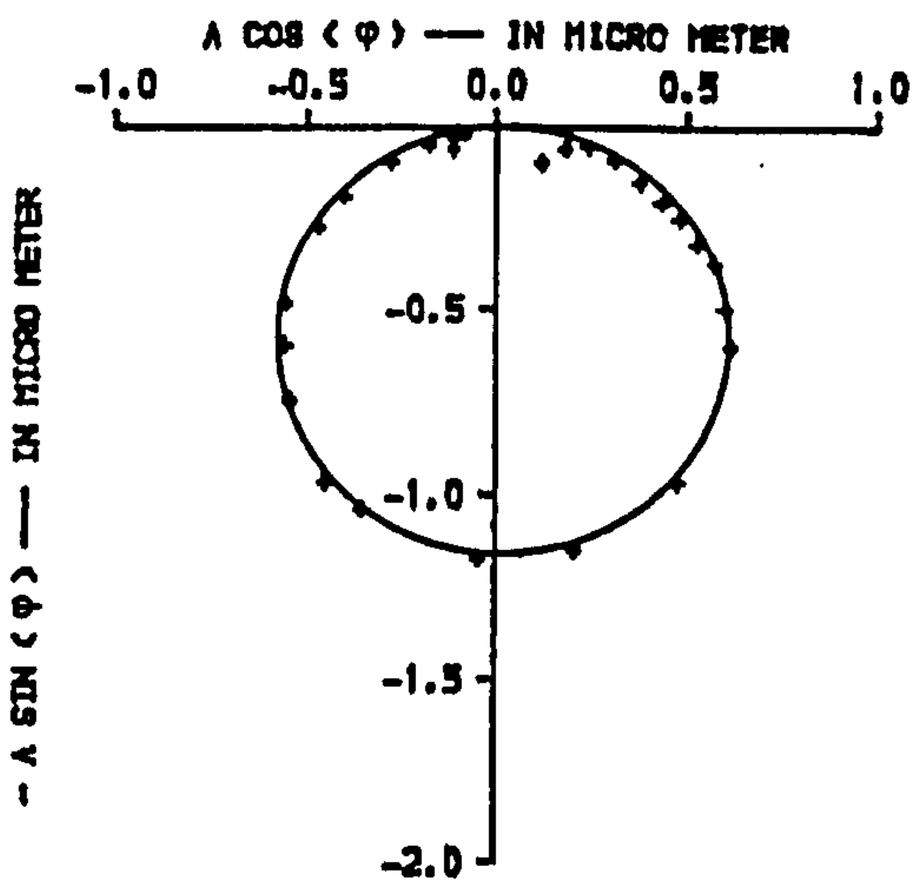

B. AFTER APPLYING FIRST LOADING STAGE

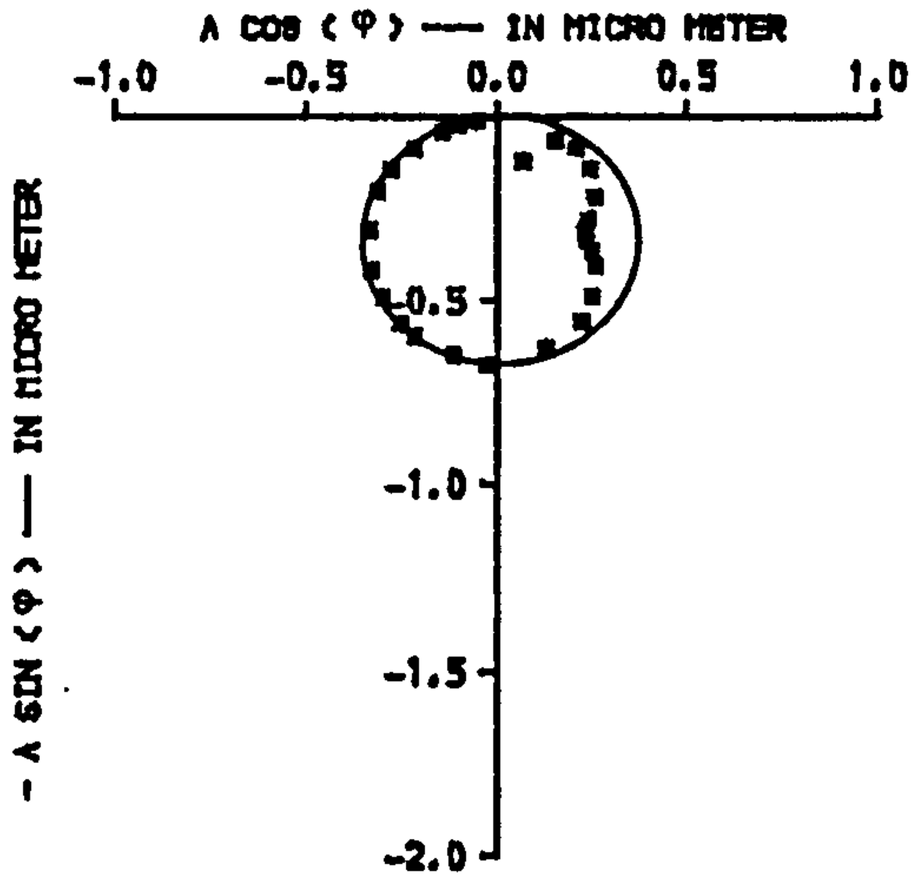

C. AFTER APPLYING SECOND LOADING STAGE

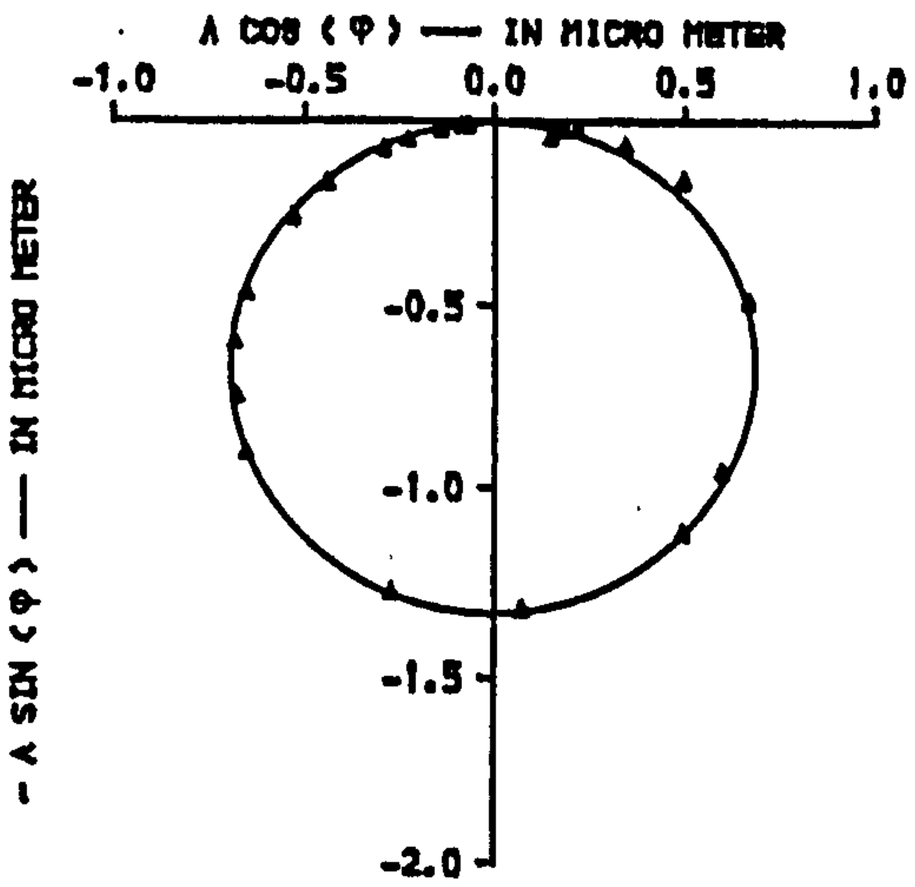

D. AFTER APPLYING THIRD LOADING STAGE

NOTES :

φ : phase angle between force of excitation and beam response

A : displacement amplitude of beam

FIG.7.27. POLAR DIAGRAMS OF BEAM-3 (FB/L2), FULLY BONDED, SECOND MODE, AT QUARTER SPAN, DIAGONAL SPLITTING CRACK PATTERN.

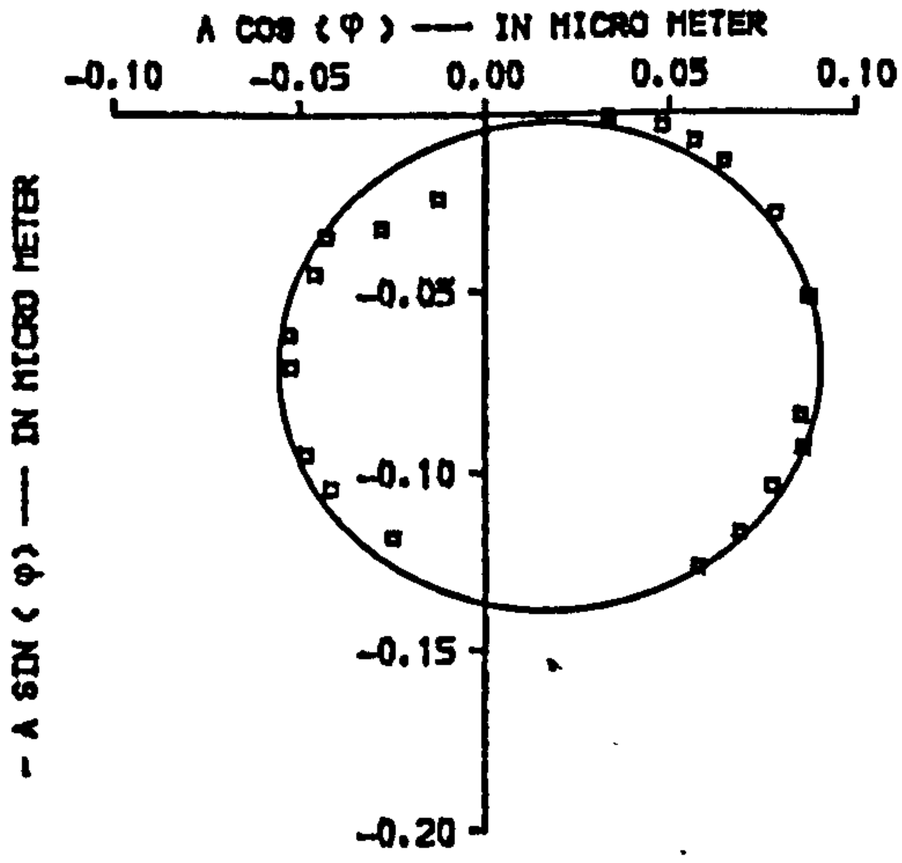

A. BEFORE APPLYING FIRST LOADING STAGE

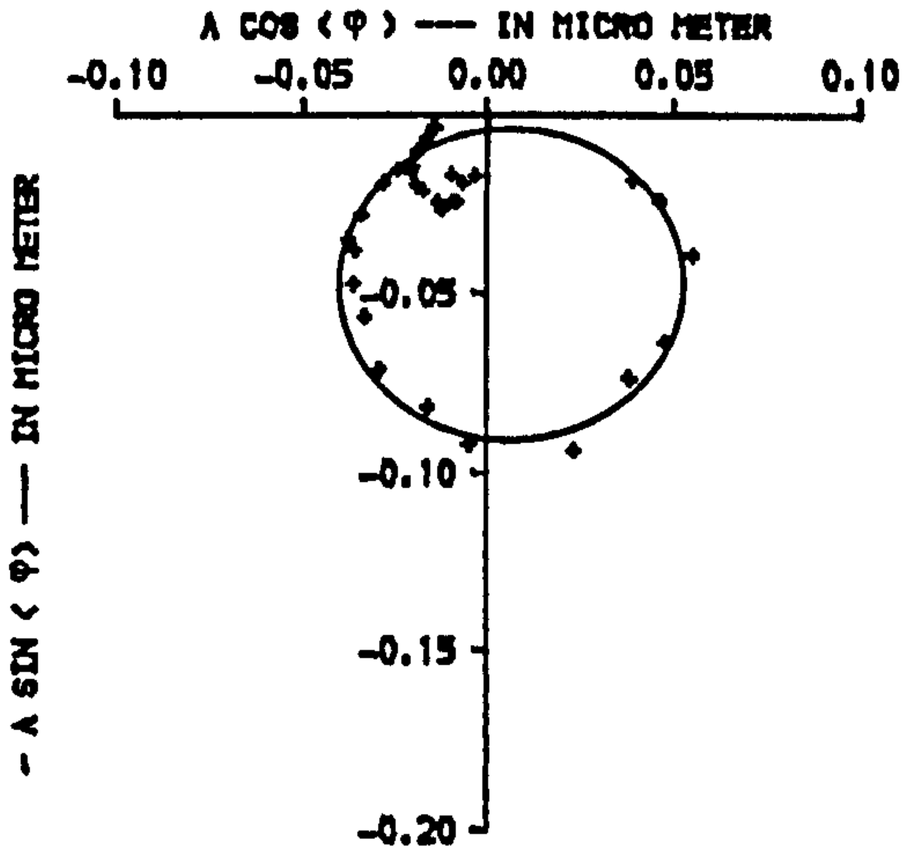

B. AFTER APPLYING FIRST LOADING STAGE

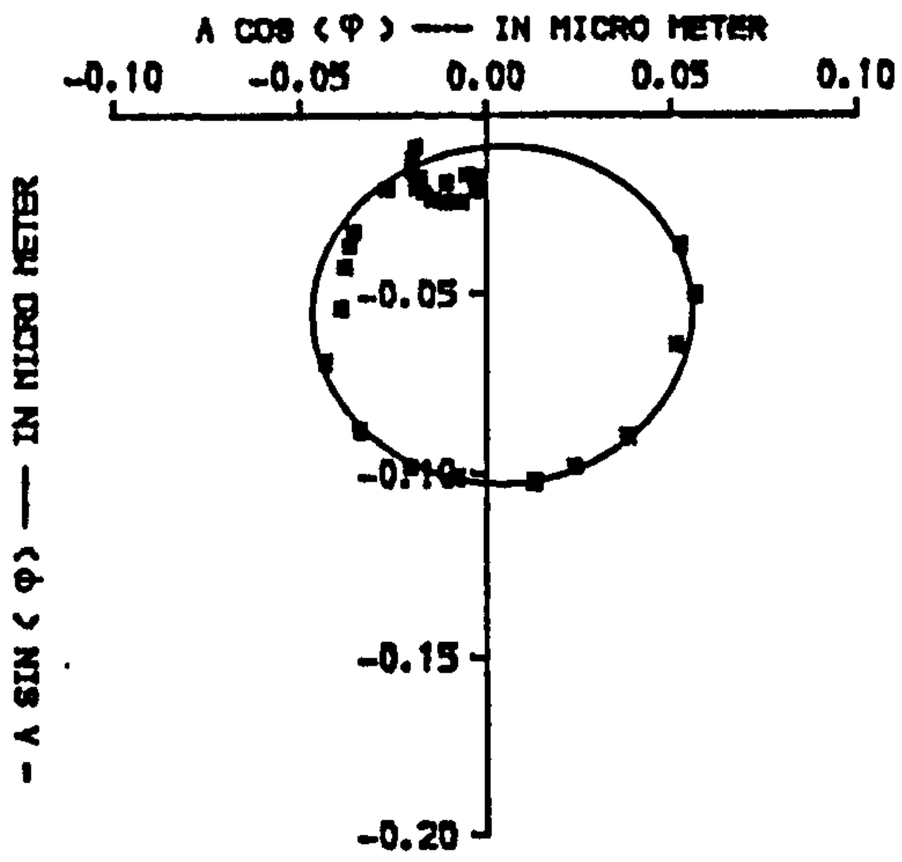

C. AFTER APPLYING SECOND LOADING STAGE

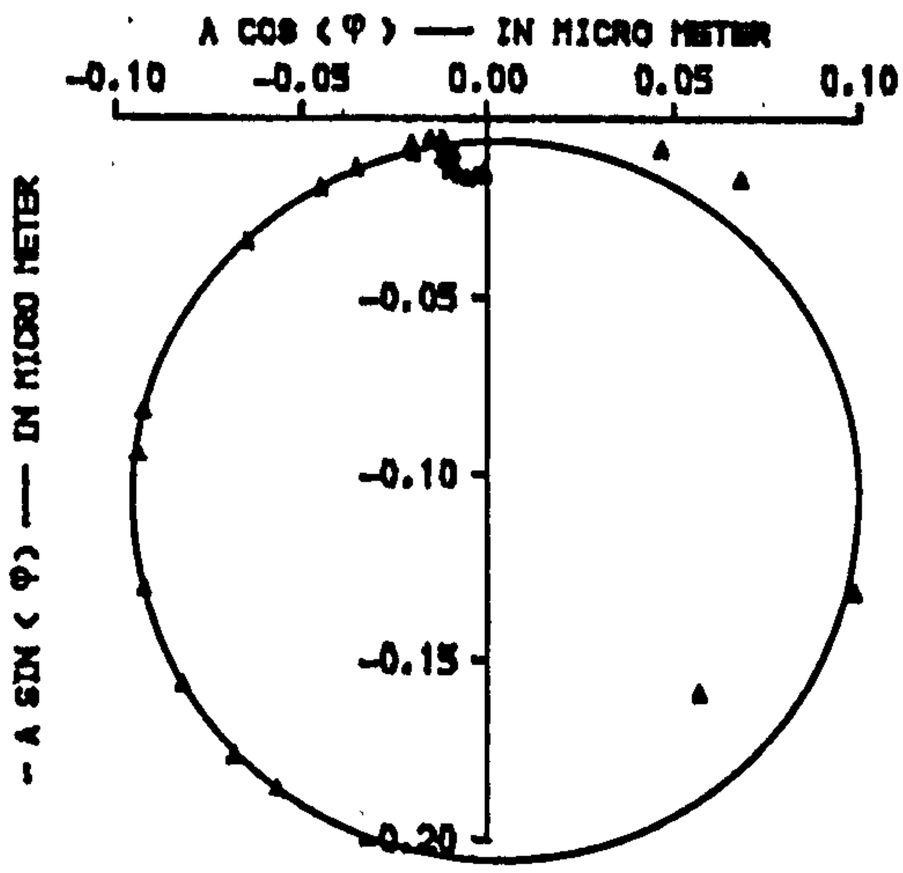

D. AFTER APPLYING THIRD LOADING STAGE

NOTES :

φ : phase angle between force of excitation and beam response

A : displacement amplitude

FIG.7.28. POLAR DIAGRAMS OF BEAM-3 (FB/L2), FULLY BONDED, THIRD MODE, AT A SIXTH SPAN , DIAGONAL SPLITTING CRACK PATTERN.

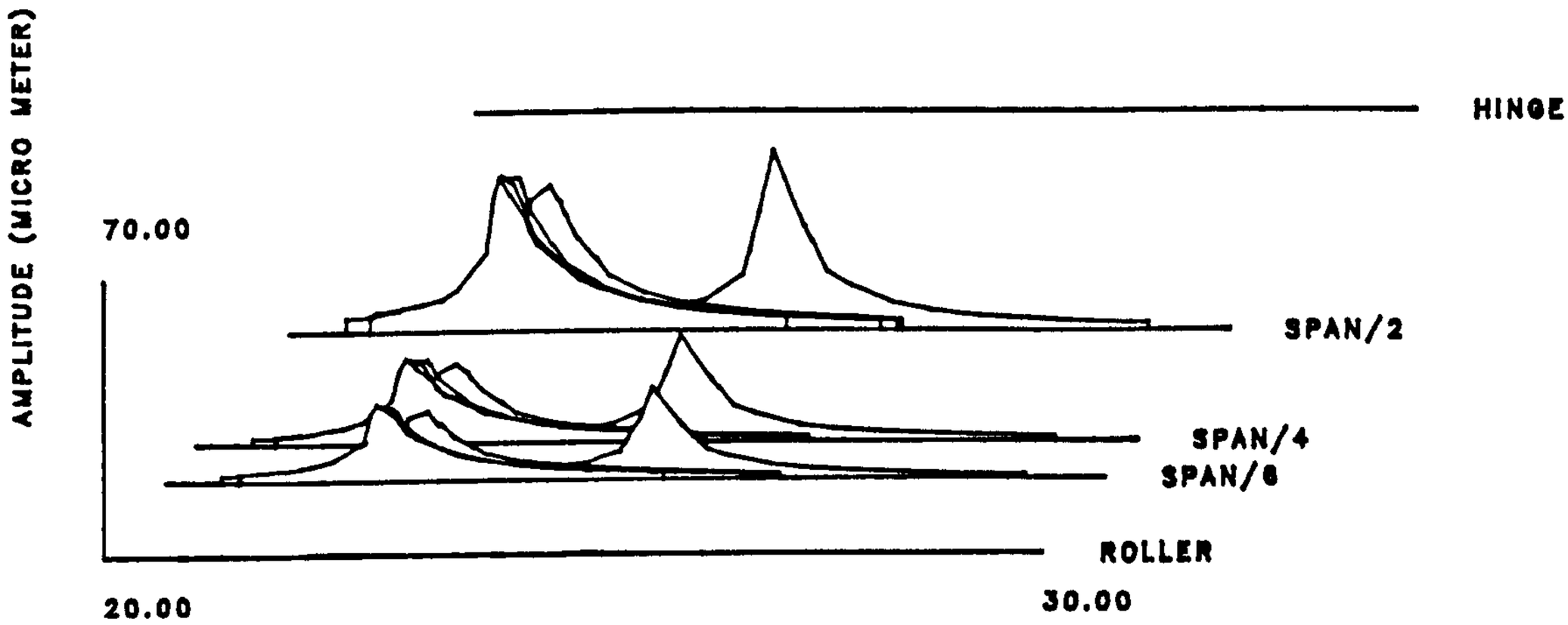

FIG.7.29.RESPONSE SPECTRA, BEAM-4 (PB/L2) SUBJECT TO SIX LOADING STAGES, PARTIALLY BONDED, DIAGONAL SPLITTING CRACK PATTERN, FIRST MODE.

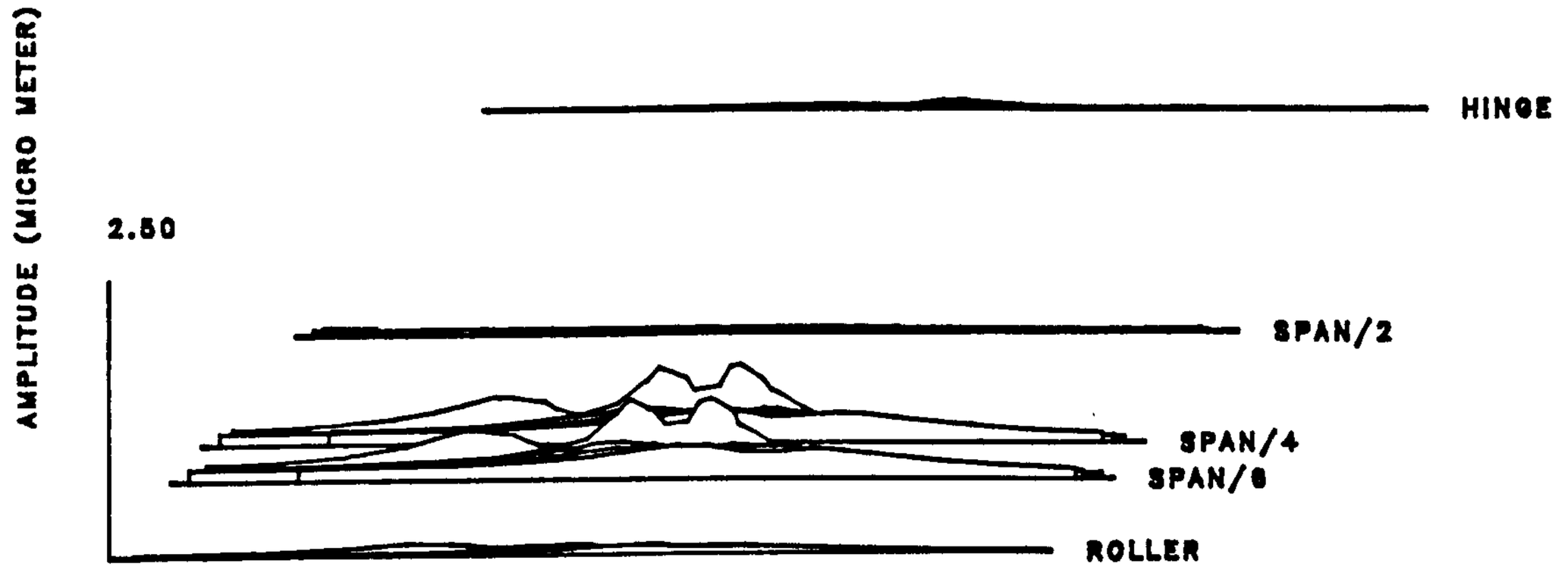

FIG.7.30.RESPONSE SPECTRA, BEAM-4 (PB/L2) SUBJECT TO SIX LOADING STAGES, PARTIALLY BONDED, DIAGONAL SPLITTING CRACK PATTERN, SECOND MODE.

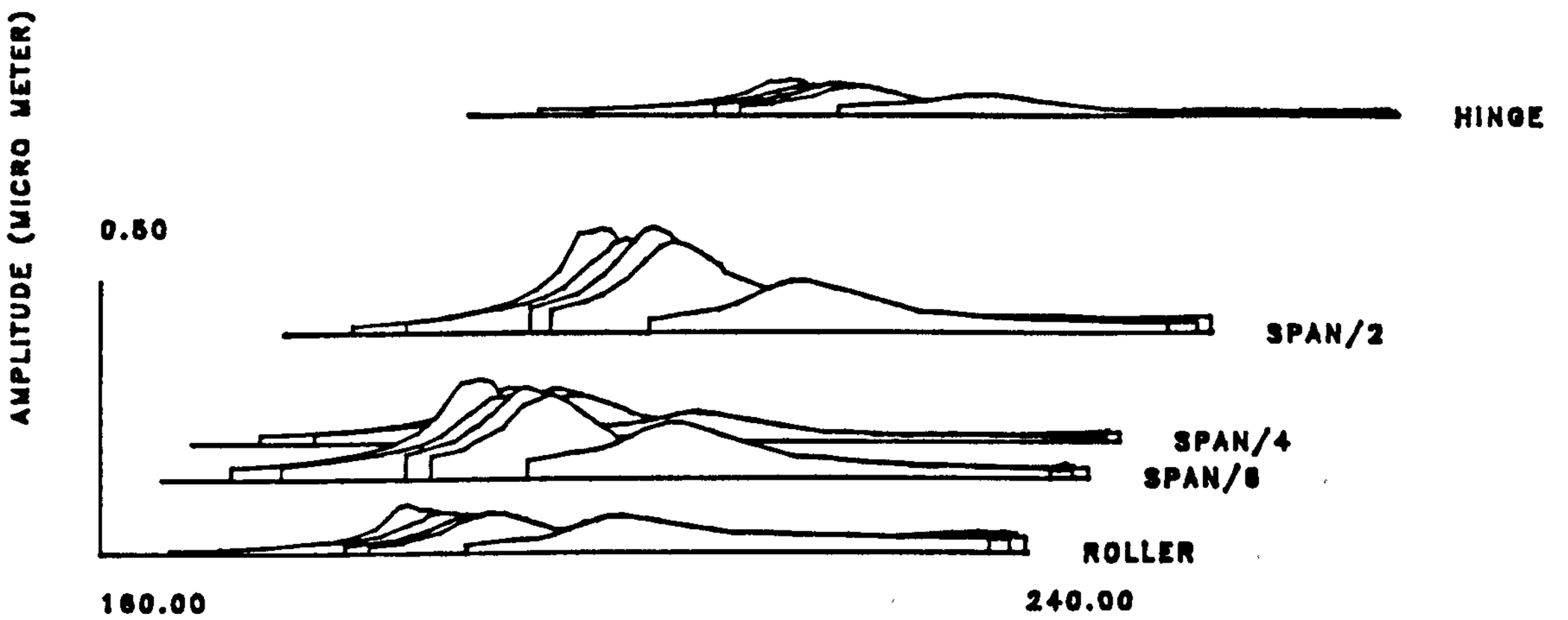

FIG.7.31. RESPONSE SPECTRA, BEAM-4 (PB/L2) SUBJECT TO SIX LOADING STAGES, PARTIALLY BONDED, DIAGONAL SPLITTING CRACK PATTERN, THIRD MODE.

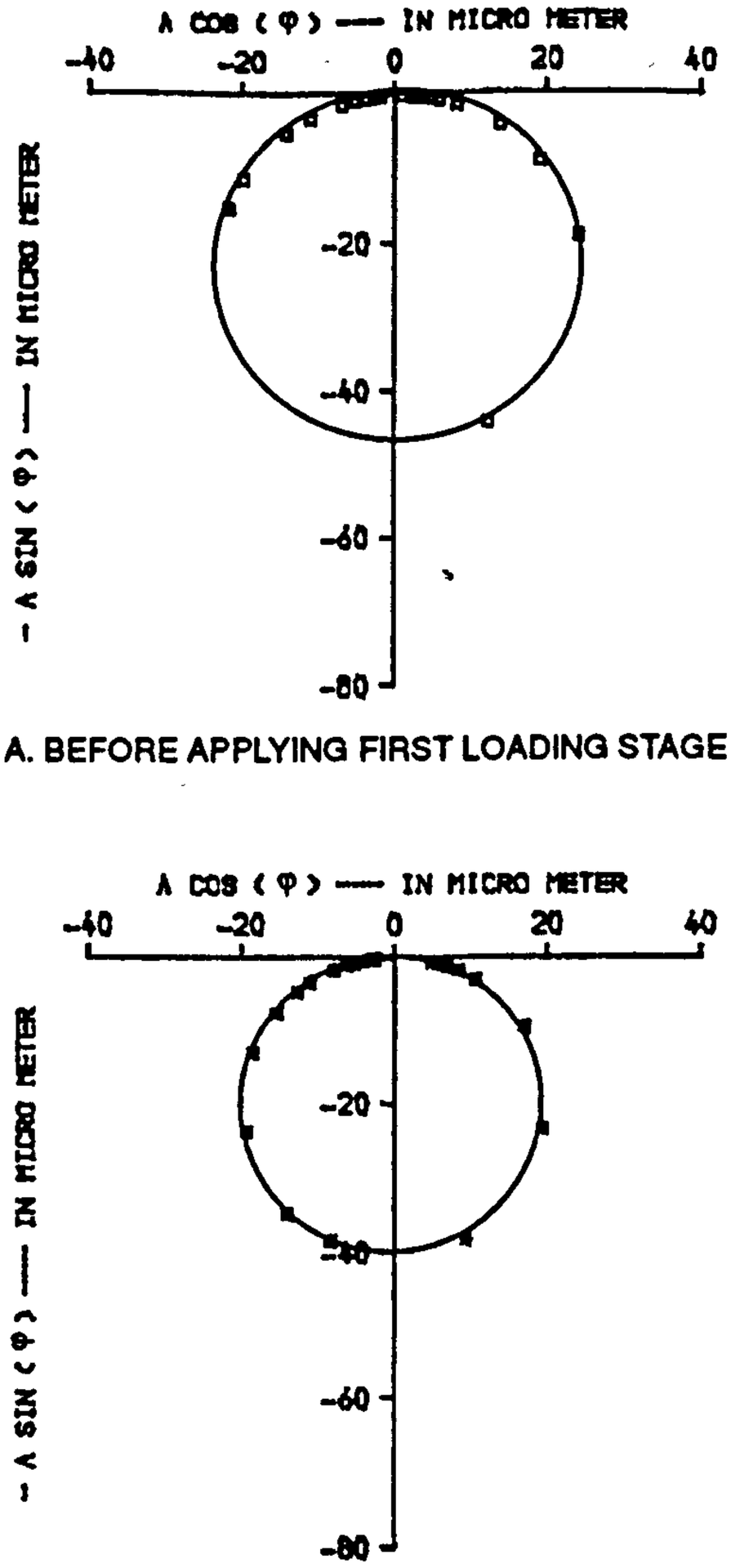

A. BEFORE APPLYING FIRST LOADING STAGE

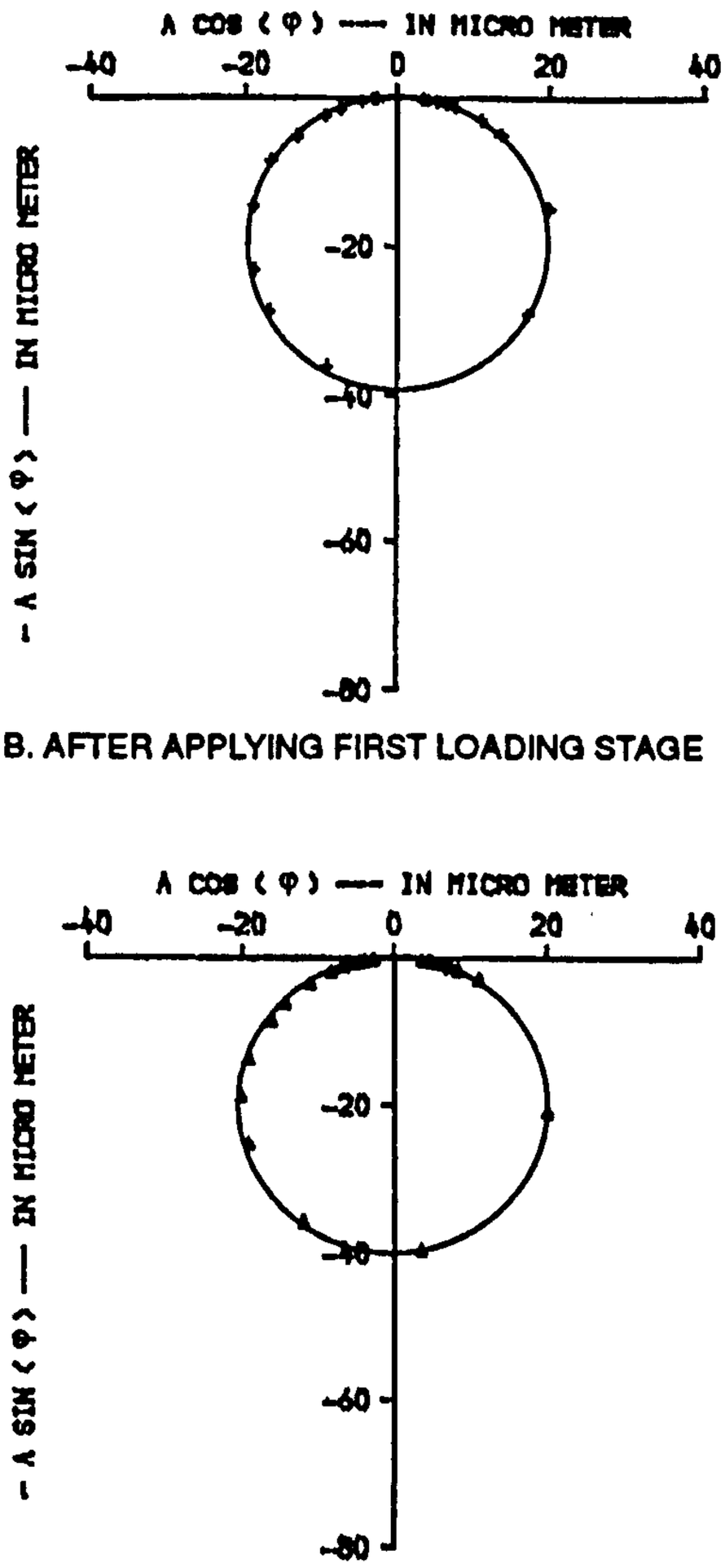

B. AFTER APPLYING FIRST LOADING STAGE

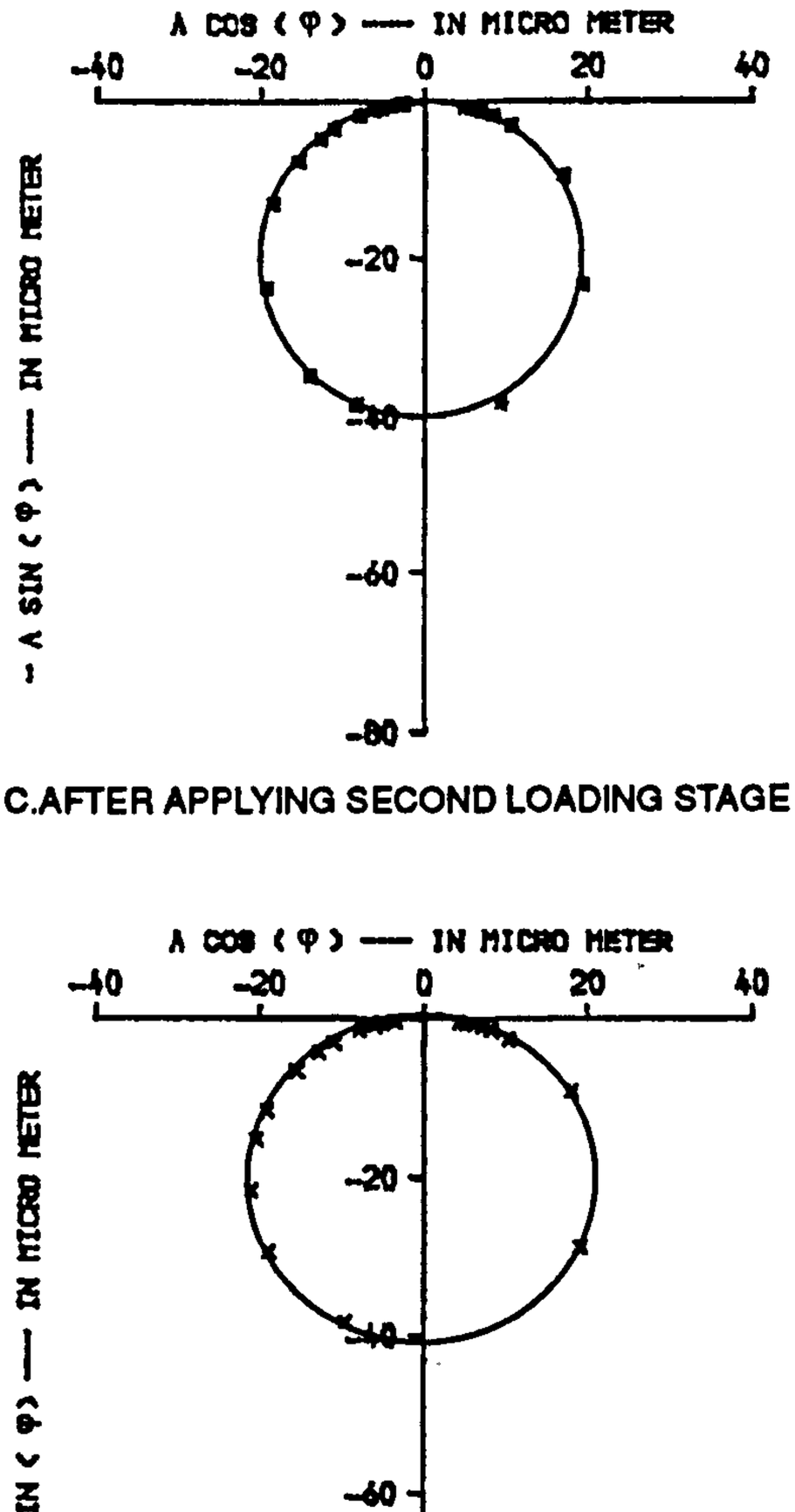

C.AFTER APPLYING SECOND LOADING STAGE

D. AFTER APPLYING THIRD LOADING STAGE

NOTES :

φ : phase angle between force of excitation and beam response

A : displacement amplitude of beam

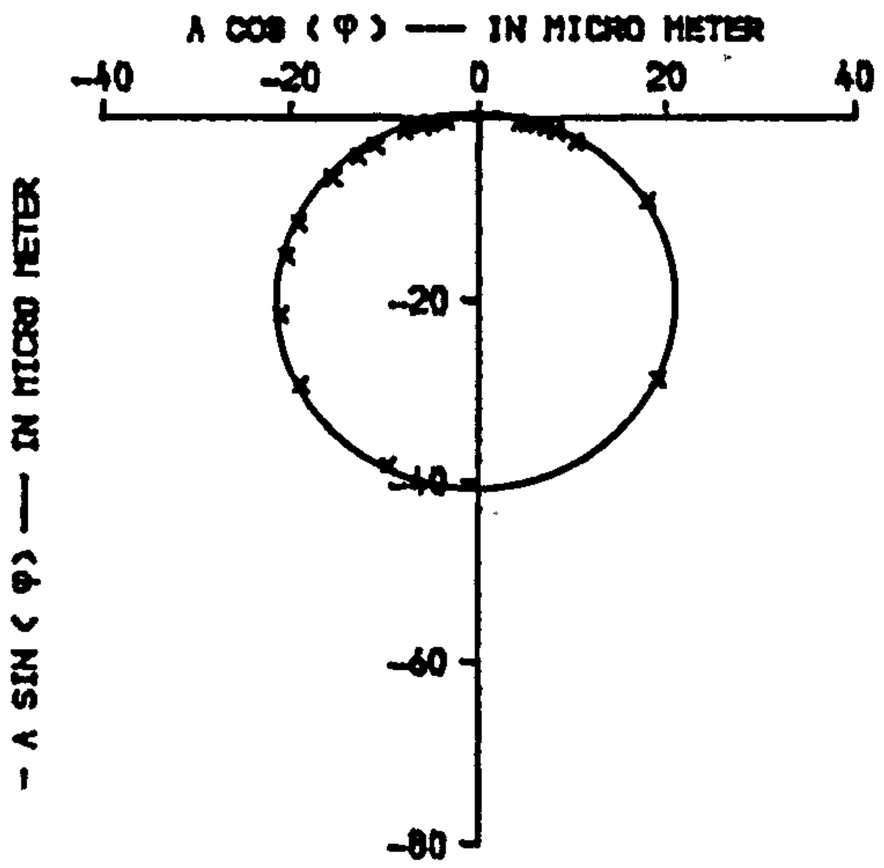

E. AFTER APPLYING FOURTH LOADING STAGE

FIG.7.32. POLAR DIAGRAMS OF BEAM-4 (PB/L2), PARTIALLY BONDED, FIRST MODE, AT MID SPAN, DIAGONAL SPLITTING CRACK PATTERN

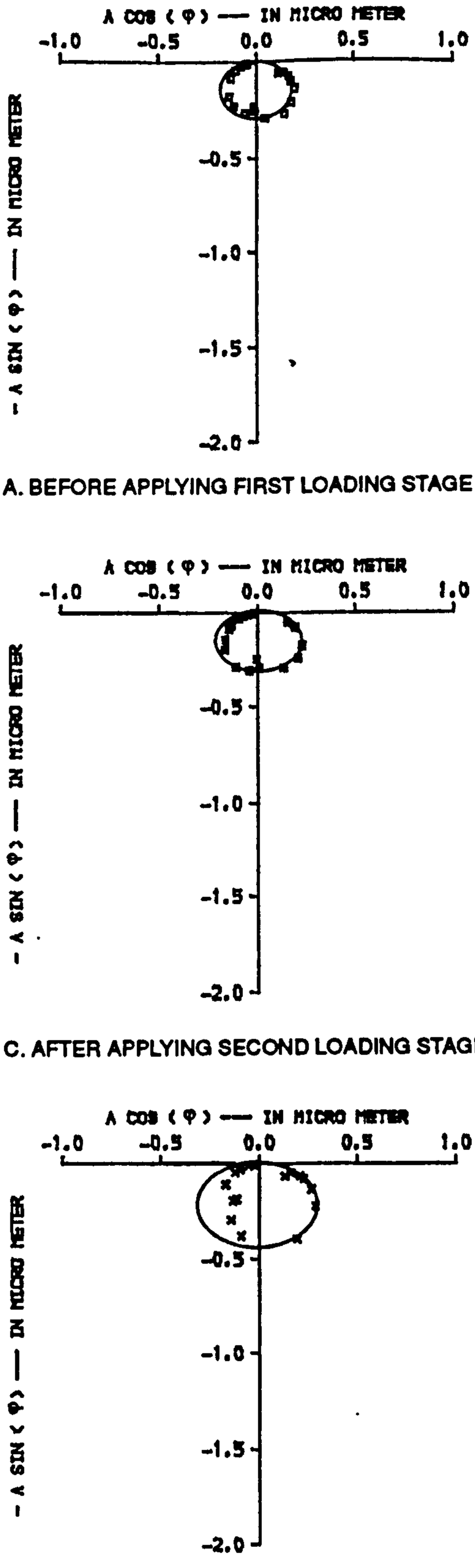

A. BEFORE APPLYING FIRST LOADING STAGE

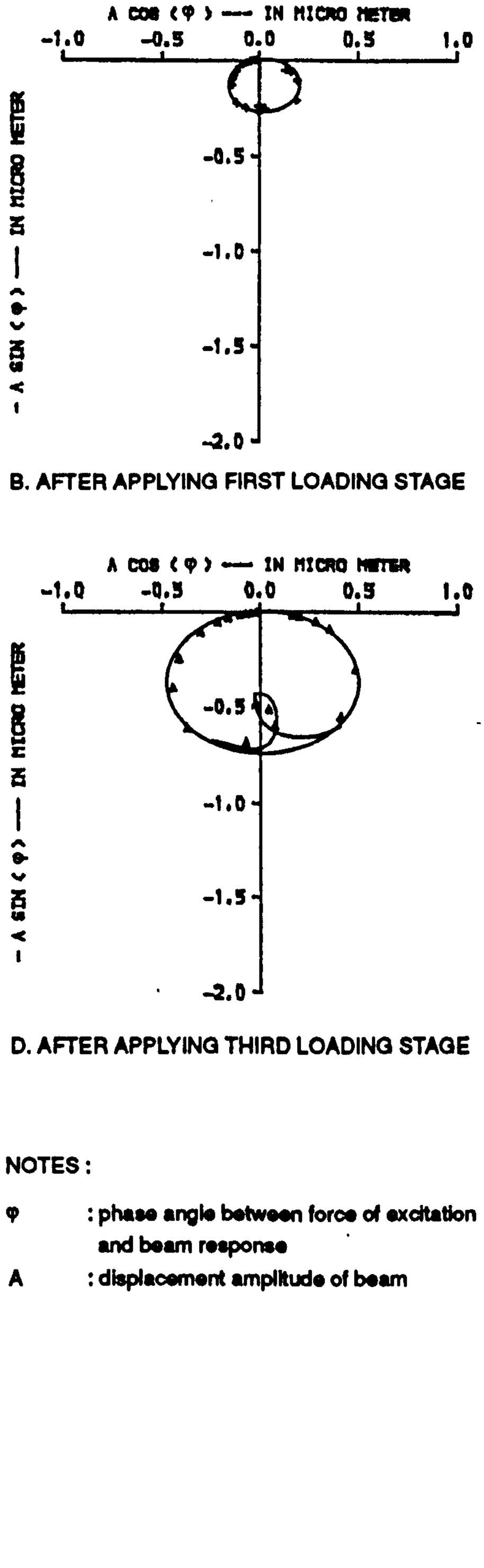

B. AFTER APPLYING FIRST LOADING STAGE

C. AFTER APPLYING SECOND LOADING STAGE

D. AFTER APPLYING THIRD LOADING STAGE

NOTES :

φ : phase angle between force of excitation and beam response

A : displacement amplitude of beam

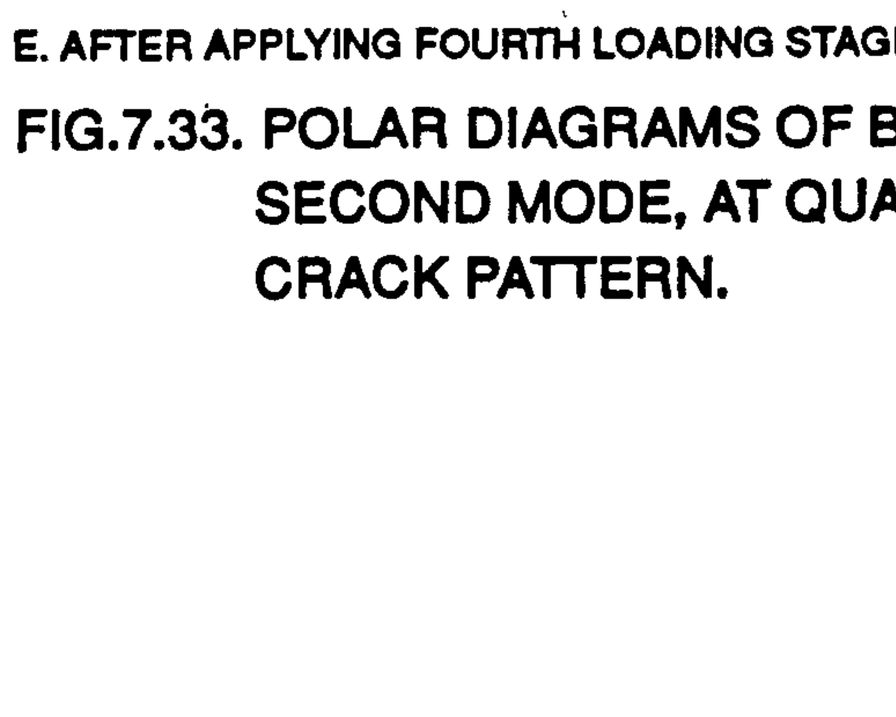

E. AFTER APPLYING FOURTH LOADING STAGE

FIG.7.33. POLAR DIAGRAMS OF BEAM-4 (PB/L2), PARTIALLY BONDED, SECOND MODE, AT QUARTER SPAN, DIAGONAL SPLITTING CRACK PATTERN.

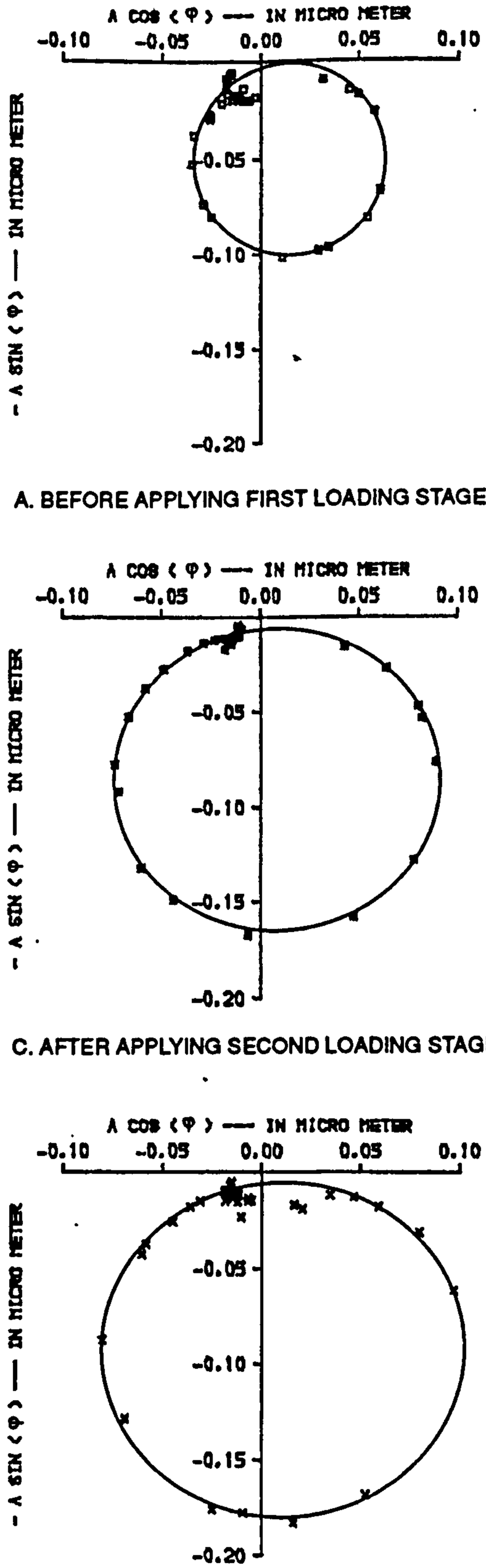

A. BEFORE APPLYING FIRST LOADING STAGE

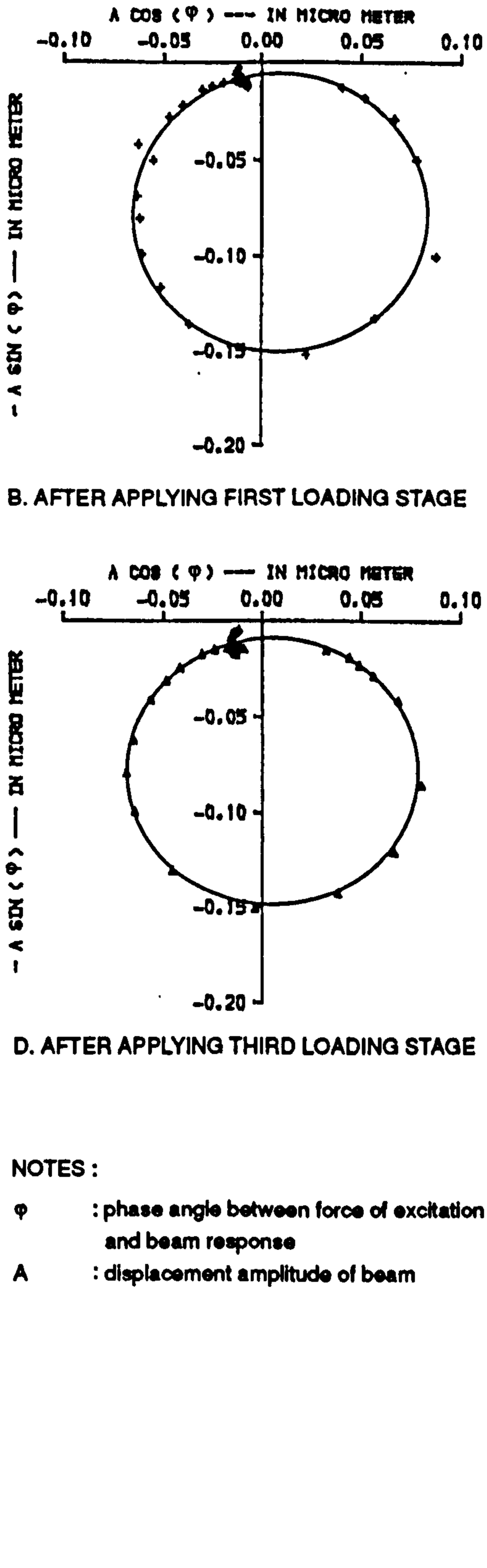

B. AFTER APPLYING FIRST LOADING STAGE

C. AFTER APPLYING SECOND LOADING STAGE

D. AFTER APPLYING THIRD LOADING STAGE

NOTES :

φ : phase angle between force of excitation and beam response

A : displacement amplitude of beam

E. AFTER APPLYING FOURTH LOADING STAGE

FIG.7.34. POLAR DIAGRAMS OF BEAM-4 (PB/L2), PARTIALL BONDED, THIRD MODE, AT A SIXTH SPAN, DIAGONAL SPLITTING CRACK PATTERN.

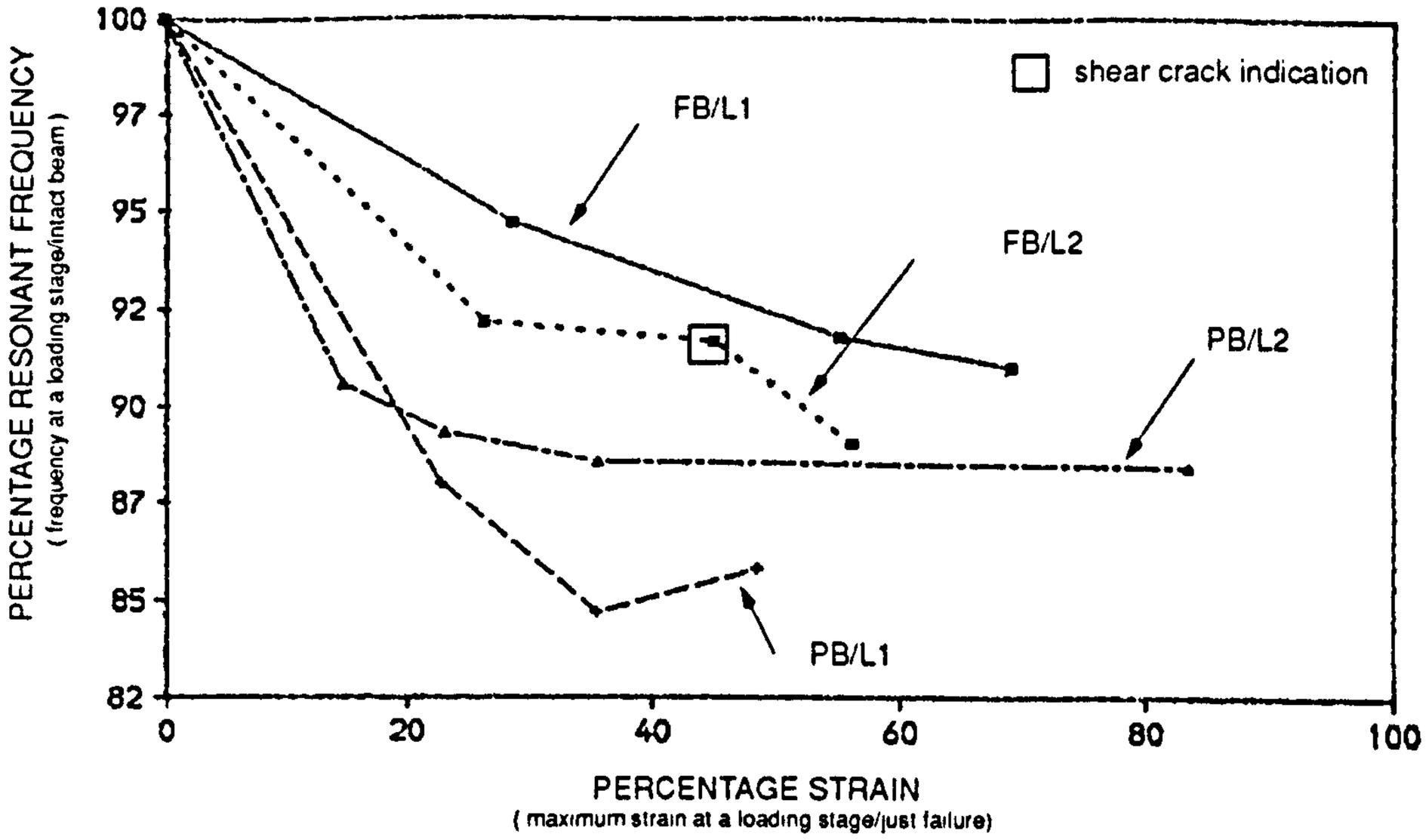

FIG.7.35. STRAIN-RESONANT FREQUENCY RELATIONSHIP OF BEAMS, FIRST MODE

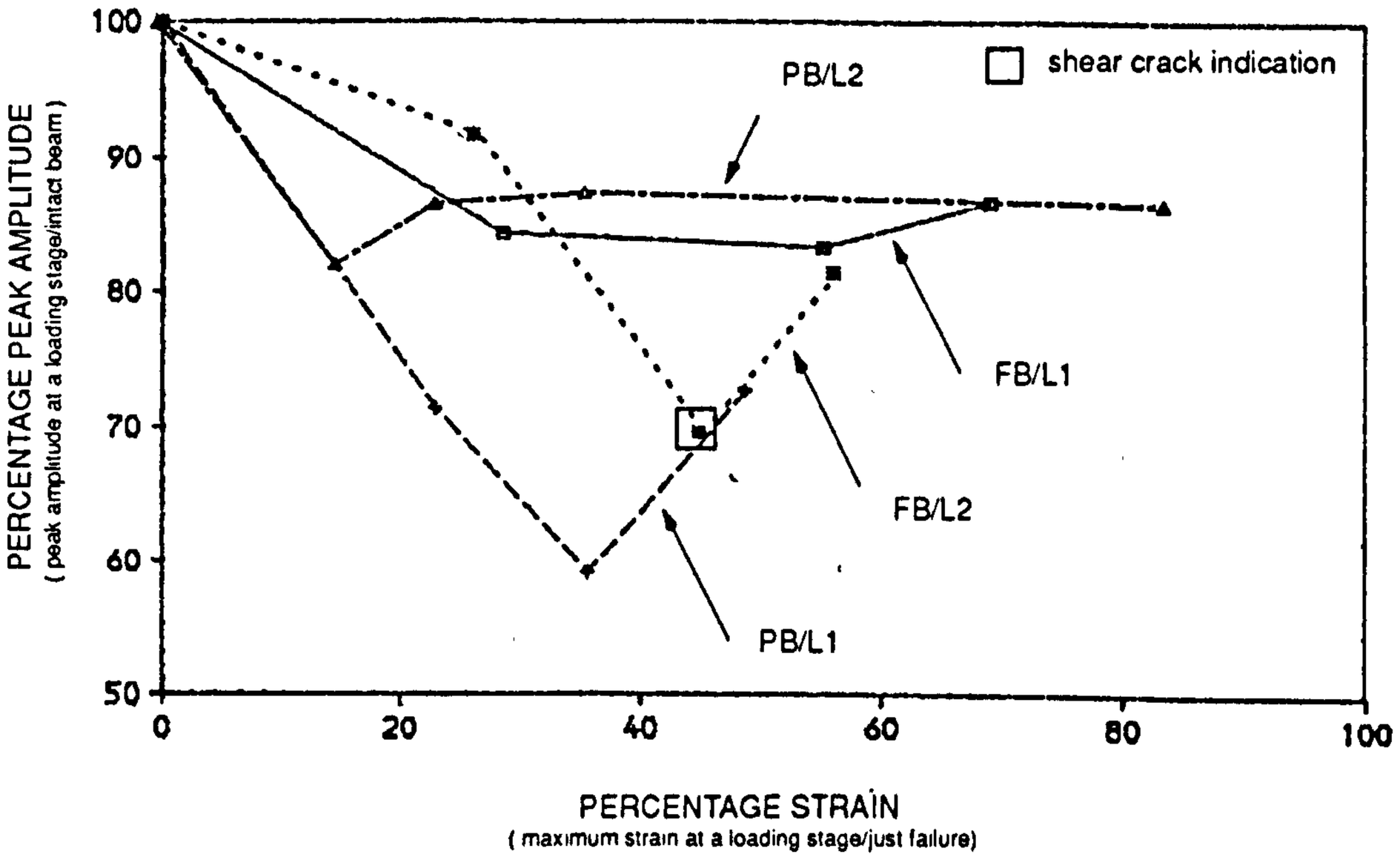

FIG.7.36. STRAIN-PEAK AMPLITUDE RELATIONSHIP OF BEAMS FIRST MODE.

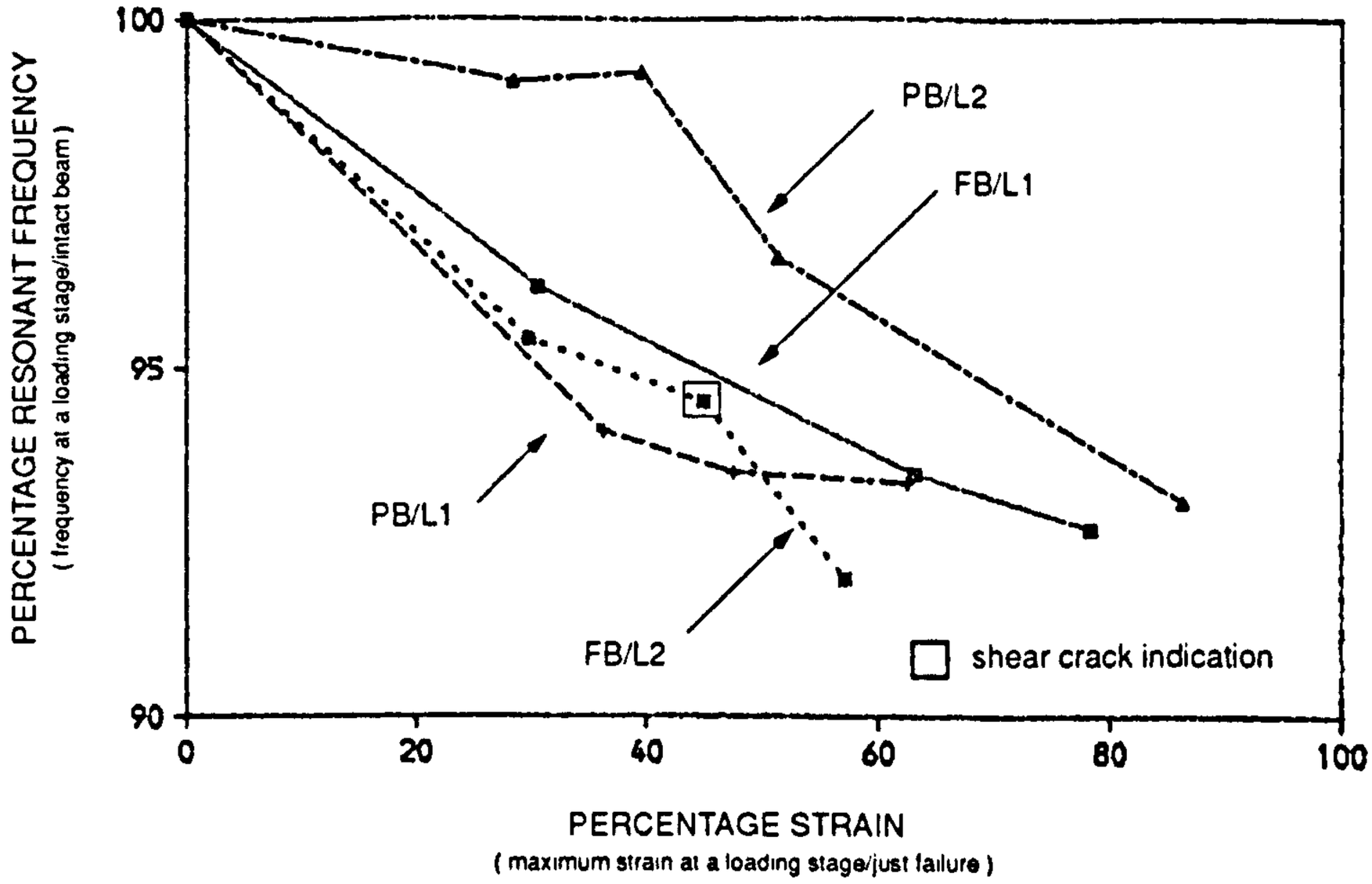

FIG.7.37. STRAIN-RESONANT FREQUENCY RELATIONSHIP OF BEAMS, SECOND MODE.

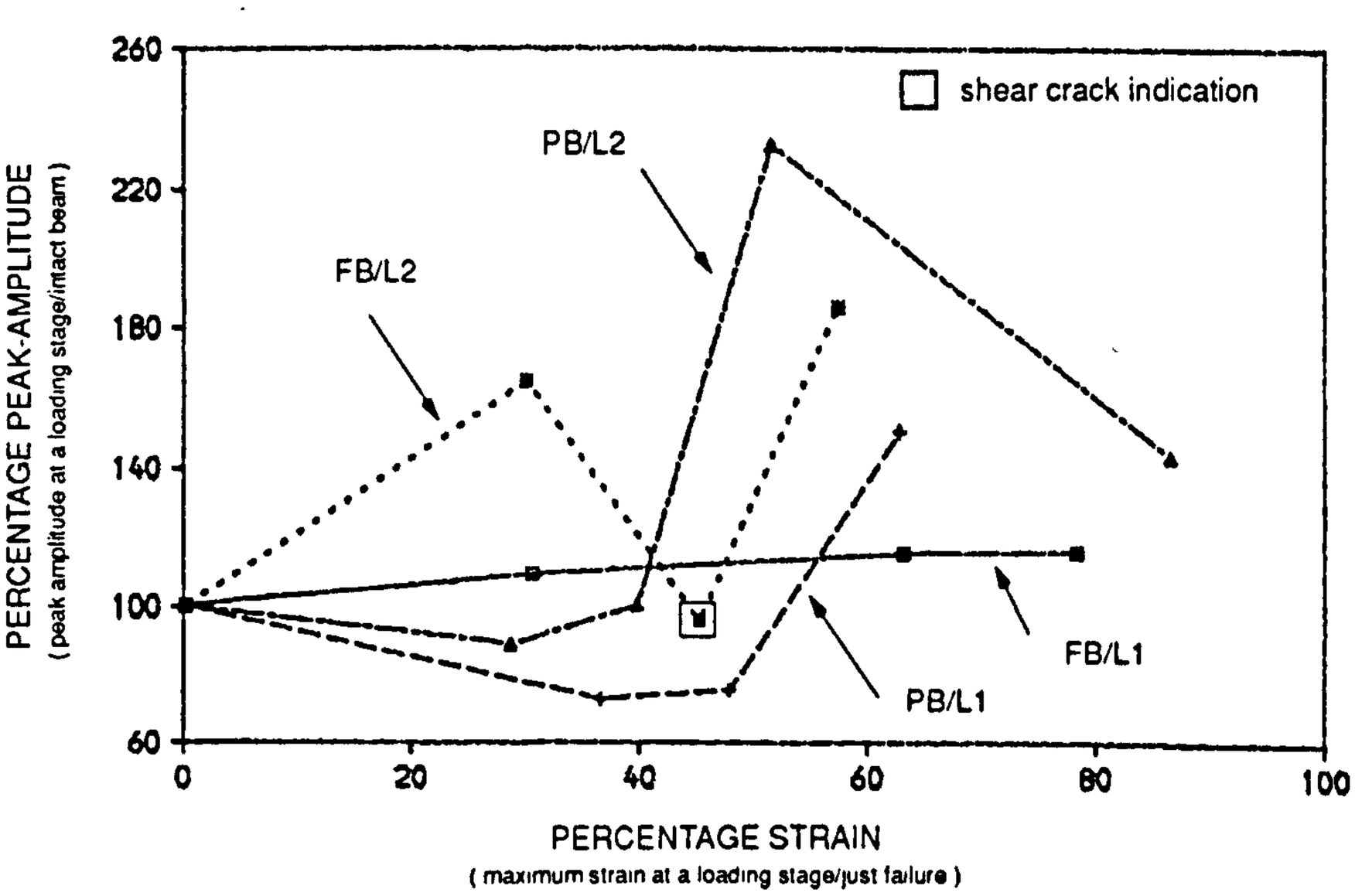

FIG.7.38. STRAIN-PEAK AMPLITUDE RELATIONSHIP OF BEAMS SECOND MODE

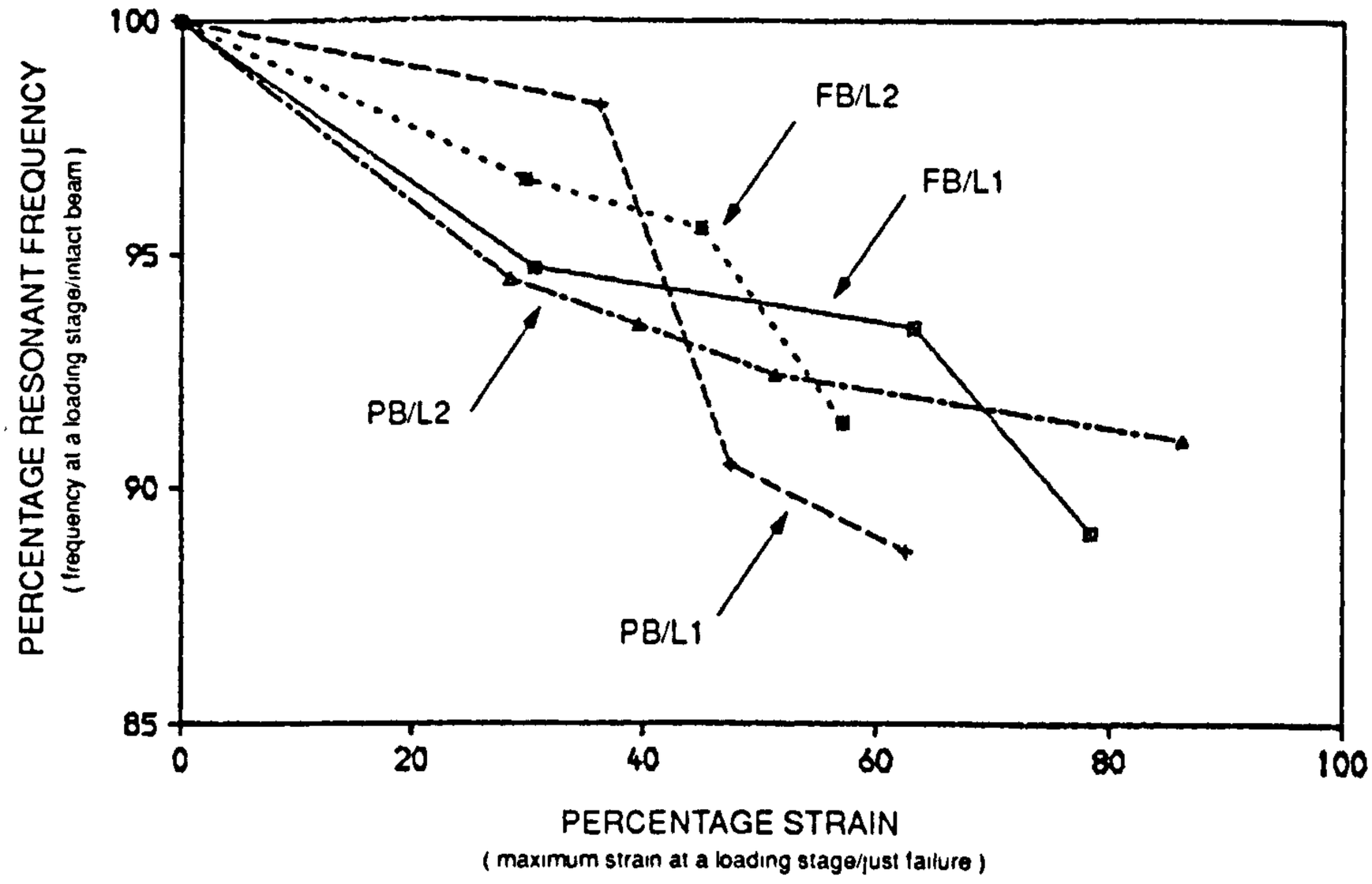

FIG.7.39. STRAIN-RESONANT FREQUENCY RELATIONSHIP OF BEAMS, THIRD MODE.

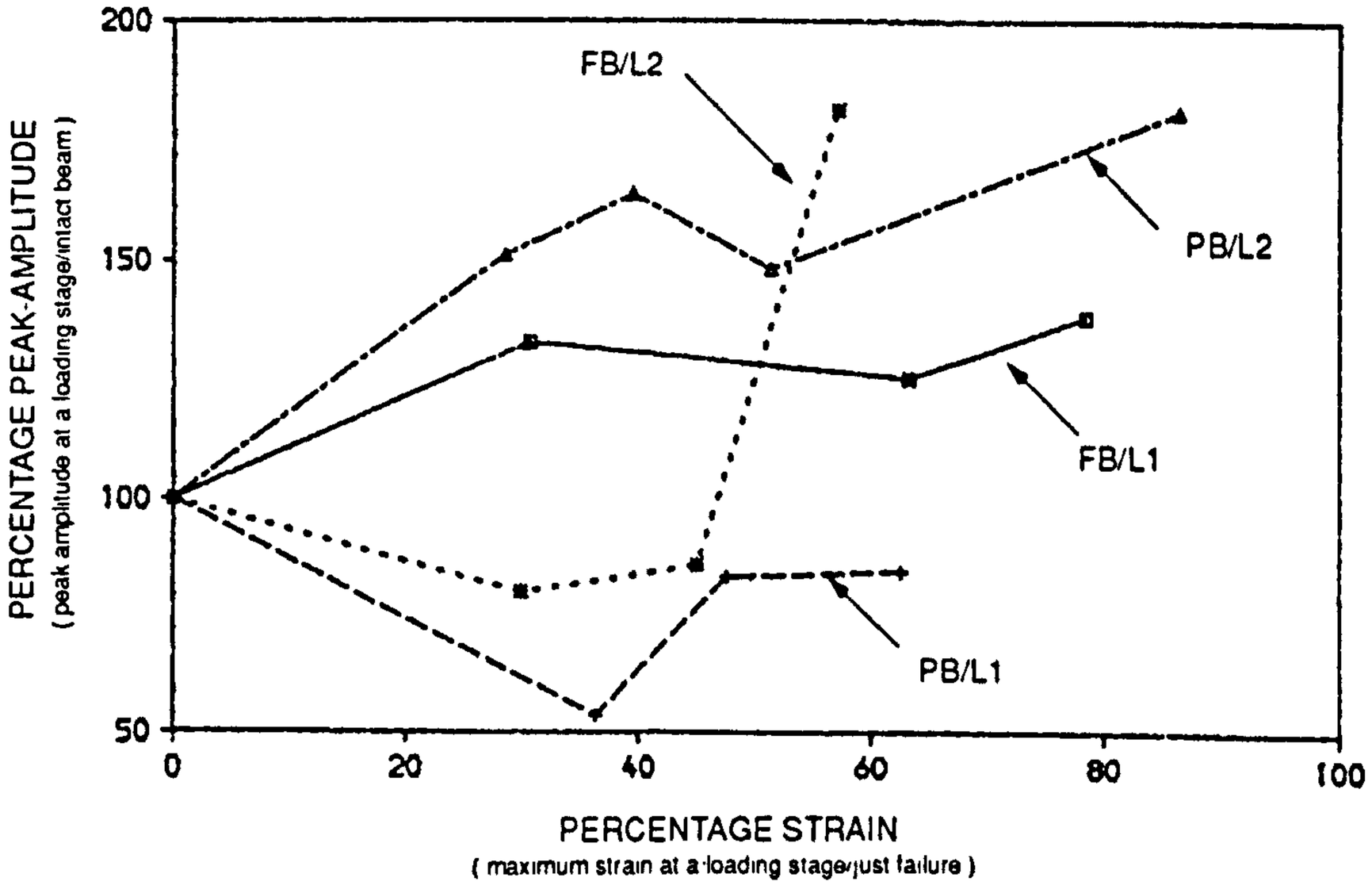

FIG.7.40. STRAIN-PEAK AMPLITUDE RELATIONSHIP OF BEAMS THIRD MODE.

TABLE 7.1. DYNAMIC PARAMETERS OF BEAMS. FIRST MODE.

Beam Code	Resonant Frequency (Hz)	Peak Amplitude (μm) *)	Load & *Strain* (%)	Force of Excitation	Loading Stages
Beam-1	24.524	57.811	---	1.340	
FB/L1	24.499	59.387	---	1.500	
	23.214	48.744	28.57	1.567	Load-1
	23.228	48.457	*30.60*	1.500	
	22.504	48.156	55.16	1.331	Load-2
	22.463	48.906	*63.17*	1.500	
	22.314	50.100	68 97	1.369	Load-3
	22.281	50.805	*78.35*	1.500	
Beam-2	25.571	43.540	---	0.619	
PB/L1	25.475	44.390	---	1.500	
	22.490	31.026	22.60	1.521	Load-1
	22.495	31.099	*36.28*	1.500	
	21.649	25.752	35.29	1.850	Load-2
	21.745	26.741	*47.57*	1.500	
	21.934	31.663	48.37	1.593	Load-3
	21.958	31.913	*62.54*	1.500	
Beam-3	24.840	51.598	---	1.139	
FB/L2	24.790	54.367	---	1.500	
	22.885	47.277	26.30	1.309	Load-1
	22.842	48.036	*29.85*	1.500	
	22.762	35.894	44.94	1.538	Load-2
	22.770	35.944	*45.00*	1.500	
	22.113	42.062	56.09	1.408	Load-3
	22.089	42.166	*57.16*	1.500	
Beam-4	25.161	45.661	---	1.348	
PB/L2	25.142	46.119	---	1.500	
	22.782	37.403	14.76	1.615	Load-1
	22.808	37.438	*28.54*	1.500	
	22.464	39.518	23.02	1.742	Load-2
	22.491	39.457	*39.60*	1.500	
	22.274	39.891	35.45	1.769	Load-3
	22.340	39.592	*51.38*	1.500	
	22.246	39.487	83.46	1.787	Load-4
	22.317	39.191	*86.35*	1.500	

Notes : cube strength of beam-1,2,3,4 are respectively 39.16, 49.02, 44.92 and 46.91N/mm^2

small numbers : parameters normalised to force of excitation (1.500 N)

*) at mid span

TABLE 7.2. DYNAMIC PARAMETERS OF BEAMS, SECOND MODE.

Beam Code	Resonant Frequency (Hz)	Peak Amplitude (μm) *)	Load & *Strain* (%)	Force of Excitation	Notes
Beam-1 FB/L1	97.838	1.293	---	0.667	

	94.070	1.365	28.57	0.795	Load-1
			30.60		
	91.432	1.445	55.16	0.711	Load-2
			63.17		
	90.647	1.525	68 97	0.750	Load-3
			78.35		
Beam-2 PB/L1	100.235	0.899	---	0.528	

	96.979	0.879	22.60	0.475	Load-1
			36.28		
	94.294	0.679	35.29	0.534	Load-2
			47.57		
	93.545	1.355	48.37	0.580	Load-3
			62.54		
Beam-3 FB/L2	97.430	0.710	---	0.632	

	92.955	1.170	26.30	0.720	Load-1
			29.85		
	92.077	0.681	44.94	0.665	Load-2
			45.00		
	89.569	1.325	56.09	0.604	Load-3
			57.16		
Beam-4 PB/L2	99.141	0.272	---	0.725	

	98.238	0.274	14.76	0.673	Load-1
			28.54		
	96.753	0.310	23.02	0.738	Load-2
			39.60		
	95.738	0.717	35.45	0.804	Load-3
			51.38		
	89.371	0.441	83.46	0.904	Load-4
			86.35		

Notes : cube strength of beam-1.2.3.4 are respectively 39.16. 49.02. 44.92 and 46.91N/mm^2
*) at quarter span

TABLE 7.3. DYNAMIC PARAMETERS OF BEAMS, THIRD MODE.

Beam Code	Resonant Frequency (Hz)	Peak Amplitude (μm) *)	Load & *Strain* (%)	Force of Excitation	Notes
Beam-1 FB/L1	215.891	0.105	---	0.632	

	204.426	0.139	28.57	0.729	Load-1
			30.60		
	201.676	0.131	55.16	0.651	Load-2
			63.17		
	192.264	0.145	68 97	0.679	Load-3
			78.35		
Beam-2 PB/L1	208.706	0.097	---	0.443	

	204.943	0.052	22.60	0.336	Load-1
			36.28		
	188.867	0.081	35.29	0.527	Load-2
			47.57		
	184.979	0.082	48.37	0.587	Load-3
			62.54		
Beam-3 FB/L2	204.064	0.121	---	0.612	

	197.110	0.097	26.30	0.481	Load-1
			29.85		
	195.010	0.104	44.94	0.599	Load-2
			45.00		
	186.521	0.219	56.09	0.555	Load-3
			57.16		
Beam-4 PB/L2	205.190	0.102	---	0.654	

	193.772	0.154	14.76	0.925	Load-1
			28.54		
	191.798	0.167	23.02	0.769	Load-2
			39.60		
	189.607	0.151	35.45	0.747	Load-3
			51.38		
	186.829	0.184	83.46	0.830	Load-4
			86.35		

Notes : cube strength of beam-1,2,3,4 are respectively 39.16, 49.02, 44.92 and 46.91N/mm^2
*) at sixth span

TABLE 7.4.POSSIBLE COMBINATIONS OF THE DYNAMIC PARAMETERS AND BEHAVIOURS OF THE POLAR DIAGRAM

	LINEAR STIFFNESS		NON LINEAR SOFT SPRING STIFFNESS	
	LOWER DAMPING	HIGHER DAMPING	LOWER DAMPING	HIGHER DAMPING
VISCOUS (A):				
1.Typical Shape	Circle to Vertically Oval	Circle to Horizontally Oval	Horizontally Oval to Circle	Flatter/Distorted
2.Orientation *)	Rotate Clock Wise	Rotate Counter Clock Wise	Not Visible	Not Visible
3.Isochrones	Straight	Straight	Bent to Left	Much Bent to Left
4.Amplitude/unit force at higher forces	Increase Amplitude	Increase Amplitude	Decrease Amplitude	Decrease Amplitude
HIGHER POLYNOMIAL (B):				
1.Typical Shape	Horizontally Oval to Circle	Horizontally Oval to Distorted	Circle to Horizontally Oval	Horizontally Oval to Distorted
2.Orientation *)	Rotate Clock Wise	Rotate Counter Clock Wise	Not Visible	Not Visible
3.Isochrones	Convex Upward	Much Convex Upward	Convex and Straight	Bent to Left
4.Amplitude/unit force at higher forces	Decrease Amplitude	Decrease Amplitude	Decrease Amplitude	Decrease Amplitude
HYSTERETIC (C):				
1.Typical Shape	Circle	Circle	Circle	Circle
2.Orientation *)	Centered about Imaginary Axis	Centered about Imaginary Axis	Centered about Imaginary Axis	Centered about Imaginary Axis
3.Isochrones	Straight	Straight	Bent to Left	Much Bent to Left
4.Amplitude/unit force at higher forces	Increase Amplitude	Increase Amplitude	Decrease Amplitude	Decrease Amplitude
COULOMB FRICTION (D):				
1.Typical Shape	Coulomb friction is independent amplitude response			
2.Orientation *)	In real structures Coulomb friction is included in			
3.Isochrones	other type/s of damping (A to C)			
4.Amplitude/unit force at higher forces	Generally Coulomb friction gives 'PEAR SHAPE'			

NOTES : *) about origin
Combinations of (A+D) and (B+D) possibly occured in the experiment of the concrete beams with shear defects.
See next page for keys.

KEYS (CONTINUED)

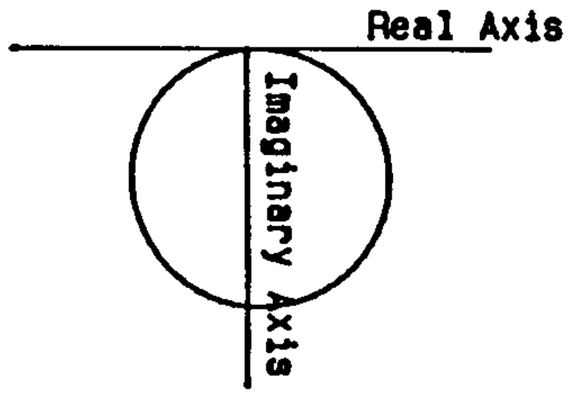

CIRCLE

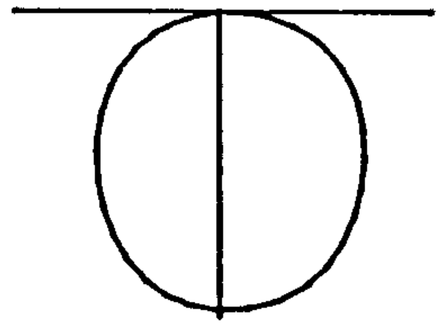

VERTICALLY OVAL

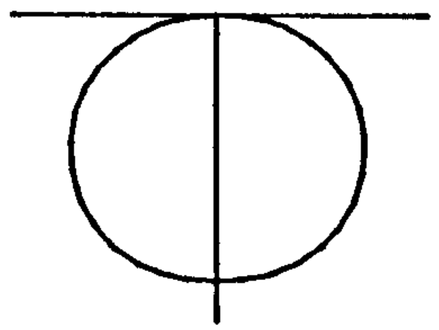

HORIZONTALLY OVAL

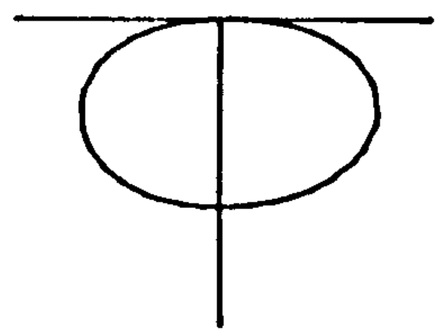

FLATTER/DISTORTED

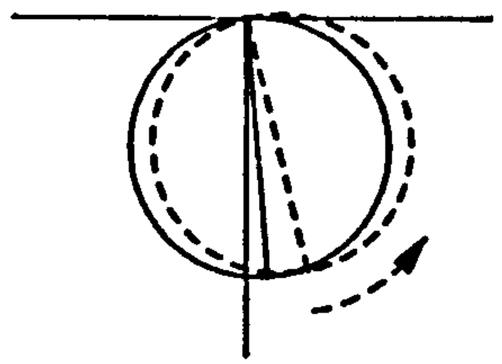

ROTATE COUNTER CLOCK WISE

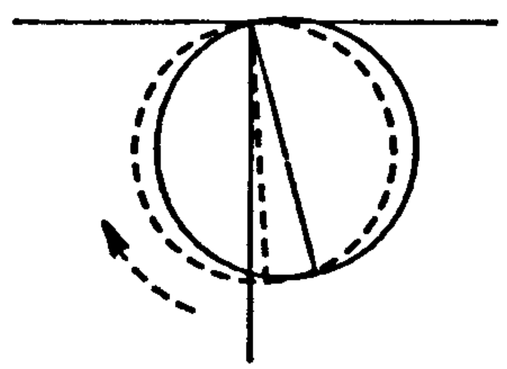

ROTATE CLOCK WISE

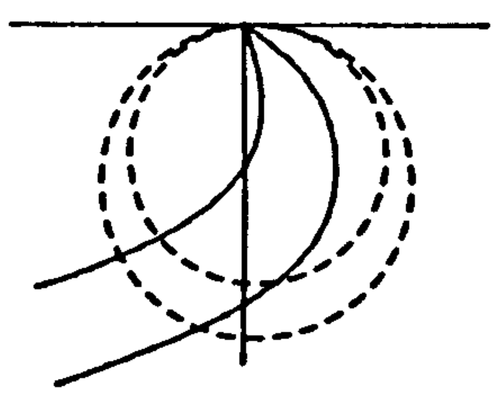

BENT TO LEFT

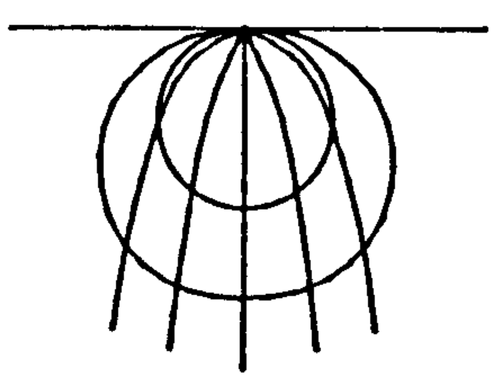

CONVEX UPWARD

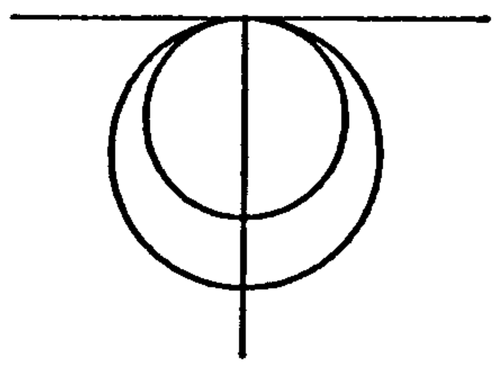

CENTERED ABOUT IMAGINARY AXIS

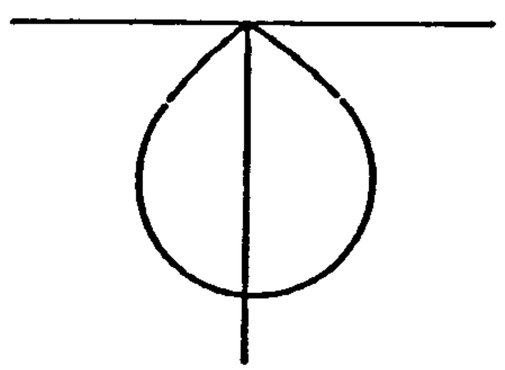

PEAR SHAPE

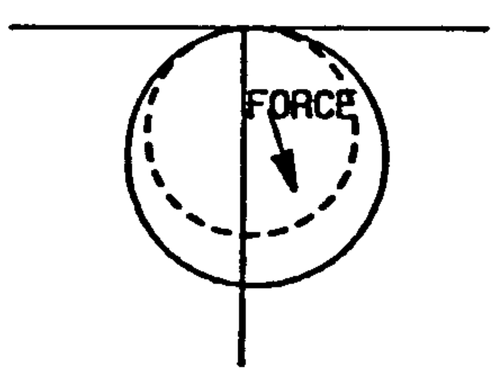

DECREASE AMPLITUDE

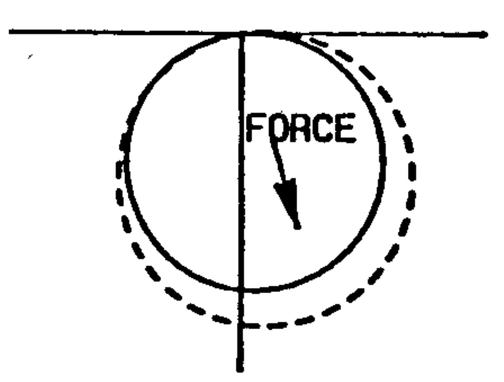

INCREASE AMPLITUDE

CHAPTER - 8

8. DISCUSSIONS.

8.1. General.

Reinforced concrete beam elements have been investigated to achieve a better understanding of the dynamic behaviour of reinforced concrete structures subjected to vibration tests. The contribution of these experiments to the analysis of defects in the reinforced structures will be discussed in this chapter.

An improved method in the determination of signal parameters provides a practical tool in the analysis of structures possessing medium to higher resonant frequencies where achieving a large number of cycles is not a problem. The improved method based on the characteristics of convolution has advantages and limits of application which will be covered in this chapter.

The experiments introduce several phenomena. The jump phenomenon may lead to confusion in understanding of the non-linear behaviour of the models unless the source of the phenomena is well understood. The practical meaning and a mathematical solution have already been discussed. The application of the mathematical solution and its merits will be discussed further in this chapter.

Two algorithms have been developed and introduced into the program to allow filter processing to be carried out in the analysis. The use of the algorithms in the program will be discussed.

The step by step loading stages used to create flexural and diagonal splitting crack pattern has shown that early diagonal splitting cracks can be identified from vibration tests. Furthermore typical loading and typical damage can also be identified.

8.2. Jump Phenomena.

It has been reported by White [15] in the study of the effect of non-linearity due to large deflections that the structure may be responding in some unspecified manner whilst the true cause may not be apparent as a result of the experimental procedure or method of analysis. This implies that any problems found during any experiments should be well understood and the solution to the problems should be determined. The jump observed whilst using the mechanical exciter and a sharp drop of amplitude when using the magnetic vibrator were phenomena which occurred in the experiments. From the associated polar diagram the jump phenomena can occur on beam systems with hinge or clamped supports where excessive force of excitation was in such that stimulated membrane effects [15]. The support system used in the experiments was hinge and roller. This did not comply with the condition required by such a jump phenomenon. The investigation using the magnetic vibrator resulted in a sharp drop of the amplitude of the moving exciter mass. This confirms that the jump phenomena does not relate to

the non-linearity but does relate to the reflected force from the excited structure. The simple two degree of freedom system which was developed provided evidence that the magnetic field of the exciter can be assumed to possess a stiffness, which together with the moving exciter mass constitutes an additional system to the dynamic degree of freedom system. From this point of view the effect of the reflected force of the structure under test on the moving exciter mass can be mathematically modeled.

The simplification of a two degree of freedom system implies that, although it does not exactly model the experiment, the effect of the force of the structure is significant. The squared frequency dependent force of excitation of the mechanical exciter resulted in lower increases of frequency of excitation when approaching resonance. At this stage the vector force of the excitation opposes the reflected force of the excited structure. The only way to increase the speed was to increase the input power. Such a situation implied in a paper on the vibration stress relief though the paper did not mention the jump phenomenon [47,48]. The jump phenomenon was started at the point where the reflected force, notably amplitude dependent, is no longer predominant. The magnetic exciter showed a decrease of amplitude since the force is proportional to the second derivative of the displacement. The reflected force of

the excited structure depends on the dynamic characteristics of the structure such as the damping ratio, mass and the stiffness. An illustration has also been given in chapter-5 that the ratio of the relative to absolute amplitudes becomes significant with decreasing stiffness in the excited beam/structure. As this relationship involves force rather than amplitude, this also depends on the quantity of the moving exciter mass and of the excited structure. This phenomenon should be considered seriously in some applications such as in the design of structural foundation for machinery and the vibratory stress relieve [47,48] where mechanical exciters are employed and the force of excitation is significant.

The true relative phase angles are also considered. The illustration shows that the measured phase angle increasingly lags behind the true phase angle as the excitation approaches resonance. This phase characteristic is dependent on the damping. A significant phase difference may be obtained at more flexible structures. This implies that phase measuring equipment, such as phase meters or resolved component indicators, which simply compare two signals, namely reference and measured, can not measure the true phase angle since the true phase angles only exist theoretically at certain conditions where the amplitude of the excited structure,B equals zero. The result of

applying phase angle measurements from such equipment on the polar diagram will cause the polar diagram to be rotated counter clock wise as the measured phase angle is always lags behind as was indicated in the experiment carried out by White [15].

The proposed practical equation relating the true and the measured phase angles discussed in chapter-5 is amplitude and phase dependent. Thus large differences in characteristics possessed by the accelerometers measuring phase angle may lead to erroneous results. About 2 to 4% amplitude difference and less than 0.187 radiant phase angle difference were found within the range of frequency investigated. As an illustration, the experiment beam-1 (FB/L1) at first mode measured 1.7255 m/sec^2 at accelerometer no.1 positioned at adjacent to the exciter, 10.060 m/sec^2 at accelerometer no.3 positioned on the moving exciter mass and 1.70257 radian measured phase angle. Using the proposed equation the true relative phase angle is found as 1.8673 radian. If the inherent error is considered, i.e. taking amplitude of accelerometer no.1 0.96 * 10.060 = 9.6428 and the measured phase angle is corrected before calculation as 1.70257-0.187 radians, the resulting relative true phase angle is 1.6940. Thus neglect of this inherent error resulted in an overestimate of about 0.1733 radians. From this point of view the polar digrams actually should be rotated about 9.2 degrees counter clock wise.

8.3. Signal Analysis.

The proposed corrective technique to achieve more reliable results for the frequency from the line spectra levels is based on the convolution process of a rectangular window function. The transform of the rectangular window in the frequency domain forms a diminishing sinusoidal wave with a main lobe and side lobes. The convolution of the rectangular window and the non-periodic signal provide a distorted main lobe. Many attempts have been carried out to reduce this distorted main lobe such as by applying other window types [25,26]. The main background of the other window types was a multiplication of the signal with a known periodic signal in such a way that the resulting signal is periodic. The digital frequency in question is then normally predicted from the behaviour of the maximum and its adjacent spectra levels such as shown in reference [10]. The proposed technique was developed from the technique shown in reference [6] where a rectangular window function is considered. The proposed direct technique applies a logic geometry on the spectra level of interest. The numerical simulations show that the error imposed in the geometry decreases as the number of cycles increases. A direct acquisition to achieve a certain number of cycles for a certain possibly maximum percentage error was some time lengthy especially for structures having low resonant frequency (less than 1Hz) with many points of

investigation. In addition a small number of cycles may also be found on structures with heavy damping when impact or 'pull-sudden release' techniques are applied. For such later structures the indirect technique may be applied to reduce error.

8.4. Programming and the Algorithms.

The program was established mainly for analyses of the data of the experiments. Several inputs relate to various pieces of equipment used in the experiment. However modifications can be made to suit other equipment settings. Since the amount of data is not critical the use of ordinary radix-2 FFT may replace the radix mixed FFT which is available in the NAG routines.

The proposed algorithms installed in the program are adequate to examine the experimental data. The number of the order of the polynomial equation depends on the frequency of interest and the attenuation factors required. As an illustration, to allow signals passes through a low pass filter with -3dB at pass band (25Hz) and -30dB at stop band (40Hz) or (40-25)Hz transition band the order of the polynomial equation is 8. If the same transition band (15Hz) and attenuation factors (-3dB and -30dB) are applied at 200Hz pass band and 215Hz stop band the order of the polynomial is 120. The associated time required using the VAXA is still less than a second.

8.5. Non-linearity.

Several aspects of non-linear behaviour were shown by the reinforced concrete beam models. These characteristics can be examined using polar diagrams obtained from the equation of motion of single degree of freedom systems as proposed by Magnus [11], White [14,15], Rades [20,21] and Tomlinson et al.[17,18].

Magnus and White [11.15] proposed an equation for systems possessing *viscous damping with non-linear stiffness*. Simulations of this equation in polar diagrams for different damping ratios but the linear stiffness parameters indicate that the increase of damping results in the rotated counter clock wise polar diagram. Furthermore for a given positive stiffness parameter (hard spring systems) but the same damping ratio indicate that the polar diagram distorts elliptically and rotate insignificantly clock wise as has also been demonstrated by White [15] in his experiment.

Rades [21] provided an equation for the single degree of freedom system possessing *hysteretic damping with non-linear stiffness*. The polar diagrams of such a system are always circular and centered at the imaginary axis for different stiffness parameters. The increase of resonant frequency with increasing force of excitation in the hard spring systems results in a rotation counter clock wise of positions of frequency on the polar diagram and analogous for soft spring systems. If the same

frequencies on the different polar diagrams are connected these form lines referred to as 'isochrones' [21] indicating the type of the spring systems. The Jump phenomenon in this case starts at points where the isochrone becomes tangent to the polar diagram.

Furthermore Rades [20] provided an equation for the single degree of freedom system for *quadratic damping with linear stiffness*. The resulting polar diagram of this system tends to elongate in the direction of the real axis as the increase of non-linear damping. The higher the quadratic damping the more distortion the polar diagram. Simulations of the equation imply that the normalised resonant amplitudes decrease as the increase of force of excitation.

Tomlinson et.al.[17,18] studied the effect of Coulomb damping on the polar diagram of lightly damped (viscous) systems. He presented an equation for the single degree of freedom system for *combined viscous damping and Coulomb friction with linear stiffness*. The resulting polar diagram is a 'pear shape'. The slightly elongated elliptical shape in the imaginary axis is due to the slightly viscous damping and the shift in y-origin position is due to the Coulomb friction.

Hasan [6] reported that damping is amplitude dependent. It was reported that a lattice tower with a U-form possessed three types of damping. Under high amplitude of excitation the structure was viscously damped. The

increase of amplitude of excitation in this region increased the damping. In contrast under low amplitude of excitation the structure was dry damped, where a decrease of amplitude of excitation increased the damping.

Such non-linearities of damping are not easily understood from the associated response spectra. In contrast the hysteretic amplitude responses or amplitude response histories with respect to load will be easily recognised from the response spectra. Thus, referring to both types of response is apparently essential in determining the precise dynamic parameters.

On the basis of the possible non-linearities mentioned above the reinforced concrete beams investigated obviously possessed non-linear soft spring behaviour with several forms of non-linear and linear viscous damping. The combined viscous damping and non-linear soft spring behaviour or the combined slightly non-linear higher order polynomial damping such as the quadratic damping and non-linear soft spring behaviour existed on the intact beams. Early flexural cracks increased damping. Several parts of beams with flexural crack pattern remained with viscous damping at the third end span. The increase of damping is always indicated by the rotation counter clock wise of the polar diagrams. In the other parts where non-linear higher polynomial damping was present the increase of damping is indicated by distorted

polar diagrams instead. Post flexural loading stages produced large wide open cracks reducing frictional area from where the opening and closing mechanism of hair line cracks existed which apparently created the higher order polynomial damping force. As a result viscous damping was more obvious as indicated by the almost circular polar diagrams.

The beam models with diagonal splitting crack patterns behaved differently just before the cracks were visible. The intact beams had viscous damping with non-linear soft spring behaviour. The increase of loading created early flexural cracks which stimulated the effect of non-linear higher order polynomial damping as shown by the distorted polar diagrams. Furthermore increase in loading created a change of load distribution. The energy concentrated in creating diagonal splitting cracks as shown by the lower increase in flexural cracks. The vibration tests showed that the distorted polar diagram slightly shift in y-origin positions. The force of excitation was partly opposed by the Coulomb friction in the shear crack regions. As a result a drastic drop of amplitude occurred at resonance. The change of loading distribution was also detected from the vibration test as a small decrease in resonant frequency. The loading stage which created visible diagonal splitting cracks partly disabled the presence of Coulomb friction damping.

8.6. Detection of Flexural and Diagonal Splitting Defects.

8.6.1. Fully bonded beam.

The reinforced concrete beams are composed of at least two different materials, i.e. the concrete and the steel, with different characteristics. At an early stage concrete can resist tensile stress. A maximum contribution of the concrete to the EI value on which the stiffness depends is achieved at this stage. The following loading stage resulted in a large shift in strain as shown in the load-strain graphs in chapter-3. The large shift in strain indicated a significant decrease in the stiffness. This was identified from the vibration tests as a significant decrease of resonant frequencies.

The flexural defects can be identified physically from the cracks which are concentrated at the third center span of the beam whilst the diagonal splitting cracks were more spread slightly over the beam length. The flexural defects were identified from the first mode as a lower decrease of percentage resonant frequency with respect to strain than the beam with diagonal splitting defects. The resonant amplitude evaluations required the associated polar diagrams. The significant drop of resonant amplitude coupled with the slight decrease of resonant frequency and a small shift in the origin position of the imaginary axis of the polar diagram

indicated the presence of early shear cracks. This indication also existed in the second mode.

The typical decreasing exponential curves presented in this research are very different from those presented by Christide et al.[5]. This is because Christide et al [5] used solid square steel bars as the models with artificially large cracks. This clearly ensured that the system possessed viscous damping with a linear stiffness. The stiffness of the steel beam related to the number of the artificially created cracks and the depth of the cracks. Once the cracks were introduced these remained open while vibration took place. As the linear stiffness is concerned the resonant frequency is independent of the force of excitation. This condition may not exist in the concrete beams even under an excessive force of excitation due to non-linear soft spring behaviour although a report on this has not been found.

Results of the work carried out by Tourk [1] was in agreement with this research. It was reported that the resonant frequencies exponentially decreased with the increase in the static bending moments.

8.6.2. Partially bonded beam.

The theoretical calculation and the experiments have revealed that the effect of unbonded part on the resonant frequencies of the beam before cracking were not significant. The resonant frequencies of this intact

beam was similar to that of the fully bonded beam. The defects were not easily identified from the relative performance of the beam with a single crack. The non-proportional load-strain distribution over the beam length in the partially bonded action may change the geometry of the beam in such a way that it became stiffer than the beam with flexural defects. This was shown as a lower decrease resonant frequency of the beam in either the first mode or the second mode. The significant drop in resonant amplitude identified as the presence of early shear cracks did not exist in this type of beam. This was possibly due to the non-proportionally load- strain distribution. Evaluation of the resonant amplitude with the associated polar diagrams revealed that more friction damping existed in the beam with flexural defects as shown by the higher decrease in amplitude. Unusual results like the increase in resonant frequency at the last vibration test of beam-2 (PB/L1) with flexural defects was questionable.

8.7. Practical Monitoring.

Several different sets of excitation applied on the concrete beam can indicate the type of non-linearity from where diagrams of force of excitation with respect to the dynamic parameters can be established. Changes of stiffness can be monitored from the curve relating the force of excitation to the resonant frequency. Since

resonant frequency relates to stiffness and mass, evaluations of stiffness from the resonant frequency should consider the changes in the existing mass, if any. Changes in the type of damping and the quantity of damping can be monitored from the diagram of force of excitation with respect to resonant amplitude. The diagrams of the normalised resonant amplitude and the resonant frequency confirmed by the polar diagrams allow predictions of the structure at different forces of excitation.

Parabolic curve fitting or any other higher polynomial curves may be used to relate the force of excitation to the resonant frequency and the force of excitation to the normalised resonant amplitude from where the relative evaluations of the dynamic parameters may be carried out.

CHAPTER - 9

9. CONCLUSIONS AND SUGGESTIONS.

9.1. Conclusions.

1. Four beams with two types of cracks pattern and two types of reinforcement have been investigated. Static and steady state vibration tests were applied stage by stage.
2. Vibration equipment used in the experiment has been calibrated and proved acceptable for the use in the experiments.
3. The jump phenomena are proved to be due not only to the non-linear stiffness but also the reflected force of the excited structure.
4. A practical equation relating absolute amplitudes to relative amplitudes and defining true relative phase angles have been developed. Evaluations of the accuracy of the equation has been discussed along with their dependence on the amplitude and phase quality of the measuring transducers.
5. A proposed direct improvement technique on the determination of signal parameters has been developed. Applications of lower number of cycles may reduce the accuracy of the technique. In addition the indirect technique may be applied for a better accuracy.
6. A program to analyse signals has been provided in which two proposed algorithms are included. The program can be used for the analysis of digital

signals from vibration tests.

7. Several possible types of non-linear damping have been demonstrated in the experiment. The typical viscous and non-linear higher polynomial damping existed mostly in the models although the typical crack pattern and intensities contributed to the type of damping.

8. The beam models showed non-linear soft spring behaviour. Typical viscous or higher order polynomial damping with lower non-linear stiffness is possessed by the intact beams.

9. Diagonal splitting crack patterns can be identified from small decrease of percentage resonant frequency and from the sharp drop of resonant amplitude on the first and second mode.

10. The experiments showed that a sharp decrease of resonant frequency indicated a large amount of residual strain exists.

11. The concrete material contributed significantly to the stiffness. The presence of single deep cracks reduced the stiffness considerably.

9.2. Suggestions for Future Research.

1. Better results may be obtained from better vibration equipment which allow precise frequency increments of less than 0.05 hz to be set up.

2. Portable exciters having self adjusted force of excitation allows various sets of force of excitation to be applied on the model without any jump phenomena with which non-linear behaviours may be investigated at higher levels of force of excitation.
3. Characteristics of damping from opening and closing of cracks in concrete structures at variable levels of force of excitation may indicate the depth of the cracks.
4. Characteristics of damping from bonding and debonding reinforcement which notably depend on the typical surface and perimeter of the reinforcement should be investigated separately from (3).
5. Early detections of various shear cracks can be further developed from experiments using beams with higher depth to span ratio.
6. The effect of reflected force should be considered in practical vibration test such as in vibratory stress relief tests and in most vibration experiments.
7. Further tests should be carried out to provide evidence of the behaviour of reinforced concrete beams subjected to increasing force of excitation levels. Beams that show clear flexural-shear type behaviour under static loading should also be studied.

REFERENCES

[1].Tourk,O.M.S., *The effect of Cracking of the Concrete on The Dynamic Characteristics of Reinforced Concrete Beams*, M.Sc. Thesis, University of Strathclyde, Glasgow. 1979.

[2].Sim,K.L., *Vibration of Concrete Beams*, M.Sc. Thesis, University of Strathclyde, Glasgow, 1980.

[3].Hashim,E.M., *Vibration of Concrete Structure*, M.Sc. Thesis, University of Strathclyde, Glasgow, 1981.

[4].Tan,C.L., *The Vibration Characteristics of Reinforced Concrete Beams under Load*, M.Sc. Thesis, University of Strathclyde, 1985.

[5].Christides.S., and Barr,A.D.S., *One Dimensional Theory of Cracked Bernoulli-Euler Beams*, Int., Jour., Mech., Sci., Vol.26, No.11/12, pp.639-648, 1984.

[6].Hassan,M., *Dynamic Characteristics of Lattice Tower with U-section Form*, Ph.D., University of Strathclyde, Glasgow, U.K., 1988.

[7].Ibanez,P., *Review of analytical and experimental techniques for improving structural dynamic models*, Welding Research Bulletin, 249, June 1979.

[8].Clough, R.W., and Penzien,J., *Dynamics of Structures*, McGraw Hill Book Company, Vol.6, Singapore, 1985.

[9].Rao,J.S., Gupta,K., *Introductory Course on Theory and Practice of Mechanical Vibrations*, Wiley Eastern, New Delhi, 1984.

[10].Harris,C.M., *Shock Vibration Analysis Hand Book*., McGraw Hill Inc., 3rd edition, 1989.

[11].Magnus,K., *Vibrations*, Blackie & Son Ltd.,Great Britain, Glasgow, 1965.

[12].Srinivasan,P., *Mechanical Vibration Analysis*, McGraw Hill, New Delhi, 1982.

[13].Warburton,G.B., *The Dynamical Behaviour of Structures* ,Pergamon Press, 1964.

[14].White,R.G., *Use of Transient Excitation in the Measurement of the Free Response of System with Non-linearities Arising from Large Deflections*, I.S.V.R., Technical Report No.27, February 1970.

[15].White,R.G., *Effects of Non-linearity Due to Large Deflections in The Resonance Testing of Structures*, Journal of Sound and Vibrations, Vol.16, No.2, pp.255-267, 1971.

[16].White,R.G., *Effects of Non-linearity Due to Large Deflections in the Derivation of Frequency Response Data from the Impulse Response of Structure*, Journal of Sound and Vibration, 29(3),pp.295-307, 1973.

[17].Tomlinson,G.R., and Hibbert,J.,H., *Identification of the Dynamic Characteristics of a Structure with Coulomb Friction*, Journal of Sound and Vibration, Vol.64, pp 233-242, 1979.

[18].Tomlinson,G.R., *An Analysis of Distortion Effects of Coulomb Damping on the Vector Plots of Lightly Damped Systems*, Journal os Sound and Vibration,

71(3), pp.443-451, 1980.

[19].Rades,M., *Parameter Identification of a Structural with Combined Coulomb and Hysteretic Damping*, Rev., Roum., Sci., Tech., Mec. Appl., Tome 27., No.2., pp.299-308, Bucharest, 1982.

[20].Rades,M., *Identification of Dynamic Characteristics of a Simple System with Quadratic Damping*, Rev.,Roum, Sci.Tech- Mec., Appl.Tome 28, No.4, pp.439-446, Bucharest 1983.

[21].Rades,M., *On The Effects of Non-linear Stiffness in Resonance Testing*, Rev., Roum., Sci., Techn., Mech., Appl., Tome28, No.6, pp.603-614, Bucharest, 1983.

[22].Schmidt,G., and Tondl,A., *Non-Linear Vibrations*, Cambridge University Press, Cambridge, London, 1986.

[23].Jordan,D.W., and Smith,P., *Nonlinear Ordinary Differential Equations*, Clarendon Press-Oxford, 1977.

[24].Brigham,E.D., *The Fast Fourier Transform*, Prentice Hall,Inc.

[25].Ramirez,R.W., *The FFt Fundamental and Concepts*, Prentice Hall, Inc., New Jersey, USA, 1985.

[26].Hamming,R.W., *Digital Filters*, Prentice Hall Inc., 2nd ed., 1983.

[27].Gold,B., and Rabiner,L.,R., *Theory and Application of Digital Signal Processing*, Prentice Hall, Inc., N.J., 1975.

[28].Peled,A and Lin,B, *Digital Signal Processing* , John

Wiley and Son, 1976.

[29].Buzdugan,G.,Mihailescu E.,Rades M., *Vibration Measurement*, Martinus Nijhoff Publishers,1986.

[30].Cooley,J.W., and J.W.Tukey, *An Algorithm for Machine Calculation of Complex Fourier Series.* Math.Computation, Vol.19, pp.297-301, April 1965.

[31].Temperton,C., *Self Sorting Mixed Radix FFT* , Journal of Computational Physics, Vol.52, pp.1-23. 1983.

[32].Temperton,C., *A note on Prime Factor FFT Algorithm*, Journal of Computational Physics, Vol.52, pp.199-205, 1983.

[33].Temperton,C., *Fast Mixed Radix Real FFT*, Journal of Computational Physics, Vol.52, pp.340-350, 1983.

[34].O'leary,C.G., *Non Recursive Digital Filtering using Cascade Fast Fourier Transformers*, IEEE Transactions on Audio and Electro Acoustics, Vol. AU-18, No.2, June 1970.

[35].Kormylo,J.J. and Jain,V.K., *Two-pass Recursive Digital Filter with Zero Phase Shift*, IEEE Transactions on Acoustics, Speech and Signal Processing, October 1974.

[36].Czarnach,R., *Recursive Processing by Noncausal Digital Filters*, IEEE. Transactions on Acoustics, Speech and Signal Processing, Vol. ASSP-30, No.3, June, 1982

[37].Chan,C., and Chen,C., *Design of FIR Digital Filters using The Wiener-Lee Decomposition Technique*, Int.,

Jour., Elect., Vol.54, No.3., pp.437-446. 1983.

[38].Kwong,C.P., *Simple Method for Computation of Wiener-Lee Decomposition*, Electronics Letters, Vol.19, No.18, Sept., 1983

[39].Chan,C., and Chen,C., *An Efficient Approach to Noncausal Filtering*, IEEE., Transactions on Acoustics, Speech and Signal Processing, Vol. ASSP-32, No.3, June, 1984.

[40].Priyosulistyo,H., *Vibration of Reinforced Concrete Beams*, M.Sc., University of Strathclyde, Glasgow, U.K., 1988.

[41].Valetsos,S.,A., and Ventura,C.,E., *Dynamic Analysis of Structures by The DFT Method*, Journal of Structural engineering, Vol.111, No.12, December 1985.

[42].Power,H.M., *The Mechanics of Bilinear Transformation*, IEEE Transactions on Education, p.114, June 1967.

[43].Davies,A.C., *Bilinear Transformation of Polynomials*, IEEE Transactions on Circuits and Systems, p.792, November 1974.

[44].Kamen,E., *Introduction to Signals and Systems*, MacMillan Publishing Co., 1987.

[45].Hartog,D.J.P, *Forced Vibration with Combined Coulomb and Viscous Friction*, Trans.ASME 53, APM 107-115,1931.

[46].Yeh,C.K.G., *Forced Vibration of a Two-Degree-of-*

Freedom System with Combined Coulomb and Viscous Damping. Journal of the Acoustical Society of America, Vol.39, pp.14-24, 1966.

[47].Claxton,R.A., *Vibratory Stress Relieving-Theory*, The Journal of the Bureau of Engineer Surveyors, Vol.10, No.1&3, 1983.

[48].Claxton,R.A., *Vibratory Stress Relieving - An Effective Alternative to Thermal Treatment for Component Stabilisation*, Heat Treatment of Metals, pp.53-59, 1991.

APPENDICES

APPENDIX A-1 : Equation of Motion of Linear Systems.

1.Single Degree Vibratory Systems.

When a displacement,x, is given to the system the equation of motion of the undamped vibratory system gives.

$$m\ddot{x} + kx = 0. \qquad (A.1)$$

The equation of a damped vibratory system gives :

$$m\ddot{x} + c\dot{x} + kx = 0. \qquad (A.2)$$

Applying a steady vibratory force on the structures can also be carried out as an alternative. The equation of a forced damped vibration system can be expressed below.

$$m\ddot{x} + c\dot{x} + kx = F(t) \qquad (A.3)$$

2. Multi Degree Vibratory Systems.

A continuous structure can be idealised as a system having a series of lumped masses, springs and dampers. This idealisation simplifies the complicated dynamic parameters which usually occur in real structures. Decoupling the equation of motion of each mass unit enable the dynamic parameters of the system to be analysed independently. The general equation of undamped multi degree vibratory systems are described the matrix below.

$$[M]\{\ddot{x}\} + [K]\{x\} = 0 \qquad (A.4)$$

where :

$$[M]\{\ddot{X}\} = \left[\begin{array}{ccc|c} m_1 & 0 & 0 & 0 \\ 0 & m_2 & 0 & 0 \\ \hline 0 & 0 & 0 & m_n \end{array}\right] \left\{\begin{array}{c} \ddot{X}_1 \\ \ddot{X}_2 \\ \hline \ddot{X}_n \end{array}\right\} \qquad (A.5)$$

$$[K]\{x\} = \left[\begin{array}{ccc|c} k_{11} & k_{12} & k_{13} & k_{1n} \\ k_{21} & k_{22} & k_{23} & k_{2n} \\ \hline k_{n1} & k_{n2} & k_{n3} & k_{nn} \end{array}\right] \left\{\begin{array}{c} x_1 \\ x_2 \\ \hline x_n \end{array}\right\} \qquad (A.6)$$

The stiffness matrix can be analysed using stiffness or flexibility methods.

Substituting $x = \bar{X}\ \mathrm{Cos}\ (pt + \alpha)$ and its derivatives into equations (A.5) and (A.6) gives

$$([K] - p^2[M])\{\bar{X}\} = 0 \qquad (A.7)$$

When stiffness,[K], and mass,[M], are given the eigen frequencies,p, as well as the eigen vectors,$\bar{X}$, can be determined from equation (A.7).

By applying the correct boundary conditions to the equation of motion given below

$$[x] = [\bar{X}](\mathrm{Cos}(pt + \alpha)) \qquad (A.8)$$

and by carrying out some iteration the amplitudes of the idealised lumped masses can be obtained.

When dealing with many lumped masses the iteration method requires a considerable amount of labourous work. Decoupling the simultanuous differential equations is an alternative solution.

Putting $\{\bar{X}\} = [E]$ and substituting this in equation (A.7) for two cases i and j and after including the scalar

quantity

$$[L_i^2] = [E_i]^T[M][E_i] \text{ or}$$

$$[1] = [e_i]^T[M][e_i] \text{ for } [e_i] = [E_i]/[L_i] \qquad (A.9)$$

where [e] is a unit eigen factor, the properties of eigen factor are as follows.

For $j \neq i$

$$[e_i]^T[M][e_j] = 0 \; ; \; [e_i]^T[K][e_j] = 0 \qquad (A.10)$$

For $j = i$

$$[e_i]^T[M][e_i] = 1 \; ; \; [e_i^T][K][e_i] = [p_i^2] \qquad (A.11)$$

Again, putting $[z] = \{\cos(pt + \alpha)\}$ and $[e] = [\bar{X}]$ into equation (A.8) gives

$$[x] = [e][z] \qquad (A.12)$$

Back substitution into equation (A.4) and multiplying by $[e]^T$ gives

$$[e]^T[M][e]\,[\ddot{z}] + [e]^T[K][e]\,[z] = 0 \qquad (A.13)$$

Referring to equation (A.11) to relate local amplitudes to overall amplitudes gives

$$[e]^T[M][e][e]^{-1} = [1][e]^{-1} \text{ or}$$

$$[e]^{-1} = [e]^T[M] \qquad (A.14)$$

Substituting equation [A.14] and applying boundary conditions into equation (A.12) gives

$$[z] = [e]^{-1}[x]$$

$$[z] = [e]^T[M][x] \qquad (A.15)$$

Equation (A.15) provides local amplitudes of the lumped mass. Using equation (A.13) the overall amplitudes can be defined.

If an external Force,F(t), is applied to the system the

equation of motion gives

$$[e]^T[M][e]\ [\ddot{z}] + [e]^T[K][e]\ [z] = [e]^T[F(t)] \quad (A.16)$$

Again, applying equation (A.9) and (A.13) into equation (A.16) the amplitudes of independent lumped masses can be obtained.

APPENDIX A-2 : Steady State Variable Forcing Function.

The Variable Forcing Function ($Fo = MR\ \omega^2$) is applied on a single degree of vibratory systems.

$$m\ddot{x} + kx + x = Fo \sin \omega t \qquad (1)$$

Apllying the particular solution $x_p = A \sin (\omega t - \varphi)$ into equation (1) and equating the harmonics yields a displacement equation of the vibrating system, x.

$$x = \frac{Fo\ \bar{D}}{k} \qquad (2)$$

where : $\bar{D}$ = is the dynamic magnification factor and equal to $\left[(1-r^2)^2 + (2dr)^2\right]^{-0.5}$

$$x = \frac{MR}{k}\ \omega^2 \left[(1-r^2)^2 + (2dr)^2\right]^{-0.5} \quad ; \text{ assuming } MR/k = 1 \text{ unit}$$

$$= \left[\omega^{-4}(1-r^2)^2 + \omega^{-4}(2dr)^2\right]^{-0.5} \quad ; \ r = \omega/p$$

$$= \left[\omega^{-4}p^{-4}(p^2-\omega^2)^2 + \omega^{-4}p^{-2}(4d^2\omega^2)\right]^{-0.5}$$

$$= \left[\omega^{-4}p^{-4}(p^4 - 2p^2\omega^2 + \omega^4) + 4\ d^2p^{-2}\omega^{-2}\right]^{-0.5}$$

$$= \left[\omega^{-4} - 2\omega^{-2}p^{-2} + p^{-4} + 4\ d^2p^{-2}\omega^{-2}\right]^{-0.5} \qquad (3)$$

The peak amplitude can be obtained by applying $\delta\ddot{x}/\delta\omega = 0$ to equation (3).

$$-0.5\left[\omega^{-4} - 2\omega^{-2}p^{-2} + p^{-4} + 4d^2p^{-2}\omega^{-2}\right]^{-1.5}$$

$$\left[-4\omega^{-5} + 4p^{-2}\omega^{-3} - 8d^2p^{-2}\omega^{-3}\right] = 0$$

$$-4\omega^{-2} + 4p^{-2} - 8\ d^2p^{-2} = 0$$

$$(\omega/p)^{-2} = (1 - 2d^2); \quad (\omega/p) = \frac{1}{\sqrt{(1 - 2d^2)}} \qquad (4)$$

$$\varphi = \tan^{-1}\left[\frac{2d\omega/p}{1-(\omega/p)^2}\right] \qquad (5)$$

The peak amplitude always occurs at $\omega/p > 1$ unless $d = 0$ or in other words the resonance occurs at $\omega/p < 1$ as seen in the table below.

d	ω/p	φ
0.05	1.0025	92.85
0.15	1.0233	98.73
0.20	1.0425	101.75
0.50	1.4142	125.26

APPENDIX A-3 : Harmonic Linearisation.

Assuming the equation of motion of a single degree vibratory system is given below.

$$m\ddot{x} + c\dot{x} + k\,(x + \gamma\, x^3) = Fo\ Cos\ \omega t$$

$$\ddot{x} + (c/m)\dot{x} + (k/m)(x + \gamma\, x^3) = Fo/m\ Cos\ \omega t$$

$$\ddot{x} + 2n\,\dot{x} + p^2(x + \gamma\, x^3) = Fo\ p^2/k\ Cos\ \omega t \qquad (1)$$

The particular solution is :

$$x_p = a\ Cos\ \omega t + b\ Sin\ \omega t$$

$$\dot{x}_p = -\ a\omega\ Sin\ \omega t + b\omega\ Cos\ \omega t$$

$$\ddot{x}_p = -\ a\omega^2\ Cos\ \omega t - b\omega^2\ Sin\ \omega t$$

$$(x_p)^3 = a^3\ Cos^3\omega t + b^3\ Sin^3\omega t + 3\ ab^2\ Sin\ \omega t^2\ Cos\ \omega t$$

$$+ 3\ a^2b\ Sin\ \omega t\ Cos^2\omega t \qquad (2)$$

Knowing : $Sin^3\omega t = -\frac{1}{4}\{3\ Sin\ \omega t + Sin\ 3\omega t\ \}$

$$Cos^3\omega t = -\frac{1}{4}\{3\ Cos\ \omega t + Cos\ 3\omega t\ \}$$

$$Sin^2\omega t = \{1 - Cos^2\omega t\ \}$$

$$Cos^2\omega t = \{1 - Sin^2\omega t\ \}$$

By ommitting higher harmonics,Sin $3\omega t$ and Cos $3\omega t$ and substituting the later trigonometric rules into equation (2) give

$$(x_p)^3 = 3ab^2\ Cos\ \omega t + 3\ a^2b\ Sin\ \omega t +$$

$$-\frac{3}{4}(a^3-3ab^2)Cos\ \omega t + -\frac{3}{4}(b^3-3ba^2)\ Sin\ \omega t \qquad (3)$$

Substituting equation (3) into equation (1) leads to :

$$-a\omega^2\ Cos\ \omega t - b\omega^2\ Sin\ \omega t + 2n\ \{-a\omega\ Sin\ \omega t + b\omega\ Cos\ \omega t\} +$$

$$p^2\ \{a\ Cos\omega t + b\ Sin\omega t\} + \gamma\ p^2\{3a^2b\ Sin\ \omega t + 3ab^2Cos\ \omega t +$$

$$-\frac{3}{4}(a^3 - 3ab^2)\ Cos\ \omega t + -\frac{3}{4}(b^3 - 3ba^2)\ Sin\ \omega t\ \}$$

$$= (Fo/k)p^2\ Cos\ \omega t$$

Equating coefficients :

$$-a\omega^2 \text{ Cos } \omega t + 2nb\omega \text{ Cos } \omega t + p^2 a \text{ Cos}\omega t + 3\gamma\, p^2 ab^2 \text{ Cos } \omega t$$

$$+-\tfrac{3}{4}-\gamma p^2 (a^3 - 3ab^2) \text{ Cos}\omega t = (Fo/k)\, p^2 \text{ Cos } \omega t$$

$$-a\omega^2 + 2nb\omega + p^2 a + 3\gamma\, p^2 ab^2 + -\tfrac{3}{4}-\gamma p^2 (a^3 - 3ab^2) = (Fo/k)\, p^2$$

$$p^2 a\{\ 1 + -\tfrac{3}{4}-\ \gamma\ (b^2 + a^2) - (\omega/p)^2\ \} + 2nb\omega = (Fo/k)p^2 \qquad (4)$$

$$-b\omega^2 \text{ Sin } \omega t - 2na\omega \text{ Sin } \omega t + bp^2 \text{ Sin}\omega t + 3\gamma p a^2 b^2 \text{ Sin } \omega t$$

$$+-\tfrac{3}{4}-\gamma p^2 (b^3 - 3ba^2) \text{ Sin } \omega t = 0$$

$$-b\omega^2 - 2na\omega + bp^2 + 3\gamma\, p^2 a^2 b + -\tfrac{3}{4}-\gamma p^2 (b^3 - 3ba^2) = 0$$

$$bp^2\{\ 1 + -\tfrac{3}{4}-\gamma\ (\ b^2 + a^2\ ) - (\omega/p)^2\ \} - 2na\omega = 0 \qquad (5)$$

Knowing $A^2 = a^2 + b^2$; $(\omega/p) = r$; $n = dp$; $A \text{ Sin } \varphi = b$;

$A \text{ Cos } \varphi = a$ and substituting into (4) and (5) give :

$$a\ \{\ 1 + -\tfrac{3}{4}-\ \gamma\ (\ A^2) - (r)^2\ \} + 2drb = (Fo/k) \qquad (6)$$

$$b\ \{\ 1 + -\tfrac{3}{4}-\ \gamma\ (\ A^2) - (r)^2\ \} - 2dra = 0 \qquad (7)$$

Multiplying equation (6) and (7) by Cos φ and Sin φ respectively give

$$a\text{Cos } \varphi\ \{\ 1 + -\tfrac{3}{4}-\ \gamma\ (\ A^2) - (r)^2\ \} + 2dr\ b\text{Cos } \varphi = Fo/k\text{Cos } \varphi$$

$$b\text{Sin } \varphi\ \{\ 1 + -\tfrac{3}{4}-\ \gamma\ (\ A^2) - (r)^2\ \} - 2dr\ a\text{Sin } \varphi = 0$$

$$\{\ 1 + -\tfrac{3}{4}-\gamma A^2 - r^2\ \}\{(a^2/A) + (b^2/A)\} = (Fo/k) \text{ Cos } \varphi$$

$$\{\ 1 + -\tfrac{3}{4}-\ \gamma\ (\ A^2) - (r)^2\ \}A = (\ Fo/k\ ) \text{ Cos } \varphi \qquad (8)$$

Multiplying equation (6) and (7) by Sin φ and - Cos φ respectively give

$$a \text{ Sin } \varphi\ \{1 + -\tfrac{3}{4}-\ \gamma(\ A^2) - (r)^2\} + 2drb \text{ Sin } \varphi = (Fo/k) \text{ Sin } \varphi$$

$$-b\text{Cos } \varphi\ \{1 + -\tfrac{3}{4}-\ \gamma(\ A^2) - (r)^2\} + 2dr\ a\text{Cos } \varphi = 0$$

$$2dr\ \{(b^2/A) + (a^2/A)\} = Fo/k\ \mathrm{Sin}\ \varphi$$

$$2drA = Fo/k\ \mathrm{Sin}\ \varphi \qquad (9)$$

Including equation (8) and (9) in the trigonometric equation $\mathrm{Cos}^2\varphi + \mathrm{Sin}^2\varphi = 1$

$$(Ak/Fo)^2\{\ 1 + -\tfrac{3}{4}-\gamma\ A^2 - r^2\}^2 + (Ak/Fo)^2\ (2dr)^2 = 1$$

Denoting $1 + -\tfrac{3}{4}-\gamma\ A^2 = r_a^2$

$$r_{1,2}^2 = r_a^2 - 2d^2 \pm \left[\left(\frac{Fo}{k}\frac{}{A}\right)^2 - 4d^2\ \{\ r_a{}^2 - d^2\ \}\right]^0 \qquad (10)$$

$$\tan\varphi = \mathrm{Sin}\ \varphi\ /\ \mathrm{Cos}\ \varphi$$

$$= \frac{2\ dr}{(1+-\frac{3}{4}-\gamma\ A^2) - r^2} = \frac{2dr}{r_a^2 - r^2}$$

$$\varphi = \tan^{-1}\left[\frac{2dr}{r_a^2 - r^2}\right] \qquad (11)$$

An other approximation :

$$\ddot{x} + 2n\ \dot{x} + p^2(\ x + \gamma\ x^3\ ) = Fo\ p^2/k\ \mathrm{Cos}(\omega t+\varphi)$$

Particular solution $x = A\ \mathrm{Cos}\ \omega t$

$$\dot{x} = -A\omega\ \mathrm{Sin}\ \omega t$$

$$\ddot{x} = -A\omega^2\mathrm{Cos}\ \omega t$$

$-A\omega^2\ \mathrm{Cos}\ \omega t + 2n\{-A\omega\ \mathrm{Sin}\ \omega t\} + Ap^2\ \mathrm{Cos}\ \omega t + \gamma p^2(A\ \mathrm{Cos}\ \omega t)^3 = Fo\ p^2/k\ \mathrm{Cos}(\omega t+\varphi)$

where $\mathrm{Cos}\ (\omega t+\varphi) = \mathrm{Cos}\ \omega t\ \mathrm{Cos}\ \varphi - \mathrm{Sin}\ \varphi\ \mathrm{Sin}\ \omega t$

$$\mathrm{Cos}^3\omega t = \tfrac{1}{4}-\{\mathrm{Cos}\ 3\omega t + 3\ \mathrm{Cos}\ \omega t\ \}$$

Equating coefficients gives

$$[-A\omega^2+Ap^2+\ \tfrac{3}{4}\ \gamma p^2A^3]\ \mathrm{Cos}\ \omega t - 2nA\omega\ \mathrm{Sin}\ \omega t = Fo\ p^2/k$$

$[\mathrm{Cos}\omega t\ \mathrm{Cos}\varphi - \mathrm{Sin}\varphi\ \mathrm{Sin}\omega t]$

$$Ap^2[1 + \tfrac{3}{4}\ \gamma\ A^2 - r^2\ ] = Fo\ p^2/k\ \mathrm{Cos}\ \varphi \qquad (a)$$

$$-2nA\omega = Fo\ p^2/k\ \mathrm{Sin}\ \varphi \qquad (b)$$

Including equation (a) and (b) in the trigonometric equation $\mathrm{Cos}^2\varphi + \mathrm{Sin}^2\varphi = 1$ give

$$\{1 + -\tfrac{3}{4}- \gamma\ (\ A^2) - (r)^2\}A = (\ \varepsilon M\ \omega^2/k\ )\ \mathrm{Cos}\ \varphi \qquad (c)$$

$$2drA = (\ \varepsilon M\ \omega^2/k\ )\ \mathrm{Sin}\ \varphi \qquad (d)$$

$$\mathrm{Sin}^2\varphi + \mathrm{Cos}^2\varphi = 1\ ;\ r_a^2 = 1 + -\tfrac{3}{4}- \gamma\ (\ A^2)$$

$$(r_a^2 - r^2)^2 = \omega^2\left[-\frac{\varepsilon M}{k^2A^2} - -\frac{4d^2}{p^2}--\right]$$

$$(\omega^2)^2 - 2r_a^2p^2(\omega^2) + r_a^4\ p^4 - \omega^2p^4\left[--\frac{\varepsilon M}{k^2A^2} - --\frac{4d^2}{p^2}--\right] = 0$$

$$(\omega^2)^2 - (\omega^2)\left[2r_a^2p^2 + -\frac{\varepsilon M p^4}{k^2A^2} - 4d^2p^2\right] + r_a^4\ p^4 = 0$$

$$(\omega^2)_{1,2} = p^2\left[r_a^2 + \frac{\varepsilon M}{2}\ [-\frac{p}{k}--\frac{}{A}]^2 - 2d^2\right] \pm p^2\left[3r_a^4 + 4d^2(d^2-2r_a^2)\right.$$

$$\left. + 2\varepsilon M\ [-\frac{p}{k}--\frac{}{A}]^2\left|-\frac{\varepsilon M}{8}[-\frac{p}{k}--\frac{}{A}]^2 + r_a^2 - d^2\right|\right]^{0.5}$$

$$(\omega/p)^2_{1,2} = \left[\ r_a^2 + \frac{\varepsilon M}{2}\ [-\frac{p}{k}--\frac{}{A}]^2 - 2d^2\right] \pm$$

$$\left[3r_a^4 + 4d^2(d^2-2r_a^2) + 2\varepsilon M\ [-\frac{p}{k}--\frac{}{A}]^2\left|-\frac{\varepsilon M}{8}[-\frac{p}{k}--\frac{}{A}]^2 + r_a^2 - d^2\right|\right]^{0.5}$$

APPENDIX A-4 : Response of Stability Boundary (Mathieu Equation).

Substituting an approximate equation : $x = A \cos \omega t + \xi$

into the equation of motion gives

$$\ddot{x} + 2n\dot{x} + p^2 x + \alpha p^2 \{x^3\} = 0 \qquad (1)$$

where : $\dot{x} = \xi'$; $\ddot{x} = \xi''$

$$\xi'' + 2n\xi' + p^2\{A\cos\omega t + \xi\} + \alpha p^2 \{A\cos\omega t + \xi\}^3 = 0 \qquad (2)$$

Knowing :

$\{A\cos\omega t + \xi\}^3 = A^3\cos^3\omega t + \xi^3 + 3A^2\xi\cos^2\omega t + 3A\xi^2\cos\omega t$

and ommitting higher harmonics such as : $A^3\cos^3\omega t$, ξ^3 , $3A\xi^2\cos\omega t$, the later equation give

$\{A\cos\omega t + \xi\}^3 = 3A^2\xi\cos^2\omega t$

Substituting $3A^2\xi\cos^2\omega t = \frac{3}{2}A^2\xi(1+\cos 2\omega t)$ in equation (2) give

$$\xi'' + 2n\xi' + p^2\xi + \frac{3}{2}\alpha p^2 A^2\xi(1+\cos 2\omega t) = 0 \qquad (3)$$

If the particular solution is expressed as $\xi_p = u\cos\omega t + v\sin\omega t$ the derivatives are described below.

$\xi_p = u\cos\omega t + v\sin\omega t$

$\xi_p' = -u\omega\sin\omega t + v\omega\cos\omega t$

$\xi_p'' = -u\omega^2\cos\omega t - v\omega^2\sin\omega t$

Back substitutions into equation (3) give

$-u\omega^2\cos\omega t - v\omega^2\sin\omega t + 2n\{-u\omega\sin\omega t + v\omega\cos\omega t\} +$

$p^2\{u \text{ Cos } \omega t + v \text{ Sin } \omega t\} + \frac{3}{2} \alpha p^2 A^2 (1 + \text{Cos } 2\omega t)(u \text{ Cos } \omega t +$

$v \text{ Sin } \omega t) = 0$ (4)

Rearranging the last part of equation (4)

$(1+ \text{Cos } 2\omega t)(u \text{ Cos } \omega t+ v \text{ Sin } \omega t) = u \text{ Cos } \omega t + v \text{ Sin } \omega t +$

$u \text{ Cos } 2\omega t \text{ Cos } \omega t+ v \text{ Sin } \omega t \text{ Cos } 2\omega t = u \text{ Cos } \omega t+ v \text{ Sin } \omega t +$

$\frac{u}{2} \text{ Cos } 3\omega t + \frac{u}{2}\text{Cos } \omega t + \frac{v}{2} \text{ Sin } 3\omega t - \frac{v}{2}\text{Sin } \omega t$

and back substitution give

$-u\omega^2\text{Cos}\omega t - v\omega^2\text{Sin}\omega t + 2n \{-u\omega \text{ Sin } \omega t + v\omega \text{ Cos } \omega t\} +$

$p^2(u \text{ Cos } \omega t + v \text{ Sin } \omega t) + \frac{3}{2} \alpha p^2 A^2 \{u \text{ Cos } \omega t + v \text{ Sin } \omega t$

$+ \frac{u}{2} \text{ Cos } 3\omega t + \frac{u}{2}\text{Cos } \omega t + \frac{v}{2} \text{ Sin } 3\omega t - \frac{v}{2}\text{Sin } \omega t \} = 0$ (5)

Again, ommitting higher harmonic orders such as Cos $3\omega t$ and Sin $3\omega t$ and equating the lower harmonics it gives

$-u\omega^2\text{Cos}\omega t + 2nv\omega \text{ Cos } \omega t + p^2\text{Cos } \omega t + \frac{3}{2}\alpha p^2 A^2 \{u \text{ Cos } \omega t +$

$\frac{u}{2} \text{ Cos } \omega t\} = 0$

$-u\omega^2 + 2nv\omega + p^2 + (\frac{3}{2} \alpha p^2 A^2)(\frac{3}{2} u) = 0$

$up^2\{ 1+\frac{9}{4} \alpha A^2 - (\omega/p)^2 \} + 2nv\omega = 0$ (6)

$-v\omega^2\text{Sin}\omega t - 2nu\omega \text{ Sin } \omega t + p^2\text{Sin } \omega t + \frac{3}{2}\alpha p^2 A^2 (v \text{ Sin } \omega t -$

$\frac{v}{2} \text{ Sin } \omega t) = 0$

$-v\omega^2 - 2nu\omega + p^2 + \frac{3}{4} \alpha A^2 v = 0$

$vp^2\{ 1 + \frac{3}{4} \alpha A^2 - (\omega/p)^2 \} - 2nu\omega = 0$ (7)

Substituting $n = dp$; $u^2 + v^2 = A^2$; $\omega/p = r$ into (6) and (7) give

$u\{ 1 + \frac{9}{4} \alpha A^2 - r^2 \} + 2drv = 0$ (8)

$v\{ 1 + \frac{3}{4} \alpha A^2 - r^2 \} - 2dru = 0$ (9)

Rearranging equations (8) and (9) give

$$\{1 + \frac{3}{2}\alpha A^2 - r^2\}^2 + (2dr)^2 - \{\frac{3}{4}\alpha A^2\}^2 = 0$$

$$r_{1,2}^2 = 1 + \frac{3}{2}\alpha A^2 - 2d^2 \pm \left[\{\frac{3}{4}\alpha A^2\}^2 - 4d^2\{1 + \frac{3}{2}\alpha A^2 - d^2\}\right]^{0.5}$$

which represents the equation of stability function.

APPENDIX A-5 : Isochrones and Stability Equations.

$m\ddot{x} + c\dot{x} + k(x + \gamma x^3) = Fo \sin \omega t$

$\ddot{x} + 2dp\,\dot{x} + p^2 x(1 + \gamma x^2) = Fo/m \sin \omega t$

Including $g = 2d\omega/p = 2dr$ gives

$\ddot{x} + 2dr(p^2/\omega)\,\dot{x} + p^2 x(1 + \gamma x^2) = Fo/m \sin \omega t$

$\ddot{x} + g\,(p^2/\omega)\,\dot{x} + p^2 x(1 + \gamma x^2) = Fo/m \sin \omega t$ (1)

Assuming $x_p = a \sin \omega t + b \cos \omega t$

$\dot{x}_p = a\omega \cos \omega t - b\omega \sin \omega t$

$\ddot{x}_p = -a\omega^2 \sin \omega t - b\omega^2 \cos \omega t$

$x^2 \simeq 0.75A^2$

Substituting into equation (1) yields

$\ddot{x} + g\,(p^2/\omega)\,\dot{x} + p^2 x(1 + 0.75\,\gamma A^2) = Fo/m \sin \omega t$

Denoting $(1 + 0.75\,\gamma A^2) = r_a^2$

$\ddot{x} + g\,(p^2/\omega)\,\dot{x} + p^2\, r_a^2\, x = Fo/m \sin \omega t$

$[(p^2 r_a^2 - \omega^2)a - gp^2 b] \sin \omega t + [(p^2 r_a^2 - \omega^2)b + gp^2 a] \cos \omega t$

$= Fo/m \sin wt$

Equating coefficients

$[(p^2 r_a^2 - \omega^2)b - gp^2 a] = 0$; $[(r_a^2 - \omega^2)b - ga] = 0$

$a = -(r_a^2 - r^2)b/g$

$Fo/m = [(p^2 r_a^2 - \omega^2)a - gp^2 b]$

$Fo/(mp^2) = [(r_a^2 - \omega^2)a - gb]$

When $r = \omega/p$; $m = k/p^2$

$$; \; b = \frac{-g\,Fo/k}{(r_a^2 - r^2)^2 + g^2} \qquad (2)$$

$$; \; a = \frac{(r_a^2 - r^2)Fo/k}{(r_a^2 - r^2)^2 + g^2} \qquad (3)$$

Instead of $x_p = a \sin \omega t + b \cos \omega t$ this can be in terms

of $x_p = A \sin(\omega t - \varphi)$. Applying trigonometry rules and equating coefficients lead to $a = A \cos \varphi$

$$b = -A \sin \varphi$$

$$a^2 + b^2 = A^2 \; ; \; A = \frac{Fo}{k\sqrt{(r_a^2 - r^2)^2 + g^2}}$$

$$A^2 = \frac{Fo^2}{k^2 \{(r_a^2 - r^2)^2 + g^2\}} \qquad (4)$$

$$(r_a^2 - r^2)^2 + g^2 = \frac{Fo^2}{k^2 A^2}$$

$$(r^2)^2 - 2r_a^2 r^2 + (r_a^2)^2 + g^2 - \frac{Fo^2}{k^2 A^2} = 0$$

$$r^2_{1,2} = r_a^2 \pm \sqrt{\frac{Fo^2}{A^2 k^2} - g^2} \qquad (5)$$

Substituting equation (4) into equations (2) and (3)

$$a = \frac{A^2}{Fo} k(r_a^2 - r^2); \quad b = \frac{-A^2 g k}{Fo} \qquad (6)$$

$$\varphi = \tan^{-1}[b/a]$$

$$\varphi = \tan^{-1}\left[\frac{-g}{(r_a^2 - r^2)}\right] = \tan^{-1}\left[\frac{g}{(r^2 - r_a^2)}\right] \qquad (7)$$

Substituting $a^2 + b^2 = A^2$ into equation (6) represents the polar equation with axes, a and b.

$$a^2 + b^2 = \frac{-Fo\, b}{g\, k}$$

Eliminating A in equation (6) the isochrones equation may be established as follows.

$$A^2 = \frac{-b\, Fo}{g_2 k}$$

$$a = \frac{A^2}{Fo} k (r_a^2 - r^2)$$

$$a = -\frac{b}{g}\{1 + 0.75\, \gamma\, A^2 - r^2\}$$

$$a = -\frac{b}{g}\{1 + 0.75\gamma(a^2 + b^2) - r^2\}$$

$$a = -\frac{b}{g}\{r^2 - 1 - 0.75\gamma(a^2 + b^2)\} \qquad (8)$$

At $a \simeq 0$ then equation (7) becomes

$$0 = -\frac{b}{g}-\{r^2-1-0.75\gamma(b^2)\} \; : \; b = \left|\frac{(r^2-1)}{0.75\gamma}\right|^{0.5} \qquad (9)$$

Back substitution into equation (7) gives

$$ga = \left|\frac{(r^2-1)}{0.75\gamma}\right|^{0.5}\{r^2-1-0.75\gamma(a^2+\left|\frac{(r^2-1)}{0.75\gamma}\right|)\}$$

$$ga = -0.75\gamma\ a^2\left|\frac{(r^2-1)}{0.75\gamma}\right|^{0.5}$$

$$a = -\frac{g}{0.75\gamma}\left|\frac{0.75\gamma}{(r^2-1)}\right|^{0.5} \qquad (10)$$

Substituting equation (9) and (10) into equation of rectangular hyperbola : ab = k yields the equation of stability function.

$$k = -\frac{g}{0.75\gamma} = \frac{4g}{3\gamma}; \quad ab = \frac{4g}{3\gamma} \qquad (11)$$

The hyperbola relationships give $A^2_{peak} = 2k$

$$A_{peak} = \sqrt{\frac{8g}{3\gamma}} \qquad (12)$$

Back substitution into equation of hyperbola (11) gives the peak frequency as follows.

$$ab = -\frac{4g}{3\gamma} \; ; \; \text{at peak } a = b \; ; \; a^2 = -\frac{4g}{3\gamma}$$

$$\frac{g^2}{(-0.75\gamma)^2}\left|\frac{0.75\gamma}{(r^2-1)}\right| = -\frac{4g}{3\gamma}$$

$$r^2 = 1 + g \; ; \; \omega_{peak} = p\sqrt{1+g} \qquad (13)$$

APPENDIX B-1 : Mix Design Procedure

Item	Reference	Values
Stage-1		
1.1. Characteristics of strength	Specified	Compressive:30N/mm2 at 28 days, proportion defective 5 per cent
1.2. Standard dev.	Fig.3	8 N/mm^2
1.3. Margin	C1	(k=1.64) x 8 =13 N/mm^2
1.4. Target mean strength	C2	30 + 13 =43 N/mm^2
1.5. Cement type	Specified	OPC
1.6. Type of aggr.		
a. Coarse		uncrushed
b. Fine		uncrushed
1.7. Free water/cement ratio	Table 2, Fig.4	0.47)use lower value
1.8. Max.free water	Specified	0.65
Stage-2		
2.1. Slump or V-B	Specified	Slump 10-30 mm
2.2. Max.aggr.size	Specified	= 20 mm
2.3. Free water cont.	Table 3	=170 kg/m^3
Stage-3		
3.1. Cement content	C3	170 / 0.44 =386 kg/m^3
3.2. Max.cement	Specified	----------
3.3. Min.cement	Specified	275 kg/m^3 -use if > 3.1
3.4. Modified free w/c ratio		----------
Stage-4		
4.1. Relative density of aggr(SSD)		2.6 t/m^3 (assumed)
4.2. Concrete dens.	Fig 5	2400 kg/m^3
4.3. Total aggregate content	C4	2400-386-170=1844kg/m^3
Stage-5		
5.1. Grad of fine agg	BS882	zone-2
5.2. Proportion of fine aggr.	Fig.6	29 to 37 say 35%
5.3. Fine aggr.cont.	C5	1844 x 0.35= 645kg/m^3
5.4. Coarse aggr.cont	C5	1844 - 645 =1235kg/m^3

	Cement(kg)	Water(kg)	Fine aggr.(kg)	Coarse aggr.(kg)
Per m^3:	386	170	645	1199

APPENDIX B-2 : Design of Fully Bonded Beam Models

1. Uncracked Condition.

Assumptions :

h = 150 mm, d = 125 mm, b = 100 mm, f_{cu} = 30 N/mm^2

f_y = 312 N/mm^2, $f_{flexural}$ = 1 N/mm^2, L = 3000 mm

Specific gravity = 24 kN/m^3, see figure (B-1).

a. Maximum Steel Area.

To provide under reinforced concrete beam models the neutral axes,x about the top compression fibre must be greater than or equal to the half depth,d. Based on this specification the maximum steel area for the individual beam model may be determined.See figure (B-2).

C_c = 0.9 X 100 (0.45 30) = 0.9 (125/2) 100 (0.45 30)

= 75937.5 N

$T_s = 0.87\ f_y\ A_s = 0.87\ 312\ A_s = 271.44\ As$

$C_c = T_s$ ---> A_s = 279.75 mm^2, <u>adopt 2Y12 = 226.19</u> mm^2

b. Cracking Moment.

To allow maximum unbalanced force on the beam model the maximum deflection before cracking has to be considered. The maximum deflection can be approximated, firstly, by determining the maximum moment before cracking. Secondly, by recalculating the equivalent distributed load. From this point of view, the equivalent maximum deflection may be obtainable.

Assumptions : $E_s = 200\ 10^3$ N/mm^2, $E_c = 26\ 10^3$ N/mm^2

$m = E_s/E_c = 7.69$, L = 3000 mm, see fig.(B-3)

Total moment about top compression fibre is equal to zero.

$0.5\ 100\ 150^2 + (7.69-1)\ 226.19\ 125 = \{(7.69 - 1)\ 226.19 + 100\ 150\}\ X$ ----> X = 79.58 mm

$I_0 = 100\ 150^3/12 + 100\ 150\ (79.58-75)^2 + (7.69-1)\ 226.19\ (125-79.58)^2 = 31561364.79$ mm^4.

$$M_{cracking} = \frac{(1)\ 31561364.79}{(125 - 79.58)} = 694878.13 \text{ Nmm.}$$

$$Q_{equivalent} = Q_{eq} = 8\ M_{cracking} / L^2 = = 0.617669 \text{ N/mm}$$

$= 0.617669$ kN/m

$Q_{self} = 0.1\ 0.150\ 24 = 0.36$ kN/m.

Thus, an extra load can be provided.

c. Maximum Deflection Before Cracking.

$$def = \frac{5\ Q_{eq}\ L^4}{384\ E_c\ I_0} = \frac{5\ \ 0.617699\ \ 3000^4}{384\ \ 26\ 10^3\ \ 31561364.79}$$

$= 0.79391$ mm

d. Natural Frequency Before Cracking.

An approximate equation derived from Rayleigh's [8] method is shown below.

$$p_i = (i\ \pi)^2 \sqrt{E_c\ I_0 / (\ q\ L^4)}$$

where : i represents the i-th frequency

q is the mass per meter of length

$E_c\ I_0 = 0.820595\ 10^6$ Nm^2, $L^4 = 81$ m^4

q = 0.36 kN/m = 360 0.102 kg/m = 36.72 kg/m

$$p_i = (i\ \pi)^2 \sqrt{\frac{EI}{m\ L^4}} = (i\ \pi)^2 \sqrt{\frac{820595}{36.72\ 81}}$$

p_1 = 163.93 rad/sec : $f_1 = p_1/2\pi$ = 26.09 Hz.

p_2 = 655.72 rad/sec : f_2 = 104.36 Hz..

p_3 = 1475.41 rad/sec : f_3 = 234.81 Hz.

e. Maximum Equivalent Point Load.

$$d_{mid\text{-}span} = \int_0^L \frac{m_1\ m_2}{E_0\ I_0} = \frac{0.4695P\ 0.5+0.1565P\ 0.6875}{E_0\ I_0} + \frac{0.013P\ 0.667+0.456P\ 0.4166}{E_0\ I_0}$$

$$= 0.5621\ P\ /\ (820595) = 6.8499\ P\ 10^{-7}\ m$$

$$= 6.8499\ P\ 10^{-4}\ mm$$

Introducing $d_{max\ before\ cracking}$ = 0.79391 mm into $d_{midspan}$ give maximum P = 1159.00 N or approximately equal to P = 118.24 kg at position shown in fig.(B-4).

2. Cracked Condition.

Assumptions :

f_{cu}= 30 N/mm^2, f_y = 312 N/mm^2. See fig.(B.2).

C_c = (0.45 30) 100 (0.9 X) = 1215 X N

T_s = 226.19 0.87 312 = 61397.01 N

$C_c = T_s$ ----> X = 50.532 mm < 0.5d = 62.5 mm

a. Ultimite Moment.

To get approximate maximum point loads when the static loading experiments are carried out. the ultimate moment has to be examined.

M_{ult}= 1215 50.53 (125 - 0.9 50.53/2) = 6278237.41 Nmm

= 6.278237 kNm

If the loading points are positioned at the third span the yield load can be approximated as follows.

$M_{ult} = P_{max}\ L/3 + Q_{self}\ L^2/8 \rightarrow P_{max} = 6.278237 - 0.405$

$P_{max} = 5.8732$ kN

b. Natural frequency.

To predict the approximate the lowest natural frequency after cracking within the elastic range the theory of elasticity for stress- strain relationships are applied in the calculation (see fig.B-5).

$T_s = 226.19\ 7.69\ f_s = 1739.4\ f_s$

$C_c = 0.5\ 100\ X\ f_c = 0.5\ 100\ X^2\ f_s/(125 - X)$

$C_c = T_s \rightarrow X^2 + 34.788\ X - 4348.5 = 0$

$X = 50.80$ mm.

$I_0 = 100\ 50.80^3/3 + 7.69\ 226.19\ (125 - 50.80)^2$

$= 13946400\ mm^4$

$EI_0 = 26\ 10^3\ 13946400 = 3.626064\ 10^{11}\ Nmm^2$

$= 0.3626064\ 10^6\ Nm^2$

$$p_i = (i\ \pi)^2 \sqrt{\frac{EIo}{q\ L^4}} = \sqrt{\frac{362606.4}{36.72\ 81}}$$

$p_1 = 108.885$ rad/sec ; $f_1 = 17.32$ Hz.

$p_2 = 435.487$ rad/sec ; $f_2 = 69.31$ Hz.

$p_3 = 979.925$ rad/sec ; $f_3 = 155.96$ Hz.

c. Shear cracks.

To create shear crack patterns on the beam model the loading points are repositioned closer to the supports in such a way that the ultimate moment is not exceeded when

shear cracks occur. Shear cracks occur at shear stress (v) exceeds $1.25v_c$. where v_c is the design shear stress and is obtainable from BS-8110 as cited in the table (B-1).

$v = V/(b\ d)$ --> $V = v\ b\ d = 1.29\ 100\ 125$

$= 16125\ N = 16.125\ kN$

$V = 0.5\ Q_{self}\ L + P$; $P = 16.125 - 0.54 = 15.585\ kN.$

The positions are obtainable by equating maximum moment due to the shear load and due to the flexural load.

Max.moment due to shear load, M_{shear} is as follows.

$M_{max} = (P + Q_{self}\ L/2)L/2 - (Q_{self}\ L/2)L/4 - P\{(L/2) - z\}$

$= (15.585 + 0.54)1.5 - (0.54)0.75 - 15.585(1.5 - z)$

$= 24.1875 - 0.405 - 23.3775 + 15.585z = 0.405 + 15.585z$

$M_{ult} = 6.2782\ kNm$

Equating $M_{ult} = M_{max}$

$6.2782 = 0.405 + 15.585\ z$; $z = 0.3768\ m$

The external point loads may be provided at positions less than 0.3768 m from supports as seen in fig.(B-6).

APPENDIX B-3 : Design of Partially Bonded Beam Model

Uncracked Condition

Assumptions :

b = 100 mm, h = 150 mm, L = 3000 mm, f_y = 30 N/mm^2.

d = 125 mm f_{cu} = 312 N/mm^2. diameter of holes within unbonded region is approximately 14 mm, see fig.(B-7).

b. Cracking Moment.

The maximum moment before cracking is obtained by excluding area of the tensile reinforcement in the unbonded region as seen in fig.(B-8). Balanced moment about the top compression fibre at the mid span determines the neutral axis,X as follows.

$0.5\ 100\ 150^2 - 2(\pi\ 14^2/4)\ 125 =$

$\{100\ 150 - 2(\pi\ 14^2/4)\}\ X$ ----> X = 73.95 mm

$I_o = 100\ 150^3/12 + 100\ 150\ (75 - 73.95)^2 - 307.87\ (125 - 73.95)^2 = 27339196\ mm^2$

$$f_{r1} = \frac{M_{max}\ y}{I_o}\ ,\ M_{max} = (1)\ 27339196\ /(125 - 73.95)$$

= 535537 Nmm = 0.535537 kNm.

c. Maximum Deflection Before Cracking.

The maximum deflection before cracking may be approximately determined by introducing $Q_{equvalent}$ to the flexural cracking moment as follows.

$M_{cracking} = Q_{eq}\ L^2/8$ -> Q_{eq} = 8 0.567037/9 = 0.47603 kN/m

Q_{self} = 0.36 kN/m < Q_{eq} --> an extra load may be provided

The equation of the deflection is defined by integrating the general equation for moment as follows (see fig.B-9).

$I_2 = 27339196\ mm^4$. $I_1 = 31561364\ mm^4$ ---> $EI_1 = 1.15\ EI_2$

Equation for region-1 (bonded) :

$$\frac{\delta^2 y_1}{\delta x^2} = \frac{-(q\ L\ X_1/2) + (q\ X_1^2/2)}{1.15\ EI_2}$$

$$\frac{\delta y_1}{\delta x} = \frac{-(q\ L\ X_1^2/4) + (q\ X_1^3/6)}{1.15\ EI_2} + A_1$$

$$y_1 = \frac{-(q\ L\ X_1^3/12) + (q\ X_1^4/24)}{1.15\ EI_2} + A_1 X_1 + A_2$$

Introducing the boundary conditions :

At $X_1 = 0m$ --> $y_1 = 0$. therefore, $A_2 = 0$

$$\text{At } X_1 = 1m \text{ --> } y_1 = \frac{-0.20833\ q}{1.15\ EI_2} + A_1 \qquad (1)$$

$$\text{--> } \frac{\delta y_1}{\delta x} = \frac{-0.58333\ q}{1.15\ EI_2} + A_1$$

$$= \frac{-0.50724\ q}{EI_2} + A_1 \qquad (2)$$

Equation for region-2 (unbonded) :

$$\frac{\delta^2 y_2}{\delta x^2} = \frac{-\{q\ L\ (1+X_2)/2\} + \{(q\ (1+X_2)^2/2\}}{EI_2}$$

$$\frac{\delta y_2}{\delta x} = \frac{-q\ L\ (X_2+X_2^2/2)/2}{EI_2} + \frac{q\ \{X_2+X_2^2+(X_2^3/3)\}/2}{EI_2}$$

$$+ A_3$$

$$y_2 = \frac{-q\ L\ (X_2^2/2+X_2^3/6)/2}{EI_2} + \frac{q\ \{X_2^2/2+X_2^3/3+(X_2^4/12)\}/2}{EI_2}$$

$$+ A_3\ X_2 + A_4$$

Introducing the boundary conditions :

$$\text{At } X_2 = 0\text{m} \longrightarrow y_2 = A_4 \tag{3}$$

$$\frac{\delta y_2}{\delta x} = A_3 \tag{4}$$

$$\text{At } X_2 = 0.5\text{m} \longrightarrow \frac{\delta y_2}{\delta x} = 0 = \frac{-0.9375\ q}{EI_2} + \frac{0.39583\ q}{EI_2} + A_3$$

$$A_3 = 0.54167\ q\ /\ EI_2 \tag{5}$$

Substituting eq.(4) and eq.(5) into eq.(2) gives

$$\frac{-0.50724\ q}{EI_2} + A_1 = A_3$$

$$A_1 = (0.54167 + 0.507243)\ q\ /\ EI_2 = 1.04891\ q/EI_2 \tag{6}$$

Substituting eq.(3) and eq.(6) into eq.(1) gives

$$\frac{-0.181145\ q}{EI_2} + A_1 = A_4$$

$$A_4 = (-0.181145 + 1.04891\ )\ q\ /\ EI_2 = 0.86775\ q/EI_2 \tag{7}$$

Substituting equation (5), (6) and (7) into the general equation of region-1 and region-2 give respectively

for region-1 :

$$y_1 = \frac{-(q\ L\ X_1^3/12) + (q\ X_1^4/24)}{1.15\ EI_2} + \frac{1.04891\ q\ X_1}{EI_2}$$

for region-2 :

$$y_2 = \frac{-q\ L\ (X_2^2/2+X_2^3/6)/2)}{EI_2} + \frac{q\ \{X_2^2/2+X_2^3/3+X_2^4/12)\}/2}{EI_2} + \frac{0.54167\ q\ X_2}{EI_2} + \frac{0.86775\ q}{EI_2}$$

where : y : deflection at respective regions, in m.

X_1 : distance from support within region-1, in m.

X_2 : distance from the third span within region-2, in m.

Substituting Q_{eq} = 0.4760 kN/m EI_2 = 710.819 kN/m^2 and X_2 = 0.5 m into equation for region-2 the approximate maximum deflection before cracking is obtainable.

$$v_2 = \frac{-0.21875\ q}{EI_2} + \frac{0.085937\ q}{EI_2} + \frac{0.2708\ q}{EI_2} + \frac{0.86775\ q}{EI_2}$$

$$= 1.00573\ q\ /\ EI_2 = 6.7353\ 10^{-4}\ m = 0.67353\ mm$$

d. Natural Frequency.

By adopting Rayleigh's method [8] the natural frequency for the partially bonded beam model may be examined. Two equations of shape function may be derived from the equations of deflection below.

For region-1 :

$$v(x)_1 = \frac{q\ (L^3\ X - 2\ L\ X^3 + X^4)}{24\ EI_1} \qquad (8)$$

For region-2 :

$$v(x)_2 = \frac{q\ (L^3\ X - 2\ L\ X^3 + X^4)}{24\ EI_2} \qquad (9)$$

Assuming $Z_1 = \frac{5\ q\ L^4}{384\ EI_1}$ and $Z_2 = \frac{5\ q\ L^4}{384\ EI_2}$ or

$$Z_2 = Z_1 (I_1 / I_2)$$

and substituting into eq.(8) and (9) give

$$v(x)_1 = \frac{3.2\ \ Z_1\ (L^3\ X - 2\ L\ X^3 + X^4)}{L^4}$$

$$v(x)_2 = \frac{3.2\ \ Z_1\ I_1\ (L^3\ X - 2\ L\ X^3 + X^4)}{I_2\ L^4}$$

The general shape function is determined as follows.

$$\psi(x)_{1,2} = \frac{3.2\ (L^3\ X - 2\ L\ X^3 + X^4)}{L^4} \qquad (10)$$

The strain energy equation is

$$V(max) = 0.5\ g\ Z_0 \int_0^L m(x)\ \Psi(x)\ \delta x$$

$$= (2)\ 0.5\ g\ Z_1 \int_0^{0.33L} m(x)\ \Psi(x)_1 \delta x +$$

$$(2)\ 0.5\ g\ Z_2 \int_{0.33L}^{0.50L} m(x)\ \Psi\ (x)_2 \delta x \qquad (11)$$

The kinetic energy equation is

$$T(max) = (2)\ Z_1^2\ (p^2/2) \int_0^{0.33L} m(x)\ [\Psi(x)_1]^2\ \delta x +$$

$$(2)\ Z_2^2\ (p^2/2) \int_{0.33L}^{0.50L} m(x)\ [\Psi(x)_2]^2\ \delta x \qquad (12)$$

Sustituting equation (10) into (11) and (12) and equating equation (11) and (12) give

$$p^2 = \frac{g\ Z_1\ [\ A + B\ ]}{Z_1^2\ [\ C + D\ ]} = -\frac{g\ [\ A + B\ ]}{Z_1\ [\ C + D\ ]}$$

where : $A = \int_0^{0.33L} m(x)\ \Psi(x)_1\ \delta x$

$$B = (I_1/I_2) \int_{0.33L}^{0.50L} m(x)\ \Psi(x)_2\ \delta x$$

$$C = \int_0^{0.33L} m(x)\ [\Psi(x)_1]^2\ \delta x$$

$$D = (I_1/I_2)^2 \int_{0.33L}^{0.50L} m(x)\ [\Psi(x)_2]^2\ \delta x$$

Introducing L = 3m. I_1 = 31561364 mm^4 . q = 360 N/m. I_2 = 27339196 mm^4 . I_1/I_2 = 1.15 g = 9.8 m/sec^2 . EI_1 = 820595 Nm^2. Z_1 = 4.62697 10^{-4}. the circular frequency can be obtained as follows.

$$\Psi(x)_1 = (3.2/L^4)\ (L^3X - 2LX^3 + X^4)$$

$$[\Psi(x)_1]^2 = (10.24/L^3)\ (L^6X^2 - 4L^4X^4 + 2L^3X^5 + 4L^2X^6 - 4LX^7 + X^8)$$

$$A = (3.2/L^4)\ m(x)\ \left[\ \{L^3(X^2/2) - 2L(X^4/4) + (X^5/5)\}\ \right]_0^{0.33L}$$

$$= 3.2\ m(x)\ 0.0493\ L = 0.15777\ m(x)\ L$$

$$B = (3.68/L^4)\ m(x) \left[\ \{L^3(X^2/2) - 2L(X^4/4) + (X^5/5)\}\ \right]_{0.33L}^{0.50L}$$

$$= 3.68\ m(x)\ (0.1000 - 0.0493)\ L = 0.18657\ m(x)\ L$$

$$C = (10.24/L^8)\, m(x)\Big[\, L^6(X^3/3) - (4/5)L^4\, X^5 + (1/3)\, L^3\, X^6 + (4/7)\, L^2\, X^7 - (1/2)\, L\, X^8 + (1/9)\, X^9 \,\Big]_0^{0.33L}$$

$$= 10.24\; m(x)\; (9.457028\; 10^{-3})\; L = 0.09684\; m(x)\; L$$

$$D = (13.54/L^8)\, m(x)\Big[\, L^6(X^3/3) - (4/5)L^4\, X^5 + (1/3)\, L^3\, X^6 + (4/7)\, L^2\, X^7 - (1/2)\, L\, X^8 + (1/9)\, X^9 \,\Big]_{0.33L}^{0.80L}$$

$$= (13.54)\; m(x)\; (\; 0.024603 - 9.457028\; 10^{-3})\; L$$

$$= 0.2050\; m(x)\; L$$

$$p^2 = -\frac{9.8\; [\; 0.15777\; m(x)\; L + 0.18657\; m(x)\; L\;]}{4.62697\; 10^{-4}\; [\; 0.09684\; m(x)\; L + 0.2050\; m(x)\; L\;]}$$

$$= 24162.40\ \text{rad}^2/\text{sec}^2.\quad p = 155.442\ \text{rad/sec}$$

$$f = p/2\pi = 24.74\ \text{Hz}.$$

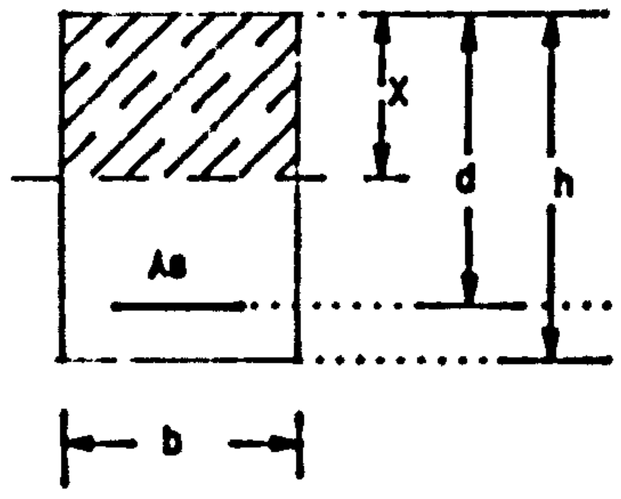

FIG.B-1.BEAM SECTION.

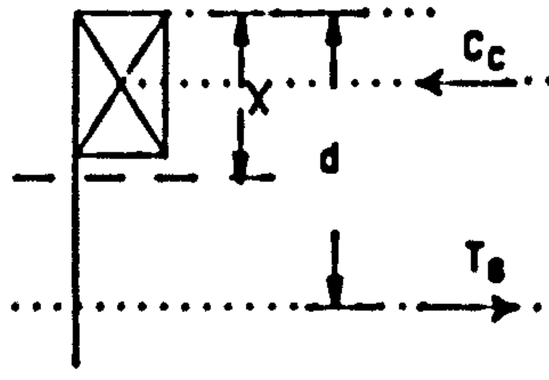

FIG.B-2.ULTIMIT STRESS DISTRIBUTION

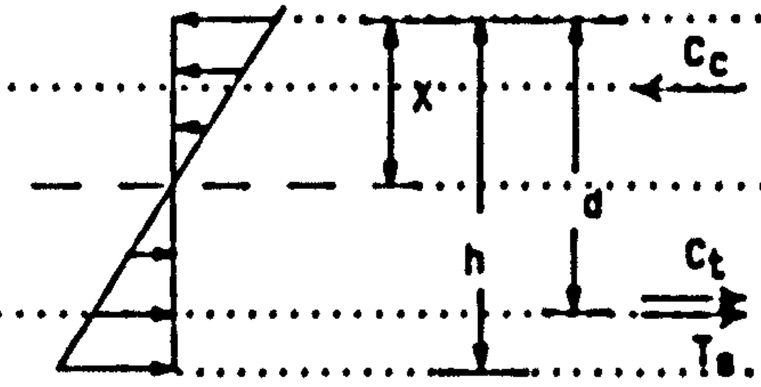

FIG.B-3.ELASTIC STRESS DISTRIBUTION

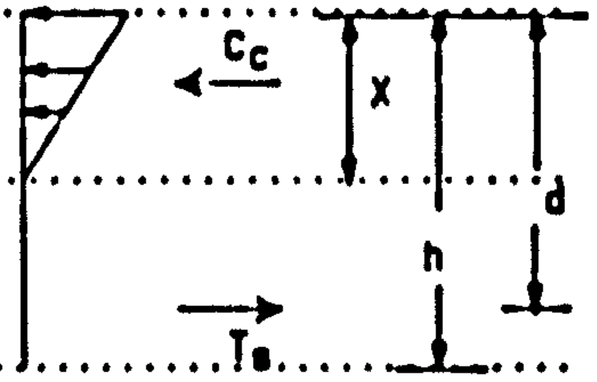

FIG.B-5.ELASTIC STRESS DISTRIBUTION

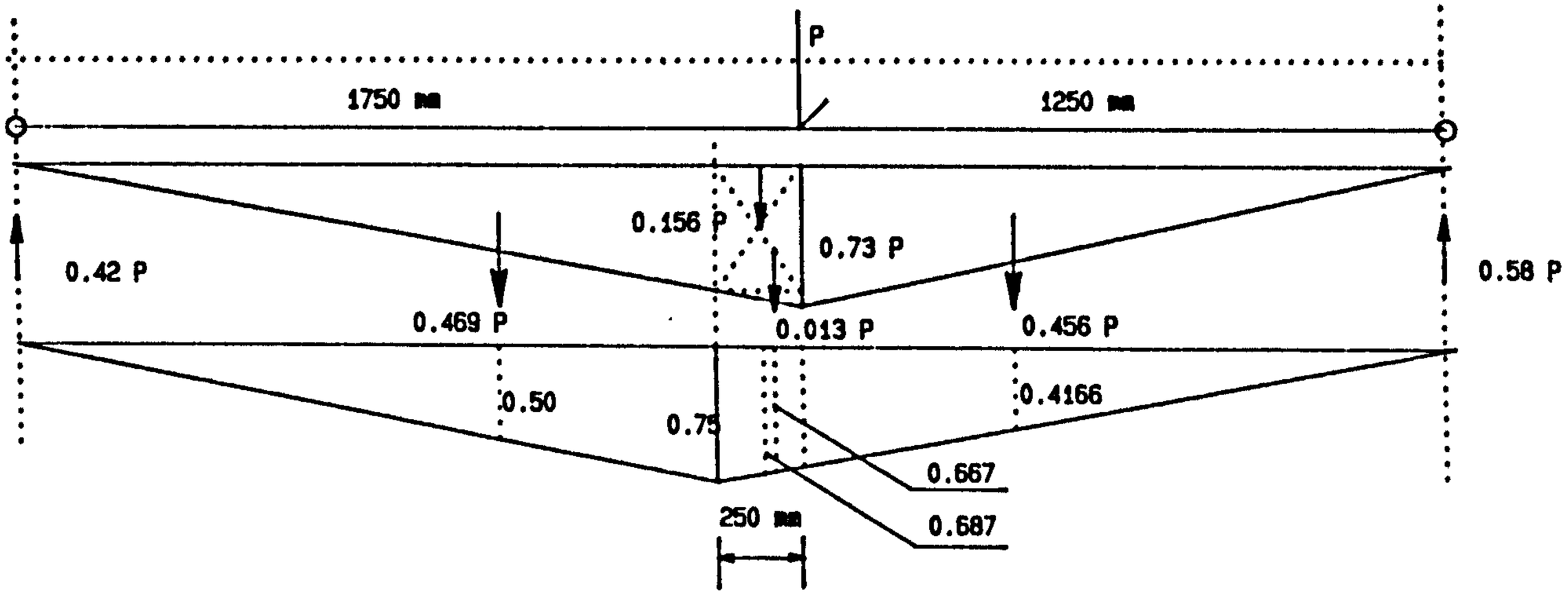

FIG.B-4.DEFLECTION AT THE MID SPAN

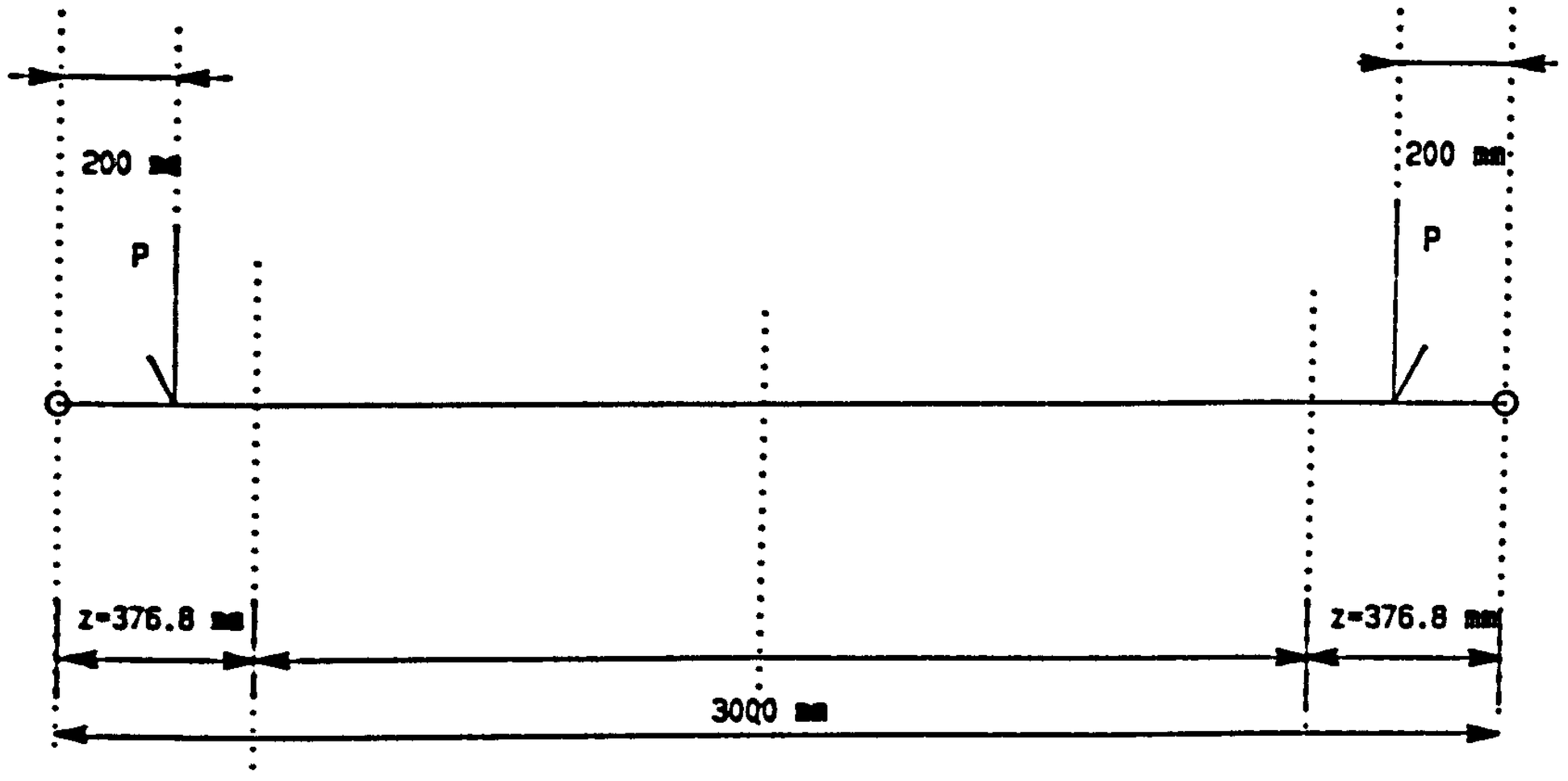

FIG.B-6.SHEAR LOAD POSITIONS

Table 3.9 Values of v_c, design concrete shear stress

$\frac{100A_s}{b_v d}$	Effective depth (in mm)							
	125	150	175	200	225	250	300	> 400
	N/mm²	N/mm²	N/mm²	N/mm²	N/mm²	N/mm²	N/mm²	N/mm²
≤ 0.15	0.45	0.43	0.41	0.40	0.39	0.38	0.36	0.34
0.25	0.53	0.51	0 49	0.47	0.46	0.45	0.43	0.40
0.50	0.67	0.64	0 62	0.60	0.58	0.56	0.54	0.50
0.75	0.77	0.73	0.71	0.68	0.66	0.65	0.62	0.57
1.00	0.84	0.81	0.78	0.75	0.73	0.71	0.68	0.63
1.50	0.97	0.92	0.89	0.86	0.83	0.81	0.78	0.72
2.00	1.06	1.02	0.98	0.95	0.92	0.89	0.86	0.80
≥ 3.00	1.22	1.16	1.12	1.08	1.05	1.02	0.98	0.91

NOTE 1 Allowance has been made in these figures for a γ_m of 1.25.

NOTE 2 The values in the table are derived from the expression:

$$0.79(100A_s/b_v d)^{1/3}(400/d)^{1/4}/\gamma_m$$

where

$\frac{100A_s}{b_v d}$ should not be taken as greater than 3;

$\frac{400}{d}$ should not be taken as less than 1.

For characteristic concrete strengths greater than 25 N/mm², the values in table 3.9 may be multiplied by $(f_{cu}/25)^{1/3}$. The value of f_{cu} should not be taken as greater than 40.

TABLE.B-1.DESIGN OF SHEAR STRESS
(CITED FROM BS-8110)

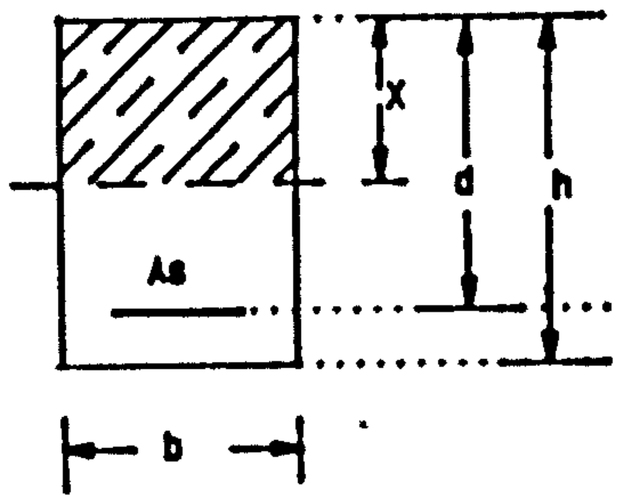

FIG.B-7.BEAM SECTION.

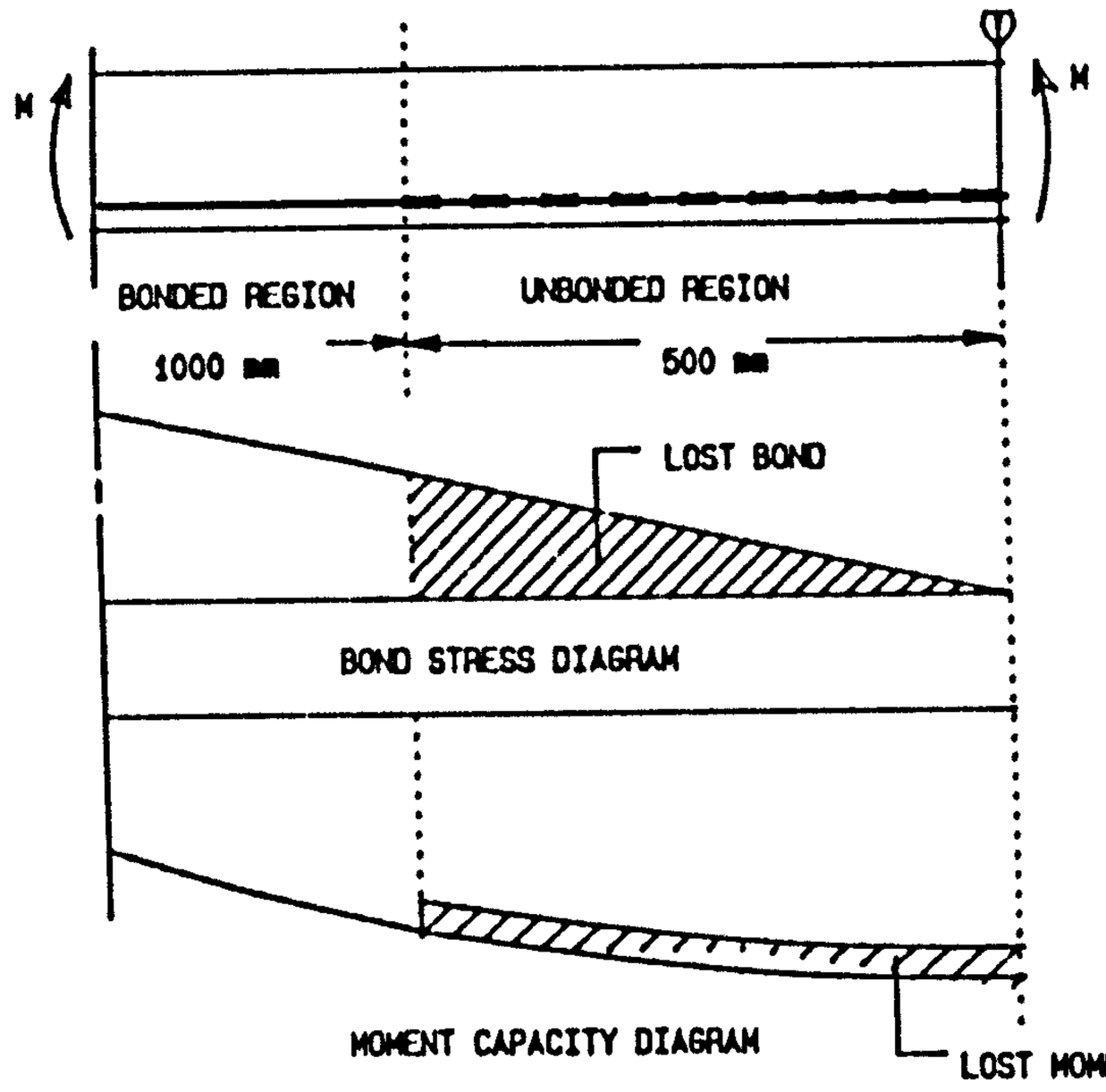

FIG.B-8.BOND STRESS AND MOMENT CAPACITY

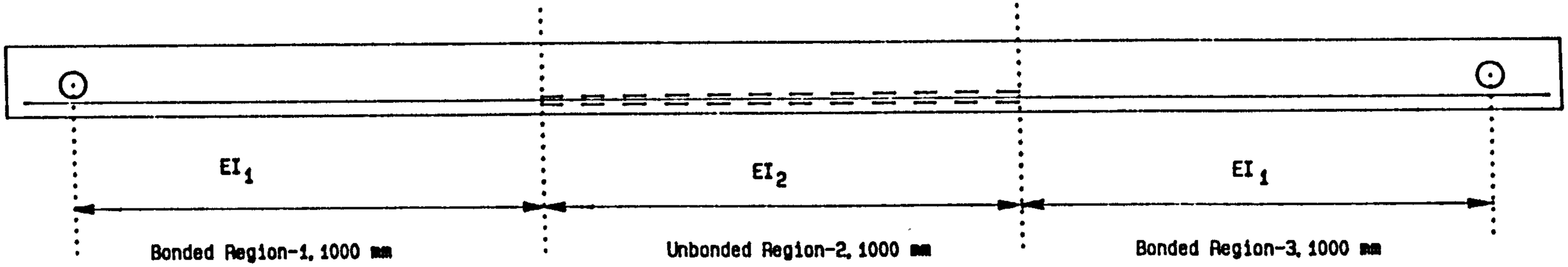

FIG.B-9.TYPICAL SET UP OF THE PARTIALLY BONDED BEAMS.

APPENDIX B-4 : STANDARD RESPONSE OF B&K ACCELEROMETERS AND SCHENCK VELOCITY PROBE T-77.

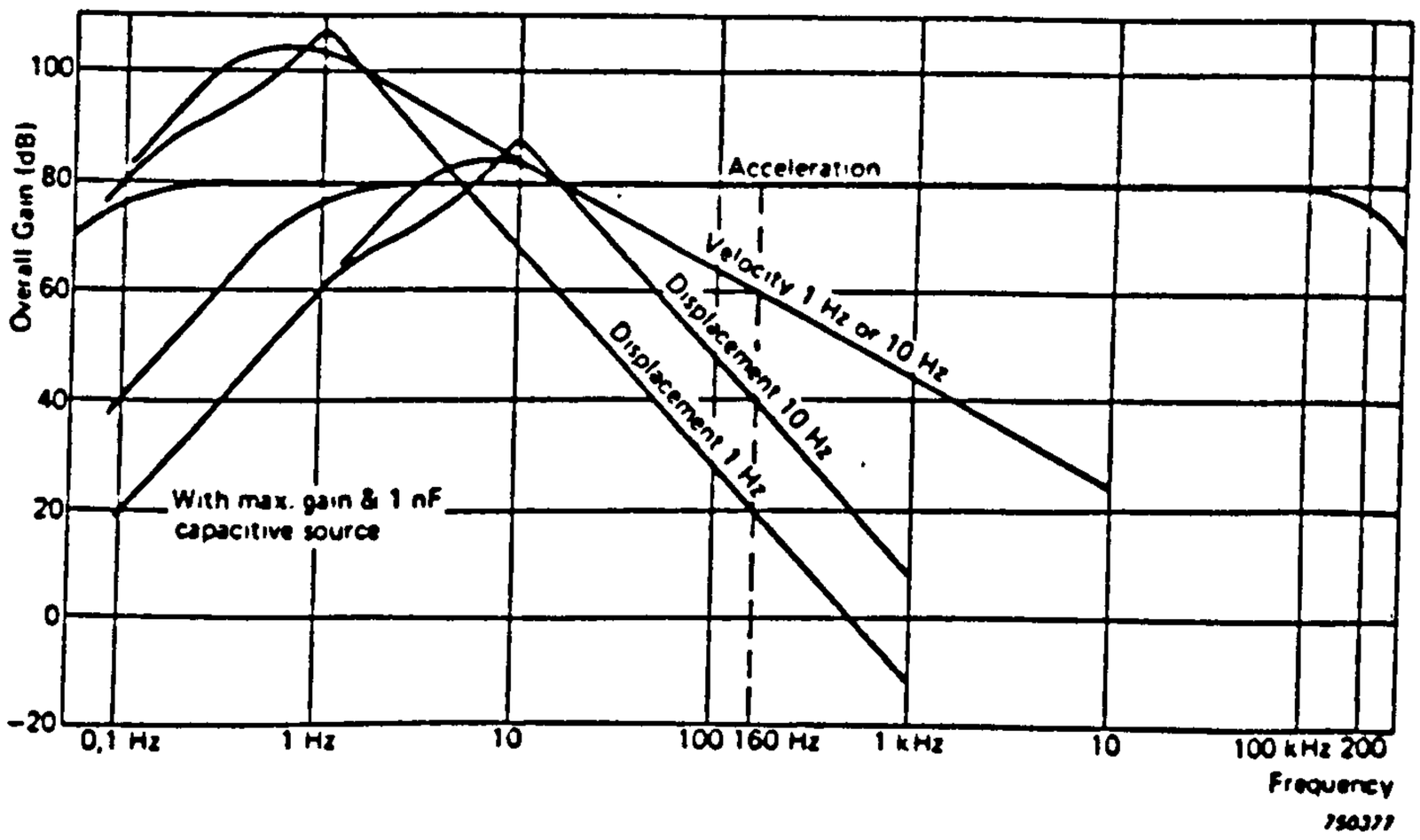

A) .CHARACTERISTICS OF ACCELEROMETER (CITED FROM B&K MANUALS)

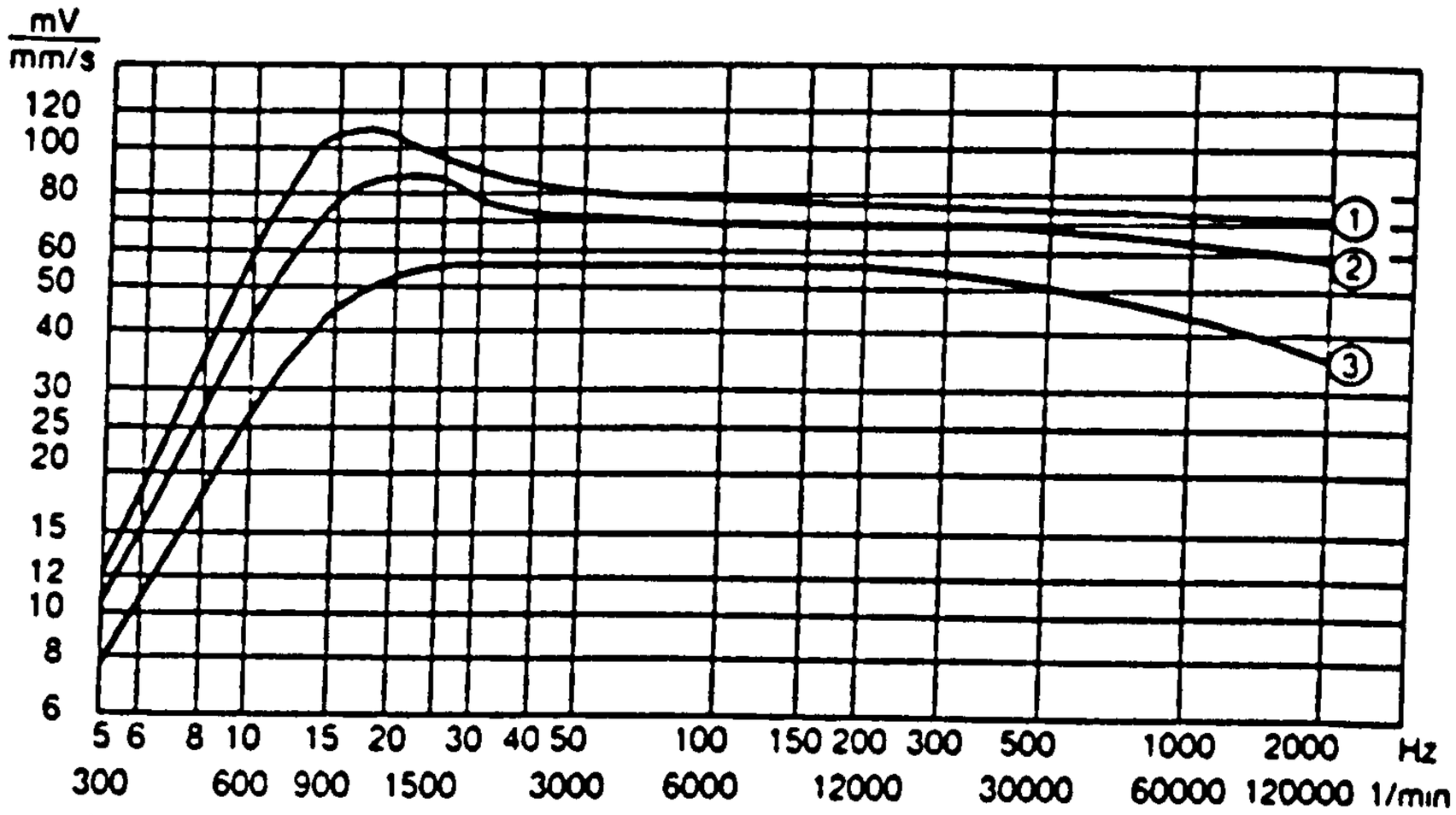

Curve	R_L	Sensitivity
①	≥ 1MOhm	75 mV/mm/s
②	27 kOhm	68 mV/mm/s
③	6.8 kOhm	53 mV/mm/s

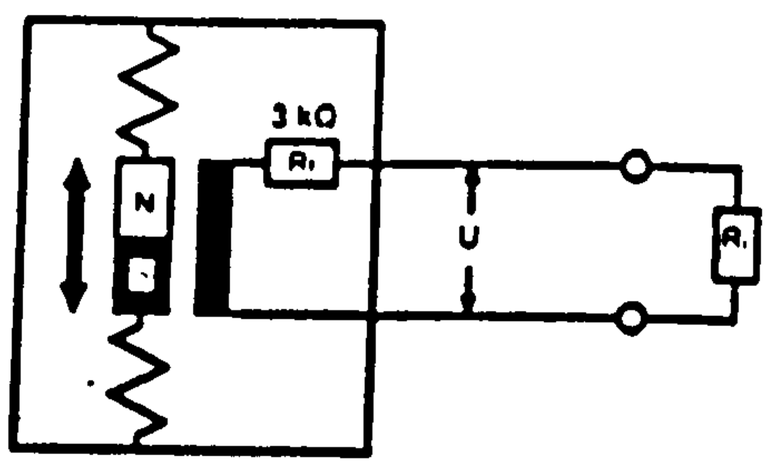

B) .CHARACTERISTICS OF VELOCITY PROBE TYPE T-77 (CITED FROM VIBROSCHENCK MANUAL)

APPENDIX C-1 : Radix Mixed FFT and Filter Programming.

```
C     ROUTINES INSTALLED IN THE VAX. MAIN FRAME: C06FPF.C06GSF. C06FKF
C     ROUTINES AVAILABLE IN THE PROGRAM : MATCHING.LOWHIGH.PASSTOP.
C     COEFF.WIND.RELIEVE

      CHARACTER*20      NAME.DNAME.FIL*1.IWIND*1.YES*1.YEZ*1.
     %                  LH*1.HI*1
      PARAMETER        (YES='Y'.YEZ='y'.LH='L'.HI='1'.
     %                  NMAX=10000)
      INTEGER           N.NC.ICH.ITYPE.NCYC.SEL
      REAL*8            PI.AVER.TOT.RTIM.TI.TT.DFR.Y(NMAX).DEVICE.
     %                  X(NMAX).GAIN(10).AVDOUT.FRANGE.VOLT.CHAN
      COMMON/MATCHING/NAME.DEVICE.IWIND

      WRITE (5.1)
      READ  (5.8) DNAME
      WRITE (5.2)
      READ  *. ICH
      WRITE (5.3) ICH
      READ  *. CHAN
      WRITE (5 4)
      READ  *. VOLT
      WRITE (5 5)
      READ  *. AVDOUTP
      WRITE (5.6)
      READ (*.9) IWIND

      OPEN (50.FILE='ORIGINAL DAT'.STATUS='NEW')
      OPEN (51.FILE='SPECTRUM.DAT'.STATUS='NEW')
      OPEN (52 FILE='FILTERED.DAT'.STATUS='NEW')
      OPEN (53.FILE='STEADYST.DAT'.STATUS='NEW')
      OPEN (80 FILE=DNAME STATUS='OLD')
      READ (80.8) NAME
      READ (80 *) N.TI
      READ (80.*) (GAIN(ICH).J=1.ICH)

      DEVICE = GAIN(ICH)*CHAN*AVDOUTP/(VOLT*2048)
      TI     = TI/1000.
      FRANGE = 1.0/TI
      TT     = TI*N
      DFR    = 1.0/TT
      PI     = 4.0*ATAN(1.0)

C     READING DATA FROM FILE AND AVERAGING

      TOT    = 0.0
      DO 10 I=1.N
      READ (80.*) (Y(I).J=1.ICH)
      TOT    = TOT+Y(I)
10    CONTINUE
      AVER   = TOT/N

      DO 50 I=1.N
      Y(I)   = Y(I)-AVER
      WRITE (50.*) RTIM.(Y(I)*DEVICE)
      RTIM   = RTIM+TI
50    CONTINUE

      ITYPE  = 1
      IF ((IWIND.EQ.YES OR.IWIND.EQ.YEZ) CALL WIND (Y.N.TI.ITYPE)

      KSTEP  = 1
      CALL MATCHING (N.TI.Y.ITYPE NCYC.KSTEP)

      WRITE (5.7)
      READ (*.9) FIL
      IF (FIL.EQ.YES.OR.FIL.EQ.YEZ) THEN
      PRINT *.'LOW/HIGHPASS(1) OR BANDPASS/STOP(2)  :'
      READ  *. SEL
      IF (SEL.EQ 1) THEN
      CALL LOWHIGH (FRANGE.PI.N.Y.TI)
      ELSE
      CALL PASSTOP (FRANGE.PI.N.Y.TI)
      END IF
      END IF

      KSTEP  = 2
      CALL MATCHING (N.TI.Y.ITYPE.NCYC KSTEP)

1     FORMAT (1X.'DATA FILENAME                              ')
2     FORMAT (1X 'CHANNEL BEING ANALYSED                     .')
3     FORMAT (1X 'ATTENUATION OF RACAL RECORDER AT CHL-:'.I2)
4     FORMAT (1X.'OUTPUT-CHARGE AMPLIFIER (V/UNIT O P)  :')
5     FORMAT (1X.'OUTPUT- (Msec-2). (Msec-1) OR (M)     :')
6     FORMAT (1X.'APPLY WINDOW (Y/N)                    :')
7     FORMAT (/.1X.'WISH TO FILTER DATA (Y/N)             :')
8     FORMAT (A20)
9     FORMAT (A1 )

      STOP
      END

C -------------------------------------------------------------

      SUBROUTINE MATCHING (ND.TI.Y.ITYPE NCYC KSTEP)

      CHARACTER*1 YES YEZ NAME*20.IWIND.FIL
      INTEGER I.IFAIL.M.N.ND.ITYPE.NCYC
      PARAMETER (MMAX=1 NMAX=10000) YES='Y' YEZ='y')
      REAL*8 PI.TI.TT.AMPL AMPH.FREQL FREQH PRI.HAS AMP ACORR
     % AMPMAX PERCEN.PREDF SW AMPLI DELPER.CONST1 PREDF1 AMPEAK
     % DEVICE.A(0.MMAX*NMAX).DFRE.FREQ TOT ANGPI.FACT.ANGMAX
      DOUBLE PRECISION U(NMAX*MMAX) V(NMAX*MMAX).WORK(2*MMAX*NMAX)
     % X(NMAX*MMAX).Y(NMAX*MMAX).TRIG(2*NMAX).ANCYC.FCORR
      COMPLEX*16 HZ(NMAX)
      COMMON/MATCHING/NAME DEVICE.IWIND
      COMMON/IYA/HZ

      IF (KSTEP.EQ.2) GOTO 22
```

```
      PRINT  *,'FREQ.RANGE INVESTIGATED (FR1 TO FR2) :'
      READ   *, FR1,FR2
      WRITE (5,1) ND,TI*1000
22    NCYC      = ND*TI*(FR1+FR2)/2
      PI        = 4.0*ATAN(1.0)
      TT        = ND*TI
      DFRE      = 1.0/TT

      DO 10 I=1,ND
      X(I) = Y(I)
10    CONTINUE

C     SUBSTITUTING NAG ROUTINE

      M    = 1
      IFAIL= 0
      CALL C06FPF(M,ND,X,'Initial',TRIG,WORK,IFAIL)
      CALL C06GSF(M,ND,X,U,V,IFAIL)

C     SELECTING MAXIMUM AMPLITUDE

      AMPMAX = 0.0
      FACT   = 1.0/SQRT(REAL(ND))
      DO 33 I=1,ND/2+1
      FREQ   = (I-1)*DFRE
      A(I)   = 2.0*FACT*SQRT(U(I)**2+V(I)**2)
      IF (AMPMAX.LT.A(I).AND.FREQ.GE.FR1.AND.FREQ.LE.FR2) THEN
      AMPMAX = A(I)
      END IF
33    CONTINUE
      IF (KSTEP.EQ.1) WRITE (5,2)

C     CALCULATING FREQUENCY AT MAXIMUM AMPLITUDE

      AML  = 0.0
      AMH  = 0.0
      AMI  = 0.0
      DO 121 I=1,ND/2+1
      IM   = I-1
      FREQ = IM*DFRE
      PERC = (AMPMAX-A(I))/AMPMAX
      IF (PERC.LE.0.001.AND.FREQ.GT.FR1.AND.FREQ.LT.FR2) THEN
      FREQL = 1.0*(IM-1)*DFRE
      FREQH = 1.0*(IM+1)*DFRE
      AMPL  = A(I-1)
      ANGMAX= -1.0*DATAN(V(I)/U(I))
      AMPEAK= A(I)
      AMPH  = A(I+1)
      DELPER= (ABS(AMPH-AMPL))*100.0/AMPEAK
        IF (DELPER.LT.0.01) THEN
        CONST = AMPH/(AMPL+AMPH+0.0000000001)
        PREDF = FREQL+ABS((FREQH-FREQL)*CONST)
        PREDF1= FREQ
        CONST1= 0.5
        GOTO 88
        ELSE
        CONST = AMPH/(AMPL+AMPH)
        PREDF = FREQL+ABS((FREQH-FREQL)*CONST)

C       AMPH>AMPL - UNDERESTIMATED (in most cases)

        IF (AMPH.GE.AMPL) THEN
        CONST1 = (AMPH/4.0+AMPEAK/2.0-3.0*AMPL/4.0)/
     %  (AMPEAK-AMPL)
        PREDF1 = FREQL+ABS((FREQH-FREQL)*CONST1)
        ELSE

C       AMPH<AMPL - OVERESTIMATED (in most cases)

        CONST1 = (2.0*AMPEAK-AMPH-AMPL)/(4.0*(AMPEAK-AMPH))
        PREDF1 = FREQL+ABS((FREQH-FREQL)*CONST1)
        END IF
      END IF

88    SW     = TT*A(I)/(4.0*PI)
      AMPLI  = AMPEAK*DEVICE

C     HANNING WINDOW CORRECTION

      IF (IWIND.EQ.YES.OR.IWIND.EQ.YEZ.AND.ITYPE.EQ.5) THEN
      ANCYC=ABS(CONST1-0.5)
      ACORR=1.0+6.827658E-03*ANCYC+8.595759E-01*ANCYC**2
     %      +7.854050*ANCYC**3
      XAMP =2.0*ACORR*AMPLI
      XFREQ=PREDF1
      ELSE

C     PEAK AND FREQUENCY ERRORS RELIEVE

        IF (ITYPE.EQ.1) THEN
        CALL RELIEVE (CONST1,FCORR,ACORR,NCYC)
        XFREQ=PREDF1*FCORR
        XAMP =ACORR*AMPLI
        END IF
      END IF
      IF (KSTEP.EQ.1) WRITE (5,3) ND,PREDF,PREDF1,XFREQ,XAMP
      HAS  = PREDF
      PRI  = XFREQ
      AMP  = XAMP
      END IF
121   CONTINUE

C     BACKUP FILE TO SPECTRUM.DAT

      WRITE (51,4) NAME
      WRITE (51,*) ND/2,'     1'
      DO 105 I=1,ND/2+1
      FREQ = (I-1)*DFRE
      A(I) = 2.0*DEVICE*FACT*SQRT(U(I)**2+V(I)**2)
        IF (U(I).EQ.0.00000000) THEN
```

```
            ANGPI= PI/2.0
            ELSE
            ANGPI= -1.0*DATAN(V(I)/U(I))
            END IF
          SW    = TT*A(I)/(4.0*PI)
          IF (I.LE.ND/2) THEN
          WRITE (51,3) I,FREQ,A(I),ANGPI
          END IF
105       CONTINUE
          WRITE (51,*) HAS,PRI,AMP

1      FORMAT(1X,'NO.OF DATA-TIME INCR.(MSECS)          :',I4,F10.6,/)
2      FORMAT(1X,'    ND      FR(HAS)      FR(AUT1)   '.
     %'   FR(AUT2)      MAX.AMP ',/,
     %'-----------------------------------------------'.
     %'--------------------------------')
3      FORMAT(1X,I6,3X,4(F12.7,1X))
4      FORMAT(A15)

       RETURN
       END

C ---------------------------------------------------------------------

       SUBROUTINE LOWHIGH (FRANGE,PI,N,XA,TI)

       PARAMETER        (MMAX=1,NMAX=10000)
       CHARACTER*2 SEL,ZF,COR
       COMPLEX*16  ZZ,Z,S,DE,FE,FH(NMAX),CC,TSCALE,
     %             A(100),B(100),C(100),D(100)
       REAL*8      PI,FR,AL,OS,AS,AC,AAL,DD,EE,TI,FRANGE,TIME,FC,FS
       DOUBLE PRECISION XA(NMAX),YA(NMAX),WORK(NMAX),Y(NMAX),X(NMAX)
       COMMON/ACC/FS,FC

       DFR    = 1.0/(N*TI)
5      WRITE (5,6),FRANGE/2,DFR
       PRINT *,'LOWPASS(L) OR HIGHPASS FILTER(H)      :'
       READ (*,1) SEL
       PRINT *,'PASSBAND (HZ) STOP BAND (HZ)          :'
       READ  *, FC,FS
       PRINT *,'MINIMUM ATTENUATION IN STOPBAND (dB) :'
       READ  *, DD
       PRINT *,'SINGLE (1) OR DOUBLE PASS (2)         :'
       READ  *, KK
       PRINT *,'ANY INPUT CORRECTION  (Y/N)           :'
       READ (*,1) COR

       IF (COR.EQ.'Y'.OR.COR.EQ.'y') GOTO 5
       CUT= (FC+FS)/2.0
       AC = 2.0*PI*FC/FRANGE
       AS = 2.0*PI*FS/FRANGE

       CC = 1.0/DTAN(AC/2.)
       OS = ABS(DTAN(AS/2.0)/DTAN(AC/2.0))
       IF (SEL.EQ.'H'.OR.SEL.EQ.'h') THEN
       CC = 1.0/CC
       OS = 1.0/OS
       END IF
       AN = 0.5*LOG10(10.0**(DD/10.0))
     %      /LOG10(OS)
       NO = AN+1.0
       WRITE (5,3),NO

C      TRANSFER FUNCTION

       DO 66 J=1,NO
       AAL    = (0.5+1.0/(2.0*NO)+1.0*(J-1)/NO)*PI
       FE     = DCMPLX( DCOS(AAL),DSIN(AAL) )
       A(J)   = DCMPLX(1.0,0.0)
       B(J)   = DCMPLX(1.0,0.0)
       C(J)   = CC-FE
       D(J)   = -(CC+FE)
       IF (SEL.EQ.'H'.OR.SEL.EQ.'h') THEN
       B(J)   = -B(J)
       D(J)   = -D(J)
       END IF
  66   CONTINUE

C      CREATING IMPULSE AND TRANSFER FUNCTION RESPONSES

       TSCALE = 1.0
       CALL COEFF (A,B,C,D,NO,TI,FRANGE,N,Y,NC,TSCALE)

       DO 33 I=1,N
       YA(I) = Y(I)
       IF (I.GT.NC) YA(I)=0.0
  33   CONTINUE

C      CONVOLUTION PROCESS

       IFAIL = 0
       CALL C06FKF (1,YA,YA,N,WORK,IFAIL)

C      SUBTRACTING TRANSIENT SIGNAL

       IF (KK.EQ.1) THEN
       NEW   = N-NC
       NL    = 0
       ELSE
       NEW   = N-2*NC
       NL    = NC
       END IF

       TOT   = 0.0
       DO 179 I=1,N
       TIME = (I-1)*TI
       IF (I.GE.NC.AND.I.LE.(N-NL)) THEN
       TOT   = TOT+XA(I)
       END IF
       WRITE (52,*) TIME,YA(I)
```

```
179   CONTINUE
      AVER = TOT/N

      N    = NEW
      TIME = 0.0
      DO 180 I=1,N
      TIME = (I-1)*TI
      XA(I)= XA(I+NC)-AVER
      WRITE (53,*) TIME,XA(I)
180   CONTINUE

   1  FORMAT (A1 )
   2  FORMAT (5(F10.5,2X))
   3  FORMAT (1X,'FILTER ORDER                                  :',I4)
   6  FORMAT (1X,'FREQUENCY RANGE-BAND AND RESOLUTION  :',2(F10.5,2X))

      RETURN
      END

C -----------------------------------------------------------------

      SUBROUTINE PASSTOP (FRANGE,PI,N,XA,TI)

      CHARACTER*2 SEL,COR,YES*1,YEZ*1,ST*1,SP*1
      PARAMETER  (NMAX=10000,YES='Y',YEZ='y',ST='S',SP='s')
      COMPLEX*16  ZZ,Z,S,DE,FE,FA3,DEN,TSCALE,TEM,SCALE,
     %            A(100),B(100),C(100),D(100),ROOT,ALF,BET
      REAL*8      AN,OS1,OS2,CC,AS1,AS2,AC1,AC2,PI,AL,
     %            FRANGE,FC2,FS2,FC1,TI,
     %            FA1,FA2,OS,AS,AC,AAL,FR,FS1
      DOUBLE PRECISION WORK(NMAX),XA(NMAX),YA(NMAX)
      COMMON/STJ/FS1,FS2,FC1,FC2

      DFR   = 1.0/(N*TI)
5     WRITE (5,3),FRANGE/2,DFR
      PRINT *,'BANDPASS(P) OR BANDSTOP(S)            :'
      READ (*,1) SEL
      PRINT *,'STOP BAND (HZ) (1) AND (2)            :'
      READ  *, FS1,FS2
      PRINT *,'PASSBAND (HZ)  (1) AND (2)            :'
      READ  *, FC1,FC2
      PRINT *,'MINIMUM ATTENUATION IN STOPBAND (dB) :'
      READ  *, D2
      PRINT *,'SINGLE (1) OR DOUBLE (2) PASS FILTER :'
      READ  *, KK
      PRINT *,'ANY INPUT CORRECTION  (Y/N)           :'
      READ (*,1) COR

      IF (COR.EQ.YES.OR.COR.EQ.YEZ) GOTO 5
      AC1= 2.0*PI*FC1/FRANGE
      AS1 = 2.0*PI*FS1/FRANGE
      AC2 = 2.0*PI*FC2/FRANGE
      AS2 = 2.0*PI*FS2/FRANGE
      ALF = 1.0/DTAN(0.5*(AC2-AC1))
      BET = (DSIN(AC1+AC2))/(DSIN(AC1)+DSIN(AC2))
      FA1 = (BET-DCOS(AS1))/DSIN(AS1)
      OS1 = -ALF*FA1
      FA2 = (BET-DCOS(AS2))/DSIN(AS2)
      OS2 = ALF*FA2
      IF (SEL.EQ.SP.OR.SEL.EQ.ST) THEN
      ALF = (DCOS(AC1)-DCOS(AC2))/(DSIN(AC1)+DSIN(AC2))
      OS1 = -ALF*1.0/FA1
      OS2 = ALF*1.0/FA2
      END IF
      IF (OS1.LT.OS2) OS=ABS(OS1)
      IF (OS2.LT.OS1) OS=ABS(OS2)
      AN  = 0.5*LOG10(10.0**(D2/10.0))/LOG10(OS)
      NO  = AN+1
      WRITE (5,4),NO

C     TRANSFER FUNCTION

      TSCALE = 1.0
      L      = 0
      DO 66 J=1,NO
      AAL    = (0.5+1.0/(2.0*NO)+1.0*(J-1)/NO)*PI
      FE     = DCMPLX( DCOS(AAL),DSIN(AAL) )
      SCALE  = ALF-FE
      DO 77 K=1,2
      L      = L+1

C     BANDSTOP FILTER

      IF (SEL.EQ.ST.OR.SEL.EQ.SP) THEN
        A(L)   = 1.0
        B(L)   = (-BET-SQRT(BET**2-1.0))
        C(L)   = 1.0
        ROOT   = (BET**2-1.0)*FE**2+ALF**2
        D(L)   = (FE*BET-SQRT(ROOT))/SCALE
          IF (K.EQ.2) THEN
          B(L)   = (-BET+SQRT(BET**2-1.0))
          D(L)   = (FE*BET+SQRT(ROOT))/SCALE
          END IF
      ELSE

C     BANDPASS FILTER

        A(L)   = 1.0
        B(L)   = 1.0
        C(L)   = 1.0
        ROOT   = (BET**2-1.0)*ALF**2+FE**2
        D(L)   = -(ALF*BET+SQRT(ROOT))/SCALE
          IF (K.EQ.2) THEN
          B(L)   = -B(L)
          D(L)   = -(ALF*BET-SQRT(ROOT))/SCALE
          END IF
      END IF

77    CONTINUE
```

```
      TEM     = TSCALE*SCALE
      TSCALE = TEM
66    CONTINUE
      NO      = 2*NO

      CALL COEFF (A,B,C,D,NO,TI,FRANGE,N,YA,NC,TSCALE)

C     CONVOLUTION PROCCESS

      DO 33 I=1,N
      YA(I) = YA(I)
      IF (I.GT.NC) YA(I)=0.0
33    CONTINUE

      IFAIL = 0
      CALL C06FKF (1,XA,YA,N,WORK,IFAIL)

C     SUBTRACTING TRANSIENT SIGNAL.

      IF (KK.EQ.1) THEN
      NEW   = N-NC
      NL    = 0
      ELSE
      NEW   = N-2*NC
      NL    = NC
      END IF

      TOT   = 0.0
      DO 179 I=1,N
      TIME = (I-1)*TI
      IF (I.GE.NC.AND.I.LE.(N-NL)) THEN
      TOT   = TOT+XA(I)
      END IF
      WRITE (52,*) TIME,XA(I)
179   CONTINUE
      AVER = TOT/N

      N     = NEW
      TIME = 0.0
      DO 180 I=1,N
      TIME = (I-1)*TI
      XA(I)= XA(I+NC)-AVER
      WRITE (53,*) TIME,XA(I)
180   CONTINUE

   1  FORMAT (A1)
   3  FORMAT (1X,'FREQUENCY RANGE-BAND AND RESOLUTION  :',2(F10.5,2X))
   4  FORMAT (1X,'FILTER ORDER                         :',I4)

      RETURN
      END

C -----------------------------------------------------------------------

C     DETERMINING COEFFICIENTS OF POLYNOMIAL FUNCTIONS
```



```
      SUBROUTINE COEFF (A,B,C,D,NO,TI,FRANGE,N,YA,J,TSCALE)

      CHARACTER*1 REP,IWIND,YES,YEZ,RE,RC
      PARAMETER   (YEZ='Y',YES='y',RE='R',RC='r')
      COMPLEX*16  F(-1:5000),Z,CC,CA(100),CB(100),TSCALE,
     %            A(100),B(100),C(100),D(100),X(100,100),HZ,
     %            XX(0:100),AA(0:100),BB(0:100),V(0:100,0:100)
      REAL*8      AL,FR,PI,AC,AS,AAL,FRANGE,YA(5000),TI,TOTCO,
     %            E(10),W(1000),DB(1000),FS,FC,FS1,FS2,FC1,FC2
      COMMON/ACC/FS,FC
      COMMON/STJ/FS1,FS2,FC1,FC2
      COMMON/IYA/HZ

      OPEN (30,FILE='IMPULSE.DAT',STATUS='NEW')
      OPEN (31,FILE='DBGAIN.DAT',STATUS='NEW')

5     PRINT *,'NO. OF FILTER COEFFICIENT (>50 ?)     :'
      READ  *, J
      PRINT *,'RECTANGULAR (R) OR HAMMING WINDOW (H):'
      READ (*,2) WIND

      DFR = 1.0/(N*TI)
      PI  = 4.0*ATAN(1.0)
      DO 10 I=1,2

      DO 15 L=1,NO
      IF (I.EQ.1) THEN
      CA(L) = A(L)
      CB(L) = B(L)
      ELSE
      CA(L) = C(L)
      CB(L) = D(L)
      END IF
15    CONTINUE

      X(1,1) = CA(1)
      X(1,2) = CB(1)

      DO 20 K=2,NO
      M         = 1
      X(K,1)    = X(K-1,1)*CA(K)
      X(K,K+1) = X(K-1,K)*CB(K)
      DO 30 M=2,K
      X(K,M)    = CA(K)*X(K-1,M)+CB(K)*X(K-1,M-1)
30    CONTINUE
20    CONTINUE

C     COEFICIENTS OF THE NUMERATOR AND DENOMINATOR

      DO 50 L=0,NO
      IF (I.EQ.2) THEN
      AA(L) = TSCALE*X(NO,L+1)
      GOTO 50
      END IF
```

```
      BB(L) = X(NO,L+1)
50    CONTINUE
10    CONTINUE

C     DECOMPOSITION OF THE RATIONAL FUNCTION BY LONG DIVISION METHOD

      DO 31 I=0,NO
      XX(I)   = AA(I)/AA(0)
31    CONTINUE

C     CREATING FACTORS

      DO 36 I=0,NO
      V(0,I)=BB(I)
36    CONTINUE
      DO 51 K=1,J
      DO 41 I=0,NO-1
      V(K,NO)   = 0.0
      V(K,I)    = XX(0)*V(K-1,I+1)-XX(I+1)*V(K-1,0)
41    CONTINUE
51    CONTINUE

C     FILTER COEFFICIENTS IN TIME DOMAIN

      TOTCO  = 0.0
      YMAX   = 0.0
      DO 100 K=0,J
      V(K,0) = V(K,0)/AA(0)
      YA(K+1)= REAL(V(K,0))
      TOTCO  = TOTCO + YA(K+1)
      IF ( YMAX.LT.ABS(YA(K+1)) ) THEN
      YMAX=YA(K+1)
      MMAX=K
      END IF
100   CONTINUE

      IF (WIND.EQ.RE.OR.WIND.EQ.RC.OR.WIND.EQ.' ') GOTO 777

C     SHIFTED HAMMING WINDOW

      ITEST = (J-MMAX)*2
      IF (ITEST.EQ.0) GOTO 5
      M     = -MMAX
      PRINT *,' '
      PRINT *,'HAMMING AND FILTER COEFFICIENTS :'
      PRINT *,'---------------------------------'
      DO 300 K=0,J
      W(K)  = 0.54+0.46*DCOS(2*PI*REAL(M)/REAL((ITEST-1)))
      M     = M+1
      WRITE (5,1) K+1,W(K),YA(K+1)
300   CONTINUE

C     WINDOWING IMPULSE

      DO 200. K=0,J
      V(K,0)  = W(K)*V(K,0)
      YA(K+1) = W(K)*YA(K+1)
200   CONTINUE

777   IF (FS.GT.0.OR.FC.GT.0) THEN
      KK  = 2
      E(1)= FS
      E(2)= FC
      ELSE
      KK  = 4
      E(1)= FS1
      E(2)= FC1
      E(3)= FS2
      E(4)= FC2
      END IF

      DO 91 L=1,KK
      FR  = E(L)
      AL  = 2.0*PI*FR/FRANGE
      Z   = DCMPLX (DCOS(AL),DSIN(AL))
      Z   = 1.0/Z
      F(-1) = 0.0
      DO 92 K=0,J-1
      F(K)  = V(K,0)*Z**(K-J+1)
      F(K)  = F(K)+F(K-1)
      HZ    = F(K)
92    CONTINUE
      DB(L)=20.*LOG10(ABS(HZ))
91    CONTINUE

      WRITE (5,4) TOTCO
      WRITE (5,3) DB(1),DB(2)
      IF (DB(3).NE.0.0) WRITE (5,6) DB(3) DB(4)
      PRINT *,'REPEATATION REQUIRED (Y/N)  . . . . . .'
      READ (*,2), REP
      IF (REP.EQ.YES.OR.REP.EQ YEZ) GOTO 5

      DO 110 L=1,J+1
      WRITE (30,*)L,,YA(L)
110   CONTINUE

C     FILTER COEFFICIENTS IN FREQUENCY DOMAIN

      DO 71 L=1,N/2
      FR = (L-1)*DFR
      AL = 2.0*PI*FR/FRANGE
      Z  = DCMPLX (DCOS(AL),DSIN(AL))
      Z  = 1.0/Z
      F(-1) = 0.0
      DO 61 K=0,J-1
      F(K)  = V(K,0)*Z**(K-J+1)
      F(K)  = F(K)+F(K-1)
      HZ    = F(K)
61    CONTINUE
      WRITE (31,1)L,,AL,,FR,ABS(HZ),20 *LOG10(ABS(HZ))
```

```
71    CONTINUE

1     FORMAT (1X,I4,2X,4(F15.10,2X))
2     FORMAT (A1)
3     FORMAT (1X,'DBGAIN AT STOPBAND - PASSBAND (1ST)  :',2X,2(F6.2,2X))
6     FORMAT (1X,'           STOPBAND - PASSBAND (2ND)  :',2X,2(F6.2,2X))
4     FORMAT (1X,'TOTTAL COEFFICICENTS ARE   --------  :',2X,F10.7)

      RETURN
      END

C -----------------------------------------------------------------------

C     RESCALING DATA BY MEANS OF WINDOWING

      SUBROUTINE WIND (B,NTD,TI,ITYPE)

      CHARACTER*20 NAMA
      INTEGER ITYPE
      REAL*8 TA,TI,PI,TT,B(10000)
      COMMON/MATCHING/NAME,DEVICE,IWIND
      PRINT *,'-------------------------------------'
      PRINT *,'INPUT TYPE OF WINDOW WEIGHTING (1-9) :'
      PRINT *,'-------------------------------------'
      PRINT *,'(1) RECTANGULAR WINDOW'
      PRINT *,'(2) EXTENDED COSINE BELL WINDOW'
      PRINT *,'(3) HALF CYCLE SINE WINDOW'
      PRINT *,'(4) TRIANGLE WINDOW'
      PRINT *,'(5) HANNING WINDOW'
      PRINT *,'(6) MODIFIED HALF CYCLE SINE WINDOW'
      PRINT *,'(7) HAMMING WINDOW'
      PRINT *,'(8) COSINE WINDOW'
      PRINT *,'(9) PARZEN WINDOW'
      PRINT *,'-------------------------------------'
      READ  *,ITYPE

      TT = TI*NTD
      PI = 4.0*ATAN(1.0)

      GOTO(100,200,300,400,500,600,700,800,900),ITYPE

C     HALF CYCLE SINE

300   DO 92 I=1,NTD
      TA=(I-1)*TI
      A=B(I)*SIN(PI*TA/TT)
      WRITE (82,1)TA,A
      B(I)=A
92    CONTINUE
      RETURN

C     TRIANGLE WINDOW

400   DO 125 I=1,NTD
      TA=(I-1)*TI
      IF (TA.LE.(TT/2)) THEN
      A=2*TA*B(I)/TT
      ELSE
      A=2*(TT-TA)*B(I)/TT
      END IF
      WRITE (82,1)TA,A
      B(I)=A
125   CONTINUE
      RETURN

C     HANNING WINDOW

500   DO 25 I=1,NTD
      TA=(I-1)*TI
      A=B(I)*(1-COS(2*PI*TA/TT))/2
      WRITE (82,1)TA,A
      B(I)=A
25    CONTINUE
      RETURN

C     EXTENDED COSINE BELL WINDOW

200   DO 22 I=1,NTD
      TA=(I-1)*TI
      IF (TA.LT.(TT/10).OR.TA.GT.(9*TT/10)) THEN
      A=B(I)*(1-COS(10*TA*PI/TT))/2
      ELSE
      A=B(I)
      END IF
      WRITE (82,1)TA,A
      B(I)=A
22    CONTINUE
      RETURN

C     COSINE WINDOW

800   DO 225 I=1,NTD
      TA=(I-1)*TI
      A=B(I)*((1-COS(2*PI*TA/TT))/2)**2
      WRITE (82,1)TA,A
      B(I)=A
225   CONTINUE
      RETURN

C     HAMMING WINDOW

700   DO 23 I=1,NTD
      TA=(I-1)*TI
      A=B(I)*(0.08+0.46*(1-COS(2*PI*TA/TT)))
      WRITE (82,1)TA,A
      PRINT *,I,TA,A/B(I)
      B(I)=A
23    CONTINUE
      RETURN
```

```
C      MODIFIED HALF CYCLE SINE

600    DO 75 I=1,NTD
       TA=(I-1)*TI
       A=B(I)*(SIN(PI*TA/TT))**3
       WRITE (82,1)TA,A
       B(I)=A
75     CONTINUE
       RETURN

C      PARZEN WINDOW

900    DO 180 I=1,NTD
       TA=(I-1)*TI
       IF(TA.LT.(TT/4).OR.TA.GT.(3*TT/4)) THEN
       A=B(I)*2*(1-ABS(2*TA/TT-1))**3
       ELSE
       A=B(I)*(1-6*(2*TA/TT-1)**2+6*(ABS(2*TA/TT-1))**3)
       END IF
       WRITE (82,1)TA,A
       B(I)=A
180    CONTINUE
100    RETURN

1      FORMAT(1X,2(2X,F20.12))
2      FORMAT (A10)

       END

C ---------------------------------------------------------------

C      SUBROUTINE IMPROVES FREQUENCY AND AMPLITUDE QUALITIES

       SUBROUTINE RELIEVE (CONST1,FCORR,ACORR,NCYC)

       INTEGER NCYC
       REAL*8 YY(30),BN(30),FCORR,ACORR,CONTS1,ANCYC,AN(30),
      %       X(1000)

       PI    =4.0*ATAN(1.0)
       CONST=ABS(CONST1-0.5)
       ACORR=1.0+2.814587*CONST-4.159906*CONST**2
      %      +8.331769*CONST**3

          AN(1) =0.162321500
          AN(2) =0.024498700
          AN(3) =0.007501950
          AN(4) =0.003197875

          BN(1) =-0.98602600
          BN(2) =-1.01939392
          BN(3) =-0.94364950
          BN(4) =-1.02845979

C      NEWTON RAPHSON

       YY(0) = 0.00000
       X(0)  = 0.005
       I=0
       DO 10 J=1,1000
       FX  = -1.626303E-18-2.233745E-03*X(I)+3.849212E-01*X(I)**2+
      %       9.528344E-01*X(I)**3+5.728516E-01*X(I)**4-CONST
       FAX = -2.233745E-03+2.0*3.849212E-01*X(I)+
      %       3.0*9.528344E-01*X(I)**2+4.0*5.728516E-01*X(I)**3
       I=I+1
       X(I) = X(I-1)-FX/FAX
       IF (ABS(X(I)-X(I-1)).LT.0.000001.AND.X(I).GT.0.0) GOTO 20
10     CONTINUE
20     ANCYC = X(I)
       DO 888 IK=1,4
       YY(IK)=YY(IK-1)+AN(IK)*(REAL(NCYC)**BN(IK))*
      %  SIN(IK*2.0*PI*ANCYC)
888    CONTINUE
       IF (CONST1 LT 0.5) THEN
       FCORR=1.0-YY(IK-1)
       ELSE
       FCORR=1.0+YY(IK-1)
       END IF

       RETURN
       END
```

APPENDIX C-2 : Waterfall Type Graphic Programming.

```
C     ROUTINES ARE INSTALLED IN THE VAX-MAIN FRAME UNDER UNIRAS-
C     UNIRASPAK PAKAGE.

      CHARACTER*100 TIT(0:10),DNAME*20,GRAPHOUT*20,SCAF*1,YES*1,
     % YEZ*1,CHOICE*1,DNAMA(20)*20,DNAM*19,NUM*10,ALT*1,KOL*1,ATT(2)
      PARAMETER (YES='Y',YEZ='y',XPOS=20.,YPOS=40.,XSC=210.,
     % YSC=130.,MEM=10000)
      INTEGER NGRAP,NGRAPHS,NGROUP
      REAL X,Y,DELTAX,DELTAY,XMIN,XMAX,AMPLI,PREDF,PREDF1,DELTA,
     % ANGE1,RANGE2,XRANGE1,YRANGE1
      DIMENSION XP(1:MEM),YP(1:MEM),X(0:MEM,30),Y(0:MEM,30),XD(30),
     % XPEAK(30,30),YPEAK(30,30),PVALU(30,30),FVALU(30,30),YM(30),
     % YD(30),FVALUP(30,30),INPEAKR(30),XL(30),YL(30),IMAX(MEM),
     % VALUM(30),FMVAL(30),NP(30),FRANGE(30),FACT(30),XM(30),
     % FAC(30),IMIN(MEM),IAD(30),ZL(10)

      PRINT *,'NAME OF FILE .....:'
      READ (*,1) DNAME
      PRINT *,'NO.OF ROWS CONTAINING GRAPHS .....:'
      READ  *, NGRAPH
      PRINT *,'NO.OF GRAPHS IN EACH ROW .....:'
      READ  *, NGROUP
      NGRAPHS =NGRAPH*NGROUP
      PRINT *,'SCALING FACTOR X & Y-AXIS(0-1.0)..:'
      READ  *, XFACT,YFACT
      PRINT *,'OVERLAPPING PICTURES (Y/N).....:'
      READ (*,2) OVER
      PRINT *,'OMITTING LINE POSITIONS (Y/N).....'
      READ (*,2) ALT
      PRINT *,'SINGLE COLOUR FOR ALL GRAPHS (Y/N):'
      READ (*,2) KOL
      PRINT *,'WISH TO ADJUST X-Y AXIS(Y/N).....:'
      READ (*,2) SCAF
      RANGE1=  0.0
      IF (SCAF.EQ.YES.OR.SCAF.EQ.YEZ) THEN
      PRINT *,'MAX RANGE OF FREQ.BAND (HZ).....:'
      READ  *, RANGE2
      PRINT *,'MIN RANGE OF FREQ.BAND (HZ) .....:'
      READ  *, RANGE1
      PRINT *,'MAX.AMPL.PERFORMED(Micro Meter)...:'
      READ  *, SCAFY
      END IF

C     READING FACTOR POSITIONING A GROUP OF GRAPHS

      DO 77 I=1,NGRAPH
      WRITE (5,4) I
      READ *, FACT(I)
      FAC(I)=FACT(I)
77    CONTINUE
      DO 78 I=1,NGRAPH*(NGROUP-1)
      FACT(I+NGRAPH)=FACT(I)
      FAC(I+NGRAPH)=FAC(I)
78    CONTINUE

      PRINT *,'PRINT BORDER DATA VALUES ONLY(Y/N):'
      READ (*,2) CHOICE
      PRINT *,'ATTRIBUTES IN X AND Y-DIRECTION ..:'

      DO 99 I=1,2
      READ (*,1) ATT(I)
99    CONTINUE
      NUM = '12345678'
      DO 688 J=1,2
      DO 589 I=20,100
      IF (ATT(J)(I-19:I).EQ.'                    ') THEN
      ATT(J) = ATT(J)(:I-19)//'$'
      IF (J.EQ.2) GOTO 590
      GOTO 688
      END IF
589   CONTINUE
688   CONTINUE

590   PRINT *,'NUMBER OF LINES OF THE TITLE .. ..:'
      READ  *, NL

C     GENERATING AND COUNTING EXACT CHARACTERS OF TITLE

      DO 88 I=1,NL
      WRITE (5,5) I
      READ (*,1) TIT(I)
88    CONTINUE
      NUM = '12345678'
      DO 788 J=1,NL
      DO 789 I=20,100
      IF (TIT(J)(I-19:I).EQ.'                    ') THEN
      TIT(J) = TIT(J)(:I-19)//'$'
      IF (J.EQ.NL) GOTO 790
      GOTO 788
      END IF
789   CONTINUE
788   CONTINUE

790   OPEN(20,FILE=DNAME,STATUS='OLD',READONLY)

      YMIN=  0.0
      XMAX=  0.0
      YMAX=  0.0
      SCA =YSC/XSC

C     READING DATA AND SORTING MAX VALUES OVER ALL DATA

      IGR = 0
      KO  = 0
      DO 10 IG=1,NGRAPHS
      IGR = IGR+1
      READ(20,3) DNAM
```

```
      READ(20,*) NP(IG),INPEAK

c     selecting main code of file (take SA from SA:CH-1)

      IF (IGR.EQ.NGRAPH) THEN
      DO 689 I=1,100
      IF (DNAM(I:I).EQ.':') THEN
      KO = KO+1
      IAD(KO)=I-1
      IGR= 0
      DNAMA(KO)= DNAM(:I-1)//'$'
      GOTO 690
      END IF
689   CONTINUE
      END IF

c     reading frequencies and amplitudes

690      DO 11 I=1,NP(IG)
         READ(20,*) AA,X(I,IG),Y(I,IG)
         IF (X(1,IG).LT.XMIN) XMIN=X(1,IG)
         IF (X(I,IG).GE.XMAX) XMAX=X(I,IG)
         IF (Y(I,IG).GE.YMAX) YMAX=Y(I,IG)
         FRANGE(IG)=XMAX
 11      CONTINUE

c     reading maximum amplitudes with frequencies at the end of files

         L   =0
         VALUM(IG)=0.00000000
         FMVAL(IG)=0.00000000
         DO 12 K=1,INPEAK
         READ (20,*) PREDF,PREDF1,AMPLI
             IF (AMPLI.NE.0.0000) THEN
             L              =L+1
             FVALU(IG,L) =PREDF
             FVALUP(IG,L)=PREDF1
             PVALU(IG,L) =AMPLI
             IF (AMPLI.GT.VALUM(IG)) THEN
             VALUM(IG)=AMPLI
             FMVAL(IG)=PREDF
            END IF
            END IF
  12     CONTINUE
         INPEAKR(IG) =L
  10  CONTINUE

C     SORTING VALUES WITHIN THE RANGE OF FREQUENCY OVER ALL DATA

      IF (SCAF.EQ.YES.OR.SCAF.EQ.YEZ) THEN
      IF (XMIN.LT.RANGE1) XMIN=RANGE1
      IF (XMAX.GT.RANGE2) XMAX=RANGE2
      YMAX=SCAFY
      END IF
      DO 20 IG=1,NGRAPHS
```

```
      IMAX(IG) =0
      IMIN(IG) =1
         DO 17 I=1,NP(IG)
         IF (X(I,IG).GT.XMAX) GOTO 17
         IMAX(IG)=IMAX(IG)+1
         IF (X(I,IG).GT.XMIN) GOTO 17
         IMIN(IG)=IMIN(IG)+1
 17      CONTINUE
            IF (IMIN(IG).EQ.0) IMIN(IG)=1
            X(IMIN(IG)-1,IG)=X(IMIN(IG),IG)
            Y(IMIN(IG)-1,IG)=0.00000
            X(IMAX(IG)+1,IG)=X(IMAX(IG),IG)
            Y(IMAX(IG)+1,IG)=0.00000
  20  CONTINUE

C     JUSTIFYING AND MODIFYING DISTANCE BETWEEN GRAPHS

      DELTAX= XFACT*(XMAX-XMIN)/(2*NGROUP)
      DELTAY= YFACT*(YMAX-YMIN)/(0.5*NGROUP)

c     modifying distance to allow additional line at most right
      DELTA = 0.2*(XMAX-XMIN)
      XMAXX = DELTA+XMAX+(NGRAPH-1)*DELTAX
      YMAXX = YMAX+(NGRAPH-1)*DELTAY
      YMINN =-0.05*YMAXX
      XMINN = XMIN-0.1*DELTA

C     UNIRAS ROUTINE

      CALL GROUTE ('S MRCOXY F')
      CALL GSURFE
      CALL GOPEN
      CALL GLIMIT(XMINN,XMAXX,YMINN,YMAXX,0.,0.)
      CALL GWBOX(1.0,SCA,0.)
      CALL GVPORT(XPOS,YPOS,XSC,YSC)
      CALL GSCALE
      CALL GCLIP

C     OVERLAP ARRANGEMENT OF GRAPHS (ART EFFECTS)

      DO 34 J=1,NGRAPHS-1
      DO 33 I=NGRAPHS,2,-1
      IF (FAC(I).GT.FAC(I-1)) THEN
      RA=FAC(I-1)
      FAC(I-1)=FAC(I)
      FAC(I)=RA
      END IF
 33   CONTINUE
 34   CONTINUE

C     PLOTTING STARTS FROM THE VERY TOP GRAPH

      IG = 0
      IGR= 0
```

```
      IC = 0
      DO 35 J=1,NGRAPHS
      IF (IGR.EQ.NGROUP) THEN
      IGR=0
      IG =0
      IC =0
      END IF
      II = 1
      IC = IC+1
      IF (IC.EQ.5.OR.IC.EQ.9.OR.IC.EQ.13) IC=1
      IF (KOL.EQ.YES.OR.KOL..EQ.YEZ) IC=1
42    IG = IG+1
      IF (IG.GT.NGRAPHS) IG=IG-NGRAPHS
      IF(FAC(J).NE.FACT(IG)) GOTO 42
      IGR= IGR+1
         DO I=IMIN(IG),IMAX(IG)+2
         II    = II+1
         IF (X(I-1,IG).LT.XMIN) X(I-1,IG)=XMIN
         IF (X(I-1,IG).GT.XMAX) X(I-1,IG)=XMAX
         XP(II)=X(I-1,IG)+DELTAX*(NGRAPH-1)*FACT(IG)
         YP(II)=Y(I-1,IG)+DELTAY*(NGRAPH-1)*FACT(IG)
         END DO
         XP(1) =XMIN+DELTAX*(NGRAPH-1)*FACT(IG)
         XP(II+1)=XMAX+DELTAX*(NGRAPH-1)*FACT(IG)
         YP(1) =YP(2)
         YP(II+1)=YP(II)
         XL(IG)=XP(II+1)+0.8*DELTA
         YL(IG)=YP(II)
      NGP = IMAX(IG)-IMIN(IG)+5
      IF (J.EQ.NGRAPHS) THEN
      XP(II+2)=XP(1)
      XP(II+3)=XP(1)
      YP(II+2)=YP(1)
      YP(II+3)=YMAX+DELTAY*(NGRAPH-1)*FACT(IG)
      NGP = NGP+2
      END IF

C     canceling overlapping pictures

      IF (OVER.EQ.YES.OR.OVER.EQ.YEZ) THEN
      CALL GSURFR(IC)
      CALL RSURF(XP,YP,NGP,0.0,1)
      ELSE
      CALL GWICOL(0.1,IC)
      CALL GVECT(XP,YP,NGP)
      END IF
35    CONTINUE

C     GENERATING AND PLOTTING BEAM'S COORDINATES

      XMMIN = 1000000000.0
      XMMAX = 0.0
      YMMIN = XMMIN
      YMMAX = XMMAX
      DO 21 K=1,NGRAPHS
      IF (XL(K).LT.XMMIN) XMMIN=XL(K)
      IF (XL(K).GT.XMMAX) XMMAX=XL(K)
      IF (YL(K).LT.YMMIN) YMMIN=YL(K)
      IF (YL(K).GT.YMMAX) YMMAX=YL(K)
21    CONTINUE

      DO 22 K=1,NGRAPH
      XL(K) = XMMIN+(XMMAX-XMMIN)*FACT(K)
      YL(K) = YMMIN+(YMMAX-YMMIN)*FACT(K)
22    CONTINUE

      IF (ALT.EQ.YEZ.OR.ALT.EQ.YES) GOTO 444
      CALL RCIRCL(XMMIN,YMMIN,0.5,2,-5.0)
      CALL RCIRCL(XMMAX,YMMAX,0.5,2,-5.0)

C     PLOTTING BEAM'S LINE AND MAXIMUM RESPONSES

      DO 23 K=1,NGRAPHS
      IC = 1+(K-1)/NGRAPH
      DO 24 J=1,INPEAKR(K)
      ZL(K) = PVALU(K,J)+DELTAY*(NGRAPH-1)*FACT(K)
      IF (FVALUP(K,J).GE.XMIN.AND.FVALUP(K,J).LE.XMAX) THEN
      IF (KOL.EQ.YEZ.OR.KOL.EQ.YES) IC=1
      CALL GWICOL(0.1,IC)
      CALL GVECT (XL(K),YL(K),0)
      CALL GVECT (XL(K),ZL(K),1)
      END IF
24    CONTINUE
23    CONTINUE

      CALL GVECT (XMMIN,YMMIN,0)
      CALL GVECT (XMMAX,YMMAX,1)
444   CALL GNCLIP

C     PLOTTING FREQUENCY AND AMPLITUDE VALUES AND ATTRIBUTES

      YAX=YPOS-15.
      YAY=YPOS+0.5*YSC
      XAY=XPOS-10.
      CALL GSCAMM
      CALL GCHARF('COMP')
      DO 222 I=1,NL
      CALL GROUTE ('S MRCOXX;E')
      CALL GCHART(1)
      CALL GCHARD(1.1)
      CALL GCHARJ(3)
      CALL GCHAR(TIT(I),XPOS+2.,YPOS-20.-5.0*I,2.5)
222   CONTINUE
      CALL GCHART(0)
      CALL GCHARF('COMP')
      CALL GCHARJ(3)
      CALL GCHAR(ATT(1),XPOS+2.,YAX,2.0)

      IF (YFACT.EQ.0.0) THEN
      XYY = XPOS+(XSC/(XMAXX-XMINN))*(XMMIN-XMINN)
```

```
      ELSE
      XYY = XYA
      END IF
      CALL GCHARC(1)
      CALL GCHAR('CODE :$',XYY,YPOS+YSC,2.0)
      IC = 0
      DO 333 KO=1,NGROUP
      IC = IC +1
      IF (IC.EQ.5) IC=1
      IF (KOL.EQ.YES.OR.KOL.EQ.YEZ) IC=1
      XCODE= XYY+6.0+KO*6.0
      CALL GCHARC(IC)
      CALL GCHAR(DNAMA(KO),XCODE,YPOS+YSC,2.0)
      IF (KO.EQ.NGROUP) GOTO 333
      CALL GCHAR('/$',XCODE+2.0*IAD(KO),YPOS+YSC,2.0)
333   CONTINUE

c     omitting symbols if values not plotted

      IF (CHOICE.EQ.YES.OR.CHOICE.EQ.YEZ) GOTO 666
      CALL GCHARC(4)
      CALL GCHAR('-      :$',XYY,YPOS+YSC-5.0,2.0)
      CALL GCHARC(1)
      CALL GCHAR('FREQUENCY$',XYY+12.0,YPOS+YSC-5.0,2.0)
      CALL GCHARC(3)
      CALL GCHAR('-      :$',XYY,YPOS+YSC-10.,2.0)
      CALL GCHARC(1)
      CALL GCHAR('AMPLITUDE$',XYY+12.0,YPOS+YSC-10.,2.0)

666   CALL GCHARA(90)
      CALL GCHARC(1)
      CALL GCHARJ(4)
      CALL GCHAR(ATT(2),XAY,YAY,2.0)

      XAT =XPOS
      YAT =YPOS+YSC
      DO 30 IG=NGRAPHS,1,-1

      CALL GROUTE ('S MRCOXX;E')
      IF (CHOICE.EQ.YES.OR.CHOICE.EQ.YEZ) GOTO 44
         DO 45 K=1,INPEAKR(IG)
         XPEAK(IG,K)=XPOS+(XSC/(XMAXX-XMINN))*(FVALUP(IG,K)+
     &   FACT(IG)*DELTAX*(NGRAPH-1)-XMINN)
         YPEAK(IG,K)=YPOS+(YSC/YMAXX)*(PVALU(IG,K)+FACT(IG)*
     &   DELTAY*(NGRAPH-1))+0.05*YSC
         IF (YPEAK(IG,K).GT.(YPOS+YSC)) YPEAK(IG,K)=YPOS+YSC+2.
         IF (XPEAK(IG,K).GT.(XPOS+XSC)) GOTO 45
         IF (FVALUP(IG,K).GE.XMIN.AND.FVALUP(IG,K).LE.XMAX) THEN
         ID = 4
         CALL GCHARF('SIMP')
         CALL GCHARJ(3)
         CALL GCHARA(90)
         CALL GCHARC(ID)
         CALL GNUMB(FVALUP(IG,K),XPEAK(IG,K),YPEAK(IG,K),2.0,4)
         ID = 3
         CALL GCHARJ(3)
         CALL GCHARA(90)
         CALL GCHARC(ID)
         CALL GNUMB(PVALU(IG,K),XPEAK(IG,K),YPEAK(IG,K)+18.,2.0,4)
         END IF
45       CONTINUE
30    CONTINUE

44       CALL GROUTE ('S MRCOXX;E')
         XRANGE2=XPOS+(XSC/(XMAXX-XMINN))*(XMAX-XMINN)
         XRANGE1=XPOS+(XSC/(XMAXX-XMINN))*(XMIN-XMINN)
         YRANGE1=YPOS-2.000
         YRANGE2=YPOS+(YSC/(YMAXX))*(YMAX)+0.1*YSC

c        plotting attributes at border

         ID = 4
         CALL GCHARJ(3)
         CALL GCHARA(0)
         CALL GCHARC(ID)
         CALL GNUMB(XMAX,XRANGE2,YRANGE1,2.0,2)
         CALL GCHARA(0)
         CALL GNUMB(XMIN,XRANGE1,YRANGE1,2.0,2)
         CALL GCHARA(0)
         CALL GCHARC(3)
         CALL GNUMB(YMAX,XRANGE1,YRANGE2,2.0,2)

C     SET THE ZERO WORLD COORDINATE

      CALL GCHAR(' $',0.0,0.0,0.1,0)
      CALL GCLOSE

1     FORMAT (A100)
2     FORMAT (A1)
3     FORMAT (A10)
4     FORMAT (1X,'INPUT POSITION OF GRAPH NO..... :',1X,I2,1X,
     %        '(0.0=BOTTOM,1.0=TOP,E.g: 0.5...etc.)')
5     FORMAT (1X,': ------- -- --- --- ----- title of line-',I1,'
     % ------------------  - - - :')

      STOP
      END
```

APPENDIX D-1 : Design of Filter.

1. Basic Concept.

A successive process of multiplication and addition of two or more functions is mathematically referred as a convolution (see fig.D-1). Filter processing is a convolution process of an unknown signal and a given signal with respect to time in the time domain form. Both the unknown and given signals can also be transformed in the frequency domain by a transformation process such as the Fourier Transformation. This transformation provides amplitude with respect to frequency instead of amplitude to time. The later form or in the frequency domain form filter processing is easily described as a multiplication of the demanded signal by one and the nondemanded signal by zero. Thus, a rectangular response having amplitudes of one in a certain range of frequency is the ideal filter response. The inverse transform of the rectangular response in the time domain form produces a diminishing sinusoidal signal with infinite time, namely an impulse filter response (see fig.D-2). Practically the impulse filter response is truncated. The truncation of this impulse filter response results in ripples in the pass band frequencies. The sharper the decay the shorter time to convolve or the shorter the delay and the better the filter. These characteristics in the frequency domain can be achieved by tapering the sharp edges of the ideal

filter response. From this point of view there have been many equations available to provide such a smoothed response. Such equations normally reduce selectivity of the filter in the transition frequency band (see fig.D-3). The steeper the slope in the transition frequency band the more selective the filter but the longer the impulse response to diminish in the time domain. In addition the ripples, namely Gibbs phenomena, in the pass band and the side lobes in the stop band frequencies affect amplitude quality of the filtered signal (see fig.D-4). In addition to considering the type of impulse used the gain factors in the pass band as well as in the stop band frequencies are of importance. The lesser the effects of the ripples and the side lobes the better the filter. These inherent characteristics represent the quality of the filter and are given as gain factors (dB gain). On the basis of the number of coefficients of the impulse response filter designs can be classified into Finite Impulse Response (FIR) and Infinite Impulse Response (IIR). The equations representing the smoothed filter response in the frequency domain are normally in term of a rational function of polynomials. From the types of equation used the filter designs can be classified into the Non-recursive Filter and the Recursive Filter which are respectively associated with the FIR and IIR. Furthermore the impulse filter signal can filter out the higher

frequencies or the lower frequencies or leave a certain frequency band and filter out the rest of the frequency band. These filters are referred as lower pass, high pass, and band pass - band stop respectively (see fig.D-2).

It is obvious that certain types of impulse filter response are applicable for certain work. In the following descriptions the IIR-Butterworth filter will be discussed.

2. Mathematical Basis.

A convolution of two functions can be expressed mathematically as follows.

$$y(n) = \sum_{k=-\infty}^{k=\infty} x(k)\ h(n-k) \qquad (1)$$

Assuming the system is linear-time invariant the later equation can be expressed as follows.

$$y(n) = \sum_{k=-\infty}^{k=\infty} h(n)\ x(k-n) \qquad (2)$$

where h(m) must be causal/physically realizable and be infinite.

The general convolution of a digital signal is then given below.

$$y(n) = \sum_{k=0}^{k=N} c_k\ x(n-k) + \sum_{k=1}^{k=M} d_k\ y(n-k) \qquad (3)$$

If $d_k = 0$ equation (3) equals to equation (1) representing the non-recursive filter type.

The transform of the convolved function $y(n)$ can be derived by assuming equation (3) as follows.

$$y_n = x_n + a\,y_{n-1}$$

$$y_n z^{-n} = x_n z^{-n} + a\,y_{n-1} z^{-n}$$

$$Y(z) = X(z) + a\,y_{n-1} z^{-(n-1)}\, z^{-1}$$

$$Y(z) = X(z) + a\,z^{-1}\{Y(z) + Y(-1)\}$$

Assume $Y(-1) = 0$

$$Y(z) = X(z) + a\,z^{-1}\,Y(z)$$

$$X(z) = \{Y(z) - a\,z^{-1}\,Y(z)\}$$

$$Y(z) = X(z)/(1 - a\,z^{-1})$$

$$Y(z) = \frac{z\;X(z)}{(z - a)} \qquad (4)$$

Applying $x_n = e^{(j\omega t)n}$ and using Z-transform rule $b^n = z/(z-b)$ for $b = e^{j\omega t}$, $X(z) = z/(z-e^{j\omega t})$.

Substituting the later $X(z)$ into eq.(4) give

$$Y(z) = \frac{z^2}{(z-a)(z-e^{j\omega t})} \qquad (5)$$

Solution to eq.(5) can be obtained by using partial fraction expansion as follows.

$$\frac{Y(z)}{z} = \frac{C1}{z} + \frac{C2}{(z-a)} + \frac{C3}{(z-e^{j\omega t})}$$

$$C1 = \frac{Y(z)}{z}\, z \Big|_{z=0} = 0$$

$$C2 = \frac{Y(z)}{z}\,(z-a) \Big|_{z=a} = \frac{z(z-a)}{(z-a)(z-e^{j\omega t})} \Big|_{z=a}$$

$$= \frac{a}{(a-e^{j\omega t})}$$

$$C3 = \frac{Y(z)}{z}\,(z-e^{j\omega t}) \Big|_{z=e^{j\omega t}} = \frac{z(z-e^{j\omega t})}{(z-a)(z-e^{j\omega t})} \Big|_{z=e^{j\omega t}}$$

$$= \frac{e^{j\omega t}}{(e^{j\omega t}-a)}$$

$$Y(z) = \frac{az}{(z-a)\,(a-e^{j\omega t})} + \frac{ze^{j\omega t}}{(e^{j\omega t}-a)(z-e^{j\omega t})} \qquad (6)$$

Inverse of equation (6) gives

$$y_n = \frac{a}{(a-e^{j\omega t})}\, a^n + \frac{e^{j\omega t}}{(e^{j\omega t}-a)}\, e^{(j\omega t)n}$$

$$= \frac{-a^{n+1}}{(e^{j\omega t}-a)} + \frac{e^{j\omega t}}{(e^{j\omega t}-a)} e^{(j\omega t)n} \qquad (7)$$

The first part of equation (7) represents the transient and the second part represents the steady state signal. Relationships between coefficients of filter,a and phase angle,ω for non-periodic truncation can be examined from the Z-plane in fig.(D-5).

$$d^2 = s_1^2 + s_2^2$$

$$s_1 = \cos \omega t - a \quad ; \quad s_2 = \sin \omega t$$

$$d^2 = (1 + a^2 - 2a \cos \omega t)$$

Transfer function, $|H| = 1/d$

$$|H| = 1/(1 + a^2 - 2a \cos \omega t)^{-1/2}$$

$$\psi = \omega t - \delta = \omega t - \tan^{-1}\left[-\frac{\sin \omega t}{\cos \omega t - a}\right] \qquad (8)$$

$$\frac{e^{j\omega t}}{(e^{j\omega t}-a)} = |H| e^{j\psi}$$

$$= e^{j\psi} /(1 + a^2 - 2a \cos \omega t)^{-1/2} \qquad (9)$$

Equations (8) and (9) prove that the phase angle and the amplitude depend on the frequency,ω and the filter coefficients,a.

If X(f) and H(f) are the transforms of the signal,x(t) and h(t) the process can also be provided as a multiplication of the individual transform as follows.

$$Y(f) = X(f) \cdot H(f)$$

Inverse transform of Y(f) is not necessary equal to convolution of x(t) and y(t) unless they are periodic.

3. Types of Filter.

a. Low-pass Filter.

IIR-Butterworth type will be discussed further because it is simple to understand and is flexible to adjust in the pass, transition and stop bands [28.37].

Derived from an analog filter Laplace transform of the filter function as described in reference [28] gives

$$H(s) = -\frac{1}{B_n(s)} \tag{10}$$

where $B_n(s)$ is a polynomial of degree n with roots at

$$e^{j(0.5n+0.5+k)\pi/n} \tag{11}$$

Relationships between analog and digital filter as seen in fig.(D-6) show that

$$z = e^{j\omega T} = e^{j\lambda}, \text{ thus } \omega T = \lambda. \tag{12}$$

Including $\omega = 2\pi f$ and $T = 1/F_s$, where F_s is a sampling frequency (2 x Nyquist freq.) and substituting into equation (2.36) gives

$$\lambda = 2\pi f/F_s \text{ or } f = \lambda F_s/2\pi.$$

Relationships between the analog and digital cut-off frequencies can be described as follows.

$$A_c = 2\pi f_c/F_s \quad \text{and} \quad A_s = 2\pi f_s/F_s \tag{13}$$

$$s = c\,\frac{(z-1)}{(z+1)} \quad \text{for} \quad c = \text{Cot}(A_c/2) \tag{14}$$

An analog cut-off frequency ratio can be set using a formula below.

$$\Omega_s = \tan(A_s/2) \,/\, \tan(A_c/2) \tag{15}$$

Noting the prescribed attenuation (At in dB) in the stop band and in the passband the required minimum degree of the polynomial function (n) can be established using the

equation below.

$$n = 0.5 \frac{\text{Log}(10^{A_t/10} - 1)}{\text{Log}(\Omega_s)} \qquad (16)$$

The transfer function H(z) is established by substituting the appropriate n into equation (10) and s into equation (11).

b. High pass filter.

The procedure is similar to the low pass (see fig.D-7) filter with exception that

$$C = \text{Tan}\,(A_c/2) \; ; \; s = C\,\frac{(z+1)}{(z-1)} \quad \text{and}$$

$$\Omega_s = \text{Tan}(A_c/2) \;/\; \text{Tan}(A_s/2)$$

c. Band pass and band stop filter.

The procedure is slightly different from the low pass and high pass filters. The analog to digital relationships are shown in fig.(D-8). Two pass band and stop band frequencies must be given. As a result of these two transition bands the equivalent equations are expressed below.

$$s = \alpha \frac{z^2 - 2\beta z + 1}{z^2 - 1}$$

$$\alpha = \text{Cot}[(A''_c + A_c)/2] \quad ; \quad \beta = \frac{\text{Sin}\,(A_c + A''_c)}{\text{Sin}\,A_c + \text{Sin}\,A''_c}$$

$$\left.\begin{aligned} \Omega_s &= \alpha(\beta - \text{Cos}A''_s)/\text{Sin}A''_s \\ \Omega_s &= \alpha(\beta - \text{Cos}A''_s)/\text{Sin}A''_s \end{aligned}\right\} \text{ select maximum value}$$

4. Application.

Most recursive filters such as the IIR-Butterworth filter posses flexibility in justifying the gain factors

in the pass and stop frequency bands. Inevitably the IIR-Butterworth results in a large amount of transients [35,36] and to eliminate the phase delay a two-pass filter processing is required [34]. To cope the problem a non-recursive filter based on the recursive IIR-Butterworth was established [37,39]. The procedures are as follows.

1. Determine the analog pass band and stop band frequencies (A_c and A_s) using equation (13).
2. The slope of the transition band,Ω is determinable from equation (15).
3. Equation (16) leads to the degree of the polynomial equation required,n
4. The roots of the polynomial equation is determinable from equation (11).
5. The complete analog transfer function,H(s) is obtainable in equation (10) by setting the polynomial equation of degree-n in the denominator as (s-a)(s-b)(s-c)(s-..... etc.
6. The Z-transfer function is determinable by substituting equation (14) into equation (10).

This recursive transfer function may be applied directly to the program. To reduce executable time and transients in the time domain the Wiener-Lee decomposition method [38] can be applied. The technique enables the inverse transform process of the z-form to be carried out in a simple way.

7. For this specific IIR-Butterwoth filter the long division method may also be used as the algorithm is available (see chapter-7).

9. The resulting series of the z-form can be truncated for the purpose of efficiency. The arbitrarily truncation may result in a non-periodic impulse response. This non-periodic impulse response reduces the gain factor in the stop band frequencies. To improve the later problem a shift Hamming window may be applied [37].

10. The fast convolution process is then carried out. The length of the transients is obtainable from the number of coefficients given when truncation is made.

Similar procedures can be carried out for the high-pass and band pass/stop filters.

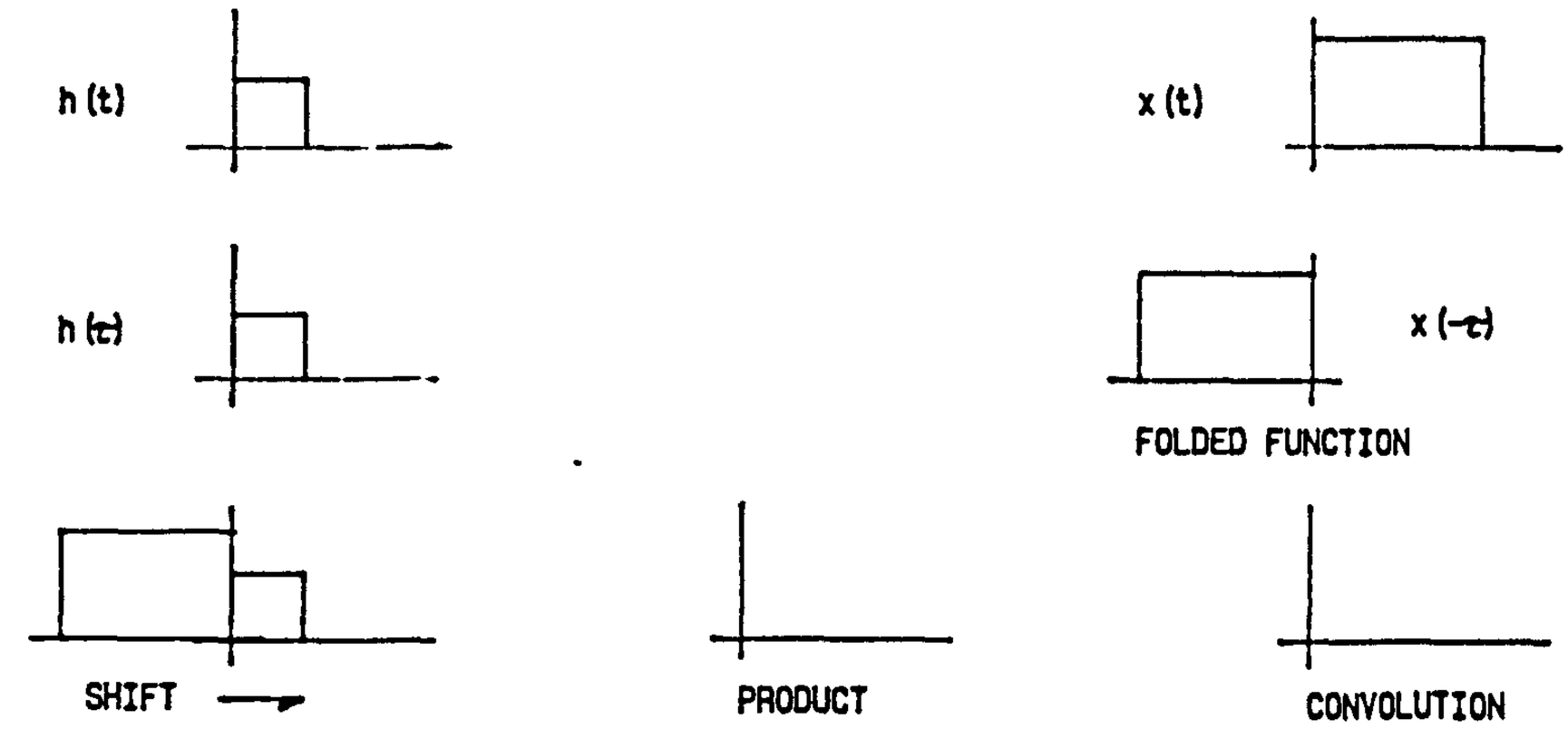

FIG.D-1.CONVOLUTION PROCESS

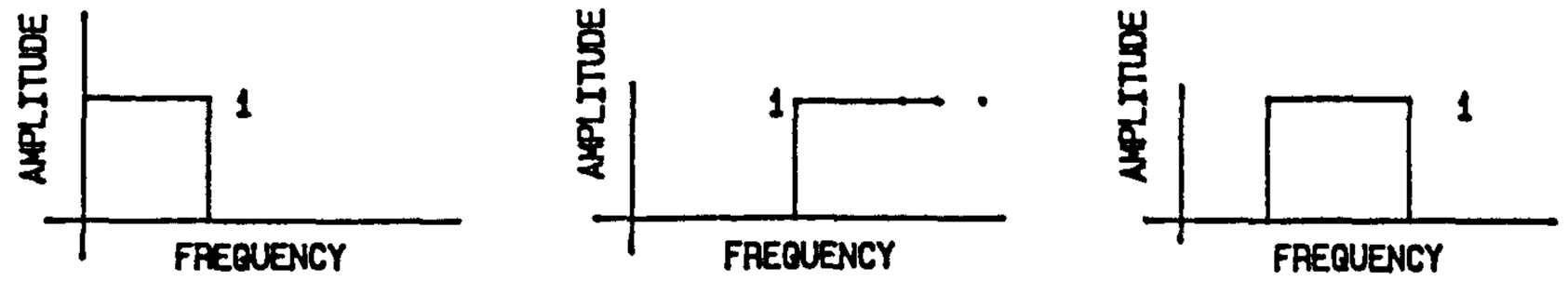

FIG.D-2.IDEAL FILTER.

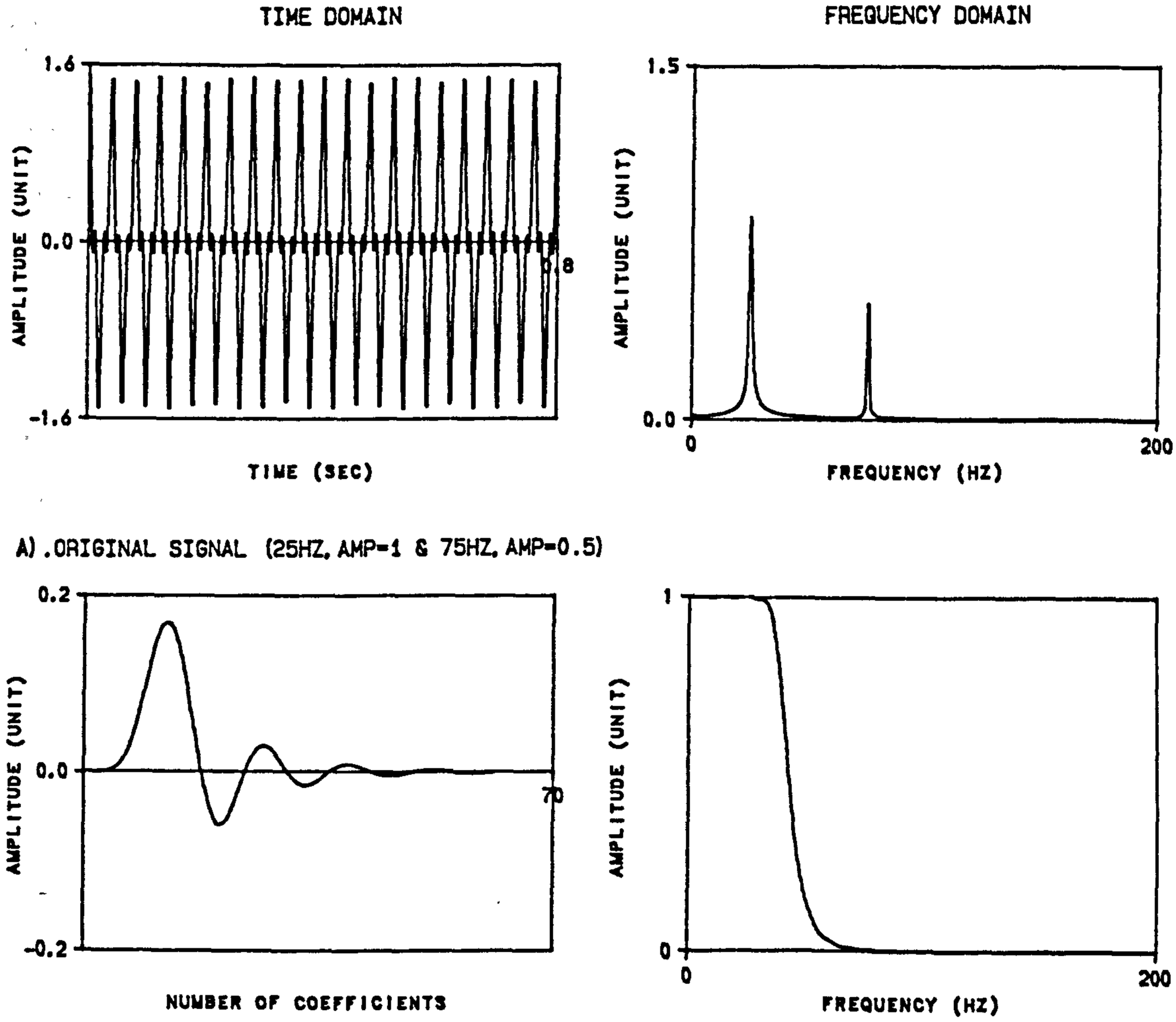

A) .ORIGINAL SIGNAL (25HZ, AMP=1 & 75HZ, AMP=0.5)

B) .IMPULSE FILTER RESPONSE, LOW-PASS, 40-60 HZ TRANSITION BAND,
GAIN FACTOR 30 dB, 60 COEFFICIENTS.

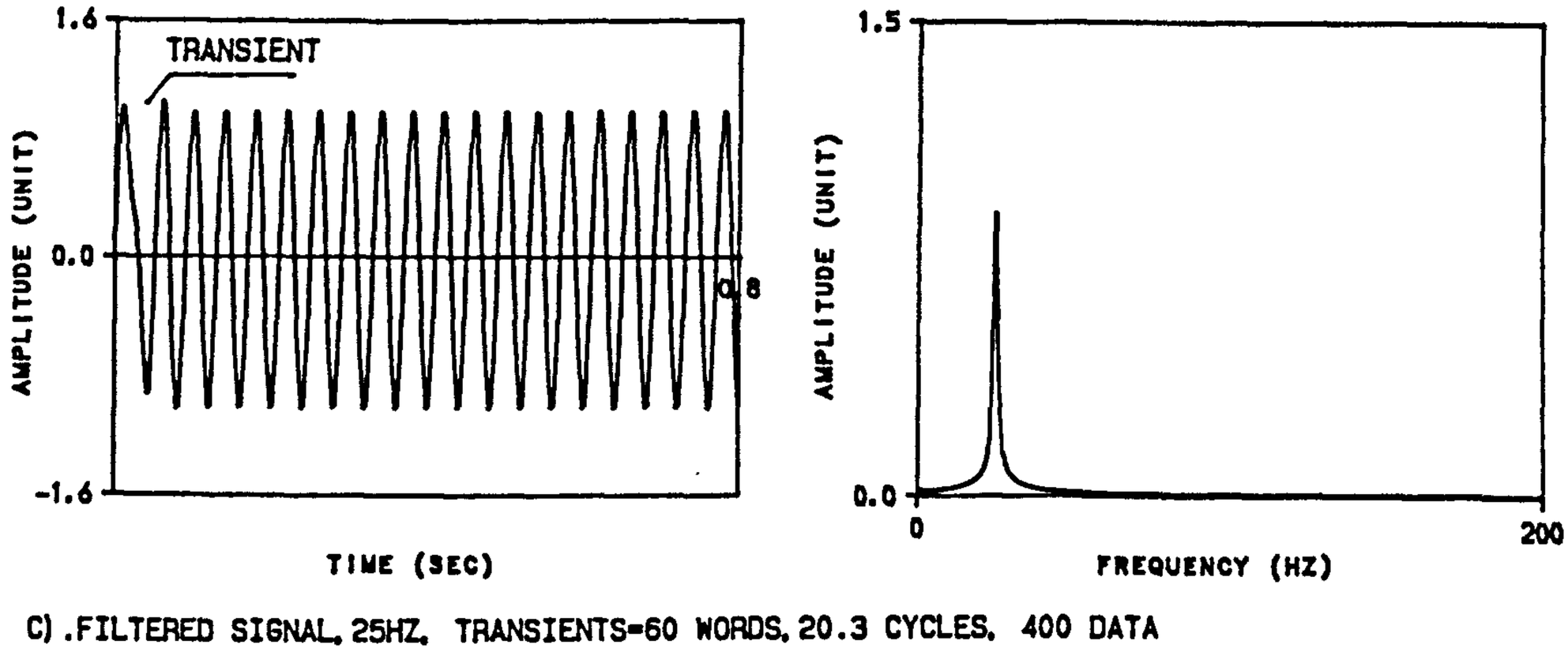

C) .FILTERED SIGNAL, 25HZ, TRANSIENTS=60 WORDS, 20.3 CYCLES, 400 DATA

FIG.D-3.FILTER PROCESSING IN TIME DOMAIN AND IN FREQUENCY DOMAIN USING LOW PASS FIR-BUTTERWORTH TECHNIQUE.

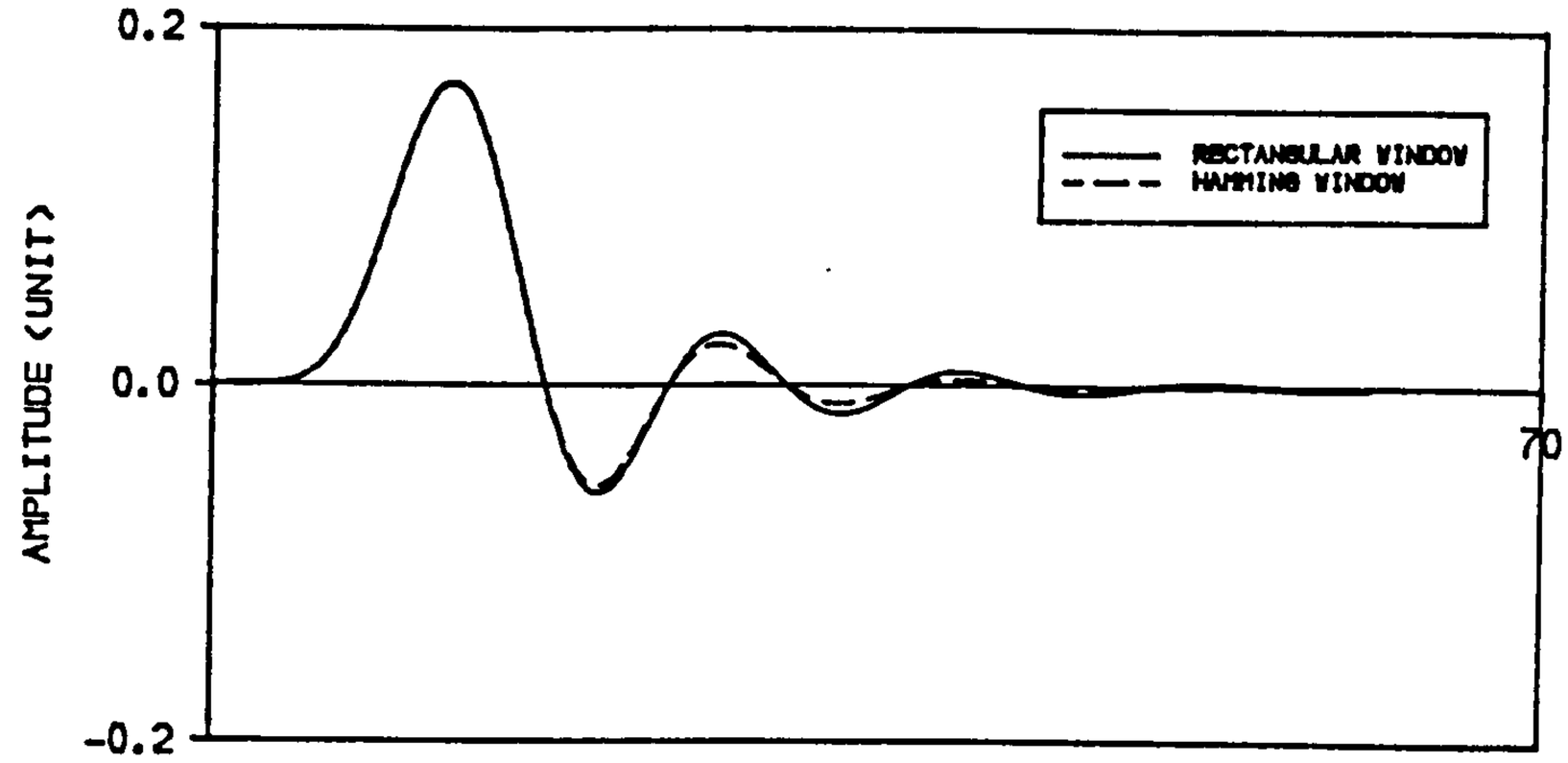

A).IMPULSE FILTER RESPONSE IN TIME DOMAIN

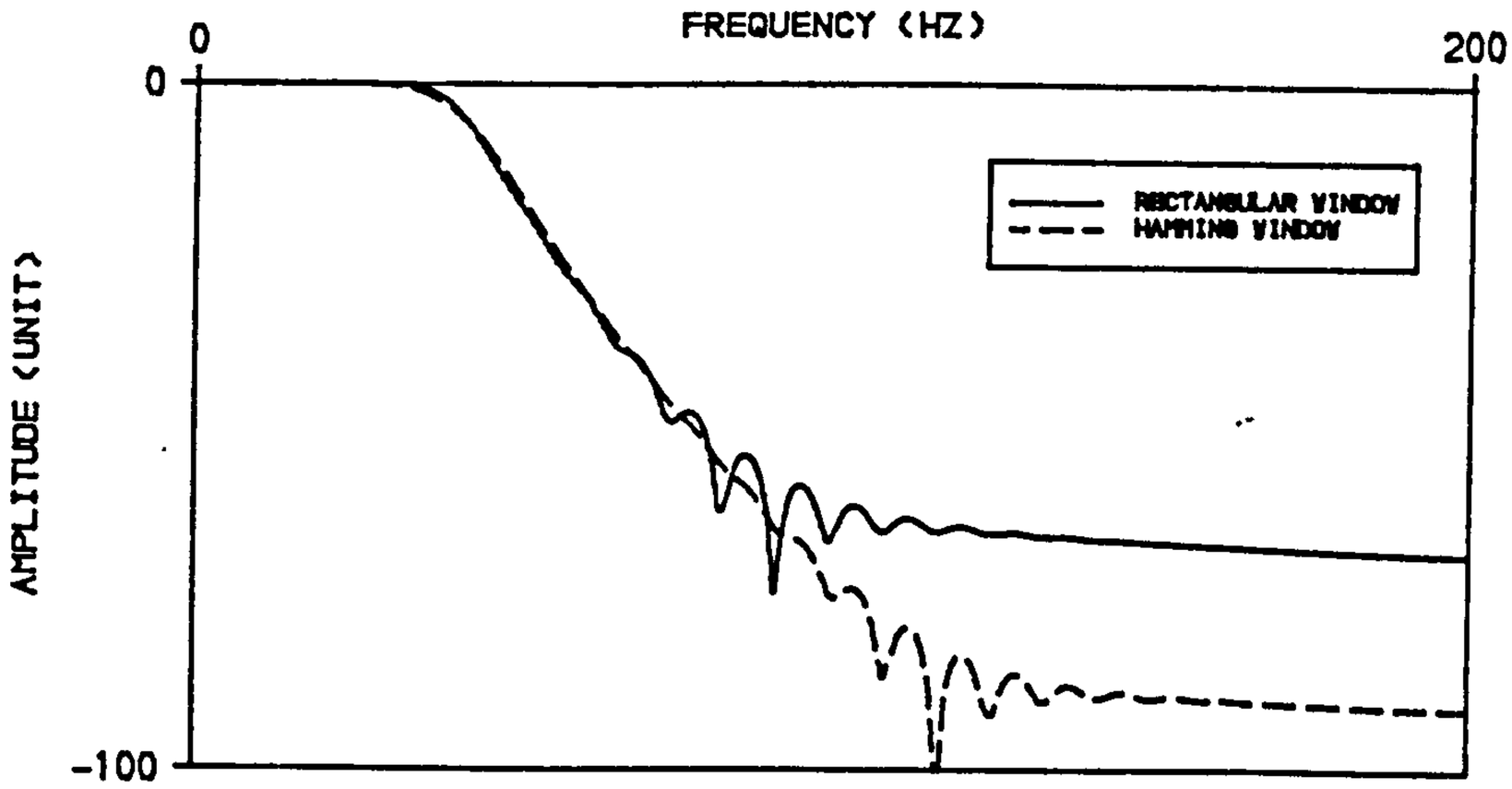

B).IMPULSE FILTER RESPONSE IN FREQUENCY DOMAIN

FIG.D-4.EFFECT OF APPLYING HAMMING WINDOW FUNCTION ON IMPULSE RESPONSE AND GAIN FACTOR

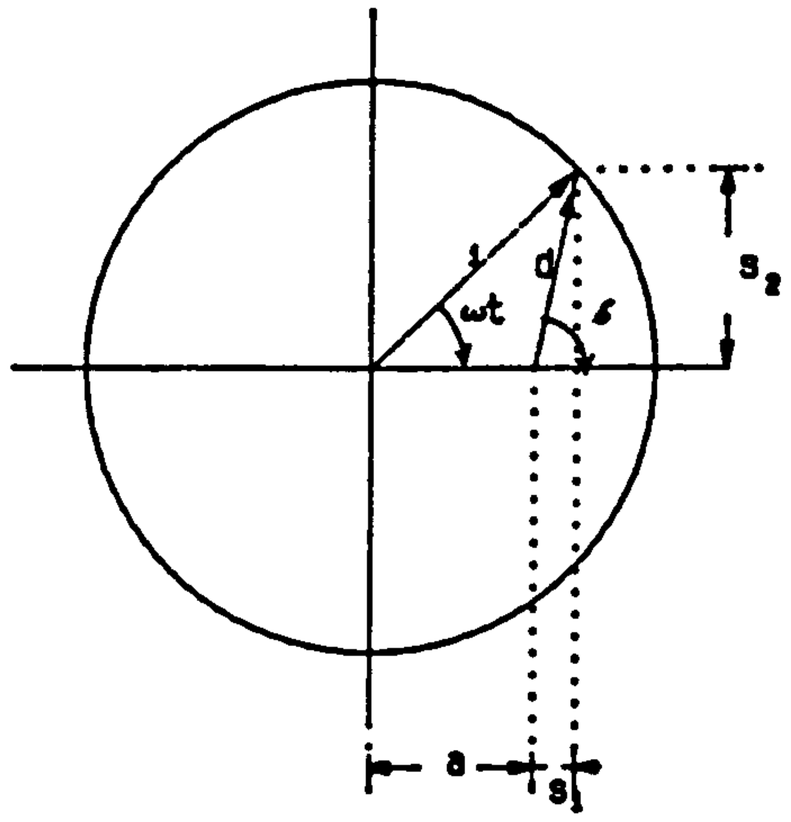

FIG.D-5.FILTER PROCESSING IN THE Z-PLANE

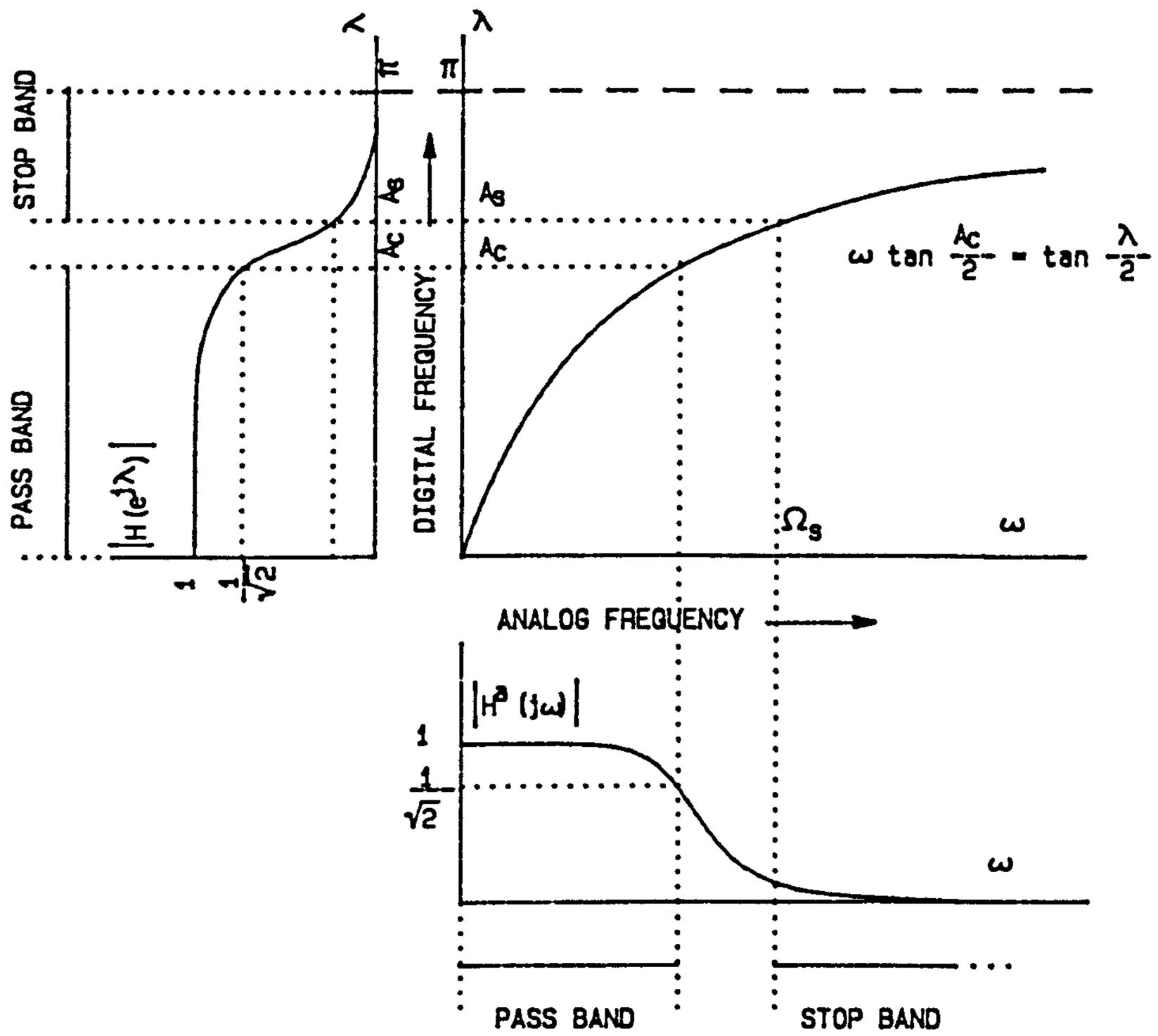

FIG.D-6.ANALOG LOW PASS TO DIGITAL LOW PASS TRANSFORMATION

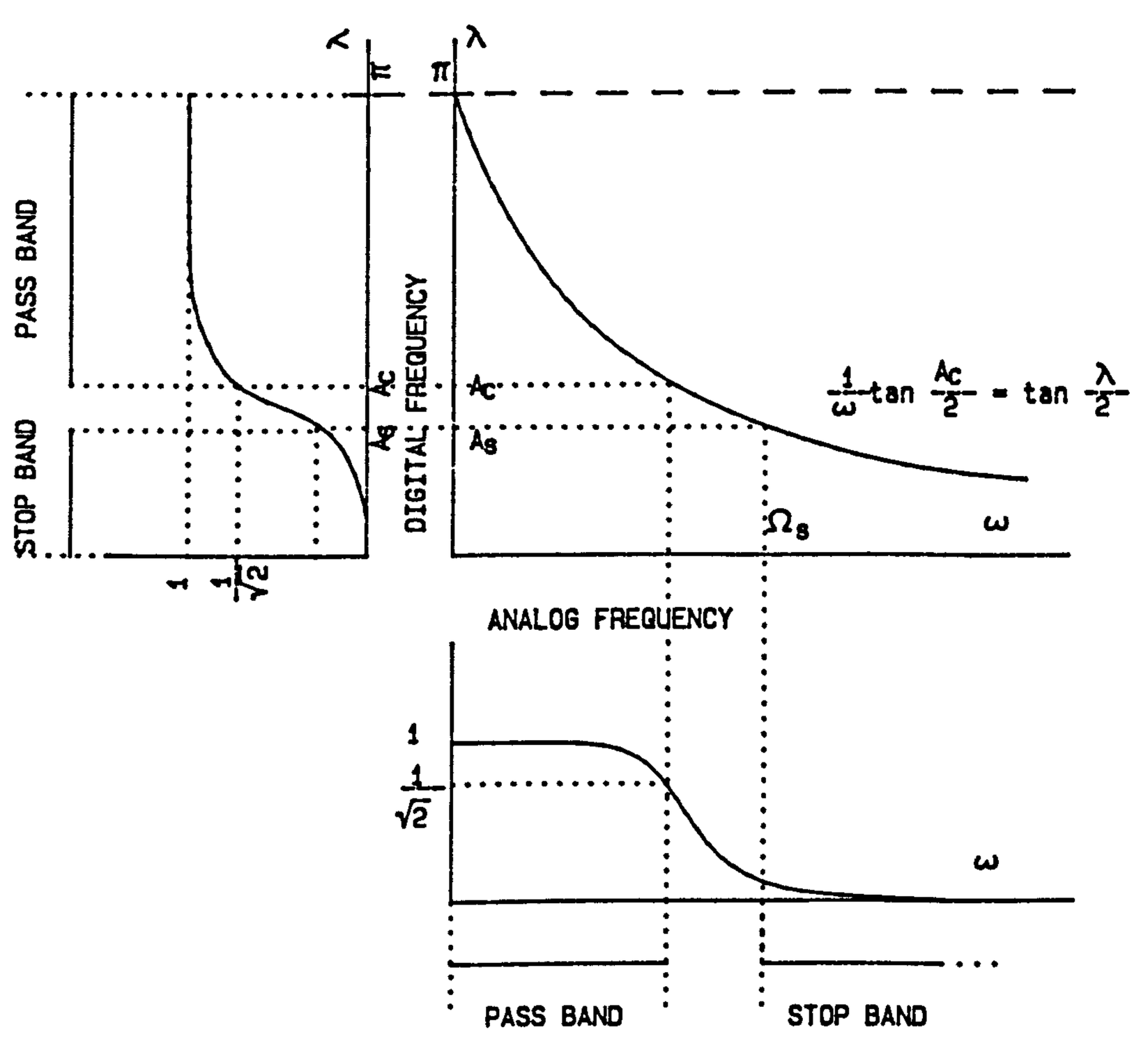

FIG.D-7.ANALOG LOW PASS TO DIGITAL HIGH PASS TRANSFORMATION

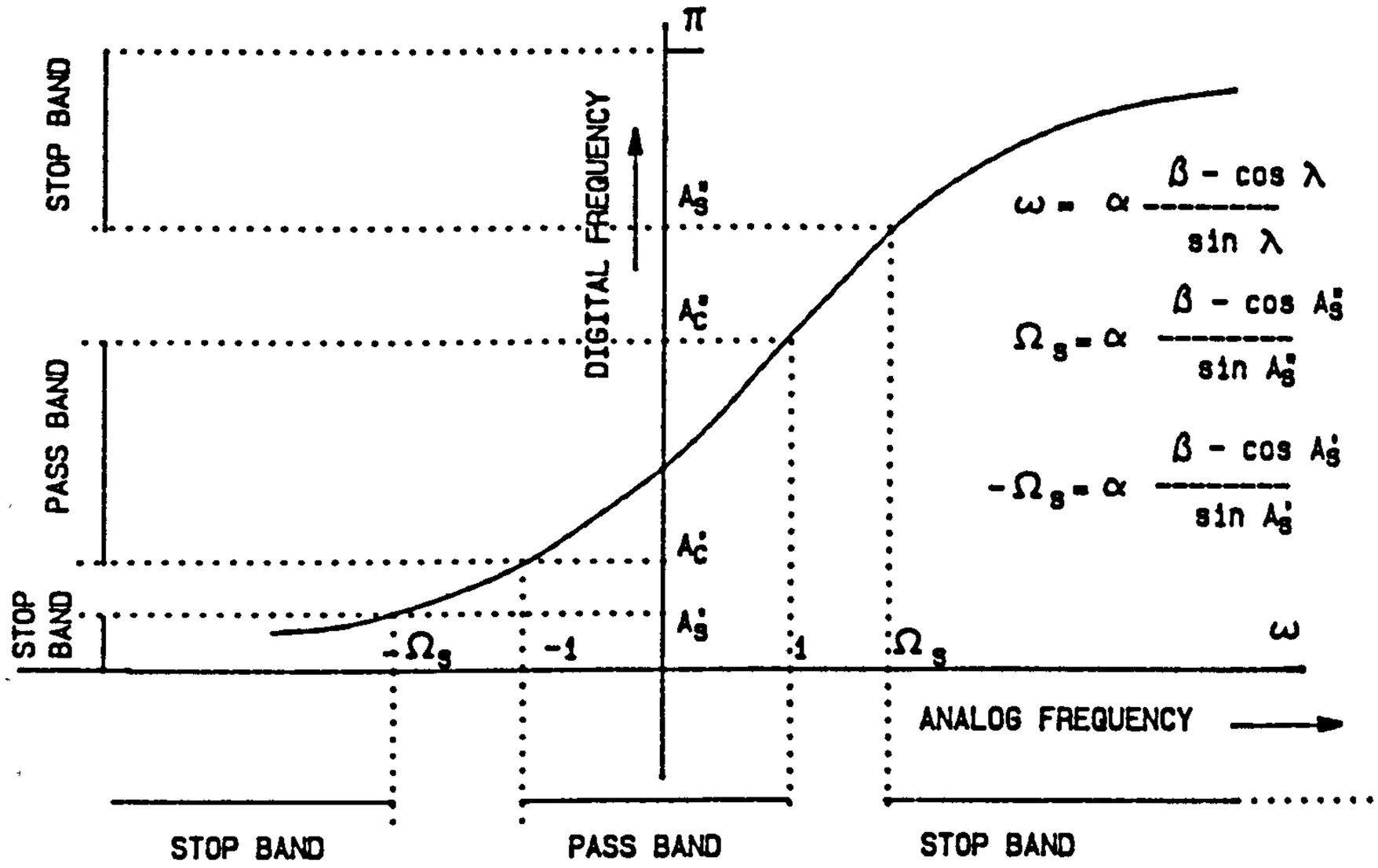

FIG.D-8.ANALOG LOW PASS TO DIGITAL BAND PASS TRANSFORMATION

APPENDIX - E.1.1 : SETS OF FORCE OF EXCITATION FOR BEAM-1, FULLY BONDED, FLEXURAL CRACK PATTERNS, FIRST MODE.

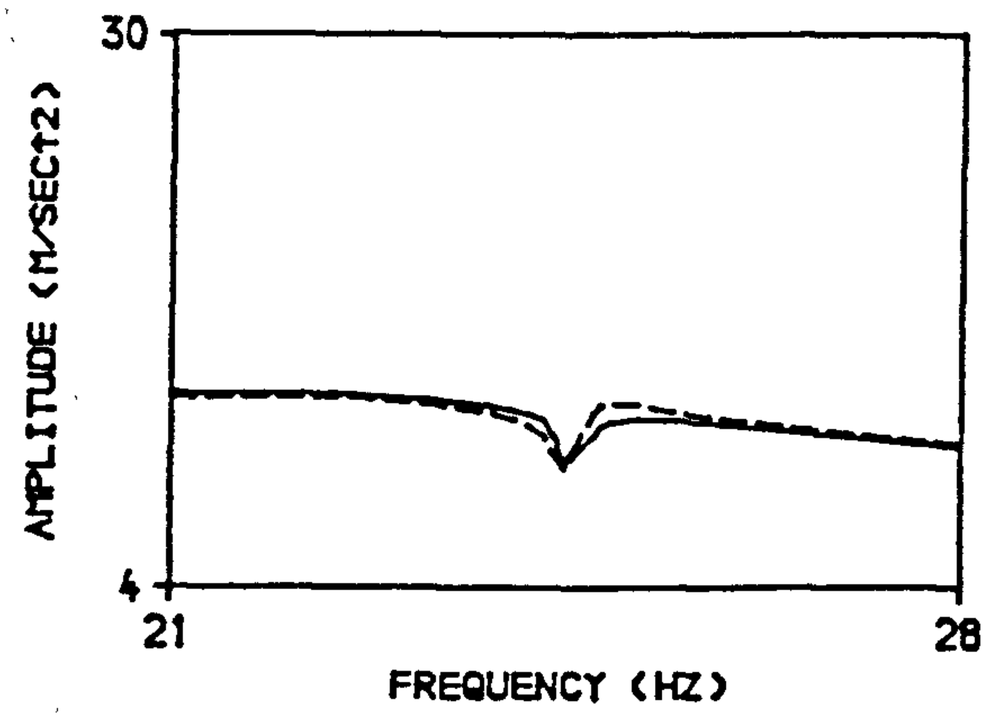

A.BEFORE APPLYING FIRST LOADING STAGE.

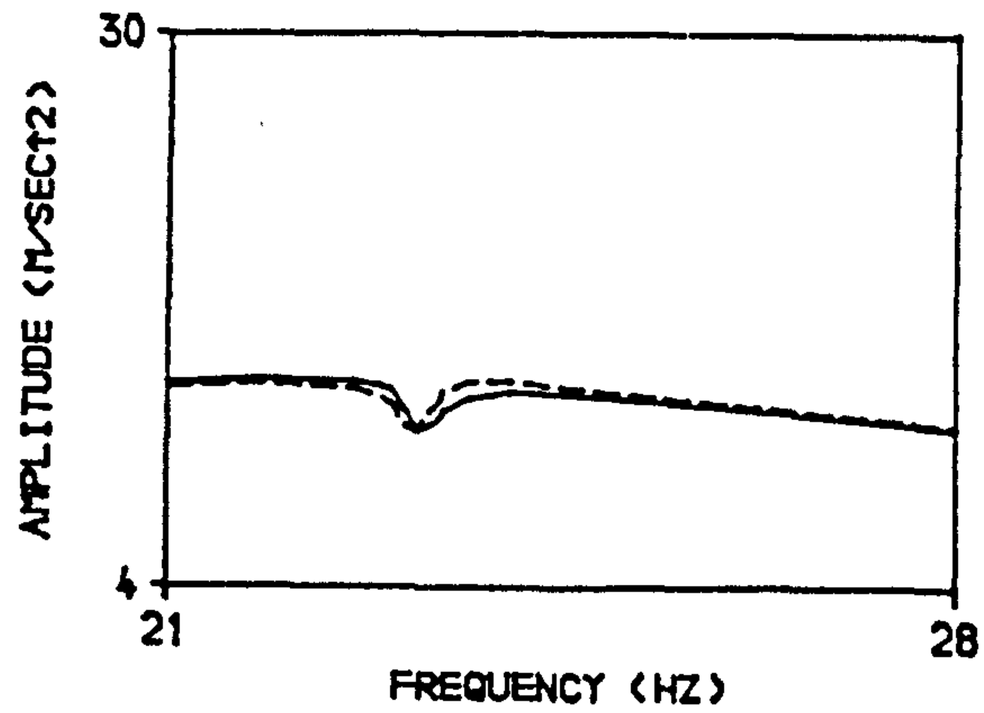

B.AFTER APPLYING FIRST LOADING STAGE.

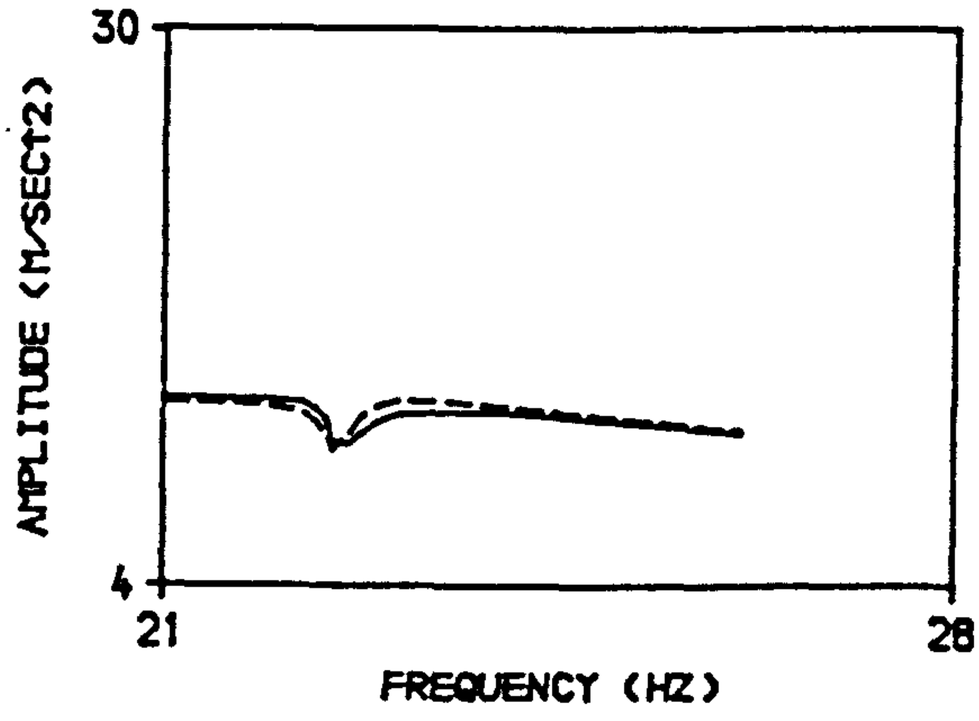

C.AFTER APPLYING SECOND LOADING STAGE.

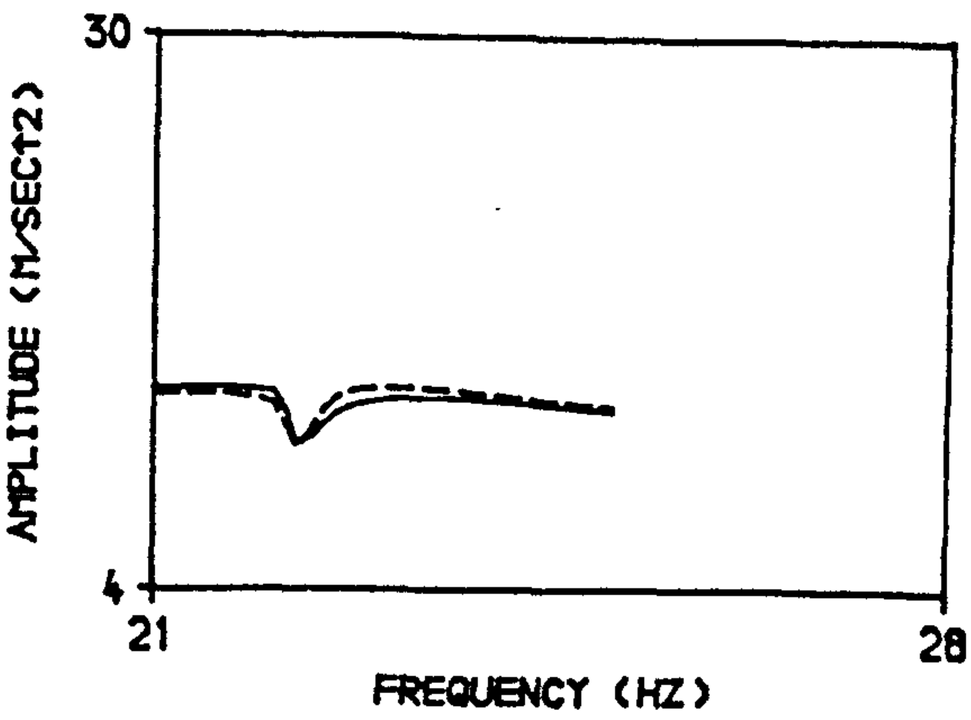

D.AFTER APPLYING THIRD LOADING STAGE.

NOTES :

——— : ABSOLUTE ACCELERATION (M/SEC^2).

------ : RELATIVE ACCELERATION (M/SEC^2)

FORCE : MOVING EXCITER MASS * RELATIVE ACCELERATION
(m) (a)

m : 0.12853 kg.

APPENDIX - E.1.2 : SETS OF FORCE OF EXCITATION FOR BEAM-1, FULLY BONDED, FLEXURAL CRACK PATTERNS, SECOND MODE.

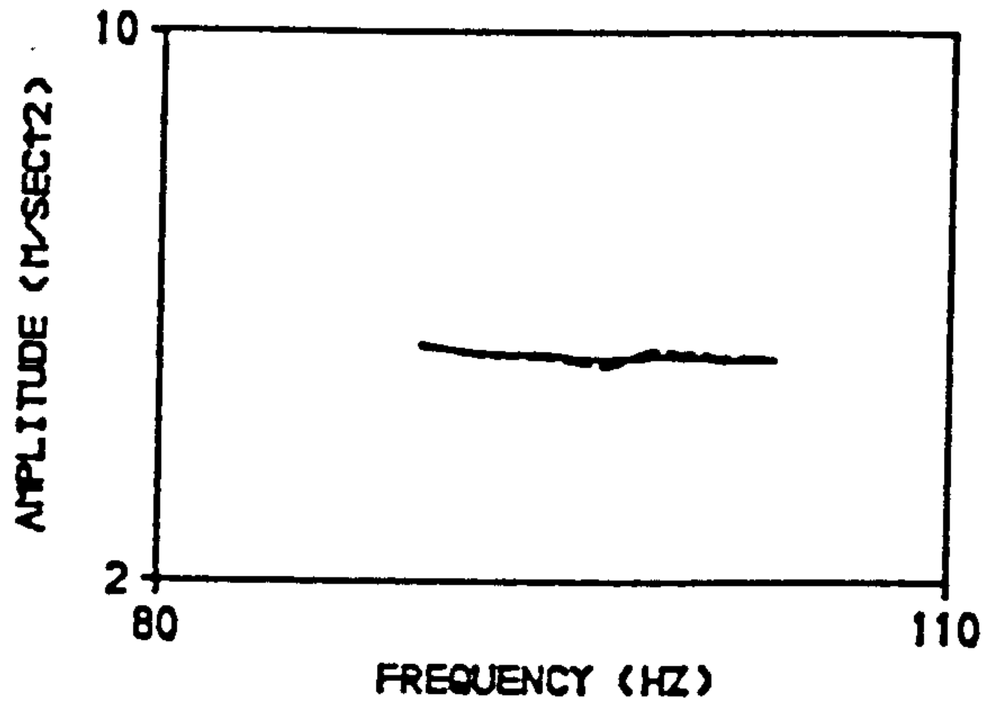

A.BEFORE APPLYING FIRST LOADING STAGE.

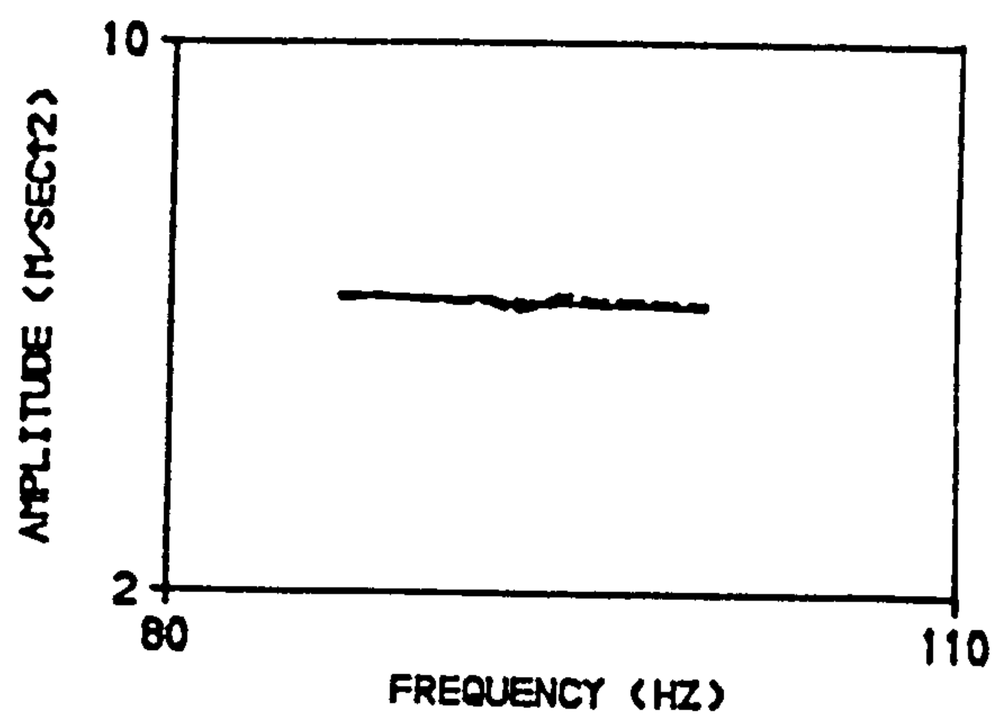

B.AFTER APPLYING FIRST LOADING STAGE.

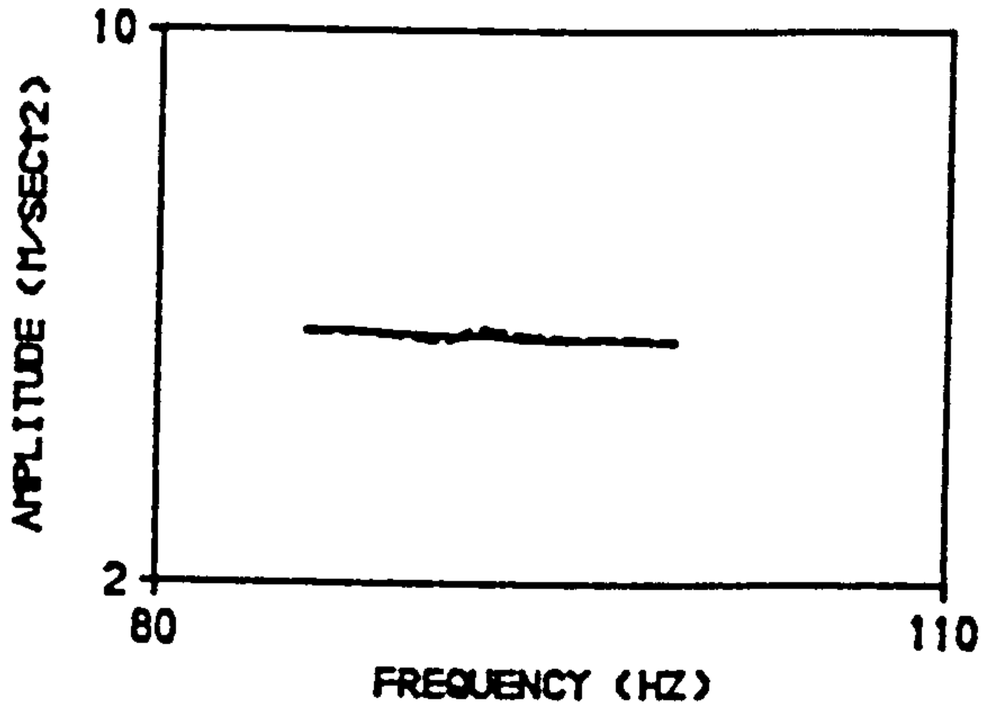

C.AFTER APPLYING SECOND LOADING STAGE.

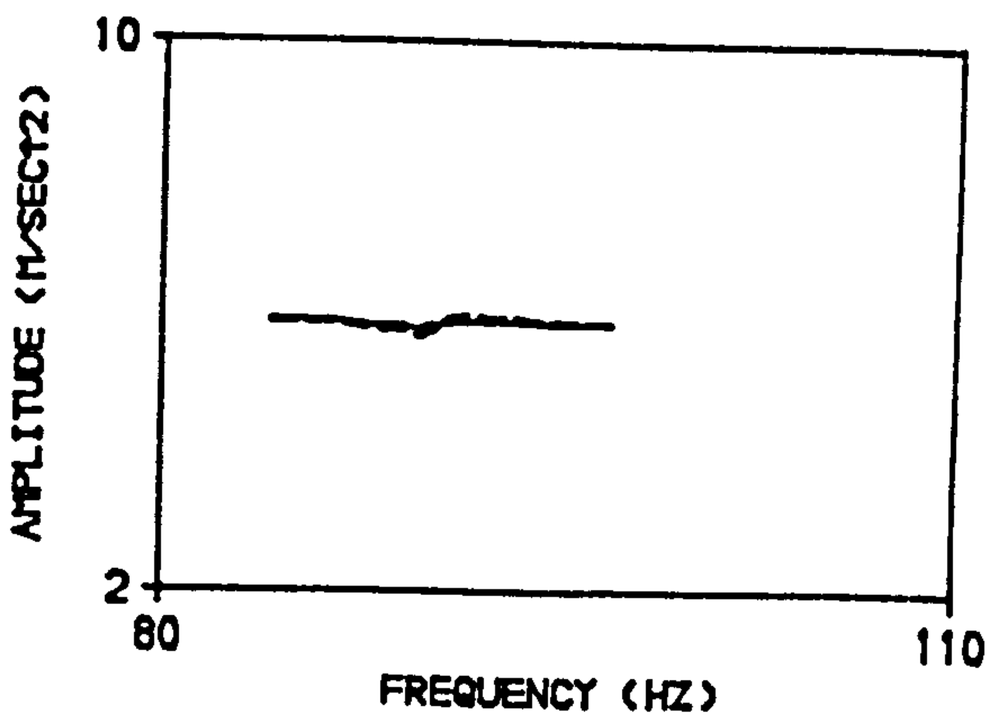

D.AFTER APPLYING THIRD LOADING STAGE.

NOTES :

——— : ABSOLUTE ACCELERATION (M/SEC^2).

------ : RELATIVE ACCELERATION (M/SEC^2)

FORCE : MOVING EXCITER MASS * RELATIVE ACCELERATION
(m) (a)

m : 0.12853 kg.

APPENDIX - E.1.3 : SETS OF FORCE OF EXCITATION FOR BEAM-1, FULLY BONDED, FLEXURAL CRACK PATTERNS, THIRD MODE.

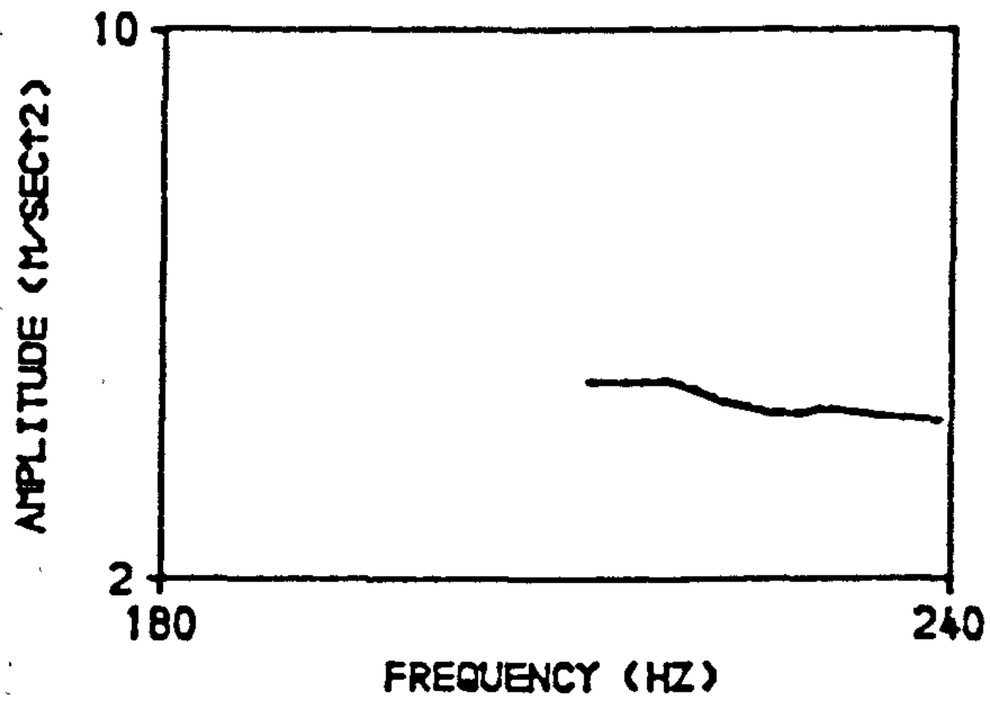

A.BEFORE APPLYING FIRST LOADING STAGE.

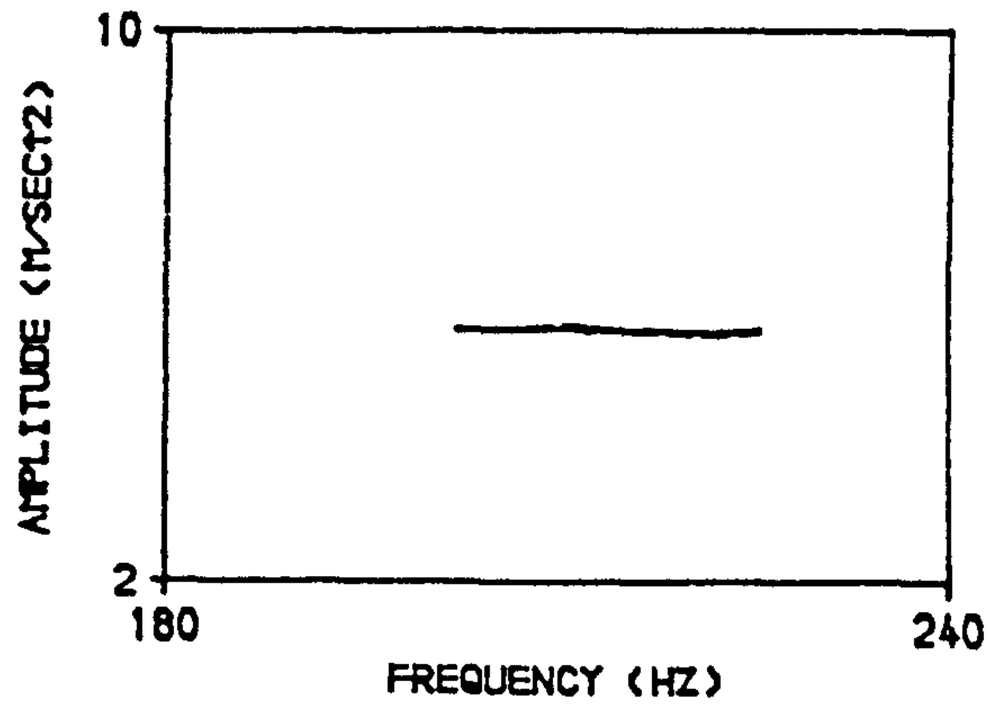

B.AFTER APPLYING FIRST LOADING STAGE.

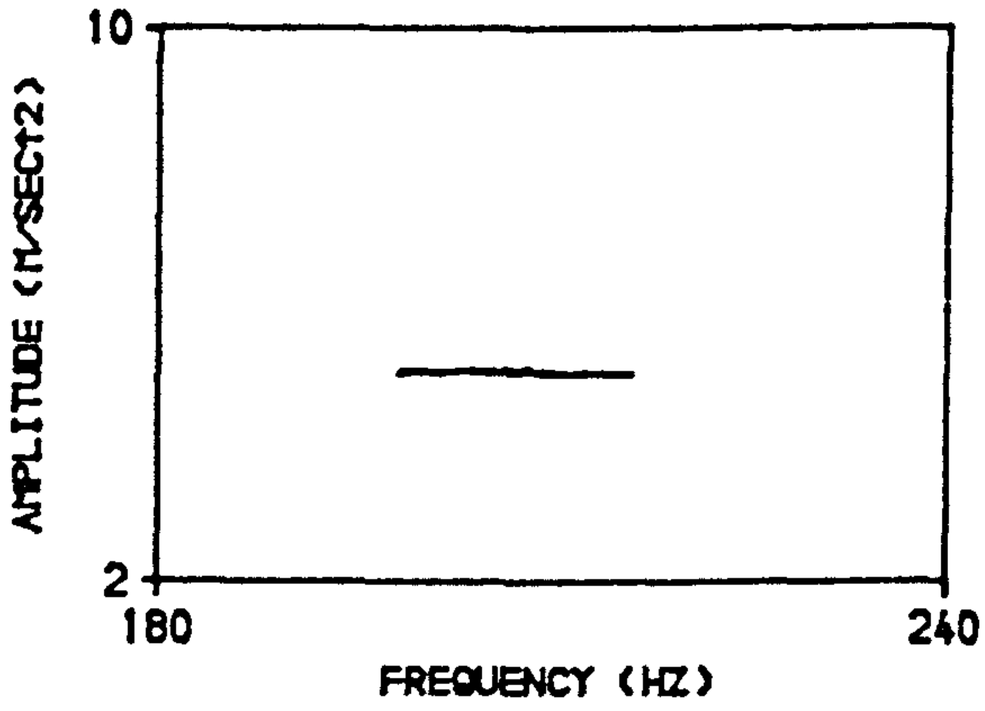

C.AFTER APPLYING SECOND LOADING STAGE.

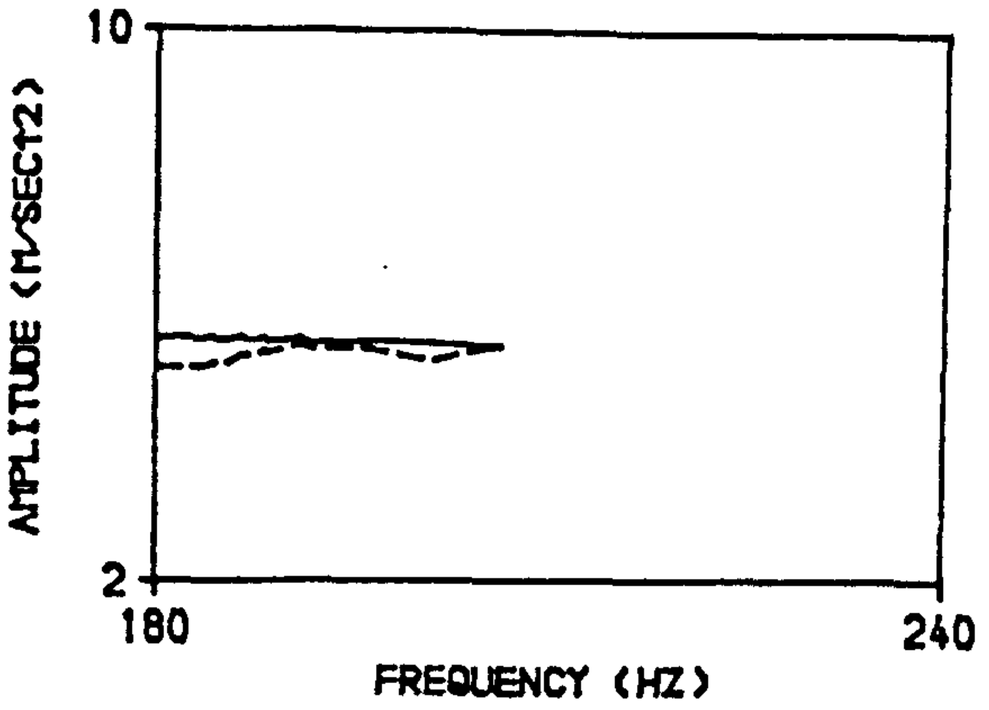

D.AFTER APPLYING THIRD LOADING STAGE.

NOTES :

——— : ABSOLUTE ACCELERATION (M/SEC^2).

------ : RELATIVE ACCELERATION (M/SEC^2)

FORCE : MOVING EXCITER MASS * RELATIVE ACCELERATION
(m) (a)

m : 0.12853 kg.

APPENDIX - E.2.1 : SETS OF FORCE OF EXCITATION FOR BEAM-2, PARTIALLY BONDED, FLEXURAL CRACK PATTERNS, FIRST MODE.

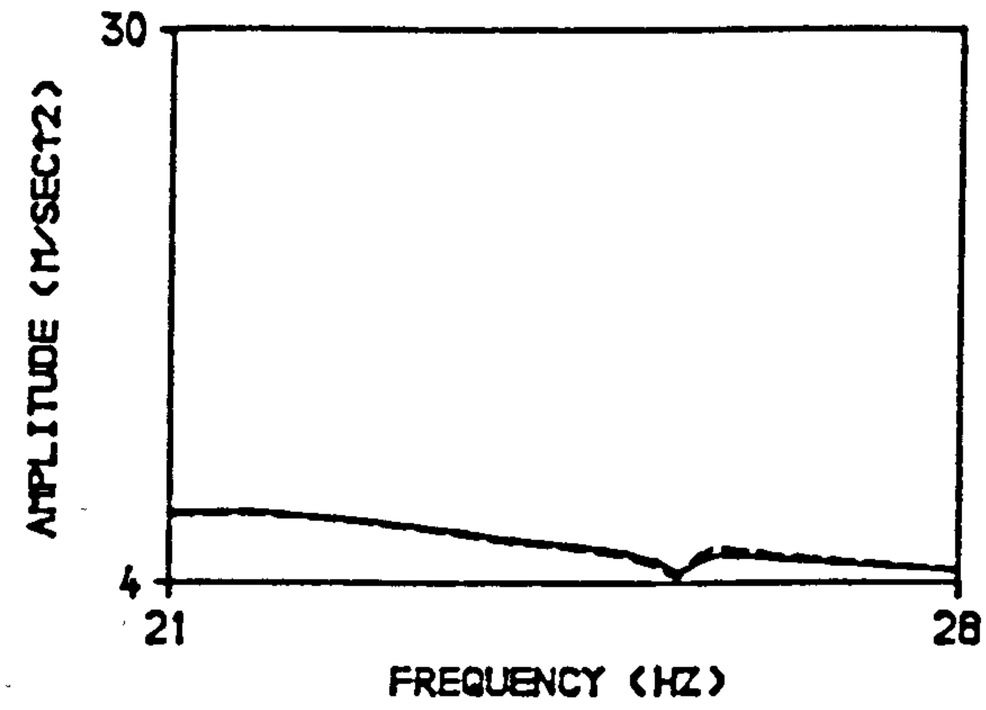

A.BEFORE APPLYING FIRST LOADING STAGE.

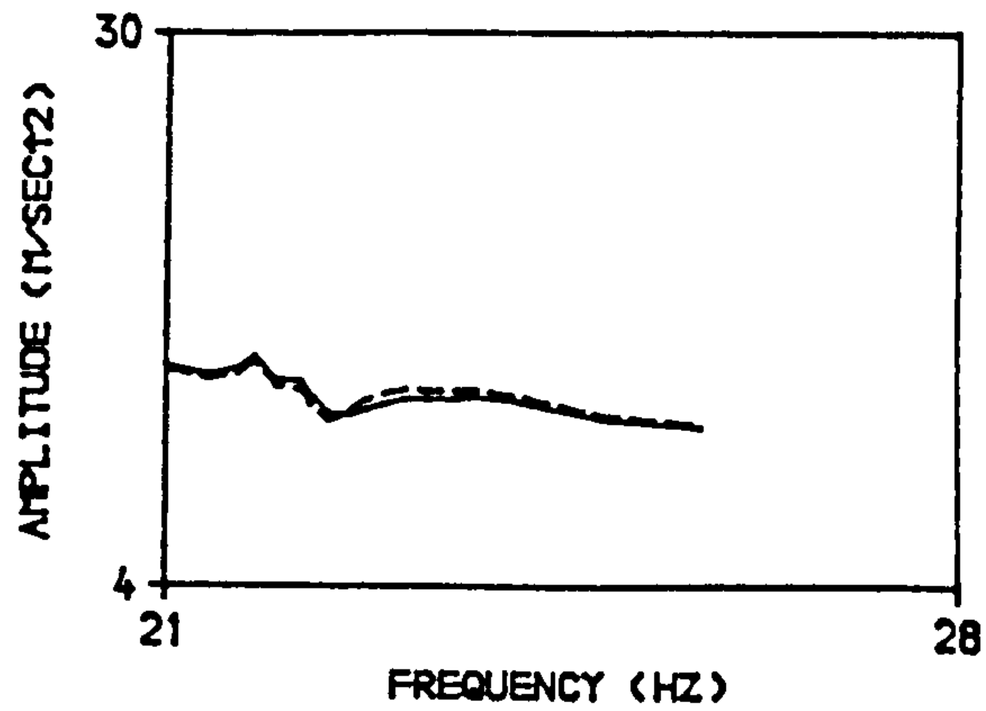

B.AFTER APPLYING FIRST LOADING STAGE.

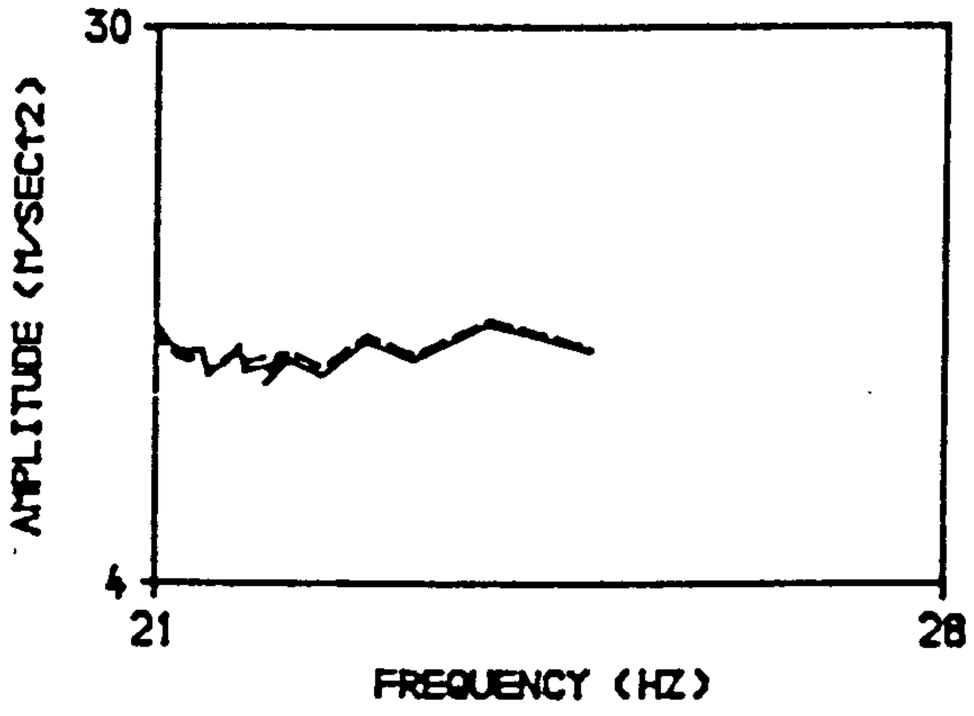

C.AFTER APPLYING SECOND LOADING STAGE.

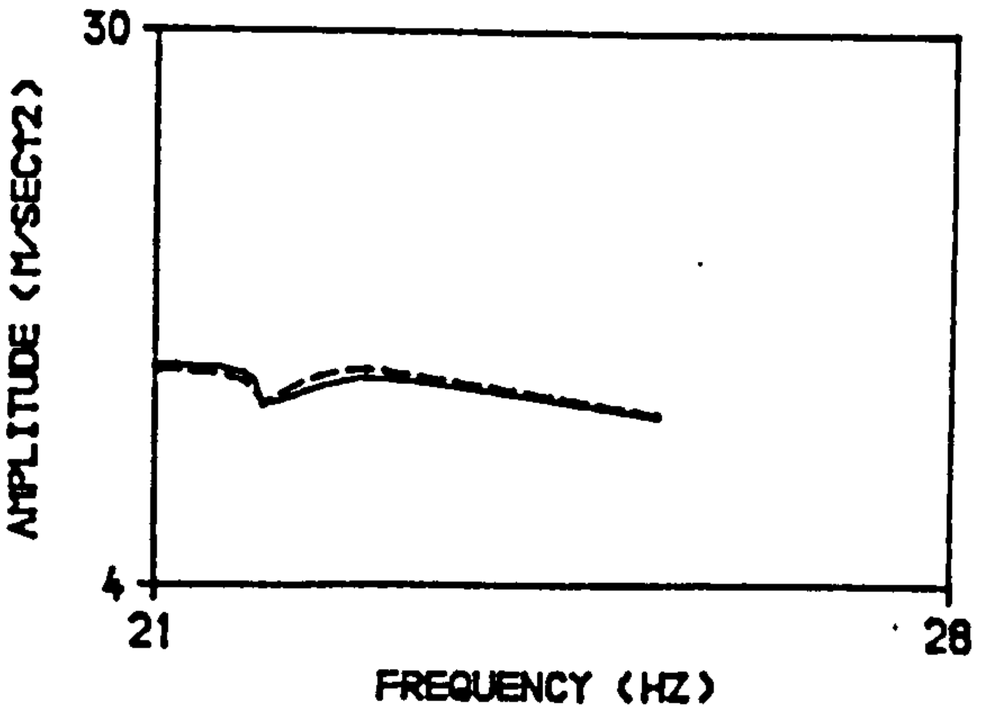

D.AFTER APPLYING THIRD LOADING STAGE.

NOTES :

——— : ABSOLUTE ACCELERATION (M/SEC^2).

------ : RELATIVE ACCELERATION (M/SEC^2)

FORCE : MOVING EXCITER MASS * RELATIVE ACCELERATION
(m) (a)

m : 0.12853 kg.

APPENDIX - E.2.2 : SETS OF FORCE OF EXCITATION FOR BEAM-2, PARTIALLY BONDED, FLEXURAL CRACK PATTERNS, SECOND MODE.

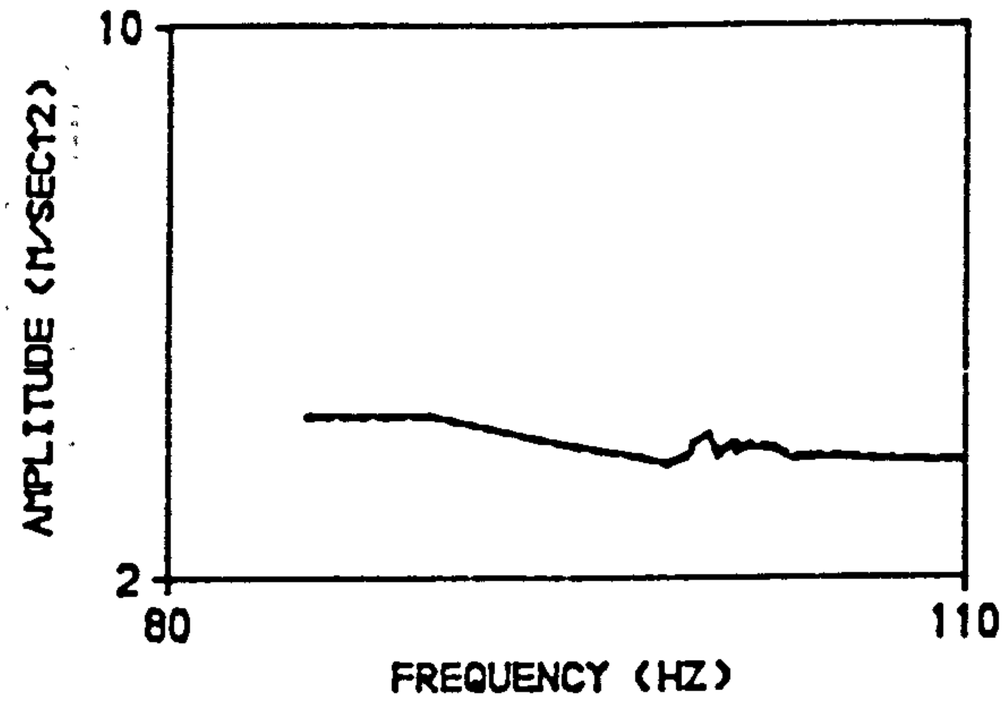

A.BEFORE APPLYING FIRST LOADING STAGE.

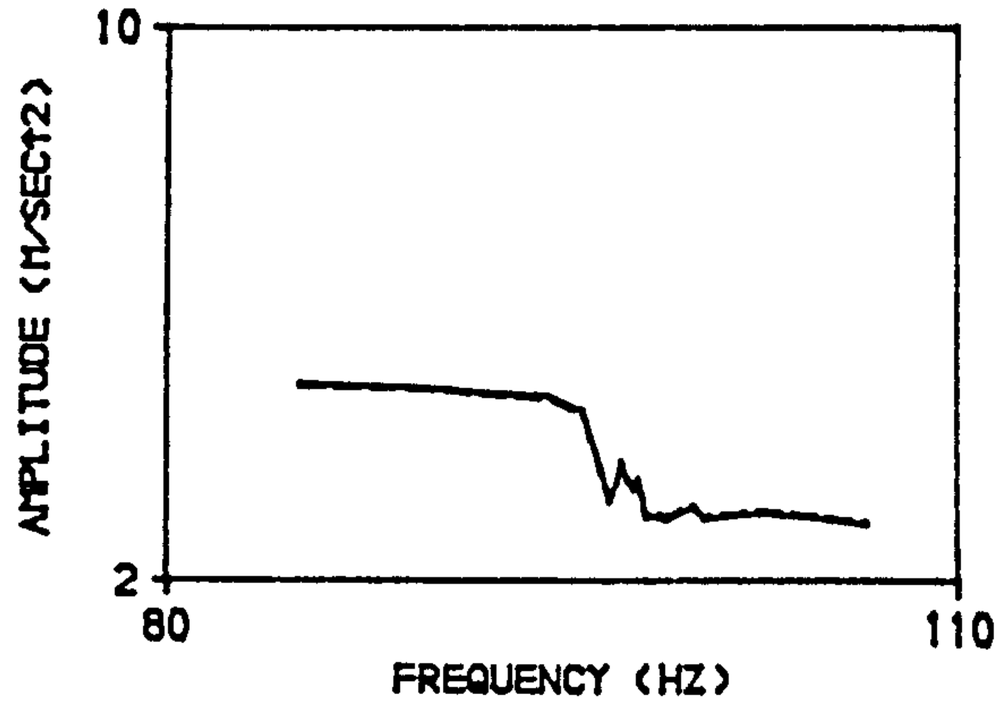

B.AFTER APPLYING FIRST LOADING STAGE.

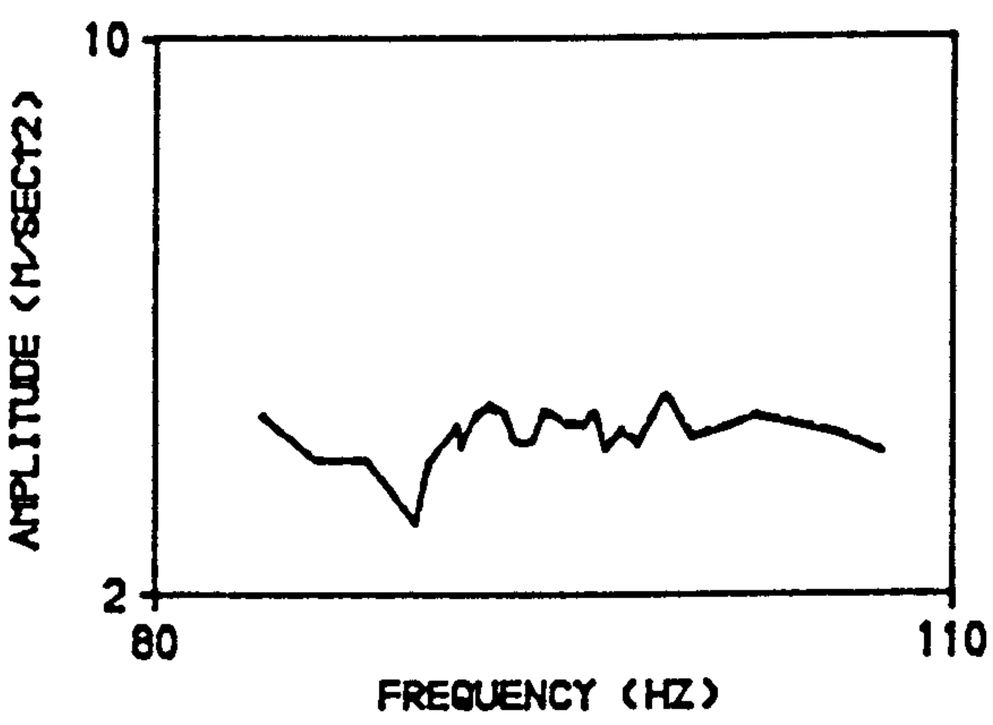

C.AFTER APPLYING SECOND LOADING STAGE.

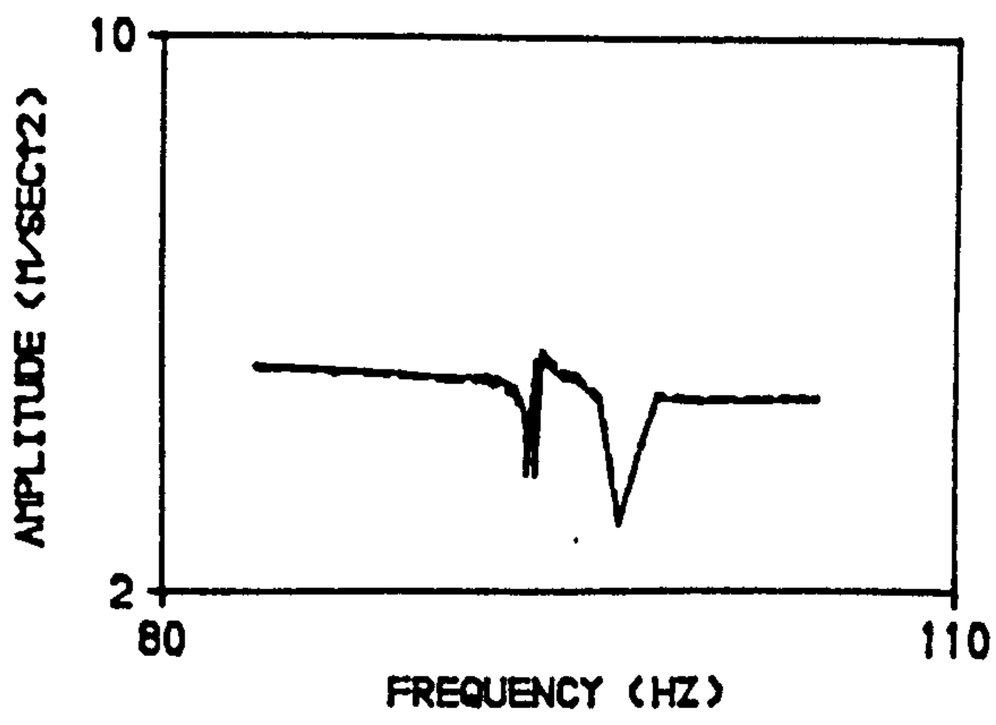

D.AFTER APPLYING THIRD LOADING STAGE.

NOTES :

——— : ABSOLUTE ACCELERATION (M/SEC^2).

------ : RELATIVE ACCELERATION (M/SEC^2)

FORCE : MOVING EXCITER MASS * RELATIVE ACCELERATION
(m) (a)

m : 0.12853 kg.

APPENDIX - E.2.3 : SETS OF FORCE OF EXCITATION FOR BEAM-2, PARTIALLY BONDED, FLEXURAL CRACK PATTERNS, THIRD MODE.

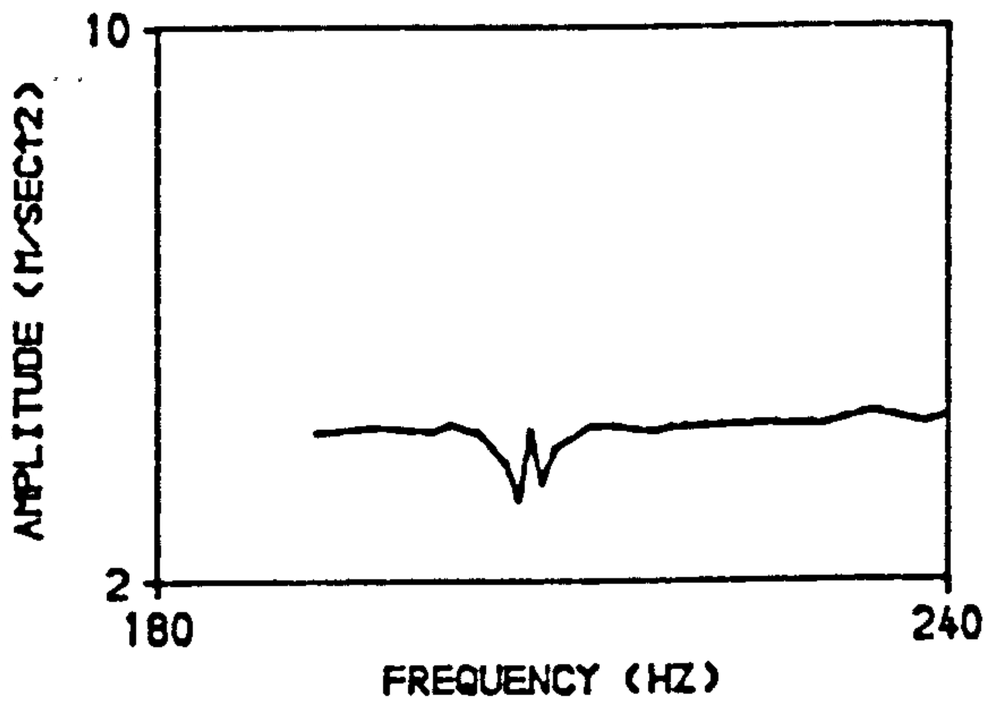

A.BEFORE APPLYING FIRST LOADING STAGE.

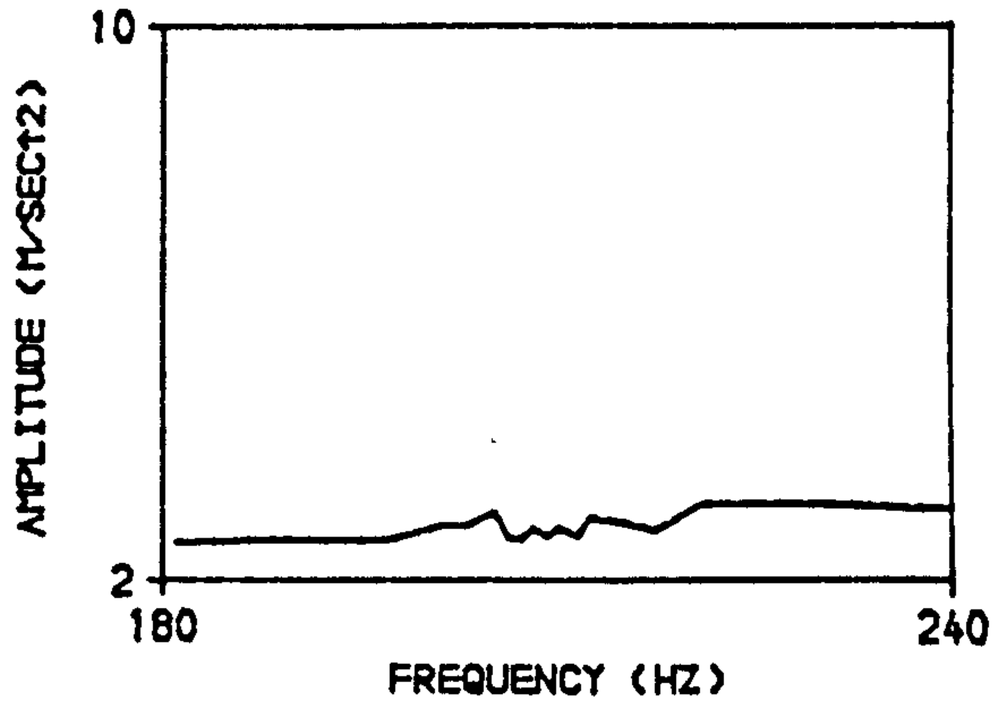

B.AFTER APPLYING FIRST LOADING STAGE.

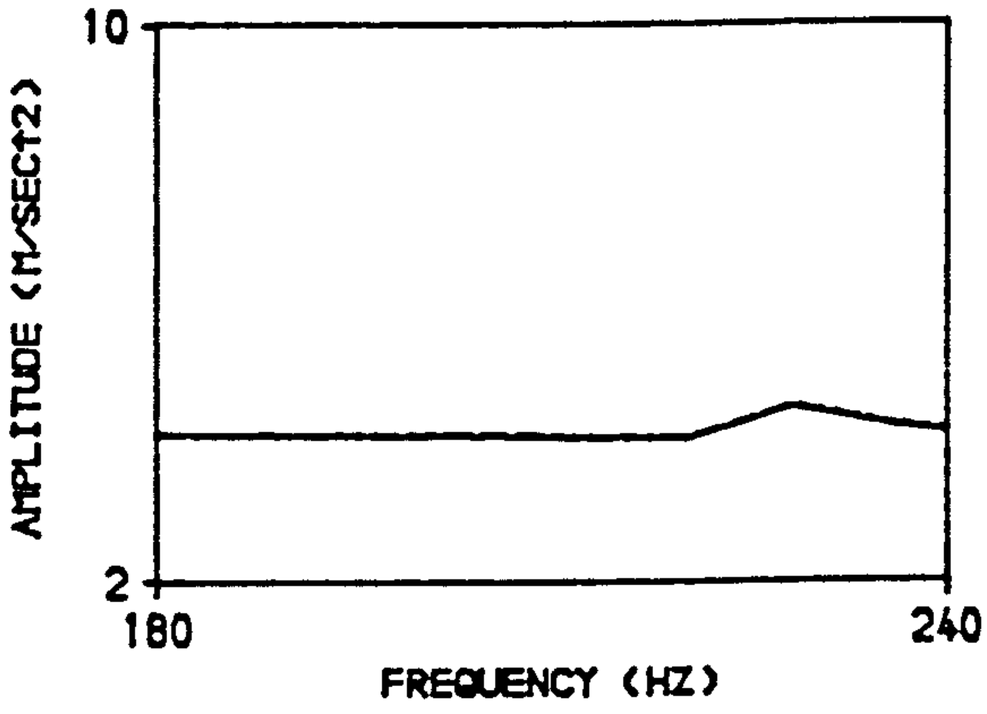

C.AFTER APPLYING SECOND LOADING STAGE.

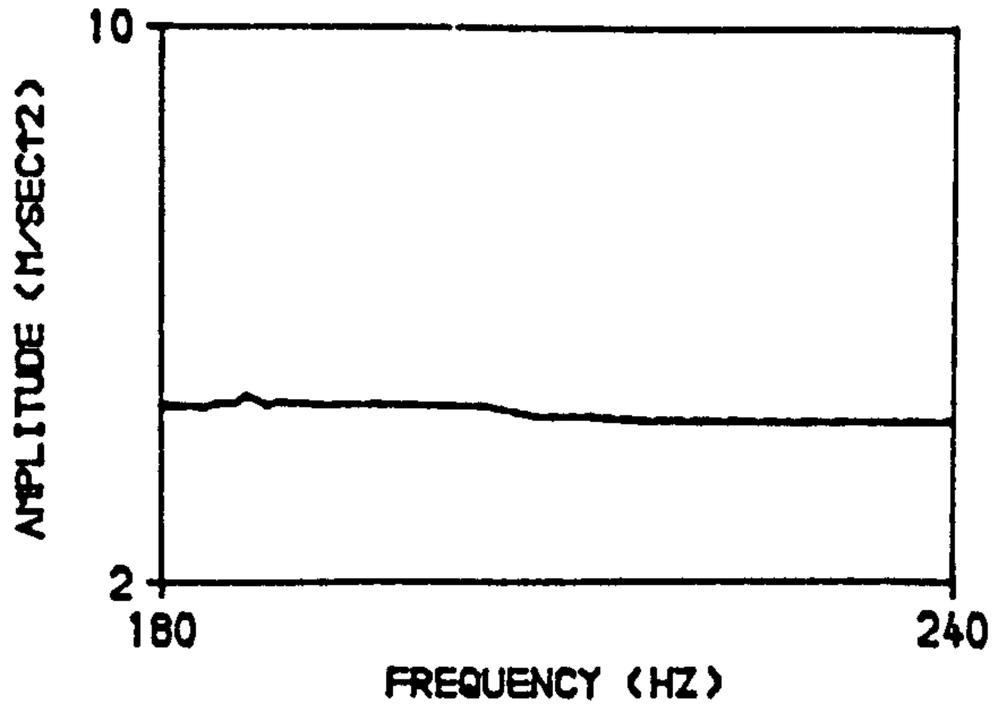

D.AFTER APPLYING THIRD LOADING STAGE.

NOTES :

——— : ABSOLUTE ACCELERATION (M/SEC^2).

------ : RELATIVE ACCELERATION (M/SEC^2)

FORCE : MOVING EXCITER MASS * RELATIVE ACCELERATION
(m) (a)

m : 0.12853 kg.

APPENDIX - E.3.1 : SETS OF FORCE OF EXCITATION FOR BEAM-3, FULLY BONDED, DIAGONAL SPLITTING CRACK PATTERNS, FIRST MODE.

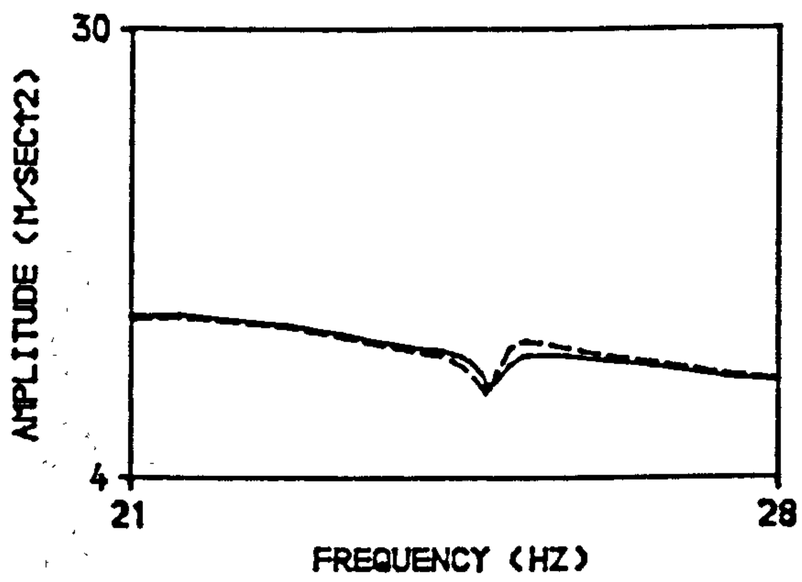

A.BEFORE APPLYING FIRST LOADING STAGE.

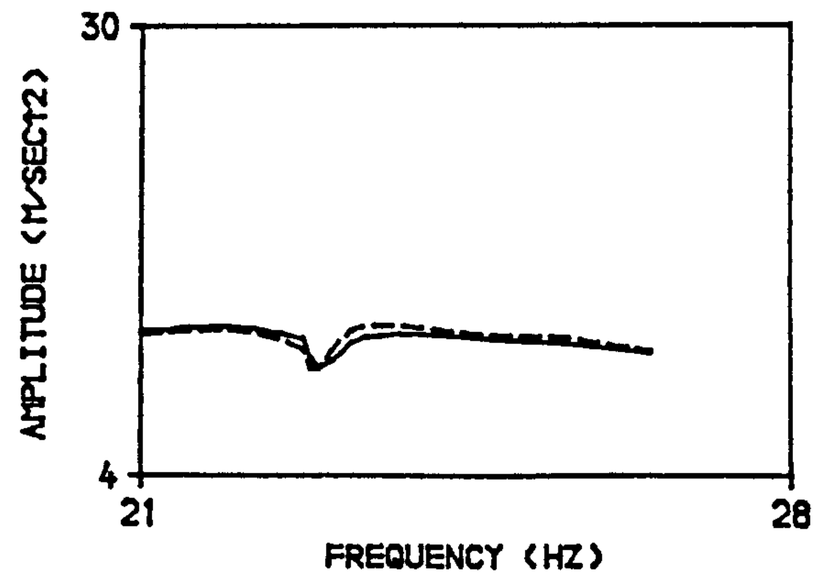

B.AFTER APPLYING FIRST LOADING STAGE.

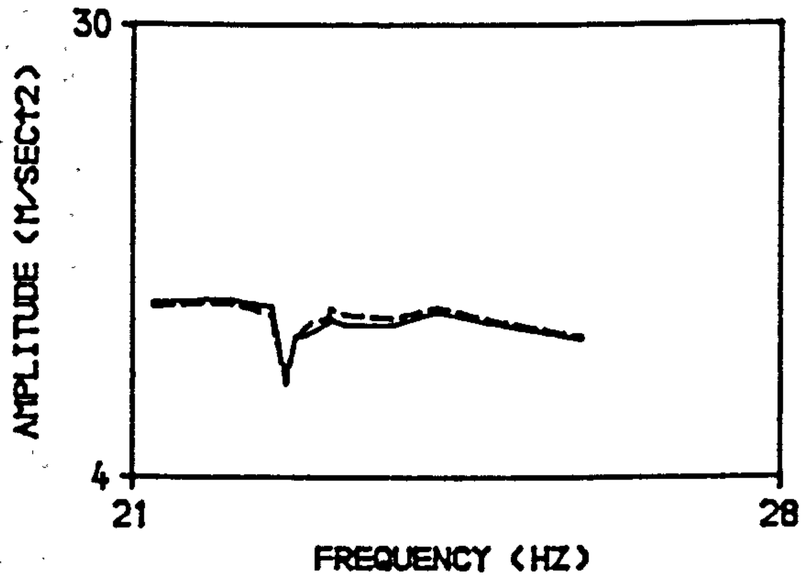

C.AFTER APPLYING SECOND LOADING STAGE.

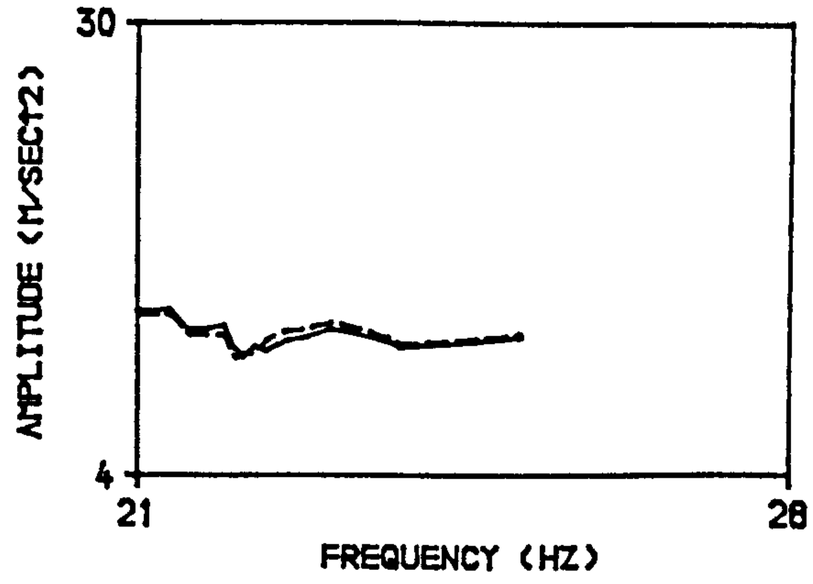

D.AFTER APPLYING THIRD LOADING STAGE.

NOTES :

——— : ABSOLUTE ACCELERATION (M/SEC^2).

------ : RELATIVE ACCELERATION (M/SEC^2)

FORCE : MOVING EXCITER MASS * RELATIVE ACCELERATION
(m) (a)

m : 0.12853 kg.

APPENDIX - E.3.2 : SETS OF FORCE OF EXCITATION FOR BEAM-3, FULLY BONDED, DIAGONAL SPLITTING CRACK PATTERNS, SECOND MODE.

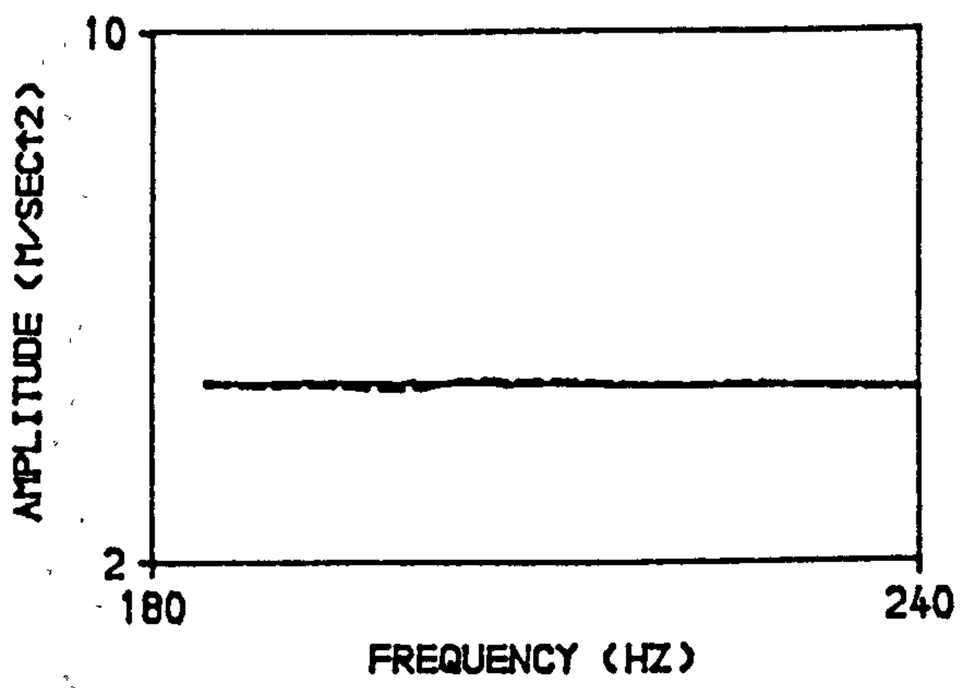

A.BEFORE APPLYING FIRST LOADING STAGE.

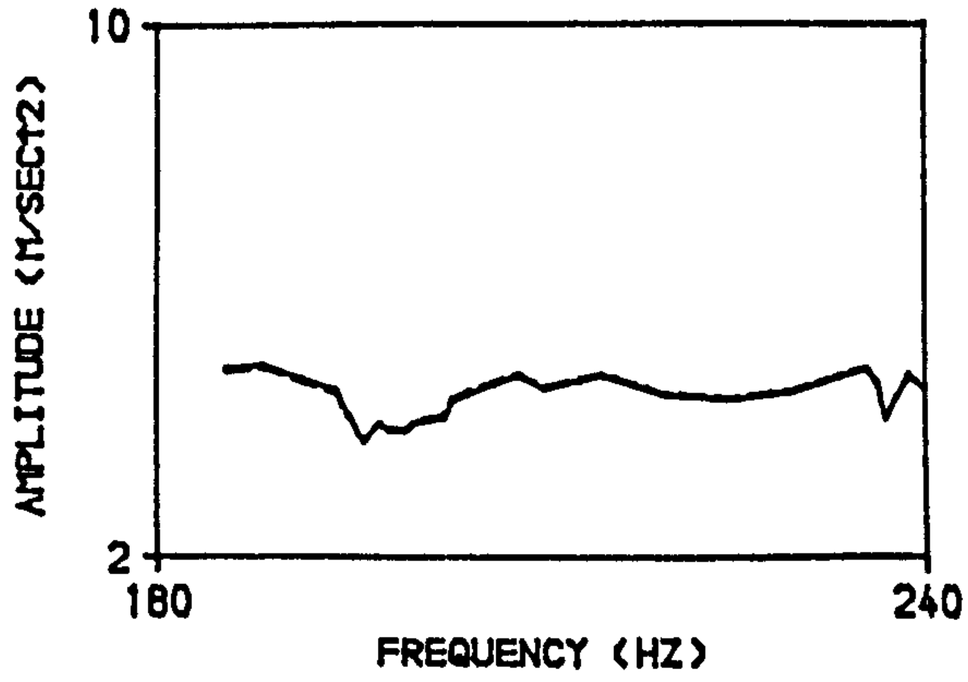

B.AFTER APPLYING FIRST LOADING STAGE.

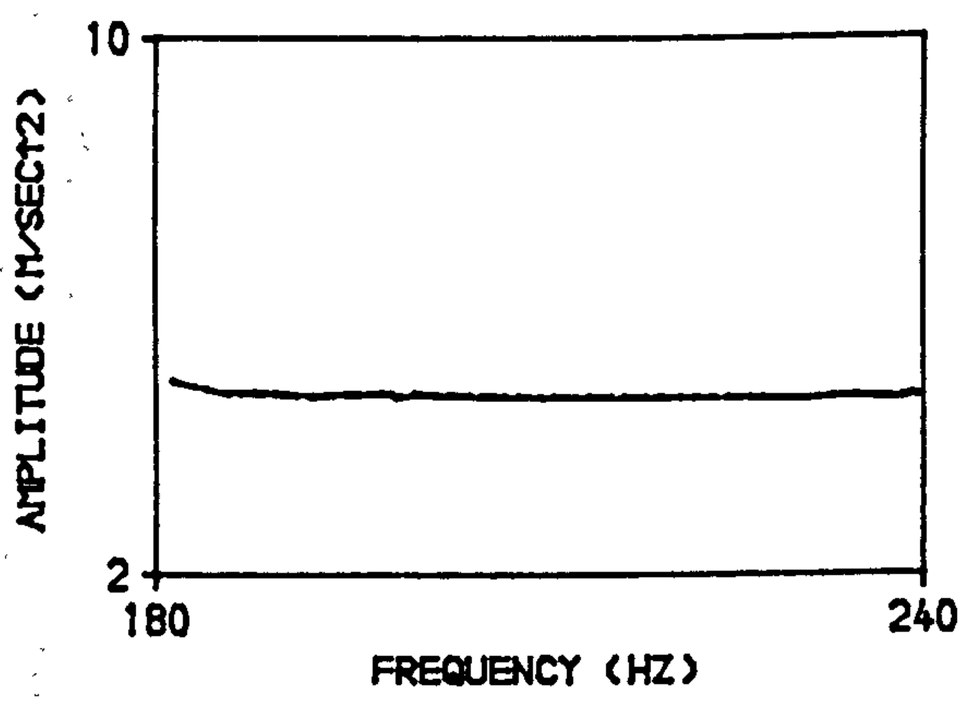

C.AFTER APPLYING SECOND LOADING STAGE.

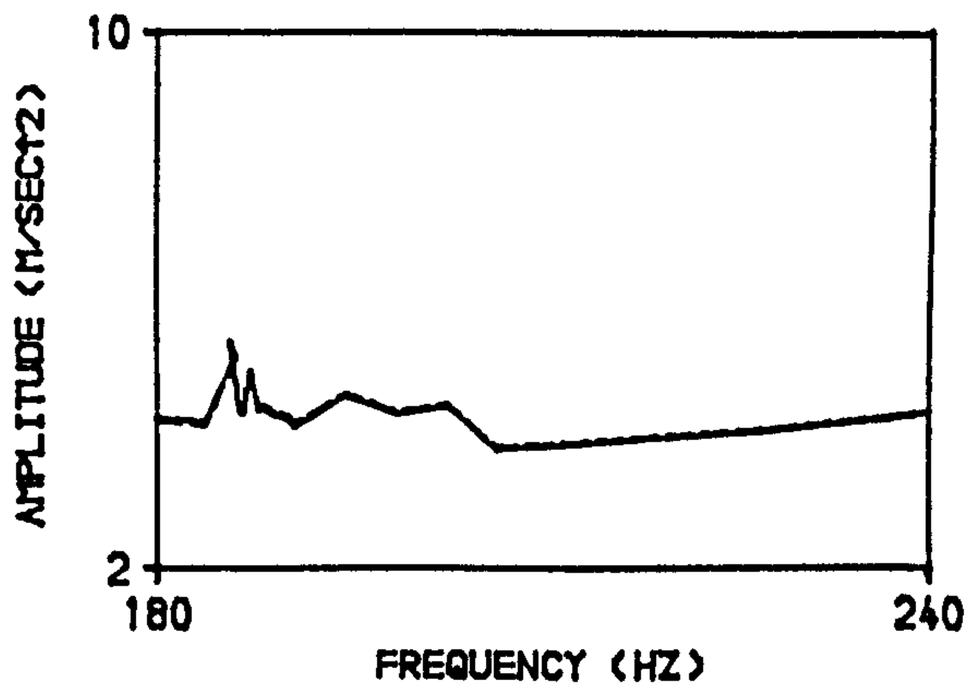

D.AFTER APPLYING THIRD LOADING STAGE.

NOTES :

——— : ABSOLUTE ACCELERATION (M/SEC^2).

------ : RELATIVE ACCELERATION (M/SEC^2)

FORCE : MOVING EXCITER MASS * RELATIVE ACCELERATION
(m) (a)

m : 0.12853 kg.

APPENDIX - E.3.3 : SETS OF FORCE OF EXCITATION FOR BEAM-3, FULLY BONDED, DIAGONAL SPLITTING CRACK PATTERNS, THIRD MODE.

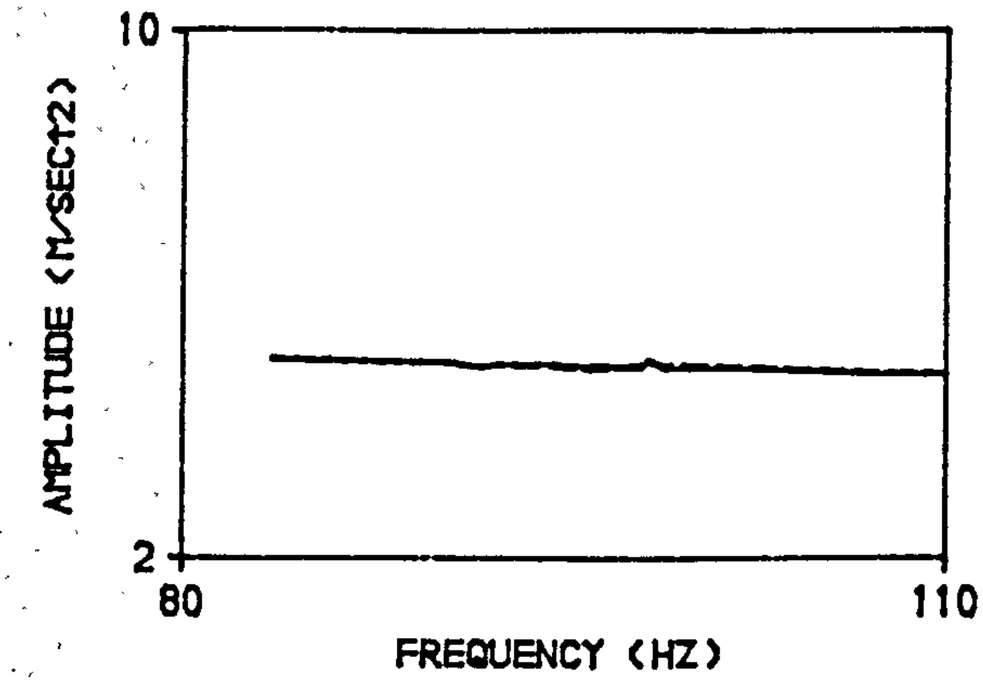

A.BEFORE APPLYING FIRST LOADING STAGE.

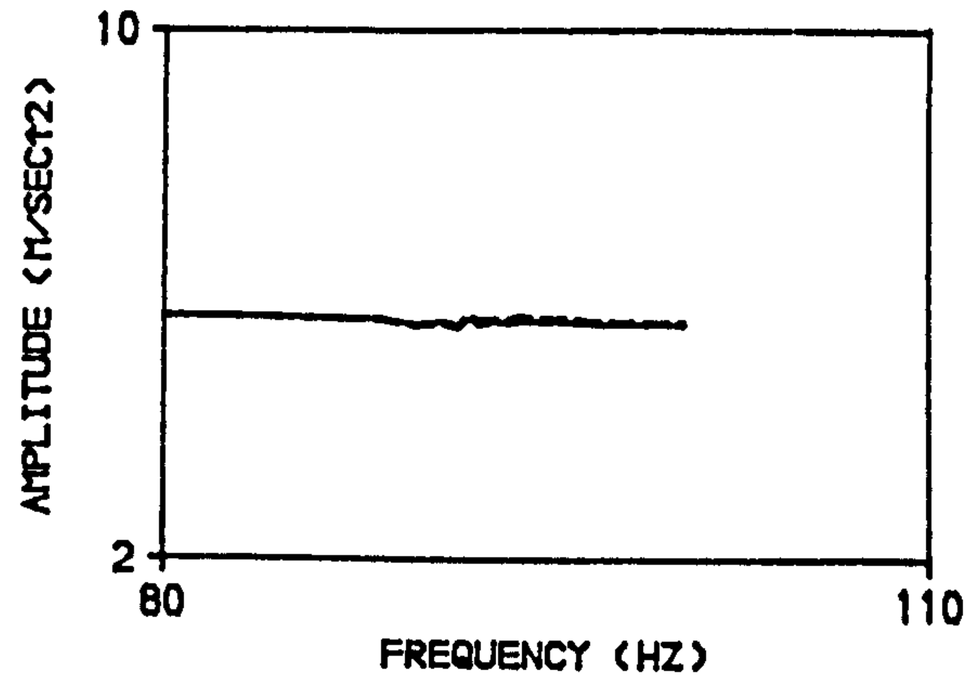

B.AFTER APPLYING FIRST LOADING STAGE.

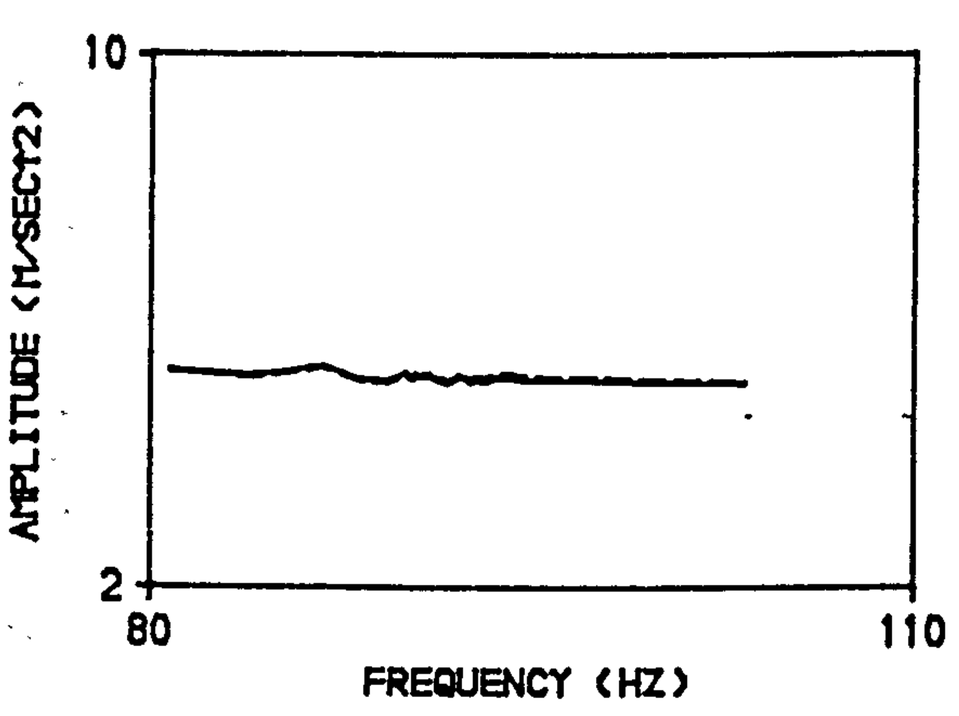

C.AFTER APPLYING SECOND LOADING STAGE.

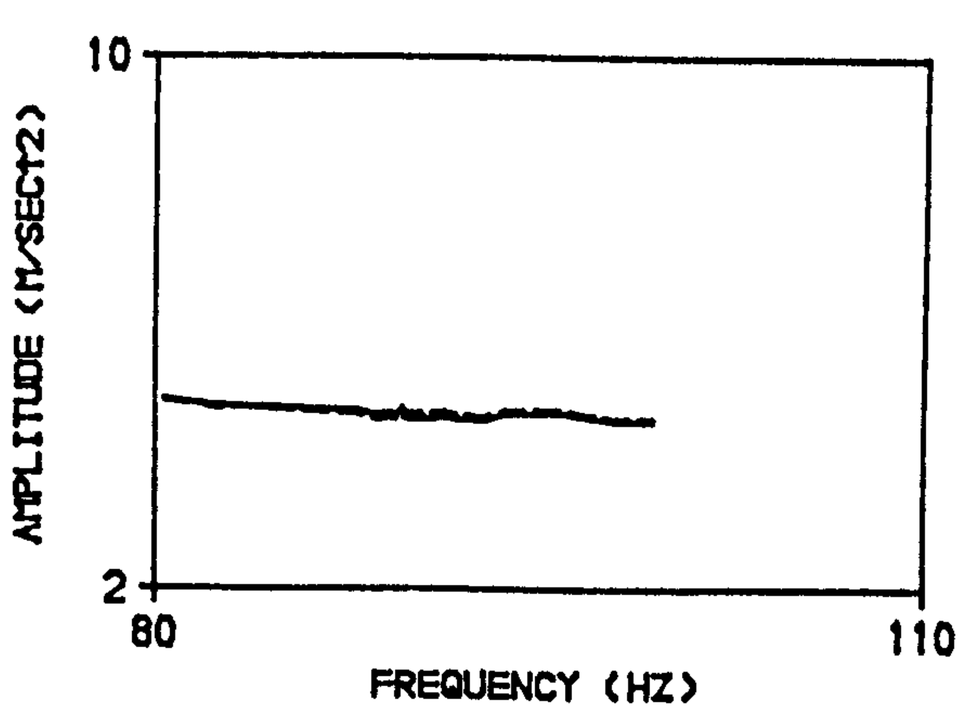

D.AFTER APPLYING THIRD LOADING STAGE.

NOTES :

——— : ABSOLUTE ACCELERATION (M/SEC^2).

------ : RELATIVE ACCELERATION (M/SEC^2)

FORCE : MOVING EXCITER MASS * RELATIVE ACCELERATION
(m) (a)

m : 0.12853 kg.

APPENDIX - E.4.1 : SETS OF FORCE OF EXCITATION FOR BEAM-4, PARTIALLY BONDED, DIAGONAL SPLITTING CRACK PATTERNS, FIRST MODE.

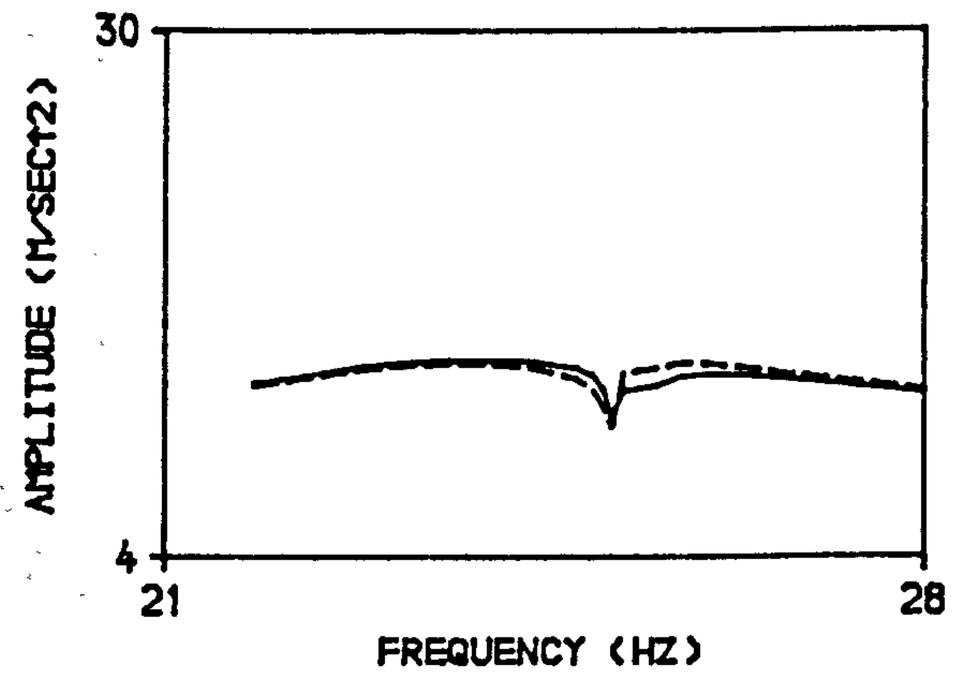

A.BEFORE APPLYING FIRST LOADING STAGE.

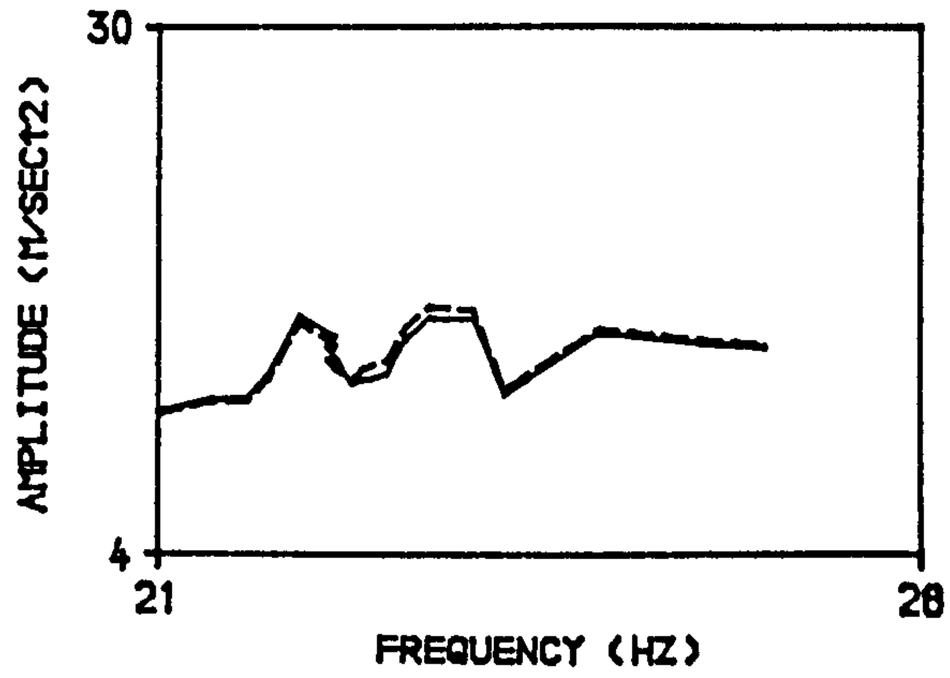

B.AFTER APPLYING FIRST LOADING STAGE.

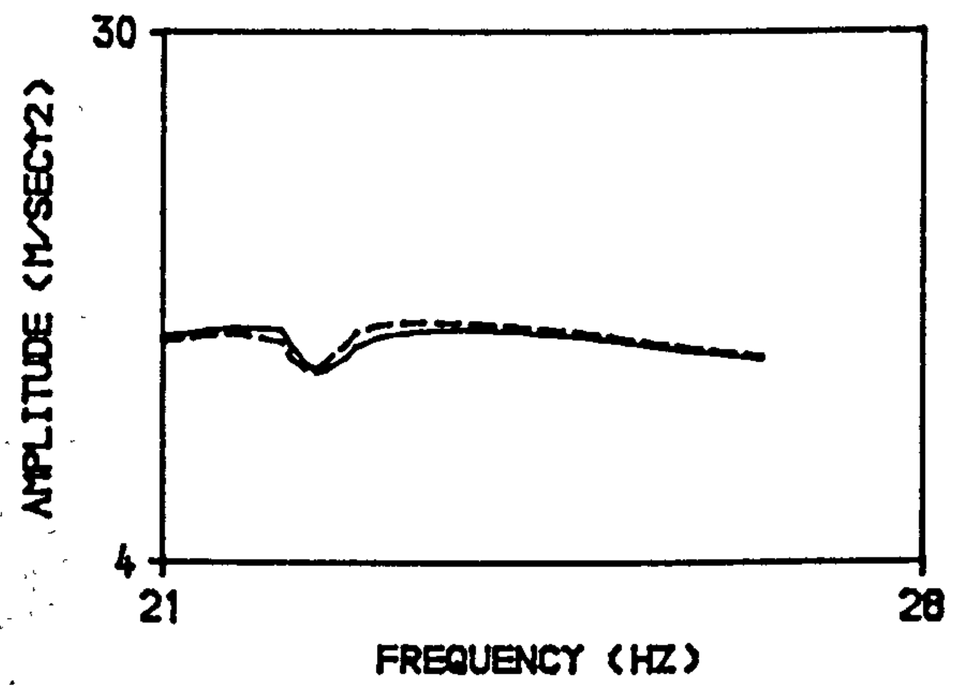

C.AFTER APPLYING SECOND LOADING STAGE.

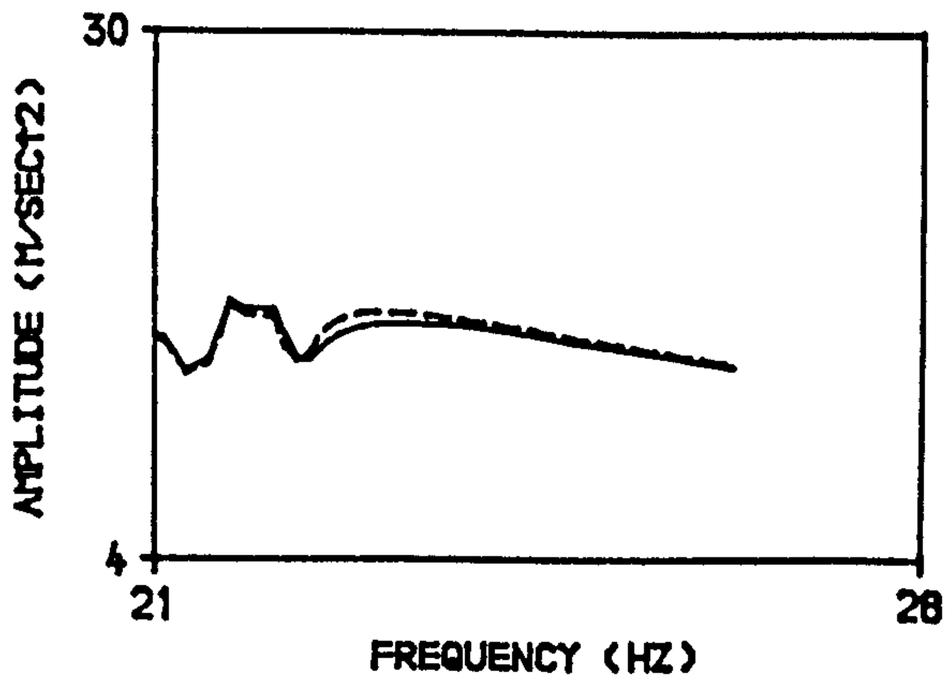

D.AFTER APPLYING THIRD LOADING STAGE.

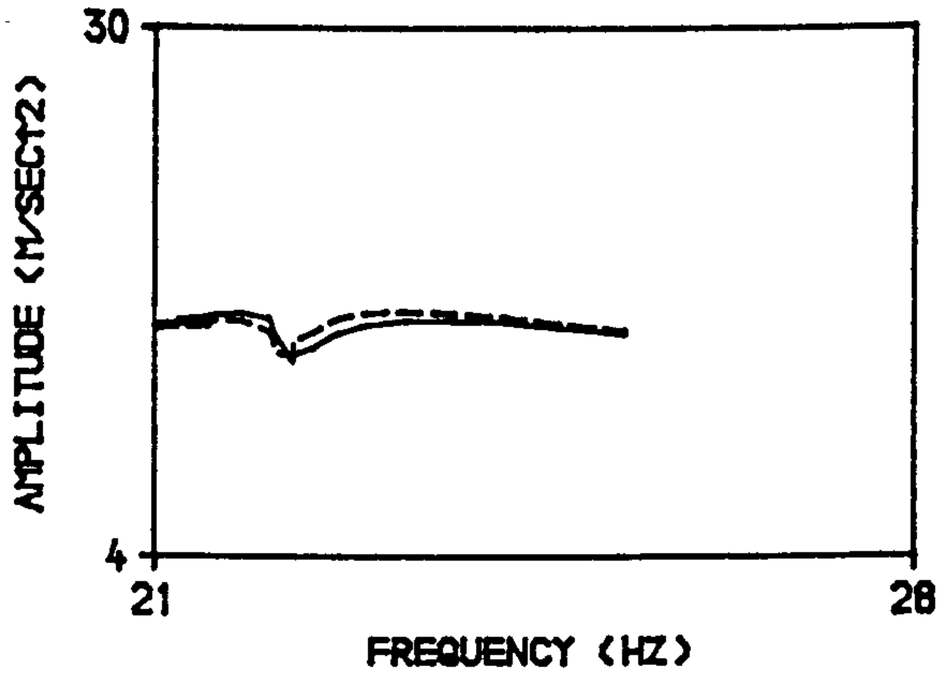

E.AFTER APPLYING FOURTH LOADING STAGE.

NOTES :

——— : ABSOLUTE ACCELERATION (M/SEC^2).

------ : RELATIVE ACCELERATION (M/SEC^2)

FORCE : MOVING EXCITER MASS (m) * RELATIVE ACCELERATION (a).

m : 0.12853 kg.

APPENDIX - E.4.2 : SETS OF FORCE OF EXCITATION FOR BEAM-4, PARTIALLY BONDED, DIAGONAL SPLITTING CRACK PATTERNS, SECOND MODE.

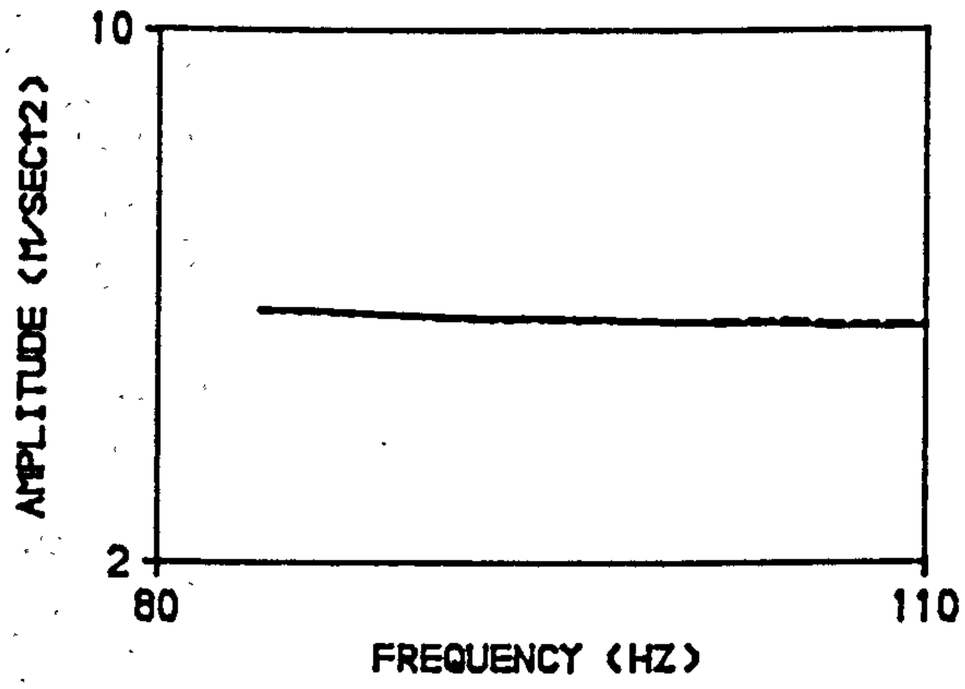

A.BEFORE APPLYING FIRST LOADING STAGE.

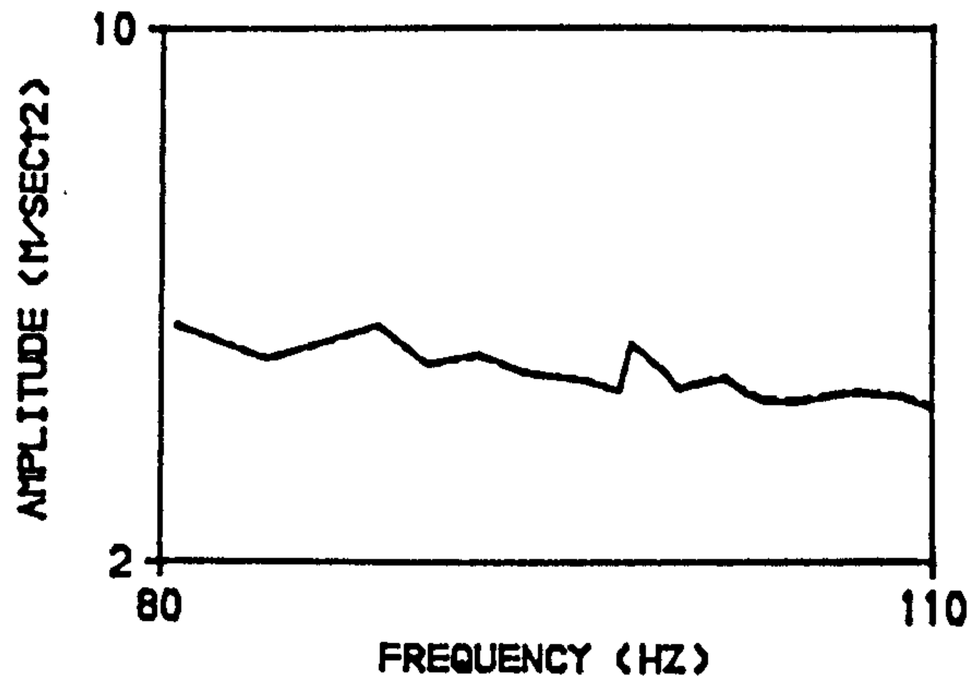

B.AFTER APPLYING FIRST LOADING STAGE.

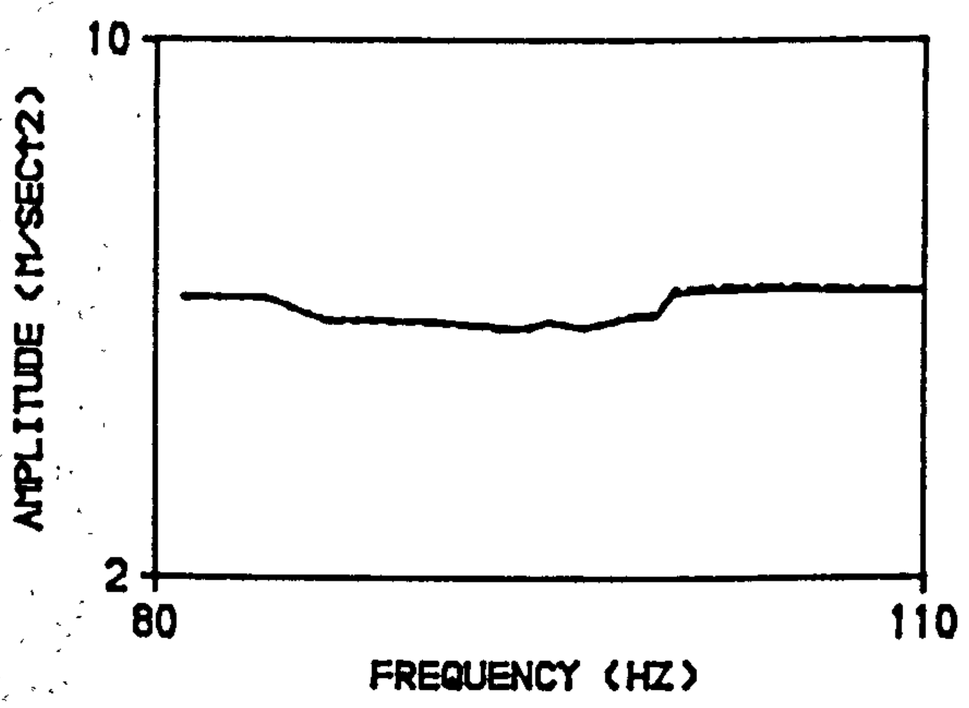

C.AFTER APPLYING SECOND LOADING STAGE.

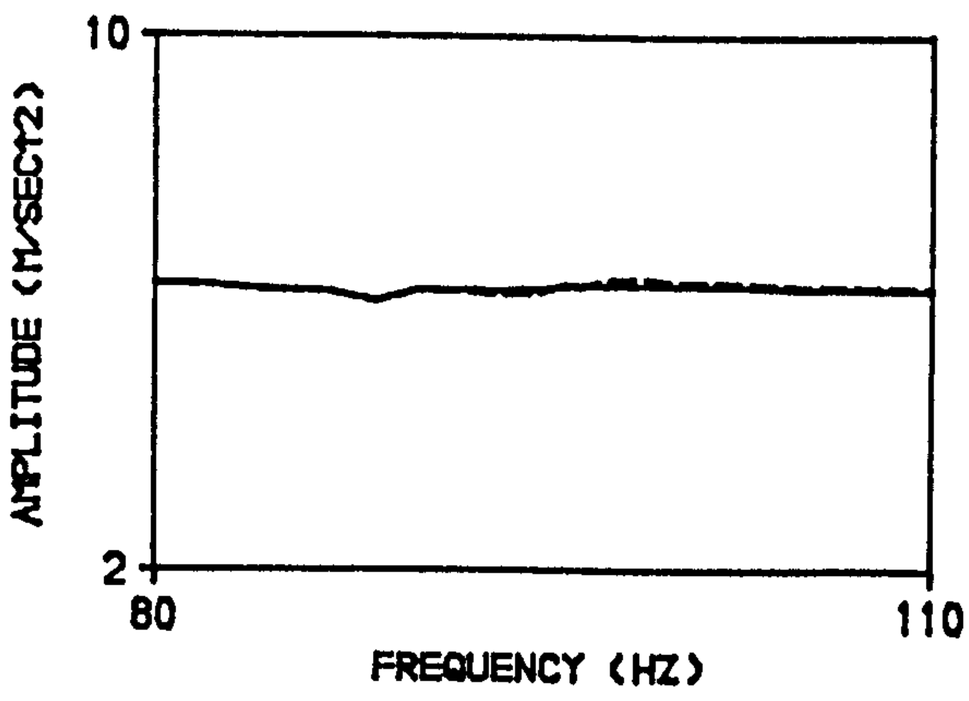

D.AFTER APPLYING THIRD LOADING STAGE.

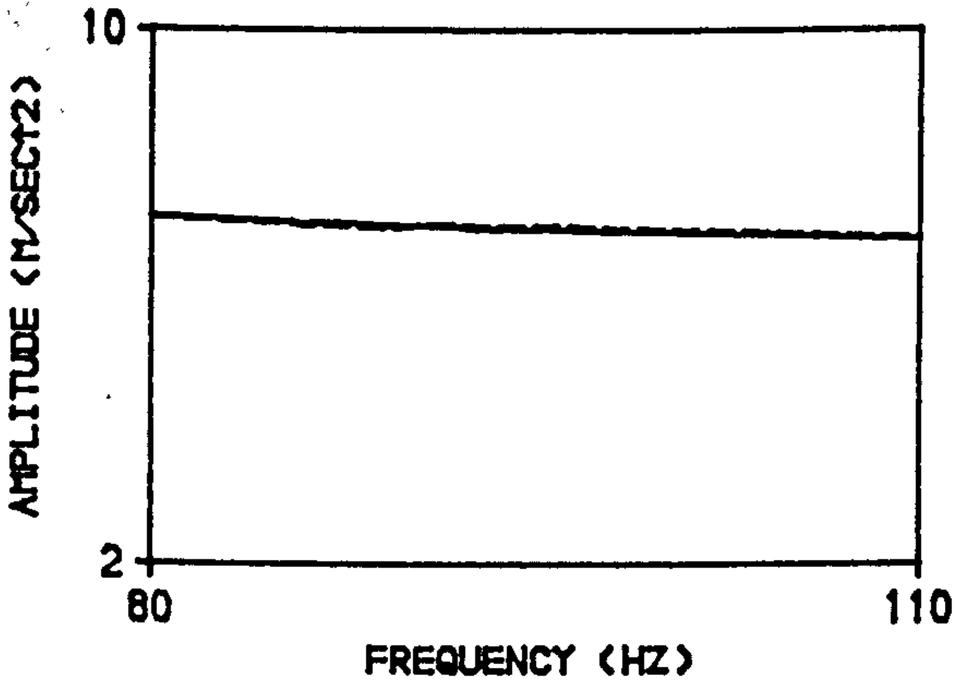

E.AFTER APPLYING FOURTH LOADING STAGE.

NOTES :

——— : ABSOLUTE ACCELERATION (M/SEC^2).

------ : RELATIVE ACCELERATION (M/SEC^2)

FORCE : MOVING EXCITER MASS (m) * RELATIVE ACCELERATION (a).

m : 0.12853 kg.

APPENDIX - E.4.3 : SETS OF FORCE OF EXCITATION FOR BEAM-4, PARTIALLY BONDED, DIAGONAL SPLITTING CRACK PATTERNS, THIRD MODE.

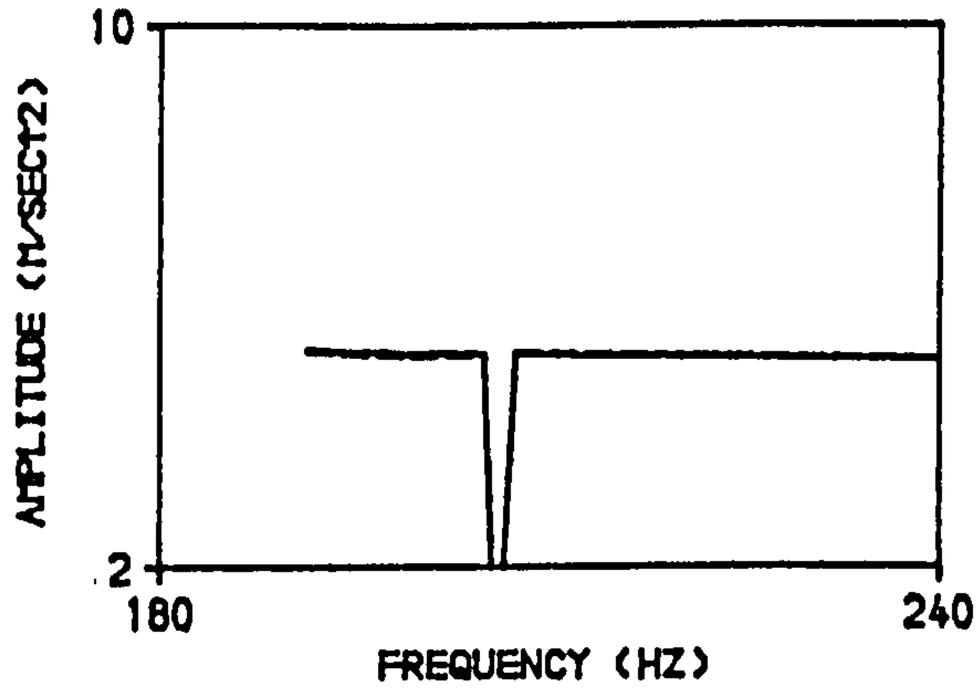

A.BEFORE APPLYING FIRST LOADING STAGE.

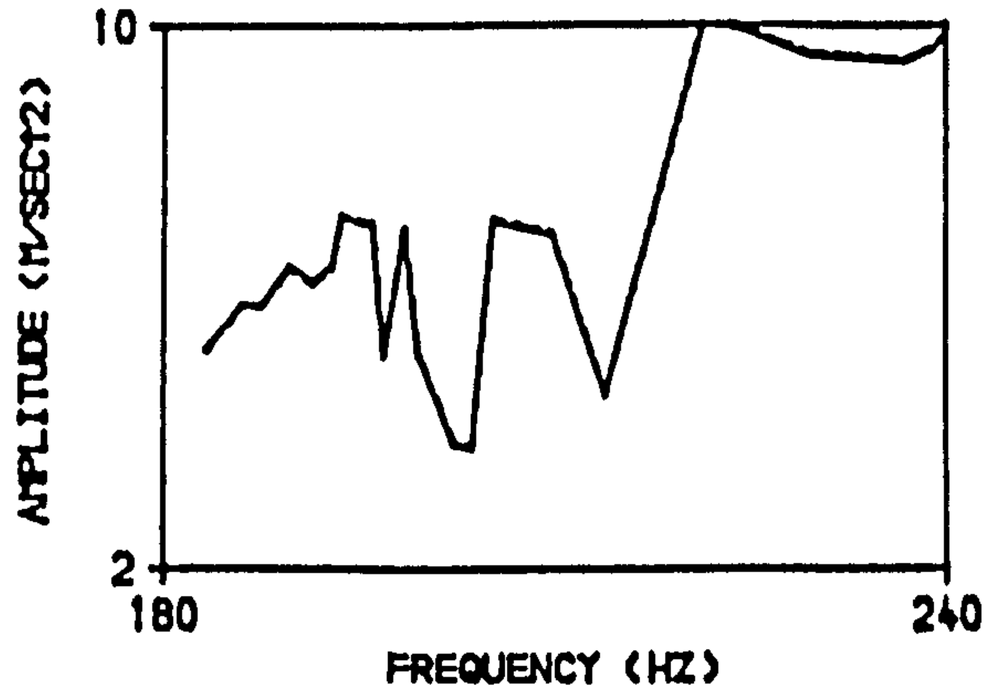

B.AFTER APPLYING FIRST LOADING STAGE.

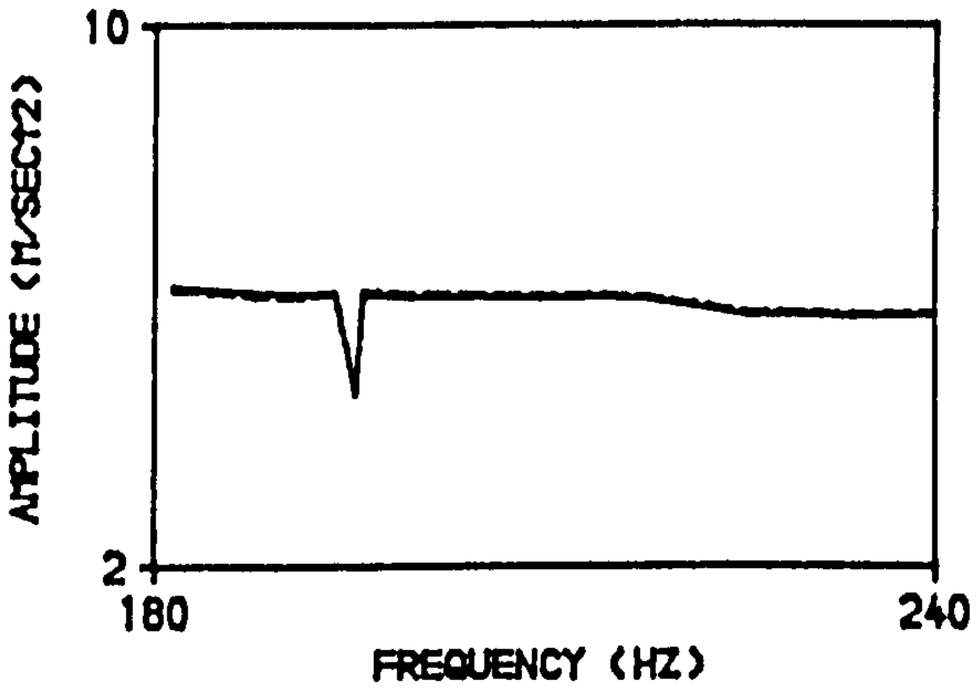

C.AFTER APPLYING SECOND LOADING STAGE.

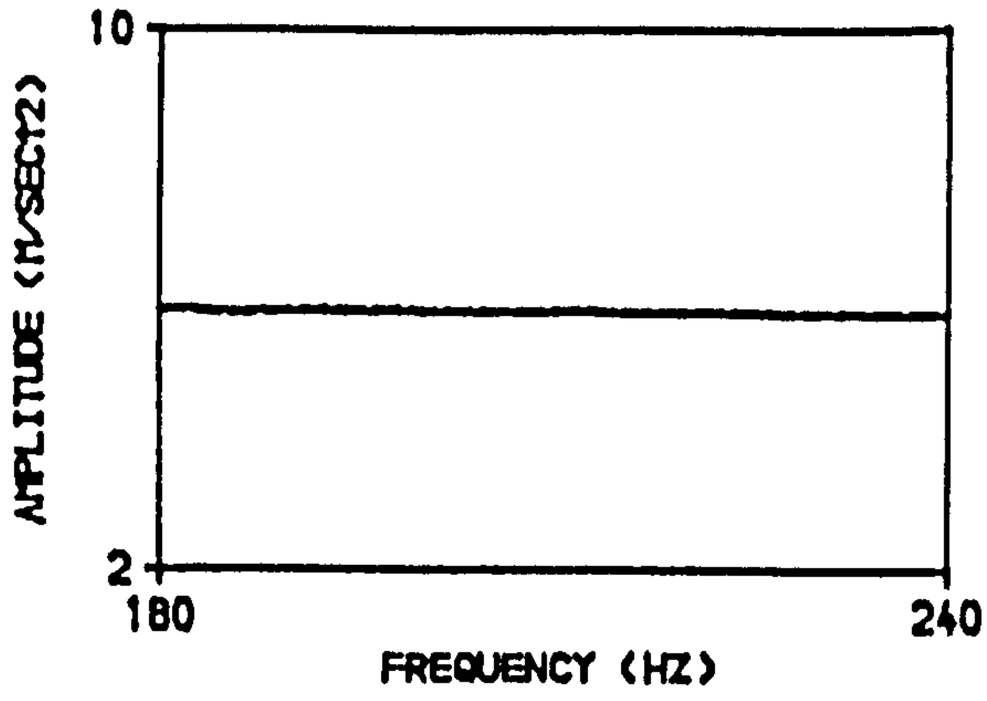

D.AFTER APPLYING THIRD LOADING STAGE.

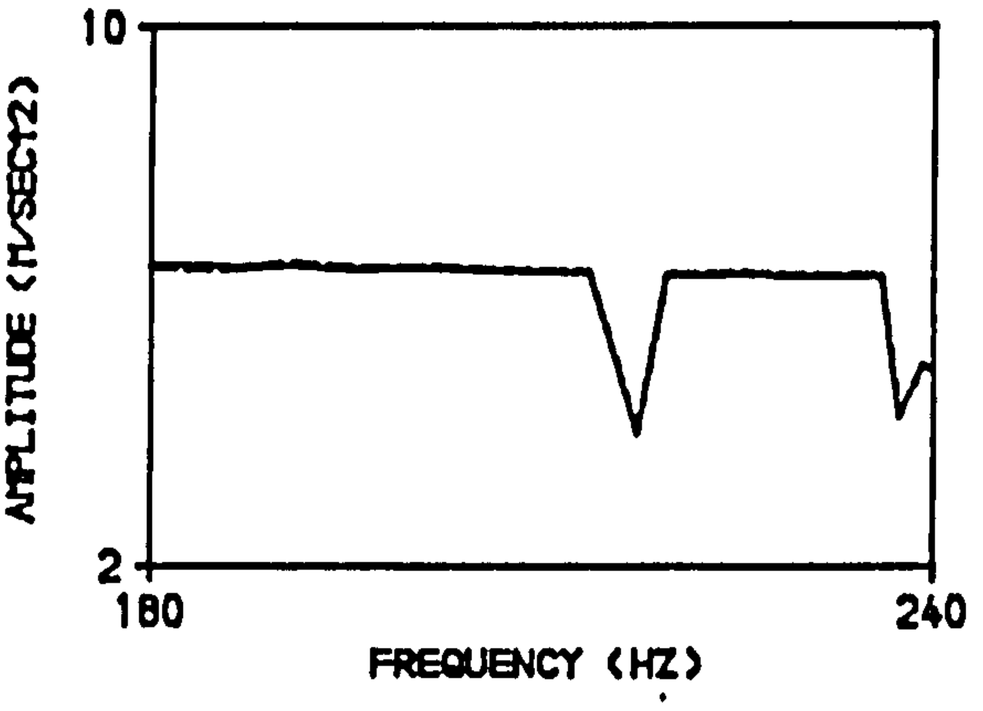

E.AFTER APPLYING FOURTH LOADING STAGE.

NOTES :

——— : ABSOLUTE ACCELERATION (M/SEC^2).

------ : RELATIVE ACCELERATION (M/SEC^2)

FORCE : MOVING EXCITER MASS (m) * RELATIVE ACCELERATION (a).

m : 0.12853 kg.

APPENDIX E-5 : CURVE FITTING

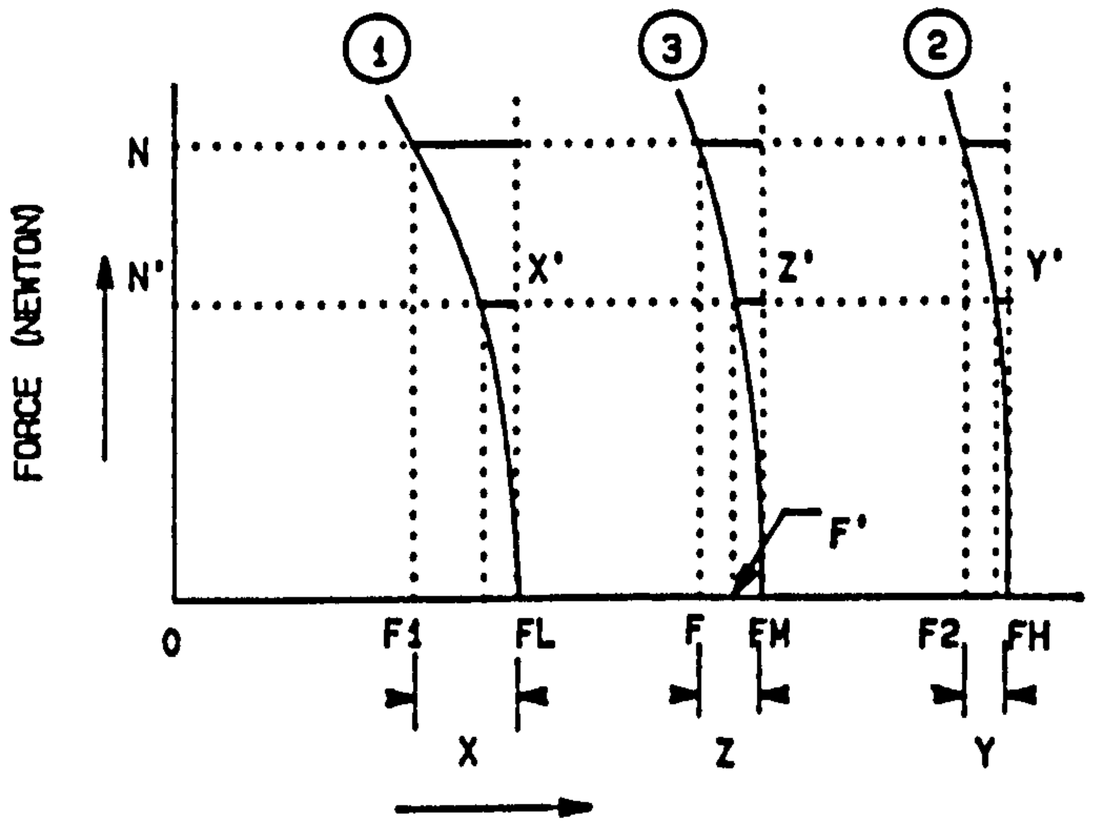

NOTES :

- FH=HIGHER FREQUENCY
- FL=LOWER FREQUENCY
- FM=INTERMEDIATE FREQUENCY
- 1 = 2 = FITTED CURVES
- 3 = INTERPOLATED CURVE
- N = GIVEN FORCE
- N'= NORMALISED FORCE IN QUESTION
- F = GIVEN FREQUENCY
- F'= FREQUENCY IN QUESTION

$$Z = \frac{(F2-F) * (X-Y)}{(F2-F1)} + Y \qquad Z' = \frac{(FH-FM) * (X'-Y')}{(FH-FL)} + Y' \qquad F' = FM - Z' = F + (Z-Z')$$

A. CURVES CORRECTING RESONANT FREQUENCIES.

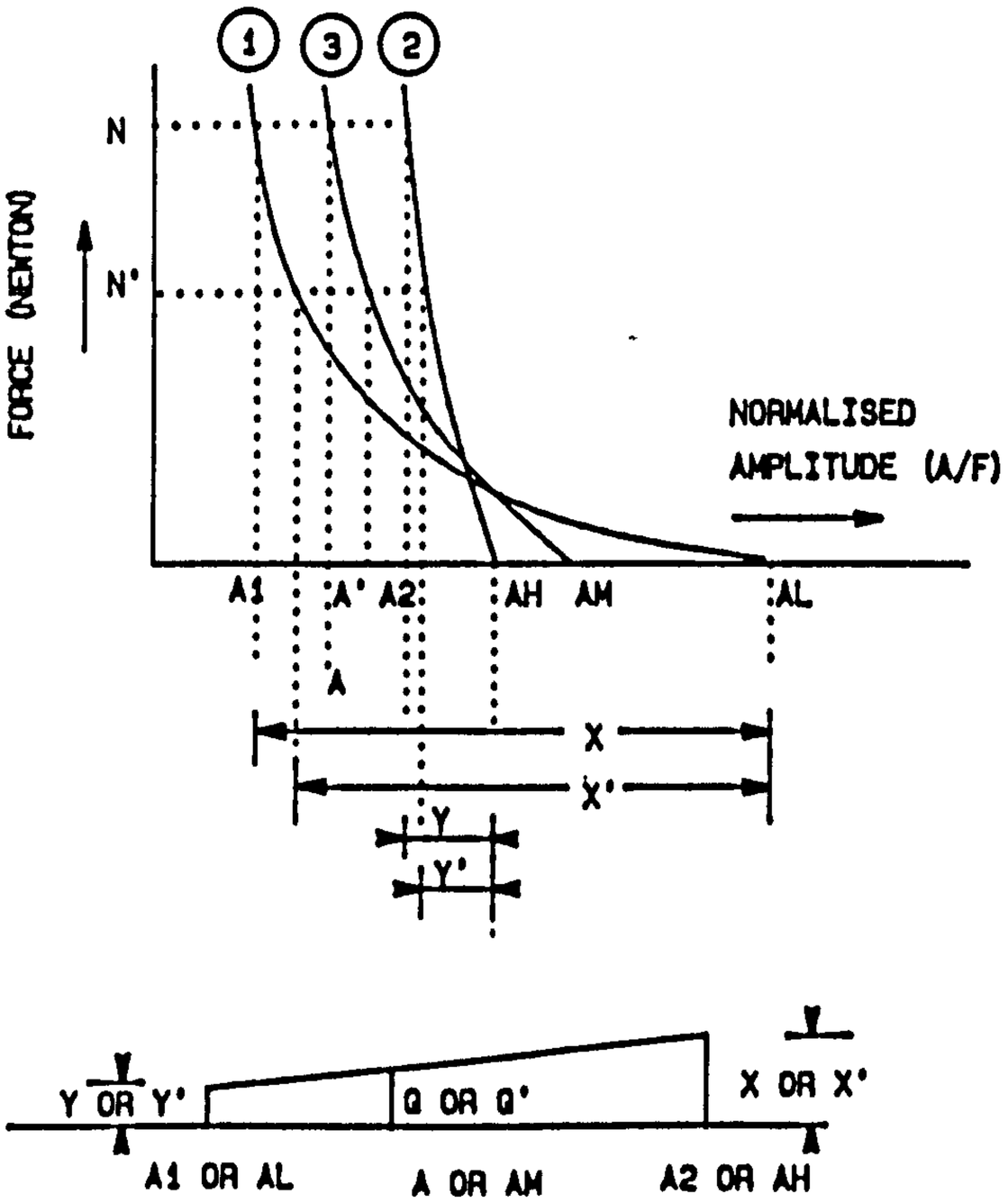

NOTES :

- AH=HIGHER AMPLITUDE
- AL=LOWER AMPLITUDE
- AM=INTERMEDIATE AMPLITUDE
- 1 = 2 = FITTED CURVES
- 3 = INTERPOLATED CURVE
- N = GIVEN FORCE
- N'= NORMALISED FORCE IN QUESTION
- A = GIVEN AMPLITUDE
- A'= AMPLITUDE IN QUESTION

$$Q = \frac{(A2-A) * (X-Y)}{(A2-A1)} + X$$

$$Q' = \frac{(AH-AM) * (X'-Y')}{(AH-AL)} + X'$$

$$A' = AM - Q' = A + (Q-Q')$$

B. CURVES CORRECTING RESONANT AMPLITUDES.